

Pieter van Gelder, Dirk Proske & Han Vrijling (Eds.): 7th International Probabilistic Workshop,
25-26 November 2009
Delft, The Netherlands 2009
TU Delft
ISBN: 978-3-00-025048-4

This book contains information obtained from authentic and highly regarded sources. Reprinted material is quoted with permission, and sources are indicated. A wide variety of references are listed. Reasonable efforts have been made to publish reliable data and information, but the authors and editors cannot assume responsibility for the validity of all materials or for the consequence of their use.

Neither the book nor any part may be reproduced or transmitted in any form or by any means, electronic or mechanical, including photocopying, microfilming, and recording, or by any information storage or retrieval system, without prior permission in writing from the editors.

The editors have no responsibility for the persistence or accuracy of URLs for external or third-party internet websites referred to in this book, and do not guarantee that any content on such websites is, or will remain, accurate or appropriate.

**Proceedings
of the
7th International
Probabilistic Workshop**

**25-26 November 2009
Delft, The Netherlands**

Edited by

P.H.A.J.M. van Gelder

D. Proske

J.K. Vrijling

Preface

Universities and Institutions from The Netherlands, Austria and Switzerland jointly organized the 7th International Probabilistic Workshop. This fact is not surprising: Humans and human settlements in these three countries are heavily exposed to natural hazards. Major areas and communities in The Netherlands are situated under sea level and facing the risk of sea dike failure and drowning. Also in Switzerland and Austria, humans are exposed to certain mountain risks such as flash floods, rock falls, debris flows, landslides or avalanches.

The recognition of such hazards and risks is mandatory when living under such conditions. Furthermore since resources are limited, one has to evaluate the hazards and has to decide which risks have to be dealt with first. The 7th International Probabilistic Workshop deals with the evaluation of risks by the application of probabilistic methods. Such probabilistic methods are now common in many different fields, not only in natural risk assessment but also in technical, health or social risk assessment. This diversity has already become visible during the history of the conference. Whereas the first two conferences were held in Dresden strongly related to structural engineering, the third conference in Vienna already showed a move to mountain risk topics. The year later in Berlin, the conference focused strongly on material testing. This topic was extended in Gent with major contributions dealing with the structural material concrete. In Darmstadt many different fields from earthquake engineering to debris flow barriers were discussed. The contributions for the conference this year are divided into five parts:

- Probabilistic Modelling in Structural Engineering
- Theoretical advances in Probabilistic Modelling
- Probabilistic Modelling for Flood Risks
- Probabilistic Modelling of Infrastructure
- Probabilistic Modelling for Geotechnical Engineering

In total 40 papers have been published in this proceedings after peer review. We thank all authors for their contributions to this conference. We also thank all reviewers who have been going through the papers.

Next year, the conference will be held in Szczecin in Poland and therefore we can assume, that risks related to the sea and ship engineering may come up again.

The organizers wish you an interesting workshop, many stimulating discussions but also some time to enjoy the nice city of Delft.

The Editors

Conference Chairman

Dr. Ir. P.H.A.J.M. van Gelder

Organizing Committee

Prof. drs. Ir. J.K. Vrijling
TU Delft,
Section of Hydraulic Engineering
P.O. Box 5048
2600 GA Delft, The Netherlands
J.K.Vrijling@tudelft.nl

Dr. Ir. P.H.A.J.M. van Gelder
TU Delft,
Section of Hydraulic Engineering
P.O. Box 5048
2600 GA Delft, The Netherlands
P.H.A.J.M.vanGelder@tudelft.nl

Drs. H.R.N. van Erp
TU Delft,
Section of Hydraulic Engineering
P.O. Box 5048
2600 GA Delft, The Netherlands
H.R.N.vanErp@tudelft.nl

Dr.-Ing. habil. D. Proske
University of Natural Resources and
Applied Life Sciences, Vienna
Institute of Mountain Risk Engineering
Peter Jordan-Strasse 82
1190 Vienna, Austria
dirk.proske@boku.ac.at

Dr. Ir. R.D.J.M Steenbergen
TNO Built Environment and Geosciences
Van Mourik Broekmanweg 6
P.O. Box 49
2600 AA Delft, The Netherlands
Raphael.Steenbergen@tno.nl



TU Delft, Section of Hydraulic Engineering, The Netherlands
University of Natural Resources and Applied Life Sciences, Vienna
Department of Civil Engineering and Natural Hazards, Austria
TNO Built Environment and Geosciences, Delft, The Netherlands

The conference has been supported by



TNO Built Environment and Geosciences, Delft, The Netherlands



European Safety and Reliability Association - ESRA

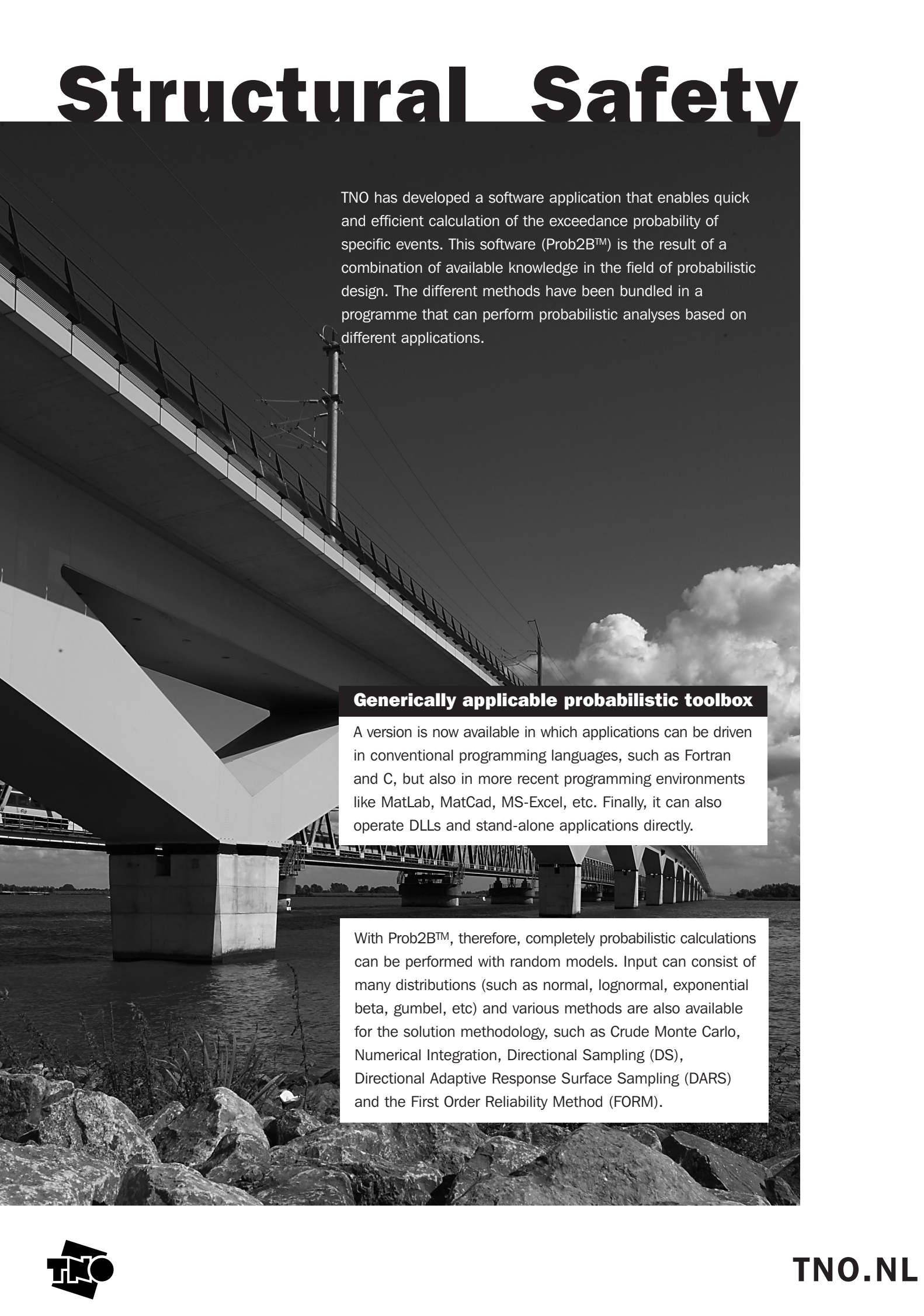


Axpo Kernenergie AG

Scientific Committee

B. Ale, Delft, Netherlands
K. Bergmeister, Vienna, Austria
C. Bucher, Vienna, Austria
H. Budelmann, Braunschweig, G.
R. Caspeepele, Ghent, Belgium
B. Ellingwood, Atlanta, USA
M.H. Faber, Zuerich, Switzerland
D. Frangopol, Lehigh, USA
P. van Gelder, Delft, Netherlands
J. de Gijt, Delft, Netherlands
C.-A. Graubner, Darmstadt, Germany
L. Gucma, Szczecin, Poland
M. Holicky, Praha, Czech Republic
M.J. Kallen, Delft, Netherlands
G. Mancini, Torino, Italy
R. Melchers, Callaghan, Australia
F. Nadim, Oslo, Norway
U. Peil, Braunschweig, Germany
D. Proske, Vienna, Austria
T. Schweckendiek, Delft, Netherlands
R. Steenbergen, Delft, Netherlands
A. Strauss, Vienna, Austria
P.D. Spanos, Houston, USA
L. Taerwe, Gent, Belgium
M.C. ten Veldhuis, Delft, Netherlands
P. Vermeer, Stuttgart, Germany
H. Vrijling, Delft, Netherlands
T. Vrouwenvelder, Delft, Netherlands

Structural Safety



TNO has developed a software application that enables quick and efficient calculation of the exceedance probability of specific events. This software (Prob2B™) is the result of a combination of available knowledge in the field of probabilistic design. The different methods have been bundled in a programme that can perform probabilistic analyses based on different applications.

Generically applicable probabilistic toolbox

A version is now available in which applications can be driven in conventional programming languages, such as Fortran and C, but also in more recent programming environments like MatLab, MatCad, MS-Excel, etc. Finally, it can also operate DLLs and stand-alone applications directly.

With Prob2B™, therefore, completely probabilistic calculations can be performed with random models. Input can consist of many distributions (such as normal, lognormal, exponential beta, gumbel, etc) and various methods are also available for the solution methodology, such as Crude Monte Carlo, Numerical Integration, Directional Sampling (DS), Directional Adaptive Response Surface Sampling (DARS) and the First Order Reliability Method (FORM).

Contents

Preface		i
Part I: Keynote Lectures on Probabilistic Modelling		1
Probabilistic budgeting and time-planning	J.K. Vrijling and P.H.A.J.M van Gelder	3
Losses due to spillage at Gariep Dam	D.J. de Waal and A.Verster	23
Part II: Probabilistic Modelling in Structural Engineering		
Application of biostatistics in the analysis of fatigue data in bond research	L. Eckfeldt and M. Curbach	37
Use of reliability analysis in engineering practice - possible applications and examples	T. Braml and M. Keuser	61
Combined production and conformity control of concrete with acceptance cusum control charts	R. Caspeele and L. Taerwe	73
Probabilistic design for cracking of concrete structures	M. Holicky, J. Retief and J. Wium	87
Influence of a combined vague-informative prior on the assessment of characteristic concrete strength	R. Caspeele and L. Taerwe	99
Reliability analysis of static equilibrium	M. Holicky and M. Sykora	111
Integrative reliability assessment of concrete structures	A. Strauss and K. Bergmeister	119
Part III: Theoretical advances in Probabilistic Modelling		
Determination of design spectrum compatible evolutionary spectra via Monte Carlo peak factor estimation	A. Giaralis and P. D. Spanos	129
Reliability of reinforced structural elements in existing structures subjected to shear force	A.Fischer, J. Schnell, T. Braml and M.Keuser	145
Probabilistic assessment of performance criteria for egress design	C. Albrecht and D. Hosser	163
Sensitivity analysis of partial safety factors to the design of offshore steel structures	A. Kolios, I. Jusoh and F. Brennan	177
A method of risk ranking for international transportation projects	E. A. Gamez and A. Touran	187
Introducing nested sampling	N. van Erp and P.H.J.A.M. van Gelder	205

Influence of the model creation methodology on the failure probability of gust exposed structures	E. Bombasaro	219
Characteristic concrete strength based on compression tests using either vague prior information or using prior information from rebound tests	R.D.J.M. Steenbergen and A. H.J.M. Vervuurt	229
Assessing the probability of material failure in Cantilever stone stairs	D. O'Dwyer A. O'Connor and O. Bashorun	239
Seismic risk assessment of unreinforced and prestressed masonry by means of probabilistic simulations	S.T. Sperbeck and H. Budelmann	251
Modeling of imprecise distribution functions by uncertain stochastic moments within the maximum entropy formulation	T. Most	265
Probabilistic sensitivity of limit states of structures. The Monte Carlo simulation	M. Skowronek	281

Part IV: Probabilistic Modelling for Flood Risks

Non-parametric continuous Bayesian belief networks for Earth Dam Safety	O. Morales Napoles and D.J. Delgado-Hernández	295
Extension of the probabilistic evacuation decision model	K. Wojciechowska	313
Determination of safety levels for quay wall structures	J. Böckmann and J. Grünberg	327
A qualitative approach to assess flood risk associated with landfills	C. Neuhold and H.P. Nachtnebel	343
Risk management of concrete flood protection walls by application of Bayesian networks	J. Marengwa and J. Retief	359
Probabilistic service life prediction of hydraulic structures under abrasion loads	M. Vogel and H.S. Müller	385
Probabilistic method of minimal safety depth evaluation for maximal ferries approaching to Ystad port	L. Gucma and M. Gucma	397

Part V: Probabilistic Modelling of Infrastructure

A probabilistic framework to determine the probability of collapse for bridges subject to vessel collision	M. Davidson and G. Consolazio	415
Scenario characteristics affect the risk of fatalities after accidents with chlorine and ammonia at a category III of evidence	F. van Boven	427

Basis for risk management of vehicle bridges located on seismic zones	D. De-León-Escobedo and D. J. Delgado-Hernández	439
Evaluating the characteristics of marine pipelines inspection data using probabilistic approach	Z. Mustafa, G. Shams and P.H.A.J.M van Gelder	451
Road traffic load model for weight restricted bridges	D. Proske and S. Loos	465
Comparison of current probabilistic approaches for budget estimating for transportation projects	P. Bakhshi and A. Touran	479
Risk Assessment of Petroleum pipelines using a combined analytic hierarchy process - Fault Tree Analysis	A. W. Dawotola, P.H.A.J.M van Gelder and J.K Vrijling	491

Part VI: Probabilistic Modelling for Geotechnical Engineering

Updating piping probabilities with survived loads	T. Schweckendiek and W. Kanning	505
Contributions to probabilistic soil modelling	M. Huber, A. Moellmann, P. A. Vermeer and A. Bárdossy	519
Reliability of reinforced masonry walls subjected to in-plane shear	E. Brehm, J. E. Dickie and S. L. Lissel	531
The subset simulation applied to the reliability analysis of a nonlinear geotechnical finite element model	I. Papaioannou, H. Heidkamp, A. Düster, E. Rank and C. Katz	543
A modified approach to the polluter-pays-principle that accounts for the value of groundwater resources and its impact on statistical decision-making	E.K. Paleologos	557

Part I

Keynotes

on

Probabilistic Modelling

Probabilistic Budgeting and Time-Planning

J.K. Vrijling and P.H.A.J.M. van Gelder
Delft University of Technology

Abstract: In this paper an overview is given of the principles of probabilistic budgeting and time planning. Uncertainties related to normal – and special events are described. Analytical expressions are presented. To deal with correlations between special events, an alternative for the classical product moment correlation coefficient is proposed.

1 Introduction

The management and control of the costs and the duration of civil engineering projects have been studied in literature since the early 1970's [5, 3, 7, 8]. Apart from uncertainties concerning quantities and production times (such as unit prices and wages), uncertainties involving economics and “influences from the outside world” (essentially changes in the design of the project), the difficulties in modelling the budgeting and time-planning are caused by the long period over which a civil engineering project is stretched. This period starts when the social demand for change is felt and the first plan for the project is outlined. The end of the period can be set at the delivery of the final product and the settlement of the bill.

The estimate of the budget is an approximation of the real costs. If all knowledge and facts have to be expressed in one single number, as is often required, discrepancies between the estimate and the finally realised costs cannot be avoided. Normally, in comparisons between the original estimate of the building costs and the total expenses at the end of the project, no correction is incorporated for the overall increase in prices. In Table 1, the exceedence of the budgets for the hydraulic engineering projects of the reclamation of some IJsselmeerpolders is given [1]:

Table 1:

Polder:	Exceedence
Wieringermeerpolder	12%
Northeast polder	16%
Easterly Flevoland	- 3%

The difference in accuracy between an estimate of the budget in an early stage of the project (the study-of-plan phase) and the final estimate (builder’s specifications at the start of the engineering) is illustrated in the next table [3]:

Table 2:

Project	Difference in % of the final costs	
	Estimate in study-of-plan phase	Estimate in Builder’s specifications phase
Haringvliet locks	77%	22%
Grevelingen dam	- 19%	22%
Volkerak dam	56%	23%
Brouwers dam	- 39%	- 18%

Often final project costs exceed their estimate. Historical estimates of the budget at the Ministry of Public Works in The Netherlands (Rijkswaterstaat) [4] clearly show a pattern of increase of costs and delay in work (which, due to inflation and loss of interest, also increases the costs):

Table 3:

Project	Start	Planned		Reality	
		Mf	years	Mf	years
Noordhollands Canal	1818	4	5	12.5	7
Haarlemmer lake	1837	8.4	5 (?)	13.8	21
Nieuwe Waterweg	1858	5	5	36.8	38
Maas & Waal	1864	6.5	10	24.7	44

In road-construction projects there were (and there are) large fluctuations in the differences between the estimated budgets and the real costs as well. For road-construction projects in The Netherlands from 1980 up to 1985, differences between estimates in the pre-design phase and the real costs as a percentage of the real costs are given in the following histogram:

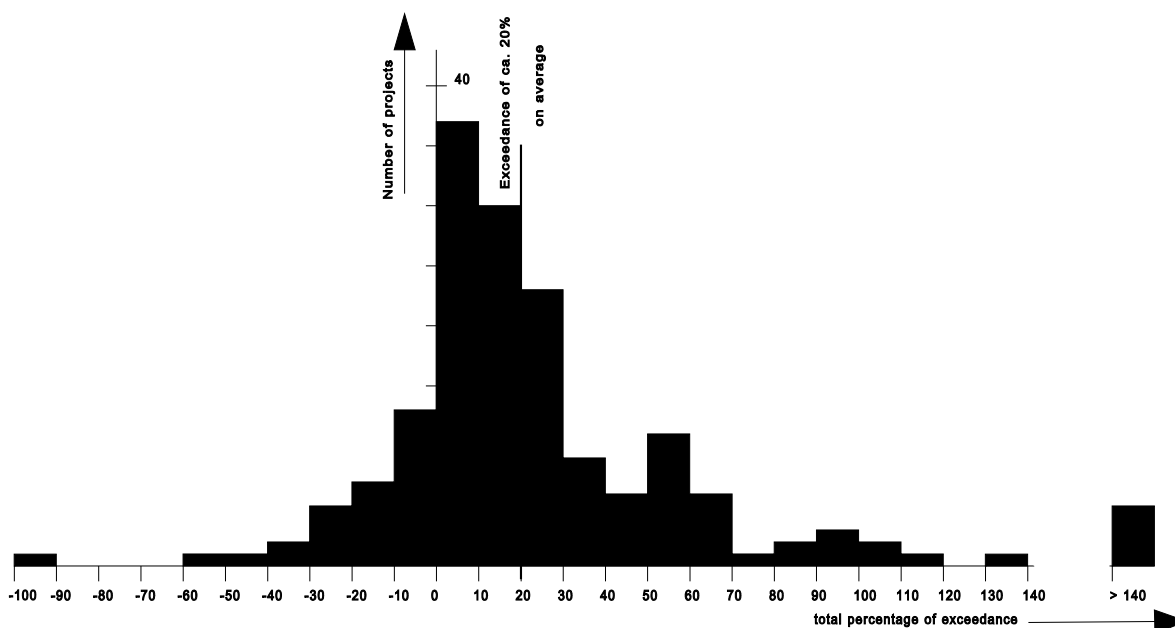


Figure 1.

Publications on exceedance of the estimates of budgets in other countries show the same tendency [2] and [5].

2 The classical approach to budget estimates and time-planning

From early days, the calculation of estimates of the budget and time-planning schemes are based on the most likely values. Uncertainty of the decision maker is expressed as an increase of the deterministic final amount by a certain percentage of that amount.

Uncertainty regarding the budget estimate or the time-planning scheme is not constant during the project. The later on in the project an estimate of the budget or a time-planning scheme is made, the more about the project is known and the decision maker’s uncertainty concerning the estimated amounts of money and duration of the activities will be less than in the early stages of the project. A classification of project phases in order of time is given in Table 4. The project parts in the phase at hand are estimated or planned in detail, for other parts in other phases the estimates are determined roughly.

Table 4:

Class	Project phase
D	study-of-plan
C	pre-design
B	pre- builder’s specifications
A	builder’s specifications

Because of the decision maker’s greater uncertainty in the early phases of the project, it is of no use to make detailed estimates and time-planning schemes for phases to come. Making an

estimate of the budget in detail for builder's specifications when the project is still in the study-of-plan phase will turn out to be a waste of time, although in the early stages more detailed estimates and time-planning schemes (or parts of those) are made.

Budget-estimates

First, some examples of specifications of budget estimates in several phases of a project are given.

Estimate of the budget, Class D (Study-of-plan phase)

<i>1 viaduct</i>	×	<i>price of 1 viaduct</i>	=	<i>item viaduct</i>
<i>5 km of road</i>	×	<i>price per km of road</i>	=	<i>item road</i>
<i>1 tunnel</i>	×	<i>price per tunnel</i>	=	<i>item tunnel</i>
				----- +
				<i>Total of Direct costs</i>
				<i>Indirect costs</i>
				----- +
				<i>Primary costs</i>
				<i>Additional costs</i>
				<i>Miscellaneous¹⁾</i>
				----- +
				<i>Basic estimate</i>
				<i>Unforeseen²⁾</i>
				----- +
				<i>Estimate (ex. VAT)</i>
				<i>VAT</i>
				----- +
				<i>Study-of-plan phase estimate</i>

In the successive phases the items of the class D- estimate are worked out in more detail. An example is given in the following class B- estimate.

Estimate of the budget, class B (Pre-builders specifications phase):

<i>800 m³ soil</i>	×	<i>price per m²</i>	=	<i>item "soil"</i>
<i>800 m³ concrete</i>	×	<i>price per m³</i>	=	<i>item "concrete"</i>
<i>1 ton reinforcement</i>	×	<i>price per ton</i>	=	<i>item "reinforcement"</i>
<i>800 m² formwork</i>	×	<i>price per m²</i>	=	<i>item "formwork"</i>
				----- +
				<i>Subtotal viaduct</i>

The other items are detailed analogously.

In a class A-estimate (estimate for builders specifications) the prices per m³, m² or ton are determined in more detail, based on working methods and quantities. In an estimate in this

1) In "Miscellaneous" those costs are categorized which are known but which are not specified. For a study-of-plan phase estimate these could be: land (has to be bought) preparation, deflection of conduit-pipes and water courses, temporary diversion of traffic, etc..

2) "Unforeseen" is taken as an additional percentage on the Basic estimate here. If there is little insight in the character of the item Unforeseen then this way of calculation is applicable.

phase, time and equipment are taken into consideration. Contractors prefer this method of estimating.

A sub-item of the item SOIL of the partial project ROAD from the class D-estimate (5 km of road) is chosen as an example of specification of an item in a class A- estimate:

For the delivery and processing of 80,000 m³ of soil for the partial project "road" the costs of the following means of production are estimated:

<i>Delivery at the quay by ship</i>	80000 m ³	×	<i>price per m³</i>	= <i>partial item 1</i>
<i>Lease of an unloading plant</i>	80 days	×	<i>day tariff</i>	= <i>partial item 2</i>
<i>Transport to location (by cars)</i>	800 days	×	<i>day tariff</i>	= <i>partial item 3</i>
<i>Equipment for processing and compaction</i>	85 days	×	<i>day tariff</i>	= <i>partial item 4</i>
			----- +	
			<i>Subtotal soil</i>	

The price per m³ of processed soil is calculated by division by the volume in m³ (here: 80,000).

In principle, the estimate of Direct costs (an example of which was given for a class D-estimate at the bottom of the previous page) follows from an addition over all N partial items of the multiplication of quantity, h_i, and the prices per unit, p_i (see the calculation scheme of the budget estimate on the next page). Indirect costs can be calculated by an additional percentage, %₁, which is a fixed percentage of the Direct costs.

Additional costs and Miscellaneous can both be expressed as a percentage %₂ of the Primary costs. As stated above, additional costs are established as a percentage of the preceding part of the estimate. The Total estimate can thus be expressed as a function of the total of the Direct costs. A percentage of (the part of) the afore calculated estimate is called an additional percentage ¹⁾.

In any phase of the project such percentages can differ. Generally, the Total estimate, in which the additional percentages are included, is calculated from the total Direct costs:

$$Estimate = \left(\prod_{j=1}^M (1 + \%_j) \right) \left(\sum_{i=1}^N h_i p_i \right)$$

in which:

M = the number of additional percentages

%_{*j*} = the *j*th addition over the foregoing subtotal

N = the number of cost items in the Direct costs

1) An additional percentage (for example the percentage Unforeseen) can be seen as a random variable or as a deterministic constant. For example the percentage VAT was fixed at 17.5% for a long time. It can be regarded as a fixed constant, unless it is expected to be changed in the future. Then, introducing the percentage VAT as a random variable is an option. In 2009, VAT is 19%.

h_i = the quantity of the i^{th} item in the Direct costs

p_i = de unit price in the i^{th} item in the Direct costs.

Time-planning

In an estimate of the budget the unit prices have to be multiplied by their quantity and then added. In a time-planning only the duration or the lengths of time of all activities have to be added and no multiplication is needed:

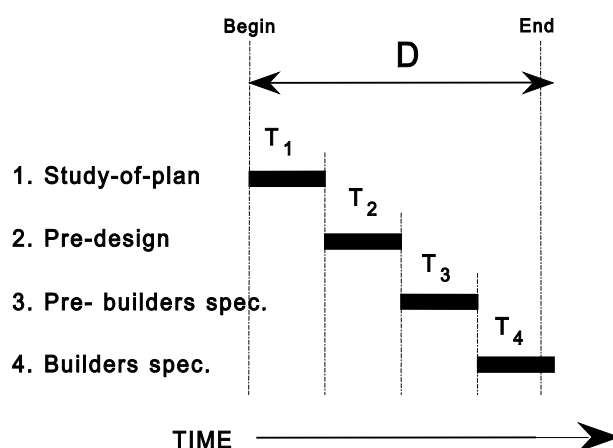


Figure 2.

The duration of the project, D , equals:

$$D = \left(\sum_{i=1}^N T_i \right)$$

in which:

i = rotation number of the activity

T_i = duration of the activity i

N = number of activities (in Figure 2: $N = 4$).

If the various activities succeed each other in time the time-planning is simple. Example: In a small building pit, pile driving cannot be started before digging of the pit is completed. The digging hinders pile driving too much.

Usually not all activities succeed each other in time. Various activities are (partially or totally) executed simultaneously. A consecutive activity can often only be started when more than one preceding activity have been completed.

In the figure below it is shown that the pre-builder's specifications phase can only be started when the pre-design phase has been completed and the licences have been granted. Both the

activities have to be completed before the pre-builder's specifications phase can be started. If two activities are executed in parallel (in Figure 3: the pre-design phase and the granting of licences) the time-planning can be sketched as follows:

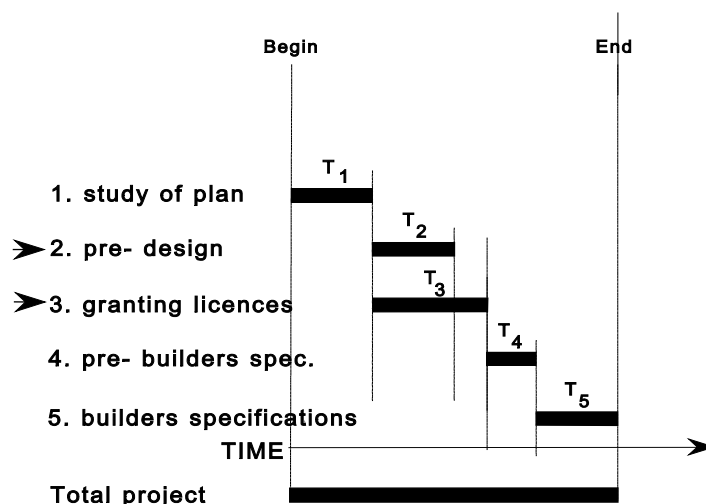


Figure 3.

In this example there are two time-paths:

$$D_a = T_1 + T_2 + T_4 + T_5$$

$$D_b = T_1 + T_3 + T_4 + T_5$$

The total duration of the project, D_{tot} , is the maximum amount of time according to the duration of the various time-paths: $D_{tot} = \max(D_a, D_b)$.

In the example in Figure 3, the duration of the activities 1, 3, 4 and 5 determine the duration of the total project, D_{tot} . It is said that these activities form the *critical time-path* (critical path for short).

3 Uncertainty concerning budget estimates and time-planning

In order to express one's uncertainty about the estimate or the time-planning, probabilistic techniques are employed. If the random character of the cost items or the duration of the various activities are taken into account, the budget estimate or time-planning of the project is said to be statistically controlled.

The estimated amount of money or the planned duration of a project can be interpreted in various ways, depending on what the person who estimates or plans has in mind. Does he or she focus on an estimate of the mean costs or duration (the expected values) or on the amount that is most likely (the mode of the costs or the duration)? In the first case it is commonly assumed that the costs or the duration are normally distributed. The mean and the mode then

coincide. In the second case other (skewed) probability density functions are possible. Triangular probability density functions are often used for this purpose.

In addition to the mode or the mean of the estimate of the budget or the time-planning, the deviation from it (or the spread around it) is important. The size of the margin depends on the phase the project is in and on the required reliability with which the budget or the planned duration (quantification of the estimate or time-planning plus margin) will not be exceeded.

Considering the first point (size of the margin depends on the phase the project is in), in an early stage of the project one is much more uncertain about the budget estimate or the planned duration than in a later stage. Estimates and time-plans are often classified according to the phase of the project they were made in. Characteristic numbers for the magnitude and for the spreading around costs items depend on the project phase. For time-planning such characteristic numbers are not (yet) available.

4 Classification of uncertainty

Uncertainty can be classified in three categories:

- ◆ uncertainty related to Normal events;
- ◆ uncertainty related to Special events;
- ◆ project uncertainty.

Uncertainty related to Normal events

Although the costs items in a Basic budget estimate of a project become increasingly clear in the course of time, and the estimate becomes more accurate, many causes of uncertainty will remain as long as the project is not finished. With the necessary changes made, this can be applied to time-planning. The degree of uncertainty can be classified as follows:

1. There is no cause of uncertainty. The item concerned is deterministic. This concerns costs items or activities that are known exactly in size or duration. If, for example, the contract settling the purchase of land has been signed, this amount of money is known exactly. An “activity” with deterministic duration is the tide. The duration (along the North Sea coasts) is “exactly” 12 hours 25 minutes.

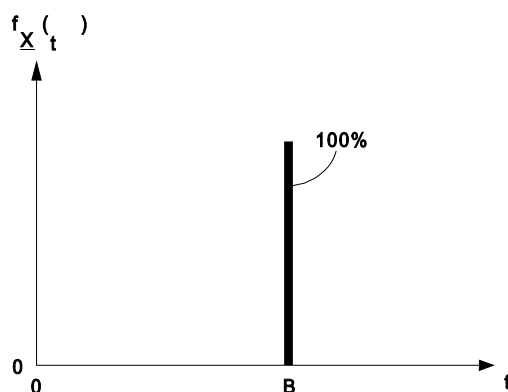


Figure 5.

2. Often the costs are not so uniquely determined and one is uncertain about the duration of an activity. When the negotiations are still in progress, there is a notion about how much money the land (meant in point 1) will cost, but one cannot be certain. An example of uncertainty about the duration of an activity is a barge with heavy draught that has to be towed over a sill. Suppose this can only be done at high tide. (The keel clearance has to be sufficient). Usually the final costs or the spreading around the point in time of arrival at the sill will be within a band width. The probability density can then be as indicated in Figure 6.

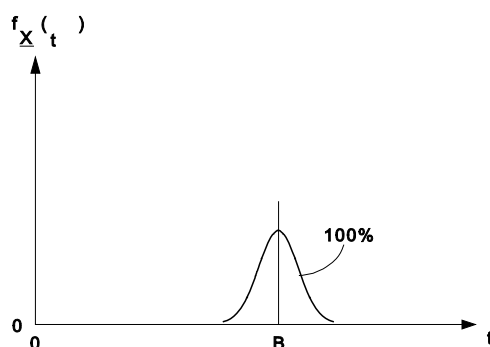


Figure 6.

Uncertainty related to Special events

Often another type of uncertainty plays a role with the evaluation of costs of a project or its duration, namely uncertainty caused by the Unforeseen or by Special events (mainly calamities). Two criteria characterize a Special event: the first is that it is not meant to occur and the second is that occurrence is not likely. The probability of occurrence, p , is small (less than 0.05), but if the event occurs, the consequence (damage or exceedence of the duration, B) is large. The probability of no occurrence (and accordingly: no damage or exceedence of the duration) is $1 - p$. In a “classical” estimate of the budget or time-planning such events are seldom taken into account. Contractors insure against such events, associated with small probabilities but with large consequences. In a statistically controlled estimate or time-planning the probabilities and the consequences can be indicated as follows:

- Figure 7 shows the mass density of a Special event as a function of the damage or exceedence of the duration.

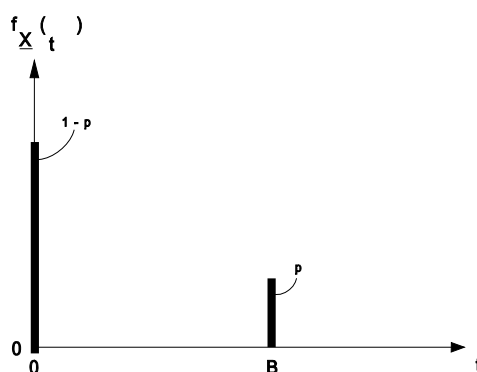


Figure 7.

- The probability density function of a “Special event”, of which the consequences (the damage or the duration) are subject to uncertainty, could be as is illustrated in Figure 8.

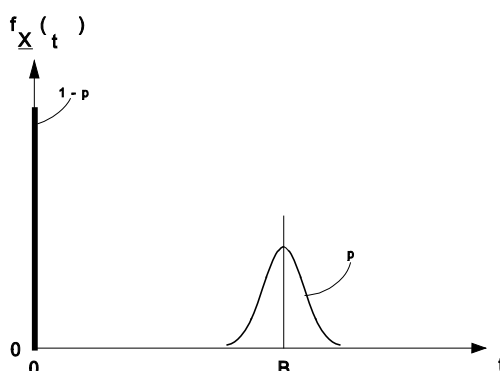


Figure 8.

Project uncertainty or plan uncertainty: variants

- In the study-of-plan phase several variants have to be considered and estimated (and sometimes planned). Beforehand, one is not certain which variant will be chosen (for example a tunnel, a ferry or a bridge for a road crossing of a river). Only at the end of the pre-design phase a decision is made. Awaiting the choice, elaborating and estimating (and eventually time-planning) several variants mainly meet the uncertainty. Sometimes, the decision between the variants is so unpredictable that all variants are considered equally likely. Sometimes one variant is preferential and it is unlikely that another one will be chosen.

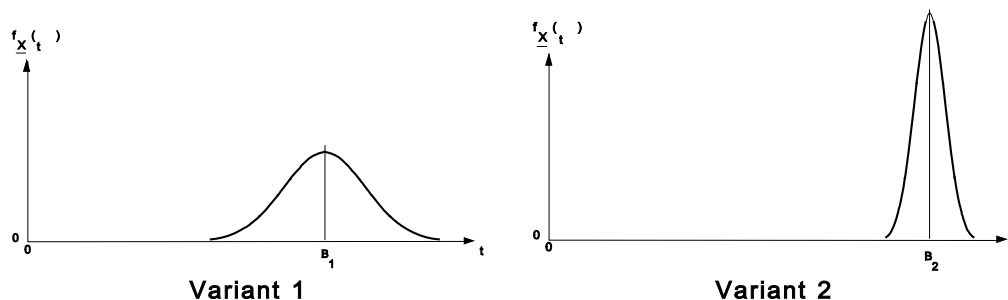


Figure 9.

If more than one variant is estimated or planned, the problem could be that the estimate of the budget is required to be one total amount of money or the time-planning should be one total duration. One estimate of the budget or one time-planning (possibly with a margin or expressed as a probability density function) for presentational purposes is then acquired rationally by weighing each variant by its (estimated) probability of selection. The following figure presents the result for two variants.

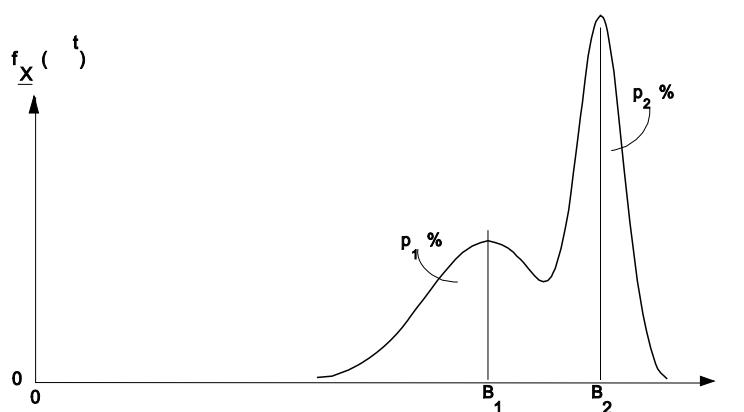


Figure 10.

The disadvantage is that the result is not recognized as a reasonable estimate or time-planning of each of the individual variants.

The classified uncertainty and the formulae to calculate the associated means and the standard deviations of the probability-weighted consequence (the related risks) are summarized in the following table. Mutatis mutandis the formulae hold for a time-planning with only one time-path.

Table 5:

	Case	mean	standard deviation	Description

Normal events	1	B	0	A deterministic amount of money, B , expressed in units of money
	2	B	σ_B	A stochastic amount of money, with mean B , and some spreading, σ_B .
Special events	3	$p \times B$	$\sqrt{p \times (1-p) \times B^2}$	An event with probability of occurrence p that has a deterministic consequence B .
	4	$p \times B$	$\sqrt{p \left((1-p) B^2 + \sigma_B^2 \right)}$	An event with probability of occurrence p that has a statistic consequence with mean B and some spreading, expressed by σ_B .
Plan uncertainty	5	$p_1 B_1 + p_2 B_2$	$\sqrt{p_1 (B_1^2 + \sigma_{B1}^2) + p_2 (B_2^2 + \sigma_{B2}^2) - (p_1 B_1 + p_2 B_2)^2}$	There are two (or more) variants, each associated with a probability of realization, p_i . Their probabilities add up to one as it is certain that one of the variants will be selected.

The spreading for an item of the estimate increases with the related uncertainty. In the first case in Table 5, one is absolutely certain about the size of the sum, B . The standard deviation equals zero. In the second case there is some uncertainty. The spreading, σ_B , is smaller than the expected value, B . (If this were not so, the estimate of the item was of no significance. It then suggests that there is not the vaguest idea of the size of B .) In case of Special events (cases 3 and 4), one is not certain if there will be costs (damage) at all. The probability that there will be costs is p ($p \ll 1$). There is a larger probability ($1 - p$) that there will be no costs. In fact the risk¹): (probability \times consequence = $p \times B$) is estimated. If the Special event occurs, the estimated amount of money ($p \times B$) is not nearly enough to cover the costs (B). According to this, the third case is associated with a larger spread (in the order of $B \times \sqrt{p}$) than in the case of a Normal event. So the spreading for Special events is approximately $\frac{1}{\sqrt{p}}$ times the expected value $p \times B$.

¹ From a mathematical point of view the estimates of Normal events are estimates of the risks as well. The probability of occurrence of Normal events is 1 (or 100% certainty).

5 Calculation formulae for probabilistic budgeting

Monte Carlo simulations can be easily used in budgeting and time planning problems, but many expressions in budgeting and time planning problems can also be derived analytically.

Assume that X and Y are random variables (of for instance prices and amounts) with PDF's f and g respectively. The following four functional operators are often encountered in budgeting and time planning problems:

$$Z=X+Y, U=X-Y, V=XY \text{ and } W=X/Y$$

Then the PDF's of Z, U, V and W are, respectively, given by:

$$f_Z(z) = \int f(x)g(z-x) dx$$

$$f_U(u) = \int f(u+y)g(y) dy$$

$$f_V(v) = \int f(x)g(v/x) |x|^{-1} dx$$

$$f_W(w) = \int f(xw)g(x) |x| dx$$

In textbooks on statistics the following relation is proven:

$$E(XY) = E(X)E(Y)$$

$$Var\left(\sum_{i=1}^n a_i X_i\right) = \sum_{i=1}^n a_i^2 Var(X_i) + 2 \sum_{i=1}^n \sum_{j=i+1}^n a_i a_j Cov(X_i, X_j)$$

Furthermore it is possible to derive the following property for the product of random variables:

$$Var(V) = Var(X)Var(Y) + E^2(X)Var(Y) + E^2(Y)Var(X)$$

If exact calculations are not possible, the following approximation rules can be used (using Taylor's formula):

$$g(X) = g(m_X) + (X - m_X) \frac{dg(x)}{dx} \Big|_{x=m_X} + \frac{(X - m_X)^2}{2} \frac{d^2 g(x)}{dx^2} \Big|_{x=m_X} + \dots$$

From this, we can derive:

$$E(g(X)) \approx g(E(X))$$

$$\text{Var}(g(X)) \approx \text{Var}(X) [g'(m_x)]^2$$

If the coefficient of variation of X is less than c , the error involved in these approximations is less than c^2 . In particular, the following useful approximations in budgeting and time planning models can be used:

$$E(\sqrt{X}) \approx \sqrt{E(X)}, \quad \text{Var}(\sqrt{X}) \approx \frac{\text{Var}(X)}{4E(X)}$$

$$E(X^{-1}) \approx \frac{1}{E(X)}, \quad \text{Var}(X^{-1}) \approx \frac{\text{Var}(X)}{E^4(X)}$$

6 Dependent Bernoulli distributed random variables for special events

The notation $X \sim \text{BBG}(p_1, G_1)$ is used for a random variable X which has a probability p_1 of the occurrence of an event with consequences G_1 .

Mean and standard deviation of X are:

$$\mu = p_1 * G_1$$

$$\sigma = G_1 * \sqrt{p_1(1-p_1)}$$

Extensions to this univariate random variable by allowing 'horizontal and vertical uncertainties' in p_1 and G_1 are described by Van Gelder [10].

Dependence

The classical product-moment correlation coefficient of Pearson is usually used as a measure for dependence between two random variables. This correlation coefficient however, can only be applied for normal distributed random variables. For non-normal distributions, the correlation structure should be described differently. In the remainder of this section, a suggestion for such structure is proposed.

Bivariate BBG's

The following 4 situations can be distinguished:

1. X and Y are independent
2. X and Y 100% positively dependent
3. X and Y 100% negatively dependent
4. X and Y partially dependent

Situation 1

Assume $X \sim \text{BBG}(p_1, G_1)$ and $Y \sim \text{BBG}(p_2, G_2)$ and independence, then the following probability table can be derived:

Table 6.

X \ Y	0	G2	Sum
0	$(1-p_1)(1-p_2)$	$p_2(1-p_1)$	$1-p_1$
G1	$p_1(1-p_2)$	p_1p_2	p_1
Sum	$1-p_2$	p_2	1

Situation 2

If X and Y are completely positive dependent, then it follows,

- if $X=0$ then $Y=0$

- if $X=G_1$ then $Y=G_2$.

Using conditional probabilities: $P(Y=0|X=0) = 1$ and $P(Y=G_2|X=G_1) = 1$.

From which it follows: $P(X=0 \text{ and } Y=0) = P(X=0)*P(Y=0|X=0)=1-p_1$

and

$$P(X=G_1 \text{ and } Y=G_2) = P(X=G_1)*P(Y=G_2|X=G_1)=p_1$$

and

$$P(X=0 \text{ and } Y=G_2) = P(X=0)*P(Y=G_2|X=0)=0$$

and

$$P(X=G_1 \text{ and } Y=0) = P(X=G_1)*P(Y=0|X=G_1)=1-p_1.$$

Which can be summarized in the following probability table:

Table 7.

X \ Y	0	G2	Sum
0	1-p1	0	1-p1
G1	0	p1	p1
Som	1-p2	p2	1

From this table, it follows that $1-p1=1-p2$.

Therefore, BBG distributed X and Y can only be 100% positively correlated if $p1=p2$.

Situation 3

If X and Y are completely negatively dependent, then it follows that:

- if $X=0$ then $Y=G2$
- if $X=G1$ then $Y=0$.

The following probability table can be derived:

Table 9.

X \ Y	0	G2	Sum
0	0	1-p1	1-p1
G1	p1	0	p1
Som	1-p2	p2	1

Requirement: $p1=1-p2$.

BBG distributed X and Y can only be 100% negatively correlated if $p1+p2=1$.

Situation 4

X and Y are partially dependent from eachother:

- if $X=0$ then $Y=0$ with probability $a1$ and $Y=G2$ with probability $1-a1$
- if $X=G1$ then $Y=0$ with probability $b1$ and $Y=G2$ with probability $1-b1$.

Table 10.

X \ Y	0	G2	Sum
0	$(1-p1)a1$	$(1-p1)(1-a1)$	1-p1
G1	$p1b1$	$p1(1-b1)$	p1
Sum	1-p2	p2	1

Requirement: $(1-p_1)a_1+p_1b_1=1-p_2$

BBG distributed X and Y can only be partially correlated if:

$$a_1+p_1(b_1-a_1)=1-p_2.$$

Situation 4 is the most general situation. Situations 1, 2 and 3 can be derived directly from situation 4 with the following choices for a_1 and b_1 :

Table 11.

	Choice for a_1 and b_1
Situation 1 (independend)	$a_1=1-p_2, b_1=1-p_2$
Situation 2 (100% positively dependent)	$a_1=1, b_1=0$
Situation 3 (100% negatively dependent)	$a_1=0, b_1=1$

We conclude that the correlation structure between 2 BBG distributed $X \sim \text{BBG}(p_1, G_1)$ and $Y \sim \text{BBG}(p_2, G_2)$, needs to be described by 2 constants a_1 and b_1 which satisfy the following 3 boundary conditions:

$$0 \leq a_1 \leq 1$$

$$0 \leq b_1 \leq 1$$

$$a_1+p_1(b_1-a_1)=1-p_2.$$

Complete positive dependence is reached when $a_1 \rightarrow 1$ and $b_1 \rightarrow 0$ and $p_1 \rightarrow p_2$.

Complete negative dependence is reached when $a_1 \rightarrow 0$ and $b_1 \rightarrow 1$ and $p_1 \rightarrow 1-p_2$.

7 Conclusions

Budgeting and time planning should be handled by probabilistic methods in order to deal with uncertainties prior to the start of the project. Correlations between events need special attention, in particular the correlation structure between special events. Analytical solutions are presented in this paper and a correlation structure is proposed.

8 Literature

- [1] Belgraver, H., H. Kleibrink, The Markerwaard, government investments in environmental ordering, (De Markerwaard, overheidsinvestering in de ruimtelijke ordening) in Dutch, Economische Statistische Berichten nummer 3445, February 1984
- [2] The Economist, Under water over budget, October 1989

- [3] Goemans, T., H.N.J. Smits, Costs control of a mega-project, the Eastern Scheldt works, (Kostenbeheersing van een mega-project: de Oosterschelde werken) in Dutch, Economische Statistische Berichten nr. 3478, October 1984
- [4] Heezik, A. van, 200 years of estimates at the Ministry of Public Works, an exploration, (200 jaar ramingen bij Rijkswaterstaat, een verkenning) in Dutch, Ministerie van Verkeer en Waterstaat, Directoraat-Generaal Rijkswaterstaat, 's Gravenhage, March 1994
- [5] Merewitz, I., Cost overruns in public works, Benefit/cost and policy analysis, Aldine Publishers, Chicago, 1973
- [6] Vrijling, J.K. en A.C.W.M. Vrouwenvelder, Lecture notes b3, Probabilistic Design, (Collegedictaat b3, Probabilistisch Ontwerpen) in Dutch, Faculty of Civil Engineering of the Technical University Delft, 1984.
- [7] Vrijling, J.K., Lecture for N.A.P. DACE (Dutch Association of Cost Engineers) seminar - 6 November 1990 - Are project costs controllable) Lecture IV: The influence of time on the controllability of projects, (Lezing voor N.A.P. DACE (Dutch Association of Cost Engineers) seminar - 6 November 1990 - Projects kosten beheersbaar? Lezing IV: De invloed van de tijd op de kostenbeheersing van projecten) in Dutch.
- [8] Vrijling, J.K., Syllabus for the course within the framework of the Project Estimates Infrastructure and in the framework of the Post Academical Course: "Foreseen, unforeseen or uncertain?", (syllabus bij de cursus voor het Project Ramingen Infrastructuur en bij de Post Academische Cursus: "Voorzien, onvoorzien of onzeker?") in Dutch, 1995.
- [9] Vrijling, J.K. et al., The RISMAN- method, a method for the management of risks of large infrastructure projects, (De RISMAN-methode, een instrument voor het risicomangement van grote infrastructuurprojecten) in Dutch, gezamenlijke uitgave van Gemeentewerken Rotterdam, NS Railinfrabeheer, RWS Bouwdienst, RWS Directie Zuid-Holland, TU Delft en Twijnstra Gudde,1996.
- [10] Gelder, P.H.A.J.M. van (2000), Statistical Methods for the Risk-based design of Civil Structures, Phd-thesis, Delft University of Technology.

Losses due to Spillage at Gariep Dam

D.J. de Waal and A. Verster

Department Mathematical Statistics and Actuarial Science University of the Free State,
Bloemfontein, S.A.

Abstract: Spillage at the Gariep Dam in the Orange river in South Africa causes financial losses to ESKOM, the main supplier of electricity in Southern Africa. ESKOM manage the outlet of water through 4 hydro turbines each having an outlet capacity of $160 \text{ m}^3/\text{s}$. Floods occur from time to time and can cause spillage over the dam wall. The aim is to manage the outlet of water through the turbines such that the **Risk of Spillage is** minimized given the constraints specified by the Department of Water Affairs and Forestry. They formulated a curve on the water level of the dam such that there is water available for irrigation purposes downstream. ESKOM is free to use water above the curve, but if it gets below the curve, they are restricted to the amount they let out. In this presentation a generalized Burr-Gamma model is presented to model spillage to care for the heavy tail in the data and a parameter is introduced to take care of the inflated zeros. Small tail probabilities are estimated and high quantiles are predicted under the model. Comparisons of this model with other models such as Exponential and lognormal are shown.

1 Introduction

The Gariep Dam lies in the upper Orange River and is the largest dam in South Africa. It has a net capacity of 5943 million m^3 . ESKOM, the National supplier of electricity, operates a hydro power station at the dam wall consisting of 4 turbines, each with a maximum water outlet of $153 \text{ m}^3/\text{s}$. With a total outlet of $612 \text{ m}^3/\text{s}$, ESKOM can manage the water to a reasonable extent, but floods occur from time to time in the catchment area and causes spillage of water over the dam wall with large financial losses to ESKOM. The aim is to manage the water through the turbines such that the risk of spillage is minimized under constraints specified by the Department of Water Affairs and Forestry. One constraint for example is an operating curve that specifies a minimum water level in the dam that must be left for irrigation purposes. If the water level reaches this minimum, ESKOM is not allowed to use water for generating power. On the other hand, the amount of electricity generated is small relative to the total amount ESKOM generate and is mainly for supply when the demand is high like in the winter months, June – August. To prevent spillage, ESKOM needs some prediction of inflows. The inflows are usually high in the summer months October to April when heavy rains can occur in the catchment areas.

We will be looking at the annual total volume of discharges of the Orange River into the dam and at the total annual volume of water spilled. Figure 1 shows the annual volume of spillage over the period 1971-2006.

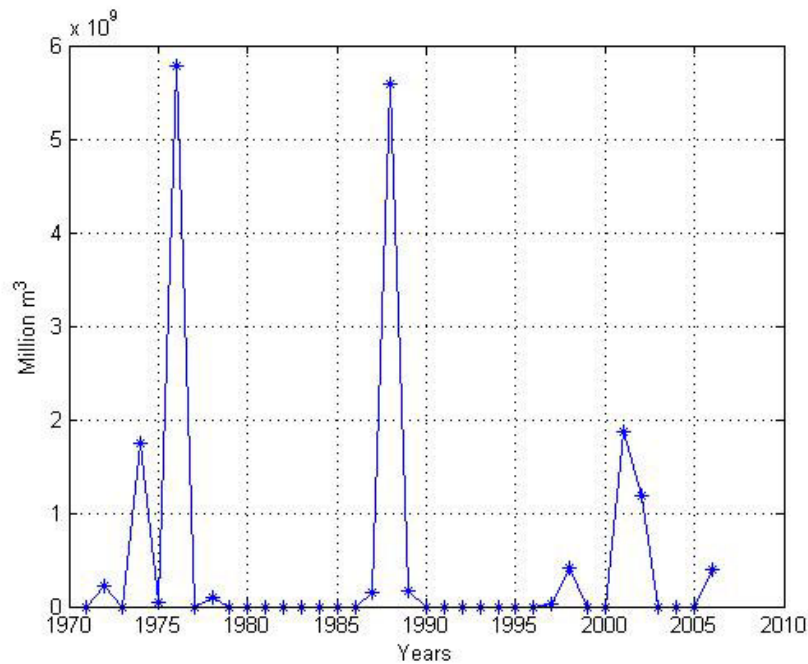


Figure 1: Annual spillage in million m^3 at Gariep Dam

The total volume of spillage that occurs over the 36 years is $1.7693 \times 10^{10} m^3$ which implies a financial loss of R76,950,708 if calculated against a rate of R4.35/1000 m^3 . Spillage occur not every year and over the 36 years of data, only 13 years recorded spillage. As can be seen from figure 1, two years show quite extreme losses. Table 1 shows a frequency table of the data with 11 bins.

Table 1: Frequency table on annual spillage in $m^3/10^7$ over 36 years.

x	0	31	89	146	204	262	319	377	435	492	550	Tot
f req	23	8	0	2	1	0	0	0	0	0	2	36

We will fit three distributions to the spillage data like the Exponential, Lognormal and Generalized Burr-Gamma [2]. We will also consider a bivariate lognormal fit to spillage and inflow jointly.

The aim is to predict future losses and to consider the risks involved for ESKOM if the management of the water and environmental conditions continue to stay the same. We will consider various distributions as possible candidates to model the losses, such as Exponential, Lognormal, Generalized Burr-Gamma (GBG) and the bivariate lognormal. An important issue to take care of in the analysis of the losses, is the inflated zeros with the number of years when no losses occur.

2 Exponential fit

Although we expect the Exponential distribution is not a good choice to model the losses, we mainly choose it to show the explicit steps of the analysis. Denote the annual spillage (losses) in m^3 (cubic meters) by the random variable X and we assume that the observations are independently $\text{Exp}(\lambda)$ distributed with λ the expected annual losses if spillage occurs. The density function is given by

$$\begin{cases} f(x) = \theta, & x = 0 \\ ((1 - \theta) / \lambda) \exp(-x / \lambda), & x > 0. \end{cases}$$

θ indicates the probability of no spillage.

Let $x = (x_1, \dots, x_n)$ denote a random sample of n observations with r non zeros and let

$$\bar{x}_r = \frac{1}{r} \sum_{i=1}^n x_i$$

be the mean spillage per year conditional spillage occurs. The likelihood function is then given by

$$Like(\theta, \lambda | x) = \theta^r (1 - \theta)^{n-r} \lambda^{-r} e^{-\frac{r}{\lambda} \bar{x}_r}$$

Assuming the Jeffreys prior on λ and a uniform prior on θ , independent of each other, namely

$$\pi(\theta, \lambda) \propto \frac{1}{\lambda},$$

the posterior becomes

$$\pi(\theta, \lambda | x) \propto \theta^r (1 - \theta)^{n-r} \lambda^{-r-1} \exp\left(-\frac{r}{\lambda} \bar{x}_r\right) \quad (1)$$

It is clear from (1) that the joint posterior becomes the product of a $\text{Beta}(r+1, n-r+1)$ and inverse $\text{Gamma}(r, \frac{1}{r\bar{x}_r})$ distribution. The posterior predictive density of a future Z becomes

$$\begin{cases} \text{pred}(z|x) = E(\theta|x), & z = 0 \\ E((1 - \theta))E\left(\frac{1}{\lambda} e^{-\frac{z}{\lambda}} | x\right), & z > 0 \end{cases}$$

$$\begin{cases} = \frac{n - r + 1}{n + 2}, & z = 0 \\ \frac{r + 1}{n + 2} \frac{1}{x_r} \left(1 + \frac{z}{rx_r}\right)^{-r-1}, & z > 0. \end{cases} \quad (2)$$

The posterior predictive density of Z conditional on $Z > 0$ follows from (2) as a generalized Pareto($\frac{1}{r}, \bar{x}_r$). The predictive tail probability of Z becomes

$$\begin{cases} P(Z \geq z|x) = 1, & z = 0 \\ \frac{r+1}{n+2} \left(1 + \frac{z}{r\bar{x}_r}\right)^{-r}, & z > 0. \end{cases} \quad (3)$$

The quantile at tail probability p is given by

$$z = \left[\left(\frac{n+2}{r+1} p \right)^{-1/r} - 1 \right] r\bar{x}_r. \quad (4)$$

An Exponential QQ-plot shown in figure 2, indicates that the Exponential distribution does not fit well, especially in the tail. The two extreme points are not accounted for. We have to consider a heavier tail distribution such as a distribution in the Pareto domain.

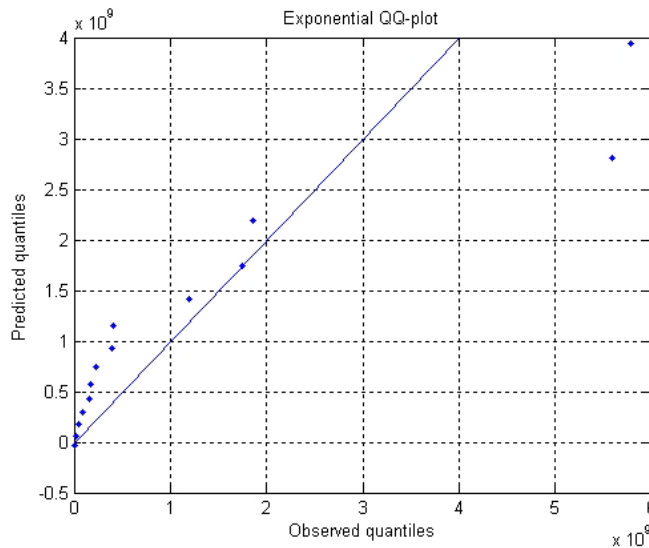


Figure 2:

Exponential QQ-plot

To calculate the risk of spillage in terms of money for a future year, we need the expected value of a future spillage. From (2) and the result by EMBRECHTS et al [4], it follows that

$$E(Z) = \frac{(1+r)r^2\bar{x}_r}{(n+2)} = 1.8121 \times 10^9 \text{ m}^3.$$

Taking the loss in rand of spillage against R4.35/1000 m^3 , we obtain the future annual risk as R7882.5 million. This is a large risk according to the Exponential model. We will consider a heavy tail model in the next section.

3 Generalized Burr-Gamma fit

The GBG distribution is defined as [3] as follows: Let $X \sim \text{GBG}(\alpha, \beta, \kappa, \xi)$, then the distribution function is given by

$$F(x) = \Gamma(\kappa, \log(1 + \xi(xe^\alpha)^{1/\beta}) / \xi), \quad x > 0 \quad (5)$$

The parameter κ denotes the scale parameter and ξ the extreme value index. The other two parameters α and β are functions of location, scale and spread of the distribution. $\Gamma(\kappa, y)$ denotes the incomplete gamma integral with scale parameter κ and location parameter one. This distribution generalizes the Burr and the Gamma distributions and falls in the Pareto class.

Various ways of estimating the four parameters can be considered. See for example Beirlant et al, [2] for a method. The approach we followed here is to estimate μ and σ as the mean and standard deviation of $-\log(X)$ on the spillage $X > 0$ below the threshold $t = 5 \times 10^9$. The threshold is obtained from a Pareto quantile plot of the data and t is selected as the value where a straight line seems to fit for large X . For more detail on the Pareto quantile plot see, Beirlant et al, (2008). After estimating μ and σ , we assume them as fix. The extreme value index ξ and scale parameter κ is then estimated through BAYES procedure. Since κ is the scale parameter for a Gamma distribution as can be seen from (5), we put the JEFFREYS prior on κ , (see [6]) and a uniform for ξ independently of each other, namely

$$\pi(\kappa, \xi) \propto \sqrt{\kappa\psi(\kappa)^2 - \psi'(\kappa) - 1} \quad (6)$$

$\psi(\kappa)$ is the digamma function and $\psi'(\kappa)$ is the trigamma function.

α and β appearing in (5) can be written in terms of μ and σ as $\beta = \sigma / \sqrt{\psi'(\kappa)}$ and

$\alpha = \mu + \beta\psi(\kappa)$ [2]. The posterior of κ and ξ is not available in an explicit form, but can be simulated using the fact from (5) that

$$\log(1 + \xi(Xe^\alpha)^{1/\beta}) / \xi \quad (7)$$

is distributed $\text{Gamma}(\kappa, 1)$. Selecting κ and ξ from a large number (approximately 2000) of simulated values from the joint posterior given the spillages and taking the means of the simulated values as the estimates of ξ and κ , we obtain the following estimates: $\hat{\kappa} = 5.02, \hat{\xi} = 0.0214, \hat{\alpha} = -14.7442, \hat{\beta} = 3.0632$. The GBG density with these estimates substituted is shown in figure 3 and the probability plot (figure 4) shows the goodness of fit of the GBG. The Kolmogorov-Smirnov (KS) measure $\text{KS} = \max|F - F_n|$ for the GBG is substantial smaller than that for the Exponential fit. The values are indicated on the graph.

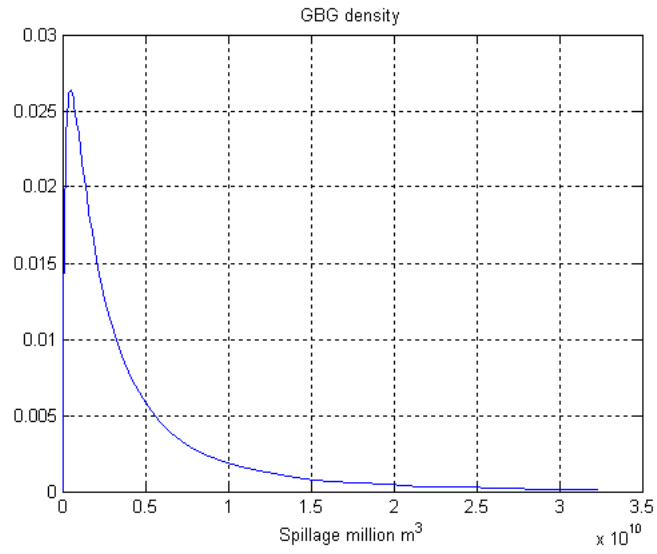


Figure 3: GBG density fitted to 13 years of annual spillage

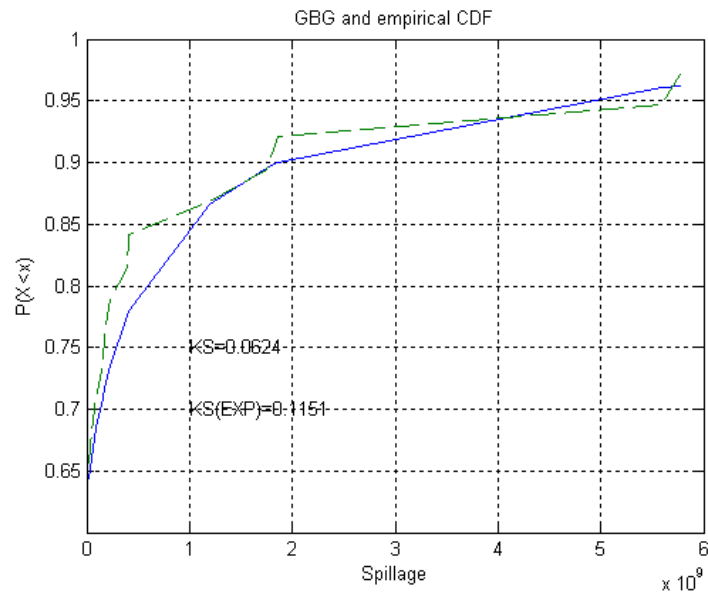


Figure 4: Probability plot showing goodness of fit (-- Emp cdf)

The predictive spillages can be simulated using a discretization of the predictive cdf

$$P(Z < z | x) = \theta + (1 - \theta) \iint_{\Omega} F(z | \kappa, \xi) \pi(\kappa, \xi | x) d\kappa d\xi. \quad (8)$$

F is given by (5) assuming the fix values for μ and σ and the parameter space $\Omega = \{\kappa > 0, \xi > 0\}$. π denotes the posterior of κ and ξ . θ is replaced by the estimate $\hat{\theta} = \frac{n-r+1}{n+2}$. 500 simulated predicted values from the Exponential, Lognormal and GBG are shown in Boxplots in figure 5. The Lognormal predictions are obtained from the predictive t distribution [5,6].

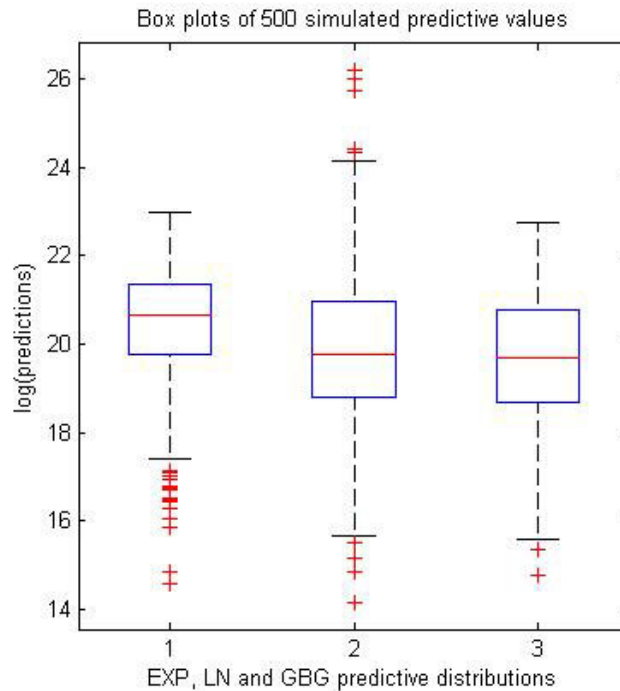


Figure 5: Boxplots of 500 predictive values on log scale from Exponential (1), Lognormal (2) and GBG (3) fits.

The Boxplots give an indication of the predictive distributions for the three models, but in the next section the differences between the models came out clearer if we consider the risks of spillage.

4 Risk of spillage

A recent definition of risk given by AVEN [1] is: A way of expressing uncertainty related to future observable quantities. We will express risk on spillage as the predictive probability $P(ZR > z|x)$ where ZR denotes the annual spillage in rand per thousand m^3 water.

These risks were calculated from the predictive distributions for the three models Exponential, Lognormal and GBG and shown in figure 6.

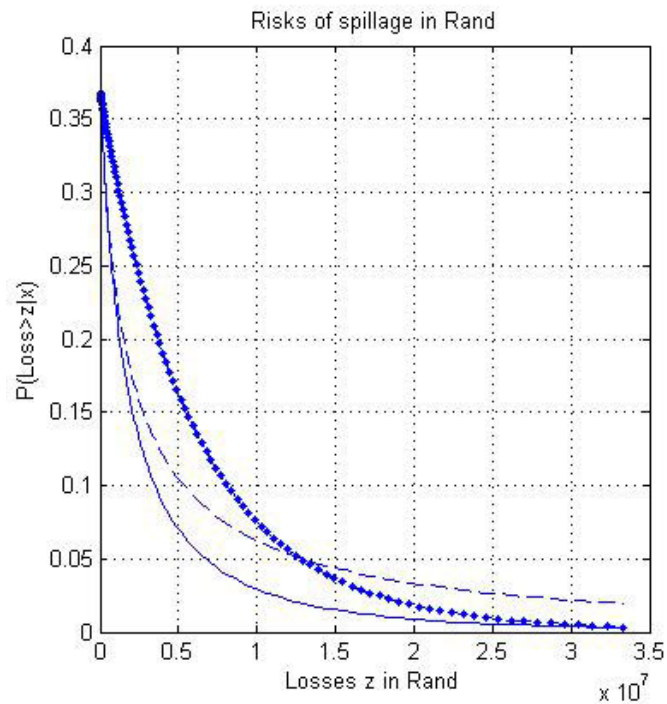


Figure 6: Risks according to an Exponential (.-), Lognormal (--), and GBG(-) models

From the graphs we get a risk of about 0.075 of getting a loss of R10 million using the Exponential model compared to 0.0625 for the lognormal and 0.0125 for the GBG model. The risk according to the GBG model is five times smaller for such a loss compared to the risk under the Lognormal which is quite substantial.

5 Bivariate model

The question arises what role the inflow to dam has on the spillage. This is a valid question and we want to address this here. The proposed model is the bivariate Lognormal where we assume that the annual volume inflow (x) and annual volume spilled (y) are jointly Lognormal(μ, Σ) distributed.

The model is given by

$$\begin{cases} f(x,y) = \theta f_1(x|y=0), & x>0 \\ (1-\theta)f_2(x,y|y>0), & x,y>0 \end{cases} \quad (9)$$

where θ is the probability of no spillage, f_1 is the univariate Lognormal density function and f_2 is the bivariate Lognormal density function. The data on log scales for the $n = 13$ years of spillage are shown in table 2. The first column indicating years, the second column spillage and the third inflow in million m^3 . The estimates are $\hat{\mu} = [19.6713, 9.2296]$ and $\hat{\Sigma} = \begin{bmatrix} 3.4084 & 0.5869 \\ 0.5869 & 0.1591 \end{bmatrix}$. The predictive distribution of future $Z =$ (Spillage, Inflow) is a bivariate t distribution ([5], pp 192, 193) with mean $\hat{\mu} = [19.6713, 9.2296]$ and covariance $S = \frac{(n-1)(n+1)}{n} \hat{\Sigma}$. The prior used is $\pi(\mu, \Sigma^{-1}) \propto |\Sigma|^{3/2}$.

The degrees of freedom are $\nu = n - 2$. The bivariate distribution of $\exp(Y)$ and $\exp(X)$ is displayed through contours shown in figure 7 with the data points indicated by stars.

Table 2: $y = \text{Log}(\text{Spillage})$, $x = \text{Log}(\text{Inflow})$ for 13 years at Gariep Dam

Years	y	x
1	19.2312	9.0861
2	21.2802	9.5072
3	17.6712	8.9001
4	22.4792	10.0244
5	18.3523	9.1801
6	18.84	8.9972
7	22.4451	9.7232
8	18.9411	9.2427
9	16.9233	8.7551
10	19.8294	8.8681
11	19.0424	9.2289
12	20.8969	8.9804
13	19.7943	9.4913

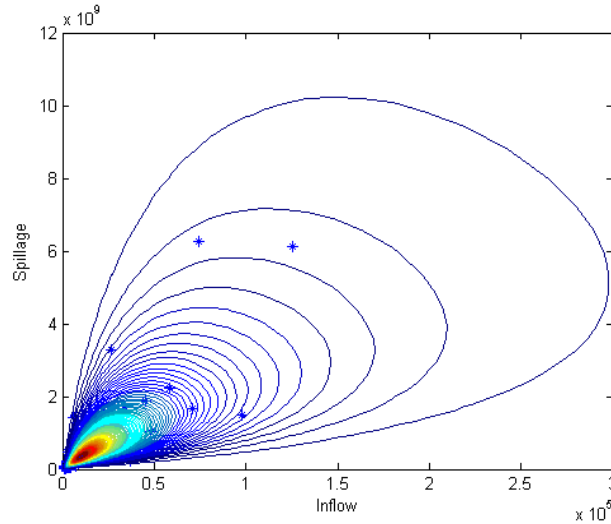


Figure 7: Contours of the bivariate predictive distribution on original scale with data points.

From these contours we notice that as the inflow gets larger, the variance of the spillage gets larger. The conditional distributions will show it more clearly.

We are interested in the conditional predictive distribution of Y given $X = x$. Let

$\hat{\mu}_{y|x} = \hat{\mu}_y - \frac{s^{xy}}{s^{xx}}(x - \hat{\mu}_x)$ be the conditional mean and $\hat{\sigma}_{y|x} = \left\{ \nu + \frac{(x - \hat{\mu}_x)^2}{s_{y \cdot x}} \right\} \frac{1}{(\nu + 1)s_{xx}}$ the

conditional variance if we let $S = \begin{bmatrix} s_{yy} & s_{yx} \\ s_{xy} & s_{xx} \end{bmatrix}$ and $S^{-1} = \begin{bmatrix} s^{yy} & s^{yx} \\ s^{xy} & s^{xx} \end{bmatrix}$. $s_{y \cdot x} = s_{yy} - \frac{s_{xy}^2}{s_{xx}}$.

Suppose the $\log(\text{Inflow}) = (9.1 \ 9.2 \ 9.3)$ and we want to predict the spillage given these three states of inflow, then according to the conditional predictive t distribution ([5], p. 196), $t(\nu + 1, \hat{\mu}_{y|x}, \hat{\sigma}_{y|x})$, we can make the predictions. Figure 8 shows Box plots on 500 simulated conditional predictions transformed to the original scale.

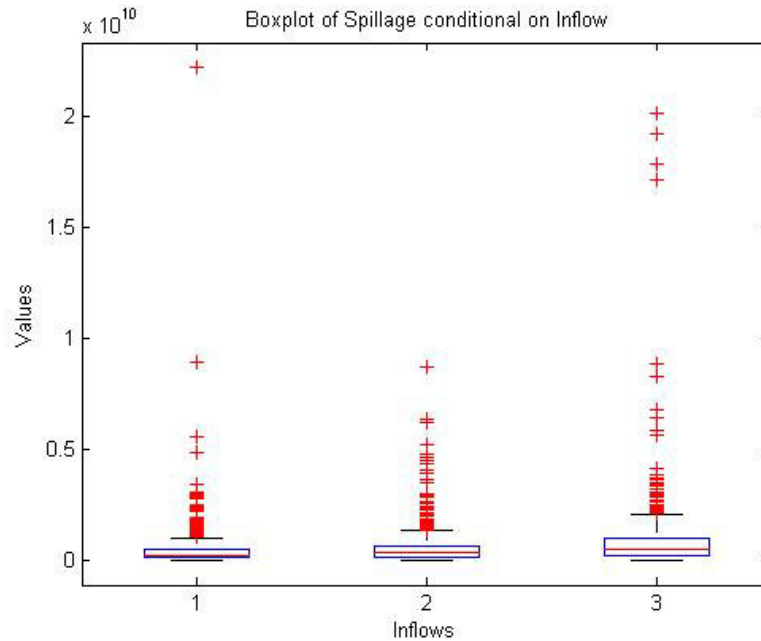


Figure 8: Box plots on 500 predictive spillage predictions conditional on inflows 8955, 9897 and 10938 million m^3

6 Conclusion

In conclusion, the model choice for prediction through the predictive density is very important. The risks can differ significantly. The GBG distribution is fairly flexible as a model for heavy tail data containing extremes and we showed that predictions for this model are possible through simulations. Although we treated the bivariate case under the lognormal, it is possible to consider the multivariate GBG as another candidate (see [3]). This will be explored in a future paper.

7 References

- [1] Aven T. (2008): Foundations of Risk Analysis. Wiley
- [2] Beirlant J.; de Waal D.J. and Teugels J.L. (2002): The Generalized Burr-Gamma family of distributions with applications in Extreme Value Analysis. Limit theorems in Probability and Statistics I, Budapest, pp 113-132. (Berkes, Csaki and Csorgo eds)
- [3] Beirlant J.; de Waal D.J. and Teugels J.L. (2000): A Multivariate Generalized Burr-Gamma distribution. South African Statist J, 34, 111-133.
- [4] Embrechts P.; Kluppelberg C. and Mikosch T. (1997): Modelling Extremal Events. Springer.
- [5] Geisser S. (1993): Predictive Inference: An introduction. Chapman and Hall.
- [6] Van Noortwijk J.M.; Kalk H.J.; Duits M.T. and Chbab E.H. (2002): Bayesian Statistics for Flood Prevention. Special report, HKV Consultants. Delft.

Part II

Probabilistic Modelling in Structural Engineering

Application of biostatistics in the analysis of fatigue data in bond research

Lars Eckfeldt, Manfred Curbach

Institute of Concrete Structures, Technische Universitaet Dresden, Germany

Abstract: The expected brittle response on high cycle fatigue loading caused major concerns for structural members made of high performance concrete (HPC) before currently considered applications in bridge engineering. A series of so-called pull-out specimens with standard reinforcing steel were tested in a program designed to study possible fatigue effects on bond. The original objective was to publish a relevant pool of data referring to so-called short bond lengths. This objective was expanded to test the application of survival analysis methods from biostatistics to conduct a fatigue analysis for civil engineering. Those explorative methods offer a better understanding of the fatigue problem and may open a new path towards interesting results in principle. The results of the performed analysis show a far lesser difference than initially expected, in the bond behaviour for HPC (High Performance Concrete) and NSC (Normal Strength Concrete). An obvious correlation to the upper bound of the cyclic load also exists. Typical fatigue diagrams like SMITH-Diagrams were produced traditionally and using logistic regression. Probability based lifetime descriptions were based on Kaplan-Meier estimates as an interesting alternative to WOEHLER($S-N$)-curves.

1 Introduction and evolution of the project

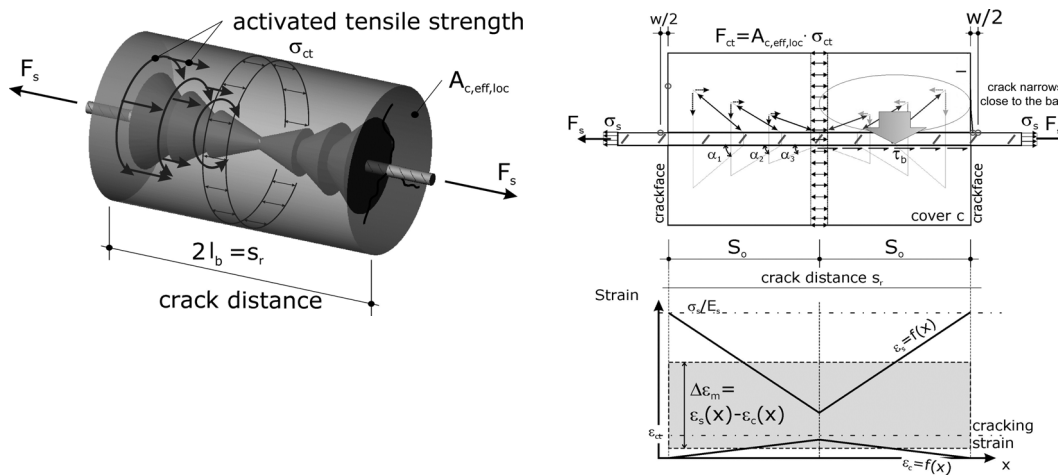
High performance concrete (HPC) as a material is well-researched and well-recognised for use in reinforced concrete structures. Current international and national building codes throughout the world impose its use with only minor restrictions. However, some countries still contest applying classes higher than $f_{ck} = 70$ MPa in bridge design as several concerns exist about such concrete's brittleness and fatigue behaviour and existing difficulties during casting. Major concerns rose over the fact, f_{ct} , increases disproportionately at a slower rate as increases occur in the compressive strength, f_c . It complicates the overtaking of design and detailing rules from NSC for HPC design. The bond between steel and concrete results

from the two important concrete properties: compressive strength and tensile strength as well as from the shape of the rebar.

Past major research, for example BALAZS [2] and REHM/ ELIGEHAUSEN [7] focused on NSC bond behaviour under fatigue loading. BALAZS proved relationships to the common idea of linear damage accumulation ("Palmgren-Miners' rule"). The subsequently described experimental program took guidance from these earlier programs with some more recent results published by ECKFELDT/ CURBACH in [10].

Typical bond tests are pull-out tests on short bond lengths and direct tension tests on long bond lengths. The first is usually preferred for parametric research the second for studies on cracking. However, transferring these results from short bond length pull-out tests to realistic long bond lengths is problematic, given the high results of ultimate bond stresses for HPC (see Tab. 4). Therefore, the focus changed towards the issue of settling practicable (that means: long) embedment lengths. This led to the bond research of monotonically loaded tests and discussions of TEPFER's [5] and GOTO's [3] approach. Combining both theories, the bond problem can be modelled as a partially cracked strut and tie system (see ECKFELDT [12], [11]).

It reopens an alternative chance to use results of those cheap bond tests on short bond lengths. Several, sequentially coupled otherwise autarkic Tepfers-Systems form a cross-over from short bond lengths results to common long bond lengths. It shows relationships between size and depth of the unknown longitudinal micro-cracks into the concrete cover (Fig. 1).



a) 3 D: ("classic" cracking approach) b) 2 D:

Fig. 1: An illustration of the complex resistance mechanism along long bond lengths in a direct tension test related to the steel loading

A strong review of the earlier performed fatigue tests revealed new possibilities from the test data even though it appears heavenly burdened by the presence of typical fatigue scatter and right censoring or truncation problems. To settle reliable predictions, it is important to be able to handle those problems. This is the point where a new performed analysis according to updated biostatistics knowledge comes into the view. However, first a rough

introduction into the test setup, the acquired data and traditionally performed fatigue data analysis is necessary, given by the next two chapters.

2 The experimental design

2.1 The pull-out specimen

The bond behaviour was studied on adapted pull-out specimens. Fig. 2 shows an example. The program tests the bar diameter and the varied clear cover. The typical undisturbed $5 d_b$ bond length in the RILEM-concept of short bond lengths reduces to $2 d_b$. The shortened bond length, l_b , ensures the bond failure occurs before the steel yields during the loading scheme. Second, the shorter bond length allows an easier fit within the general idea of analyzing the bond matter by the notion of the bar differential Δx . REHM [1] introduced the concept first and referred to the two differing sizes of the clear cover. Either it uses an ideal confined setting of the installed bar located in the centre of the specimen and m-tagged in the specimen code digits or it uses the common case of a close-to-surface casting. It resembles the more realistic bridge cover of at least 40 mm and it is r-tagged in the specimen code digits.

For this study, the bar were in an upright position with the bond zone placed opposite to the side of loading. This setting avoided constraints from the steel made bearing plate.

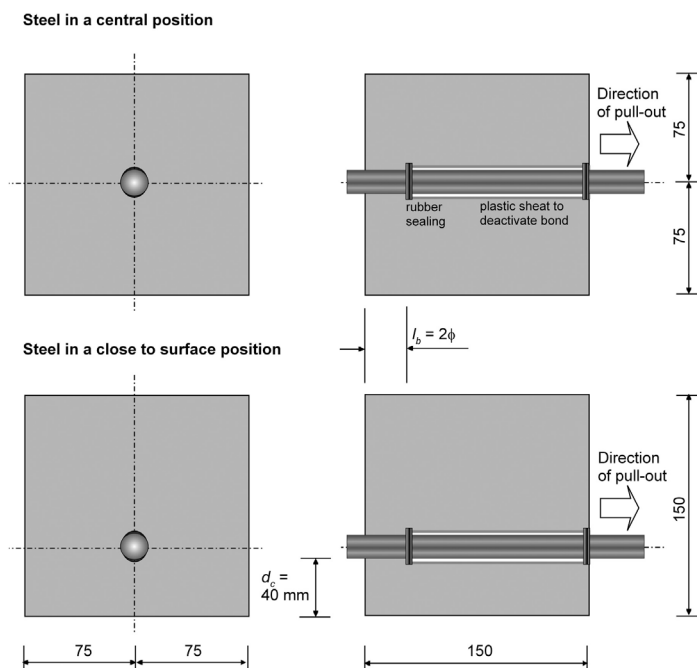


Fig. 2: Pullout specimen, geometrical design in mm

2.2 The test program

Tests plans incorporated 10, 14 and 25 mm bars with 14 mm playing a major role because of its wide use in concrete bridges. The HPC concrete grades varied from C60 to close C100. Each, of the total 15 test series conducted, consisted of 3 pull-out specimens tested on the static-monotonically increasing load to obtain the expected value (expected by statistical means) of the ultimate bond stress and bond-slip curves. The other 4 pull-out specimens of one series were tested under a high-cyclic sinusoidal loading. The frequency was kept constant in the test between 3 to 6 Hz with $f = 5$ Hz as the most used loading rate. The stress range, the difference between the upper and lower stress level extremes, was constantly applied. The tests run until specimen collapse or 1 million load cycles reached, whichever occurred first. The upper and lower bounds of bond stressing are ratios of the normalizing mean bond strength, f_b . Such calibrating bond stress came from previously measured, single monotonic tested specimen to achieve comparability among the series (Fig. 3). All surviving pull-out specimens were finally tested against a monotonic load increase until the bond fully failed.

All 4 specimens of the cyclic tested portion of a series were subject to the same testing boundaries. The upper and lower stress levels according to the 3 a priori static tests changed from series to series. This ensured, the results would show evidence if the fatigue resistance of the bond area depended on the upper and lower stress levels, the stress range or the mean stress. Several routine data (i.e. compressive stress f_c ; modulus of elasticity E_{cm} ; tensile splitting strength f_{ct}) was also gained. The table Tab. 1 shows the experimental plan. It also provides the relation to the tested cyclic loading as sketched out in Fig. 3. It illustrates the sinusoidal load cycles. All cyclic tests were performed force controlled.

Tab. 1: Geometric data for the test specimens and loading scheme

No.	Series	a , mm	d_b , mm	l_b , mm	c , mm	c/d_b	l_b/d_b	$f_{b,min}/f_{b(ult)}$	$f_{b,max}/f_{b(ult)}$	$f_{b,mean}/f_b$
1	1809	150	14	28	68	4.9	2	0.35	0.55	0.450
2	0110	150	14	28	68	4.9	2	0.35	0.70	0.525
3	1610	150	14	28	68	4.9	2	0.35	0.85	0.600
4	1711	150	14	28	40	2.9	2	0.15	0.70	0.425
5	2611	150	14	28	40	2.9	2	0.15	0.85	0.500
6	1112	150	14	28	40	2.9	2	0.15	0.55	0.350
7	1501	150	14	28	40	2.9	2	0.55	0.70	0.625
8	3001	150	14	28	40	2.9	2	0.35	0.70	0.525
9	1202	150	14	28	40	2.9	2	0.35	0.70	0.525
10	1902	150	14	28	40	2.9	2	0.55	0.85	0.700
11	1203	150	10	30	40	4	3	0.35	0.70	0.525
12	0204	150	10	20	40	4	2	0.35	0.70	0.525
13	0705	150	14	28	40	2.9	2	0.35	0.55	0.450
14	1405	150	14	28	40	2.9	2	0.35	0.85	0.600
15	0207	150	25	50	40	1.6	2	0.35	0.70	0.525

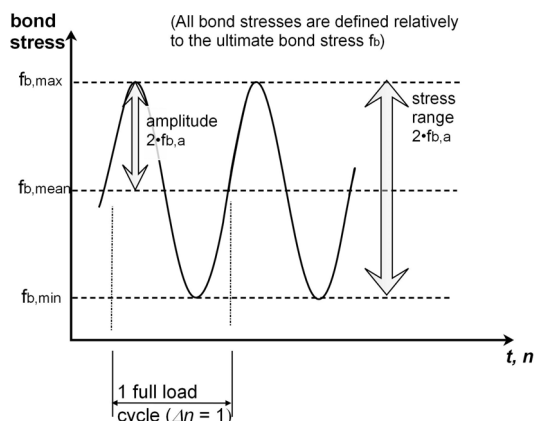


Fig. 3: Explanations of definitions used within Tab. 1

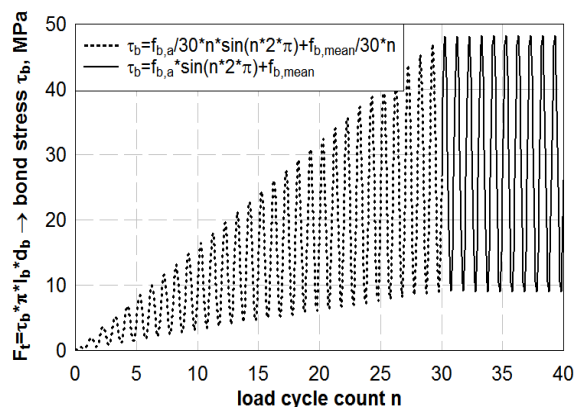


Fig. 4: Turn-up sequence (test# 6r282611). load history applied to reach the full amplitude

2.3 The test set-up

The tests used a hydraulic, dynamic enabled test-rig (Fig. 5). The test specimen hung from the upper bearing beam using coupler and hanger elements. The pulling direction for the rebar was downward while an underlay reduced the constraining influence of the bearing plate. It comprised of a deformable plastic material and the bonded zone located at the opposite side of the specimen. The following data was recorded:

- transferred force F by a load cell beneath the bearing plate [in kN].
- slip on the load-free end of the bar, s_0 [in mm] by an inductive longitudinal displacement transducer (LDT)

The bond stress τ_b was simply calculated as a mean shear stress at the bar surface:

$$\tau_b = \frac{F}{\pi \cdot d_b \cdot l_b} \quad (1)$$

The load could not be applied at once but was usually turned-up in a sequence of about 30 load cycles with increasing amplitude until the needed stress level was reached. The load cycle count 30 refers to $lg n \sim 1.5$. Fig. 4 shows the load history of the turn-up sequence.

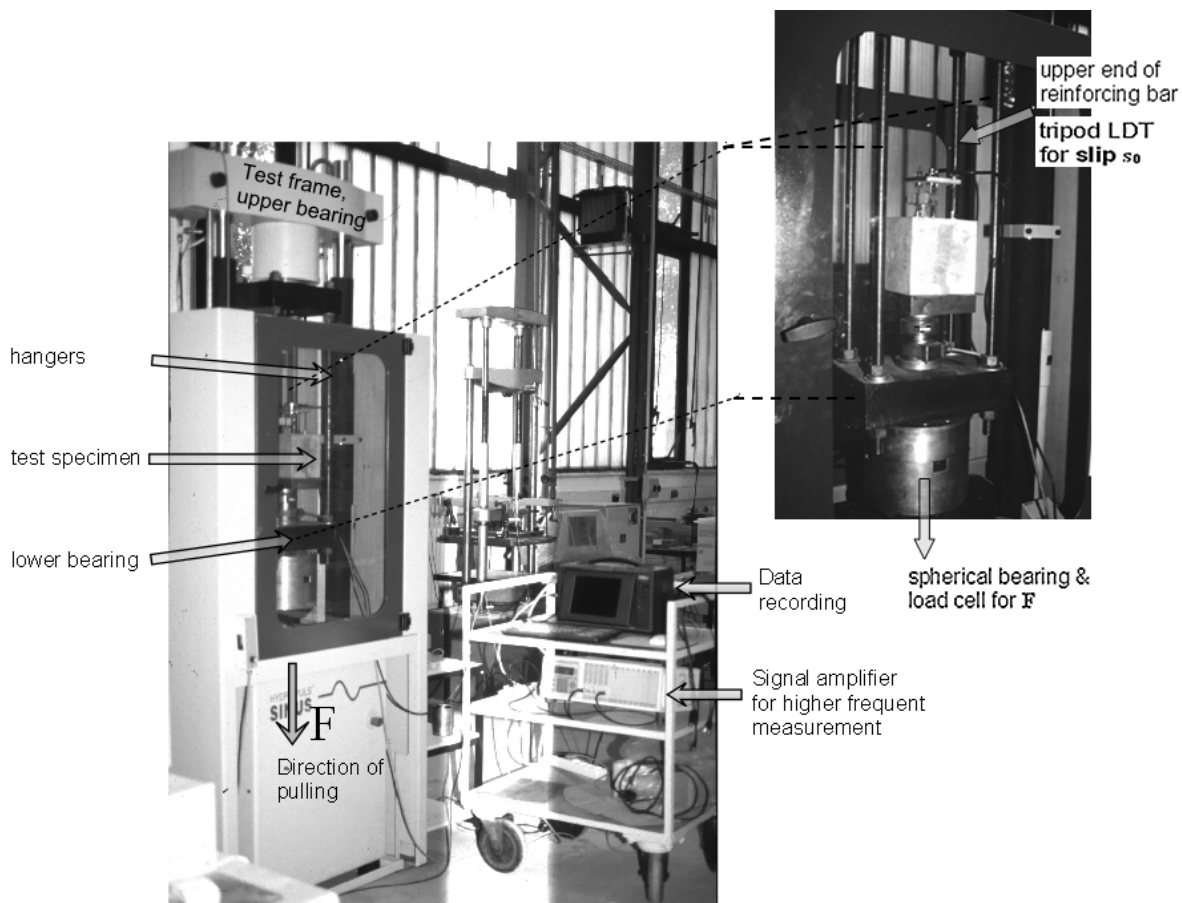


Fig. 5: Test set-up for the experimental program

3 Results from standard fatigue analysis

3.1 Material data

The measured routine data provided mean values for the tensile (splitting) strength f_{ct} , compressive strength f_c and the modulus of elasticity E_{cm} . Numbers in italic in Tab. 3 point to the lack of availability of enough data for some series. Therefore, values are assigned based on the assumed systematic relations drawn from recorded data. The rebar of type BSt 500S is in compliance with the German DIN 488. The steel data of Tab. 2 provide a frame of reference based on a quality check by the contractor and standard demands.

Tab. 2: Steel characteristics

Steel type	$d_{b,mm}$	f_y, MPa	f_t, MPa	E_s, MPa
BSt 500S	10; 14; 25	>500	>550	210000

Tab. 3: Concrete characteristics

No.	Series	f_c , MPa	f_{cc200}	f_{ct} , MPa	E_c , MPa
1	1809	89.38	105.02	5.57	38467
2	0110	73.64	88.69	5.30	41900
3	1610	70.71	85.56	4.57	38553
4	1711	79.15	94.50	5.20	41549
5	2611	77.00	92.25	5.15	41146
6	1112	82.74	98.23	5.37	42206
7	1501	81.16	96.59	5.28	42777
8	3001	92.07	107.73	5.07	43787
9	1202	57.32	70.87	4.40	36394
10	1902	94.32	109.98	6.33	45715
11	1203	94.60	110.26	4.93	43443
12	0204	87.65	103.27	5.45	43074
13	0705	90.06	105.70	5.97	46070
14	1405	83.72	99.24	5.26	42382
15	0207	73.99	89.06	5.03	42554

3.2 Survived load cycles

The most straightforward result that these fatigue tests provided was the number of survived load cycles under the applied loading regime. Cyclic loading stopped automatically after 1,000,000 load cycles. This regime censors the experimental program on the right as well as unexpected steel failures do. The specific test parameters (stress range, upper and lower bound bond stress) of the dynamic tests were based on the average bond strength, f_b (Tab. 4) from the three previously conducted static tests of each series.

 Tab. 4: Results from pre- and post tests on the series' bond strength f_b ($l_b = 2(3) d_b$, Tab. 1)

No.	Series	monotonic loading					after 10^6 applied load cycles			
		d_b , mm	f_b , MPa	$s_0(f_b)$, mm	$\tau_{b,0.1}$, MPa	test failure mode	$f_{b,1mill}$, MPa	$s_0(f_{b,1mill})$, mm	test failure mode	
1	1809	14	66.62	0.52	55.62	sliding	59.88	0.187	splitting	
2	0110	14	64.93	0.50	56.04	sliding	65.69	0.486	sliding	
3	1610	14	53.79	0.43	43.61	sliding			sliding	
4	1711	14	47.66	0.28	43.24	splitting	49.03	0.122	splitting	
5	2611	14	57.30	0.27	50.22	splitting			splitting	
6	1112	14	51.44	0.24	38.29	splitting	57.92	0.195	splitting	
7	1501	14	57.58	0.33	44.67	splitting	55.43	0.257	splitting	
8	3001	14	60.01	0.23	51.21	splitting	63.25	0.307	splitting	
9	1202	14	40.86	0.39	31.60	splitting	41.06	0.327	sliding	
10	1902	14	67.32	0.29	56.88	splitting			splitting	
11	1203	10	45.54	0.19	36.98	sliding	46.65	0.416	sliding	
12	0204	10	42.97	0.40	37.22	sliding	49.53	0.335	splitting	
13	0705	14	62.68	0.92	51.07	splitting	62.18	0.283	sliding	
14	1405	14	62.96	0.46	52.13	splitting			splitting	
15	0207	25	24.84	0.08	23.73	splitting	30.22	0.101	splitting	

According to HUANG ET. AL [25] one would expect the bond stress at $f_{b(ult)} \sim 0.45 \cdot f_{ck}$. The values in Tab. 4 are different because of the latent influence of a limited c/d_b -ratio and the bonded zone set on the opposite side of the loaded end of the specimen (see ECKFELDT [12] for more detailed explanation). Tab. 5 presents the results in both, decimal or common (decadic) logarithmic scales.

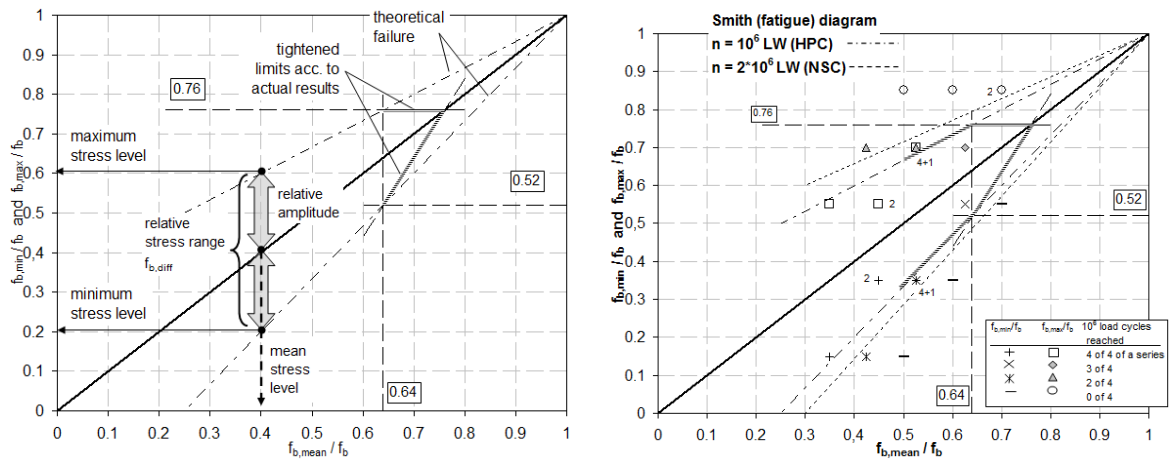
Tab. 5: n and $lg(n)$ survived load cycles, sorted according to specimen# within a series

No.	Series	# 4	# 5	# 6	# 7	# 4	# 5	# 6	# 7
1	1809	1000000	1000000	1000000	1000000	6	6	6	6
2	0110	61049	159771	1000000	1000000	4.786	5.203	6	6
3	1610	3284	27118	-	-	3.516	4.433	-	-
4	1711	729057)**	787153)**	1000000	1000000	5.863	5.896	6	6
5	2611	42	122	490	56584	1.623	2.086	2.690	4.753
6	1112	1000000	1000000	1000000	1000000	6	6	6	6
7	1501	97014	1000000	1000000	1000000	4.987	6	6	6
8	3001	1000000	1000000	1000000	1000000	6	6	6	6
9	1202	1000000	1000000	1000000	1000000	6	6	6	6
10	1902	87)*	116582	132041	367052	1.934	5.067	5.121	5.565
11	1203	982328)**	1000000	1000000	1000000	5.992	6	6	6
12	0204	1000000	1000000	1000000	1000000	6	6	6	6
13	0705	1000000	1000000	1000000	1000000	6	6	6	6
14	1405	158	947	44532	126918	2.199	2.976	4.649	5.104
15	0207	1000000	1000000	1000000	1000000	6	6	6	6

)* extreme value,)** unexpected, early steel failure

3.3 A glance at classic fatigue diagrams

The objective of the first analysis was to produce typical fatigue diagrams depicting the bond case present. The results were used to produce a SMITH-diagram (drawn according to an assumed dependency on the upper, mean and lower stress level). To help to understand the principles of the SMITH-diagram [22], Fig. 6 a) explains its general interpretative idea. Further firsthand results were basic WOEHLER(S-N)-lines (see Schijve [23] for details) relying on the limited data and conservatively ignoring the statistical impact of censored data. Fatigue-diagrams for RC typically refer to a failure envelope of 10^6 or $2 \cdot 10^6$ load cycles. The stress limits that allow to beyond this number are cross-referred as technical fatigue strength or the practical fatigue limit. The engineer believes failure is nearly unlikely to occur after passing this milestone. However, it is seldom full proven for concrete members and a rest of uncertainty always remains.



a) Principle boundary envelopes as the important information in a SMITH-diagram b) Smith-diagram based on acquired data

Fig. 6: Approach towards a SMITH-diagram based on acquired data and construction aids

The failure envelope in Fig. 6 b) was defined around the tests with load regimes where no failure occurred. It shows very basically and roughly an estimated survival mark. Fig. 6 b) also includes necessary corrections based on the results. The suggested failure envelope by REHM/ELIGEHAUSEN [7] is added to allow for comparison with normal strength concrete (NSC) and $2 \cdot 10^6$ load cycles.

An obvious problem for the prospective user of this freely drawn diagram is that there comes no probabilistic information with such a defined failure envelope. Does it show for a mean bond stress an expected value (estimator) or a conservative characteristic value of the possible amplitude? In this particular case no precise statements about the expected lines of longevity (10%-percent failure) or prompt failure (90%-percentile failure in fatigue tests) can be summarized from Fig. 6 b). The censoring on the right hand side by limiting tests to 10^6 load cycles remained as an untreated problem. There is no obvious justification for expecting the median $f_{b,max}/f_b$ -ratio to reach an allowance of more than 0.8.

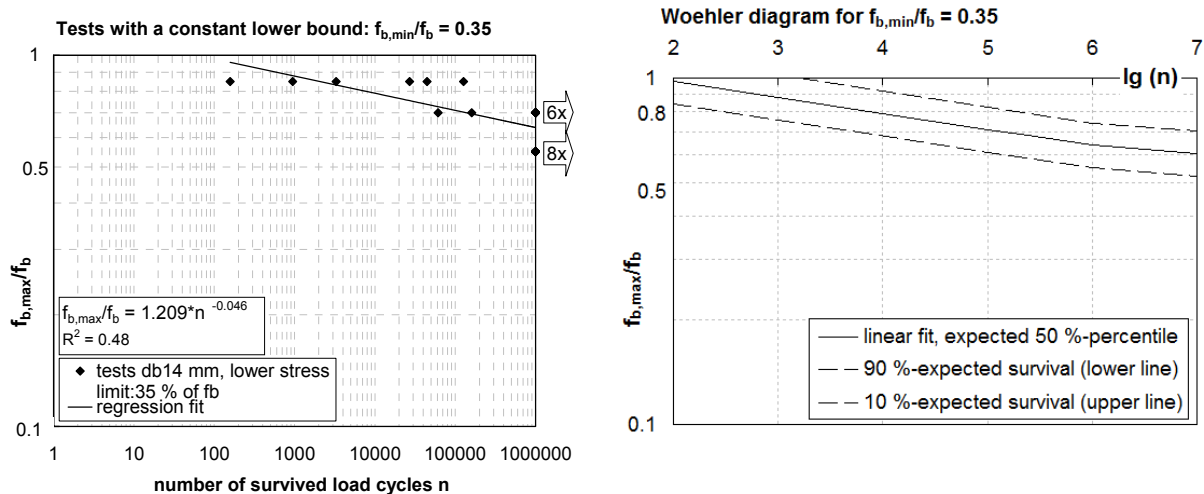
The experimental design did not take aim on a stress-life test according to WOEHLER (see [23]) usually performed in stress-blocks when the fatigue behaviour of the reinforcing steel is under research. However, it was tried to retrieve WOEHLER-like information from the recorded data but it was necessary to set the $S-N$ -curves on fixed lower stress bounds.

The WOEHLER-diagrams are set up using double common logarithmic scaling forming the WOEHLER-lines. They incorporate the HAIBACH improvement [9] for the slope for $n > 10^6$:

$$k_2 = 2k_1 - 1 \tag{2}$$

where: k_1 is the slope of the WOEHLER-line before reaching 10^6 load cycles referring to the so-called Basquin relation $S_a^{k_1} \cdot N = \text{constant}$.

Fig. 7 shows the data group for tests with $d_b = 14$ mm based on fixed lower bounds for the bond loading to 35% of the static ultimate bond stress. In the diagrams on the right, 10 %-lines and 90 %-lines are added to give estimates of prompt failure or longevity.



a) Expected $S-N$ -line and test results

b) Estimated $S-N$ -line with 10%- and 90%-percentiles

Fig. 7: WOEHLER-(fatigue) diagram for different relative stress levels for a $d_b = 14$ mm and a relative lower stress bound of $f_{b,min}/f_{b,ult} = 0.35$

4 Fatigue life as a survival problem

4.1 Why looking over to survival analysis?

The analysis above faces two major drawbacks, the right censoring/ truncation and the relation to important HPC-properties E_c and f_{ct} .

The simple question of interest is: Will the specimen under certain repeated loading fail or not? The more abstract question in design arises therefore: Will the specimen/ structural member under verification "survive" the fatigue loading or not?

Obviously, there exist some so-called dichotomous variables, *Failure mode (Fm)* and *censoring status (censstat)* in the game. These are variables bound to two states, for example 0 or 1, failed or not failed, censored or not censored, event yes/ not or even opposing. If such states are in some relation to time, there exist various methods for treatment in biostatistics and epidemiology. For fatigue life analysis and in difference to such models, we might use the load cycle number n or its logarithmic transform as a time replacement. In fact, the load cycle number can be defined by time over the loading frequency.

4.2 Hazard and survival - terms explained

The general idea is, to provide a model that returns a survival probability, a hazard ratio or hazard probability of reaching the failure state. This would enable to draw direct the fa-

tigue diagrams for the estimators on the demanded representative probability. Intervals of confidence (CI) accompany such results as measures of quality for model responses.

A survival function $S(t)$ describes the survival probability under defined parameters. The survival function results from the CDF (*-cumulative distribution function*) $F(t)$ stating the failure probability:

$$S(t) = 1 - F(t) \quad (3)$$

If the failure rate on a certain time needs verification, the *hazard ratio* (or *hazard function*) gains importance:

$$h(t) = f(t) / S(t) = \frac{f(t)}{1 - F(t)} = - \left(\frac{dS(t)}{S(t)} \right) \quad (4)$$

Such a ratio can be also expressed by suitable time-step functions, relating it to explanations given by KLEINBAUM [15]:

$$h(t) = \lim_{\Delta t \rightarrow 0} \frac{P(t \leq T < t + \Delta t | T \geq t)}{\Delta t} \quad (5)$$

The cumulative hazard function denotes $H(t)$ and derives from:

$$H(t) = -\ln(1 - F(t)) = -\ln(S(t)) \quad (6)$$

The average hazard rate \bar{h} out of the gained survival experience is in a descriptive way:

$$\bar{h} = \text{number of failures} / \sum_{n=1}^n t_i \quad (8)$$

If several variables influence the survival of a specimen, a measure of single exposure to an effect is the hazard ratio (HR) in comparison to the average hazard function. For the fatigue problem, either n or $\lg n$ replaces the time t in the above equations.

$$HR = h_E(t) / \bar{h}_E(t) \quad (9)$$

4.3 Use of the logistic regression in model building

The only result seeming of primary interest is a failure probability indicating failure or not. This is transferable in form of a 1 or 0 decision. So, it becomes necessary to introduce a mathematical function that limits the results effectively to the interval $[0;1]$. So far, it is basically a binomial concept.

It is possible to describe such results by the way of calculating the probability of either 1 or 0 state in the dependency on certain parameters (*factors*).

$$P(Y = 0) = (1 + e^{-z})^{-1} \quad (10)$$

This function yields results between 0 and 1 and is called the *logistic function*. The function (10) simplifies to:

$$P(Y = 0) = \frac{e^z}{1 + e^z} \quad (11)$$

The introduction of $z = \beta_0 + \beta_1 \cdot x$ allows a linear fit to a representative or calculated probability.

$$P(Y = 0) = \frac{e^{\beta_0 + \beta_1 \cdot x}}{1 + e^{\beta_0 + \beta_1 \cdot x}} \quad (12)$$

The single parameter x in (12) can take arbitrary arguments but the function always returns values between 0 and 1. Extending the same idea more general on many parameters, the formula of a *logit-transform* would emerge:

$$\text{logit}(p(X)): \quad \ln\left(\frac{P(X)}{1 - P(X)}\right) = \ln(\text{odds}(p)) = \beta_0 + \beta^T X \quad (13)$$

$$\text{where:} \quad X = \begin{bmatrix} x_1 \\ \vdots \\ x_n \end{bmatrix}; \quad \beta = \begin{bmatrix} \beta_1 \\ \vdots \\ \beta_n \end{bmatrix}$$

The logit-transform is the logarithm of the ratio between probability and complementary probability showing the chance of something to happen. After reshaping it returns boundaries on parameters for the wanted event probabilities at the 90 %, 50 % and 10 % level for survival based on suitable data. The source of data is arbitrary and might be not only medical or pharmaceutical. It could also describe the life states of engineering parts and even the results of in fatigue verifications since the assumption of independent tests is widely secured within the data.

Inspired by this appealing idea and the binomial starting point, the available recordings of the fatigue tests need certain reshaping and conversion to fit within the assumptions. Fig. 8 pictures a typical recoding of the failure states for the overall test duration of 1 million load cycles. One test includes a failure event the second shows a so-called run-out meaning it passed 1 million load cycles without failure. A discretisation of the time to failure or load cycles to failure count n into 11 observation steps simplifies the situation (see table attached to Fig. 8).

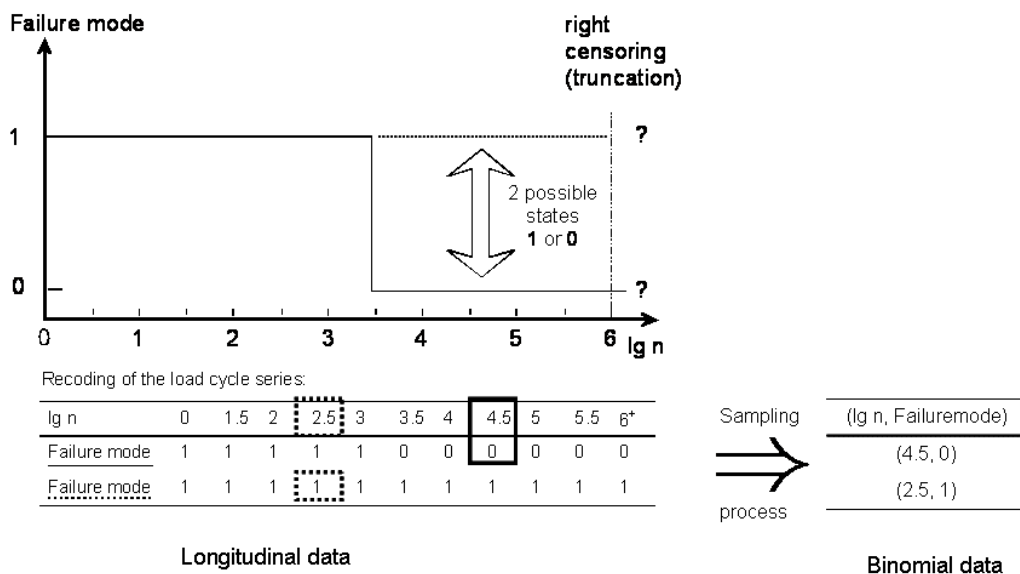


Fig. 8: The recoding concept for fatigue tests

The examples within Fig. 8 show two fatigue tests converted into longitudinal data. However, it still bears an underlying latent process starting always with a sequence of 1's. Sampling pairs of $(\lg n; Failuremode)$ for every test restores independent data samples. Such a sampling process converts the longitudinal observation into binomial data. It is noteworthy that the sampling might result in (2; 1) instead of (4.5; 0) for the 1st example of Fig. 8 with the same chance.

Models gained from such data won't return results like minimum fatigue strength or maximum fatigue strength but probabilities of survival under given parameters. It direct supports fatigue diagrams, reliability estimations and explorative parameter research. If necessary, it provides an easy link to further probabilistic approaches and the reliability assumptions.

4.4 Familiarize with the logistic regression concept for fatigue

Further tests on the given data used the R PROGRAM [16] for statistical computing. The fatigue test program presumed the ratio $f_{b,max}/f_b$ being of decisive influence on the achieved number of load cycles to failure. By reviewing Tab. 5 it becomes clear, no failure at all occurred over 10^6 load cycles if $f_{b,max}/f_b$ was 0.55. The research efforts therefore concentrate on fatigue tests $f_{b,max}/f_b = [0.70; 0.85]$.

The available test recording for $f_{b,max}/f_b = 0.70$ consists of 8 series á 4 specimen = 32 specimens tested. Unfortunately, the longitudinal recording of observation data presents a lack of independence among observations in its sequence. This sequential and discrete recording of the *Failuremode* variable's state with increasing $\lg n$ can be handled as repeated measure. To "reinstall" independence, always one of the 11 possible observation stages $\lg n, \lg n \in \{0; 1.5, 2.0; 2.5; \dots; 6.0\}$ step 0.5} is drawn by an univariate sampling process. Repeated for 32 times with replacement, it attaches every sampled $\lg n$ to a specimen number 1 to 32. In a second sampling, this order of 32 specimens is also randomized without

replacement using random permutations. Accordingly, the pair (#specimen, $\lg n$) is available and a fully randomized sample of 32 binomial data combinations ($\lg n$, *Failuremode*) can be extracted from the full set of longitudinal data in Tab. 6. Repeating this for 500 times produces a set of 16000 binomial data pairs combinations. The program GNUmeric 1.7.10 [17] produced sufficient accuracy in random sampling.

Tab. 6: Information of Tab. 5 for tests with $f_{b,max}/f_b = 0.70$ converted into binomial data

# speci- men	Series- ref.	$\lg n$											<i>1 random sample</i>		
		0	1.5	2.0	2.5	3.0	3.5	4.0	4.5	5.0	5.5	6.0 ⁺	<i>binom. data</i>		
		#	\lg <i>n</i>	<i>Failure-</i> <i>mode</i>											
1	0110#4	1	1	1	1	1	1	1	1	0	0	0	23	6.0	1
2	0110#5	1	1	1	1	1	1	1	1	1	0	0	13	0.0	1
3	0110#6	1	1	1	1	1	1	1	1	1	1	1	26	3.5	1
4	0110#7	1	1	1	1	1	1	1	1	1	1	1	4	5.5	1
5	1711#4	1	1	1	1	1	1	1	1	1	1	0	12	5.0	1
6	1711#5	1	1	1	1	1	1	1	1	1	1	0	16	0.0	1
7	1711#6	1	1	1	1	1	1	1	1	1	1	1	8	3.5	1
8	1711#7	1	1	1	1	1	1	1	1	1	1	1	19	4.5	1
9	1501#4	1	1	1	1	1	1	1	1	0	0	0	20	2.5	1
10	1501#5	1	1	1	1	1	1	1	1	1	1	1	21	4.0	1
11	1501#6	1	1	1	1	1	1	1	1	1	1	1	1	5.0	0
12	1501#7	1	1	1	1	1	1	1	1	1	1	1	25	2.5	1
13	3001#4	1	1	1	1	1	1	1	1	1	1	1	28	5.0	1
14	3001#5	1	1	1	1	1	1	1	1	1	1	1	30	5.0	1
15	3001#6	1	1	1	1	1	1	1	1	1	1	1	22	6.0	1
16	3001#7	1	1	1	1	1	1	1	1	1	1	1	6	3.5	1
17	1202#4	1	1	1	1	1	1	1	1	1	1	1	14	5.5	1
18	1202#5	1	1	1	1	1	1	1	1	1	1	1	11	4.0	1
19	1202#6	1	1	1	1	1	1	1	1	1	1	1	24	5.0	1
20	1202#7	1	1	1	1	1	1	1	1	1	1	1	7	6.0	1
21	1203#4	1	1	1	1	1	1	1	1	1	1	0	3	3.0	1
22	1203#5	1	1	1	1	1	1	1	1	1	1	1	18	6.0	1
23	1203#6	1	1	1	1	1	1	1	1	1	1	1	10	6.0	1
24	1203#7	1	1	1	1	1	1	1	1	1	1	1	32	4.5	1
25	0204#4	1	1	1	1	1	1	1	1	1	1	1	29	5.0	1
26	0204#5	1	1	1	1	1	1	1	1	1	1	1	15	1.5	1
27	0204#6	1	1	1	1	1	1	1	1	1	1	1	27	5.5	1
28	0204#7	1	1	1	1	1	1	1	1	1	1	1	2	2.5	1
29	0207#4	1	1	1	1	1	1	1	1	1	1	1	31	1.5	1
30	0207#5	1	1	1	1	1	1	1	1	1	1	1	9	1.5	1
31	0207#6	1	1	1	1	1	1	1	1	1	1	1	17	4.5	1
32	0207#7	1	1	1	1	1	1	1	1	1	1	1	5	1.5	1

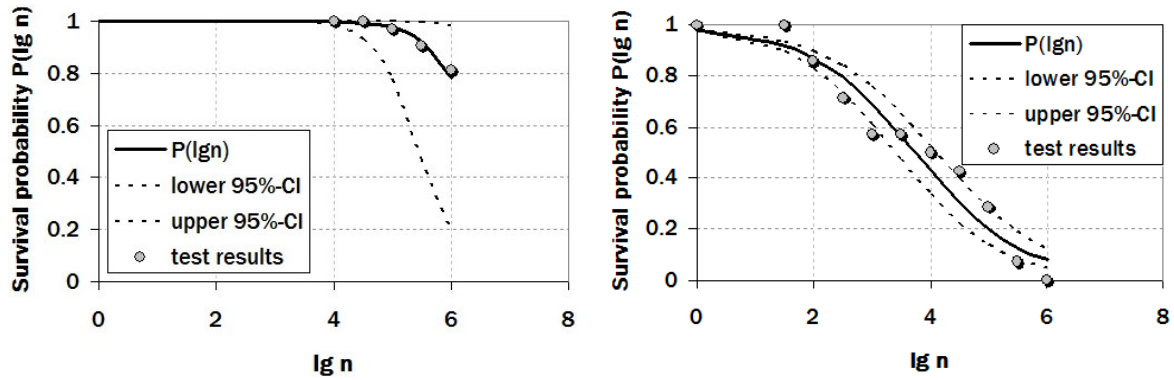
The regression database leading to equation (14) used an overall of 500 random samples based on Tab. 6. One obtains a first model for the estimated survival probability:

$$P\left(\text{Failuremode} = 1 \left| \frac{f_{b,max}}{f_b} = 0.70 \right.\right) = \hat{S}(\lg n) = \frac{\exp(16.0863 - 2.4678 \cdot \lg n)}{1 + \exp(16.0863 - 2.4678 \cdot \lg n)} \quad (14)$$

Confidence intervals have been calculated under assumed normal distribution:

$$\begin{aligned} \widehat{\beta}_i \pm z_{1-\alpha/2} \cdot se(\widehat{\beta}_i) & \quad [i = 0;1] \\ \widehat{\beta}_i \pm 1,96 \cdot se(\widehat{\beta}_i) & \quad 95\% - CI \end{aligned} \tag{15}$$

The next diagram shows the expected value of survival as estimator and the 95%-confidence intervals on the survival probability:



a) $f_{b,max}=0.70 f_b$

b) $f_{b,max}=0.85 f_b$

Fig. 9: Survival probability as a function of applied load cycles

From Fig. 9 a), it becomes immediately clear the confidence in the expected survival is fading away for load cycle numbers larger than 10^5 . That is because of the fact that 32 Specimens allow many random permutations of observations. The same procedure has to be repeated for $f_{b,max}=0.85 f_b$ with longitudinal data in Tab. 7.

Tab. 7: Information of Tab. 5 for tests with $f_{b,max}/f_b = 0.85$ converted into binomial data

# speci- men	Series- ref.	lg n												1 random sample binom. data		
		0	1.5	2.0	2.5	3.0	3.5	4.0	4.5	5.0	5.5	6.0 ⁺	#	lg n	Failure- mode	
		1	1610#4	1	1	1	1	1	1	0	0	0	0	0	2	6,0
2	1610#5	1	1	1	1	1	1	1	0	0	0	0	3	2,0	0	
3	2611#4	1	1	0	0	0	0	0	0	0	0	0	8	3,0	1	
4	2611#5	1	1	1	0	0	0	0	0	0	0	0	4	6,0	0	
5	2611#6	1	1	1	1	0	0	0	0	0	0	0	13	3,5	1	
6	2611#7	1	1	1	1	1	1	1	1	0	0	0	14	5,0	1	
7	1902#4	1	1	0	0	0	0	0	0	0	0	0	11	1,5	1	
8	1902#5	1	1	1	1	1	1	1	1	1	0	0	12	2,5	1	
9	1902#6	1	1	1	1	1	1	1	1	1	0	0	7	2,0	0	
10	1902#7	1	1	1	1	1	1	1	1	1	1	0	6	4,5	1	
11	1405#4	1	1	1	0	0	0	0	0	0	0	0	5	3,5	0	
12	1405#5	1	1	1	1	0	0	0	0	0	0	0	9	2,5	1	
13	1405#6	1	1	1	1	1	1	1	1	0	0	0	1	3,5	1	
14	1405#7	1	1	1	1	1	1	1	1	1	0	0	10	4,5	1	

The logistic regression in a dataset of 500 binomial samples as displayed in Tab. 7 yields:

$$P\left(\text{Failuremode} = 1 \mid \frac{f_{b,\max}}{f_b} = 0.85\right) = \hat{S}(\lg n) = \frac{\exp(4.05552 - 1.08468 \cdot \lg n)}{1 + \exp(4.05552 - 1.08468 \cdot \lg n)} \quad (16)$$

The standard error (*se*) estimates from the regression statistics form again the base for the 95%-confidence intervals. They seem optimistic but the base for Fig. 9 a) and b) are repeated measures where the test design and subsequently the observations itself were not fully randomized. Instead, the estimators were results of an artificially randomized sample.

Of course there are still several drawbacks. Forecasting load cycles above 10^6 is not possible and no special care is taken of right censored data in $f_{b,\max}/f_b = 0.70$. The influence of other parameters remained hidden.

4.5 The coverage of more than one candidate predictors

The next objective is to cater for the influence of $f_{b,\min}/f_b, f_{b,\max}/f_b$ -ratios and $\lg n$ together on the survival probability. The calculation method used here, is the multiple logistic regression, an expansion of the above. The estimators of the $\beta_1, \beta_2, \beta_3$ -factors are based on maximum likelihood (ML) estimations. Another problem before going in computation is the randomization of the existing tests and time series. The results from 58 tested specimens belong in the multiparameter study set. Data of these specimens must be randomized and 500 samples combined.

The choice of suitable parameters for the final model suggestion uses the deviance residuals and the AIC-criterion intended by AKAIKE [18].

$$\begin{aligned} AIC &= -2 \cdot \ln(\text{likelihood}) + 2 \cdot k \\ \text{for small sample sizes, } (n / k < 40): AIC_c &= AIC + \frac{2k \cdot (k + 1)}{n - k - 1} \end{aligned} \quad (17)$$

where: n is the number of observations (tests)

k is the number of parameters

A stepwise test procedure is applied to possible model arrangements. A stepwise high decline of the AIC suggests a valuable effect and a vote to consider integration in the final model. However, there exists evidence that, model fits using the AIC information have a tend toward overfitting. Therefore looking for the physical meaning of variables (stress levels, strengths, modulus of elasticity) provides support in decisions. It helps that possible interactions are often already well-researched. Integration of variables or their interaction effects should be only considered when the combined effect can be mathematically specified. This is different from the biostatistics analysis core where for example treatment effects only generalize interaction effects.

The following expressions (m1) to (m5) show possible model configurations for linear models. The term $I(x:y)$ stands for the interaction term with specified relation between x and y or by $x:y$ without specification.

$$(m1) \quad P(\text{Failuremode} = 1) = f(\lg n; \frac{f_{b,\max}}{f_b}; \frac{f_{b,\min}}{f_b})$$

$$(m2) \quad P(\text{Failuremode} = 1) = f(\lg n; \frac{f_{b,\max}}{f_b}; \frac{f_{b,\min}}{f_b}; f_{ct}; E_{cm})$$

$$(m3) \quad P(\text{Failuremode} = 1) = f(\lg n; \frac{f_{b,\max}}{f_b}; \frac{f_{b,\min}}{f_b}; f_{ct}; (E_{cm} ?); I(f_{ct} / E_{cm}))$$

$$(m4) \quad P(\text{Failuremode} = 1) = f(\lg n; \frac{f_{b,\max}}{f_b}; \frac{f_{b,\min}}{f_b}; f_{ct}; (E_{cm} ?); I(f_{ct}^2 / E_{cm}))$$

with the interaction effect pointing to concrete brittleness definitions

$$(m5) \quad P(\text{Failuremode} = 1) = f(\lg n; \frac{f_{b,\max}}{f_b}; \frac{f_{b,\min}}{f_b}; f_{ct}; E_{cm}; I(f_{ct} \cdot E_{cm}))$$

In cases of uncertainty, the model selection might be based on the BIC (SCHWARTZ'S *Bayesian Information Criterion*-R package BMA for automated model selection considering posterior probabilities). However, the separate integration of E_{cm} seems not necessary and it might be worth to check only interaction terms in (m3) and (m4) instead. The BIC results show also no further need for an inclusion of f_{ct} as a separate term into models (m3) and (m4). Further, no theory exists that supports an inclusion of the interaction term in (m5). Therefore (m5) is expelled from the analysis. Its best AIC seems only to benefit from a kind of "artefact" property in the data.

The resulting and remaining models would be therefore:

$$P(Fm. = 1) = \hat{S}(\lg n; \frac{f_{b,\max}}{f_b}; \frac{f_{b,\min}}{f_b}) = \frac{\exp(31.23 - 1.373 \cdot \lg n - 32.71 \cdot \frac{f_{b,\max}}{f_b} + 5.006 \cdot \frac{f_{b,\min}}{f_b})}{1 + \exp(31.23 - 1.373 \cdot \lg n - 32.71 \cdot \frac{f_{b,\max}}{f_b} + 5.006 \cdot \frac{f_{b,\min}}{f_b})} \quad (18),$$

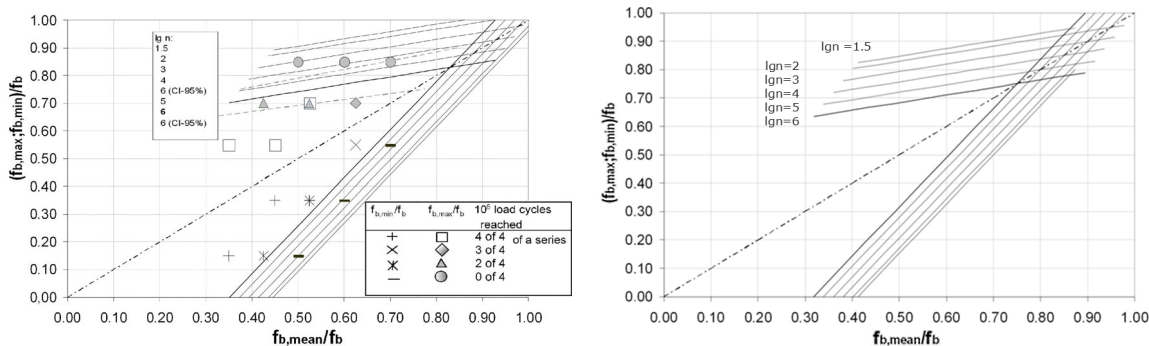
$$P(Fm. = 1) = \frac{\exp(29.30 - 1.373 \cdot \lg n - 31.86 \cdot \frac{f_{b,\max}}{f_b} + 5.509 \cdot \frac{f_{b,\min}}{f_b} - 0,665 \cdot f_{ct} + 0.000109 \cdot E_{cm})}{1 + \exp(29.30 - 1.373 \cdot \lg n - 31.86 \cdot \frac{f_{b,\max}}{f_b} + 5.509 \cdot \frac{f_{b,\min}}{f_b} - 0,665 \cdot f_{ct} + 0.000109 \cdot E_{cm})} \quad (19),$$

$$P(Fm. = 1) = \frac{\exp(33.69 - 1.374 \cdot \lg n - 31.94 \cdot \frac{f_{b,\max}}{f_b} + 5.655 \cdot \frac{f_{b,\min}}{f_b} - 26170 \cdot \frac{f_{ct}}{E_{cm}})}{1 + \exp(33.69 - 1.374 \cdot \lg n - 31.94 \cdot \frac{f_{b,\max}}{f_b} + 5.655 \cdot \frac{f_{b,\min}}{f_b} - 26170 \cdot \frac{f_{ct}}{E_{cm}})} \quad (20),$$

$$P(Fm. = 1) = \frac{\exp(31.52 - 1.374 \cdot \lg n - 32.32 \cdot \frac{f_{b,\max}}{f_b} + 5.592 \cdot \frac{f_{b,\min}}{f_b} - 1286 \cdot \frac{f_{ct}^2}{E_{cm}})}{1 + \exp(31.52 - 1.374 \cdot \lg n - 32.32 \cdot \frac{f_{b,\max}}{f_b} + 5.592 \cdot \frac{f_{b,\min}}{f_b} - 1286 \cdot \frac{f_{ct}^2}{E_{cm}})} \quad (21),$$

given $f_{b,\max}/f_b > f_{b,\min}/f_b$. Fm stands for "Failuremode".

A turnover into needful fatigue diagrams is possible by some simple assumptions. Smith diagrams can be successively drawn for the expected values (Fig. 10 a)) or the lower 10%-percentile (Fig. 10 b)) to secure against early failure. Model (18) founds the base for both Smith-diagrams. They integrate the original results and can be compared with Fig. 6 b):



a) Expected failures for several parameter combinations (incl. 95%-CI on $\lg n = 6$) b) $\lg n$ -lines for a 90%-survival

Fig. 10: Survival probability as a function of applied load cycles

Within the next snapshot (Fig. 11) of a Smith-diagram, a comparison between the rough model $m1$ (equation (18)) and the more sophisticated models ($m2$) to ($m4$) is drawn. It can be stated the differences between model ($m3$) and ($m4$) are minor. The same is true about the supposed influence of the modulus of elasticity E_{cm} and the tensile strength f_{ct} . Looking over it closer, there exists a small shift towards a decrease in the fatigue resistance for higher concrete grades. A correlation to the ratio f_{ct}^2/E_{cm} in the model ($m4$) shows the influence of an increasing brittleness.

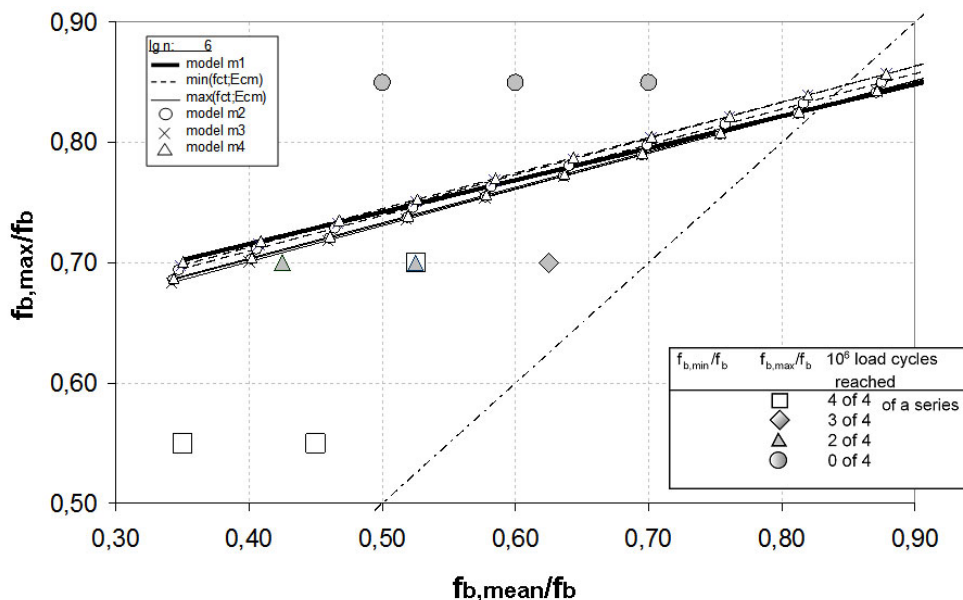


Fig. 11: Influence of concrete tensile strength and modulus of elasticity within test range, $\{\min(f_{ct}; E_{cm}) = (4.40 \text{ MPa}; 36394 \text{ MPa}), \max(f_{ct}; E_{cm}) = (6.33 \text{ MPa}; 45715 \text{ MPa})\}$.

Imposing E_{cm} or f_{ct} in the models causes the question of scale effects compared to the major effect of the relative upper bond stress ratio. However, by reviewing the tried range of f_{ct}/E_{cm} to E_{cm} , there were no major changes detected related to a quality difference in the response. It seems therefore reasonable to state, differences in the concrete grade did not heavily inflict the failure characteristics.

WOEHLER-diagrams are of interest for damage accumulation calculations. A transformation of results from the model (mI), equation (18), into a WOEHLER-like shape is easily performed. The lower stress level is fixed to a constant $f_{b,min}/f_b \in \{0.15; 0.35; 0.55\}$. The evolving function out of equation (18) is then:

$$\frac{f_{b,max}}{f_b} = \frac{\ln\left(\frac{P}{1-P}\right) - \beta_0 - \beta_1 \cdot \lg n - \beta_3 \cdot \left(\frac{f_{b,min}}{f_b}\right)_{\in(0.15;0.35;0.55)}}{\beta_2} \quad (22)$$

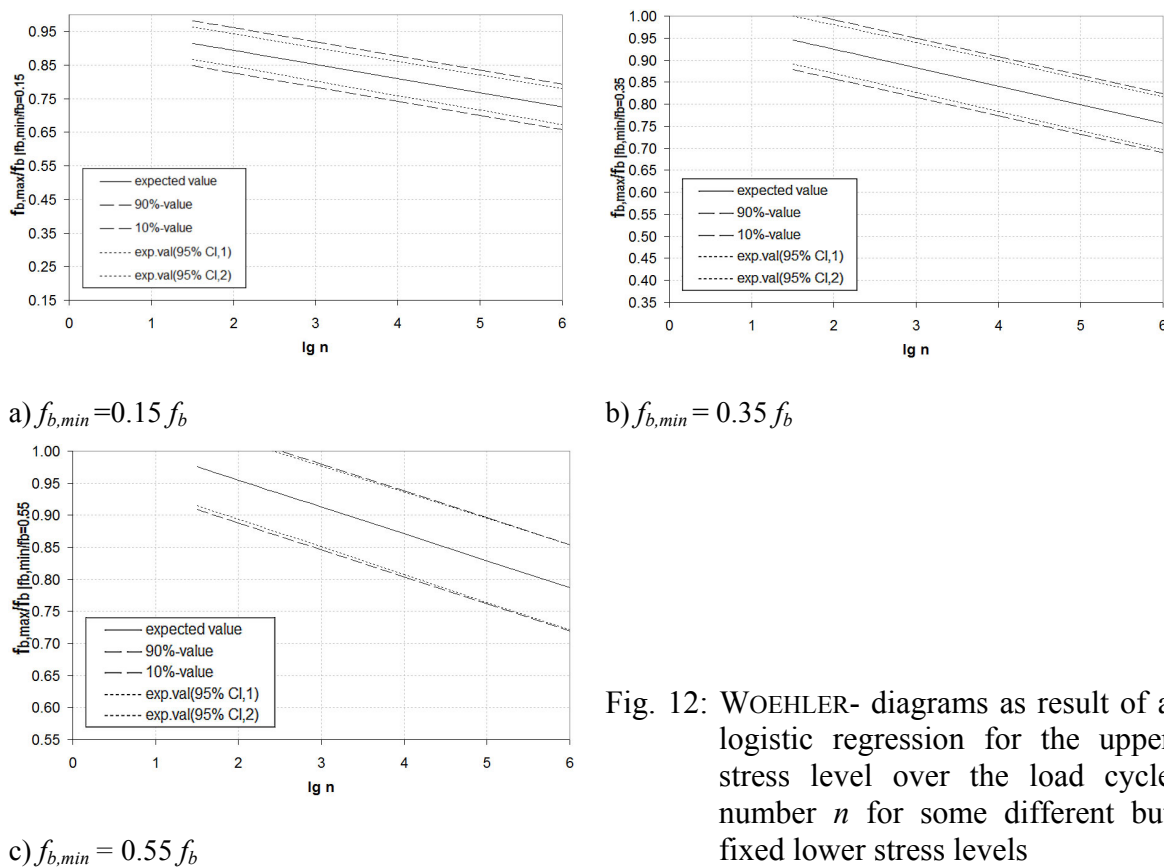


Fig. 12: WOEHLER- diagrams as result of a logistic regression for the upper stress level over the load cycle number n for some different but fixed lower stress levels

The resulting WOEHLER-diagrams enable for a comparison with the presented results in Fig. 7. However, no statement is possible on load cycle counts with $\lg n < 1.5$ because this range lies within the automated turn-up sequence to achieve the final amplitude (Fig. 4). Also, a connection to the Smith-diagram can be setup by substituting the $f_{b,min}/f_b$ - term:

$$\frac{f_{b,max}}{f_b} = \frac{\ln\left(\frac{P}{1-P}\right) - \beta_0 - \beta_1 \cdot \lg n - \beta_3 \cdot \left(-\frac{f_{b,max}}{f_b} + 2 \cdot \frac{f_{b,mean}}{f_b}\right)_{\in(0.15;0.35;0.55)}}{\beta_2} \quad (23)$$

4.6 Median survival in censored fatigue data based on KAPLAN-MEIER-estimations

Some problems remained still unsolved. Run out values in $\lg n = 6$ truncated tests are an important issue. Using them as uncensored, shifts these models on the conservative side if it comes close to the truncation point. KAPLAN-MEIER-estimations [24], [14] are a suitable way of producing sensible survival estimations while caring for censored data. In addition, the early steel failures in the series 1711 and 1203 (Tab. 5) could be taken censored from n load cycles of failure onwards if censoring is applied in a strong sense. Comprehensive information of the previous subchapter depends on an artificially randomized set of data gained from resampling of the original data. KAPLAN-MEIER allows a step backwards to the genuine set of data. These data are already sufficient to estimate expected survival probabilities. The KAPLAN - MEIER - Method returns an empirical estimator of the survival probability as a function of time. We may use n or $\lg n$ respectively as substitutes for time:

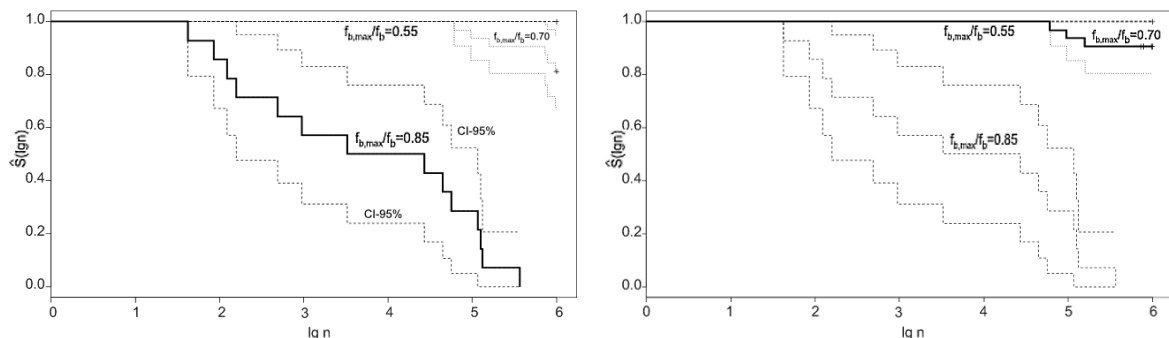
$$\hat{S}(\lg n_i) = \prod_{n_i < N} \left(\frac{r_i - f_i}{r_i} \right) = \prod_{n_i < N} \left(1 - \frac{f_i}{r_i} \right) \quad (24)$$

where: $r(n_i)$ is the number of specimen still without event (failure) on a certain n_i ,
 $f(n_i)$ is the number of specimen failed until a certain n_i ,
 N is the maximum number of applied load cycles.

The variance estimation according to Greenwood forms the base to calculate the CI:

$$\text{CI-95\%:} \quad \hat{S}(\lg n_i) \pm z_{\alpha/2} \cdot \sqrt{\widehat{\text{Var}}(\hat{S}(\lg n_i))} \quad (25)$$

$$\text{where: } \widehat{\text{Var}}(\hat{S}(\lg n_i)) = \left(\hat{S}(\lg n_i) \right)^2 \cdot \sum_{n_i < N} \left(\frac{f_i}{r_i \cdot (r_i - f_i)} \right) \text{ and } z_{\alpha/2} = 1,96 \quad (26)$$



a) Plot with marked censoring (+)

b) Censoring of steel failure treated as unrealistic failure in testing

Fig. 13: KAPLAN-MEIER-Plots of the survival estimates

For the benefit of a symmetric CI, the KALBFLEISCH and PRENTICE (in GREENWOOD [20]) modification towards an exponential CI was left aside. The R-package "survival" (Therneau, Lumley [19]) provides the library for calculating Kaplan-Meier-estimates. The data was subdivided either to the upper $f_{b,max}/f_b$ (Fig. 13) or to the lower stress bound $f_{b,min}/f_b$ (Fig. 14). A different trial on the event status *censstat* instead of *Fm-failuremode* shows a different outcome for $f_{b,max}/f_b = 0.70$ in Fig. 13 b).

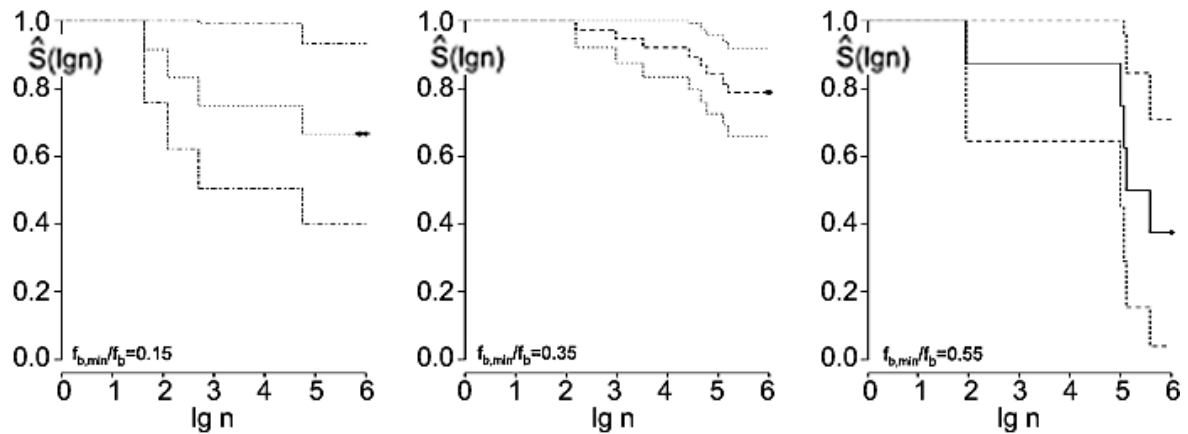


Fig. 14: Kaplan-Meier-Estimates of $f_{b,min}/f_b$ -grouped data with 95%-confidence band (+ marked censoring)

Looking to the also presumed dependency on $f_{b,min}/f_b$ (Fig. 14) it remained unclear whether a high lower bond stress bound is overall favourable or not. In the upper survival probabilities a higher $f_{b,min}/f_b$ stress bound increases the number of survived load cycles. However, higher $f_{b,min}/f_b$ stress bounds bear also a tendency of being more prone to a higher failure progression on a logarithmic scale. For $f_{b,max}/f_b$ - and $f_{b,min}/f_b$ -differenced cases, a much larger 95%-CI has been calculated than for the resampled data set. The level of uncertainty for the survival estimates matches the experience during fatigue testing. It suggests an analysis with more advanced methods to gain better certainty in the influence that $f_{b,min}/f_b$ might develop. Finally a statement on the mean and median survival according to KAPLAN-MEIER is possible (Tab. 8).

Tab. 8: Median and (restricted) mean survived load cycles

Constant Parameter	Restricted mean survival $\lg(n_{rmean})$	Median survival $\lg(n \hat{S} = 0.5)$	Lower 95%-CL for median survival, $\lg(n)$
$f_{b,max}/f_b = 0.55$	6.0	∞	∞
$f_{b,max}/f_b = 0.70$	5.91	∞	∞
$f_{b,max}/f_b = 0.85$	3.69	3.97	2.69
$f_{b,min}/f_b = 0.15$	4.93	∞	4.75
$f_{b,min}/f_b = 0.35$	5.60	∞	∞
$f_{b,min}/f_b = 0.55$	5.08	5.34	5.07

The median is found as calculated estimate $\hat{S}(\lg n) = 0.5$. The mean of survived load cycles results restricted based on the number of survived load cycles until first censoring occurred. Only for $f_{b,min}/f_b = 0.55$ or $f_{b,max}/f_b = 0.85$, the values of median survival fall far

below 1 million load cycles. The 95%-confidence interval for median survival evolve horizontally if the line $\hat{S}(\lg n) = 0.5$ crosses the confidence limits. It shows that also tests with $f_{b,min}/f_b = 0.15$ bear a latent danger of a median survival within 1 million load cycles.

5 Conclusion

The original question was: How does the bond behaviour of reinforcing steel change in fatigue, when HPC instead of NSC is used? After reviewing the results of an extensive program of fatigue loaded pull-out specimens the answer is:

There is no evidence that a higher modulus of elasticity and tensile strength of HPC had much influence on improving or worsen bond in fatigue compared to the better researched NSC. The most influencing factors are undoubtedly the relative upper stress level first and the lower stress level second. Results show $f_{b,max}/f_b = 0.7$ brings already a notable probability of failure before reaching the technical fatigue limit. Choosing $f_{b,max}/f_b = 0.55$ as an upper boundary would be therefore a decision towards the safe side valid for the whole range of possible average stress levels (see Fig. 10 b)). Decisions on the allowable lower bound $f_{b,min}/f_b$ should not be made without connecting it to $f_{b,max}/f_b$. For small lower stresses the high stress ranges and therefore amplitudes to $f_{b,max}/f_b$ are unbeneficial. For high $f_{b,min}/f_b$ stress bounds, the high mean stress level seems causes severe problems. The suggested models (18) or (23) allow a fine-tuning among relative $f_{b,max}$, $f_{b,min}$ and $f_{b,mean}$ levels.

SMITH- and WOEHLER-diagrams are classic and typical presentations of fatigue issues. However, the common way to achieve such results is a costly way. Modern biostatistics provide interesting alternatives to produce such important presentations and to handle limited and censored datasets. They help to produce direct formulas for the WOEHLER - problem. The influence of The AIC or BIC indicators provide far better aids for confirmation of the parameter effect as the commonly used significance levels. KAPLAN-MEIER-estimates, originated in medicine, provide an interesting analysis alternative to the WOEHLER-diagrams common in engineering.

Datasets cannot be arbitrarily high expanded without paying a certain price. The advantage is, the mean and therefore the main model stabilizes. However, the given confidence intervals are probably to optimistic. Likely workarounds could be setting up bootstrapping strategies within the original data pool.

The successes by performing simple bioinformatics and survival approaches in the steps towards the searched information/presentation of fatigues issues look very promising. They should encourage researchers to look for advances abroad the beaten track.

6 Acknowledgement

The authors acknowledge the financial and kind support of the DAfStb, Deutscher Ausschuss für Stahlbeton (German Committee for Reinforced Concrete).

7 Literature and further material

- [1] Rehm, G.: Über die Grundlagen des Verbundes zwischen Stahl und Beton. Heft 138 des DAfStb, W. Ernst & Sohn, Berlin 1961
- [2] Balazs, G. L.: Fatigue of Bond. *ACI Materials Journal*. V. 88, November- December 1991, pp. 620-629
- [3] Goto, Y. and Otsuka, K.: Studies on Internal Cracks Formed in Concrete Around Deformed Tension Bars. *ACI Journal*. Proceedings V. 68, No.4, April 1971, pp. 244-251
- [4] Bolotin, V. V.: Mechanics of Fatigue. *CRC Mechanical Engineering Series*. CRC Press, Boca Raton, 1998
- [5] Tepfers, R.: A Theory of Bond Applied To Overlapped Tensile Reinforcement Splices For Deformed Bars. Publication 73:2. Chalmers University of Technology Göteborg, Division of Concrete Structures, 1973, 328 p.
- [6] Gaede, K.: Versuche über die Festigkeit und die Verformung von Beton bei Druck-Schwellbelastung. Heft Nr. 144 des DAfStb, Berlin: W. Ernst & Sohn 1962.
- [7] Rehm, G. and Eligehausen, R.: Einfluß einer nicht ruhenden Belastung auf das Verbundverhalten von Rippenstählen. *Journal Betonwerk-und Fertigteil -Technik*, Heft 6/1977.
- [8] FIP-CEB: High Strength Concrete. State of the Art Report, FIP SR 90/1, CEB Bulletin d'Information No. 197, London: FIP 1990
- [9] Haibach, E.: Betriebsfeste Bauteile, Konstruktionshandbücher Band 38, Berlin Heidelberg: Springer-Verlag 1992
- [10] Eckfeldt, L. and Curbach, M.: Bond Behaviour of High Performance Concrete (HPC) and Reinforcing Steel Under Fatigue Loading. *Proceedings of the 3rd Int. PhD-Symposium in Civil Engineering 2000 Vienna*, Vienna 2000, pp. 67-76
- [11] Eckfeldt, L.: Control of Cracking for Concrete Bridges - the performance of calculation models. *Proceedings of the 7th International Conference on Short and Medium Span Bridges*, Montreal 2006 (AN-019, 11 pages)
- [12] Eckfeldt, L.: Möglichkeiten und Grenzen der Berechnung von Rissbreiten in veränderlichen Verbundsituationen (Opportunities and limits of crack control in respect to varying bond situations), Dissertation. Dresden 2005, published online: <http://nbn-resolving.de/urn:nbn:de:swb:14-1138179912681-09751>
- [13] Harrell jr., F. E.: Regression Modeling Strategies: With Applications to Linear Models Logistic Regression and Survival Analysis. *Springer Series in Statistics*, Springer, New York 2001, 568p.

- [14] Sachs, L. and Hedderich, J.; *Angewandte Statistik: Methodensammlung mit R*. Springer-Verlag 2006, 702p.
- [15] Kleinbaum, D. G.: *Survival Analysis: A Self-Learning Text. Statistics in the Health Sciences*, Springer-Verlag 1995, 324p.
- [16] R Development Core Team (2007). *R: A language and environment for statistical computing*. R Foundation for Statistical Computing, Vienna, Austria. ISBN 3-900051-07-0, URL: <http://www.R-project.org>.
- [17] McCullough, B. D.: *Fixing Statistical Errors in Spreadsheet Software: The Cases of Gnumeric and Excel*. 2004, (http://www.csdassn.org/software_reports/gnumeric.pdf)
- [18] Akaike, H.: A new look at the statistical model identification. *IEEE Transactions on Automatic Control*, 19 (6), 1974, pp. 716-723
- [19] S original by Therneau, T. and ported by Lumley, T.: *Survival analysis, including penalised likelihood*. R package version 2.32.
- [20] Sawyer, S.: *The Greenwood and Exponential Greenwood Confidence Intervals in Survival Analysis*. Handout, 2003. URL: www.math.wustl.edu/~sawyer/handouts/greenwood.pdf
- [21] Cohen, A. C.: *Tables for Maximum Likelihood Estimates: Singly Truncated and Singly Censored Samples*. *Journal:Technometrics*, Vol. 3, No. 4 (Nov., 1961), pp. 535-541
- [22] Smith, J. H.: *Some experiments on fatigue of metals*. *J. Iron Steel Inst.* 82 (1910), 2. p. 246-318
- [23] Schijve, J.: *Fatigue of Structures and Materials*. Kluwer Academic Publishers, New York 2004
- [24] Kaplan, E.L. & Meier, P. (1958). "Nonparametric estimation from incomplete observations". *Journal of the American Statistical Association* **53**: 457–481
- [25] Huang, Z.; Engström, B.; Magnusson, J.: *Experimental and analytical studies of the bond behaviour of deformed bars in high strength concrete*. Fourth International Symposium at the Utilization of High Strength/ High Performance Concrete, Vol. 3, Laboratoires des Ponts et Chaussées, Paris 1996

The interested reader may download illustrating datasets and R-scripts of the discussed analysis from:
URL: http://www.tu-dresden.de/biwitb/mbau/forschung/rissbreiten_stb.html
(The import lines must be altered to the final storage path of the datasets).

Use of reliability analysis in engineering practice – possible applications and examples

Thomas Braml, Manfred Keuser

Institute for Structural Engineering, University of the German Armed Forces, Munich, Germany

Abstract: The requirement for the reliability based assessment of structures in civil engineering has risen significantly in recent years. The basis for probabilistic analysis is carried out using the codes developed by the Joint Committee of Structural Safety (JCSS) [12]. The software tools have been developed in the last few years, for example [2, 17]. For existing structures the structural analysis does not provide a forecast in the way that the planning of new buildings does. With a probabilistic analysis like FORM/SORM the additional information of the existing structure can be considered more adequately than with the current semi-probabilistic safety concept. In individual cases, the additional use of a probabilistic analysis is very helpful as a complement to an engineer opinion on the basis of the current safety concept in the codes. Using these additional results the investigation program of the structure can be planned cost-efficiently and the material properties or the loads with the highest influence on reliability can be examined with monitoring systems, for example. The paper illustrates in two examples the extension of the assessment of existing structures with probabilistic methods. Currently, in engineering practice the probabilistic methods are only a supplement to the conventional calculation on the basis of the codes, because the methods are not recognised by the German government.

1 Introduction

Due to the increasing stock of older buildings, the assessment of such buildings in terms of structural safety affected by damage or by changes in usage is gaining importance. Generally, the static recalculation for such an existing structure is based on the current codes which have been developed for the design of new buildings. However, an analysis for an existing structure is not the same as for a new structure. For existing structures the structural analysis does not provide a forecast in the way that the planning of new buildings does, because essential information about the building, e.g. the material strength, is readily at hand and this information can be validated with the use of non-destructive methods and with monitoring systems. In Germany there are additional documents which allow such a modification of the partial safety factors for use in practice. In Table 1 there is a summary

of the current developments. At the moment these documents in Table 1 are not recognised by the German government. With the use of probabilistic methods there are great advantages for the assessment of an existing structure. For example, with a sensitivity analysis for the different limit states the influence of the basic variables of the resistance and of the loads can clearly be shown. The extent of the necessary investigations to be carried out on the existing structure can be chosen on the basis of the results of a sensitivity analysis. Focusing on the essential aspects leads to lower investigation costs.

2 Current safety concepts in the codes

2.1 Design of new buildings

The Eurocode: “Basis of Structural Design [8]” is the basis code for the application of the safety concepts for the design of new buildings in Europe. The Eurocode is based on the safety concept with partial safety factors. In appendices B and C the code gives information on how to perform an analysis with probabilistic methods. Every country in the EU has a National Annex to the various Eurocodes. In Germany it is the DIN 1055-100, Grundlagen der Tragwerksplanung, [6] for [8]. The DIN 1055-100 includes the principles of limit state design and the partial safety factors for building construction. The partial safety factors for other constructions and for different materials are regulated in every specific design code for the different materials. Appendix B of DIN 1055-100 is not established by the German government [15]. So for an analysis with the reliability index β , acceptance by the government is required in individual cases.

In Germany, the partial safety factors for loads and resistance for the design of new buildings are fixed. A reduction of the partial safety factor for the concrete resistance from 1.50 down to 1.35 [5] is only allowed for prefabricated structural elements.

2.2 Safety concepts for existing structures

In DIN 1055-100 [6], in the Eurocode [8] and in specific codes for different materials there are no regulations for modifying the partial safety factors in the case of existing structures for the semi-probabilistic safety concept. In Germany there are additional documents which allow such a modification of the partial safety factors for use in practice. In Table 1 there is a summary of the current developments. The values from DIN 1045-1 [5] (column 2) show the reference values without modification.

Table 1: Modified partial safety factors for existing structures (columns 3 to 5)

1	2	3	4	5
	DIN 1045-1 [5]	DAfStb Heft 467 [18]	Richtlinie Belastungsversuche an Massivbauwerken [3]	Betonkalender 2009 [9]
Dead load – general γ_G	1.35	1.35	1.35	1.35
Dead load – existing structure γ_G	1.35	1.15	1.15	1.35
Live Loads γ_Q	1.50	1.50	1.50	1.5
Concrete γ_C	1.50	1.40	1.40	1.20 – 1.50
Reinforcing steel γ_S	1.15	1.10	1.10	1.05 – 1.15

For the use of the modified partial safety factors you have to do precise investigations on the existing structure, e.g. establish the measurements of the concrete strength and steel yield strength. The details are shown in the codes. At the moment the documents in Table 2 [3], [9], [18] are not recognised by the German government. In individual cases you can use the regulations with permission from the government and the checking engineer for particular construction projects.

For a probabilistic analysis, the Joint Committee on Structural Safety (JCSS) has published the document "Assessment of existing structures" [13]. This document contains instructions for inspection techniques, for reliability updating such as the Bayes theory and for tentative target reliability indices β . The tentative target reliability β in [13] is differentiated to the relative cost of safety measures and to the consequences of failure. For a typical building the required reliability index β decreases by $\Delta\beta = 0.5$ for the assessment of an existing structure compared to the design of a new structure.

In [16] there is a recommendation for the adjustment of the reliability index β with regard to inspection performance, system behaviour and risk category. The target reliability for existing structures can decrease by $\Delta\beta = 0.25$ up to 0.5 compared to the design of new structures.

The safety concept with optimization reliability is currently extended to the Life Quality Index (LQI) which includes reliability-oriented optimal designs of technical facilities and structures. For existing structures there are at present no proposals.

3 Benefits of a probabilistic analysis for practical use

3.1 Overview of the probabilistic methods

The following Table 2 gives an overview of the various current safety concepts.

Table 2: Overview of the safety concepts

Safety concept	Level	Reliability dimension	General equation
Conventional deterministic	0	Central safety factor γ (R = Resistance, S = Stress)	$\gamma = R / S \geq \text{erf } \gamma$
Semi-probabilistic	1	Partial safety factors for Resistance R (γ_R) and for Stress S (γ_S)	$R / \gamma_R \leq \sum (\gamma_S * S)$
Probabilistic approximation	2	Reliability index β	existing β – required $\beta \geq 0$
Probabilistic accuracy	3	Probability of failure p_f	permissible p_f – exist. $p_f \geq 0$
Economic optimum	4	Permissible probability of failure p_f , Required reliability index β	Optimization reliability

The Level 0 method uses a conventional deterministic design equation with one central safety factor γ . The Level 1 safety concept uses different partial safety factors for the loads and for the resistance. The reliability index β will be calculated with probabilistic approximation methods such as the First Order Reliability Method (FORM) or the Second Order Reliability Method (SORM) at Level 2. In the Level 3 safety concept the probability of failure p_f will be calculated. The Level 4 concept uses the total expected cost of the design

as the optimization criterion. The acceptable design maximizes the utility function, which describes the difference between the benefits and costs associated with a particular design.

In practice, the current design codes are usually based on a Level 1 safety concept philosophy. However, the partial factors for the load and resistance factors are derived using Level 2 methods. At present, Level 3 and Level 4 methods are used mainly in advanced research or for the design of critical structures.

3.2 Sensitivity analysis

The α factors in a sensitivity analysis indicate the influence of the load and resistance variables on the reliability index. In the case of existing structures, they show clearly which characteristics of the load and resistance model should be taken into special consideration and are determined for the probability of failure. Figure 1 shows the influence of the basic variables on the reliability index for the limit state function of shear capacity without reinforcement for a reinforced concrete slab.

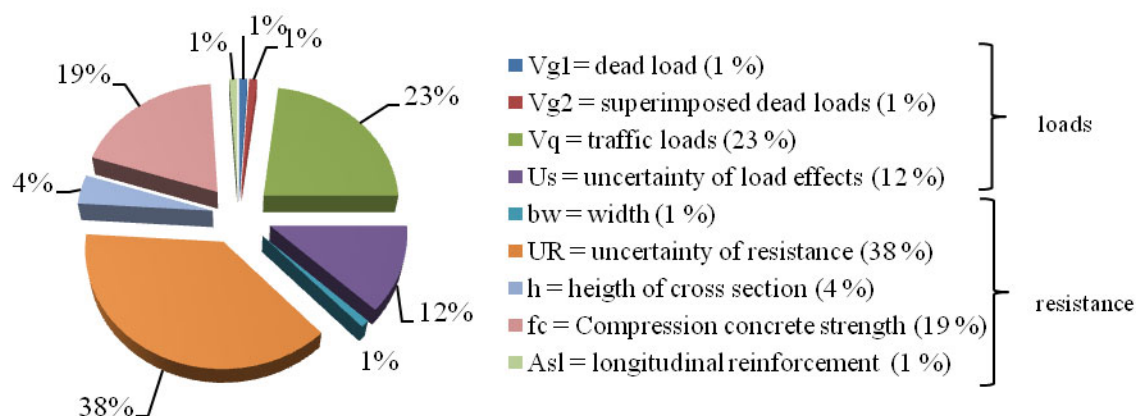


Fig. 1: Illustration of the percentage distribution of the sensitivity factors α^2

In such a case the investigation of the concrete compressive strength is important. The investigation program can be planned cost-efficiently when the priorities of the inspection are clear.

3.3 Use of monitoring data for the probabilistic analysis

If more information about a structure and its use is available, the uncertainty of the loads and of the resistance decreases. For a probabilistic analysis the coefficient of variation for the considered basic variables may become smaller. The influence of such a decrease on the reliability index β is significant. [20] shows statistical and probabilistic aspects associated with the determination of the required number of sensors for a monitoring system. For a practical application, the simple method with a decrease of the coefficient of variation on the basis of the monitoring data is advisable. The evaluation of the results of monitoring has to be carried out for use in the probabilistic analysis. For use in engineering practice with the current codes, the partial safety factors for a static calculation can be calculated

according to [19] from the modified reliability index β with the information from a monitoring system.

4 Examples for the practical use of probabilistic methods

4.1 One of the oldest flat slabs in Munich

A static recalculation was carried out on one of the oldest flat slabs in Munich. An extensive investigation was necessary [10] on account of some damage to the slab, for example corroded reinforcement, and some modification in the top floor. The investigation includes

- Measurement of the geometry and the dead loads from heater and roof
- Taking of drilling cores with determination of carbonation, chloride and compression concrete strength
- Measurement of the steel yield strength on samplings

Figure 2 shows the hall with the groundplan dimensions of 62 m x 30 m. The height of the columns is 8.80 m. The columns are separated by a distance of 6 m. Figure 3 shows the corroded reinforcement of the flat slab in the area of a column.



Fig. 2: View of the hall and the flat slab



Fig 3.: Corroded reinforcement in the area of a column

Several drilling scores were taken from the flat slab, Figures 4 and 5. The evaluation was carried out according to the code DIN EN 13791 [4]. With the results of the laboratory tests and according to table 1 of [4], the compressive concrete strength is C20/25. As we expected, there is no influence of chloride in the flat slab. The corrosion of the reinforcement results from carbonation of the concrete.



Fig. 4: Drilling score taken from the flab slab



Fig.5: Point of withdrawal

A linear and nonlinear finite element analysis was carried out [11] using the results of the investigations [10]. The chosen safety concept was the semi-probabilistic safety concept with the modified partial factors for existing structures as shown in table 1. The relevant areas of the slab are the corroded reinforcement above the supports and the punching shear reinforcement. To compare the results from the finite element analysis a probabilistic analysis for the bending moment capacity and the punching shear was additionally done.

The limit state function for punching shear without shear reinforcement can be written according to [5] as:

$$g(v_{R,ct}) = U_{R,ct} * \left[\frac{0,2965 * \left(1 + \sqrt{\frac{200}{d * 1000}} \right) * \eta_1 * \left(100 * \sqrt{\frac{A_{stx}}{b_x * d} * \frac{A_{sty}}{b_y * d} * f_c} \right)^{0,5}}{*(v_g + v_A + v_Q + v_S)} \right] * (h - d_1) - \quad (1)$$

The terms in (1) are shown in table 3. The factor 0,2965 has been calculated from the factor of [5] with the partial safety factor for the concrete of $\gamma_c = 1,5$: $\frac{0,21}{\gamma_c} = \frac{0,21}{1,5} = 0,14$ (design value). The mean value is then calculated with an LN – distribution and a coefficient of variation with 5 % to 0,2965.

Tab. 3: Statistical properties of basic variables for punching shear of the flat slab (1)

Basic variables	Name of basic variables	Symbol	Distribution type	Dimension	Mean	Standard deviation	
Material properties	Compression concrete strength factor	f_c	LN	MN/m ²	33	4.95	
		η	Det.	-	1	-	
Geometric data	Height of cross-section	h	N	m	0.157	0.00785	
	Distance of bars to the slab bottom	d_1	N	m	0.035	0.00035	
	Distance of bars to the slab top side	d	N	m	0.122	0.00366	
	Reinforcement in x-direction	A_{slx}	N	m ²	0.00098	$1.098 \cdot 10^{-5}$	
	Reinforcement in y – direction	A_{sly}	N	m ²	0.00106	$2.12 \cdot 10^{-5}$	
Model uncertainty	Uncertainty of resistance	$U_{R,et}$	LN	-	1.0	0.25	
	Uncertainty of load effect	U_E	LN	-	1	0.2	
Actions	Dead load	v_{G1}	N	MN/m	0.0372	0.00148	
	Superimposed dead loads	v_{G2}	N	MN/m	0.0054	0.00022	
	Live loads	v_Q	GUMBEL	MN/m	0.00378	0.00095	
	Snow loads		v_s	GUMBEL	MN/m	0.00462	0.00231

The following table shows a comparison of the results of the finite element analysis with the probabilistic analysis for punching shear and for the additional analysis with the ultimate bending moment. The probabilistic analysis has been carried out with [17].

Table 4: Comparison of different safety concepts

Safety concept	Ultimate limit state	Occupancy rate	Reliability index β / probability of failure p_F
Semi-probabilistic with modified partial factors (according to column 3 in table 1)	Bending moment	103 %	-
	Punching shear	87 %	-
Probabilistic FORM result	Bending moment	-	$\beta = 4.616 / p_F = 1.95 \cdot 10^{-6}$
	Punching shear	-	$\beta = 5.385 / p_F = 3.64 \cdot 10^{-8}$

The results from an analysis with the safety concept from the codes can be compared with an additional probabilistic analysis. Furthermore, a sensitivity analysis shows the influence of the basic variables from table 3 to the reliability index β . In special cases more investi-

gations for the decisive material properties or the loads of the existing structure can be carried out and the coefficient of variation can decrease.

4.2 Evaluating existing post-tensioned concrete bridges

For some of the post-tensioned concrete bridges in Germany tension wires are used with high susceptibility to stress corrosion cracking as we know nowadays (steel types St 145/160 Neptun N40, St 145/160 Sigma Oval “first generation”, St 145/160 Sigma Oval “new generation” and St 145/160 from steelworks Hennigsdorf in former East Germany).

Due to this high corrosion susceptibility, the structures are characterized by fracture behavior determined by sudden collapse rather than giving any preannouncement of failure. Special evaluation is necessary in order to be able to use these bridges in the future with a minimized risk of sudden collapse. In the 1990ies, recommendations on how to handle these bridges were therefore worked out by König et al [1, 14].

The basic idea of the recommended approach is the consideration of the gradual failure of tendons. The question is whether or not any cross-section of the girder would be able to bear the unusual load combination after tendon failures lead to cracking as a result of bending. In this case the damage can be noticed before the structure fails, and the bridge displays pre-announcing behaviour (“crack-before-collapse-criterion”).

In addition to the static calculation according to [1, 14], a probabilistic analysis has been done to illustrate the influence of the material properties and the loads on the ultimate limit state. The investigation program has been modified on the basis of these results

The representative bridge is a 3-span multi-girder bridge built in 1967. It was built in one construction stage without coupling joints. The longitudinal section consists of three spans of 37 m, 46 m and 37 m (Figure 1).

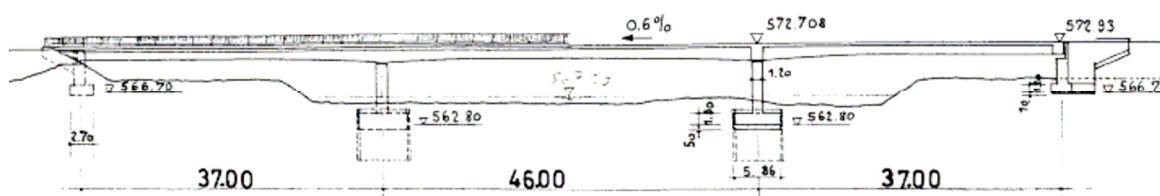


Fig. 6: Longitudinal section of representative bridge

The width between the handrails measures 10 m, which allows two-lane traffic of 3,5 m width for each lane and additionally a pavement on each side of the bridge. The cross-section is a double-webbed T-beam with a variable constructional height of 1,43 m to 2,0 m for the end spans and of 2,0 m to 1,53 m () for the mid span (Figure 2). The bridge had originally been designed for load class 60 (60t vehicle) according to DIN 1072 (edition of 1967 [7]).

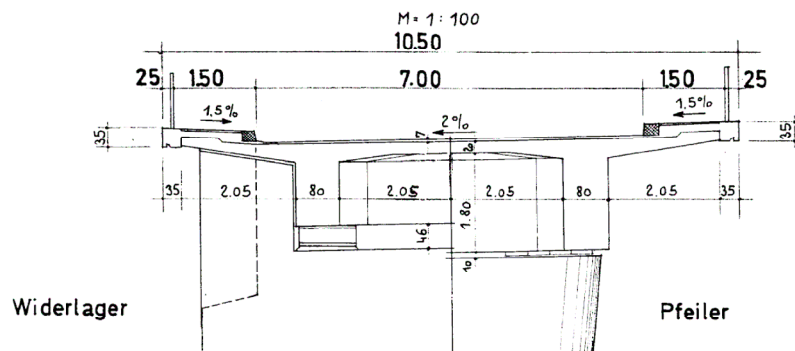


Fig. 7: Cross-section at abutment station (left) and at pier station (right)

The calculation of the probability of failure p_f and of the reliability index β was made by use of STRUREL software [17]. The results for the ultimate limit state with the remaining sectional areas of prestressing steel confirm the findings from the analysis according to [1, 14]. In addition, the calculation yields sensitivity factors α for all random variables x_i of the loads and the resistance of the system. Figure 3 shows the influence of the variables. On the load side it is the traffic and on the resistance side it is the cross-section of the tendons and the yield strength of the prestressing steel. For the assessment of the bridge the change in these two values has the most influence on the reliability and bearing capacity. These results confirm the approach in the recommendation [1, 14].

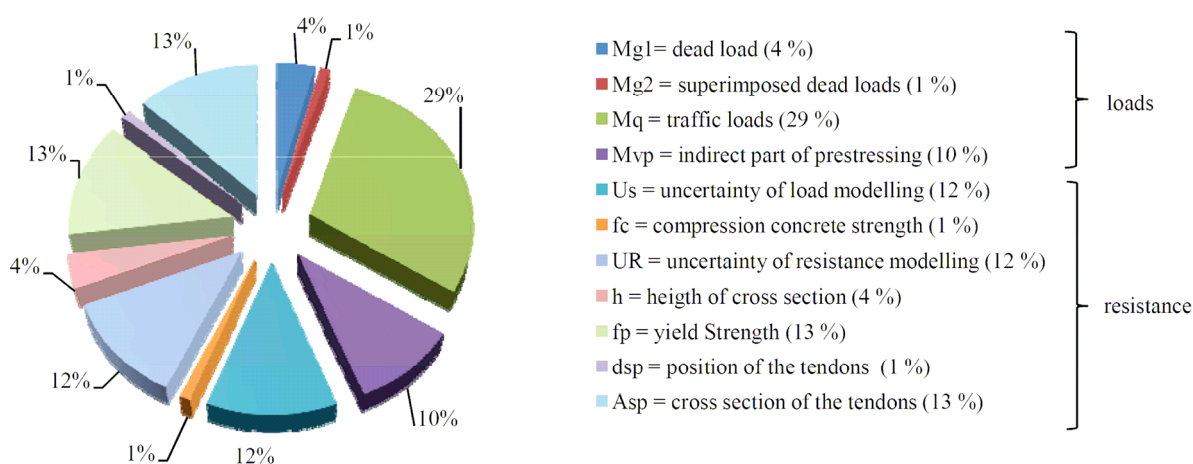


Fig. 8: Illustration of the percentage distribution of the sensitivity factors α^2 to show the influence of the individual basic variables for the reliability index

5 Conclusion

With the combination of the semi-probabilistic safety concept from the current codes and the full probabilistic methods, the assessment of structures can be done very well. Especially for expert reports in individual cases, the investigation program can be planned target-oriented and cost-efficiently. If more information from a structure is available, there is less uncertainty concerning loads and resistance. For a probabilistic analysis the coefficient

of variation for the considered basic variables may become smaller. The two examples have illustrated this in the assessment of one of the oldest flat slabs in Munich and in the evaluation of a post-tensioned concrete bridge.

Literature

- [1] Bundesminister für Verkehr, Abteilung Straßenbau: „Empfehlungen zur Überprüfung und Beurteilung von Brückenbauwerken, die mit vergütetem Spannstahl St 145/160 Neptun N40 bis 1965 erstellt wurden“, July 1993
- [2] Code Calibration Program, March 2003. Faber, M. H., Kübler, O., Köhler J., Swiss Federal Institute of Technology, Institute of Structural Engineering, Group on Risk and Safety, Zürich
- [3] Deutscher Ausschuss für Stahlbeton: Richtlinie Belastungsversuche an Massivbauwerken, Ausgabe September 2000
- [4] DIN EN 13791, Bewertung der Druckfestigkeit von Beton in Bauwerken oder in Bauwerksteilen, CEN 2007
- [5] DIN 1045-1, Ausgabe August 2008, Tragwerke aus Beton, Stahlbeton und Spannbeton – Teil 1: Bemessung und Konstruktion
- [6] DIN 1055-100, Ausgabe März 2001, Einwirkungen auf Tragwerke, Teil 100: Grundlagen der Tragwerksplanung, Sicherheitskonzept und Bemessungsregeln
- [7] DIN 1072: „Straßen- und Wegbrücken – Lastannahmen“, German Code, 1967 edition, Beuth Verlag, Berlin, Germany, 1967
- [8] EN 1990: Eurocode – Basis of structural design, 2002
- [9] Fingerloos, F., Schnell, J.: Tragwerksplanung im Bestand, Betonkalender 2009, Teil 2, S. 2 – 51, Ernst & Sohn Verlag, Berlin 2009
- [10] Gutachterliche Stellungnahme, Teil 1, Bauzustandsanalyse
- [11] Gutachterliche Stellungnahme, Teil 2, Statische Untersuchung
- [12] Joint Committee on Structural Safety (JCSS): Probabilistic Model Code 12th draft. <http://www.jcss.ethz.ch>, 17.05.2002
- [13] Joint Committee on Structural Safety (JCSS), Probabilistic Assessment of Existing Structures, RILEM Publications S.A.R.L, January 2001
- [14] KÖNIG, G.; TUE, N. and POMMERENING, D.: “Schadensablauf bei Korrosion der Spannbewehrung”, Deutscher Ausschuss für Stahlbeton (DAfStb), Issue 469, Beuth Verlag, Berlin, Germany, 1996
- [15] Liste der als Technische Baubestimmungen eingeführten technischen Regeln, Vollzug des Art. 3 Abs. 2 Satz 1 der Bayerischen Bauordnung (BayBO); Bekanntmachung des Bayerischen Staatsministeriums des Innern vom 28. November 2008 Az.: IIB9-4132-014/91
- [16] Melchers, R. E.: Structural reliability and prediction. John Wiley & Sons Ltd., Chichester, Australien 1999

- [17] Reliability Consulting Programs (RCP) 2004. STRUREL, a Structural Reliability Analysis Program-System, COMREL & SYSREL: Users Manual. Munich: RCP Consult
- [18] Schäfer, H. G., u. a: Verstärken von Betonbauteilen, Sachstandsbericht; Deutscher Ausschuss für Stahlbeton, Heft 467. Berlin, Köln: Beuth, 1996
- [19] Spaethe, G.: Die Sicherheit tragender Baukonstruktionen . Springer – Verlag, Berlin 1992
- [20] Strauss, A. , Frangopol, Dan M.; Sunyong, K.: Structural Monitoring under Uncertainty, 6.th. International Probabilistic Workshop, Technische Universität Darmstadt, Darmstadt, November 2008

Combined production and conformity control of concrete with acceptance cusum control charts

Robby Caspeele, Luc Taerwe
Magnet Laboratory for Concrete Research
Faculty of Engineering, Department of Structural Engineering
Ghent University, Belgium

Abstract: Production and conformity control are most often used as separate tools in the quality control process of concrete production. However, both methods can be combined in a way so that conformity control is used as a steering element for the production process. This paper describes a methodology for the design of appropriate V-masks for cusum control charts in case of a combined production and conformity control, satisfying multiple criteria such as the average run length (ARL) and the average outgoing quality limit (AOQL). Monte Carlo simulations are used in order to calculate operating characteristic curves (OC-curves) associated with different cusum charts. The influence of autocorrelation between test results is investigated and discussed. As a result, proper design guidelines for a combined production and conformity control of concrete are presented.

1 Introduction

The ultimate objective of concrete production is to make concrete which complies with the specifications and to do this in an cost-effective way. After an initial test period, a uniform level of performance is aimed for. In order to control the production process, control charts can be used to detect significant changes in performance. This production control allows a continuous monitoring of the production process and thus enables producers to make fast adjustments towards the mixing proportions or the constituent materials, in order to meet the specifications or to reduce the material cost of the concrete.

Conformity control, on the other hand, has another objective. It is used in order to assess whether the produced concrete lots obtain a characteristic strength which is conform the specified concrete class. However, this quality inspection is rarely monitored in a continuous way and thus does not allow to make adequate adjustments of the process.

In practice, both methods are used separately or complementary, but without coherency regarding the decision making. Each method has certain advantages and limitations for inspecting the quality of the production. However, both methods can be combined in an efficient way, so that the conformity control is used as a steering element in the production process of concrete.

2 Production control based on cusum control charts

2.1 Principle

A cumulative sum control chart (cusum) is well adapted to detect abrupt jumps in the process level which persist for some time [1]. Concrete production is indeed subjected to such jumps [2], which justifies the use of cusum control charts for the production control of concrete. Generally, cusum charts have 3 major advantages in comparison to standard control charts [3]:

1. Changes in mean level can be easily detected visually by a change in slope of the chart.
2. The point at which the change in slope appears, can be located easily, which is very useful in helping to discover the cause of the change.
3. The improved efficiency – in comparison to standard control charts – for changes between 0.5σ and 2σ . This means that, in this region, changes can be detected approximately twice as quickly or, if preferred, can be detected in the same period of time, but with much smaller sample sizes.

GIBRA provides a historical overview of the developments in cusum control charts in [4], which was supplemented by WOODALL with more recent developments in [5]. Guidelines for practical applications can be found in the standards ISO/TR 7871 [6], BS 5703-2 [7] and BS 5703-3 [8]. In order to clarify this control chart procedure, the basic principles are outlined in the following.

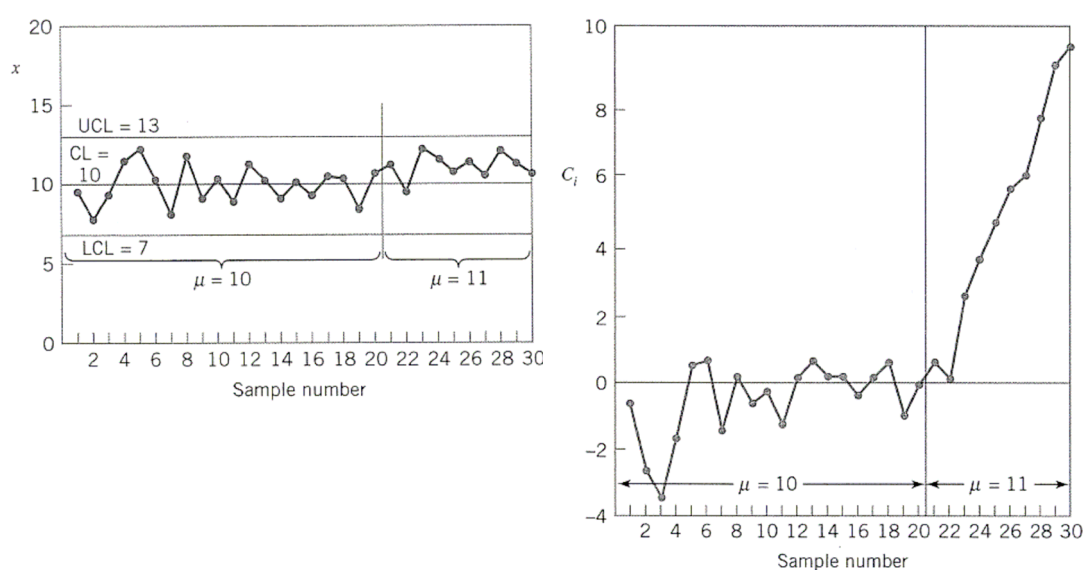
For a set of observations x_j , a cusum chart plots the cumulative deviations from a specified target value μ_0 against the sequence of results i , thus yielding [9]:

$$C(i) = \sum_{j=1}^i (x_j - \mu_0) \quad (1)$$

In most cases a normalized cusum is used, where the value of the standard deviation σ is assumed to be known from past experience or estimated from about 20 sample sets [10]

Consider, as an example, the observations plotted in Figure 1. The graph in Fig. 1 (a) illustrates a standard (Shewhart) control chart, based on 20 random observations of a normal distribution with mean 10 and variance 1, followed by 10 observations of a normal distribution with mean 11 and the same variance. As can be seen, the graph does not provide

graphical evidence for detecting an out-of-control warning. The graph in Fig. 1 (b), however, plots the same observations in a cusum chart. Here, the change in mean is clearly visible.



(a) Example of a Shewhart control chart (b) Example of a CUSUM control chart

Fig. 1: Graphical representation of simulated random observations in control charts [11]

However, a visual inspection is unsatisfactory for most applications. An appropriate decision criterion is necessary, which can be based on a V-mask procedure.

2.2 Decision making based on V-masks

A V-mask consists of a V-shaped decision boundary with the vertex pointing horizontally forward (cf. Fig. 2). A V-mask is characterized by 2 parameters, namely the distance d ahead of the most recently added point O in the graph and the angle θ between the obliques and the horizontal. A lack of process control is indicated when a previously plotted point falls outside the limbs of the V-mask. The graph is recommenced or an appropriate correction is made when the process mean is reset after an out-of-control warning [12]. An illustration of such a V-mask is given in Figure 2.

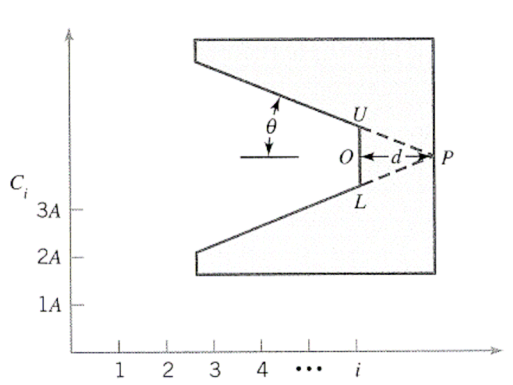


Fig. 2: Illustration of a typical V-mask [10]

The parameters d and θ can be translated to the parameters k and h of a tabular cusum according to the following transformation rules [11, 13]:

$$\begin{cases} k = A \tan \theta \\ h = Ad \tan \theta = dk \end{cases} \quad (2)$$

with A the horizontal distance on the V-mask plot between successive points in terms of a unit distance on the vertical scale.

Several techniques are available in literature in order to make an appropriate choice for these parameters, mostly based on the average run length (ARL), which is the number of samples that are required – on average – to yield the first out-of-control warning. These methods can be categorised by the requirements that are specified:

- The parameters k and h of a cusum chart can be selected to yield approximately a specified value ARL_0 and ARL_1 at the acceptable quality level μ_0 and rejectable quality level μ_1 respectively [3,14]. ARL_0 is typically called the in-control ARL.
- The parameter k is depending only on the shift δ that one wants to detect (i.e. $k = \delta/2$, with δ in terms of σ). The parameter h is then chosen based on the required in-control ARL_0 , according to the graphs provided by GOLDSMITH & WHITFIELD [12], the more accurate graphs from LUCAS [15] or the nomograms from GAN [16].
- The parameters d and θ can be selected directly by specifying the in-control and out-of-control probabilities, using JOHNSON's formula [11]. However, this method does not seem to be very accurate [11].

As a general guideline, the choice of $h = 5.0$ and $k = 0.5$ seems to yield very good properties for a cusum chart [3], which is also suggested as a standard choice in the standards ISO/TR 7871 [6] and BS 5703-2 [7].

When one wants to use the ARL of a cusum as a basis for the parameter selection, different techniques are available to calculate this ARL. A computer program is provided by VANCE [14]. GOLDSMITH & WITHFIELD [12], LUCAS [15] and GAN [16] provide graphs for reading of the ARL at different δ . Finally, WOODALL & ADAMS recommend the ARL approximation given by SIEGMUND because of its simplicity. For a one-sided cusum with parameters h and k , SIEGMUND's approximation yields [11]:

$$ARL = \frac{\exp(-2\Delta b) + 2\Delta b - 1}{2\Delta^2}, \Delta \neq 0 \quad (3)$$

with $\Delta = \delta - k$ for the upper one-sided cusum and $\Delta = -\delta - k$ for the lower one-sided cusum, $b = h + 1.166$ and $\delta = (\mu_1 - \mu_0)/\sigma$. For $\Delta = 0$ one can use $ARL = b^2$. Finally, for calculating the ARL of a two-sided cusum, based on the ARL^+ for the upper one-sided cusum and the ARL^- for the lower one-sided cusum, the following relation can be used [3,11,13]:

$$\frac{1}{ARL} = \frac{1}{ARL^+} + \frac{1}{ARL^-} \quad (4)$$

3 Using cusum charts for acceptance control

3.1 Combining production and conformity control

In 1957, FREUND already presented a technique to combine the use of a Shewhart control chart with the principles of acceptance sampling [4]. This is known as the acceptance control chart [10]. When a value falls outside the acceptance control limit, the process is rejected and the operator must then take whatever actions are specified [10] in order to make sure that the produced quality attains the specified quality. Practical guidelines regarding such acceptance Shewhart control charts are provided in ISO 7966 [17].

However, as mentioned in section 2.1, cusum charts are a more appropriate choice in case of concrete. Moreover, the design of the acceptance charts is based on a traditional approach for parameter selection based on an acceptable quality level (AQL) and limiting quality (LQ). Currently, the design of conformity control is commonly based on the average outgoing quality limit principle (AOQL) – originally proposed by GOVINDARAJU [18]. This method was also used in order to derive the current conformity criteria in the European Standard EN 206-1 [19], based on the work done by TAERWE [2,20].

Similarly to the investigation of conformity criteria, acceptance control charts can be analyzed by calculating their operating characteristic curves (OC-curves). These curves give the probability of acceptance P_a in function of the fraction defectives θ , which is the fraction of the realized (but unknown) concrete strength distribution lower than the specified characteristic strength f_{ck} ($\theta = P[X \leq f_{ck}]$) [5]. Thus, OC-curves represent the ability to distinguish “good” from “bad” production, through the quantification of producers and consumers risks [19]. In case of control charts, no analytical expressions are available for the associated OC-curves, but these can easily be calculated using Monte Carlo simulations.

A fairly objective method for the evaluation of these OC-curves is provided by the average outgoing quality limit concept (AOQL) [17,19]. The AOQL is the worst average quality of the outgoing (or accepted) concrete, in terms of fraction defectives. If θ is the incoming quality, then the average outgoing quality AOQ is given by the function $P_a \theta$ [2,17,19]. The AOQL is the maximum of this AOQ function and thus the highest (or worst) expected value of the outgoing quality. Based on the definition of the specified characteristic strength, the AOQL is set to 5%. This leads to a boundary curve $AOQL = (\theta P_a)_{max} = 5\%$ for the OC-curves of decision criteria and enables to make a parameter selection. The current conformity criteria for concrete strength in the European Standard EN 206-1 [19] are also based on this parameter selection criterion.

A cusum chart for acceptance control is characterized by 4 variables, namely the parameters of the V-mask k and h (or d and θ), the number of samples n over which the V-mask

is evaluated as a conformity criterion and the target value μ_0 . The target value can also be rewritten as:

$$\mu_0 = f_{ck} + \lambda\sigma \quad (5)$$

yielding λ as an alternative expression of the 4th parameter of an acceptance cusum control chart (independent of the specified f_{ck}).

In case of concrete conformity control, only specifications are given regarding a minimal concrete strength (see [19]). As a result of this, a proper decision rule for an acceptance cusum control chart is the following:

- When a point of the cusum chart crosses the lower limb of a specified V-mask, corrective actions are suggested – although not mandatory – in order to retain an economic concrete design.
- When a point of the cusum chart crosses the upper limb of a specified V-mask, the investigated samples are regarded as not conform and corrective actions are mandatory.

Based on this decision rule, only the upper limb of the cusum, has to be taken into account when calculating corresponding OC-curves.

Values for the parameters k and h (or d and θ) can be derived based on the principles outlined in section 2.2, mostly based on ARL requirements. As mentioned is the same section, a cusum chart with $h = 5$ and $k = 0.5$ seems to behave well for production control [3,6,7]. Apparently, in the UK a cusum chart with parameters $h = 8.1$ and $k = 1/6$ is commonly used for production control of concrete. Based on (3), the ARL for a shift of 1σ from the target value is approximately 9 for a one-sided control chart and the in-control ARL approximately 321. In comparison to these values, a standard (one-sided) cusum chart with $h = 5$ and $k = 0.5$ has an ARL for detecting a shift of 1σ from the target value of about 10 and an in-control ARL of approximately 938.

The value n has to be decided upon the frequency of concrete testing. When the test rate is sufficiently high (providing more than 35 test results in a limited time period of f.e. less than 2 months), a value of $n = 35$ is suggested in order to achieve a low probability of rejecting the concrete lot. For a low test rate, a value of $n = 15$ is suggested, based on the comparable conformity control suggested in EN 206-1 [19]. A much larger value is not advisable, due to the fundamental objective of conformity control to check whether a plant at certain regular time intervals produces concrete which complies with the specifications.

Finally, the values for the parameter λ , defining a minimal target value so that the requirements for conformity control (in terms of AOQL) are achieved, are given in the following.

3.2 Influence of the target value on the AOQ

The influence of the specified target value (or more specifically the λ value) on the AOQ is investigated through Monte Carlo simulations in case of the standard choice of $h = 5.0$ and $k = 0.5$ (as mentioned in sections 2.2 and 3.1). 100000 sets of n independent observations from a standard normal distribution are generated and transformed according to different values for the fraction defectives θ . The cusum chart for these observations is calculated and the probability of acceptance is determined according to the V-mask under consideration. This way, the OC-curve of a certain cusum chart can be calculated.

For the standard V-mask with $h = 5.0$ and $k = 0.5$, Figure 3 illustrates the OC-curves associated to λ values 1.645, 2.0 and 2.5 for $n = 15$ and $n = 35$ observations respectively. The associated AOQ-curves are depicted in Figure 4. From these graphs it can be seen that an increase of the target value (or λ value) corresponds to a shift of the OC-curve towards lower fraction defectives and decreases the AOQL. An increase of the number of samples n , which is taken into account for the conformity assessment, corresponds to an increase of the slope of the OC-curve and also decreases the AOQL. Finally, both an increase of n or λ leads to a shift of the AOQ-curve towards lower fraction defectives.

3.3 Influence of autocorrelation

Most concrete strength records reveal a significant autocorrelation between consecutive test results [21]. This autocorrelation can be modelled using an autoregressive process of order 2 with parameters derived in [2,21,22] based on the analysis of extensive concrete strength records from Belgian ready-mixed concrete plants. In the framework of Monte Carlo simulations, this AR(2) model is implemented using Equation (6) for the calculation of consecutive random realizations of a standard normal distribution.

$$u_k = 0.4 \cdot u_{k-1} + 0.2 \cdot u_{k-2} + \varepsilon_k \quad (6)$$

with u_k the k^{th} autocorrelated standard normally distributed number
 ε_k a normally distributed random number with mean 0 and variance 0.8.

The OC and AOQ-curves associated to the cusum charts analysed in §3.2 are depicted in Figures 5 and 6 respectively in case of autocorrelated observations. In comparison with the simulations for independent observations, the OC-curves show a smaller slope, the AOQL is lower and the AOQ-curves are slightly shifted to the higher fraction defectives.

An analysis of the influence of autocorrelation on the ARL associated with different cusum control charts is available in [12,23,24], in case of first order autoregressive processes. Generally, it is found that autocorrelation decreases the average run length, which is also expected based on the mentioned results regarding the OC-curves.

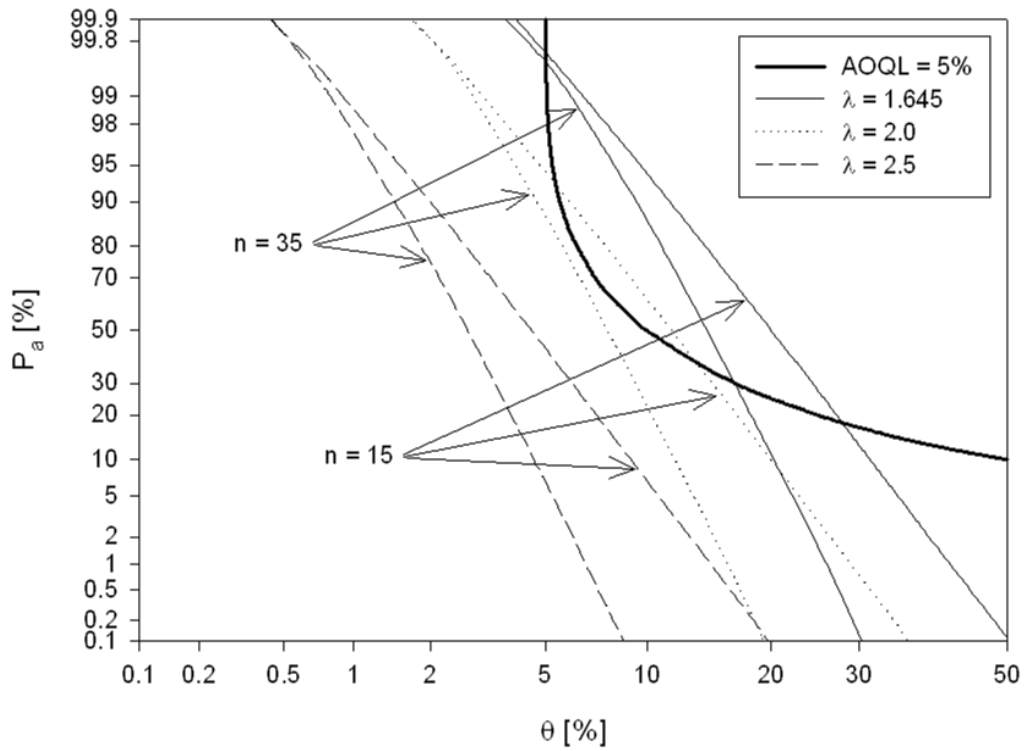


Fig. 3: OC-curves associated to acceptance cusum control charts with parameters $h = 5.0$ and $k = 0.5$ for different λ values (independent observations)

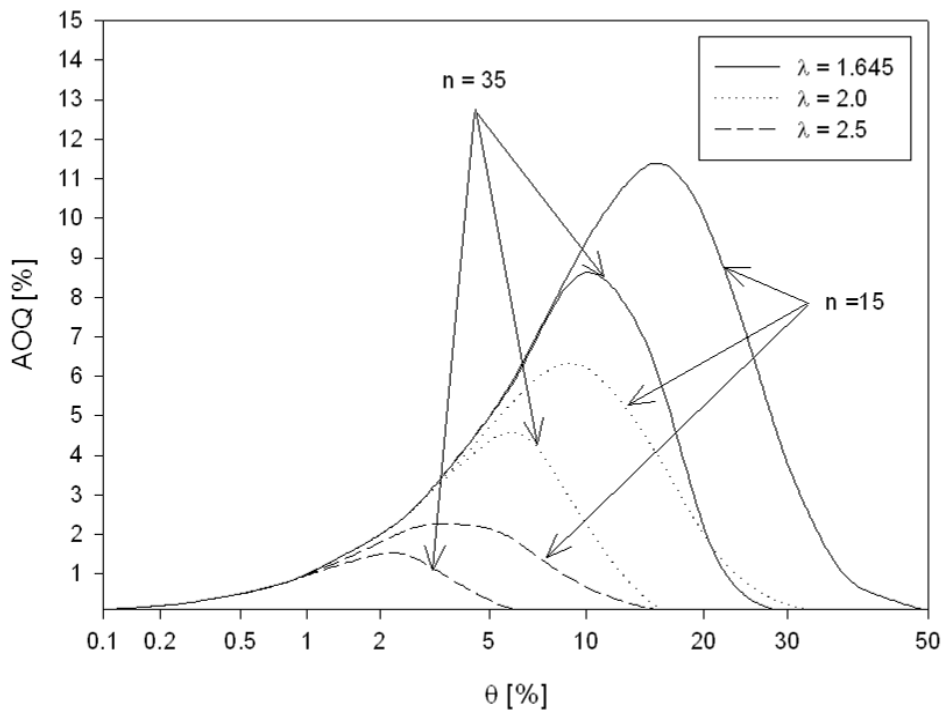


Fig. 4: AOQ-curves associated to acceptance cusum control charts with parameters $h = 5.0$ and $k = 0.5$ for different λ values (independent observations)

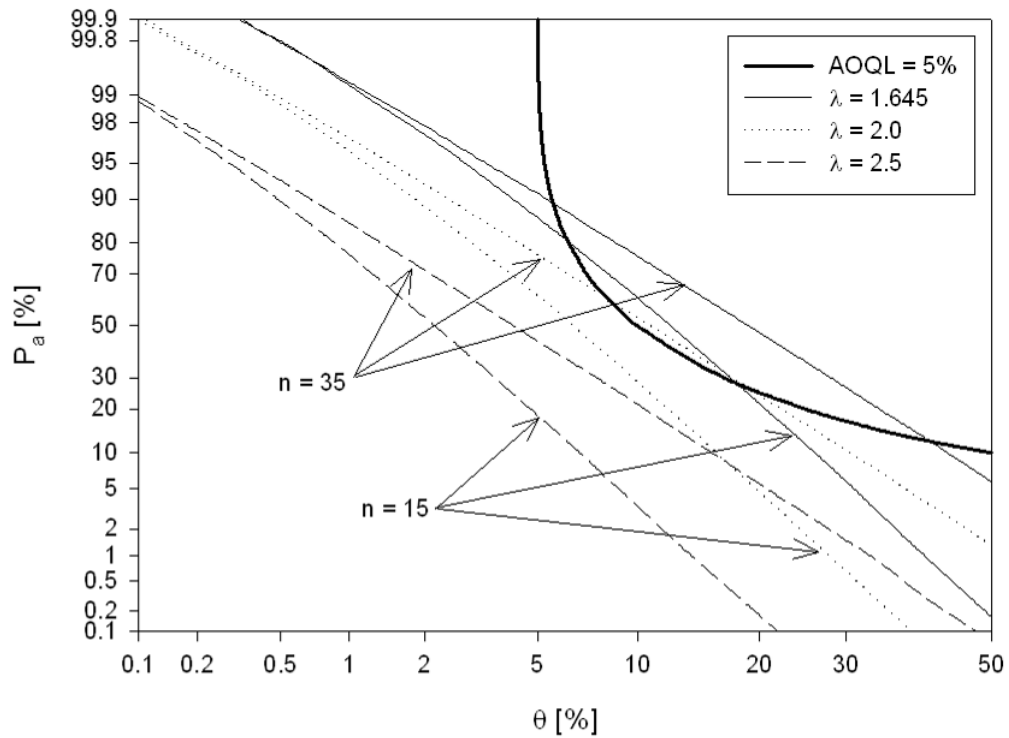


Fig. 5: OC-curves associated to acceptance cusum control charts with parameters $h = 5.0$ and $k = 0.5$ for different λ values (autocorrelated observations)

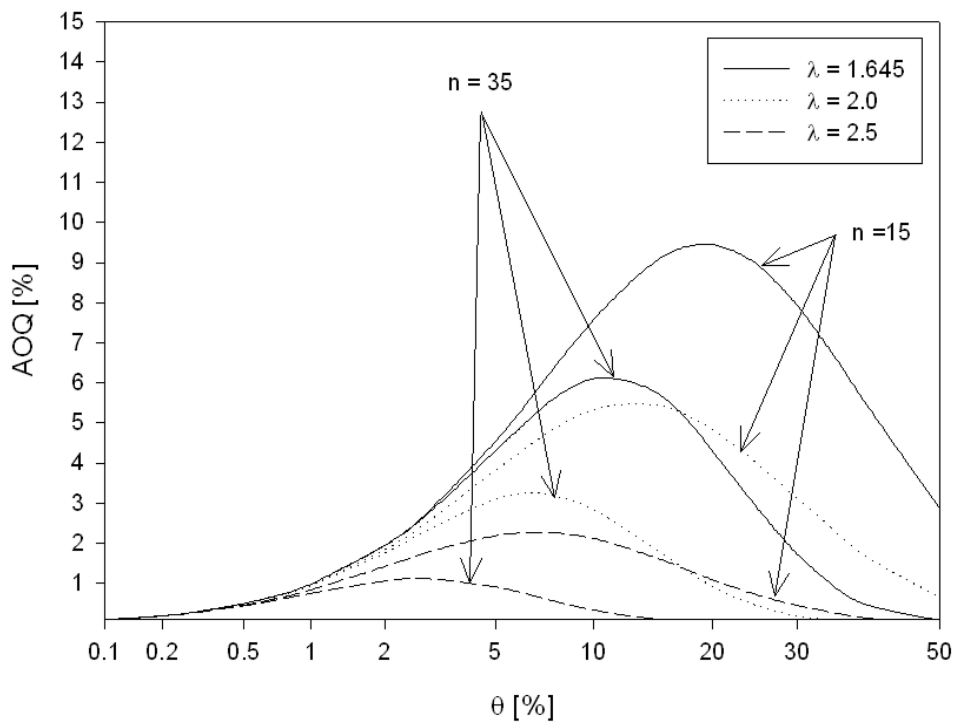


Fig. 6: AOQ-curves associated to acceptance cusum control charts with parameters $h = 5.0$ and $k = 0.5$ for different λ values (autocorrelated observations)

3.4 Guidelines on the choice of target values

Based on the same methodology as described in sections 3.2 and 3.3, the required λ values can be calculated in order to obtain an AOQL of 5%. Table 1 provides such λ values for independent and autocorrelated observations as well as for $n = 15$ and $n = 35$.

The OC and AOQ-curves associated to an acceptance control chart with parameters $h = 5.0$, $k = 0.5$ and target values according to Table 1 are depicted in Figures 7 and 8. The same conclusions as drawn in sections 3.2 and 3.3 can be repeated here. Note that the AOQL = 5%, as was required. Finally, also the probability of acceptance (or the probability of rejectance) associated to an in-control or out-of-control production can be obtained from Fig. 7.

Tab. 1: Values for λ corresponding to an AOQL = 5%

		Independent observations		Autocorrelated observations	
		n = 15	n = 35	n = 15	n = 35
k = 1.00	h = 1	2.12	2.08	2.08	1.94
	h = 2	2.30	2.25	2.23	2.06
	h = 3	2.43	2.33	2.35	2.14
	h = 4	2.53	2.40	2.45	2.21
	h = 5	2.62	2.45	2.55	2.26
	h = 6	2.71	2.49	2.64	2.32
	h = 7	2.79	2.53	2.72	2.36
	h = 8	2.87	2.57	2.80	2.41
	h = 9	2.94	2.60	2.89	2.45
	h = 10	3.02	2.64	2.96	2.49
k = 0.50	h = 1	1.63	1.59	1.58	1.44
	h = 2	1.80	1.75	1.73	1.56
	h = 3	1.93	1.83	1.85	1.64
	h = 4	2.03	1.90	1.95	1.71
	h = 5	2.12	1.95	2.05	1.76
	h = 6	2.21	1.99	2.14	1.82
	h = 7	2.29	2.03	2.22	1.86
	h = 8	2.37	2.07	2.31	1.91
	h = 9	2.44	2.10	2.39	1.95
	h = 10	2.52	2.14	2.47	1.99
k = 0.25	h = 1	1.38	1.33	1.33	1.19
	h = 2	1.55	1.50	1.48	1.31
	h = 3	1.68	1.58	1.60	1.39
	h = 4	1.78	1.65	1.70	1.46
	h = 5	1.87	1.70	1.80	1.51
	h = 6	1.96	1.74	1.89	1.57
	h = 7	2.04	1.78	1.98	1.61
	h = 8	2.12	1.82	2.06	1.66
	h = 9	2.19	1.85	2.14	1.70
	h = 10	2.27	1.89	2.22	1.74

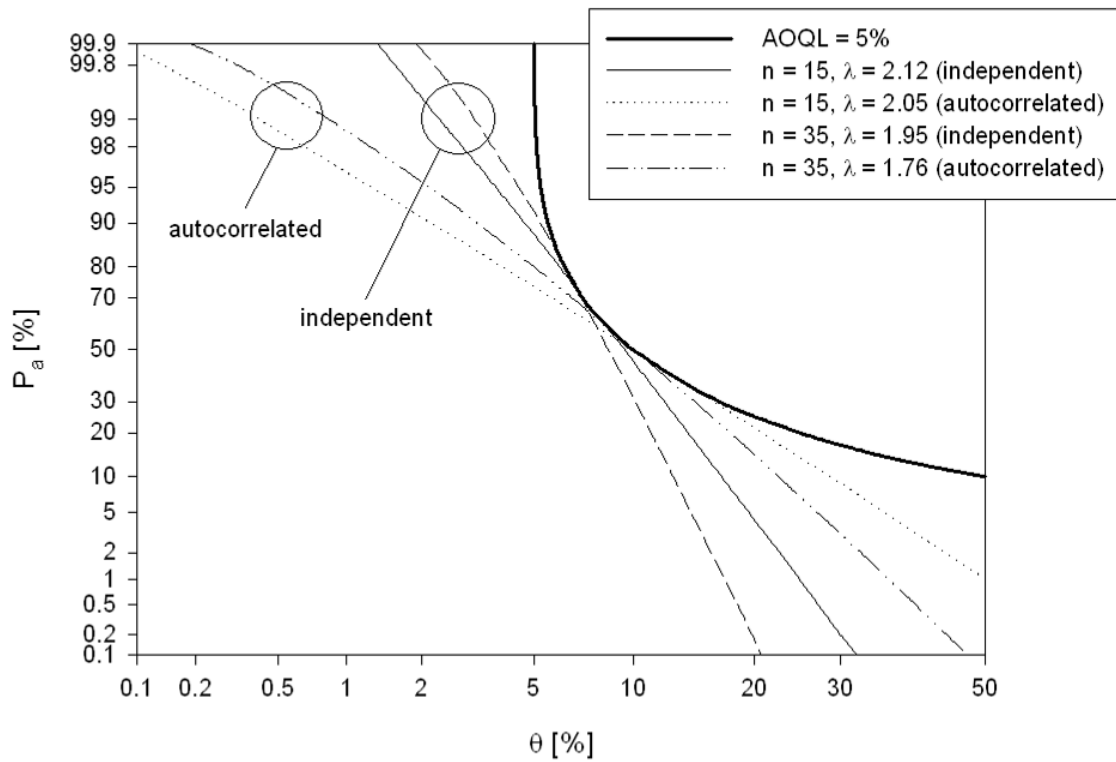


Fig. 7: OC-curves associated to acceptance cusum control charts with parameters $h = 5.0$ and $k = 0.5$, optimized with respect to an AOQL = 5%

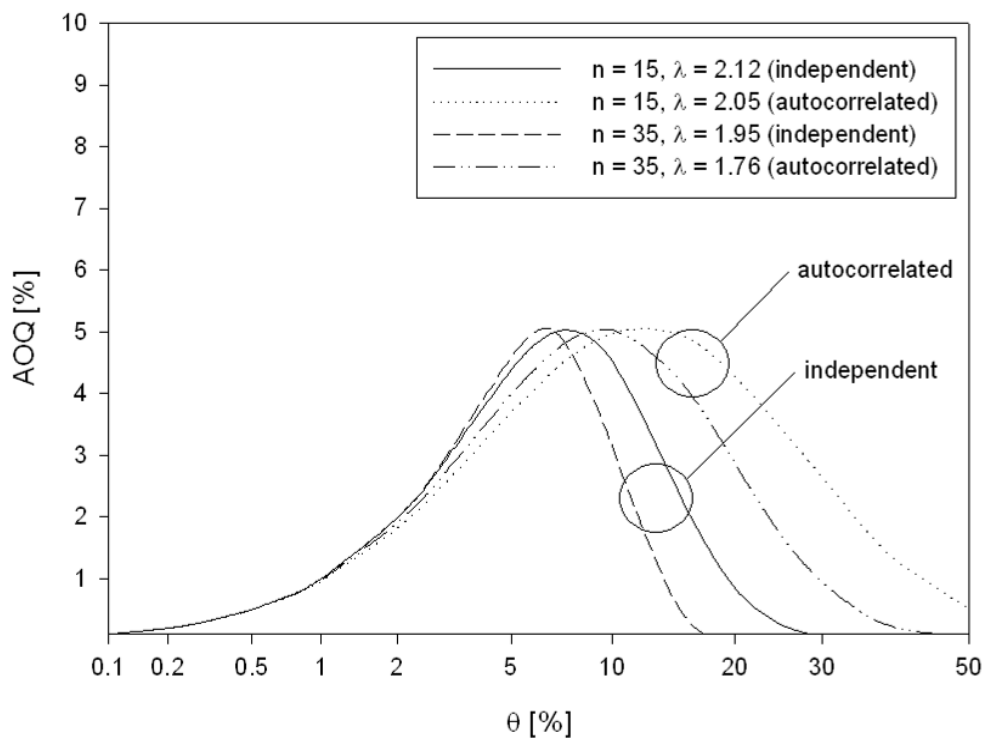


Fig. 8: AOQ-curves associated to acceptance cusum control charts with parameters $h = 5.0$ and $k = 0.5$, optimized with respect to an AOQL = 5%

4 Conclusions

Basic aspects regarding the production control of concrete based on cusum control charts are provided and guidelines for the choice of V-masks for decision making are provided.

In order to combine this type of production control with conformity assessment, a methodology for the design for such acceptance cusum control charts is presented and analyzed. This way, conformity assessment is used as a steering element in the production process of concrete and an economic process control system is achieved.

The influence of target values is investigated for independent and autocorrelated observations and suggestions for appropriate target values are provided in order to achieve the requirements based on the AOQL principle.

Finally, the proposed methodology for the design of an acceptance cusum control charts for a combined production and conformity control of concrete can be summarized as follows:

1. Chose appropriate values for the parameters k and h of the cusum V-mask, based on the guidelines provided in sections 2.2 and 3.1.
2. Based on the intensity of inspection, chose $n = 15$ or $n = 35$ according to the guidelines in section 3.1.
3. Use Table 1 to select an appropriate λ value and calculate the target strength as $\mu_0 = f_{ck} + \lambda\sigma$, with σ based on previous monitoring and controlled through another control scheme.
4. If necessary, check whether the in-control probability of acceptance corresponding to $\theta_0 = \Phi^{-1}(-\lambda)$ is acceptable, using numerical simulations.

5 Acknowledgements

ROBBY CASPEELE is a Research Assistant of the FWO Research Foundation of Flanders. The authors wish to thank the FWO for the financial support on the research project "Probabilistic formulation of the influence of conformity control on the strength distribution of concrete and the safety level of concrete structures by means of Bayesian updating techniques".

6 References

- [1] Juran, J.M.; Gryna, F.M. & Bingham, R.S.: *Quality Control Handbook (third edition)*. McGraw Hill, New York, 1979.
- [2] Taerwe, L.: *Aspects of the stochastic nature of concrete strength including compliance control (in Dutch)*. Doctoral thesis, Ghent University, Ghent, Belgium, 1985.
- [3] Ewan, W.D.: When and how to use cusum charts. *Technometrics*, 5(1), 1963, pp. 1-22.
- [4] Gibra, I.N.: Recent developments in control chart techniques. *Journal of Quality Technology*, 7(4), 1975, pp. 183-192.
- [5] Woodall, W.H.: The design of CUSUM quality control charts. *Journal of Quality Technology*, 18(2), 1986, pp. 99-102.
- [6] ISO/TR7871: *Cumulative sum charts – Guidance on quality control and data analysis using CUSUM techniques*. ISO Standard, 1997.
- [7] BS5703-2: *Guide to data analysis, quality control and improvement using cusum techniques – Part 2: Introduction to decision-making using cusum techniques*. British Standard, 2003.
- [8] BS5703-3: *Guide to data analysis, quality control and improvement using cusum techniques – Part 3: Cusum methods for process/quality control using measured data*. British Standard, 2003.
- [9] Page, E.S.: Cumulative Sum Charts. *Technometrics*, 3(1), 1961, pp. 1-9.
- [10] Woods, R.F.: Effective, economic quality through the use of acceptance control charts. *Journal of Quality Technology*, 8(2), 1976, pp. 81-85.
- [11] Montgomery, D.C.: *Introduction to Statistical Quality Control (fifth edition)*. John Wiley & Sons, USA, 2005.
- [12] Goldsmith, P.L. & Whitfield, H.: Average run lengths in cumulative chart quality control schemes. *Technometrics*, 3(1), 1961, pp. 11-20.
- [13] Wetherill, G.B.: *Sampling Inspection and Quality Control*. Methuen and Co, London, 1969.
- [14] Vance, L.C.: Average run lengths of cumulative sum control charts for controlling normal means. *Journal of Quality Technology*, 18(3), 1986, pp. 189-193.
- [15] Lucas, J.M.: The Design and use of V-mask control schemes. *Journal of Quality Technology*, 8(1), 1976, pp. 1-12.
- [16] Gan, F.F.: An optimal design of CUSUM quality control charts. *Journal of Quality Technology*, 23(4), 1991, pp. 279-286.

- [17] ISO7966: *Acceptance control charts*. ISO Standard, 1993.
- [18] Govindaraju K. (1990), Single sampling plans for variables indexed by AQL and AOQL, *Journal of Quality Technology*, Vol. 22, No. 4, pp. 310-313.
- [19] EN 206-1: *Concrete – Part 1: Specification, performance, production and conformity*. European Standard, CEN, 2000.
- [20] Taerwe, L.: A general basis for the selection of compliance criteria. *IABSE Proceedings P-102/86*, 1986, pp. 113-127.
- [21] Taerwe, L.: Serial correlation in concrete strength records. In: *Special Publication ACI SP-104*, Lewis H. Tuthill International Symposium on Concrete and Concrete Construction, Detroit, 1987, pp. 223-240.
- [22] Taerwe, L.: Influence of autocorrelation on OC-lines of compliance criteria for concrete strength. *Materials and Structures*, 20, 1987, pp. 418-427.
- [23] Johnson, R.A. & Bagshaw, M.: The effect of serial correlation on the performance of CUSUM tests. *Technometrics*, 16(1), 1974, pp. 103-112.
- [24] Bagshaw, M. & Johnson, R.A.: The effect of serial correlation on the performance of CUSUM tests. *Technometrics*, 17(1), 1975, pp. 73-80.

Probabilistic Design for Cracking of Concrete Structures

M. Holický¹, J. Retief², J. Wium²

¹ Klokner Institute, Czech Technical University in Prague, Czech Republic

² University of Stellenbosch, South Africa

Abstract: Serviceability limit states including cracking are often controlling the design of reinforced concrete structures. As a rule the crack width due to loading is a random variable of considerable scatter and uncertainty. The model provided in current codes of practice is accepted to assess the sufficiency of code requirements and design procedures. As an example crack widths of water retaining structures are investigated in detail using probabilistic methods of structural reliability. Results of deterministic and probabilistic design are critically compared. It appears that current codes are rather conservative and probabilistic approach may lead to considerable economic effects. Further research should concentrate on theoretical models of basic variables and probabilistic optimization of serviceability criteria.

1 Introduction

Cracking of concrete structures is inevitable due to certain characteristics of the material. This is a phenomenon which is accepted in structural design procedures, and methods for designing concrete structural elements allow for crack development. In many structures crack width is not a dominant design condition, and suitable allowance is made for limitations on concrete cracking by compliance with reinforcement detailing requirements specified in design standards. However, for special circumstances it may be necessary to specifically include procedures in the design process to limit the width of cracks. Such conditions may include temperature effects, structural restraint, or the specific purpose of the structure as found in concrete water retaining structures.

In special cases therefore, designers need to verify concrete crack widths against specified criteria. Structural design standards provide guidelines for the calculation of crack widths in concrete structures. Criteria for evaluation of calculated crack widths are then expressed as limiting values depending on performance requirements such as durability or the effectiveness of containment.

This paper presents a probabilistic evaluation of the crack width calculation for a specific case in the design of concrete water retaining structures. The paper considers the general crack width calculation procedures given by CEN 2004 [3] (EN 1992-1-1) and limits for water retaining structures as specified by CEN 2006a [4] (EN 1992-3).

The background to this evaluation is that in South Africa, a design standard is being drafted for concrete water retaining structures which uses EN 1992-1-1 and EN 1992-3 as reference standards. Traditionally concrete water retaining structures have been designed in South Africa to BSI [1] (BS 8007). With the replacement of this code in the UK by BS EN 1992 1-1 and EN 1992-3, the implications of adopting a standard based on these standards for South Africa are being investigated.

2 Background

The main steps in setting up a reliability model for cracking of concrete structures can be aligned with the *basis of structural design* as presented in CEN 2002 [2] (EN 1990) and the Draft South African Standard, SABS [12] (SANS/DSS 10160-1).

The main elements of the design verification scheme as it can be applied to the reliability assessment of water retaining structures as discussed by WIUM [13] consist of establishing (i) the scope of application from a survey of representative structures, (ii) the controlling limit state to be cracking (iii) the need to confirm a suitable level of reliability (iv) representation of the relevant actions (hydrostatic load, thermal, shrinkage and creep strains) and their combinations (v) structural behavior and the associated mechanics models (vi) compilation of basic variables (vii) the influence of construction procedures and the associated quality management procedures related to curing and thermal effects.

In this paper only a limited selection of the range of conditions for which reliability assessment should be done is reported, to pilot a more comprehensive investigation.

3 Representative water retaining structure

From a survey of South African practice in the construction of concrete reservoirs, the following configuration is selected to be sufficiently representative of the distinctive characteristics of water retaining structures to serve as scheme for investigating its reliability performance: Cylindrical reservoirs with a diameter/height ratio of four are typically used for storage capacities up to 10 ML using reinforced concrete, with a wall thickness of 250 mm. Concrete classes of 25/30 are used with OPC and 30/37 for mixes with reduced heat of hydration.

Differentiated reliability levels apply to the respective serviceability limit states in increasing steps of (i) nominal limitation of cracking (ii) ensuring sufficient durability as related to the exposure of the surface (iii) compromising the containment functionality of the structure where tensile stresses occur across the section width. The action effect of tensile

hoop stress is directly related to the hydrostatic pressure of the water. The combination with thermal, shrinkage and creep actions is defined to be outside the scope of the present investigation.

Present South African practice limits cracks widths to 0.2mm as stipulated by BS 8007. In EN 1992-3 crack width is limited to 0.05 – 0.2mm, depending on the height-wall-thickness ratio. This is further discussed below.

4 Scope of investigation

For probabilistic calibration of reliability elements the following items were selected for consideration in this study from the items identified above :

- load combinations to be considered for the analysis of cracking,
- classification of the hydrostatic pressure,
- limits to crack width.

Taking account of the discussion above, the Eurocodes EN 1992-1-1 and EN 1992-3 and the *Designers Guide to EN 1992-1-1 and EN 1992-1-2* NARAYANAN & BEEBY [11], some recent studies by MARKOVÁ & HOLICKÝ 2000 [9] and 2001 [10], the fundamental aspects mentioned above are discussed further and provisional recommendations, supplementary to those given by WIUM [13], are offered.

4.1 Load combinations

Cracking is commonly considered as one of the serviceability limit states analyzed using an appropriate combination of actions. Quasi-permanent combination and frequent combinations of actions are recommended for the verification of cracking in Eurocode EN 1992-1-1 and EN 1992-3. According to EN 1992-3 the quasi-permanent combination of actions is also used for liquid retaining and containment structures to provide an adequate assurance that cracks do not pass through the full width of a section. Thus, the quasi-permanent combination seems to be generally accepted and used in the following study.

However, for the verification of the crack width as a critical and irreversible load effect in water retaining structures, the most severe, characteristic load combination may be adequate. This seems to be also supported by WIUM [13]. Particularly, for important water retaining structures with significant consequences of malfunctioning, the characteristic combination of actions is recommended.

The quasi-permanent combination may be used provided that the hydrostatic pressure is considered as a permanent load or variable load with combination factors ψ equal to unity (see the following notes on the classification of hydrostatic pressure). However, the assumption of quasi-permanent combination may still lead to somewhat lower load effects than the characteristic combination. Methods of probabilistic optimization may be used to specify the appropriate reliability level and ψ factors of all variable actions.

4.2 Classification of the hydrostatic pressure

In accordance with CEN 2006b [5] (EN 1991-4), actions caused by water may be classified as permanent and/or variable actions depending on the variation of their magnitude with time. Hydrostatic pressure in water retaining structures seems to be almost fixed and its variation with time is negligible. It is therefore justifiable to classify the hydrostatic pressure in water retaining structures as a permanent action. Alternatively, the hydrostatic pressure may be considered as variable actions having the combination factors ψ equal to unity due to its negligible variation with time (see the previous aspect). This approach, used in Eurocodes, is considered in this study.

4.3 Limiting crack width

In accordance with the Eurocodes EN 1992-1-1 and EN 1992-3, appropriate limits to crack width should be selected taking into account the required function of the structure. However, it appears that limits recommended in literature and codes are mostly based on past experience. The limiting value 0.2 mm is indicated in EN 1992-1-1. EN 1992-3 recommends for those cracks which can be expected to pass through the full thickness of the section, limits ranging from 0.05 mm (for high ratios of the hydrostatic pressure to the wall thickness of the reinforced concrete wall, greater or equal to 35) up to 0.2 mm (for low ratios up to 5). In accordance with NARAYANAN & BEEBY [11], practical experience shows that cracks, with a width of less than 0.2 mm, which pass through a section, will leak somewhat initially but will quickly seal themselves.

Thus, it appears that the limiting value of 0.2 mm represents a reasonable requirement for common water retaining structures even when cracks pass through the full width of a section. Considering however that EN 1992-3 limits cracks widths over a range of values as mentioned under section 3 above, this paper investigates the effects of the limiting values of 0.05mm and 0.2mm. The ultimate choice of a value may depend on structural conditions, possible consequences of structure malfunctioning and relative costs of serviceability improvements.

5 Fundamental concepts in Eurocodes

5.1 Crack width

Verification of cracking is mostly based on semi empirical formulae supported by experimental evidence, experience and structural detailing as stipulated in EN 1992-1-1 and EN 1992-3. A number of different approaches leading to considerably diverse results may be found in literature and codes of practice such as BSI [1], NARAYANAN & BEEBY [11] MARKOVÁ & HOLICKÝ 2000 [9] and 2001 [10]. The following probabilistic study is based on the concepts accepted in Eurocodes. Basic relationship for the assessment of crack width w is written in the form of simple compatibility condition given in EN 1992-1-1.

$$w_m = S_{rm} \varepsilon_m \quad (1)$$

where w_m is the mean crack width, S_{rm} the mean crack spacing and ε_m the mean strain in between the two adjacent cracks. The mean crack spacing S_{rm} can be assessed using a semi empirical formula given in EN 1992-1-1

$$S_{rm} = 2 c + 0.25 k_1 k_2 \phi / \rho_{\text{eff}} \quad (2)$$

where c denotes concrete cover, k_1 is a coefficient taking into account bond properties of the reinforcement (a value 0.8 for high bond and 1.6 for smooth bars), k_2 is a coefficient depending on the form of stress distribution (a value 0.5 for bending, 1.0 for pure tension), ϕ is the bar diameter and ρ_{eff} the effective reinforcement ratio $A_s/A_{c,\text{eff}}$. Here A_s is the reinforcement area and $A_{c,\text{eff}}$ is the effective concrete area surrounding the reinforcing bars. Detailed instructions on how to determine the area $A_{c,\text{eff}}$ are provided in EN 1992-1-1. Note that $A_{c,\text{eff}}$ is usually smaller than the concrete area A_c considered normally for the reinforcement ratio of flexural or compressive members and, consequently, the effective reinforcement ratio ρ_{eff} may be greater than the commonly used reinforcement ratio ρ .

The mean strain ε_m for reinforced concrete members (non prestressed) may be calculated from the expression from EN 1992-1-1

$$\varepsilon_m = \varepsilon_{sm} - \varepsilon_{cm} = \frac{\sigma_s - k_t f_{ct,\text{eff}} (1 + \alpha_e \rho_{\text{eff}}) / \rho_{\text{eff}}}{E_s} \geq 0.6 \frac{\sigma_s}{E_s} \quad (3)$$

where ε_{sm} is the mean strain in reinforcing bars, ε_{cm} the mean strain in surrounding concrete, σ_s is the stress in tension reinforcement at the crack section, k_t is a factor dependent on the duration of the load (0.6 for short term loading, 0.4 for long term loading), $f_{ct,\text{eff}}$ is the mean of the tensile strength of the concrete, effective at the time when the cracks may first develop ($f_{ct,\text{eff}} \leq f_{ctm}$) and α_e is the ratio modulus E_s/E_{cm} .

5.2 Design condition

To verify the mean crack width, w_m is multiplied by the factor β_w ($= 1.7$) and compared to the limiting crack width w_d . Thus, it is required that

$$w_k \approx \beta_w w_m < w_d \quad (4)$$

It is assumed that the product $w_k \approx \beta_w w_m$ is called the characteristic value of the crack width, which is supposed to be equal to the upper 5 % fractile of the crack width w . The required value w_d is considered as a deterministic quantity (for water retaining structures up to 0.2 mm).

5.3 Load combinations

The quasi-permanent combinations of actions are usually considered in design verification of crack width as follows :

$$G_k + L_k + \psi Q_k \quad (5)$$

Here G_k denotes the characteristic value of the permanent load G , L_k the characteristic value of the liquid load L , (considered similarly as the permanent load, $\mu_L = L_k$), Q_k the characteristic value of the variable load Q , ψ is the combination factor for the variable load Q . In some cases (for example in case of a wall of water retaining structures) the liquid load L can be considered only (effect of other loads are negligible).

In design verification of the ultimate limit states the partial factors for all actions should be considered as recommended in EN 1990, for the liquid load L the partial factor should be considered as $\gamma = 1.2$ as recommended in EN 1991-4.

6 Probabilistic formulation

6.1 The limit state function

Random behavior of crack width w can be analyzed using equation (1) where all input quantities are considered as random variables. Thus in general

$$w = S_r \varepsilon \quad (6)$$

Here w denotes the crack width, S_r the crack spacing and ε the strain as random variable. The crack spacing S_r is assumed to be described by equation (2), the strain ε by equation (3) where all input quantities are considered as random variables having the means equal to nominal values. In equation (3) the lower bound $0.6 \sigma_s/E_s$ is not considered in the following reliability analysis.

The theoretical model for strain ε is partly based on experimental observation. Its uncertainty is taken into account by a factor θ expressing model uncertainty. In the following analysis the required crack width w_d is considered as a deterministic value. Then the limit state function g may be written in a simple form

$$g = w_d - \theta w \quad (7)$$

Here the random crack width is given by equation (7), (2) and (3). The model uncertainty θ is considered as an additional random variable (having the mean equal to unity and coefficient of variation 10 %).

6.2 Theoretical models of basic variables

All the quantities entering equations (2), (3) and (7) including the model uncertainty θ are in general random variables. Some of them (having relatively small variability) are, however, approximated by deterministic values. Theoretical models (including type of distribution and their parameters) of all variables used in the following reliability analysis of crack widths of a water reservoir are indicated in Table 1. General guidance is taken from JCSS

[8] as extracted and presented by HOLICKÝ [7,], with information on reinforcement cover given in Example 3.5. The model for concrete tensile strength is derived from Table 3.1 of EN 1992-1-1. Nominal provision is made for modeling uncertainty.

Table 1: Theoretical models of basic variables.

Name	Symbol X	Unit	Distribution	Char. value X_k	The mean μ_X	St. dev. σ_X
Cross section depth	h	m	Normal	0.25	0.25	0
Cross section width	b	m	Det	1.00	1.00	0
Cover of reinforcem.	c	m	Gamma	0.04	0.04	0.01
Reinforcement diam.	ϕ	mm	Det	20 (16)	20 (16)	0
Tensile strength	f_{ct}	MPa	LN	2.0	2.9	0.55
Steel modulus	E_s	GPa	Det	200	200	0
Concrete modulus	E_c	GPa	Det	33	33	0
Creep coefficient	φ	-	Det	2	2	0
Coefficient-reinforc.	k_1	-	Det	0.8	0.8	0
Coefficient-tension	k_2	-	Det	1	1	0
Coefficient-long term	k_t	-	Det	0.4	0.4	0
Liquid pressure	L_k	kN/m ²	Normal	70	70	3.5
Limiting crack width	w_{lim}	mm	Det	0.2 (0.05)	0.2 (0.05)	0
Model uncertainty	θ	-	LN	1.00	1.00	0.10

The following abbreviations are used in Table 1: Normal - for normal distribution, Gamma - for gamma distribution, LN - for log-normal distribution, Det - for deterministic value. Note that the model uncertainty θ is supposed to cover uncertainties in some variables that are indicated as deterministic quantities.

7 Reliability analysis

7.1 An example of water reservoir

As an example of probabilistic design for cracking a cylindrical water reservoir with diameter $D = 28$ m, height 7 m (the maximum water pressure $L_k = 70$ kN/m²) and wall thickness 0.25 m is considered. Crack width is analyzed in the wall only under pure tension due to water pressure. The maximum characteristic force in the wall is thus

$$N_s = D L_k / 2 = 980 \text{ kN} \quad (8)$$

The basic reinforcement area $A_0 = 0.0027$ m² in the wall is determined considering the ultimate limit state of tensile capacity of the wall using the load factor $\gamma = 1.2$, thus the design force $N_d = \gamma N_s = 1176$ kN.

It is common that the basic reinforcement A_0 must be increased to an acceptable value A in order to control cracking. For the data given in Table 1 the enhancement factors given by ratio A/A_0 follow from general equations (1) to (3). For deterministic design for crack

width control according to EN 1992-1-1 the enhancement for the crack limit $w_{lim} = 0.20$ is more than a factor of 2, and for the crack limit $w_{lim} = 0.05$ it is more 5, depending on the steel diameter. In the following analysis these outcomes of the deterministic calculation are compared in detail with results of probabilistic analysis.

7.2 Probabilistic analysis

Crack width of the reservoir wall exposed to pure tension is analyzed considering the limit state function (7) and theoretical models of basic variables given in Table 1. Two diameters of the reinforcing bars $\phi = 20$ mm and $\phi = 16$ mm, and two crack width limits $w_{lim} = 0.2$ mm and $w_{lim} = 0.05$ mm are taken into account. Figure 1 shows variation of the failure probability with the increasing area A/A_0 within the range from 1 to 2.5 for $w_{lim} = 0.2$ mm.

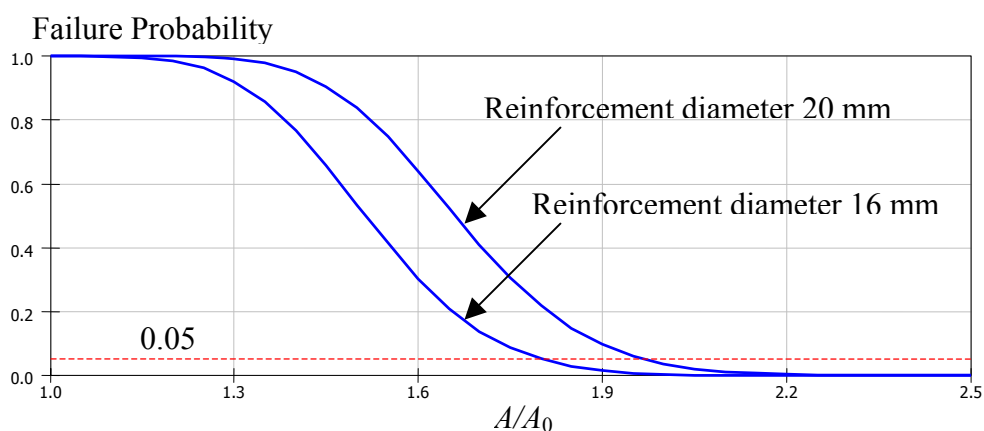
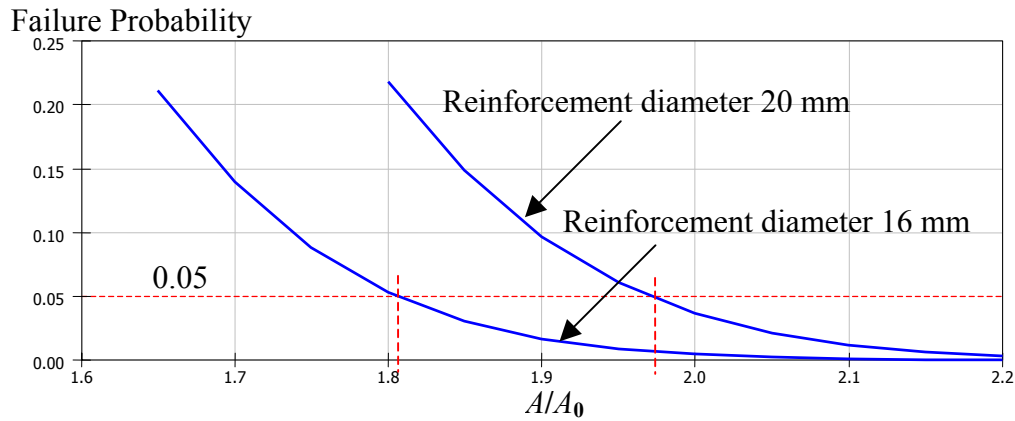


Fig. 1: Variation of serviceability failure probability with the reinforcement ratio A/A_0 for the crack width limit $w_{lim} = 0.2$ mm.

It follows from Figure 1 that without substantial enhancement of reinforcement area the crack width would exceed the required limit $w_{lim} = 0.2$ mm with a very high probability. The basic reinforcement area A_0 should be increased approximately by the factor of 2 to comply with required crack width. Figure 1 also indicates failure probability level 5 % accepted in EN 1992-1-1 for verification of serviceability limit states including crack widths, see NARAYANAN & BEEBY [11] §8.3.4 and Gulvanessian *et al* [6] §8.3.2.

To estimate desired enhancement of reinforcement area more accurately, Figure 2 shows variation of the failure probability with the reinforcement ratio A/A_0 in a limited interval of the ratio A/A_0 from 1.6 to 2.2. It appears that when the reinforcement diameter is 16 mm the basic reinforcement area A_0 should be increased by the factor 1.81, when the reinforcement diameter is 20 mm and by the factor 1.95.



F

ig. 2: Variation of serviceability failure probability with the reinforcement ratio A/A_0 for the crack width limit $w_{lim} = 0.2$ mm.

It is interesting to note that if the required crack width w_{lim} is limited to 0.05 mm, then the reinforcement area A_0 should be increased substantially more than when the limiting crack width is 0.20 mm. Figure 3 shows variation of the failure probability with the reinforcement ratio A/A_0 for $w_{lim} = 0.05$ mm. It follows from Figure 3 that the reinforcement area ratio A/A_0 less than about 3, the crack width $w_{lim} = 0.05$ mm will be almost certainly exceeded. Obviously the reinforcement ratio A/A_0 should be about 4.

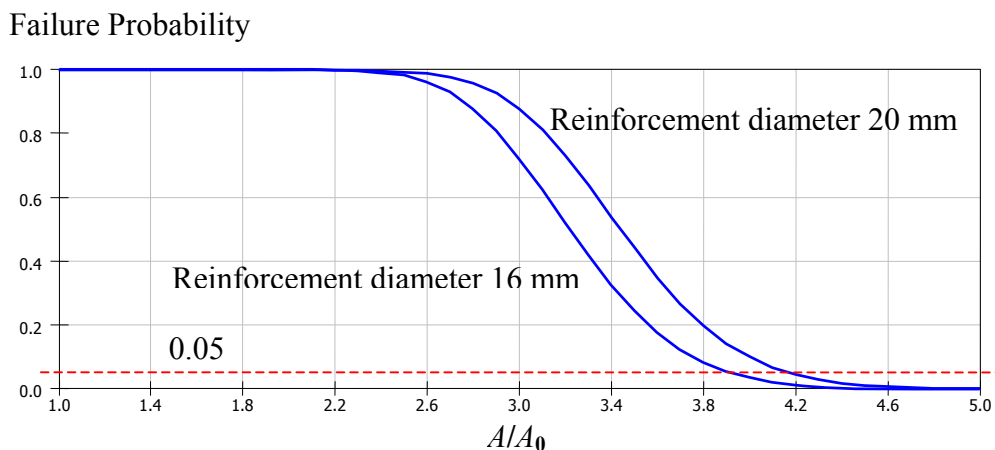


Fig. 3: Variation of serviceability failure probability with the reinforcement ratio A/A_0 for the crack width limit $w_{lim} = 0.05$ mm.

Figure 3 further indicates that the basic reinforcement area A_0 should be increased by the factor of about 4 not to exceed the crack width limit with the probability 5%. Figure 4 shows variation of failure probability within the limited interval of the ratio A/A_0 from 3.8 to 4.4. This detail graph could be used for more accurate estimates of necessary enhancement.

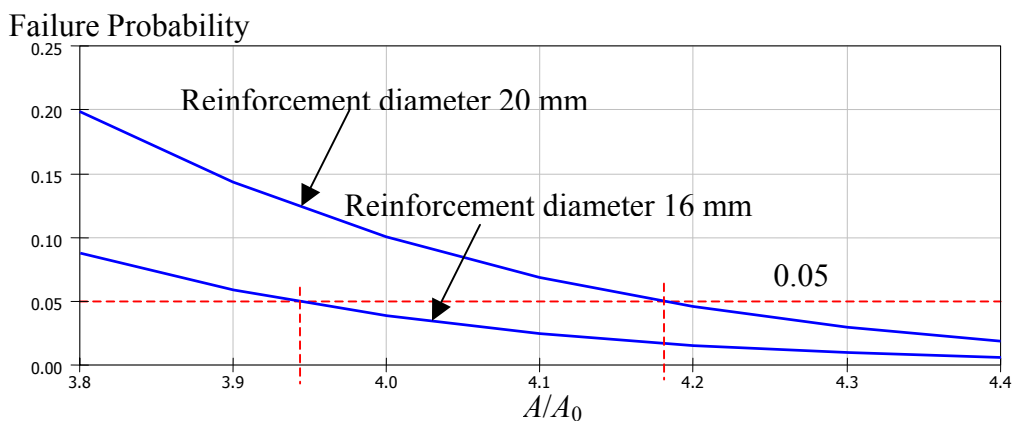


Fig. 4: Variation of serviceability failure probability with the reinforcement ratio A/A_0 for the crack width limit $w_{lim} = 0.05$ mm.

It follows from Figure 4 that the basic reinforcement area A_0 should be increased by the factor 3.94 when the reinforcement diameter is 16 mm and by the factor 4.18 when the reinforcement diameter is 20 mm. This substantial enhancement of reinforcement may have considerable economic consequences.

7.3 Comparison of deterministic and probabilistic analysis

Table 2 provides a summary of deterministic and probabilistic analysis of cracking in the water reservoir. Obviously, reinforcement ratios A/A_0 obtained by deterministic design are systematically greater than corresponding values obtained by probabilistic analysis.

Table 2: Reinforcement area enhancement ratio A/A_0 based on deterministic/probabilistic design.

	Crack limit $w_{lim} = 0.20$ mm	Crack limit $w_{lim} = 0.05$ mm
Reinforcement diameter 16 mm	2.04/1.81 (= 1.13)	5.05/3.94 (= 1.28)
Reinforcement diameter 20 mm	2.26/1.95 (= 1.16)	5.47/4.18 (= 1.31)
Approximate ratio of deterministic/probabilistic enhancement	≈ 1.15	≈ 1.3

Table 2 indicates that in the case of the crack width limit $w_{lim} = 0.05$ mm the reinforcement ratio A/A_0 is greater by about 30 %, and in the case of the crack width limit $w_{lim} = 0.20$ mm it is greater by about 15 % (as shown at the last row of the Table 2). It appears that the degree of conservatism of current codes increases with increasing (more severe) requirements on crack width and increasing reinforcement diameter.

The probabilistic analysis may obviously have considerably economic effects. However, the accepted reliability level corresponding to probability of 5% of exceeding the required limiting crack width is not rationally justified and may not be an optimum choice. It is therefore suggested to verify the requirements for crack widths and their reliability using methods of probabilistic optimization.

The probabilistic optimization would make it possible to balance cost of measures used for increasing the reliability level and cost of expected consequences due to an infringement of the required crack width limits. Possible measures to increase reliability may include enhancement of reinforcement area, surface treatment of the reservoir wall and other possible actions. Consequences of crack limits infringement may include leakage of the reservoir and possible requirement for its repair that may further induce other unfavorable situations.

8 Concluding remarks

1. The probabilistic analysis of crack width in a water reservoir presented here confirms previous experience that basic reinforcement areas required by the ultimate limits state must be considerably enhanced to control crack widths.
2. Deterministic methods accepted in current codes for verification of cracking seem to provide a conservative assessment of crack widths.
3. The degree of conservatism of current design standards increases with the increasing requirements on crack widths.
4. The applications of probabilistic methods on verification of crack width may lead to positive economic effects.
5. Further research of crack width verification should concentrate on the optimization of required crack width limits and on improvement of theoretical models for basic variables including model uncertainty.
6. The increased conservatism for reduced crack widths identifies the need to establish suitable crack width criteria to be adopted in a draft South African standard for water retaining structures.

9 References

- [1] BSI: BS 8007:1987, British Standard: *Code of practice for design of concrete structures for retaining aqueous liquids*, British Standards institute, 1987.
- [2] CEN, 2002: EN 1990:2002, *Basis of structural design*. European Committee for Standardization (CEN), Brussels.

- [3] CEN, 2004: EN 1992-1-1:2004, Eurocode 2: *Design of Concrete Structures, General rules and rules for building*, 2004. European Committee for Standardization (CEN), Brussels.
- [4] CEN, 2006a: EN 1992-3:2006, Eurocode 2: *Design of concrete structures Part 3: Liquid retaining and containment structures*, June 2006. European Committee for Standardization (CEN), Brussels.
- [5] CEN, 2006b: EN 1991-4:2006, Eurocode 1 *Actions on structures Part 4 : Silos and tanks*, June 2006. European Committee for Standardization (CEN), Brussels.
- [6] Gulvanessian, H., Calgaro, J.-A., Holický, M.: *Designer's guide to EN 1990*, Thomas Telford, 2002.
- [7] Holický, M.: *Reliability analysis for structural design*. ISBN 978-1-920338-11-4. SUN PReSS 2009 www.africansunmedia.co.za .
- [8] JCSS: *Probabilistic model code*. JCSS working materials, <http://www.jcss.ethz.ch/>.
- [9] Marková, J., Holický, M., 2000: Probabilistic Analysis of Crack Width, *Acta Polytechnica* Vol. 40 No. 2/2000, Prague, Czech Republic, 2000, pp. 56-60.
- [10] Marková, J., Holický M., 2001: Credibility of Design Procedures. *Acta Polytechnica*. 2001, vol. 41, no. 4-5, s. 74-78. (See also *International Conference on Advanced Engineering Design*. Glasgow: University of Glasgow, 2001, s. 407-412).
- [11] Narayanan, R.S., Beeby, A.: *Designers Guide to EN 1992-1-1 and EN 1992-1-2*, Thomas Telford, 2005.
- [12] SABS: SANS/DSS 10160 Part 1 *Basis of structural design*. Draft South African Standard, South African Bureau of Standards, Pretoria, 2009.
- [13] Wium, J. A.: Progress Report to the Water Research Commission, Project K5-1764, The development and calibration of South Africa's National Standard for water retaining structures, University of Stellenbosch, September 2008.

Acknowledgement. This study has been partly funded by the Czech Science Foundation as a part of the research project GAČR 103/09/0693 „Assessment of Safety and Risk of Technical Systems”.

Influence of a combined vague-informative prior on the assessment of characteristic concrete strength

Robby Caspeele, Luc Taerwe
Magnet Laboratory for Concrete Research
Faculty of Engineering, Department of Structural Engineering
Ghent University, Belgium

Abstract: Annex D of the European Standard EN 1990 ‘Basis of structural design’ allows to determine the characteristic in-situ compressive strength f_{ck} from n test results, using a prediction method which is referred to as a ‘Bayesian procedure with vague prior distributions’. The assumption of a vague or uniform prior results in a conservative approach in cases where only a limited number of test results are available. However, in case of concrete, prior information is available in literature based on the investigation of an extensive number of test results. The Bayesian framework for the estimation of the characteristic strength according to EN 1990 is investigated. In order to account for prior information on concrete strength distributions, a Bayesian methodology based on a combined vague-informative prior is presented for the estimation of the characteristic in-situ concrete strength. More specific, prior distributions for the standard deviation of concrete strength are analyzed and generalized so that this information can be used for the assessment of concrete compressive strength from a limited number of test results. Because prior information is taken into account, the uncertainty regarding the standard deviation of the predictive strength distribution can be reduced, resulting in a more appropriate estimation model in cases where only a few test results are available.

1 Introduction

Repair and upgrading of existing structures is becoming more and more important and has an increasing economic significance. The assessment of existing structures thus becomes of crucial importance in decision making. In case of concrete structures, the estimation of the characteristic strength values from limited data is a difficult, but important task. Based on the European Standard EN1990 [1], which is in accordance with ISO Standards ISO 2394 [2], ISO 12491 [3] and ISO 13822 [4], the characteristic in-situ compressive strength

f_{ck} may be determined from n test results, using a prediction method which is referred to as a ‘Bayesian procedure with vague prior distributions’.

The assumption of a vague or uniform prior results in a conservative approach in cases where only a limited number of test results are available, mostly due to a large sample standard deviation. When for example only 3 concrete compressive strength results are available and the sample standard deviation is found to be 8 MPa, this is very unlikely to be the actual standard deviation of the total population, based on available information on concrete strength distributions.

However, in case of concrete, prior information on concrete strength can be found in literature or country-specific prior information can be determined, based on normal-gamma or lognormal-gamma distributions. In case of the assessment of the characteristic strength from a limited number of test samples, the use of a combined vague-informative prior is of particular interest.

2 Informative priors for the standard deviation of concrete strength

Parameters for the joint prior density function of the mean and standard deviation of the concrete strength X , i.e. $f'_{M\Sigma}(\mu, \sigma)$, can be obtained from an extensive database on strength results from different concrete plants, using the maximum-likelihood method. In [5] prior parameters for concrete strength distributions are derived for different concrete types and concrete strength classes, based on a large data collection of concrete production in Southern Germany. In the latter paper, concrete cube strength is assumed to be log-normally distributed. Therefore, the parameters of the prior distributions are given in case of lognormal-gamma distributions. These parameters are summarized in Table 1 for different concrete types and different concrete strength classes, based on the following expression for the lognormal-gamma distribution [5,6,7]:

$$f'_{M,\Sigma}(\mu, \sigma) = \frac{\sqrt{n'}}{\sqrt{2\pi}\mu\sigma^*} e^{-\frac{1}{2}\left(\frac{\ln \mu - \bar{x}'}{\sigma^*/\sqrt{n'}}\right)^2} \times \dots \quad (1)$$

$$\dots \frac{\left(\frac{1}{2}v'(s^*/\sigma)^2\right)^{\frac{v'}{2}-1} \exp\left(-\frac{1}{2}v'(s^*/\sigma)^2\right)}{\Gamma(v'/2)} \frac{v' s^{*2}}{\sigma^3}$$

$$\text{with } \sigma^* = \sqrt{\ln(\delta^2 + 1)}$$

$$\delta = \sigma/\mu$$

$$s^* = \frac{\exp(\bar{x}')}{\exp(-s'^2/2)} \sqrt{\exp(s'^2) - 1}.$$

Table 1: Prior parameters for concrete strength distributions based on lognormal-gamma distributions [5]

	Concrete grade					
	C15	C25	C35	C45	C55	
Site mixed concrete	\bar{x}'	3.40	3.65	3.85	-	-
	n'	1.0	2.0	3.0	-	-
	s'	0.15	0.12	0.09	-	-
	ν'	3.0	4.0	4.5	-	-
Ready-mixed concrete	\bar{x}'	3.40	3.65	3.85	3.98	-
	n'	1.5	1.5	1.5	1.5	-
	s'	0.14	0.12	0.09	0.07	-
	ν'	6.0	6.0	6.0	6.0	-
Concrete for precast elements	\bar{x}'	-	3.80	3.95	4.08	4.15
	n'	-	2.0	2.5	3.0	3.5
	s'	-	0.09	0.08	0.07	0.05
	ν'	-	4.5	4.5	5.0	5.5

As an example, the joint prior density function for ready-mixed concrete from a C25 concrete class is illustrated in Figure 1, based on the parameters given in Table 1.

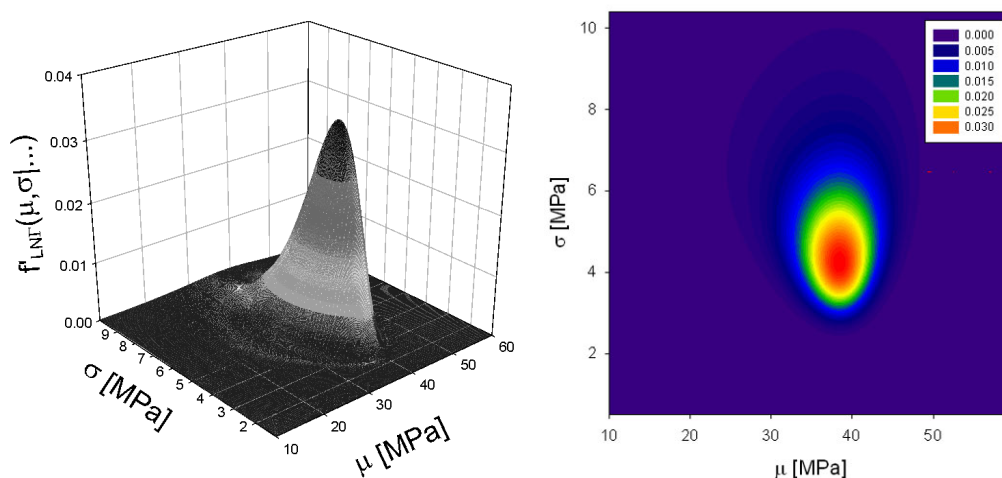


Figure 1: Prior joint probability distribution $f'_{M,\Sigma}(\mu, \sigma)$ for concrete class C25 in case of ready-mixed concrete

Further, in [5] it was also mentioned that the suggested prior information does not differ substantially from that of other countries. In [12], the suggested prior information was compared to results obtained in Belgium, yielding also comparable results. Finally, also recent investigation of current Belgium concrete mixtures do not show significant differences. So, it is concluded that this information provides proper prior information with respect to the objectives of this paper. Nevertheless, more appropriate country-specific priors can be calculated and taken into account in the following.

When concrete strength has to be assessed from a limited number of test samples, the previously mentioned prior information cannot be used straightforward. Since the concrete strength class is unknown, a vague prior has to be used for the mean μ . However, the prior information on the standard deviation σ is very useful in order to make less conservative estimations regarding the characteristic concrete strength in cases where only a limited number of test results are available. Therefore, the prior information on σ has to be generalized irrespective of the concrete class. This is done by simulating Monte Carlo samples from a temporary distribution which is defined as the piecewise maximum of all probability density functions corresponding to the different concrete classes of a particular concrete type. Using the maximum-likelihood principle, estimators for the prior parameters s' and ν' can be obtained for the following natural conjugate prior distribution [6,7]:

$$f'_{\Sigma}(\sigma) \propto \sigma^{-1}(\sigma^2)^{-(\nu'/2+1)} \exp\left(-\frac{\nu' \sigma^2}{2\sigma^2}\right) \tag{2}$$

which is an Inverse- χ^2 distribution.

The generalized prior parameters for different concrete types are summarized in Table 2. In figures 2-4 the prior distributions of σ for different concrete classes are compared with the calculated generalized priors in case of site mixed concrete, ready mixed concrete and concrete for precast elements respectively.

Table 2: Generalized prior parameters for $f'_{\Sigma}(\sigma)$

	s'	ν'
Site mixed concrete	4.44	3.17
Ready mixed concrete	4.11	4.71
Concrete for precast elements	3.66	3.57

3 EN 1990 method for determining the characteristic concrete compressive strength

Under the assumption of a normal distribution for the population, the posterior predictive characteristic concrete strength, based on a Bayesian method with vague prior information is given by the following equation [1,8,9]:

$$\hat{f}_{ck} = \bar{x}(1 - k_n V_X) \tag{3}$$

with $V_X = s/\bar{x}$, the sample coefficient of variation
 $k_n = t_{n-1;0.05}\sqrt{1+1/n}$, a coefficient depending on n
 $t_{\nu,\alpha}$ the α -fractile of a t-distribution with ν degrees of freedom.

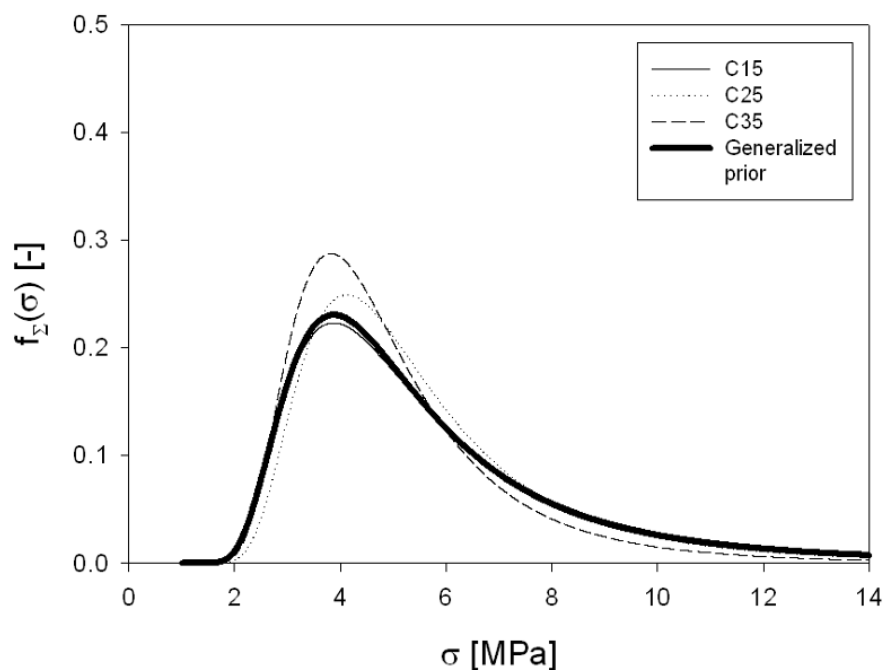


Figure 2: Comparison of prior distributions for the standard deviation of the strength of site mixed concrete

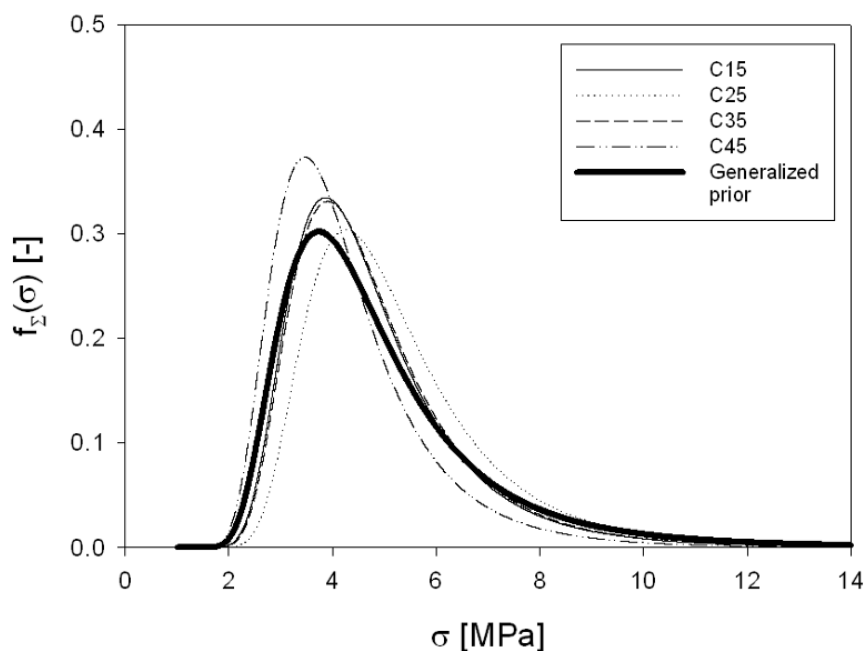


Figure 3: Comparison of prior distributions for the standard deviation of the strength of ready-mixed concrete

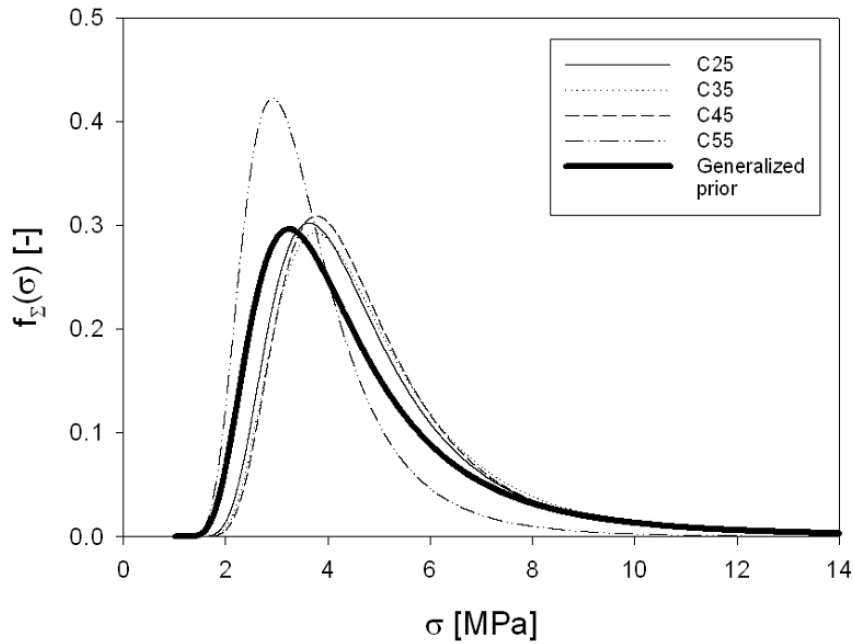


Figure 4: Comparison of prior distributions for the standard deviation of the strength of concrete for precast elements

4 Bayesian estimation method based on a combined vague-informative prior

In case when prior information is available with respect to the standard deviation, a new Bayesian method based on a combined vague-informative prior is proposed. It can be shown that the posterior predictive characteristic concrete strength is then given by the following equation:

$$\hat{f}_{ck} = \bar{x} \left(1 - k_n^* V_X \right) \tag{4}$$

with $k_n^* = t_{\nu''; 0.05} \sqrt{1 + 1/n} \frac{s''}{s}$, an equivalent coefficient de-

pending on n , s and s''

$\nu'' = \nu' + n$, the posterior degrees of freedom

$s'' = \sqrt{\frac{1}{\nu''} \left[\nu' s'^2 + (n-1) s^2 \right]}$, the posterior standard de-

viation.

In case of concrete, the values for ν' and s' given in Table 1 can be used or country-specific parameters can be derived from an extensive national database, based on the same methodology.

5 Comparison between the use of vague and combined vague-informative priors

A comparison of the coefficients k_n and k_n^* is given in Table 3 in case of ready-mixed concrete (with prior parameters $s' = 4.11$ MPa and $\nu' = 4.71$). Since for a vague-informative prior k_n^* is function of the sample standard deviation s , the k_n^* values are calculated for different values of s , ranging from 2 MPa to 7 MPa. Due to the small number of degrees of freedom, the influence of the prior parameters decreases quickly with an increasing number of test results. From Table 3 it can also be concluded that for most sample standard deviations, the coefficient k_n^* in case of a vague-informative prior is smaller than the corresponding coefficient k_n in case of vague prior information.

Table 3: Comparison of coefficients k_n and k_n^* in case of ready-mixed concrete

	n						
	3	4	5	10	15	∞	
vague prior (k_n)	3.37	2.63	2.34	1.92	1.82	1.64	
vague-informative prior (k_n^*)	s = 2 MPa	3.78	3.43	3.20	2.60	2.35	1.64
	s = 3 MPa	2.66	2.47	2.34	2.05	1.93	1.64
	s = 4 MPa	2.13	2.03	1.96	1.81	1.76	1.64
	s = 5 MPa	1.84	1.78	1.75	1.69	1.67	1.64
	s = 6 MPa	1.66	1.64	1.63	1.62	1.62	1.64
	s = 7 MPa	1.54	1.54	1.55	1.58	1.59	1.64

In order to compare both Bayesian methods quantitatively, Monte Carlo simulations are performed according to the sampling theory as explained in for example [10]. For different values of the standard deviation σ of the concrete strength population, 100000 estimates \hat{f}_{ck} of the characteristic concrete compressive strength are determined according to the two previously described methods, in case of ready mixed concrete with proper prior parameters according to Table 2.

The probability for overestimating f_{ck} is illustrated in Figure 5. From this graph, it can be concluded that the Bayesian method with a combined vague-informative prior is less biased than the method described in EN 1990 (based on a vague prior) in case of large σ values, thus yielding less conservative results.

In order to investigate the effect of autocorrelation between consecutive test results, an AR(2)-autoregressive process with parameters derived by TAERWE [11] is implemented for the random sample generation. Figure 6 illustrates the influence of autocorrelation on the probability of overestimating f_{ck} . Due to autocorrelation, the probability for overestimating f_{ck} increases in comparison to independent observations. Nevertheless, the conclusions drawn from Figure 5 in case of independent observations remain valid.

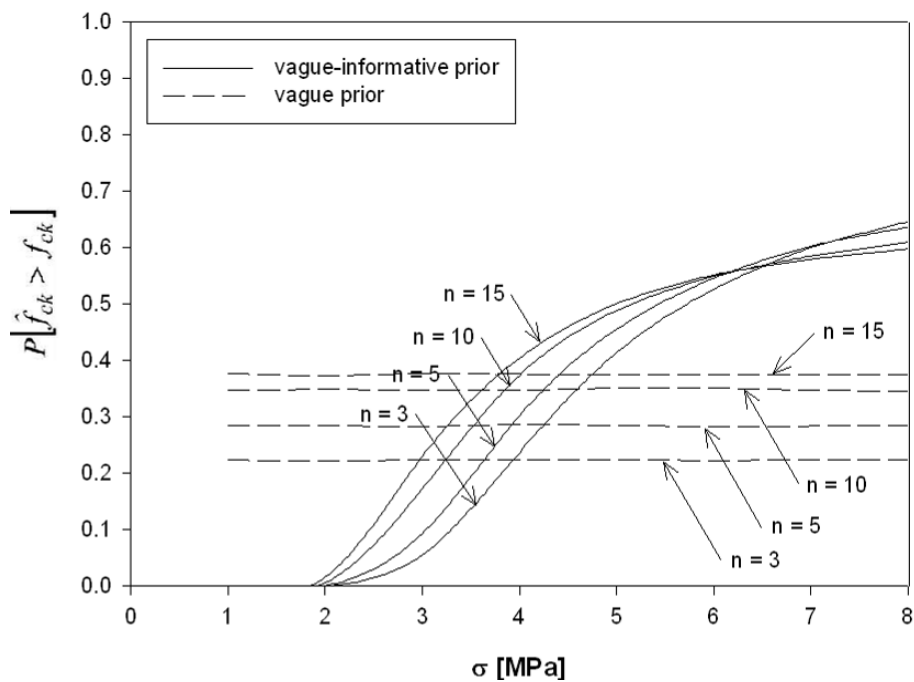


Figure 5: Comparison on the probability for overestimating the characteristic concrete strength in case of independent observations

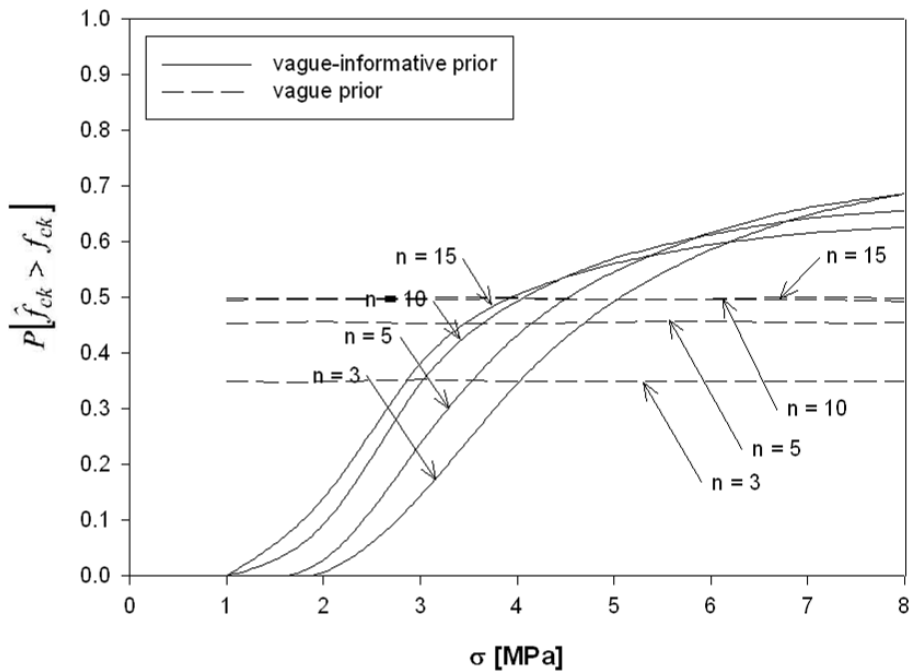


Figure 6: Comparison on the probability for overestimating the characteristic concrete strength in case of autocorrelated observations

The normalized sample mean is shown in Figure 7. In case of a small number of test results, the estimated characteristic strength is significantly lower than the real characteristic strength of the distribution, irrespective of the standard deviation of the population. In comparison to the assumption of a vague prior, the estimated characteristic strength based on the Bayesian method with a combined vague-informative prior is found to be less conservative. Only in case of a high standard deviation, the estimated characteristic strength is slightly higher than the real characteristic strength of the population (an overestimation), but – as already mentioned earlier – this situation is unlikely to occur frequently. The effect of autocorrelation on the normalized sample mean is illustrated in Figure 8. Due to autocorrelation the sample mean decreases. This effect is again more pronounced in case a Bayesian method with vague priors is used. The conclusions drawn from Figure 7 in case of independent observations remain however still valid.

The sample coefficient of variation is given in Figure 9 and illustrates the variability of the estimated characteristic strength. This variability increases with an increasing standard deviation of the population. From Figure 9 it can be concluded that the application of a Bayesian method with a combined vague-informative prior reduces the variability of the estimates significantly. Finally, Figure 10 illustrates that autocorrelation decreases the sample coefficient of variation in case of vague priors, but increases the sample coefficient of variation in case of combined vague-informative priors in comparison to independent observations. Nevertheless, the use of vague-informative priors still reduces the sample coefficient of variation significantly when only a few test results are available.

6 Conclusions

- In order to estimate the characteristic concrete strength from test samples, EN 1990 (which is consistent with ISO 2394, ISO 12491 and ISO 13822) provides a Bayesian method based on vague prior information. In practice however, the assumption of a vague prior results in a conservative approach in cases where only a limited number of test results are available, mostly due to a large sample standard deviation. Therefore, the use of a combined vague-informative prior is recommended.
- A practical formula for the estimation of the characteristic concrete strength based on combined vague-informative priors is given by Equation (4). Prior parameters for the distribution of the standard deviation of the population are derived, based on available data in literature. These prior parameters are given in Table 2. Some practical values for the coefficient k_n^* are provided in Table 3.
- The differences between the use of a vague and a combined vague-informative prior are investigated through Monte Carlo simulations, also taking into account the influence of possible autocorrelation between consecutive test results. Because prior information is taken into account, the uncertainty regarding the standard deviation of the predictive strength distribution can be reduced, resulting in a more appropriate estimation model.

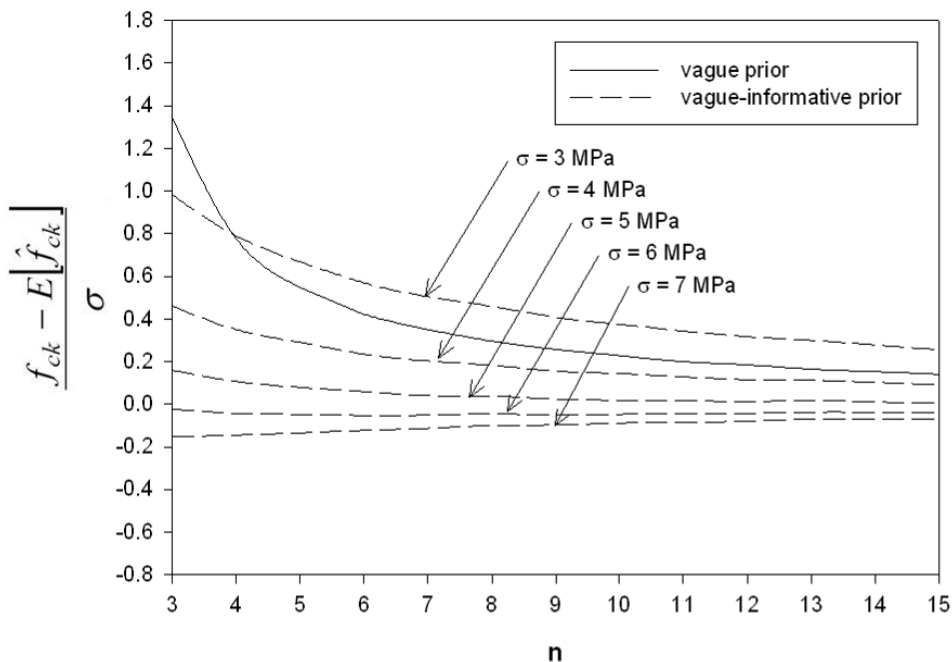


Figure 7: Normalized sample mean of the estimated characteristic concrete strength based on a Bayesian method with a vague or a combined vague-informative prior (independent observations)

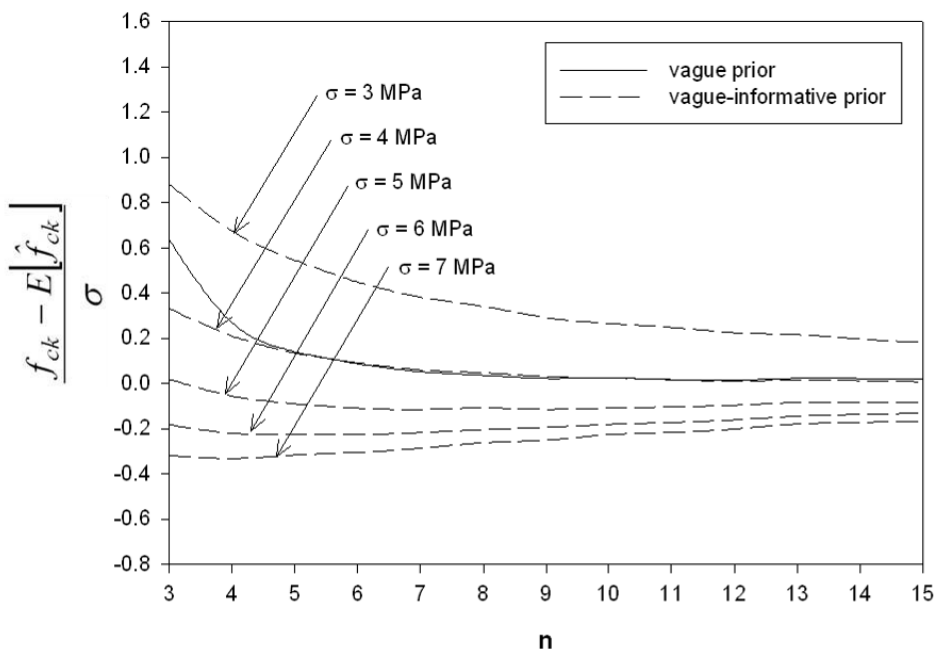


Figure 8: Normalized sample mean of the estimated characteristic concrete strength based on a Bayesian method with a vague or a combined vague-informative prior (auto-correlated observations)

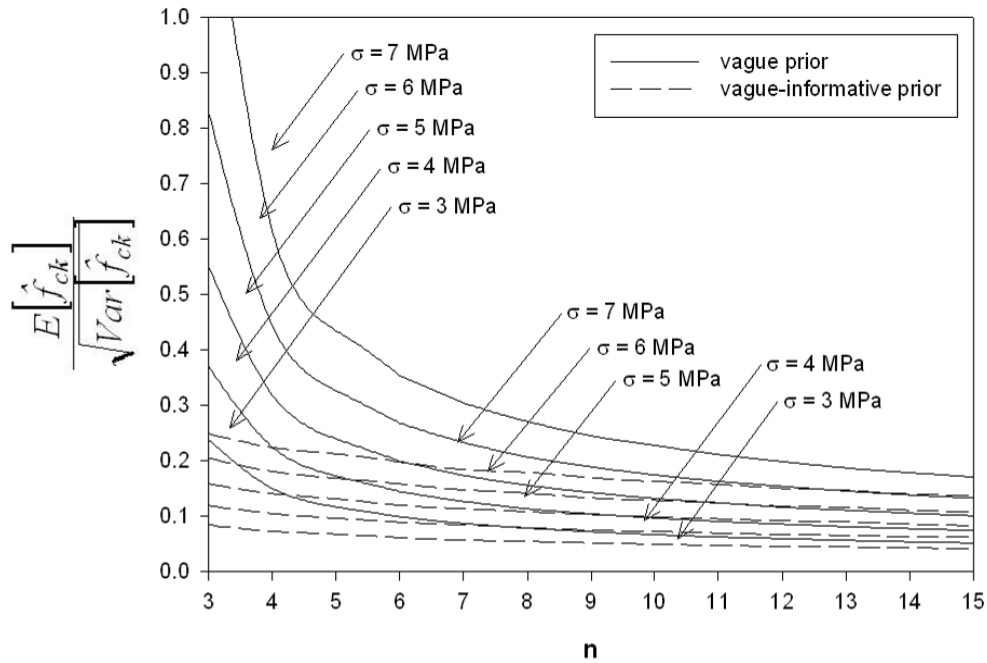


Figure 9: Sample coefficient of variation of the estimated characteristic concrete strength based on a Bayesian method with a vague or a combined vague-informative prior (independent observations)

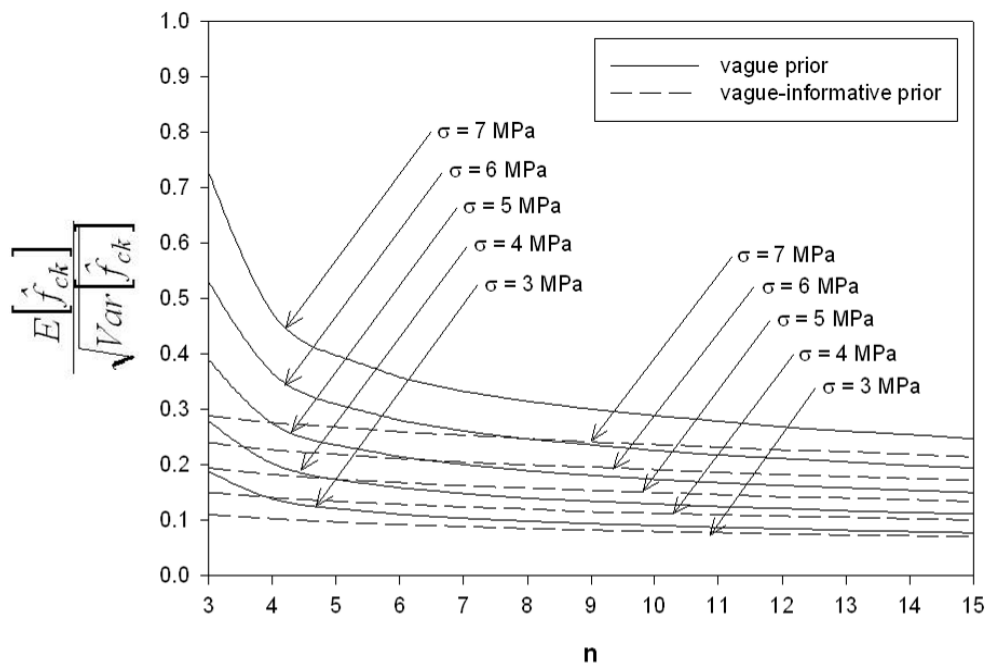


Figure 10: Sample coefficient of variation of the estimated characteristic concrete strength based on a Bayesian method with a vague or a combined vague-informative prior (autocorrelated observations)

7 Acknowledgements

ROBBY CASPEELE is a Research Assistant of the FWO Research Foundation of Flanders. The authors wish to thank the FWO for the financial support on the research project "Probabilistic formulation of the influence of conformity control on the strength distribution of concrete and the safety level of concrete structures by means of Bayesian updating techniques".

8 References

- [1] EN 1990: *Eurocode 0: Basis of structural design*. European Standard, CEN, 2002.
- [2] ISO 2394: *General principles on reliability for structures*. ISO Standard, 1998.
- [3] ISO 12491: *Statistical methods for durability control of building materials and components*. ISO Standard, 1997.
- [4] ISO 13822: *Basis for design of structures – Assessment of existing structures*. ISO Standard, 2003.
- [5] Rackwitz, R.: Predictive distribution of strength under control. In: *Materials and Structures*; 16(94), 1983, 259-267.
- [6] Box, G. & Tiao, G.: *Bayesian Inference in Statistical Analysis*. Addison-Wesley Publishing, USA, 1973.
- [7] Gelman, A.: *Bayesian Data Analysis (2nd edition)*. Chapman & Hall/CRC, USA, 2004.
- [8] Diamantidis, D. et al.: *Probabilistic Assessment of Existing Structures*. RILEM Publications S.A.R.L., France, 2001.
- [9] Gulvanessian, H. & Holický, M.: *Designers' Handbook to Eurocode 1*. Thomas Telford, London, 1996.
- [10] Ang, A.H.-S. & Tang, W.H.: *Probability concepts in engineering (second edition)*. John Wiley & Sons, New York, 2007.
- [11] Taerwe, L.: Analysis and modeling of autocorrelation in concrete strength series. In: Proske, D., Mehdiانpour, M & Guçma, L (eds.): *Proc. 4th International Probabilistic Symposium*, 12-13 October, Berlin, Germany, 2006, 29-43.
- [12] Taerwe, L.: *Aspects of the stochastic nature of concrete strength including compliance control (in Dutch)*. Doctoral thesis, Ghent University, Ghent, Belgium, 1985.

Reliability analysis of static equilibrium

Milan Holický, Miroslav Sýkora
 Czech Technical University in Prague, Klokner Institute

Abstract: Limit state of static equilibrium is an essential ultimate limit state to be verified in persistent and transient design situations of construction works. In the present study the static equilibrium of a cantilevered beam and motorway gantry is analyzed considering traditional probabilistic models for permanent and variable actions. It is shown that the alternative sets of partial factors recommended in EN 1990 for stabilizing and destabilizing action effects lead to different and mostly insufficient reliability levels (reliability index around 3). Span ratios and correlation between favourable and unfavourable permanent actions influence predicted reliability levels. With increasing correlation the reliability increases. More conservative factors than those recommended in EN 1990 are proposed for verification of common structures by the partial factor method. For verification of important and costly structures, application of probabilistic reliability analysis is advised.

1 Introduction

Current codes of practice (ISO 2394 [1], EN 1990 [2]) require verification of all relevant limit states in all appropriate design situations. The limit state of static equilibrium (EQU) is an important ultimate limit state that may have serious consequences and should be considered for construction works in both, persistent and transient design situations. In accordance with EN 1990 [2] it should be verified that

$$E_{d,dst} \leq E_{d,stb} \tag{1}$$

with $E_{d,dst}$ the design action effect of destabilizing actions
 $E_{d,stb}$ the design action effect of stabilizing actions.

The effect of destabilizing and stabilizing actions $E_{d,dst}$ and $E_{d,stb}$ shall be determined considering combination of actions (6.10) given in EN 1990 [2]. The partial factors for unfavourable and favourable permanent and variable actions recommended in the Annex A1 and A2 of EN 1990 [2] are given in Tab. 1.

Tab. 1: Partial factors for permanent and variable actions G and Q in persistent and transient design situation recommended in Annex A1 and A2 of EN 1990 [2].

		Table A1.2(A), Buildings			Table A2.4(A), Bridges
Action	Symbol	Alternative 1	Alternative 2, more unfavourable from two sets		
		Set of partial factors			
		{1}	{2}	{3}	{4}
Unfavourable permanent	$\gamma_{G,\text{sup}}$	1,1	1,35	1,0	1,05
Favourable permanent	$\gamma_{G,\text{inf}}$	0,9	1,15	1,0	0,95
Unfavourable variable	γ_Q	1,5	1,5	1,5	1,5

The partial factors for all unfavourable variable actions γ_Q are considered by the common value 1,50 (zero for favourable variable actions). In Annex A2 of EN 1990 [2] some reductions of γ_Q are allowed for unfavourable construction loads (1,35), pedestrian actions (1,35) and rail traffic actions (1,45). In addition this Annex provides an alternative set of partial factors when the verification of static equilibrium also involves the resistance of structural elements (similarly as for buildings in A1.2(A) in EN 1990 [2]).

Note that some national standards required verifying the static equilibrium using “the global safety factor” s for which the value 2 was specified. The global factor s can be written as

$$s = E_{k,\text{stb}} / E_{k,\text{dst}} \quad (2)$$

with $E_{k,\text{dst}}$ the characteristic effect of destabilizing actions
 $E_{k,\text{stb}}$ the characteristic effect of stabilizing actions.

This study attempts to compare the reliability level reached using the recommended partial factors given in Tab. 1, with previous requirements for the global safety factor s and with reliability levels commonly accepted for structural members (reliability index $\beta = 3,8$ for a 50-year reference period). Two examples are analysed in detail: cantilevered beam and motorway gantry.

2 Cantilevered beam

A cantilevered beam indicated in Fig. 1 is a typical structural element that should be always checked for the limit state of static equilibrium. The beam is exposed to two permanent actions g_1 and g_2 , and two independent variable actions q_1 and q_2 . Correlation of the two permanent actions g_1 and g_2 is described by a coefficient of correlation $\rho_{g_1g_2}$ (0 for independent actions and 1 for fully dependent actions).

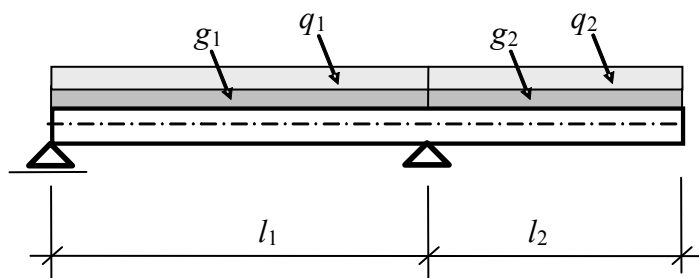


Fig. 1: A cantilevered beam

The design condition (1) is rewritten as

$$\gamma_{g2}g_{k2}\alpha^2 + \gamma_{q2}q_{k,2}\alpha^2 \leq \gamma_{g1}g_{k1} \quad (3)$$

with α the span ratio l_2 / l_1 .

The span ratio α is considered within an interval $\langle 0; 1 \rangle$. The maximum characteristic value q_{k2} of the variable action q may be derived from equation (3) as follows

$$q_{k2} \leq \frac{\gamma_{g1}g_{k1} - \gamma_{g2}g_{k2}\alpha^2}{\gamma_{q2}\alpha^2} \quad (4)$$

The limit state function can be written as

$$Z = g_1 - g_2\alpha^2 - q_2\alpha^2 \quad (5)$$

with Z the reliability margin.

Relationships (3), (4) and (5) could be generalized to describe more complicated structural conditions, for example when additional actions should be taken into account. Model uncertainties in determination of action effects may be included.

In the following it is considered that the beam is designed in such a way that the characteristic value q_{k2} is equal to its maximum value given by relationship (4).

3 Basic variables

The three random basic variables g_1 , g_2 and q_2 enter the limit state function (5) while the span ratio α is considered as a deterministic quantity. Theoretical models of the random variables are indicated in Tab. 2. Commonly used models, supported by the working materials of JCSS [3] and the study by GULVANESEAN and HOLICKÝ [4], are accepted. The same characteristic value g_k is considered for both permanent actions g_1 and g_2 (though the actions g_1 and g_2 may be different).

Fifty-year maxima of the unfavourable variable action q_2 (corresponding to a 50-year reference period for the reliability index) are taken into account. In the general example the favourable variable action q_1 is considered to be intermittent with significant intervals of

load not present. Therefore, it is likely that the 50-year maximum of q_2 will occur when q_1 is not acting and favourable effects of q_1 are (conservatively) neglected. In a specific case combination of time-variant loads could be analysed in more details.

Tab. 2: Theoretical models of basic variables.

Basic variable	Symbol X	Distribution	Characteristic value X_k	The mean μ_X	The standard deviation σ_X
Favourable permanent	g_1	Normal	g_k	g_k	$0,08 g_k$
Unfavourable permanent	g_2	Normal	g_k	g_k	$0,08 g_k$
Unfavourable variable	q_2	Gumbel	eq. (3)	$0,6q_k$	$0,21q_k$

Considering the theoretical models given in Tab. 2, relationship (3) for the maximum characteristic value q_k can be expressed as

$$\frac{q_k}{g_k} \leq \frac{\gamma_{g1} - \gamma_{g2}\alpha^2}{\gamma_{q2}\alpha^2} \quad (6)$$

Assuming the maximum load ratio q_k / g_k , the global safety factor s follows from relationships (2) and (6) as

$$s = \gamma_{q2} / (\gamma_{g1} - \gamma_{g2}\alpha^2 + \gamma_{q2}\alpha^2) \quad (7)$$

Obviously, the maximum global factor s is achieved for very small α (approaching zero). It follows from equation (7) that the factor s is much less than the commonly accepted value 2 ($s < \gamma_{q2} / \gamma_{g1} < 1,5 / 0,9 = 1,67$).

4 Reliability analysis

To analyze the simple limit state function given by equation (5) and determine reliability index β , the reliability software Comrel® is used. Fig. 2 and 3 show variation of β and the maximum load ratio q_k / g_k (6) with the span ratio α for the two extreme coefficients of correlation $\rho_{g1g2} = 0$ (independent permanent actions) and 1 (fully dependent permanent actions).

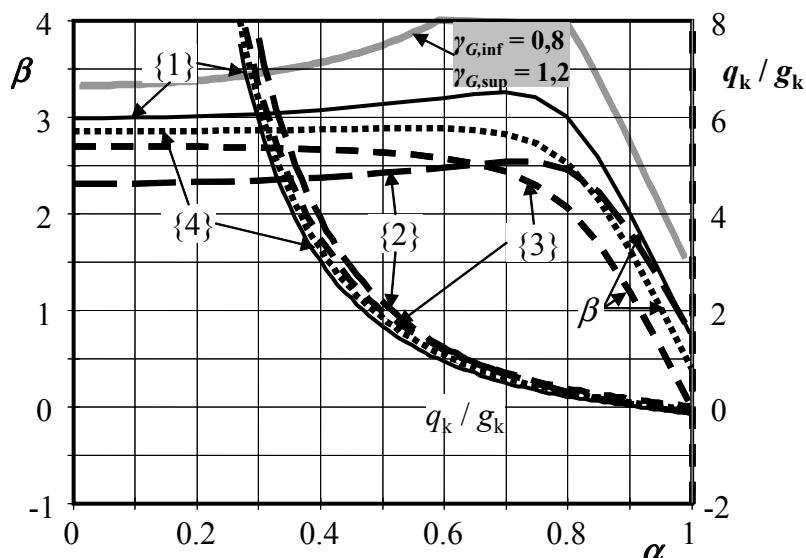


Fig. 2: Variation of the reliability index β (left-hand vertical axis) and the maximum load ratio q_k / g_k (right-hand vertical axis) with the span ratio α , for the partial factors sets {1}, {2}, {3}, {4} and $\rho_{g_1g_2} = 0$

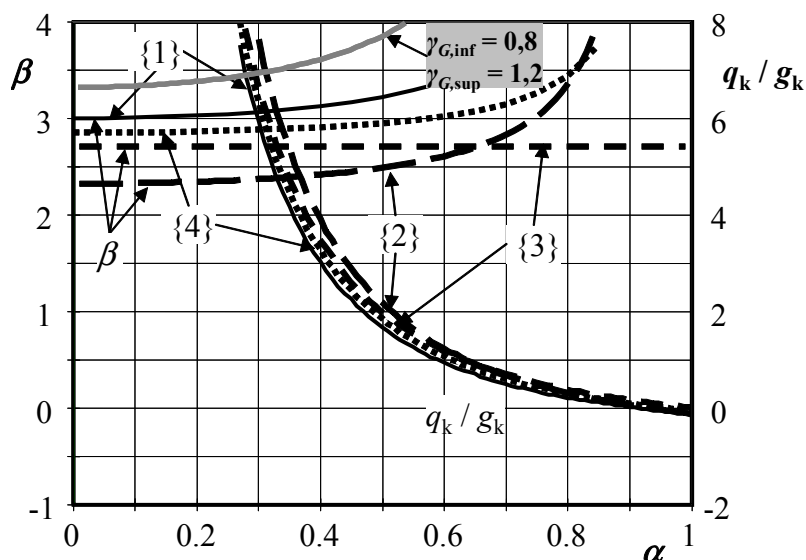


Fig. 3: Variation of the reliability index β and the maximum load ratio q_k / g_k with the span ratio α , for the partial factors sets {1}, {2}, {3}, {4} and $\rho_{g_1g_2} = 1$

It follows from Fig. 2 and 3 that the coefficient of correlation $\rho_{g_1g_2}$ may significantly affect the resulting reliability level only for span ratios α greater than 0,6. The recommended factors provide insufficient reliability level (β around 3). More conservative factors $\gamma_{G,inf} = 0,8$ and $\gamma_{G,sup} = 1,2$ are thus proposed for verification of common structures.

Note that the coefficient of variation for the permanent actions 0,08 (Tab. 2) represents an average value. It might be in some cases of transient design situation somewhat high, in other cases of permanent design situation slightly lower. Therefore, the above analysis provides indicative information that should be critically reviewed, particularly when a structural element is sensitive to the limit state of static equilibrium.

5 Motorway gantry

A motorway gantry supporting traffic information boards is another example of a structure to be verified for the limit state of static equilibrium. As obvious from Fig. 4, the gantry is subjected to the destabilizing wind load Q while the stabilizing action effects are due to the total self weight of the gantry and foundations G .

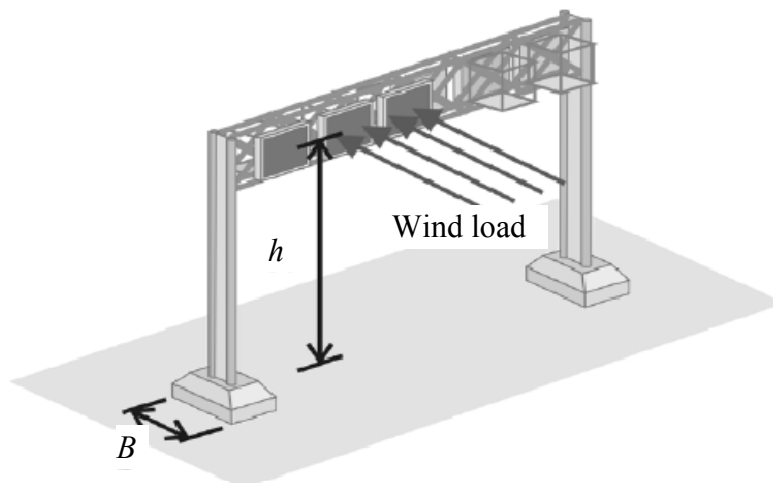


Fig. 4: A motorway gantry exposed to wind load

The limit state condition (1) can be written as

$$\gamma_Q Q_k h \leq 0,5 \gamma_G G_k B \quad (8)$$

with h the height of the gantry
 B width of the footing.

Note that earth pressure on foundations is neglected. The minimum footing width B follows from equation (8) as

$$B \geq \frac{2\gamma_Q Q_k h}{\gamma_G G_k} \quad (9)$$

It follows from equations (8) and (9) that the global safety factor against loss of static equilibrium is as in the previous example $s = \gamma_Q / \gamma_G < 2$. The limit state function can be written as

$$Z = 0,5BG - Qh \quad (10)$$

with B the minimum value obtained from equation (9).

The two random variables G and Q enter the limit state function (10). Their theoretical models, accepted from GULVANESSIAN and HOLICKÝ [4], are indicated in Tab. 3. Dimensions B and h are considered as deterministic quantities.

Tab. 3: Theoretical models of basic variables.

Basic variable	Symbol X	Distribu- tion	Characteristic value X_k	Mean μ_X	Standard deviation σ_X
Favourable permanent	G	Normal	G_k	G_k	$0,10G_k$
Unfavourable variable	Q	Gumbel	Q_k	$0,7Q_k$	$0,25Q_k$

Similarly as in the example of the cantilevered beam, reliability of the motorway gantry is analysed by the software Comrel®. It is shown that the reliability against the limit state of static equilibrium seems to be insufficient similarly as in the previous example. Fig. 5 shows variation of β and the minimum dimension ratio B/h (given by relationship (9)) with the load ratio Q_k/G_k for selected partial factors γ_G and γ_Q . The recommended factors for favourable permanent action $\gamma_G = 0,9$ and $0,95$ seem to provide insufficient reliability level (β around 3). More conservative value $\gamma_G = 0,8$ is proposed to be used in verification of common cases.

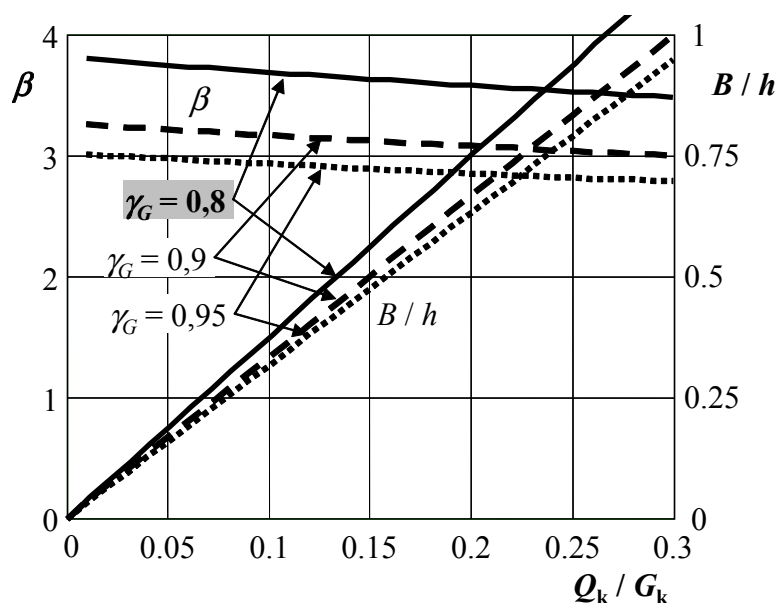


Fig. 5: Variation of the reliability index β and the minimum dimension ratio B/h with the load ratio Q_k/G_k for selected partial factors γ_G and γ_Q .

The example of motorway gantry confirms findings of the first example that the partial factors recommended presently for verification of the static equilibrium may lead to insufficient reliability levels (β significantly less than 3,8 for a reference period of 50 years). More conservative partial factor for unfavourable permanent actions $\gamma_{G,\text{inf}} = 0,8$ seems to be appropriate. However, in case of complicated and economically demanding structures, probabilistic reliability methods should be preferably applied.

6 Concluding remarks

The following concluding remarks can be drawn from the reliability study of static equilibrium of a cantilevered beam and motorway gantry:

- (1) Partial factors recommended in present codes of practice for verification of the limit state of static equilibrium correspond to the global safety factors lower than 1,7.
- (2) The partial factors recommended for verification of static equilibrium yield rather low reliability levels (obtained reliability index β around 3).
- (3) Different sets of partial factors may lead to considerably different reliability levels.
- (4) The reliability of a cantilevered beam depends on the coefficient of correlation between favourable and unfavourable permanent actions and on the span ratio.
- (5) With increasing coefficient of correlation the reliability level increases; particularly for span ratios greater than 0,6 the correlation affects significantly the resulting reliability.
- (6) For partial factor verification of the limit state of static equilibrium, more conservative partial factors for permanent actions are proposed (0,8 and 1,2).
- (7) In case of important and costly structures, probabilistic methods of structural reliability should be preferably applied; target reliability levels should be reviewed taking into account consequences of an equilibrium failure.

Acknowledgement. This study has been conducted at the Klokner Institute, Czech Technical University in Prague, Czech Republic, within the framework of the research project GA103/08/1527 Global safety formats for design of concrete structures supported by the Czech Science Foundation.

7 Literature

- [1] ISO 2394. 1998. General principles on reliability for structures. ISO.
- [2] EN 1990, 2002. Basis of structural design, CEN.
- [3] JCSS: Probabilistic model code. JCSS working materials, <http://www.jcss.ethz.ch/>, 2002.
- [4] Gulvanessian, H., Holický, M., 2005. Eurocodes: Using reliability analysis to combine action effects, Proceedings of the Institution of Civil Engineers, Structures and Buildings, Thomas Telford. August.

Integrative Reliability Assessment of Concrete Structures

Alfred Strauss, Konrad Bergmeister
Univ. of Natural Resources and Life Sciences, Vienna

Abstract: In structural engineering, the determination of the safety level at serviceability and at bearing capacity is essential during the design, construction and maintenance phases of a structure. Generally, safety levels are subject to a temporal change, as mechanical and chemical changes take place in material properties due to natural and man-made environmental impacts as well as changes in the applied actions (e.g. change of the user's behavior). In design codes, the level of safety is defined by means of semi-probabilistic safety concepts (SPSC) in order to cover uncertainties and unknown parameters of the design, construction and maintenance phases. The concepts of the partial safety and load combination factors guarantee a boundary of the safety level for a group of structure types (e.g. concrete structures or steel structures) and action types. In the integrative assessment structure-specific uncertainties and unknown parameters are analyzed in detail. This allows for a more realistic representation of the safety level due to the obtained additional information. The primary objective of this paper is to discuss the methodology of the integrative assessment for a highway bridge, which was abandoned in 2008. In particular, the reconstruction of the time course of the safety level during the entire life cycle of this bridge was carried out.

1 Introduction

In engineering there are well developed tools for the assurance of the planned lifetime. These tools have to be applied during different construction periods (i.e., during (a) design, (b) construction, and (c) maintenance). For instance, the already well established partial safety factor concept influences the design phases directly, by demanding minimum characteristic input quantities, limit state considerations (e.g. Ultimate Limit State (ULS) and Serviceability Limit State (SLS)), load combinations and special solution procedures. These concept is based on a philosophy that quarantines (a) at least a failure probability p_f smaller than 10^{-6} ($\beta \geq 4.7$) per year, as shown in Table 1, and (b) the reliability over the planned lifetime.

In addition, an *extended supervision*, will cause efforts and costs in design, production, and maintenance, but will also result at least in a failure probability p_{fe} smaller than 10^{-6} as characterized in EN1990 [1]. The integrative element of extended supervision allows the inclusion of structural specific properties. For instance, Table 1 portrays essential steps within the static modelling and (a) associated quantities and formats recommended for the

EN1990 based verification procedure, and (b) required efforts in design, production, maintenance, in order to meet specific supervision priorities.

In addition, the EN1990 code provides as an additional integrative element the *modification of the partial safety factors format* by a K_{FI} factor. The factor K_{FI} addresses the importance of the structure and the frequency of usage by consequence classes CC (see, Table 2). The consequence classes CC (RC) together with the inspection levels IL, shown in Table 3, yield the K_{FI} factor, which can be used for the reduction of the partial safety factor format of the resistance side (e.g., $K_{FI} = 0.9$ for RC1 and DSL 2) or for the increase in the safety.

Tab. 1: Design philosophy acc. to EN1990 and EN1992

Quantities	En19xx	Extended supervision in
Environment	Exposition classes	Design, Maintenance
Material	Characteristic values	Design, Production, Maintenance
Geometry	Characteristic values	Design, Production
Loads	Characteristic values	Design, Maintenance
Load Combinations	Service limit states	Design, Maintenance
	Ultimate limit states	
System Analysis	Linear / Non Linear	Design, Production, Maintenance
Design – Cross Section	Linear / Non Linear	Design, Production, Maintenance
Reliability, r	$r = 1 - p_f$; with $p_f \leq 1 \times 10^{-6}$	$r_e = 1 - p_{fe}$; with $p_{fe} \leq p_f$

Tab. 2: Consequence Classes based on the structural importance and frequency of usage acc. to EN1990

Frequency of usage	Importance		
	Low Greenhouses	Medium Hotels, Schools	High Convention
High	-	CC3	CC3
Medium	CC2	CC2	CC3
Low	CC1	CC2	CC3

Tab. 3: K_{FI} adjustment based on consequence classes and the inspection level acc. to EN1990

Consequence Classes	Inspection level		
	DSL 1 IL 1	DSL 2 IL 2	DSL 3 IL 3
RC 3 ($\beta = 5.2$)	-	$K_{FI} = 1.1$	$K_{FI} = 1.0$
RC 2 ($\beta = 4.7$)	-	$K_{FI} = 1.0$	-
RC 1 ($\beta = 4.2$)	$K_{FI} = 1.0$	$K_{FI} = 0.9$	-

The concept has to be considered as an indirect integrative element, since it does not address the measured quantities (e.g., material strength properties, environmental conditions) explicit but takes care on the demanded safety format and inspection level of a building. A higher level of integrative design with respect to the previous discussed concepts is provided by non linear computational methods and non linear computational methods combined with probabilistic methods [2]. The EN19xx family allows the application of non linear computational methods in design and maintenance, in order to capture the real behavior and the performance of new structures and existing structures at discrete time points and in consequence during their lifetime [3].

These methods differ from the former discussed code based methods in essential steps, for instance, in using (a) statistical based input properties, (b) incremental loading procedures, and (c) statistical based structural response assessment procedures (e.g., expressed by a reliability index β [4]) or a global safety format assessment, among others [5] (Table 4). Figure 1 shows some non-linear computed structures performed in cooperation with Cervenka Consulting. Non linear computational methods in the design, require the stipulation of load combinations, and the reinforcement in advance. Possible procedure for the non-linear analysis during design of engineering structures are given in [6].

Despite the high integrative capability of non linear analysis methods in capturing the real environmental and structural properties there is also an increase in the risk not to match the real properties and in consequence to cause an inescapable failure due to the loss of the safety margin guaranteed by the partial safety factor concept. Therefore, extended supervision and investigation of the explicit and implicit parameters necessary methods or procedures have to be associated with the previously discussed non linear analysis in order to reduce the risk caused due to misjudgement of input parameters. An efficient method in reducing the risk is the combination of probabilistic with NL computational analysis concepts as provided in the SARA tool [9].

Tab. 4: Principles of non linear computational methods acc. to EN1990 and EN1992

Quantities	En19xx	Non linear analysis
Environment	Exposition classes	Advanced models
Material	Mean values	e.g., ATENA [7]
Geometry	Characteristic values	
Loads	Characteristic values	Incremental load steps
Load Combinations	Service limit states	Incremental load steps
System Analysis	Linear / Non Linear	Reinforcement (e.g., adopted from a linear design procedure [8])
Cross Section Verification	Linear / Non Linear	Stress- Strain- fields, Cracks
Reliability, r	r expressed by a reliability index β [4]	Global Safety factor Cervenka et al.[5]

The probabilistic analysis is an element of the EN1990 and provides the structural response as statistical quantities. It allows the explicit computation of the failure probability p_f comparing action characteristics S with the associated resistance characteristics R . In consequence, an increased risk due to a non linear analysis can be faced (a) by the treatment of input parameters as disperse quantities, (b) the detection of the contribution of input parameters on the structural response using the probabilistic based sensitivity analysis, (c) the adjustment of the failure probability due to enhanced investigation of disperse input parameters. Finally, the previously discussed five methods are presented in Table 5 with respect to (a) the integrative aspects (e.g., incorporation of the structural specific properties originating from environment, material, production among others) and (b) the analyses associated risk. The medium and high integrative of the non linear and the probabilistic analysis is evident. Nevertheless, the non linear analysis bears an additional risk in misinterpreting of input parameters, whereas this risk can be reduced by a probabilistic analysis.

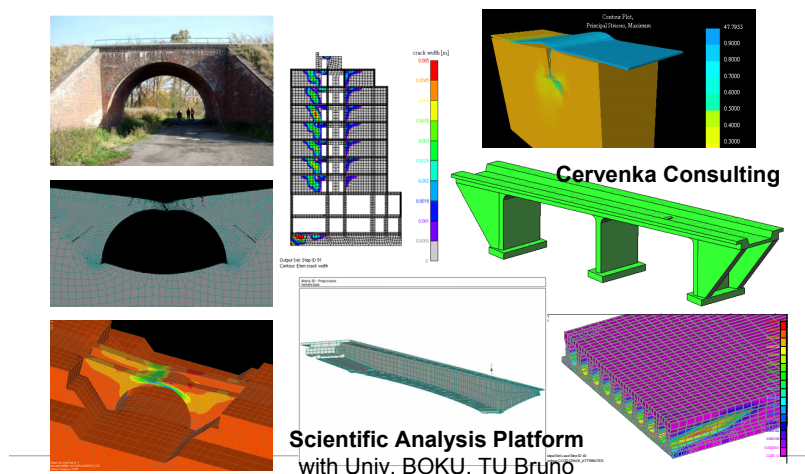


Fig. 1: Typical examples of non linear computed structures (adopted from [7])

Tab. 5: Integrative level and associated risk of design methods

Analysis technique	Integrative level	Risk, R_i
EN19xx	low	constant
EN, extended supervision (ES)	low	decrease
EN19xx, K_{FI} adjustment (K_{FI})	moderate	constant
EN19xx, Non linear analysis (NA)	medium	increase
EN19xx, Probabilistic analysis (PA)	high	decrease

2 Verification of the integrative level

The previously described methods will have a direct effect on the time horizon and the associated costs. In consequence, the cost quantities will affect the decision for one of the methods. For instance, Table 6 presents in a quantitative manner costs associated with design, production and maintenance with respect to the traditional code design (0-Variant).

The cost associated efforts will have an effect on the failure probability and in consequence on the risk, as shown in the last two rows of Table 6. In general the constants in cost due to accidental failure can be assumed constant except the K_{FI} adjustment method according to EN1990, which focuses on the importance of the structure and the frequency in use. Furthermore, monitoring will effect next to the additional cost the failure probability and in consequence the risk. Therefore, decision guidance needs the incorporation of accident failure cost or risk based failure cost as presented in Table 6. The sum of these costs can be used to compute a benefit factor with respect to the 0-Variant cost of the traditional code design. Finally the highest benefit, B (at least larger equal 0) from one of the five methods will argue for its application.

Tab. 6: Benefit based decision guidance

Cost		Analysis method				
		EN	ES	K_{FI}	NA	PA
Design, C_D	Detailing	0 Variant	S	S	A	A
	Computation		S	S	A	A
Production, C_P	Conformity		S	S		
	Structure		S	S		
Maintenance, C_M	Detailing		S			
Monitoring, C_{Mo}						
Failure Probability, p_f		0.9	0.4 – 0.9	0.9	0.9 – 1.1	0.4 – 0.9
Accident-Failure, C_A		1.0	1.0	0.5 – 1.2	1.0	1.0
Risk, $R_i = C_A \times p_f$		0.9	0.4 - 0.9	0.4 – 1.1	0.9 – 1.1	0.4 – 0.9
$C^x = C_D + C_P + C_M + C_{Mo} + R_i$		C^0	C^{ES}	C^K	C^{NA}	C^{PA}
Benefit, $B = 1 - C^x/C^0$		0	B^{ES}	B^K	B^{NA}	B^{PA}

S = efforts in supervision, A = efforts in analysis

3 Application

Marktwasser Bridge is a foreshore bridge leading to a Danube-crossing which is currently being built. Although initially conceived as ordinary bridge with bearings and expansion joints the design was redone to meet the changed specifications issued by the building-owner, who wanted to explore the possibilities a jointless design provides – namely reduced costs in maintenance and reduction of traffic obstructions during necessary construction work.

Marktwasser bridge is a three span continuous plate structure with spans of 19.50 m, 28.05 m and 19.50 m respectively consisting of two separate structures for both directions, one accommodating 2, the other one 5 lanes. Subsequently only the latter is considered. Figure 2 show the 2D FEM and the reinforcement layout of one half of the discussed structure. Apart from being built without pre-stressing the main aspects of design are a crossing angle of 74° between center-line and integral abutments, a deck width of around 19.37 m excluding two cantilevers of 2.5 m each and a construction height of 1.0 m. Around both middle supports the deck shows a haunch going from 1.0 m to a total of 1.6 m to account for the negative bending moment. In the following investigation the structure was loaded by a constant temperature field of 15° K, since a monitoring system has been installed for the assessment of the structure during design and the first year out of traffic.

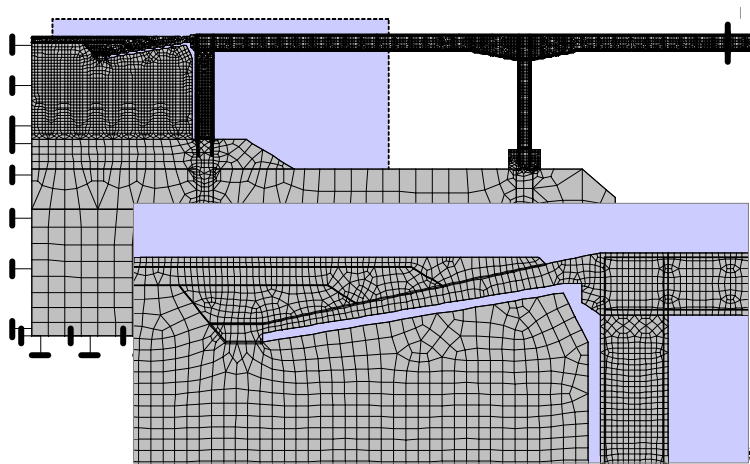


Fig. 2: Details of the FEM layout of the Marktwasser-Bridge S33.24

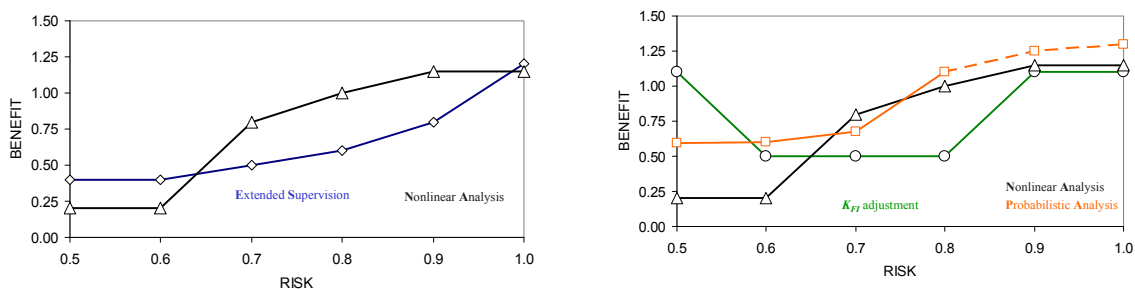


Fig. 3: Benefit versus Risk of the nonlinear analysis and the code based analysis using an extended supervision concept

In a first approach, there was a high in interest in the selection of the most efficient analysis method in order to capture the realistic structural behavior and the existing risk. Based on the cost data and cost analysis performed within the diploma thesis of Hirute Abebe [10] a benefit analysis shown in Table 6 has been performed for the five previously discussed analysis methods. The risks are normalized with respect to the maximum. The analysis demonstrated, as shown in Fig.3, an explicit relationship between an increase in benefit and the increase in risk for (a) the extended analysis, (b) the NL analysis, and (c) the probabilistic analysis. In particular, the probabilistic analysis indicates the most benefit with respect to the risk range of the Marktwasser Bridge. The benefit-risk distribution of the probabilistic analysis is portrayed only up to a 0.8 risk quantity, since the probabilistic analysis will be used (e.g. detailed investigation of the random input quantities) to reduce the risk instead of maximizing the benefit in this risk region.

In addition to the previous performed comparison of analyses methods with respect to the benefit, it was of interest to investigate the effect of inspection or production level, which can be expressed by the coefficient of variations (COV) of random variables, on the risk and in consequence on the benefit. The model used for the probabilistic analysis and its stochastic parameters are presented in Figure 4. The investigation focused on the structural behavior loaded by its body weight and the temperature gradient of 15°C.

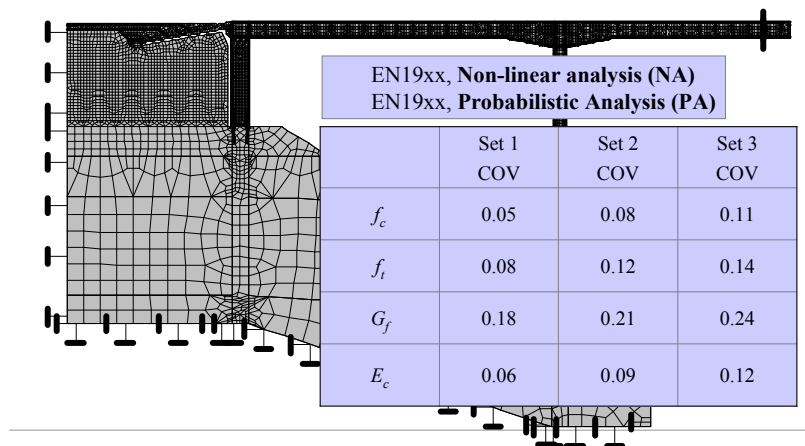


Fig. 4: Probabilistic Model of the Marktwasser-Bridge S33.24

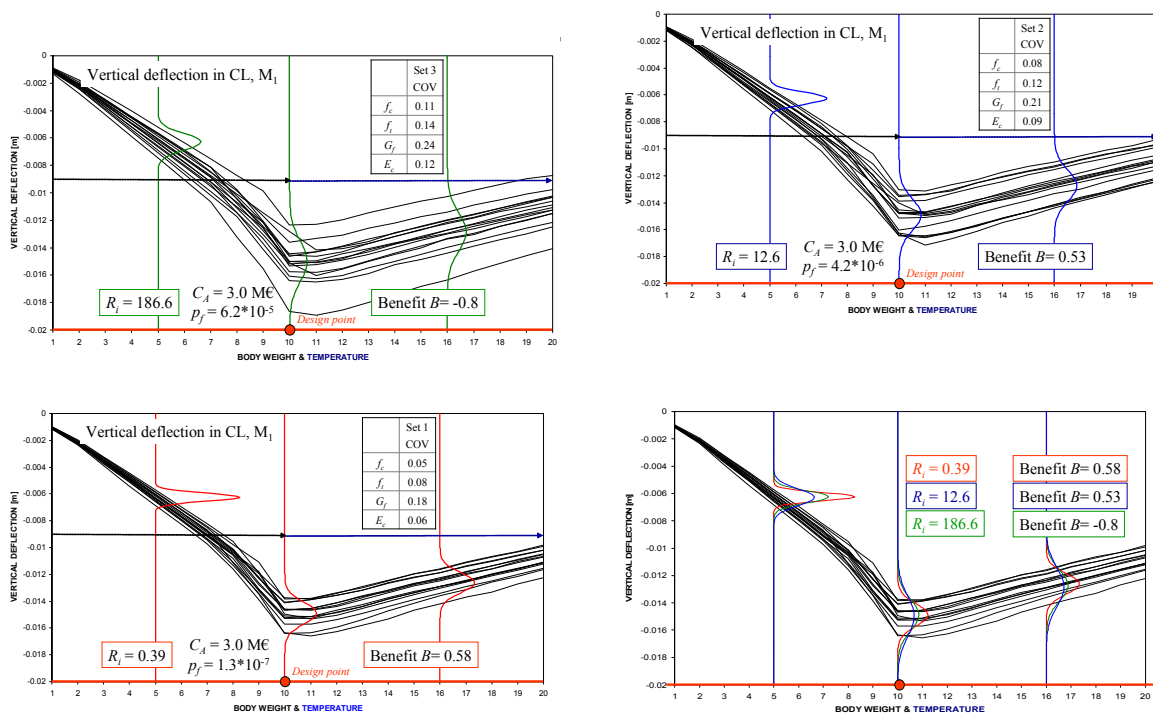


Fig. 5: Risk, failure probability and benefit with respect to the vertical deflection in the Centerline of the Marktwasserbridge using the third stochastic set of random variables

The investigation assumed a vertical deflection of 20 mm in the centreline (CL) of the structure as critical resistance (R) for a service limit state consideration. The results showed a clear increase in benefit from -0.8 to 0.58 (see Figs.5) with increasing inspection or production control, which is indicated by smaller disperse stochastic models. Neverthe-

less, the decreasing increment between the stochastic set 2 and 1 indicates an movement towards the optimum. A more precise inspection or production restrictions (e.g., smaller variation in stochastic quantities) will decrease the benefit due to higher costs in design, production and inspection.

4 Conclusions

There are several procedures and analyses methods available for the design and layout of new engineering structures and the assessment of existing engineering structures according to the new EN Code family. Nevertheless, in many cases users are not aware about the integrative ability of the methods and the associated risks. This paper presents an benefit based approaches for the effective selection of analysis methods, and the verification of proper inspection and monitoring procedures.

5 References

- [1] EN1990: Eurocode - Basis of structural design *EN 1990*. Brüssel, Belgium (2002):.
- [2] Strauss, A.; Bergmeister, K.; Hoffmann, S.; Pukl, R.; Novak, D.: Advanced life-cycle analysis of existing concrete bridges. *J Mater Civil Eng*, 20, (2008): pp. 9-19.
- [3] Bergmeister, K; Novak, D; Pukl, R; Cervenka, V.: Structural assessment and reliability analysis for existing engineering structures, theoretical background. *Struct Infrastruct Eng.*, 5(4), (2009) pp. 267-275.
- [4] Zilch, K; Zehetmaier, G.: Bemessung im konstruktiven Betonbau. Nach DIN 1045-1 und DIN EN 1992-1-1. 2. Auflage, Berlin: Springer, (2008).
- [5] Cervenka V.: Global Safety Format for Nonlinear Calculation of Reinforced Concrete structures. Ernst&Sohn, Berlin, *Beton und Stahlbetonbau* 103, Special Edition. (2008) pp.37-42.
- [6] Strauss, A.; Bergmeister, K.; Wendner, R.; Lehky, D.; Novak, D.; Pukl, R.: Risked based design aspects for concrete structures. In: Austrian Society for concrete- and Construction Technology, *Innovative concrete Technology in Practice* (2009).
- [7] Červenka V, Červenka J, Pukl R.: “ATENA – an Advanced Tool for Engineering Analysis of Connections. Connections between Steel and Concrete,” *RILEM Publications Ens France* 2001; pp. 658-667.
- [8] Strauss, A.; Geier, R.; Wendner, R.; Bergmeister, K.; Frangopol, D.: Integrale Brücken und deren Zuverlässigkeitsaspekte unter Einbeziehung von Monitoring. In: Jürgen Feix, Andreas Andreatta, *Innsbrucker Bautage 2009, Innsbrucker - Massivbau und Brückenbau*, Band 3; ISBN: 978-3-902571-98-4.
- [9]. Bergmeister, K.; Novak, D.; Strauss, A.; Pukl, R.: Structural Analysis and Reliability Assessment, SARA Part I. In: Baidar Bakht, Aftab Mufti, *Structural health Monitoring and Intelligent Infrastructure, ISHMII, The 3rd International Conference on Structural Health Monitoring of Intelligent Infrastructure*, November 14 - 16, 2007, Vancouver.
- [10] Hirute, A. Cost model comparison for concrete structures. Master Thesis, Department für Bautechnik + Naturgefahren; Universität für Bodenkultur; (2009) (in progress)

Part III

Theoretical advances in Probabilistic Modelling

Determination of design spectrum compatible evolutionary spectra via Monte Carlo peak factor estimation

Agathoklis Giaralis¹, Pol D Spanos²

¹School of Engineering and Mathematical Sciences, City University, London, UK

²George R. Brown School of Engineering, Rice University, Houston, TX, USA

Abstract: The problem of generating ensembles of artificial non-stationary earthquake accelerograms compatible with a given (target) response/design spectrum is cast on a stochastic basis. The design spectrum of the European aseismic code provisions (EC8) for various soil conditions and damping ratios is used as a paradigm of a design/target spectrum. The generated accelerograms are construed as realizations of a non-stationary random process; they are characterized in the frequency domain by a parametrically defined evolutionary power spectrum (EPS). An appropriate least squared optimization problem is formulated for the determination of the parameters of the EPS. The solution of this problem involves the incorporation of a “peak factor” which is used to relate the target spectrum to the EPS in a probabilistic context. To this end, a comprehensive Monte Carlo study is undertaken to estimate numerically the statistical properties of the peak factor from appropriately computed populations, and to derive polynomial expressions for the median frequency-dependent peak factors (peak factor spectra). These expressions are used in conjunction with the herein adopted optimization problem to determine EPSs compatible with the EC8 design spectrum. The derived median peak factor spectra yield an excellent level of agreement between the EC8 spectrum and the ensemble average and median response spectra of simulated EPS-compatible ensembles of accelerograms.

1 Introduction

Typical dynamic loads applied to various structured facilities by the natural environment such as those associated with the action of earthquakes, winds and sea waves exhibit an inherent level of uncertainty. This uncertainty can be readily incorporated in structural design procedures by representing the induced dynamic loads in a statistical manner via the concept of a stochastic process.

Note that, contemporary code provisions regulating the aseismic design of structures represent the input seismic loads by means of analytically defined response/design spectra (e.g. [4]). This practice allows for considering linear dynamic response-spectrum based types of analyses which significantly facilitates the design of ordinary structures (e.g. [5]). Nevertheless, by its definition, a design spectrum neither corresponds to an individual earthquake record associated with a certain seismic event nor to a specific stochastic process. In this respect, design spectra cannot be straightforwardly considered in conjunction with dynamic time-history analyses which involve the complete knowledge of the acceleration trace (accelerogram) of the motion of the ground. The incorporation of these kinds of analyses is commonly mandated by regulatory agencies in the design of special structures and facilities of critical importance. In this context, aseismic code provisions require the representation of the seismic severity by means of suites of design spectrum compatible accelerograms. That is signals whose average response spectrum is in agreement with a prescribed (elastic) design spectrum satisfying specific “compatibility criteria”. Such accelerograms can be derived either by manipulation of field recorded ground motions, or by generation of time-histories belonging to an appropriately defined stochastic process which is consistent with the given design spectrum (see e.g. [7], [25] and references therein).

To this end, various researchers have proposed methods to relate a response/design spectrum to a power spectrum characterizing a stationary stochastic process (e.g. [8]; [17]; [16]). This relation necessitates the consideration of the so-called “peak factor” which is closely associated with the first passage problem of the response of stochastically excited linear single-degree-of-freedom (SDOF) systems (see e.g. [26]). Obviously, assigning a stationary process to a response/design spectrum involves a rather restrictive limitation in dealing with an inherently non-stationary phenomenon (i.e. the strong ground motion during a seismic event). Nevertheless, a very limited number of research studies have considered the case of relating an evolutionary power spectra (EPS) characterizing a non-stationary random process to a given response/design spectrum. The main difficulty in this case, is that no reliable expressions for the peak factor exists. Certain previous studies (e.g. [10]; [27]; [20]; [11]; [12]) have provided numerical results associated with the peak response and the first passage problem of linear SDOF systems excited by non-stationary input processes. However, the considered input EPSs have been somewhat arbitrarily selected as either modulated white noise, or colored noise having a boxcar envelop function. Obviously, these forms of EPSs have limitations in modelling seismic acceleration processes.

In this study, a formulation originally proposed by SPANOS and VARGAS LOLI [23] and recently extended by GIARALIS and SPANOS [7] and SPANOS et al. [25] is adopted to relate a parametrically defined EPS to the design spectrum prescribed by the European code provisions (EC8) [4]. It involves the solution of an inverse stochastic dynamics problem and necessitates the consideration of a peak factor. The adopted parametric form of the EPS is used as a mathematical instrument to facilitate the solution of the aforementioned problem and to capture adequately the main features of the EC8 spectrum. Upon determining of the EPS, an efficient filtering technique is employed to generate EC8 design spectrum compatible non-stationary artificial accelerograms. Further, a comprehensive Monte Carlo analysis is undertaken to estimate the statistical features of the peak factor and of other quantities of engineering interest associated with the first passage problem for non-stationary excitations compatible with the EC8 design spectrum. Special attention is focused on deriving frequency and damping dependent median peak factors compatible with

the EC8 spectrum. These are incorporated in the aforementioned formulation to achieve enhanced level of compatibility of the derived artificial accelerograms with the EC8 spectrum compared to the previous study of GIARALIS and SPANOS [7] which have assumed a constant peak factor value. The level of compatibility is assessed by comparison of the average and the median response spectra of ensembles of the generated artificial signals with the EC8 design spectrum.

2 Theoretical Background

2.1 Relation of an evolutionary power spectrum to a design spectrum

Let the acceleration process $u_g(t)$ of the ground motion due to a seismic event be modelled as a uniformly modulated non-stationary stochastic process. That is,

$$u_g(t) = A(t)y(t), \quad (1)$$

where $A(t)$ is a deterministic time dependent envelop function and $y(t)$ is a zero-mean stationary stochastic process. The exponential modulated function [1]

$$A(t) = Ct \exp\left(-\frac{b}{2}t\right), \quad (2)$$

is adopted herein to model the non-stationary features of the strong ground motion intensity exhibited by typical field recorded seismic accelerograms. The parameter $C > 0$ is proportional to the intensity of the ground acceleration process while the parameter $b > 0$ controls the shape of the envelope. Assuming that $A(t)$ varies slowly with time, the process $u_g(t)$ can be characterized in the frequency domain via a two-sided evolutionary power spectrum (EPS) $G(t, \omega)$ given by the expression [18]

$$G(t, \omega) = |A(t)|^2 Y(\omega). \quad (3)$$

In the latter equation $Y(\omega)$ denotes the power spectrum of the stationary stochastic process $y(t)$. In this study, the Clough-Penzien (CP) spectrum given by the expression [6]

$$Y(\omega) = \frac{1 + 4\zeta_g^2 \left(\frac{\omega}{\omega_g}\right)^2}{\left(1 - \left(\frac{\omega}{\omega_g}\right)^2\right)^2 + 4\zeta_g^2 \left(\frac{\omega}{\omega_g}\right)^2} \frac{\left(\frac{\omega}{\omega_f}\right)^4}{\left(1 - \left(\frac{\omega}{\omega_f}\right)^2\right)^2 + 4\zeta_f^2 \left(\frac{\omega}{\omega_f}\right)^2} \quad (4)$$

with $|\omega| \leq \omega_b$.

is considered, where ω_b is a cut-off frequency beyond which $Y(\omega)$ attain negligible values of no engineering interest. This is a widely used phenomenological model which accounts

for the influence of the surface soil deposits on the frequency content of the propagating seismic waves via the effective stiffness (ω_g) and damping (ζ_g) parameters. The parameters ω_f and ζ_f control the properties of the high-pass filter incorporated by the model to suppress the low frequencies (see also [7]).

Furthermore, consider a linear quiescent unit-mass SDOF system, with ratio of critical viscous damping ζ_n and natural frequency ω_n , base-excited by the acceleration process $u_g(t)$. The relative displacement response process $x(t)$ of this system with respect to the motion of its base is governed by the equation

$$\ddot{x}(t) + 2\zeta_n\omega_n\dot{x}(t) + \omega_n^2x(t) = -u_g(t) \quad ; \quad x(0) = \dot{x}(0) = 0, \quad (5)$$

in which a dot over a symbol denotes time differentiation. Focusing on lightly damped systems (i.e. $\zeta_n < 0.1$), the response $x(t)$ is assumed to be a narrow-band process. In this case the time-evolving variance of the response process $x(t)$ can be replaced by the variance $\sigma_a^2(t)$ of its amplitude [21]. A reliable expression for the latter quantity reads [22]

$$\sigma_a^2(t) = \frac{\pi}{\omega_n^2} \exp(-2\zeta_n\omega_n t) \int_0^t \exp(2\zeta_n\omega_n \tau) G(\tau, \omega_n) d\tau. \quad (6)$$

In the practice of aseismic design of structures often only a relative displacement design spectrum $S_d(\omega_n, \zeta_n)$ is provided to the designer for the definition of the input seismic severity. This design spectrum is not related to any specific EPS. Clearly, an “inverse” stochastic dynamics problem must be considered to relate an EPS $G(t, \omega)$ defined by Eqs. (2)-(4) to a given design spectrum $S_d(\omega_n, \zeta_n)$. Following SPANOS and VARGAS LOLI [23], this problem can be formulated by relying on the equation (see also [7])

$$S_d(\omega_n, \zeta_n) = r(\omega_n, \zeta_n, G, p) \max_t \{ \sigma_a(t, \omega_n, \zeta_n, G) \}. \quad (7)$$

In Eq. (7) the so-called “peak factor” r is the critical parameter establishing the equivalence between the given design spectrum S_d and the EPS G to be determined in a statistical manner (see e.g. [26]). Essentially, it corresponds to the scalar by which one needs to multiply the peak standard deviation of the response amplitude (assumed to be equal to the peak standard deviation of the response process x) attained at some time instant $t_{max\ var}$ to reach a certain peak response level S_d with probability p . In general, the peak factor depends on the properties ζ_n and ω_n of the considered SDOF system and on the EPS of the input strong ground motion. Further discussion on the peak factor is included in sections 3.2 and 3.3 in light of numerical data obtained from Monte Carlo simulations for input EPSs associated with the design spectrum of the European aseismic code regulations [4].

An approximate point-wise solution of the inverse problem of Eq. (7) can be obtained by minimizing the error [7]

$$e = \sum_{j=1}^{2M} (S_j - q_j)^2 \quad (8)$$

$$\text{with } S_j = \begin{cases} S_d^2(\omega_{n(j)}, \zeta_n) & , j = 1, \dots, M \\ 0 & , j = M + 1, \dots, 2M \end{cases}$$

$$q_j = \begin{cases} \frac{r^2 \pi C^2 t_j^{*2} \exp(-bt_j^*)}{2\zeta \omega_{n(j)}^3} Y(\omega_{n(j)}) & , j = 1, \dots, M \\ \gamma_{j-M}^2 (2t_{j-M}^* - bt_{j-M}^{*2}) - 2\gamma_{j-M} (1 - bt_{j-M}^*) - \\ -2b + 4\zeta_n \omega_{n(j-M)} \exp(-\gamma_{j-M} t_{j-M}^*) & , j = M + 1, \dots, 2M \end{cases}$$

$$\gamma_j = 2\zeta_n \omega_{n(j)} - b$$

at a certain set of M natural frequencies $\{\omega_{n(j)}\}$ for $j=1, \dots, M$, where the symbol t_j^* denotes the time instant at which the variance $\sigma_a^2(t)$ corresponding to the linear SDOF system with natural frequency $\omega_{n(j)}$ is maximized. In all ensuing numerical results, a Levenberg-Marquardt algorithm with line search (see e.g. [14]) is used to solve the over-determined nonlinear least-square fit optimization problem of Eq. (8) for the unknown parameters $C, b, \omega_g, \zeta_g, \omega_f, \zeta_f$ of the herein adopted EPS form.

2.2 Simulation of design spectrum compatible seismic accelerograms

Clearly, an EPS $G(t, \omega)$ obtained as discussed in the previous section defines a non-stationary process $u_g(t)$ whose realizations achieve a certain level of compatibility with the given design spectrum S_d . In particular, it is expected that generated non-stationary time-histories compatible with such an EPS will constitute seismic accelerograms whose response spectra will lie close to the design spectrum S_d . Such accelerograms can be numerically generated by first synthesizing stationary discrete-time signals as sampled versions of the continuous-time stochastic process $y(t)$ appearing in Eq. (1). That is,

$$y[s] = y(sT_s) \quad , \quad s = 0, 1, \dots, N, \quad (9)$$

$$\text{with } T_s \leq \frac{\pi}{\omega_b} \text{ sampling interval}$$

where N should be selected appropriately so that $A(NT_s)$ is negligible. Next, these stationary records are multiplied individually by the corresponding discrete/sampled version of the envelop function defined in Eq. (2) to obtain the final artificial records with non-stationary intensity as Eq. (1) suggests.

In this study, stationary discrete-time signals $\tilde{y}[s]$ are synthesized by filtering arrays of discrete-time Gaussian white noise $w[s]$ with a two-sided unit-intensity power spectrum band-limited to ω_b through an autoregressive-moving-average (ARMA) filter of order (m, n) . In a practical numerical implementation setting these arrays comprise pseudo-

random numbers belonging to a Gaussian distribution with zero mean and variance equal to $\sqrt{2\omega_b}$. The aforementioned filtering operation is governed by the difference equation

$$\tilde{y}[s] = -\sum_{k=1}^m d_k \tilde{y}[s-k] + \sum_{l=0}^n c_l w[r-l], \quad (10)$$

in which c_l ($l=0,1,\dots,n$) and d_k ($k=1,\dots,m$) are the ARMA filter coefficients. Herein, the auto/cross-correlation matching (ACM) method is adopted to determine these coefficients so that the power spectrum of the process $\tilde{y}[s]$ matches the CP spectrum $Y(\omega)$ of the process $y[s]$. In this manner, the process $\tilde{y}[s]$ can reliably model the process $y[s]$. The mathematical details of the ACM method can be found in [24].

It is further noted that the non-stationary artificial records generated as discussed above are further processed to address the issue of baseline correction (e.g. [2]). This is accomplished efficiently by appropriate zero-padding and forward/backward filtering of the records using a standard Butterworth high-pass filter of order 4 and cut-off frequency 0.10Hz [3].

3 Numerical results pertaining to the EC8 design spectrum

For the purposes of this study, a Monte Carlo analysis to estimate the statistical properties of the peak factor r appearing in Eq. (7) associated with the EC8 design spectrum is performed [4]. Specifically, CP evolutionary power spectra (EPSs) compatible with the EC8 design spectrum for peak ground acceleration (PGA) of 0.36g ($g=9.81 \text{ m/sec}^2$), for three different damping ratios $\zeta_n=2\%$, 5%, and 8% and for all five soil conditions prescribed by the EC8 are considered: a total of 15 EPSs. These have been obtained as discussed in section 2.1 assuming a constant peak factor $r=\sqrt{3\pi}/4$ (see also [7]).

For each of the thus obtained EPSs a suite of 10000 spectrum-compatible non-stationary artificial accelerograms has been generated and base-line adjusted as described in section 2.2. Next, each suite is “fed” to a series of 200 linear SDOF systems with natural periods ranging from 0.02sec to 6sec. The damping ratio of these systems is set to coincide with the value of ζ_n considered in deriving each of the EPS from the corresponding EC8 spectrum. For every such system defined by the properties $T_n=2\pi/\omega_n$ and ζ_n and excited by a specific suite of accelerograms the response ensembles $(x^{(k)}(t); k=1,2,\dots,10000)$ are calculated via numerical integration of Eq. (5) [13]. Finally, populations of peak factors ($r^{(k)}; k=1,2,\dots,10000$) are computed from the above ensembles as the ratio of the population of peak responses over the maximum standard deviation of the response ensemble. That is,

$$r^{(k)}(T_n, \zeta_n, G) = \frac{\max_t \{ |x^{(k)}(t, T_n, \zeta_n, G)| \}}{\max_t \left\{ \sqrt{E \left\{ \left(x^{(k)}(t, T_n, \zeta_n, G) \right)^2 \right\}} \right\}}. \quad (11)$$

It is important to note that these peak factor populations are independent of the intensity of the excitation. Thus, they are neither influenced by the adopted PGA value assumed in the

derivation of the 15 considered EPSs nor by the value of the constant peak factor $\sqrt{3\pi/4}$ involved in this derivation. However, they do reflect the different spectral contents and effective durations (as controlled by the b parameter of Eq. (2)) of the various G EPSs; certainly they depend strongly on the dynamical properties (T_n, ζ_n) of the SDOF system considered.

3.1 Monte Carlo analysis of peak response time instants

In the course of computing the denominator of Eq. (11) two quantities need to be considered. First, is the peak value of the mean square of the response ensembles (equal to the variance since the simulated signals are base-line corrected to have zero mean value). Second is the time $t = t_{max\ var}$ at which this value is attained. Fig. 1 provides plots of both of these quantities as functions of the natural period of the SDOF systems considered for damping ratio $\zeta_n = 5\%$ for the five EC8 soil types. The spectral shapes of the variance (Fig. 1(a)) are similar to the EC8 displacement design spectrum (see [4]). And, as more flexible oscillators are considered the maximum response variance is reached at later times.

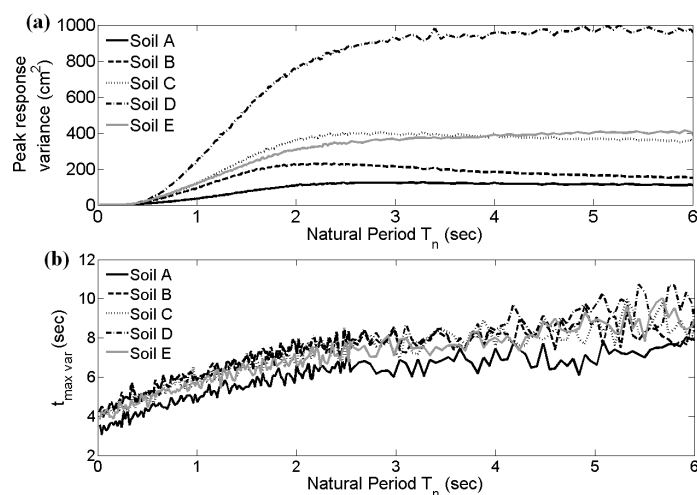


Fig. 1: Peak variances and time instants $t_{max\ var}$ at which these peak values are attained for the response ensembles pertaining to EC8 spectrum compatible EPSs for PGA= 0.36g reported in [7] ($\zeta_n = 5\%$). Ensemble includes population: 10000.

Furthermore, the computation of the numerator of Eq. (11) involves the calculation of the time instants $t_{max|x|}$ at which the peak value of each response time-history is attained. Fig. 2 shows certain plots associated with the statistical properties of the $t_{max|x|}$ populations normalized by the $t_{max\ var}$ time instants for $\zeta_n = 5\%$. Specifically, Fig. 2(a) and 2(b) plots the average and standard deviation, respectively, of these populations for all EC8 soil conditions as a function of natural period. The average spectra fluctuate around unity with small dispersion for all soil types, although a noticeable trend of linear decrease towards the longer periods exists. This result agrees with the intuition which suggests that the time instants at which the peak response and the peak response variance are obtained should be in a close agreement, on the average. Nevertheless, the standard deviation spectra reveal that there is a significant dispersion in the population of the samples (10000 for each oscillator). To

further elucidate this point, six histograms of such populations related to certain oscillators and the corresponding fitted gamma distributions (solid lines) are shown in Fig. 2. It is reported that in general the gamma distribution yielded the best parametric fitting results based on a standard maximum likelihood estimation algorithm. The gamma distribution of a random variable z reads [15]

$$f(z/\kappa, \theta) = \frac{1}{\theta^\kappa \Gamma(\kappa)} z^{\kappa-1} \exp\left(-\frac{z}{\theta}\right), z \geq 0 \quad (12)$$

$$\text{where } \Gamma(\kappa) = \int_0^\infty \exp(-t) t^{\kappa-1} dt,$$

and κ , θ are the “shape” and “scale” parameters, respectively. Similar results as the above have been observed for response ensembles corresponding to $\zeta_n=2\%$ and 8% not presented here for brevity.

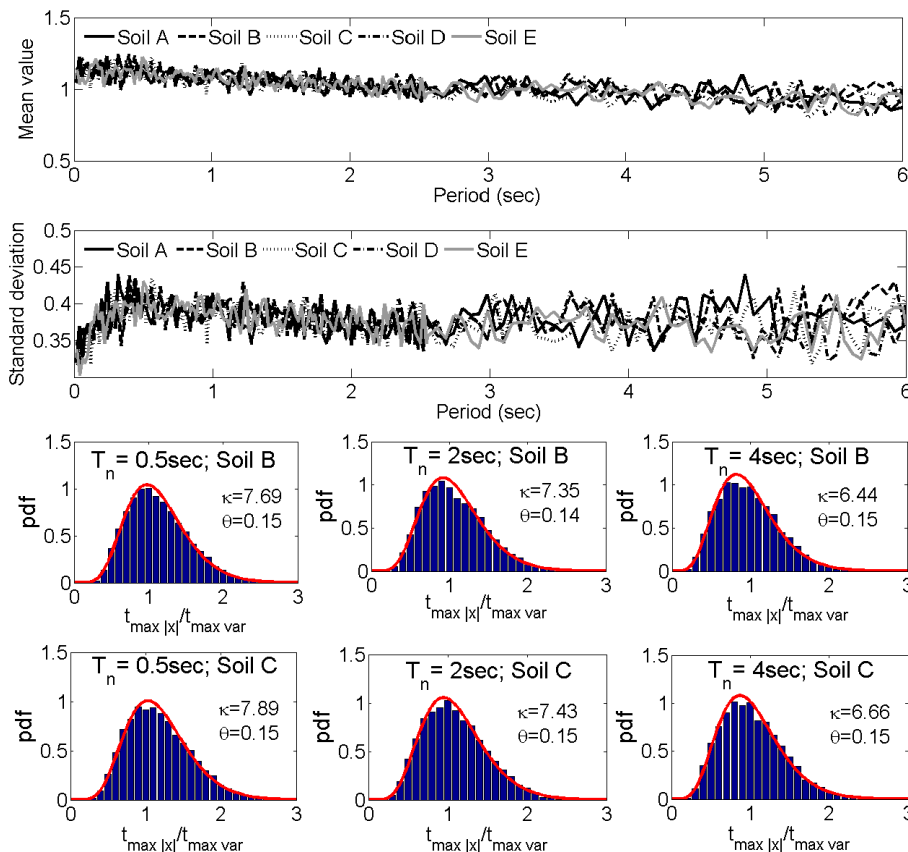


Fig. 2: Mean value spectra, standard deviation spectra, and histograms of populations of time instants $t_{\max|x|}$ at which the peak response is observed normalized by the time instants $t_{\max \text{ var}}$ at which the peak response variance is attained. The considered response ensembles are the same as in Fig. 1.

3.2 Monte Carlo analysis of peak factors

Fig. 3 collects similar results as in Fig. 2 corresponding to peak factor populations calculated by Eq. (11). In particular, the median of the peak factors plotted against the natural

period (median peak factor spectra) for all the EC8 soil conditions and for $\zeta_n = 5\%$ are shown in Fig. 3(a). These spectra possess a significant merit for the purposes of this study. Specifically, when substituted in Eq. (7) the following criterion between a design/response spectrum S_d and an EPS G is established: considering an ensemble of non-stationary samples compatible with G (i.e. generated as described in section 2.2), half of the population of their response spectra will lie below S_d (i.e. S_d is the median response spectrum). Consequently, the probability of exceedance p appearing in Eq. (7) becomes equal to 0.5. Evidently, the median peak factor possesses a complicated dependence with the natural period of linear SDOF oscillators. Interestingly, similar trends have been previously reported in the literature (see Fig. 8.17 and 8.18 in [26]). From a practical viewpoint, the most important conclusion drawn from Fig. 3(a) is that the various shapes of the underlying evolutionary power spectrum corresponding to the different EC8 shapes of the design spectrum depending on the soil conditions has a minor effect on the median peak factor spectrum. In other words, the five curves of Fig. 3(a) lie very close to each other.

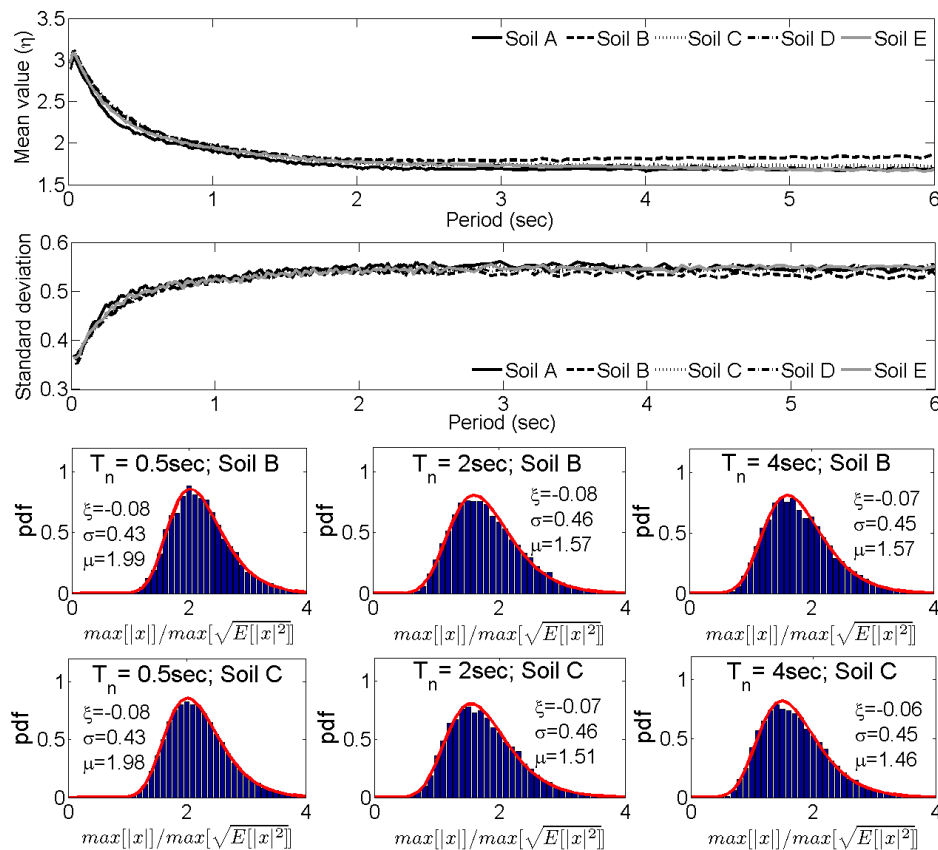


Fig. 3: Median spectra, standard deviation spectra, and histograms of populations of peak responses normalized by the peak ensemble standard deviation. The considered response ensembles are the same as in Fig. 1.

It is further noted, that the standard deviation of the peak factor populations is certainly non-negligible and it also varies for natural periods up to 1sec approximately. Then it attains a practically constant value. Moreover, histograms of peak factor populations have

been included in Fig. 3 related to certain oscillators and input EPSs. Generalized extreme value distributions given by the equation,

$$f(z/\xi, \sigma, \mu) = \frac{1}{\sigma} \exp\left(-\left(1 + \xi \frac{z - \mu}{\sigma}\right)^{-1/\xi}\right) \left(1 + \xi \frac{z - \mu}{\sigma}\right)^{-1-1/\xi} \quad (13)$$

where $1 + \xi \frac{z - \mu}{\sigma} > 0$,

have been fitted to these histograms (solid lines). In the above equation and in Fig. 3 μ corresponds to the “center of mass” of the population, σ is a “spread” factor and ξ is the “shape” factor. Note that in all cases examined the value of parameter ξ is negative. This corresponds to a “type III” extreme value distribution of the Weibull kind [9].

3.3 EC8 compatible peak factor and evolutionary power spectra

The shape of the median peak factor spectrum is relatively insensitive with respect to the shape of the corresponding evolutionary power spectrum and thus to the shape of the EC8 design spectrum. Thus, it is reasonable to consider the average of these spectral curves for the various soil conditions of EC8 and for each value of the damping ratio herein considered. Further, polynomial curve fitting can be applied to the above averaged median peak factor spectra to obtain an analytical expression to approximate the numerically derived median peak factors. The eighth-order polynomials plotted in Fig. 4 and expressed by the equation

$$\hat{r}(T) = \sum_{j=0}^8 p_j T^j, \quad 0.02 \leq T \leq 6 \text{ sec.} \quad (14)$$

approximate reasonably well the averaged median peak factor spectra. The coefficients p_j of these polynomials are given in Tab. 1.

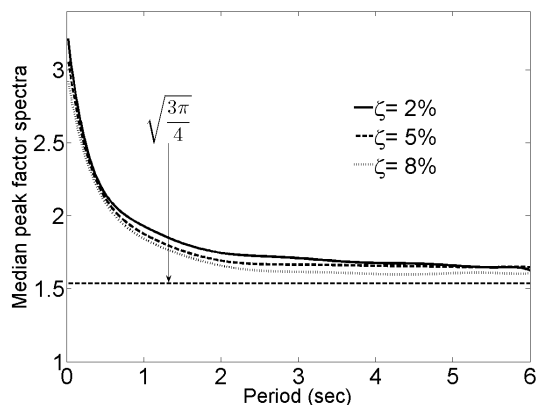


Fig. 4: Polynomial fit to the median peak factors from all soil types as defined in EC8.

Tab. 1: Coefficients of the fitted polynomials to the averaged numerically obtained median peak factor spectra from all EC8 defined soil types.

	p_0	p_1	p_2	p_3	p_4	p_5	p_6	p_7	p_8
$\zeta=2\%$	3.3079	-4.9375	8.3621	-8.3368	5.0420	-1.8983	0.4469	-0.0639	0.0051
$\zeta=5\%$	3.1439	-3.9836	5.9247	-5.3470	2.9794	-1.0439	0.2305	-0.0311	0.0023
$\zeta=8\%$	2.9806	-3.2070	4.1190	-3.1733	1.4746	-0.4144	0.0689	-0.0062	0.0002

Table 2 shows CP evolutionary power spectra compatible with the EC8 design spectrum for $PGA=0.36g$, damping ratio 5% and for all soil conditions obtained by solving the optimization problem of Eq. (7) using the frequency-dependent averaged median peak factor spectrum \hat{r} of Eq. (14). In Fig. 5 median pseudo-acceleration response spectra for ensembles of 100 baseline-corrected artificial accelerograms compatible with the CP spectra of Tab. 2 are plotted along with the corresponding target design spectrum. For comparison, average pseudo-acceleration response spectra for ensembles of 100 baseline-corrected artificial accelerograms compatible with CP spectra derived by assuming a constant peak factor equal to $\sqrt{3\pi/4}$, are also included. Clearly, the influence of the peak factor incorporated on the matching of the average response spectra of the artificial signals obtained via solving the stochastic problem of Eq. (7) is quite strong. Evidently, the use of the peak factor of Eq. (14) improves significantly the quality of this matching compared to that achieved via the constant peak factor (see also [7]). Furthermore, in terms of pseudo-acceleration spectral ordinates and for the range of natural periods that most of the ordinary structures are designed to withstand seismically induced forces a satisfactory matching is attained for the frequency-dependent peak factor. More importantly, it is noted that the shapes of the prescribed EC8 design spectra for the various soil types exhibit considerable variations. Thus, it is reasonable to argue that the average EC8 peak factor spectrum of Eq. (14) can yield results of similar quality as those of Fig. 5 for target design spectra prescribed by other contemporary aseismic code provisions, as well. Obviously, the latter claim warrants further numerical investigation.

Incidentally, the significant discrepancy of the average response spectra obtained under the assumption of a constant peak factor $\eta = \sqrt{3\pi/4}$ from the target spectrum can be readily justified by considering the deviation of the averaged median peak factor spectrum from the constant level of $\sqrt{3\pi/4}$ shown in Fig. 4.

Tab. 2: Parameters for the definition of CP evolutionary power spectra compatible with various EC8 design spectra for the frequency-dependent peak factor of Eq. (14).

Peak ground acceleration	Soil type	CP power spectrum parameters [$T_{min}=0.02, T_{max}=10$] (sec)					
		C ($cm/sec^{2.5}$)	b (1/sec)	ζ_g	ω_g (rad/sec)	ζ_f	ω_f (rad/sec)
$\alpha_g=0.36g$ ($g=981$ cm/sec^2)	A	8.08	0.47	0.54	17.57	0.78	2.22
	B	17.76	0.58	0.78	10.73	0.90	2.33
	C	19.58	0.50	0.84	7.49	1.15	2.14
	D	30.47	0.50	0.88	5.34	1.17	2.12
	E	20.33	0.55	0.77	10.76	1.07	2.03

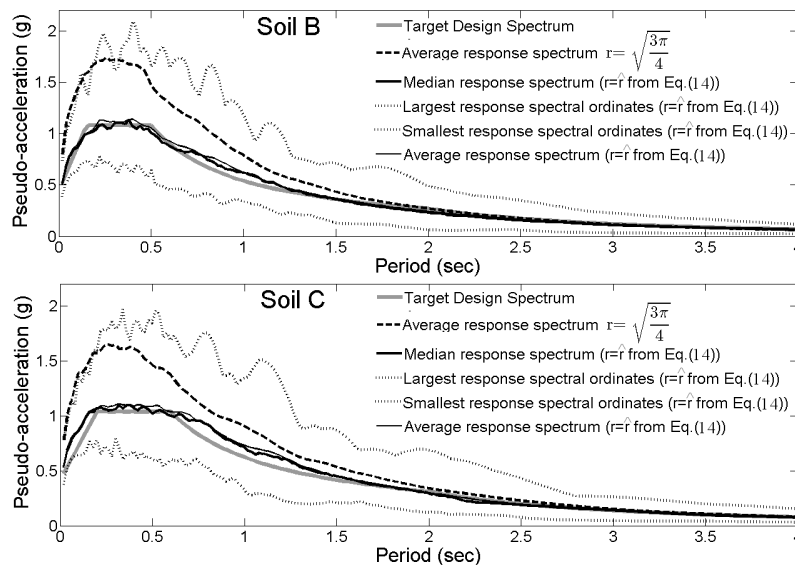


Fig. 5: Pseudo-acceleration response spectra of ensembles of 100 simulated accelerograms compatible with CP evolutionary power spectra derived by assuming a constant peak factor of $\sqrt{3\pi/4}$ and the frequency-dependent peak factor of Eq. (14).

4 Concluding Remarks

In this work, an inverse stochastic dynamics approach has been adopted to relate an evolutionary power spectrum (EPS) to a given seismic design spectrum. A solution of this problem in an approximate point-wise least-squared sense has allowed for defining a design spectrum consistent EPS characterizing a non-stationary stochastic process. Subsequently, an efficient simulation technique for producing EPS compatible non-stationary time-histories has been employed along with acausal high-pass filtering for adjusting the baseline of the simulated signals. Ensembles of thus generated signals constitute artificial seismic accelerograms whose response spectra achieve a certain level of agreement with the design spectrum.

Special attention has been given to the peak factor: a quantity which governs the relation of the EPS with a given design spectrum in a statistical manner. Specifically, using the design spectrum prescribed by the European aseismic code provisions (EC8) as a paradigm, and assuming a uniformly modulated Clough-Penzien type of EPS, a Monte Carlo analysis has been undertaken to estimate numerically median peak factor spectra pertaining to all soil conditions and various damping levels of the EC8 design spectrum. This need has been dictated by the fact that no convenient expression of the peak factor in the non-stationary case considered exists in the open literature. The consistency of the derived median peak factor spectra with the EC8 has been established by utilizing appropriately defined EC8 compatible EPSs as input spectra in the Monte Carlo analysis. Additional numerical data derived as by-products of the above analysis have been also reported to elucidate certain aspects of the response of linear SDOF systems driven by uniformly modulated colored noise processes.

The thus derived median peak factor spectra have been further incorporated in the solution of the aforementioned inverse stochastic problem to yield EC8 consistent EPSs. The achieved level of consistency has been assessed by comparing the average and median populations of response spectra of ensembles of EPS compatible artificial accelerograms. Compared with similar data from a previous study incorporating constant peak factors in the derivation of EC8 compatible EPSs [7], the average and median of the herein generated signals lie significantly closer to the EC8 spectrum. This result establishes the usefulness and practical merit of the reported EC8 compatible median peak factor and evolutionary power spectra for simulating EC8 design spectrum consistent non-stationary accelerograms to be used as input for time-history elastic and inelastic dynamic analyses for the aseismic design of critical structured facilities.

As a final note, and given the enhanced level of consistency of the derived EPSs with the EC8 design spectrum, it is suggested that these EPSs can be further considered as input spectra to perform non-stationary linear and non-linear random vibration analyses for the design of structures regulated by the EC8 provisions. In the non-linear case, the method of statistical linearization can perhaps be employed [19].

5 References

- [1] Bogdanoff, J. L.; Goldberg, J. E.; Bernard, M. C.: Response of a simple structure to a random earthquake-type disturbance. *Bulletin of the Seismological Society of America*, 51 (1961), 293-310.
- [2] Boore, D. M.; Bommer, J. J.: Processing of strong-motion accelerograms: needs, options and consequences. *Soil Dynamics and Earthquake Engineering*, 25 (2005), 93-115.
- [3] Boore, D. M.: On pads and filters: Processing strong-motion data. *Bulletin of the Seismological Society of America*, 95 (2005), 745-750.
- [4] CEN.: Eurocode 8: Design of Structures for Earthquake Resistance - Part 1: General Rules, Seismic Actions and Rules for Buildings. *EN 1998-1: 2004*. Comité Européen de Normalisation, Brussels, 2004.
- [5] Chopra, A. K.: *Dynamics of Structures. Theory and Applications to Earthquake Engineering*. Prentice-Hall, New Jersey, 2001.
- [6] Clough, R. W.; Penzien, J.: *Dynamics of Structures. Second Edition*. Mc-Graw Hill, New York, 1993.
- [7] Giaralis, A.; Spanos, P. D.: Wavelet-based response spectrum compatible synthesis of accelerograms-Eurocode application (EC8). *Soil Dynamics and Earthquake Engineering* 29 (2009), 219-235.

- [8] Kaul, M. K.: Stochastic characterization of earthquakes through their response spectrum. *Earthquake Engineering and Structural Dynamics* 6 (1978), 497-509.
- [9] Kotz, S.; Nadarajah, S.: *Extreme Value Distribution., Theory and Applications*. Imperial College Press, London, 2000.
- [10] Mason, A. B.; Iwan, W.D.: An approach to the first passage problem in random vibration," *Journal of Applied Mechanics, ASME*, 50 (1983), 641-646.
- [11] Michaelov, G.; Lutes, L. D.; Sarkani, S.: Extreme value of response to nonstationary excitation. *Journal of Engineering Mechanics, ASCE* 127 (2001), 352-363.
- [12] Morikawa, H.; Zerva, A.: Approximate representation of the statistics for extreme responses of single degree-of-freedom system excited by non-stationary processes. *Probabilistic Engineering Mechanics* 23 (2008), 279-288.
- [13] Nigam, N. C.; Jennings, P. C.: Calculation of response spectra from strong-motion earthquake records. *Bulletin of the Seismological Society of America* 59 (1969), 909-922.
- [14] Nocedal, J.; Wright, S. J.: *Numerical Optimization*. Springer-Verlag, New York, 1999.
- [15] Papoulis, A.; Pillai, S.U.: *Probability, Random Variables and Stochastic Processes. Fourth Edition*. McGraw-Hill, New York, 2002.
- [16] Park, Y. J.: New conversion method from response spectrum to PSD functions. *Journal of Engineering Mechanics, ASCE* 121 (1995), 1391-1392.
- [17] Pfaffinger, D. D.: Calculation of power spectra from response spectra. *Journal of Engineering Mechanics, ASCE* 109 (1983), 357-372.
- [18] Priestley, M. B.: Evolutionary Spectra and Non-Stationary Processes. *Journal of the Royal Statistical Society. Series B (Methodological)* 27 (1965), 204-237.
- [19] Roberts, J. B.; Spanos, P.D.: *Random Vibration and Statistical Linearization*. Dover Publications, New York, 2003.
- [20] Senthilnathan, A.; Lutes, L.D.: Nonstationary maximum response statistics for linear structures. *Journal of Engineering Mechanics, ASCE* 117 (1991), 294-311.
- [21] Spanos, P. D.: Non-stationary random vibration of a linear structure." *International Journal of Solids and Structures* 14 (1978), 861-867.
- [22] Spanos, P. D.; Lutes, L. D.: Probability of response to evolutionary process. *Journal of the Engineering Mechanics Division, ASCE* 106 (1980), 213-224.
- [23] Spanos, P. D.; Vargas Loli, L. M.: A statistical approach to generation of design spectrum compatible earthquake time histories. *International Journal of Soil Dynamics and Earthquake Engineering* 4 (1985), 2-8.

- [24] Spanos, P. D.; Zeldin, B. A.: Monte Carlo Treatment of Random Fields: A Broad Perspective. *Applied Mechanics Reviews* 51 (1998), 219-237.
- [25] Spanos, P. D.; Giaralis, A.; Jie, L.: Synthesis of accelerograms compatible with the Chinese GB 50011-2001 design spectrum via harmonic wavelets: artificial and historic records. *Earthquake Engineering and Engineering Vibrations* 8 (2009), 189-206.
- [26] Vanmarcke, E. H.: *Structural Response to Earthquakes*. Seismic Risk and Engineering Decisions. Eds: Lomnitz, C.; Rosenblueth, E. Elsevier, Amsterdam, 1976.
- [27] Zembaty, Z: A note on non-stationary stochastic response and strong motion duration. *Earthquake Engineering and Structural Dynamics* 16 (1988), 1189-1200.

Reliability of reinforced structural elements in existing structures subjected to shear force

Alexander Fischer*, Jürgen Schnell*, Thomas Braml** and Manfred Keuser**

*Institute of Concrete Structures and Structural Design, University of Technology, Kaiserslautern, Germany

**Institute for Structural Engineering, University of the German Armed Forces, Munich, Germany

Abstract: Probabilistic analyses are becoming more and more important in civil engineering. Probabilistics can be used for the calibration of partial safety factors of the semi-probabilistic safety concept of current codes as well as in the context of sustainability evaluations of existing buildings. For reinforced concrete components subjected to bending, the limit state function for structural failure can be specified clearly because of a well-defined mechanical model. By contrast, for the formulation of the mechanical model of shear carrying capacity there are still large uncertainties. The following article deals with the reliability of components in building structures subjected to shear force and should be understood as a support selecting appropriate statistical parameters of model uncertainties for probabilistic calculations. The proposed statistic parameters of model uncertainties were selected out of extensive parameter studies in view of the target reliability level.

1 Introduction

As far as existing buildings are concerned, it can be that changes in usage and related stress increase during their lifetime, resulting in a reassessment of stability and structure requirements. Basically, the assessment of the load-bearing capacity of existing buildings is made according to current standards. The problem is that the current standards have been developed for the design of new buildings, and thus can only be applied to existing buildings with restrictions and modifications. The static analysis of existing buildings is in many cases not feasible using the strict application of current regulations, because the standards have been signed on new buildings and in the partial factors the uncertainties for new structures [14] are considered.

In the recording of an existing structure, for example the material data of used materials, the dimensions and spans as well as the size and location of reinforcement can be measured and the uncertainties can decrease in comparison to the planning phase. This can be used for probabilistic structural considerations. But keep in mind that for example uncertainties can also increase due to lost information or uncertainties regarding the assessment techniques.

There is sufficient data for a probabilistic calculation for the bending moment capacity of structures using the corresponding basic variables available in the literature [21]. However there are significant deficits concerning shear action. In the formulation of the limit state for shear force stressed structures model uncertainties for the resistance and for loads plays a major role. Despite extensive analyses in recent years, the identified statistical parameters of the model uncertainties which have been identified using experiments are very diversified. With regard to the reliability assessment of existing buildings, the paper gives a position in the assessment of shear force stressed structures.

2 Limit state functions for shear force bearing capacity

The shear force failure of reinforced concrete cross-sections is, by definition, divided into three failure modes. By *flexural shear failure* the crack leading to the failure results from a bending crack. In structures with profiled tension flange a shear tension crack can appear if inclined cracks form in the web of profiled beams. These cracks are not drawn to the outside edge and they are not caused by bending cracks. This is called *shear tension failure*.

In the case of compressive strut failure, the compressive stresses in the oblique compressive struts increase so much until the pre-damaged concrete caused by shear crack initiation fails. The current assessment codes which are applied for the carrying capacity model of the general truss system quest with variable strut inclination is the basis for shear force carrying capacity including shear force reinforcement. In addition, the load-carrying effects such as crack interlocking, dowel action, and the capacity of the compression zone are activated. These effects are dominant for the capacity of structures without shear reinforcement [30, 32, 39].

To grasp the shear-load bearing, extensive theoretical and experimental researches have been carried out, but a clear solution has not yet been found. Therefore, different models for describing shear force behavior exist. In Germany, the assessment of shear force bearing capacity is on the basis of DIN 1045-1 [8]. Within the framework of probabilistic analysis, these dimensioning equations rated as limit state functions are used. In addition the model uncertainties must be taken into account and all the basic variables with their mean values must be used.

The prefactors in the analysis equations for the shear force bearing capacity in [8] were mainly determined empirically. An evaluation of the mechanical model of shear behavior can be carried out by the introduction of model uncertainty.

The limit state function for shear force stressed structures in the ultimate limit state can be written basically through the comparison of shear force stress V_S and shear force resistance V_R in major cross section:

$$g(\mathbf{R}, \mathbf{E}) = V_R - V_E = 0 \quad (1)$$

The assessment of shear force bearing capacity is divided into three failure mechanisms in accordance with [8]: The shear force bearing capacity of structures without shear force reinforcement $V_{R,ct}$, the bearing capacity of the shear force reinforcement $V_{R,sy}$ and the bearing capacity of the compressive strut $V_{Rd,max}$.

The limit state function for the shear force bearing capacity of structures without shear force reinforcement is in accordance with [8]:

$$g(V_{R,ct}) = U_{R,ct} * \left[0,20 * \left(1 + \sqrt{\frac{200}{d * 1000}} \right) * \eta_1 * \left(100 * \frac{A_{sl}}{b_w * d} * f_c \right)^{\frac{1}{3}} \right] * (h - d_1) - U_E * (V_G + V_Q) \quad (2)$$

The descriptions of the basic variables in the limit state functions are in accordance with the definition in [8]. Hereinafter the variables which are necessary and relevant for the probabilistic calculation are only explained.

$U_{R,ct}$ defines the model uncertainty for the shear force bearing capacity of a structure without shear force reinforcement. U_E refers to the model uncertainty on the load side, and U_N to the model uncertainty for a normal force. V_G defines the shear force caused by a dead load and V_Q that caused by a live load.

Great importance in (2) is placed on the probabilistic analysis adapted prefactor of 0.20, which is in [8] calculated from the term $0.15 / \gamma_c$. The value 0.15 represents the 5% quantile of the empirically determined prefactor. In [6] experimental results are listed which establish the empirical factor.

The following table 1 provides an overview of values mentioned in the literature for the empirical prefactor for various different ways of evaluating the experimental databases.

Tab. 1: Literature of the empirical factor 0,20 in (2), (N = normal distribution)

Literature	Recommended mean value	Calculated 5 % fractile	Distribution type	Coefficient of variation v_x
Reineck [30]	0.20	0.134	N	0.20
Zink [39]	0.18	0.121	N	0.20
Heft 525 DafStb [6]	0.20	0.14	N	0.18
DIN 1045-1 [8]	0.23*	0.15	N	0.20
DIN EN 1992-1 [10]	0.27*	0.18	N	0.20

* value calculated assuming the coefficient of variation

According to [30, 39], the prefactor chosen in DIN 1045-1 [8] is not on the safe side. The structural behavior of reinforced concrete components without shear force reinforcement is then a bit overestimated. This is also confirmed by the remarks in [2], in which the experimental studies of recent decades have been included [15, 16, 36]. For probabilistic analysis the model uncertainty for the shear load capacity of a reinforced concrete structures without shear force reinforcement according to [30] should be chosen lower than 1.0.

The limit state function for structures with arithmetically necessary shear force reinforcement can be calculated by:

$$g(V_{R,Sy}) = U_{R,Sy} * b * \left(\frac{A_{Sw}}{S_w} * f_y * (0,9 * (h - d_1)) * (\cot\theta + \cot\alpha) * \sin\alpha \right) - U_E * (V_G + V_Q) \quad (3)$$

The inclination of compressive struts can be calculated according to [8].

$$0,58 \leq \cot\theta \leq \frac{1,2}{1 - \frac{U_{Rd,c} * 0,425 * 1,0 * f_c^{1/3} * b_w * z}{U_E * (V_G + V_Q)}} \leq 3,0 \quad (4)$$

$V_{Rd,c}$ for the concrete capacity is already contained in (4). This has also been empirically derived from experimental results. The associated model uncertainty is defined here with $U_{Rd,c}$.

The factor 0.425 in (4) is derived from the term $c_j \cdot 0,48$ according to [8]. The roughness coefficient c_j is given by 0.5. The prefactor $0,5 \times 0,48 = 0,24$ defines a design value which implies a partial safety factor of $\gamma_c = 1,50$. Hence the 5% quantile amounts to 0.36. The transfer to the mean value of 0.425 is calculated by using a log normal distribution and a coefficient of variation of 10%.

The limit state function for the failure of the compressive strut is according to [8]:

$$g(V_{R,max}) = U_{R,max} * \frac{b_w * 0,9 * (h - d_1) * \alpha_c * 0,85 * f_c}{\cot\theta + \tan\theta} - U_E * (V_G + V_Q) \quad (5)$$

$U_{R,max}$ defines the model uncertainty for the resistance.

The coefficient α_c in (5) for the compressive strut resistance include the reduction of compressive concrete strength of cracked webs in comparison to the prismatic strength. The reduction is caused by the tensile stress from the composite effect of the compressive strut crossing reinforcement. The value α_c was determined empirically. α_c can be used of the compressive strut stays parallel to the cracks, which occur in structures by high shear force or very high levels of reinforcement, and is indicated in [23] with 0.80 to 0.85. According to [31], „Truss models with crack friction" which [8] is based on, the coefficient can be determined with $\alpha_c = 0.80$. On the basis of the plasticity theory and the model of "variable compressive strut inclination" in DIN EN 1992-1-1 [10], which permits compared to DIN 1045-1 flatter compressive struts, lower values than in [8] are defined, because the direction of the compressive struts significantly deviates from the crack direction. For example for concrete of strength class C20/25 α_c has a value of 0.552.

According to [31] "after lengthy discussions the slightly lower value $\alpha_c = 0.75$ was carefully fixed in DIN 1045-1." Basically, it centres on α_c for the probabilistic calculation of a mean value. For the other parameter studies, a mean value of $\alpha_c = 0.80$ was chosen.

With the current edition of DIN 1045-1 [8] a minimum value of shear force bearing capacity $V_{Rd,ct,min}$ for bending reinforced components without shear force reinforcement was introduced. However this is not an ultimate limit state or failure state. Therefore it is not considered further for the probabilistic calculation.

3 Model uncertainties

3.1 Model uncertainties for resistance

For the limit state function of structures with shear force reinforcement (3) a sensitivity analysis was performed to assess the influence of the basic variables for the shear force bearing capacity (figure 1).

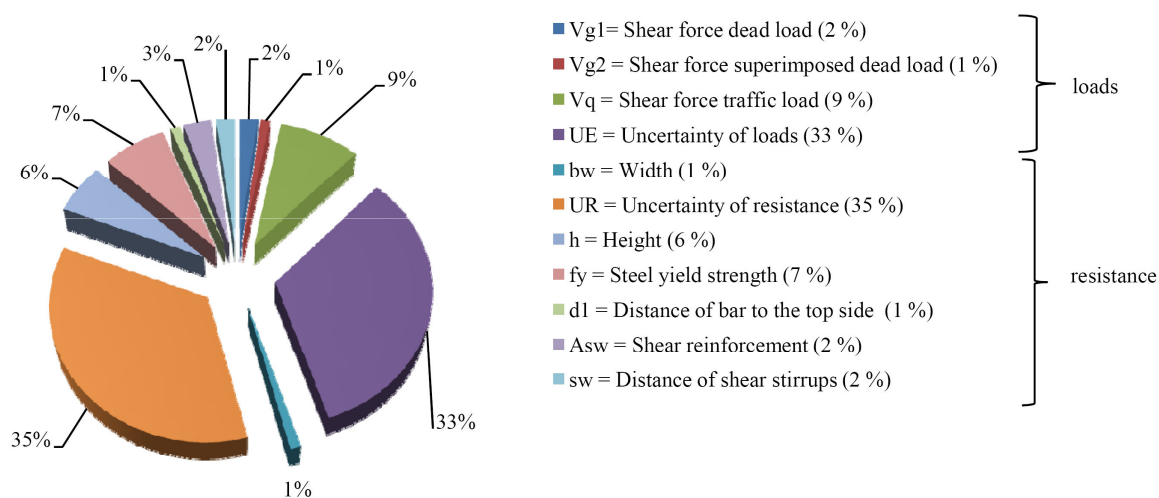


Fig. 1: Exemplary illustration of the influence of basic variables on the reliability of shear reinforced structures $g(V_{R,sv})$ according to (3) [29]

By using basic variables according to Table 4 figure 3 shows that the model uncertainties of resistance and loads have a major influence on reliability in terms of shear force failure.

The model uncertainties were determined by the interpretation of approximately 1.500 experiments [15, 16, 36]. In [2], individual national and international models for the calculation of shear force bearing capacity of reinforced concrete components without shear force reinforcement have been evaluated with regard to the destination of model uncertainty for a probabilistic calculation. It shows that the mean value of the resistance model uncertainty is 0.92 to 1.57 and the coefficient of variation varies between 18% and 42%.

In [19] the present shear force trials were categorized and evaluated in terms of use in probabilistic analysis with an indication of a model factor for the resistance model of shear force bearing capacity.

Table 2 shows an overview of proposed values in the literature for the choice of the statistical properties of the model uncertainties of the shear force bearing capacity for structures with and without shear force reinforcement.

Tab. 2: Statistical Parameters of model uncertainties concerning shear capacity in literature (LN = log-normal distribution, N = normal distribution)

Literature	Distribution type	Mean value model uncertainty	Coefficient of variation for model uncertainty
JCSS [21]	LN	1.4	25 %
Faber [13]	LN	1.0	10 % - 20 %
Brehm et.al. [2]	LN	1.0 for $V_{R,ct}$	20 %
Hansen [18]	LN/N	1.1	10 %
Model Code 90 [4]	LN/N	0.91	11 %
Nowak [26]	LN/N	1.20 for $V_{R,sy}$ 1.40 for $V_{R,ct}$	15.5 % for $V_{R,sy}$ 17.0 % for $V_{R,ct}$
Melchers [25]	LN/N	1.00 for $V_{R,sy}$ 0.93 for $V_{R,ct}$	19.0 % for $V_{R,sy}$ 21.0 % for $V_{R,ct}$
Kautsch (DIN) [22]	N/LN	1.454	26.8%

Beside in [2], [25] and [26] for the model uncertainty there are no differences between the individual failure mechanisms. Recent evaluations of the database for shear force trials according to Kautsch [22] lead to similar results to those in JCSS 2000 [21].

The evaluation of the shear force trials in [18] showed, however, that the size of mean value and coefficient of variation are very different and depend on the chosen boundary conditions such as the type of stress. Figure 2 shows the influence on the sensitivities of the various basic variables on variation of the mean value and the coefficient of variation of the resistance model uncertainty. The parameter studies have been carried out with the limit state function of structures with shear force reinforcement (3). In the variation of the mean value of the model uncertainty U_R (figure 2 left), the coefficient of variation was chosen at 15% and for the change in the coefficient of variation (figure 2 right), the model uncertainty was chosen at $U_R = 1.0$.

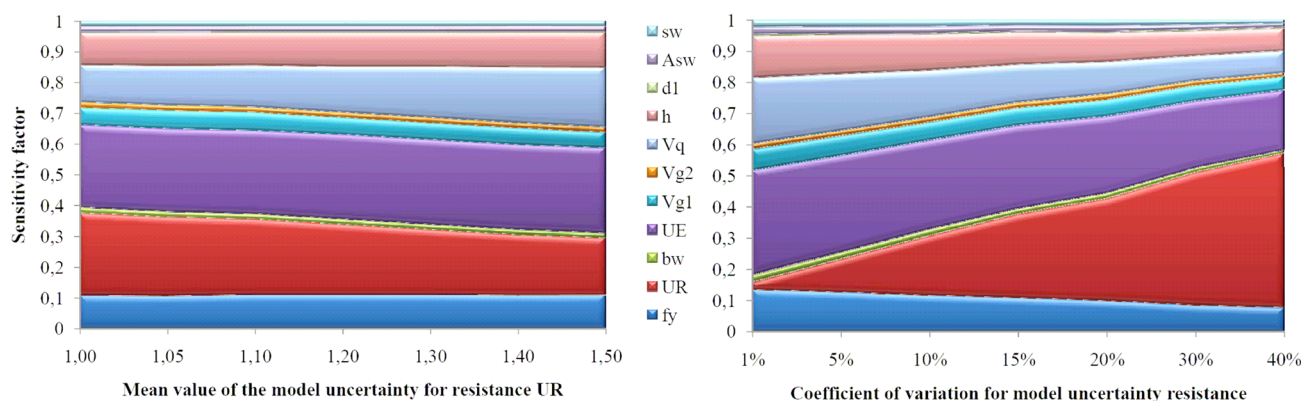


Fig. 2: Impact on sensitivity factors α_i by variation of the mean value μ_{UR} (left) and the coefficient of variation (right) of the resistance model uncertainty. Denotations are shown in Figure 3.

Furthermore, the effects with regard to the shear force capacity by changing the statistical parameters of the model uncertainty (Fig. 3) were examined.

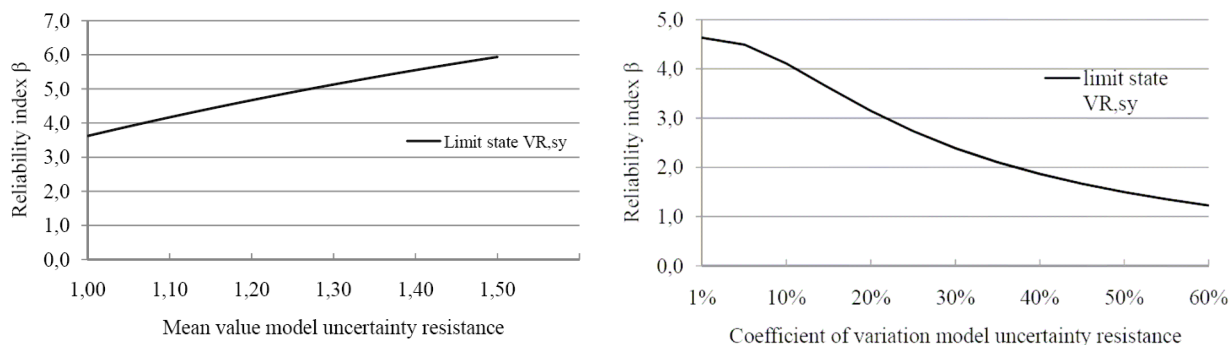


Fig. 3: Exemplary illustration of the influence of mean value μ_{UR} (left) and coefficient of variation (right) of model uncertainty on the reliability index β

3.3.2 Model uncertainties for loads

The model uncertainties in the calculation of stress resultant caused by loads result from the simplifications in the calculation itself and from the method used for the analysis of the stress resultants. One problem in determining the model uncertainty is the fact, that the stress resultants are not measurable directly.

In accordance with [21] and other literature sources such as [13, 18] the statistical parameters of the model uncertainties of the loads are listed in Table 3.

Tab. 3: Statistical Parameters of model uncertainty of loads according to [13, 18, 19, 21]

Stress resultant	Distribution type	Mean value	Coefficient of variation
Axial forces	N / LN	1.00	0.05
Moments in frames	N / LN	1.00	0.07
Moments in plates	N / LN	1.00	0.10
Shear force in frames, single load	N / LN	1.00	0.17
Shear force in frames, uniformly distributed load	N / LN	1.00	0.12
Shear force in plates, uniformly distributed load	N / LN	1.00	0.10

When a uniformly distributed load and a single load occur concurrently the higher coefficient of variation in Table 4 should be chosen.

4 Reliability Studies on Components subjected to Shear Force

Reliability studies on reinforced concrete components of existing structures subjected to shear without additional longitudinal force were realized with the statistical parameters composed in Table 4 for a reference period of 50 years. The studies are restricted to reinforced concrete components under dead and live load demands.

Tab. 4. Statistical Parameters of used basic variables (LN = log-normal distribution, N = normal distribution, GUM = Gumbel distribution)

	basis variables	type of statistic distribution	statistic parameter		Note
			$m_{x,i}/X_{k,i}$	CoV	
Resistance	Concrete compressive strength f_{cm}	LN	1.267 ¹⁾	0.1 – 0.4 ²⁾	-
	Concrete tensile strength f_{ctm}	LN	1.267 ¹⁾	0.3 – 0.4 ²⁾	-
	Steel tensile strength f_{ym}	LN	1.106	0.06	BSt I, III, IV
	Edge distance of reinforcement d_l	N	0.98	0.125	-
	Geometry b_w, h, d	N	1.00	0.02	-
Model uncertainties	Reinforcement A_s	-	1.00	const.	-
	Shear force capacity $U_{R,ct}$	LN	1.40	0.25	JCSS
	Shear force capacity $U_{R,ct}$	LN	1.454	0.268	Kautsch [41]
	Shear force capacity $U_{R,sy}$	LN	1.10	0.10	UDL
	Shear force capacity $U_{R,max}$	LN	1.10	0.15	UDL
	Shear force action $U_{E,q}$	N	1.00	0.1 – 0.15	UDL, beams
	Shear force action $U_{E,q}$	N	1.00	0.10	UDL, plates
	Design dead load V_G	N	1.00	0.066	incl. extension
	Design dead load V_G	N	1.00	0.04-0.05	pure RC comp.
	Action	Live load ³⁾ V_Q	GUM	1.10	0.20
Wind load ³⁾ V_W		GUM	1.07	0.15	-
Snow load ³⁾ V_S		GUM	1.13	0.25	-

1) for concrete compressive strength class C30/37

2) Variation of the coefficient of variation in the specified interval

3) Distribution of the maximum extreme values for a reference period of 50 year

In Table 4 X_k is the characteristic value of the basic variable. Because of a standardization for the parametric studies for the statistic parameter the mean $m_{x,i}$ divided by X_k and coefficient of variation was used. The reliability examinations are carried out in the ultimate limit state, i. e. resistance and impact are equal in the deterministic sense, based on the partial safety factors of $\gamma_c=1.50$ and $\gamma_s = 1.15$ according to [8] and of $\gamma_G=1.35$ and $\gamma_Q=1.50$ according to [9] ($Z = R - E = 0$). These characteristic values of impact and resistance were taken as a basis for responding to the probabilistic calculations [20] with their mean values by using the coefficient of variation according to Table 4. Therefore the dimensions of the mean value results by using a scale factor for standardisation to size the real mean for the different characteristic values of the basic variables. This procedure leads to the coordinates of the design point and thus the reliability of the considered failure. The advantage of this method is that the studies can be used for all kinds of concrete compressive strength and all grade of steel for example. Therefore the reliability curves in the Figures 4, 5 and 6 are representative for all concrete compressive strengths whether the coefficient of variation for the regarded concrete compressive strengths is used.

The coefficient of variation of concrete compressive strength in existing structures varies enormous and is often much higher than nowadays. At TU Kaiserslautern a lot of concrete specimens of existing structures were analysed with the result that the coefficient of varia-

tion is often in the range of $v_x = 0,30$ till $0,40$ depending on the point of time of the construction phase.

In order to describe failure subjected to shear force in accordance to section 2, three failure criterions are defined. Successively these were considered probabilistic for a load ratio of $g_k / q_k = 70 / 30$ and $50 / 50$. Subsequently the target reliability level of $\tilde{\beta}_{50} = 3.8$ is applied in all reliability diagrams for a reference period of 50 years. The failure criterions were regarded separately in dependence on the design equation of the current German code DIN 1045-1. The structural safety of all buildings in Germany have to be analysed with current codes because there are no particular codes for existing structures.

The parameters studies of $V_{Rd,ct}$ were managed on the basis of equation (2). The model uncertainties, the live load and the concrete compressive strength are decisive for the component reliability. With an increasing coefficient of variation of concrete compressive strength the sensitivity of the resistance side increases.

The model uncertainties of the resistance was chosen according to [21] with a mean of $\mu_{UR} = 1,4$ and a coefficient of variation of $v_x = 25\%$. The model uncertainty of actions was assumed with a mean of $\mu_{UE} = 1,0$ and $v_x = 15\%$.

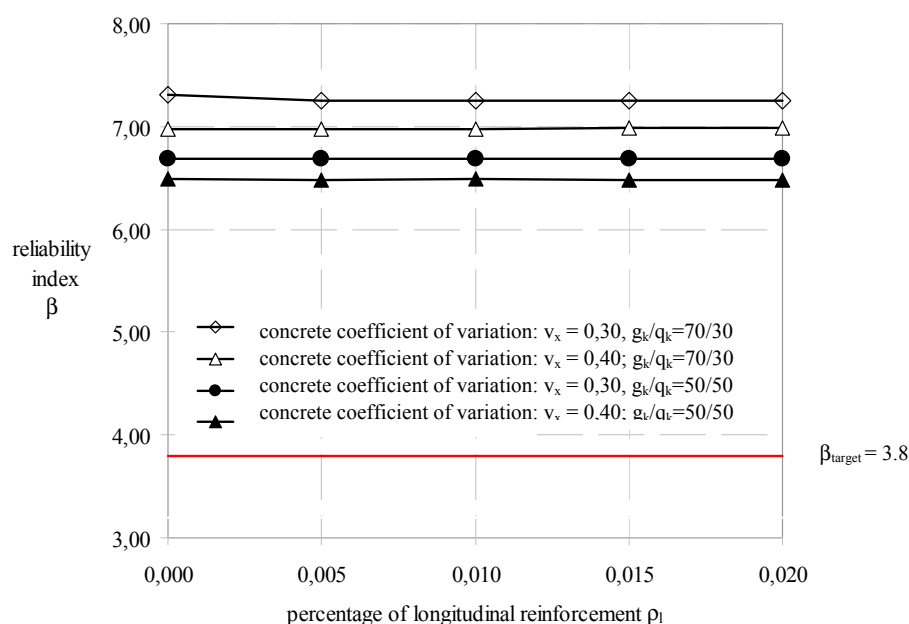


Fig. 4: Reliability of concrete structures without shear reinforcement ($V_{Rd,ct}$) due to shear loads subject to percentage of longitudinal reinforcement ρ_1 according to (2) for a reference period of 50 years with $\gamma_c = 1.50$; $\gamma_s = 1.15$ and $\gamma_G = 1.35$, $\gamma_Q = 1.50$

The verification of $V_{Rd,ct}$ provides a very high reliability independent of the statistical parameters of the model uncertainties even with a high coefficient of variation of concrete compressive strength. Even the proposal of model uncertainty U_R by Hansen [18] provides similar reliability. As Tab. 2 shows, the statistical parameters of the model uncertainty for $V_{Rd,ct}$ vary considerably. The following table discusses the reliability of selected proposals of model uncertainties in Table 2 in terms of the statistical parameters of actions and resistance written in Table 4.

Tab. 5: Reliability by consideration of model uncertainties according to Table 3 with $v_{x,\text{concrete}} = 30\%$ by utilisation of a log-normal distribution

Model	Mean model uncertainty	COV model uncertainty	Reliability index
JCSS [21]	1.40	25 %	7,26
Hansen [18]	1.10	10 %	7,92
Faber [26]	1.00	15 %	6,42
Brehm et. al. [2]	1.00	20 %	5,53
Melchers [25]	0.93	21 %	4,86

With all analyzed model uncertainties shown in Tab. 5 a very high component reliability was achieved, even with a mean value of model uncertainty U_R smaller than 1.0, as requested in [30]. This leads to the conclusion that the failure model for $V_{Rd,ct}$ in [8] is not exactly captured. For probabilistic investigations the model by Brehm et. al. [2] and Faber [13] is recommended. The results of Figure 4 and Table 5 make it clear, that probabilistic studies should be used as a convenient method for assessing the component sustainability of existing buildings.

The reliability of the diagonal tie according to (3) of the chosen truss model for the shear force transfer is rather low (Fig. 5). The model uncertainties of resistance and actions are highly decisive for reliability here. A mean of $\mu_{UR} = 1.1$ with a coefficient of variation of $v_x = 10\%$ was assumed as model uncertainty on resistance side. For model uncertainty on the action side $\mu_{UE} = 1.0$ with $v_x = 0.12$ was assumed. As a simplification, the strut inclination was used with $\cot \theta = 1.2$ according to DIN 1045 [8]. Studies on probabilistic determination of $\cot \theta$ up to (4) lead to the same reliability in the limit state of sustainability by the following performed parameter studies of $V_{Rd,sy}$, because the dimension of action and resistance side changes in the same quantity. It can be noted that the crack frictional force $V_{Rd,c}$ acting perpendicularly to the longitudinal axis of the component shows far higher values for small reinforcement percentages close to the minimum shear reinforcement than the sustainability of the tie $V_{Rd,sy}$ does. This circumstance is also confirmed by the fact that the formula for the determination of $\cot \theta$ offers values outside the defined interval in the range from 0.58 to 3.0 according to [8].

The parameter studies were done with a percentage of stirrup reinforcement in the range of $\rho_w = 1\%$ to a maximum of 2%. In addition to the model uncertainties chosen in Table 5 also model uncertainty of [22] were also used. These differ only marginally from the definitions in [21].

The limit state equation of $V_{Rd,sy}$ (3) responds very sensitively with regard to changes in the statistical parameters of model uncertainties on the action and resistance sides. A variation of the steel tensile strength is not effective, as their dispersion is very small and there is also a low sensitivity.

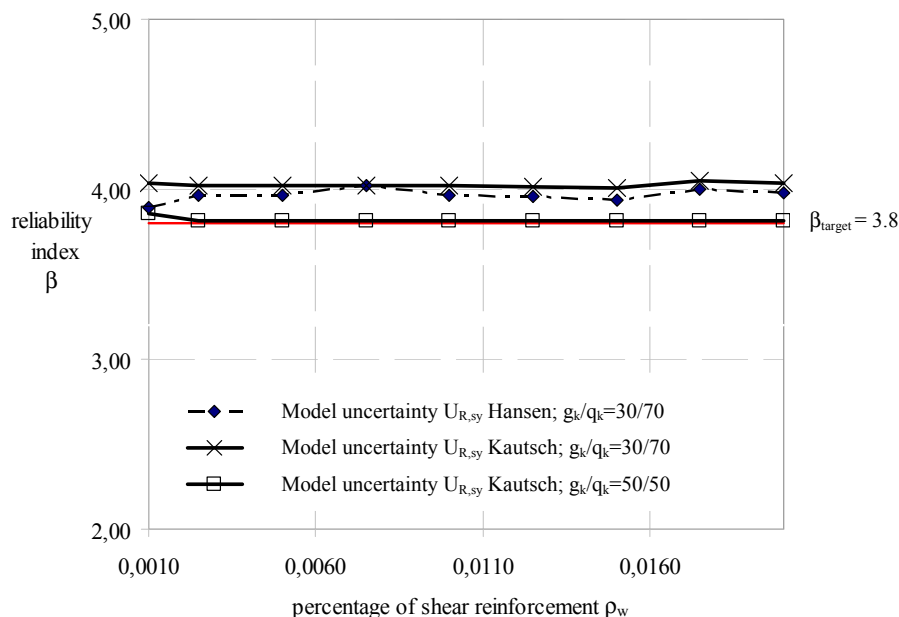


Fig. 5: Reliability of concrete structures with shear reinforcement ($V_{Rd,sy}$) due to shear load subjected to percentage of shear reinforcement ρ_w for a reference period of 50 years with $\gamma_c = 1.50$; $\gamma_s = 1.15$ and $\gamma_G=1.35$, $\gamma_Q=1.50$

Figure 6 shows the reliability of the bearing capacity of the compressive strut $V_{Rd,max}$ for different coefficients of variation. According to Table 5 a mean value of 1.10 with a coefficient of variation of 15 % is used for the model uncertainty on resistance side. For model uncertainty on action side $\mu_{UE} = 1.00$ with $v_x = 0.15$ was assumed. The choice of the statistical parameters of the model uncertainties affects the reliability only marginally.

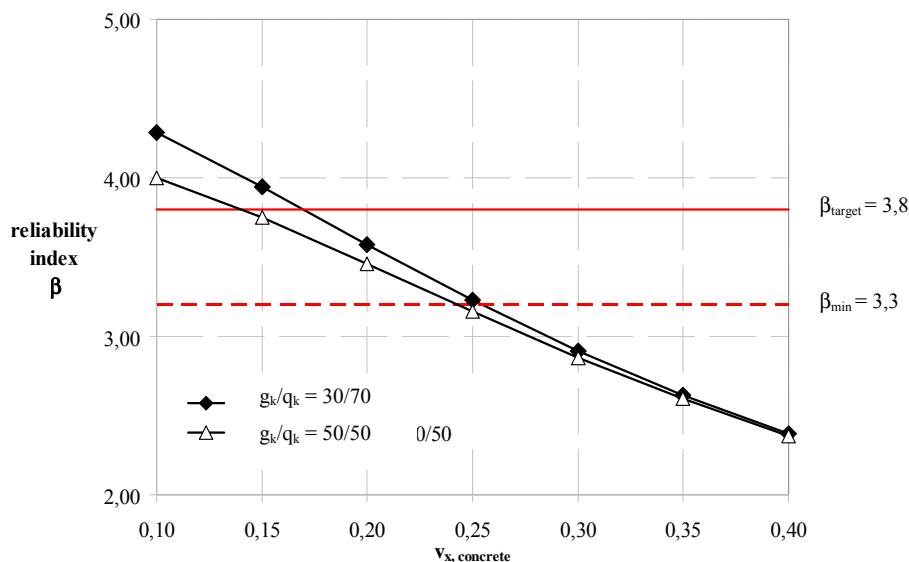


Fig. 6: Reliability of the strut due to shear load ($V_{Rd,max}$) by variation of concrete compression strength for a reference period of 50 years with $\gamma_c = 1.50$; $\gamma_s = 1.15$ and $\gamma_G=1.35$, $\gamma_Q=1.50$

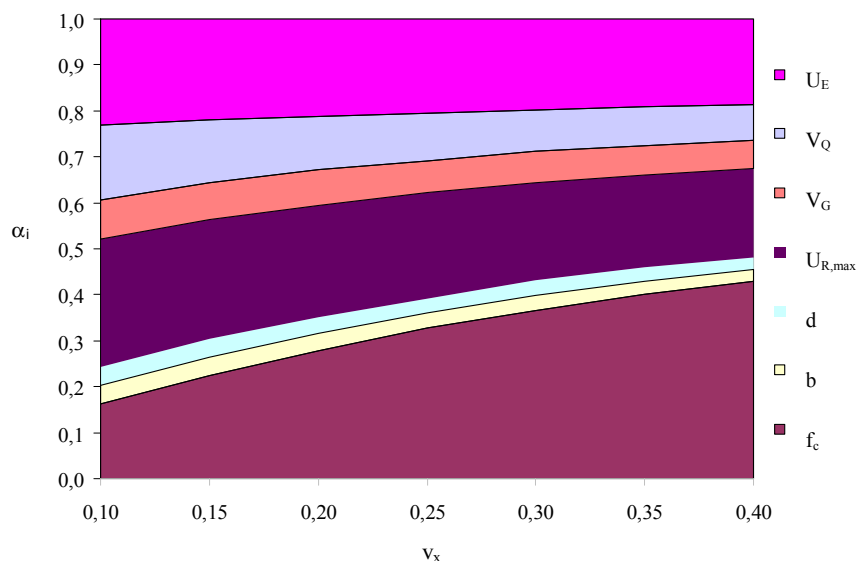


Fig. 7: Change of sensitivity factors α_i with regard to the variation of concrete compressive strength on the reliability curve $V_{Rd,max}$ according to Figure 6 (Denotations are shown in Table 4)

Figure 7 shows clearly the growth of the sensitivity of concrete compressive strength with an increasing coefficient of variation, which leads to a decrease of the component reliability shown in Figure 6.

This further denotes, that in the reliability examinations the weighting of the resistance side rises by an increasing dispersion of the concrete compressive strength.

In general the verification of $V_{Rd,max}$ is only decisive for cross sections with a high rate of shear reinforcement. For existing buildings, the verification of the strut can be relevant for the bearing capacity because of low concrete quality or wide dispersions of concrete compressive strength. Figure 6 shows that for a coefficient of variation of the concrete compressive strength which is larger than 25 % the reliability has decreased below the minimum value of the defined target reliability.

In accordance to Appendix B of DIN 1055-100 the target reliability may, however, vary within the range of $\beta_{50,min} = 3.04$ to $\beta_{50,max} = 4.04$, because of the definition of the abbreviated sensitivity factors of $\alpha_E = -0.7$ and $\alpha_R = 0.8$, when considering that the ratio of standard deviations range in the interval of $0.16 < \sigma_E/\sigma_R < 7.60$. In probabilistic studies of existing buildings a lower limit of $\beta_{50,min} = 3.3$ is proposed for the target reliability. For existing buildings this procedure is confirmed because a reduction of the target reliability of $\Delta\beta = 0.5$ is also shown in [6].

5 Results

On the basis of the probabilistic parameter studies it should be noted that for all three failure criteria subjected to shear force formulated in [8], no uniform safety level is reached. Under consideration of Table 5 there is always a high reliability for components without rated required shear reinforcement. High dispersion of the concrete compressive strength

affects the reliability of components without shear force reinforcement in existing buildings only a little.

The analysis further shows that using probabilistic studies for the assessment of the load-bearing capacity of components in existing structures is a reasonable method if a deterministic evaluation gives no sufficient results.

The limit states for $V_{Rd,sy}$ and $V_{Rd,max}$ achieve the target reliability level quite well, whereas for $V_{Rd,max}$ the size of the coefficient of variation of concrete compressive strength is of crucial importance.

The parameter studies also show that even the choice of the statistical parameters of the model uncertainties is of great importance in order to achieve the target reliability. Based on the arranged probabilistic analyses and on an extensive study of literature, the following considerations of the limit states of components under uniformly distributed loads subjected to shear force following model uncertainties were proposed:

Tab. 6: Statistical parameter for model uncertainty of shear force capacity

Failure criterion	Notation	Distribution density function	Mean model uncertainty	COV model uncertainty
$V_{Rd,ct}$	$U_{R,ct}$	lognormal	1.00	15 %
$V_{Rd,sy}$	$U_{R,sy}$	lognormal	1.10	10 %
$V_{Rd,max}$	$U_{R,max}$	lognormal	1.10	15 %

With statistical parameters of the model uncertainties for all three types of failure specified in Table 6, the target reliability level is generally achieved by using the parameters listed in Table 4. With Table 6 existing buildings which are subjected to shear force can be evaluated usefully. For calibration, the underlying safety level of $\beta = 3.8$ based on JCSS or rather DIN 1055-100 was used. This safety level has been historically developed with the experience gained from executed structures and it is consistent with the current general safety requirements as well as the required efficiency [17]. For existing buildings or new buildings with control actions the safety level can be adjusted on additional information [11, 18, 20].

For single loads near the point of support in beam structures a higher coefficient of variation of model uncertainty compared to the uniformly distributed load has to be assumed. For $V_{Rd,sy}$ and $V_{Rd,max}$ it is recommended that the coefficient of variation according to Table 7 should be increased up to 5 – 10 %.

Probabilistic considerations on types of shear force failure can also be managed with consistent statistical parameters of the model uncertainties. Thus, no differentiation in terms of failure have to be made. Here it is disadvantageous that different reliability is offered in all shear force failure types: in particular the reliability for $V_{Rd,ct}$ is on the very safe side. Therefore the values stated in Table 7 are sensible.

Tab. 7: Statistical parameter of model uncertainty when using one single statistical model for shear capacity

Shear force failure	Notation	Distribution density function	Mean model uncertainty	COV model uncertainty
V_{Rd} by uniformly distributed load	U_R	lognormal	1.10	15 %
V_{Rd} by single load	U_R	lognormal	1.40	20 % - 25 %

6 Summary

In probabilistic considerations of components subjected to shear force the selection of appropriate statistical parameters such as the model uncertainties on action and resistance side are of great importance to the component reliability. In contrast to flexural members, the structural behavior of shear force with the differentiation into various failure states is not entirely clear despite of extensive scientific research. Three failure states for components subjected to shear force are defined in [8]. On the basis of the conducted probabilistic calculations for general buildings, model uncertainties for a probabilistic calculation are proposed in Tables 6 and 7 taking into account that the reliability target has been given.

Furthermore the article acts as an appraisal aid for of the reliability in terms of the shear force failure of reinforced concrete components in existing structures in case where a deterministic verification is not successful with the partial safety factors fixed in [8] or rather [9]. In particular, the theoretical considerations of reliability of components without shear force reinforcement demonstrate impressively that probabilistic studies for assessing the sustainability of components in existing structures can be used as a reasonable method.

Based on the executed probabilistic parameter studies, it can be noted that there is no uniform safety level for the three shear force failure criteria formulated in [8].

Literature

- [1] Braml, Th.; Keuser M.: *Beurteilung der Tragfähigkeit von geschädigten Stahlbetonbrücken auf der Grundlage der Ergebnisse einer Bauwerksprüfung*, Beton- und Stahlbetonbau 104, Heft 5, S. 256 - 267, Ernst & Sohn Verlag, Berlin, 2009
- [2] Brehm, E. , Schmidt, H.; Graubner, C.-A.: *Model Uncertainties for Shear Capacity Prediction of Reinforced Concrete Members*, 6.th. International Probabilistic Workshop, Technische Universität Darmstadt, Darmstadt, November 2008.
- [3] CIB W81: *Actions on Structures, Snow Loads*, Report No. 141, Rotterdam, September 1991.
- [4] COMITE EURO-INTERNATIONAL DU BETON: *CEB-FIP Model Code 1990*, Design Code. 1993.

- [5] DAfStb Heft 206: Deutscher Ausschuss für Stahlbeton: Heft 206: *Statistische Analyse der Betonfestigkeit – Bericht von Rüschi, H., Sell, R. und Rackwitz, R.*, Verlag Ernst & Sohn, Berlin, Ausgabe 1969.
- [6] DAfStb Heft 525: Deutscher Ausschuss für Stahlbeton: *Heft 525: Erläuterungen zur DIN 1045-1*, Beuth-Verlag, Berlin, Ausgabe 09/2003.
- [7] Daus, S.: *Zuverlässigkeit des Klebeverbundes von nachträglich verstärkten Betonbauteilen – Sicherheitskonzept für den Verbundnachweis von oberflächlich geklebter Bewehrung*, Dissertation Technische Universität Darmstadt, Darmstadt 2007.
- [8] DIN 1045-1, Ausgabe August 2008, *Tragwerke aus Beton, Stahlbeton und Spannbeton – Teil 1: Bemessung und Konstruktion*, 2008.
- [9] DIN 1055-100: *Einwirkungen auf Tragwerke - Teil 100: Grundlagen der Tragwerksplanung*, Sicherheitskonzept und Bemessungsregeln; Deutsches Institut für Normung e.V., Fassung März 2001.
- [10] DIN EN1992-1-1: Eurocode 2: *Bemessung und Konstruktion von Stahlbeton- und Spannbetontragwerken - Teil 1-1: Allgemeine Bemessungsregeln und Regeln für den Hochbau*; Deutsche Fassung EN 1992-1-1:2004. Fassung Oktober 2005.
- [11] EN 1990: 2002-04: *Grundlagen der Tragwerksplanung*, Europäisches Komitee für Normungen, Brüssel.
- [12] EN-1992-1-1. *Design of Concrete Structures. Part 1: General Rules and Rules for Buildings*. European Standard. CEN: Brüssel, 2004.
- [13] Faber, M. H.: *Risk and Safety in Civil, Surveying and Environmental Engineering*. Course notes, ETH Zürich, 2005
- [14] Fingerloos, F., Schnell, J.: *Tragwerksplanung im Bestand, Betonkalender 2009*, Seite 1-51, Ernst & Sohn, Verlag für Architektur und technische Wissenschaften, Berlin 2009.
- [15] Fischer, J.: *Versagensmodell für schubslanke Balken*. Deutscher Ausschuss für Stahlbeton, Heft 480. Berlin, Köln: Beuth, 1997
- [16] Grimm, R.: *Einfluss bruchmechanischer Kenngrößen auf das Biege- und Schubtragverhalten hochfester Betone*; Deutscher Ausschuss für Stahlbeton, Heft 477. Berlin, Köln: Beuth, 1997
- [17] Grusibau: *Grundlagen zur Feststellung von Sicherheitsanforderungen für bauliche Anlagen*. NABau, Deutsches Institut für Normung e.V., Beuth Verlag GmbH, Berlin/Köln, 1981.
- [18] Hansen, M.: *Zur Auswirkung von Überwachungsmaßnahmen auf die Zuverlässigkeit von Betonbauteilen*. Dissertation, Universität Hannover, 2004.
- [19] Hosser, D.: *Tragfähigkeit und Zuverlässigkeit von Stahlbetondruckgliedern: Vereinfachte Nachweise bei beliebigen Einwirkungen und Randbedingungen*, Mitteilungen aus dem Institut für Massivbau der Technischen Hochschule Darmstadt, Heft 28, Verlag Wilhelm Ernst & Sohn, Berlin, München, Düsseldorf, 1978.

- [20] Joint Committee on Structural Safety (JCSS), *Probabilistic Assessment of Existing Structures*, RILEM Publications S.A.R.L, January 2001
- [21] Joint Committee on Structural Safety (JCSS): *Probabilistic Model Code* 12th draft. <http://www.jcss.ethz.ch>, 17.05.2002
- [22] Kautsch, R.: *Beitrag zur Nachweisführung von querkräftbewehrten Stahlbeton- und Spannbetonquerschnitten unter kombinierter Biege- und Schubbeanspruchung auf Grundlage der Erweiterten Technischen Biegelehre*, Technische Universität Kaiserslautern, Fachgebiet Massivbau und Baukonstruktion (Veröffentlichung in Vorbereitung).
- [23] Kollegger, J., Mehlhorn, G.: *Experimentelle Untersuchungen zur Bestimmung der Druckfestigkeit des gerissenen Stahlbetons bei einer Querkzugbeanspruchung*. DAFStb Heft 413, Beuth Verlag, Berlin 1990
- [24] König, G.; et al.: *Sichere Betonproduktion für Stahlbetontragwerke – Schlussbericht – DBV-Nr. 199*. Fraunhofer IRB Verlag, Stuttgart, 1998.
- [25] Melchers, R. E.: *Structural reliability and prediction*. John Wiley & Sons Ltd., Chichester, Australien 1999
- [26] Nowak, A. S.: *Bridge Strength*, in *Bridge Safety and Reliability*, edited by Dan M. Frangopol, S. 58 – 82, ASCE and SEI, Colorado, 1999
- [27] Pottharst, R.: *Zur Wahl eines einheitlichen Sicherheitskonzeptes für den konstruktiven Ingenieurbau*, Mitteilungen aus dem Institut für Massivbau der Technischen Hochschule Darmstadt, Verlag Ernst & Sohn, Berlin, 1977.
- [28] Rackwitz, R.: *Einwirkungen auf Bauwerke*. In: Mehlhorn, G. (Hrsg.): *Der Ingenieurbau: Tragwerkszuverlässigkeit, Einwirkungen*, Ernst & Sohn Verlag, Berlin, 1996
- [29] RCP: *A Structural Reliability Analysis Program-System*, Modul: COMREL, RCP GmbH. München, 2004.
- [30] Reineck, K.-H.: *Querkraftbemessung von Bauteilen mit und ohne Querkraftbewehrung in DIN 1045-1 – Erläuterungen und Vergleiche mit Versuchen*; Teilbericht zum Abschlussbericht für das DIBT-Forschungsvorhaben IV 1-5-876/98: Überprüfung und Vereinheitlichung der Bemessungsansätze für querkraftbeanspruchte Stahlbeton- und Spannbetonbauteile aus normalfesten und hochfesten Beton nach DIN 1045-1; Institut für Konstruktion und Entwurf II; Universität Stuttgart; Dezember 1999.
- [31] Reineck, K.-H.: *Hintergründe zur Querkraftbemessung in DIN 1045-1 für Bauteile aus Konstruktionsbeton mit Querkraftbewehrung*. In: *Bauingenieur* 76 (2001), Nr. 4. S. 168-179
- [32] Reineck, K.-H.: *Überprüfung des Mindestwertes der Querkrafttragfähigkeit in EN 1992-1-1 – Projekt A3*; DIBT-Forschungsvorhaben ZP 52-5-7.270-1218/05; Institut für Leichtbau Entwerfen und Konstruieren; Universität Stuttgart; Dezember 2006.
- [33] Rußwurm, D.: *Teilsicherheitsbeiwerte für Werkstoffwiderstände*, Betonwerk + Fertigteiltechnik, Heft 10, Seite 30 - 36, 1988.
- [34] Scheuermann, G.: *Beitrag zur Kombination klimatischer Lasten*; Schriftenreihe Stahlbau – RWTH Aachen, Shaker Verlag, 2002.

- [35] Sørensen, J. D.: Calibration of Partial Safety Factors in Danish Structural Codes, JCSS Workshop on Reliability based Code Calibration, Zürich 2002.
- [36] Specht, M., Scholz, H.: *Ein durchgängiges Ingenieurmodell zur Bestimmung der Querkrafttragfähigkeit im Bruchzustand von Bauteilen aus Stahlbeton mit und ohne Vorspannung der Festigkeitsklassen C12 bis C115*. Deutscher Ausschuss für Stahlbeton, Heft 453. Berlin, Köln, Beuth, 1995
- [37] Tue, N. V.: *Statistische Auswertung der Betonqualität - Folgerungen für die Bauwerkssicherheit*. Kongressunterlagen der 51. BetonTage, Neu-Ulm, 2007.
- [38] Vrouwenvelder, A. C. W. M. & Siemes, A. J. M.: *Probabilistic calibration procedure for the derivation of partial safety factors for the Netherlands building codes*, Heron Vol.32, No. 4, 1987.
- [39] Zink, M.: *Zum Biegeschubversagen schlanker Bauteile aus Hochleistungsbeton mit und ohne Vorspannung*; aus der Reihe „Forschung für die Praxis“ am Institut für Massivbau und Baustofftechnologie der Universität Leipzig; Stuttgart, Leipzig: B. G. Teubner Verlag, 2000.

Probabilistic Assessment of Performance Criteria for Egress Design

Cornelius Albrecht, Dietmar Hosser

Institute of Building Materials, Concrete Construction and Fire Protection (iBMB),
University of Braunschweig (Institute of Technology), Germany

Abstract: In this paper, a probabilistic analysis of life safety criteria for egress design is performed using a Latin Hypercube Monte Carlo sampling and the common methods of event history analysis, namely the Kaplan-Meier estimator and Greenwood's formula to assess the vulnerability and the confidence bounds. The vulnerability curves found for the criteria will be compared and analyzed and methods for design and criteria selection are presented. Furthermore, a correlation analysis reveals the influence of the input parameters on the times to untenability. It was found that the fire growth rate, expressed as time to reach a fire size of 1MW is the governing parameter.

1 Introduction

Providing for life safety during the event of a hostile building fire is a key aspect of Fire Safety Engineering. In Germany, the safety is implicitly ensured by prescriptive building regulations, but due to the more and more complex architecture of buildings, prescriptive fire-codes are not always applicable. In these cases performance-based solutions have to be found to satisfy the required level of safety. In a performance-based approach for life safety, the time needed for safe egress (t_{required} or RSET) is compared to the time until untenable conditions are reached within the building ($t_{\text{available}}$ or ASET).

The available time can be obtained by applying performance criteria which account for the various effects of the fire on the occupants, e. g. the height, the optical density, toxic effects or the height of the "smokeless" lower air layer. For the toxic effects either single threshold values after HOSSER [1] or combined and time-integrated values according to PURSER [2] can be chosen to account for various species and exposure concentrations. The different fire effects are calculated by numerical fire simulations based on representative fire scenarios using CFAST [3] and design fires which are derived from values for fire loads, fire growth rate, heat release rate etc. These values are usually chosen as determinis-

tic values, even though they are known to be subjected to major uncertainties. These uncertainties can be regarded using stochastic models for the various fire parameters. Some models can be found in the literature, for example in the work of HOLBORN [4].

The benefit of a probabilistic analysis is not only to gain insight into the uncertain effects of the fire, but also to obtain information about the temporal variance and thus conservativeness of the criteria. Knowing the probabilities of untenability reached at a certain time, a quantification of the time-dependent risk to life can be derived, so that probabilistic requirements can be formulated as shown in NOTARIANNI [5].

2 Event History Analysis

Event history analysis is often applied to predict the likelihood of a certain event to happen at a certain time, when only a limited number of samples are available. The methodology is often times used in medical studies to estimate the effectiveness of treatments with respect to the time of occurrence of a certain event. The methodology can also be applied in fire protection engineering to estimate the probability of untenable conditions to occur at a certain time during a fire as previously shown by NOTARIANNI [5]. The following sections will briefly explain the basic ideas of event history analysis.

2.1 The Kaplan-Meier Estimator

The Kaplan-Meier Estimator, also often referred to as Product Limit Estimator, is used to predict the probability of an event to happen within a certain time interval. The advantage of this method is that the resulting maximum likelihood estimate is non-parametric and of empirical nature and hence avoids inaccuracies involved with distribution fitting and therefore can also be used for smaller sample sizes. The methodology was first published by KAPLAN and MEIER [6] and takes into account all observed events d_i and their time of occurrence t_i , so that the probability of the event to happen $\hat{S}(t)$ at the time t yields

$$\hat{S}(t) = \prod_{t_{(i)} \leq t} \frac{n_i - d_i}{n_i} = \prod_{t_{(i)} \leq t} \left(1 - \frac{d_i}{n_i} \right), \quad (1)$$

where d_i is the sample(s), where the event happened until the time t_i and n_i is the remaining number of samples at risk at time t_i .

Generalizing the formula from the set of samples to the general random variable T with $F(t)$ to be the cumulative distribution function, we get the complementary distribution function

$$S(t) = P[T > t] = 1 - P[T \leq t] = 1 - F(t), \quad (2)$$

which is often referred to as the “survivor function” of the random variable T .

2.1.1 Variance Estimation

The variance of the Kaplan-Meier Estimator based on a set of samples in the interval $t_k \leq t \leq t_{k+1}$ can be approximated using

$$\text{Var}(\hat{S}(t)) = \hat{S}(t)^2 \sum_{i=1}^k \frac{d_i}{n_i(n_i - d_i)}. \quad (3)$$

The formula is often referred to as Greenwood's Formula and is commonly used to calculate the confidence bounds. For an approximation of the 95% confidence bounds, we utilize Equation 3 to get the standard error and subsequently the confidence interval

$$95\% \text{ CI bounds} \equiv \hat{S}(t) \pm 1.96 \cdot \hat{S}(t) \left\{ \sum_{i=1}^k \frac{d_i}{n_i(n_i - d_i)} \right\}^{\frac{1}{2}}. \quad (4)$$

2.2 Censoring of data

For the accurate estimation of the likelihood of an event to happen, all data samples must contain the needed information. In case the event has already occurred prior to the observation interval, the data has to be censored. This case is called left-censoring and is only of theoretical nature for this study, as untenable conditions before the start of the fire are not possible. The right-censoring of data is more relevant for this study. Samples in which the criterion is not reached during the simulation time have to be excluded from the further analysis. As it is assumed that the egress has to be completed within 15 minutes as proposed by MEHL [7], the data is considered "right-censored, type I", meaning that the event (untenable conditions) has not occurred within the defined period of time of 900 seconds.

3 Performance Criteria for Egress Design

The evaluation of the available time for safe egress is a challenging task of fire protection engineering, as unlike structural elements which are only subject to the high temperatures, the occupants can be confronted with multiple effects of the fire. These effects that can prevent the occupants from safe egress can be the temperature as well, but also visibility or the height of the smoke layer and most of all the toxic and asphyxiant effects of the combustion products, like i.e. hydrogen cyanide (HCN) or carbon monoxide (CO). As some of the effects can occur simultaneously during a fire situation, these interactions have to be regarded as well.

Additionally, not only maximum instant threshold values can be dangerous for the occupants but also exposure to lower doses over a longer period of time. Extensive work on the modeling of those effects was done by PURSER [2] leading to the fractional effective dose concepts (FED) for heat, toxic and asphyxiant, as well as irritating effects taking into account multiple species. The basic principle of the FED values is that the sum of time-

integrated fractions of the doses of all species considered that would prevent egress must be less than 1.0 for a safe egress of an average person:

$$X_{FED} = \sum_{i=1}^n \int_t \frac{C_i}{(C \cdot t)_i} dt, \quad (5)$$

where C_i is the concentration at time t for species i and $(C \cdot t)_i$ is the specific exposure dose that prevents safe egress.

The account for weaker populations, the threshold for the FED_{tox} is usually chosen to be 0.3. All criteria and the threshold values considered in this study are summarized in Table 1. The values are taken from the relevant literature HOSSER [1] and PURSER [2]. Additionally, other values around those thresholds are used to test for the temporal variance of the criteria.

Tab. 1: Performance Criteria and Threshold values used in this study

Effect	Criterion	Threshold Value	Reference/Reason
Smoke	Layer Height	2.5m	HOSSER [1]
		1.8m	Avg. body height
		1.0m	Crawl height
Thermal	Max. Temperature	50°C	HOSSER [1], Tab. 8.1
		100°C	HOSSER [1], Tab. 8.1
		180°C	Thermal Shock
	Heat Flux	2.5 kW/m ²	Pain
		4.0 kW/m ²	Instant Burns
10.0 kW/m ²		Instant Death	
	$FED_{thermal}$	1.0	Incapacitation
Toxic	Carbon Monoxide	200ppm	Medium Exposure Limit
		500ppm	Short Exposure Limit
	FED_{toxic} (with HCN)	0.3	PURSER [2]

4 Fire Scenario and Simulation

As the focus of this paper should mainly be on the utilization of the probabilistic methods, a very simple scenario was assumed. For the calculation of the ASETs, a rectangular room of around 180m² (14.4m by 12.4m) was modeled with a height of 3.8m. The fire scenario was chosen to be follow a αt^2 -curve according to HOSSER [1]. This assumption is based on the work of HESKESTAD [8], who found that the heat release rate of a fire will increase quadratically over time during the fire development phase. α is a multiplier to consider different growth rates. The growth rates are dependent on the type of combustibles and normally correspond to a fire growth up to 1MW to occur between 75 and 600 seconds depending on the occupation. After reaching the maximum heat release rate, it will remain constant until 70% of the fire load is consumed and will then progress into a linear decay, as shown in Fig. 1.

The uncertain variables used herein are the fire load density, the maximum rate of heat release, the fire growth rate as well as the species yields for carbon monoxide (CO), soot and hydrogen cyanide (HCN). The stochastic models can be found together with the relevant literature in Table 2.

The fire and the effects were simulated with the zone model CFAST [3]. The model basically divides the room into three zones: the plume zone, the upper (smoke) layer and the lower (smokeless) layer. The model has been widely used in the area of fire protection engineering and has the advantage of a low computational cost, as an average simulation run only takes about 5-10 seconds. The disadvantage is the rather coarse approximation and the averaging within the zones. A better approximation would be the use of computational fluid dynamics (i.e. FDS [9]), which requires far longer computation times in the range of hours to days per simulation. Hence, a Monte Carlo simulation is out of scale for recent computers to be calculated within a reasonable time. For that reason, the zone model was chosen to demonstrate the applicability.

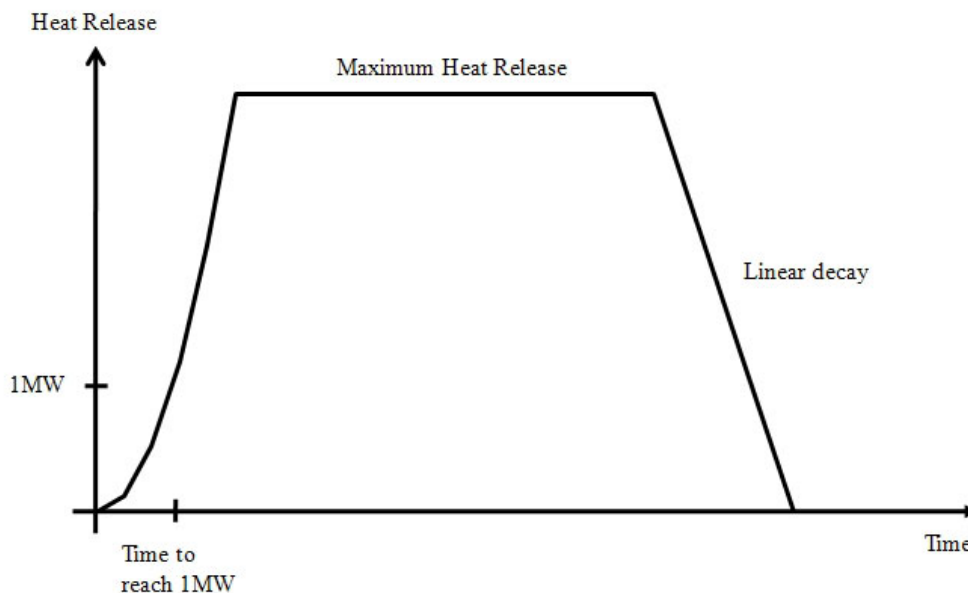


Fig. 1: Course of the heat release rate of the fire scenario

Tab. 2: Stochastic input parameters of the fire simulation model

Parameter	Distribution	Mean / Lower	Std.Dev. / Upper	Source
Fire Load Density	Gumbel-max	300 MJ/m ²	90 MJ/m ²	BSI [10]
Max. Heat Release	Normal	2.5 MW	0.5 MW	ZEHFUSS [11]
Fire Growth Rate	Normal	225s	45s	YUNG [12]
CO-yield	Uniform	0.01 g/gCO ₂	0.2 g/gCO ₂	PEACOCK [13]
Soot-yield	Uniform	0.005 g/gCO ₂	0.08 g/gCO ₂	PEACOCK [13]
HCN	Uniform	0.001 g/g	0.01 g/g	PEACOCK [13]

Based on the above assumptions and models, a Monte Carlo simulation was carried out using Latin Hypercube sampling for a better representation of the random space. Because

of the low per-annum probability of a hostile fire to occur and grow beyond the stage of fire initiation, only the random space of $\pm 2\sigma$ (standard deviations) around the means was scanned for the fire load density and the maximum heat release rate. This is reasonable, as two standard deviations in each direction represent more than 95% of all cases. Due to the occupancy, the time to reach 1MW was chosen to be between medium (300s) and fast (150s) according to the BSI [10] and YUNG [12], which leads to a mean value of 225s. To account for the uncertainty of this parameter, the standard deviation was chosen to be 45s, so that times from 135s to 315s are included in the simulations. This assumption is in approximate accordance with the values found by HOLBORN [4] for public buildings.

The yields are chosen to be uniform distributed due to a lack of better stochastic models and were used within their whole range from the lower to the upper bound.

Due to the low computational time required, it was possible to run 2500 simulations for the scenario. As an assembly room of $>200\text{m}^2$ is required to have smoke and heat exhausting system (SHE) by German fire codes (MVSTÄTTVO [14]), the scenario was simulated with and without a SHE of a required 1% of the floor space (2m^2) to check for the impact of such a system on the time to reach the tenability limits. The doors were also dimensioned according to the fire codes.

5 Results of the Analyses

In the following section an introduction is given on how to interpret the results of the survival analysis and how to compare the various criteria as well as to compare different designs. A detailed analysis of all the outcomes would go far beyond the scope of this paper. In this example, two designs of the same room with the same fire scenario described above will be compared: with and without smoke and heat exhaustion system (SHE).

Figure 2 shows the empirical survivor functions of the various criteria tested for the design with SHE system installed. It should be noted here that most of the thresholds were not reached in the lower “smokefree” layer of the fire due to the exhaustion. Even though the smoke layer falls below 2.5m within a maximum of 200 seconds, none of the designs simulated had the smoke layer fall below 1.8m. In that case all the data was censored and therefore no curve could be plotted.

The empirical survivor plots can be utilized to gain probabilistic information about the times to untenability in the room together with the probability of survival. Taking the heat flux not to exceed $2.5\text{kW}/\text{m}^2$, for example, we can obtain that in 90% of the cases, there are 290 seconds or more until the criteria is reached and even 400 seconds in 50% of the cases. Figure 2 also shows the different criteria and their time-dependent transgression which enables us to obtain information about the conservativeness of each threshold criterion.

Figure 3 exemplary shows the complementary empirical CDF for the time to reach a layer height of 2.5m in the SHE scenario. Additionally, the 95% confidence bounds are plotted. In this case the confidence interval is rather narrow as none of the 2500 simulations had to

be censored from this dataset. Nevertheless an analysis of the confidence interval is recommended for small datasets or datasets that have a high percentage of censored data.

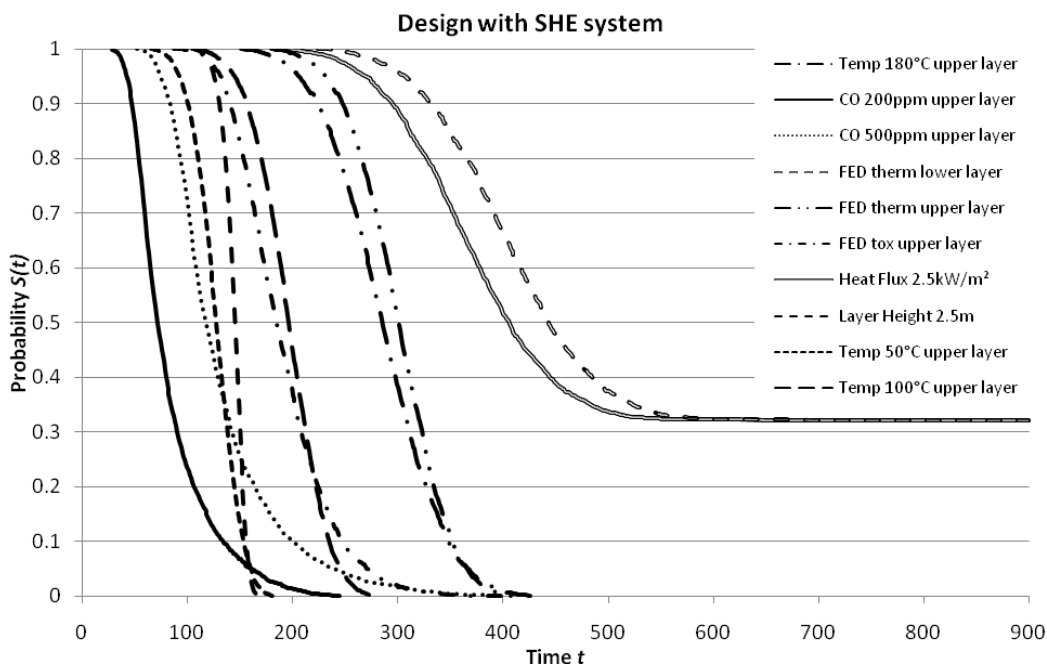


Fig. 2: Complementary empirical CDFs of the threshold criteria in the scenario with SHE

Figure 4 exemplary shows a comparison between the designs with and without a SHE system installed providing a good illustration on how to interpret the criteria: the comp. emp. CDFs of the times of the layer height to fall below 2.5m are nearly parallel with a rather steep course compared to the comp. emp. CDFs of the times to reach a heat flux of 2.5kW/m². In qualitative terms, a steep comp. emp. CDF describes a very small variance of the criterion with regard to time. Being close together, the curves show that the impact of the SHE is not very distinct with regard to this criteria.

Nevertheless it should be stated that for the design without SHE, the layer height fell below 1.8m in all cases in less than 200 seconds, whereas none of the 2500 simulations of the design with SHE installed had the smoke layer fall below 1.8m, which implies a “smokefree” escape in at least 2500 of 2501 cases, which corresponds to a probability of failure (p_f) of at least 4E-4. This example shows the importance of the correct selection of the criteria.

The times to reach a heat flux of 2.5kW/m² show a larger variance in time and the SHE has a large impact on this criterion. With a SHE system installed, a heat flux of 2.5kW/m² is not reached in about 32% of the simulated cases.

Figure 5 shows an overlapping of the comp. emp. CDFs of two criteria for the scenario without SHE system installed. In this case it seems difficult to make a reasonable choice between the two criteria, as both can be the more or the less conservative choice: the temperature is more conservative between 220s and 530s, whereas the FED toxic is more conservative thereafter.

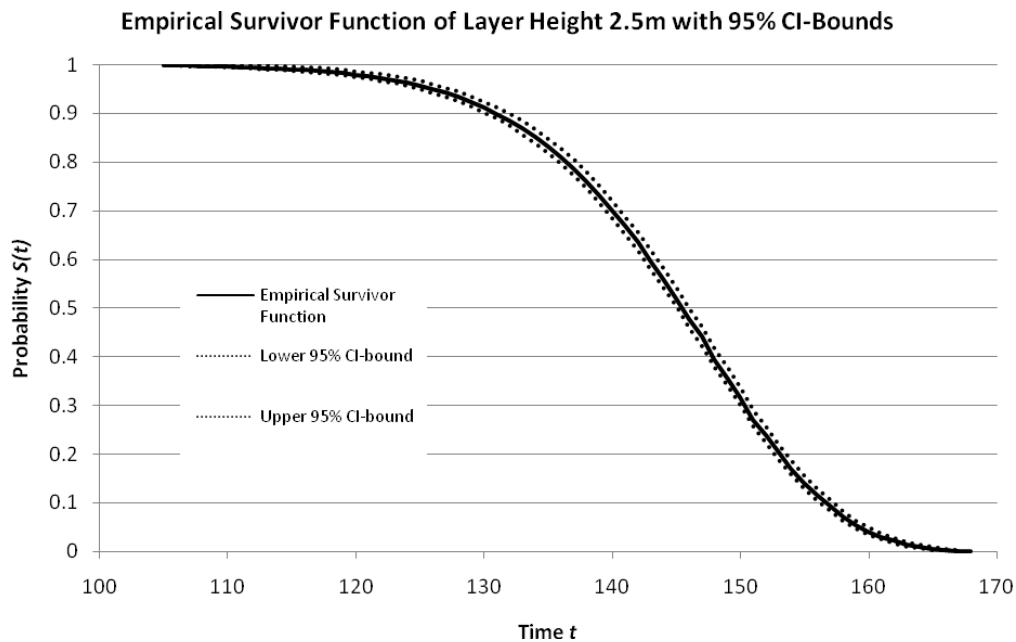


Fig. 3: Complementary empirical CDF of time to reach a layer height of 2.5m in the SHE scenario together with the 95%-confidence bounds

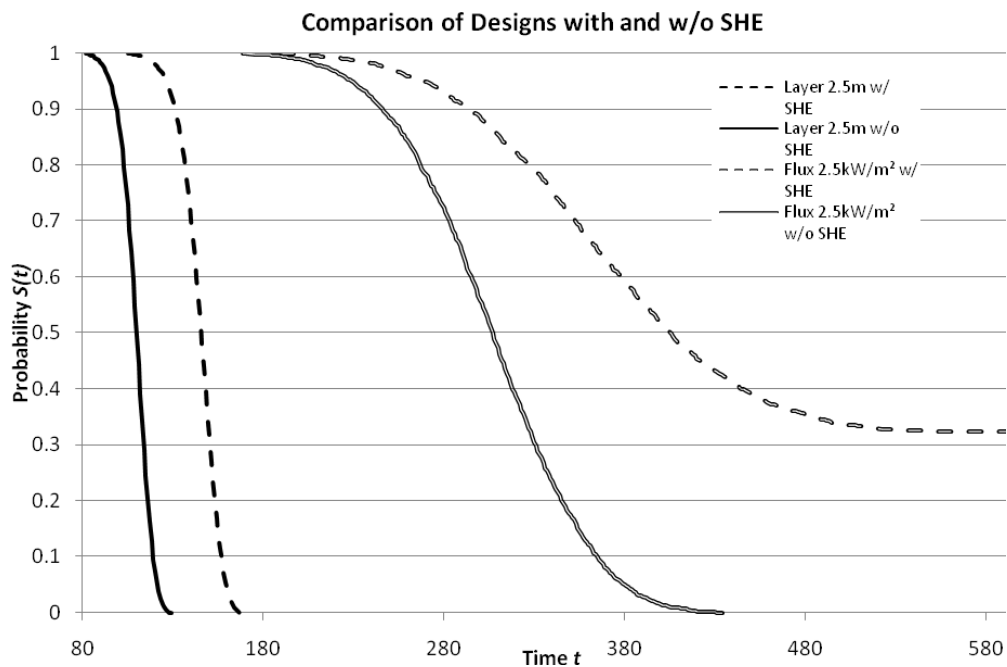


Fig. 4: Comparison of two criteria for the two scenarios

A simple decision aid can be a closer look at the time differences Δt between the two criteria for each simulation, as shown in Figure 6. As the time to reach a temperature of 100°C is subtracted from the time to reach the FED toxic, negative values imply that the FED toxic is more conservative, while positive results denote a conservativeness of the time to reach the temperature of 100°C. Sorting the data and normalizing by the number of total simulations, we get an empirical cumulative distribution function of Δt . Figure 6 provides information about the two criteria, for example that the FED toxic is more conservative in 43% of the cases, while the temperature criteria is in 57%. Those difference plots can also be used for the comparison of different designs.

A method described by NOTARIANNI [5] considers more than only one criterion. In this case we want to obtain the empirical probability of having 400s or more for egress considering both criteria stated above (FED toxic and temp. 100°C). In this case we can simply divide the number of simulations where both criteria provided times to untenability of more than 400s by the total number of simulation. From Figure 5 we can obtain that the probability of having more than 400s for the FED toxic is 72% and for the temp. 100°C is 64%. Figure 6 graphically shows the (lower) probability of 57% of having 400s or more when considering both criteria at the same time. Naturally, this method can be used for multiple criteria, but should only be used if a sufficient number of simulation runs are available for a reasonable approximation. In this case, no censoring was used.

The brief analyses show that event history analysis can be utilized for the probabilistic evaluation of performance criteria for egress designs. The results show how the criteria varies in time and in comparison with other criteria and designs. The plots of the empirical “survivor” functions show the probability of the room to become untenable in case of a fire. The course of the plot over the time after fire ignition provides details about the available egress time and the temporal variance of the criterion for any chosen probability or vice versa gives information about the probability of tenability of a chosen required egress time. Testing different criteria each with different threshold values also makes it easier to identify the appropriate criterion depending on the goal of the analysis (for example: the most conservative).

A decision between two criteria or designs can be made by simple subtraction of the times to untenability for each scenario and normalization to obtain the empirical distributions of the differences Δt . This set of very simple analyses provides the designer with a powerful tool to quantitatively decide and verify a design or the threshold criterion to use.

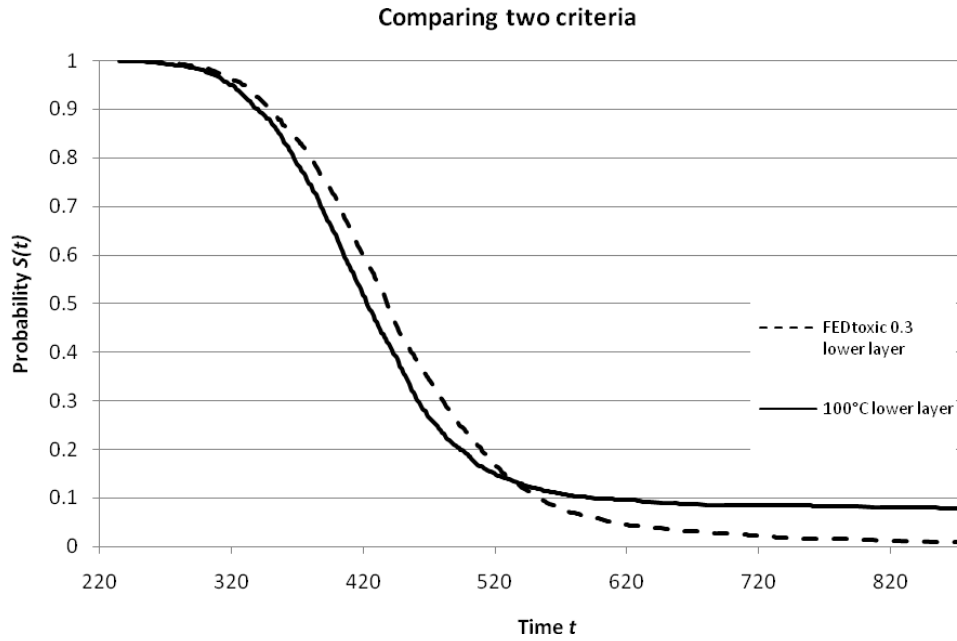


Fig. 5: Overlapping of the comp. emp. CDFs of two criteria

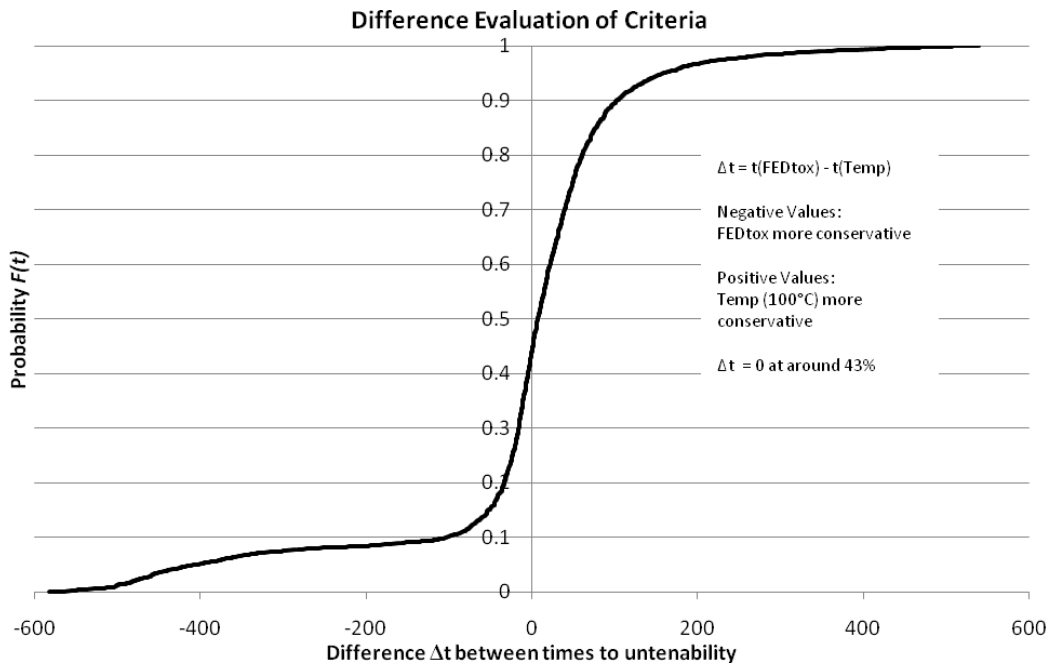


Fig. 6: Evaluation of the differences two criteria

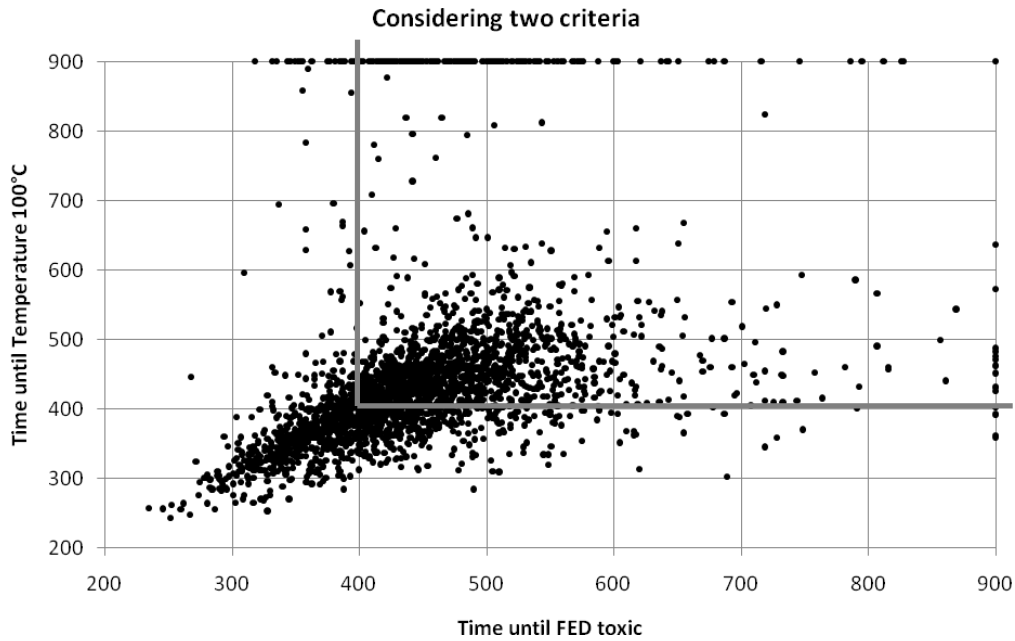


Fig. 7: Considering multiple criteria

6 Parameter Correlation

To analyze the linear correlation between input and output parameters, a hypothesis test is carried out using the correlation coefficients ρ_i . Hypothesizing that the correlation between input and output is not significant to a chosen significance level of 95% (H_0), the alternative hypothesis states, that the correlation is to be considered significant (H_1). The null hypothesis has to be rejected if the test statistic t_i is greater than the critical value of the t -distribution (student distribution) with a $\alpha/2$ significance level and $(n-2)$ degrees of freedom ($t_i > t_{\alpha/2; n-2}$). The test statistic is calculated

$$t_i = \frac{|\rho_i|}{\sqrt{1-\rho_i^2}} \sqrt{n-2}, \quad (6)$$

where ρ_i denotes the calculated correlation coefficient and n is the number of samples.

It should be noted that a significant mathematical correlation does not automatically imply a causal correlation between two parameters, so that a qualitative analysis of the causal correlation must be carried out to identify those coincidental correlations.

6.1 Results of Correlation Analysis

A correlation analysis with subsequent hypothesis testing to a 95% significance level was carried out according to Equation 6 for the parameters to test for linear correlation with the times to untenability. The results show, that the fire load has no significant impact on any of the times to reach a criterion. This is most likely due to the fact that the fire load only impacts the duration of the fire in the chosen αt^2 -fire model. Due to the given distribution of the fire load, the overall duration of the fire exceeds the 900s simulation limit and therefore will not impact the time to untenability. Hence, a “safety” factor on the fire load would not provide any additional safety for the occupants.

The fire growth rate expressed by the time of the fire to grow to 1MW has highly significant impact on the times to untenability for all criteria. This seems reasonable considering the fire scenario and the model used and also corresponds very well with the findings of FORELL [15], who also found the growth rate to have significant impact on the times to untenability.

Additionally, a high significance of the CO-yields and the HCN-yields on the times to reach the FED toxic values could be observed which confirms the qualitative assumption. Naturally, the CO-yields also play a major role in the times to untenability for the maximum CO concentration, whereas the maximum heat release rate (HRR) significantly contributes to the times to reach the temperature thresholds.

The correlation analysis is not limited to input vs. output parameters, but can also be utilized to test for inter-dependencies of the output parameters. Expectedly, an analysis shows that there is a high correlation between the criteria that are based on the same parameters, for example the temperature thresholds and the FED thermal or the FED thermal and the heat flux. The FED toxic and the maximum allowable CO concentrations are also significantly correlated but not with a correlation coefficient near one, as the HCN has a significant impact on the FED toxic.

A mathematically significant correlation was found between the soot yield and the temperature criteria, which is considered to be either coincidental or related to the influence of the heat release rate on both criteria (spurious relationship).

7 Conclusions

Non-parametric event history analysis is often times used in medical studies to test for the impact of a treatment, when not enough patients are available to utilize parametric distributions. This paper showed the applicability of this methodology to problems of fire protection engineering, where occupants are confronted with the impacts of the fire. In this study, a sufficient number of simulations runs could be performed to gain accurate information about the behavior of the criteria in the $\pm 2\sigma$ random space around the means.

For future analyses, simulations based on computational fluid dynamic (CFD) models have to be considered to gain more detailed information about the effects of the fire on the occupants, also considering the location within a room, as well as more complex geometries (i.e. atria in shopping malls), which cannot be reasonably approximated with zone models. As the high computational costs will not allow for a high number of simulations within a reasonable time, the methodology can be used to estimate confidence bands for the times to untenability with far less simulation runs.

A correlation analysis showed that the fire growth rate has the most significant impact on the time to untenability, which is in accordance with the findings of FORELL [15]. On the other hand it was found that the fire load has no significant influence on the times to untenability when using the fire scenario model described.

8 References

- [1] HOSSER, D. (ed.), “Leitfaden Ingenieurmethoden des Brandschutzes (Guidelines for Fire Safety Engineering),” German Fire Protection Association (vfdb) Technical Report TB 04/01, Altenberge, Braunschweig, May 2009
- [2] PURSER, D.A., “Toxicity assessment of combustion products,” The SFPE Handbook of Fire Protection Engineering (4th ed). DiNenno P.J. (ed.). National Fire Protection Association. Quincy. MA 02269. 2008
- [3] JONES, W. et al., “CFAST – Consolidated Model of Fire Growth and Smoke Transport (Version 6) – Technical Reference Guide”, Gaithersburg, MD, May 2008
- [4] HOLBORN, P., NOLAN, P. & GOLT, J. “An Analysis of Fire Sizes, Fire Growth Rates and Times between Events using Data from Fire Investigations”, Fire Safety Journal, 2004, 39, 481-524
- [5] NOTARIANNI, K.A., “Uncertainty”, Chapter 4, Section 5, Handbook of Fire Protection Engineering, 3rd Edition, DiNenno, P.J., Editor, Society of Fire Protection Engineers, 2002
- [6] KAPLAN, E.L. & MEIER, P. “Nonparametric Estimation from Incomplete Observations”, Journal of the American Statistical Society, Vol. 53, No. 282 (June 1958), pp. 457-481
- [7] MEHL, F.: “Richtlinien für die Erstellung und Prüfung von Brandschutzkonzepten” In: Hosser, D. (Editor): Praxisseminar Brandschutz bei Sonderbauten. Institut für Baustoffe, Massivbau und Brandschutz der TU Braunschweig, Issue 178, 2004.
- [8] HESKESTAD, G.: “Engineering Relations for Fire Plumes”. Fire Safety Journal, 1984, pp. 25-32.

- [9] MCGRATTAN, K. (ed.), “Fire Dynamics Simulator (Version 5), Technical Reference Guide,” National Institute of Standards and Technology Report NIST SP 1018, Gaithersburg, MD, 2009
- [10] British Standards “Fire safety engineering in buildings”, BSI DD 240, 1997
- [11] J. ZEHFUSS, D. HOSSER, “A parametric natural fire model for the structural fire design of multi-storey buildings”, Fire Safety Journal, Volume 42, Issue 2, March 2007, p115-126
- [12] YUNG, D., “Principles of Fire Risk Assessment in Buildings”, John Wiley and Sons, 2009
- [13] PEACOCK, D. et al, “Characteristics of Fire Scenarios in Which Sublethal Effects of Smoke are Important”, Fire Technology, 40, p127-147, 2004
- [14] IS-Argebau, “Musterverordnung über den Bau und Betrieb von Versammlungsstätten – MVStättV”, June 2005
- [15] FORELL, B., “Niveau der Personensicherheit von Versammlungsstätten – Nachweis nach vfdb-Leitfaden”, Proceedings of the 56th Jahresfachtagung der vfdb, Leipzig, May 2007, p294-317

Sensitivity analysis of partial safety factors to the design of offshore steel structures

A. Kolios¹, I. Jusoh², F. Brennan¹

¹ Offshore Engineering and Naval Architecture Group, Cranfield University, United Kingdom

² Universiti Teknologi Malaysia, Skudai, Johor. Malaysia.

Abstract: Use of design standards is nowadays the most widely used design method providing structures that achieve minimum levels of reliability. Partial safety factors incorporate sources of uncertainty of each acting load, forming load combinations that should be considered for the critical loading of the structure. Optimization of offshore structures where wind, wave and environmental loads act demands analytical derivation of those factors. Structures of large scale can benefit from this calibration procedure, resulting to lighter and more economic designs with predicted performance throughout their service life. This paper presents a sensitivity analysis of the partial safety factors of an offshore jacket reference structure.

1 Introduction

The essential requirement of structural design is to produce structures with an adequate safety level, able to withstand design loads throughout its service life. Design analysis starts from the formulation of the loading models followed by structural modelling and later the response analysis of the structure. Typical loading formulation adopted in the analysis gives the results in the form of several response analysis such as strength utilization ratio, reliability index and failure path.

Use of safety factors is an important consideration and inclusion in the design process in order to achieve the safe final design. Several design codes are considered in this respect; among others are the API code, the ISO design code as well as the Eurocodes. Commonly, the design procedures are mainly based on structural limit states. However, modern design codes and procedures, have adopted a new approach introducing partial safety factors. In this paper a sensitivity analysis of partial safety factors in the design of a typical offshore structure is investigated.

The study started with structural modeling using typical finite element program, DNV SESAM and related structural analysis followed the standard design procedure presented in [1]. Having a structure designed as close as possible to the requirements of the standard and based on a load combination of the acting loads with weight factor

equal to 1, each of the safety factors was gradually increased and the effect on the utilization factor of the critical parts is measured. Later a simultaneous combination between two loads was studied and finally for that set of cases the variation of the total mass of the structure in order to resist the applied loads is calculated and presented. The useful findings of this study are summarized in the conclusions of this paper.

2 Design Of Offshore structures

2.1 Offshore Structures

The challenge of offshore structures is that very large scale structures have to be designed against considerable environmental phenomena. Wind and wave effects are much more severe as we move further away from shore. Corrosion is another factor that gradually diminishes the load bearing capacity of the structure. In addition, the action of those loads is continuous and the structure's service life can exceed 40 years.

A typical fixed steel offshore structure may be described as a structure comprising by tubular members (tubes and pipes) extended from the seabed to certain level above the sea water level. The structure is kept in place on the sea bed piled and should safely remain stationary over its intended design life. It is intentionally designed to support a topside and transmit all lateral and vertical loads to the seabed. An analytical description of a jacket structure will be carried out in the later paragraphs.

2.2 Design Standards

Relevant Design Standards, provide analytical methodologies for the design, construction and inspection of offshore structures. Based on rules and calculations, they incorporate good engineering practice in order to achieve adequate designs giving guidelines for calculations, characteristic values of loads and propose safety factors and load combinations. Petroleum industry has assisted crucially the process of systematic design of offshore structures, due to their high demands on reliability and safety.

API RP-2A: "Recommended Practice for Planning, Designing and Constructing Fixed Offshore Platforms" [1], standard of American Petroleum Institute (API), which today has reached its 21st edition, was introduced in 1969 and has been the basis for the design of most offshore fixed installations around the world. In 1993 it was published in a limit state design layout [2]. Lloyd's, later published the "LRS Code for Offshore Platforms" [3] in 1988 and recently in 2007, Germanischer Lloyd, published the "Guideline IV – Industrial Services: Offshore Technology" [4]. Det Norske Veritas published "DnV: Rules for the classification of Offshore Installations" [5] in 1989, and recently in 2008 the "Offshore Standard OS-C101: Design of offshore steel structures, General – LRFD Method" [6]. Finally from 2007 the International Standardization Organization (ISO) has introduced a series of standards, the most relevant to the above is "ISO 19902:2007 Petroleum and Natural Gas Industries – Fixed Steel Offshore Structures" [7].

2.3 Partial Safety factors

Safety factors are magnification factors that incorporate all sources of uncertainty of a design, taking into account unforeseen extremes throughout its life time by increasing the characteristic values of loads in order to achieve structures of accepted reliability. Use of Partial Safety Factors (PSFs) (Limit States Method) is the development of the Global Safety Factor Method. Compared to the later, use of PSFs, provides optimized results of design considering each design load's uncertainty individually.

Derivation of the appropriate PSFs is a crucial decision the engineer has to make in order to provide a safe and economically feasible design. Design Standards give typical values of PSFs for acceptable target reliability levels. More modern standards, such as the Euro-codes provide analytical methodologies for the deterministic derivation of the safety factors considering every structure individually for the loads it may undergo. Therefore, PSFs values cannot be verified without knowledge of real properties of load bearing structural members [8]. This is a demanding probabilistic procedure that calibrates the values given by the standards targeting to the same levels of reliability. The structure's probability of failure is analyzed in dependence on values of partial safety factors of material, permanent loading and long time variable loading.

In [8] a study of the effect of partial safety factors on the design reliability using fuzzy numbers can be found. Other researches [9-11] also investigated the application of partial safety factors for tubular joint design as well as random wave overtopping respectively.

3 Jacket Structures

3.1 Structural Model

Offshore Jacket is a common design of offshore structures that are able to operate in depths between 25 and 50 meters. Widely used in oil and gas platforms they have been operated for more than 50 years. They are constructed by vertical and inclined tubular members (legs) connected together to a space-framed truss structure (bracing). The structure can be modeled using finite element methods (FEM) to derive its response to the loads acting on it. Suitable boundary conditions and assumptions must be taken into consideration in order to realistically represent the interaction of the structure to the seabed. In a typical jacket, the legs of the platform extend towards the direction of the seabed by a length approximately equal to that of the legs. Commonly piles are of smaller cross section than the legs, and frequently, separate pipes are used inside the legs that go through them and extend to the bottom. This increases significantly the stiffness of the overall structure.

A typical four-legged structure was used in this analysis to estimate the utilization factor of the fixed offshore structure. The basic static as well as dynamic responses of the structure were analyzed. The scope of this study is to investigate the effects of variation of partial safety factors as refer to several design codes with respect to structural loading and response under design loading conditions. The consideration of the loads applied to the structure and the assumptions considered will be discussed briefly in the paragraphs below.

3.2 Applied Loads

The loads experienced by offshore structures are mainly from environmental sources which includes wave, wind and current. Other loading contribution is mainly from dead loads, construction loads, live loads, as well as operational loads [1].

3.2.1 Wind Load

Most current design methods for wind loads assumed that the wind is a static load – that a fixed value which does not vary with time. In reality, a wind profile consists of a mean flow, plus a time-varying gust called turbulence. Therefore the real wind imposes both a static load due to the mean flow, and a dynamic load due to turbulence. The mean and turbulent contributions added together give a vector quantity which varies randomly in magnitude and direction.

Wind loads are calculated using the following drag type relationship;

$$F_{wi} = \frac{1}{2} \rho C_{wi} A_p V_{wi}^2$$

Where; C_{wi} is the shape coefficient and ρ is the density of air, A_p is the projected area of the structural component subjected to wind and V is the wind velocity. Values of C_{wi} for the topside of the structure considered as a square block and the leg of jacket exposed to wind are 2.0 and 0.6 respectively [12].

3.2.2. Wave Load

Accurate mathematical description of typical wave motions may only be possible by non-linear spectral methods. It has been found reasonable for many purposes to resort to finite wave theories such as Linear wave theory, first and higher order Stoke to describe discrete characteristics. Linear wave also known as ‘regular waves’ are commonly used for estimating loading on offshore structures which will in practice be loaded by ‘irregular waves’. These regular waves are sinusoidal in nature where as their height increases the crest becomes steeper and troughs flatter. There are several types of regular wave theories that may be used in the loading estimation of offshore structure. In this study the simple analysis is adopting a Linear Wave Theory.

The theory for wave forces on cylindrical bodies faces the total force as being composed of a drag component due to shear and inertia component due to fluid acceleration. Thus, for a small cross sectional element of axial length, ds , in a circular cylinder of diameter D , the total load may be estimated using Morison equation:

$$f_T = f_D + f_i$$

Where; f_D is drag force per unit length and f_i is an inertia force per unit length.

Wave force per unit length:

$$f = \frac{1}{2} \rho C_D D |u|u + \frac{\pi}{4} \rho C_M D^2 \frac{\partial u}{\partial t}$$

Where: ρ is density of sea water, C_D is the drag coefficient, C_M is the inertia coefficient and u is horizontal water particle velocity.

The total force on the cylinder immersed in water depth d :

$$F = \int_0^d f ds = \int_0^d \left[\frac{1}{2} \rho C_D D |u|u + \frac{\pi}{4} \rho C_M D^2 \frac{\partial u}{\partial t} \right] ds$$

While the effect of current flow in the Morison equation is included in the following relationship:

$$f = \frac{1}{2} \rho C_D D |u|u + \frac{\pi}{4} \rho C_M D^2 \frac{\partial u}{\partial t} + \frac{1}{2} \rho C_D D u_c^2$$

Where: u_c is the current velocity.

3.2.2 Functional Loads

Functional are loads which may vary in magnitude, position and direction during the period under consideration, and which are related to operations and normal use of the installation. For an offshore wind turbine, operation loads are the thrust and the overturning moment due to wind acting on the tower. In an offshore oil and gas platform operation loads are those occurring due to the operation of the drilling machinery etc.

3.3 Load Combinations

Several loading conditions are applicable in response analysis depending on variation in water depth, topside loads, wind velocities, marine growth, miscellaneous appurtenances and angle of wave attack. In base case design study only one set of loading condition is adopted to represent the structural response as a reference to later load cases.

In practice several methods may be adopted in calculating wave loading and structural response. Good understanding of the factors affecting the fluid loading and structural response are required in order to make the right selection of a suitable overall method and the detailed application of the method in the analyses themselves.

The first step in performing structural response analysis is to develop appropriate probabilistic models for the basic loads and resistance variables. The main sources of uncertainty affecting the loading is the extreme wind speed, the extreme current

speed, the spectral form of the extreme sea state, the extent of the marine growth, the hydrodynamics forces (given water particle velocities and accelerations) and deck loads.

Loadings on any offshore structural element comes from two distinct sources namely internal loads which are transferred from adjacent elements members as well as external loads predominantly from waves, wind and current. Transferred loads are estimated using Finite Element program while loads due to waves are estimated using Morison`s equation and Stokes wave theory.

The principal differences between base case loading models and more realistic models come from the direction of approach of wave, wind and current. The main assumption in the base case is that all environmental parameters are assumed to act unidirectionally onto the structure. In reality the probability of this happening is very small.

Stress utilization for any structural element under axial tension and bending or compression and bending may be estimated by the following relationship [1]:

$$\frac{f_a}{0.6F_y} + \frac{f_b}{F_b} \leq 1.0$$

Where: f_a is allowable axial stress, f_b is bending stress, F_y is yield stress, and F_b is allowable bending stress

3.4 Model assumptions

For the purposes of this study, a common Jacket structure was selected and modeled as is shown on Figure 1. It is an assembly of tubular members of various diameter sizes to form the structure. The 95 m height structure has a square dimension of 30.4x30.4 m at the sea bed and 15x15 m with vertical and horizontal X-bracing and slope of legs 1:10.

The water depth is considered to be 80 m and the total height of the platform 95 m. A wave load of period equals 13 sec and significant wave height of 20.5 m was applied following data of API. Wind load was modeled as constant force acting on the top of the structure parallel to the sea surface that equals 50 tn. In the top of the jacket, concentrated masses where considered on the top of each leg with total mass of 200tn adding an extra gravitational load on the structure. The self weight of the structure was taken into account. Flooding of legs and drag of the jacket were also considered.

An assumption was made regarding the pile-soil interaction considering the jacket to be fixed on the seabed. For the purpose of this study, this simplification does not influence the results significantly.

The basis for design was the utilization factor proposed by the API and referred to above. The baseline case was a critical design of the reference structure for the most critical case, considering a load combination of the sum of wave, wind and gravity loads with PSFs of 1. Comparisons were made based on this case.

21 Sep 2009 11:35
v.0.1
Analysis4

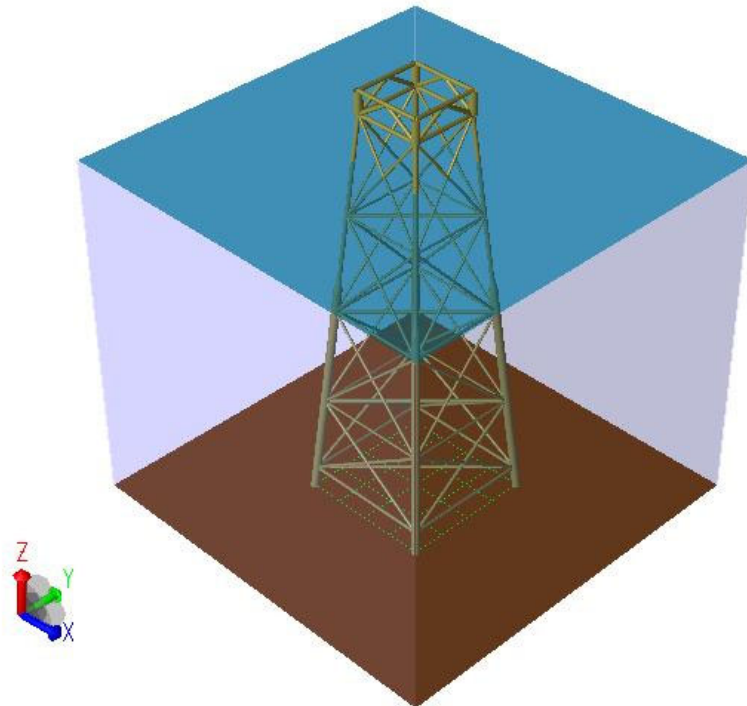


Figure 1: Reference jacket structure

3.5 SESAM Software

The analysis of all 51 cases considered was made using the DNV GeniE SESAM software which has the capacity to handle individually the loads acting on an offshore structure using its sub programs/routines [13]:

- Wajac, Waves on frame structures (Jackets)
- Sestra, Structural Finite Element Analysis (FEA)
- Splice, Pile-Soil interaction

4 Sensitivity Analysis

4.1 Utilization factor

The parameters examined in this study were the response of the structure to variation of the PSFs. Beginning with variation of the wave PSF and keeping the other factors equal to 1, the same procedure took place for the wind and the gravitational loads. After that, a set of cases was examined considering the simultaneous variation of the wave and wind load (gravitational PSF equal 1). Figures 2-4, present the response of

the utilization factor to the variation of the PSFs for each case. The first point of each graph is just below 1, proving critical initial design of the structure.

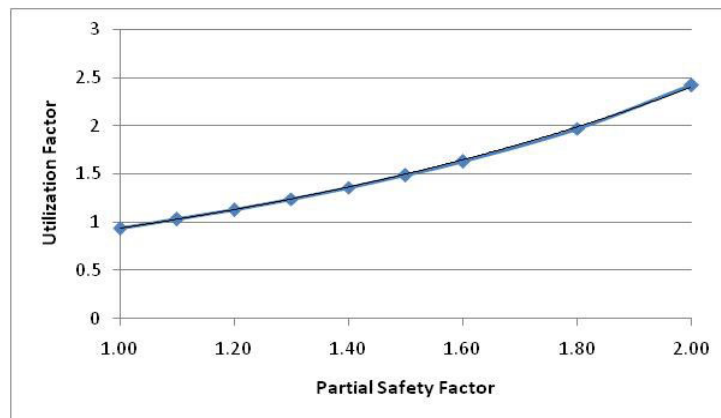


Figure 2: Variation of Utilization Factor as a function of wave PSF

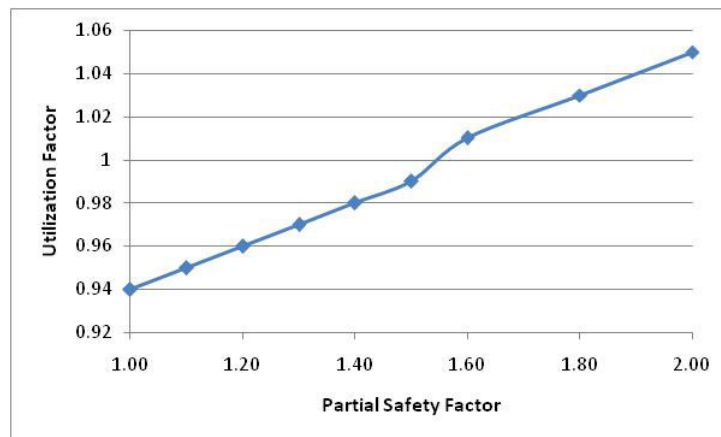


Figure 3: Variation of Utilization Factor as a function of wind PSF

From the figures above, it can be observed that variation of the wave PSF causes an exponential increase ($\exp \alpha \sim 0.938$) of the Utilization Factor, demanding drastical increase in the load capacity of the structure. Therefore larger and more expensive structures should be designed and therefore larger structures. This variation can increase the Utilization factor by 2.57 times when doubling the safety factor. In the case of wind loads, increase of the PSF causes a linear ($\lambda=1.12$), less significant effect on the structure. The same procedure on gravitational loads causes same results as the wave loads.

Simultaneous variation of wave and wind PSFs was considered for 9 cases. The results, as presented on the three dimensional graph below, shows an increase to the Utilization factor of almost 3 times from 0.94 when both values equal 1, to 2.86 when both values equal 2.

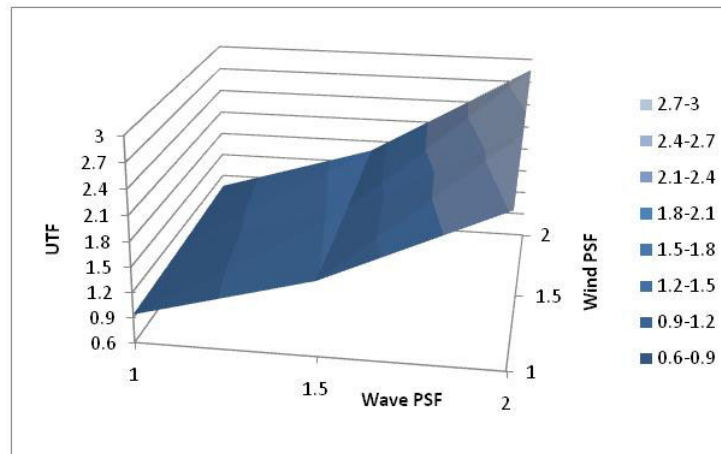


Figure 4: Variation of Utilization Factor as a function of wind and wave PSFs

4.2 Total Mass

The 9 cases of the last comparison were modified in order to comply marginally with standards. These modifications refer to changes in the cross sections of the legs and the bracing of the structure. The results are presented as mass variations. Figure 5, incorporates this data in a three dimensional graph. Variation of the total mass of a percentage of approximately 63% is obvious.

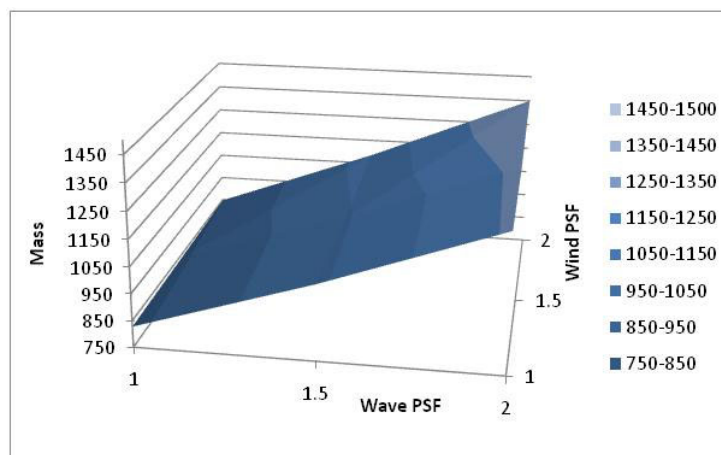


Figure 5: Variation of Total Mass as a function of Wind and Wave PSFs

5 Conclusions - Discussion

The results presented above indicate that the effect of the Partial Safety Factors on the resulting design is significant and therefore special effort should be taken for their determination in order to achieve reliable structures. This implies that analytical derivation of PSFs can optimize structural design and result to more economical structural designs, avoiding unwanted over conservativeness.

Considering those results reversely, structures, can achieve different levels of reliability when located in different environments since the corresponding Utilization Factors become less and therefore the reserve capacity of the structure increases. This is due to the fact that different PSFs and therefore load combinations refer to different

load conditions. For commercial designs that lead to construction of multiple identical structures, this can be translated to different life cycle performance for each of them, allowing them to utilize their loading capacity to withstand all the actual acting loads, determining the inspection and maintenance schedule as well as the total service life of the structure.

Future work of this study is the calculation of the reliability for each of the cases examined according to the PSFs used. In addition, the reliability of a structure under different load conditions will be considered.

6 References

- [1] American Petroleum Institute, “API RP2A-WSD, Recommended practice for planning, designing and constructing fixed offshore platforms - working stress design. (API RP2A-WSD). 20th Edition, Washington. 2002.
- [2] American Petroleum Institute, “API RP 2A – LRFD: Recommended Practice for Planning, Designing and Constructing Fixed Offshore Platforms – Load and Resistance Factor Design”, 1st Edition, 1993
- [3] Lloyds Registers, “LRS code for offshore Platforms”, 1988
- [4] Germanischer Lloyd, “Guidelines for offshore technology, Part IV – Industrial Services, Part 6: Offshore Technology”, 2007
- [5] Det Norske Veritas, “DnV: Rules for the classification of Offshore Installations”, 1989
- [6] Det Norske Veritas, “DnV Offshore Standard OS-C101: Design of offshore steel structures, General – LRFD Method”, 2008
- [7] International Organization for Standardization, “ISO 19902:2007 Petroleum and Natural Gas Industries – Fixed Steel Offshore Structures”, 2007
- [8] Kala, Z., “Influence of partial safety factors on design reliability of steel structures – probability and fuzzy probability assessment. Journal of Civil Engineering and Management. Vol XIII, No. 4.”, 2007
- [9] Song, R., Tjelta, E. And Bai, Y., “Reliability based calibration of safety factors for tubular joints design“. Proc of the 8th ISOPE Conf. Montreal. Canada, 1998
- [10] Lee, C-E and Kwon, H.J, “Reliability analysis and evaluation of partial safety factors for random wave overtopping”, KSCE Journal of Civil Engineering Vol 13, 2009
- [11] Burdekin F. M., “General Principles of the use of safety factors in design and assessment”, Journal of Engineering Failure Analysis, 2006
- [12] Aquirre, J.E. and Boyce, T.R., “Estimation of wind forces on offshore drilling platforms”, The Royal Institution of Naval Architects, London. Spring Meeting, 1973
- [13] Det Norske Veritas, “DNV SESAM User Manual, GeniE Vol. 1: Concept design and analysis of offshore structures“, 2005

A method of risk ranking for international transportation projects

Eduardo A. Gamez¹, Ali Touran²

¹ Risk Manager - Global Program Management, AECOM. 66 Long Warf, Boston, MA 02110, USA

² Assoc. Prof., Dept. of Civil & Env. Engrg., Northeastern Univ., Boston, MA 02115, USA

Abstract: This paper describes a research effort to create a tool to facilitate and promote the use of risk assessment methodologies for owners of projects in developing countries and ensure projects finishing as predicted on-time and on-budget. The research consisted of an in-depth analysis of 89 highway projects sponsored in part by the World Bank and constructed in 60 countries. These projects were reviewed for their cost and schedule performance and for identifying major risk factors that affected their performance. Twenty risk factors were identified and categorized according to a proposed framework. This is a major contribution because it demonstrates that major highway projects in developing countries can be managed more effectively by focusing on relatively few risk factors.

The final product of this research effort is a model called Risk Management Template. Risk Management Template provides a user-friendly tool for identifying, filtering and ranking project risks by following a number of clearly defined steps. This methodology is developed to rank the risks affecting future transportation projects by considering the impact of each risk factor on project schedule and the probability of occurrence of each risk factor. The impact was quantified using a multiple linear regression model on the sample. The combined effect of the risk impact and probability are presented in the form of iso-risk plots. These plots provide an effective means for ranking the risk factors which in turn will allow the owners to focus on the most important risk factors for a given project. The risk impact functions will be combined with probability of occurrence using Monte Carlo simulation to arrive at the expected risk impacts on project budget and schedule. Once these risk factors are identified and quantified, the management can more effectively mitigate their impact.

1 Introduction

Risk management in infrastructure projects has been the subject of multiple research and conferences for the last 15 years in the industry. However there is a limited amount of research done in what Baccarini and Archer (2001) called the vital link between risk identification and risk management: the risk ranking. Grey (2005) claims that having identified the risks in a project, there will not always be sufficient resources to address them all. The objective of this paper is to introduce a new method for ranking and prioritizing risks in a transportation project, allowing users to make an educated selection of the risk factors to be managed.

2 Data collection

The data used in this research was collected from the World Bank records of highway projects executed in developing countries. The ex-post data in transportation infrastructure is rarely reported, especially in developing nations where reporting and documentation processes are not comprehensive and sophisticated. It was found in The World Bank an entity that has a thorough process with a standardized set of documents that are developed through the life of a project, and more importantly it is committed, since its creation in 1945, to fund infrastructure projects in developing nations. Transportation is the second largest sector the World Bank invests in, only after law and justice and public administration. Transportation funding represents 15% of the Bank's \$23,600 million annual budget (World Bank annual report 2006).

Once a project sponsored by the World Bank is completed, the Bank's supervising team generates a document called "Implementation Completion Report" (ICR). This report summarizes the overall process starting at the project inception, original and modified objectives, achievements, sustainability and lessons learned. This document also provides data of original and actual investment and duration and the supervisory team from the Bank assigns a rating to the outcome of the project from the sponsor's viewpoint. The term "sponsor" for these projects is used to designate the entity that principally contributes funding to the project and usually takes no part in the project implementation. As an example, the World Bank is a major sponsor in all the projects reported in this paper. Project implementation is the function of the host country (owner or owner agency).

There are multiple benefits for using this source of data:

1. The documents were consistent in format, terminology and criteria.
2. The spread of the data was broad coming from 60 developing countries in 5 continents.
3. The data dates ranged from 1991 to 2007 and accounted for \$27 billion worth of work.
4. The evaluation process performed by the World Bank was consistent from project to project. About 60% of the projects in the sample also had a mid-term evaluation re-

port. These documents were reviewed for this paper and overall, provided a comprehensive assessment of project performance using a consistent approach. This cannot be claimed about other databases consisting of projects that are evaluated by various agencies or firms.

The sample studied consists of the entire slate of highway projects from the World Bank web database, using the search criteria: *transport projects* and *implementation completion results reports*. From among these projects all projects containing highway construction as principal component were collected. As a result of this process, the Implementation Completion Reports (ICR) of 89 Transportation projects was carefully reviewed and relevant data were extracted.

In order to analyze the projects' performance we were interested in the traditional dimensions: Cost and Schedule. Every Implementation Completion Report (ICR) provides detailed information for the total cost, and reports the World Bank and the counterpart's contributions. Typically the Bank covers a portion of the investment and the host country, either with local funds or with additional sponsors, covers the balance. For the purposes of this research, we have used the total project cost.

For the analysis, "cost performance" has been defined as actual cost of work divided by the budgeted cost of work in percentage points. Budgeted cost is defined as the original estimate or forecast at the time of decision to build a project; and actual cost is defined as the real recorded cost at the time of project completion. Thus, a project with a percentage lower than 100% means that the project finished under budget.

$$\text{Cost Performance} = \frac{\text{Actual Cost}}{\text{Budgeted Cost}} \times 100\% \quad (1)$$

Also, "schedule performance (delay)" has been defined as the difference of actual and estimated duration of the project in percentage points of estimated duration. Estimated duration is defined as the forecasted duration at the time of decision to build a project; actual duration is defined as the actual time it took to complete the project.

$$\text{Schedule Performance (Delay)} = \frac{(\text{Actual Duration} - \text{Estimated Duration})}{\text{Estimated Duration}} \times 100\% \quad (2)$$

For the statistical analysis, Kolmogorov-Smirnov test of Goodness of Fit (Ang and Tang 1975) is used to verify if normal distributions can be assumed for the populations. The reason for this is that most statistical tests of hypotheses are based on the assumption of normality for the underlying populations. Binomial distribution test is used for comparing both sides of a distribution around a purposefully selected fixed value (i.e.: 0% cost over/under run). This test is used to determine the proportion of the results obtained for a variable (cost or schedule over/under run). If the proportion is statistically similar to a 50%:50% chance, then we can say that the values of performance of the measured variable is random, otherwise it shows a tendency that is driven by something different than by chance. In general the study uses regression analysis and various tests of hypothesis and the respective *p*-values are reported for every case (SPSS Ver. 16.0.1). Following Flyvbjerg's *et al.* (2003) definition: *p*-value < 0.01

is considered highly significant, p -value <0.05 significant, and larger p -values assume that deviation could be due to chance.

3 Categorization of the data

The projects in the sample covered a total investment of \$27 billion (actual cost) distributed in projects of different sizes. Table 1 shows a breakdown of number of projects per project size.

Tab. 1: Number of projects per size

	Number of projects	% of the total
Projects < \$100mm	32	36%
\$100mm < P < \$500mm	40	45%
Projects > \$500mm	17	19%

The duration of the projects ranged from 24 month to 92 month, with most common duration around 60 months (5 years). These durations are original estimated durations. Table 2, shows the statistical values of estimated durations for the sampled projects.

Tab. 2: Statistics of estimated project durations in months

	Estimated Duration of projects (months)
Mean	59
Standard Deviation	12
Minimum	24
Maximum	92

4 Cost and schedule performance

This study analyzed projects' performance along two dimensions: Cost and Schedule. Therefore, the data extracted from the World Bank's ICRs were: original cost estimate, actual cost, original project start (the date the Bank loan becomes effective), estimated project finish and the actual project finish.

In addition the implementation completion reports (ICR) clearly identified those projects that presented significant change in scope of work. And, it was observed that despite the fact that some projects experienced change in scope, the actual cost and schedule values were always compared with the originally estimated values. Because of this, the data analysis uses only the subset of projects that have not presented a significant change in scope. This trimming of data will reduce the sample from 89 to 65 projects and will guarantee that the performance analysis is based on comparison of actual versus estimated values for the same scope.

A Kolmogorov-Smirnov test of normality has been performed for values of cost and schedule performance (delay) for the subset of projects. With p -values of: 0.760 and 0.331 the test of hypothesis could not be rejected, therefore it can be said that cost and schedule performance values in the projects with no change in scope follow a normal distribution; and this is important for the simplification of the data analysis going forward. Table 3, presents the cost performance statistics of projects that did not report a significant change in scope.

Tab. 3: Cost performance

COST PERFORMANCE	
# of projects	65
Mean cost performance	95%
Standard deviation	17.2%
95% confidence interval for mean	91% - 99%
Minimum	48%
Maximum	125%
Under budget cases	59%
Over budget cases	39%
On-budget cases	2%

Using the data from Table 3, the following observations can be made:

- The likelihood of a random project finishing under budget is 59% and the likelihood of cost overrun is 39%; 2% of projects finished on-budget.
- The mean of the actual cost is on average 5% less than the original estimate (SD=17.2) and this difference is statistically significant (p -value=0.020) when compared with an on-budget scenario.
- We cannot reject the hypothesis that underestimates are as common as overestimates. (p -value=0.130, binomial distribution test)

The results reported above present a somewhat unexpected finding. Most authors reporting on transportation project performance have observed a tendency of projects to finish significantly over budget. As an example, Flyvbjerg *et al* (2002) reported that 86% of the transportation projects that they studied finished over budget, compared to only 39% computed from the data presented here. Furthermore, Flyvbjerg's *et al* (2002) reported significant evidence that cost deviation was not a result of chance or error, but instead due to a deliberate underestimation of costs; whereas the data analyzed in this report does not present a significant trend other than random error for cost performance.

Flyvbjerg's *et al* (2002) analysis was done on projects that were mainly implemented in developed countries: 94% of projects were in Europe and North America. Whereas 100% of the data used in our analysis comes from developing countries. Developing countries have different challenges to overcome: government and political instability, shortages of adequately trained manpower, limited resources (material, equipment), low productivity, and financial limitations (Jaselskis and Talukhaba,1998). While underestimation seems to be the norm in

developed nations (Flyvbjerg *et al* 2002), overestimation seems to be more frequent in developing countries, at least on international development transportation projects funded by the World Bank. We can only make this statement for projects sponsored by the World Bank.

Schedule delay, is widely used as an indicator of performance in construction projects. The statistical values used to analyze the schedule performance of the dataset are presented in Table 4, comparing actual durations at the project completion with those estimated before project start. As defined before, “schedule performance” or “delay” is defined as the difference of actual and estimated duration of the project in terms of percentage points of estimated duration.

Tab. 4: Schedule performance

SCHEDULE PERFORMANCE (DELAY)	
# of projects	65
Mean cost performance	35%
Standard deviation	25%
95% confidence interval for mean	29% - 41%
Minimum	0%
Maximum	100%
Probability of delay	88%
# of projects with 0% delay	8

Using the data from Table 4, the following observations can be made:

- The likelihood of a random project to finish late is 88%; while the likelihood of a project to finish on-schedule or ahead are 12%.
- The mean schedule delay is 35% of the original estimate (SD=25%), and it is highly significant compared to an on-schedule scenario (p-value<0.001)
- We reject with high significance the hypothesis that projects finishing with schedule delays are as common as projects meeting the schedule or finishing ahead of schedule (p-value<0.001, binomial distribution test), meaning that the chances that a project is finished late is much higher than finishing on time.

These findings clearly indicate that schedule performance pose a larger challenge to these projects compared to cost performance. Overpromised schedules are the rule rather than the exception and the magnitudes of actual delay are significant. Consequently, whenever schedule is a constraint, there is a high risk of failing to finish the scope of work. Lastly, it is evident that schedules are being significantly less controlled and more poorly predicted in developing countries than budgets.

5 Risk identification

Risk is an uncertain event that, if occurs, has an undesirable effect on at least one project objective (e.g., time, cost, scope, quality) (PMI 2004). Yet it was only during the last 15 years that the construction industry has started to utilize risk techniques and methodologies as a standard practice, especially in some sectors of the industry. From all indications, the use of risk assessment techniques is going to increase in the coming years (Touran 2006; Molenaar 2005).

In this section the process of risk identification is described based on the review of the projects collected for the data analysis. A systematic review system is then used to study and analyze the 89 transportation projects mentioned earlier. A unified risk catalog listing the risk factors affecting these projects is developed and a discussion is presented regarding the frequency of each risk factor in the analyzed projects.

Even though the performance analysis described earlier considered only the projects with no scope change, the risk analysis takes into consideration the entire sample of 89 projects. By doing this, important risk factors like “Change in project scope” are also considered.

In addition to the original and actual quantitative information, we were able to extract from the World Bank’s Implementation Completion Reports (ICR) the “major factors affecting implementation and outcome”. We call these the project Risk Factors. The texts of the ICRs are written in a descriptive prose form. Therefore, the identification of the risk factors was an interpretation effort by the authors. For each project, the risk factors present were identified and tallied. The number of times a risk appeared in the sample was counted and the frequency rate was calculated by dividing this count by the total number of projects (*i.e.*, 89).

It was also observed that from the 89 projects studied only a relatively limited number of 20 risks factors were identified. We could not find any explicit guideline from the World Bank that gives the evaluators a catalog of risks to choose from; meaning that these factors represents evaluators’ own observation of the hindrances to the project success. It was further confirmed in conversation with a World Bank officer that this section of the reports are open ended for the evaluators to present their actual observations, and do not follow a predetermined catalog of risk factors. Thus, the limited number of factors seems to be an unbiased set of events that are proven to have affected the projects from an outsider’s perspective (nor owner nor contractor).

For this reason, Table 5 is proposed to be used as a register for documenting and identifying major risks factors in international transportation projects at an early phase. This register of risks will set the stage for a mitigation strategy. As stated before, having a unified system for risk documentation ensures consistency of reporting between projects and allows a meaningful comparison between similar projects in terms of risk performance. In this table, the frequency rate (the number of projects affected by a specific risk factor divided by 89) of each risk factor is also presented.

Tab. 5: Risk identification catalog

Risk #	Risk factor	Frequency rate (%)
R1	Political / Social Instability	28%
R2	Political interference	24%
R3	Force Majeure (nature)	31%
R4	Change in country priorities	15%
R5	Lack of security in work areas	6%
R6	Lack of private sector support	3%
R7	Sponsor delays	3%
R8	Lack of counterpart funds or delay in allocation.	47%
R9	Macro-economic volatility	36%
R10	Disbursement difficulties	29%
R11	Crisis in the region (Financial or Market implications)	19%
R12	Contractor / Designer delays or inefficiency	38%
R13	Change in project scope	27%
R14	Institutional changes	39%
R15	Procurement delay	42%
R16	Ineffective management of agency	34%
R17	Slow land acquisition by agency	12%
R18	Central - local agencies miscommunication	28%
R19	Delay compiling data by agency (Sponsor requirements)	22%
R20	Limited implementation experience	20%

A good risk identification catalog is important for the overall risk ranking exercise and ultimately for better managing the threats faced by a project. The frequency rates presented can be used as a starting point for estimating the probability of occurrence of each factor in future projects when no other information is available.

The number of factors identified in the relatively large sample and the assumed constraint of resources to manage all of them, highlights the importance of finding a reliable ranking system to ensure that proper attention is placed to manage the most significant risk factors. The study of these higher level risk factors at an early stage from the owner's perspective can be of great benefit for implementing a timely risk management plan that will have a strong influence on the project outcome and more importantly help the predictability of the project. Understanding those difficulties is needed to provide owners with better tools to set up successful projects and/or programs.

6 Risk assessment

The performance analysis described above indicated that schedule issues pose a more significant problem to infrastructure projects in developing countries than cost issues. Additionally, significant evidence was found in schedule performance indicating that the main problems in this type of projects are either intentional duration underestimation, or a lack of effective schedule controls. This problem was not found when evaluating cost performance for which

we concluded that the cost performance was more controlled in our sample and its inaccuracy may be a product of random estimation error, rather than a deliberate action.

The challenge is to find how prediction indicators can help owners improve forecasting realistic schedules, and give them the tools necessary for more accurate implementations. In this study, “Risk Analysis” techniques are used to find these prediction indicators. Additionally, the historical data is used to provide reference indications to aid project predictability and project control.

The risk analysis method is a four step process described in detail by Touran (2006). It consists of (1) Risk identification, (2) Risk quantification, (3) Risk mitigation and (4) Implementation of the Mitigation plan.

Similar studies linking risk factors to performance variables have been done in the past using statistical methods like lineal regressions and correlation analysis (Morrow, 1998; Kaming et al., 1997; Chua et al., 1999). In the following section we will cover the use of a statistical method to assess the impact that these factors have over the projects.

6.1 Methodology

The statistical method used to assess the impact of each risk factor is Multiple Lineal Regression. The primary goal of this method is to understand and quantify the relationship between the independent variables (i.e.: risk factors) and the dependent variable (i.e.: delay) (Tamhane and Dunlop, 2000). The model proposes to fit the relationship between those variables in a lineal form.

The Multiple Lineal Regression approach takes into consideration the correlation between factors. The correlation coefficients (ρ) and the significance value for each combination of risk factors (p -value) were calculated using a computer package (SPSS v.16.0). It was observed that even though the correlation coefficients are not great, there are instances of statistically significant relationships between some factors (e.g.: R2 and R4 present low $\rho=0.295$ but significant p -value <0.005).

In addition to the cost and schedule variables extracted from the ICRs, the rating of the outcomes was also recorded. This rating presents from the World Bank’s evaluators point of view the level of satisfaction a project achieved in terms of scope completed. If a project was classified as Highly Satisfactory (HS) or Satisfactory (S), then it means that most or all of its major scope items were completed. A project classified as Unsatisfactory (U) means that the scope of work was not completed (World Bank, n.d.). We observed that some factors present significant correlation with scope completion (e.g.: R4 with p -value=0.011). Therefore, the variable “Scope Completion” will be included as a dummy variable in the regression model and will take values of “0” for U projects and values of “1” for HS and S projects.

The Multiple Lineal Regression model has been designed to have delay as the dependent variable, the 20 risk factors as independent variables and scope completion as a dummy variable. This dummy variable has only been included to adjust the values of the factors that have significant correlation with the completion of scope.

$$Y = b_0 + b_1 * X_1 + b_2 * X_2 + b_3 * X_3 + \dots + b_{20} * X_{20} + b_{sc} * X_{sc} \quad (3)$$

Where:

Y: dependent variable (i.e.: Delay)

X_j: Risk factor “j” [present = “1”, not present = “0”]

b_j: impact coefficients for risk factor “j”

X_{sc}: dummy variable for scope completion [HS = “1”, S = “1”, U = “0”]

b_{sc}: dummy coefficient for scope completion

Multifactor Analysis was also explored as a statistical method to assess the impact of each factor over the response variable. However due to the small sample size Multifactor Analysis did not provide satisfactory results, omitting the existing correlation between factors that the Regression model considers. Therefore, the most robust method identified to assess the impact distribution of each risk factor and the one used in the proposed model is “Multiple Lineal Regression”.

6.2 Risk quantification and distribution of impact

Following the Multiple Lineal Regression method from the previous section the designed model explained in Equation [3] will be used to assess the impact of the identified risk factors. The designed model will have not only the risk factors, but also a dummy variable that will represent the completion of scope of work. This dummy variable has a correlation between the risk factors and completion of scope of work and provides a correction to the calculated impact values when the correlation is significant.

Tab. 6: Risk impact results using multiple lineal regression

Risk Factor	Mean of impact	St.dev. of impact	t-test	Significance p-value
R1	12.62 %	7.69%	1.641	0.106
R2	11.46 %	8.42%	1.361	0.178
R3	- 9.51%	7.02%	-1.355	0.180
R4	10.10 %	12.38%	0.815	0.418
R5	- 19.93 %	14.69%	-1.357	0.179
R6	28.80 %	18.08%	1.593	0.116
R7	10.84 %	19.01%	0.570	0.570
R8	12.36 %	7.11%	1.737	0.087
R9	- 7.77 %	8.06%	-0.965	0.338
R10	- 13.70 %	8.20%	-1.670	0.100
R11	3.76 %	9.40%	0.400	0.690
R12	1.33 %	7.16%	0.185	0.853
R13	9.65 %	7.77%	1.242	0.219
R14	- 1.87 %	6.90%	-0.271	0.787
R15	14.32 %	7.11%	2.013	0.048

Risk Factor	Mean of impact	St.dev. of impact	t-test	Significance p-value
R16	- 5.65 %	7.70%	-0.734	0.466
R17	3.45 %	10.52%	0.328	0.744
R18	6.96 %	7.74%	0.899	0.372
R19	- 3.23 %	9.14%	-0.354	0.725
R20	- 1.31 %	9.25%	-0.142	0.888
Scope comp.	32.06 %	14.55%	-2.204	0.031
Constant	27.04 %	7.88%	3.428	0.763

The mean values of impact in Table 6 represent percentage points of original schedule that a project varies in average when affected by the respective risk factor. It is important to mention that when a risk factor is reported in the World Bank ICR document, it is because it negatively affected the project outcome. Therefore, one might expect that impact values should be positive for all risk factors. However, as we can observe in Table 6 risk factors take a broad range of values from large positive to large negative means of impact.

The observed results present a significant variability, and the calculated R of the Multiple Lineal Regression is considered small (0.536), leading us to conclude that the model presented cannot be reliably used to predict the effect of each risk factor on the project's schedule performance. However, we can use the values obtained to rank the risk factors in order of importance by impact, providing us with the necessary tool in the following model.

7 Risk ranking model

As part of this research, a risk ranking model called "Risk Management Template" has been designed to be used by owners of infrastructure projects in developing countries. It is a user-friendly tool created to filter and identify significant areas of risk, raising awareness for owners. Once the owners can identify the top relevant risk areas, they can concentrate efforts and design management actions in these significant areas. Additionally, this template provides a system for documenting the decision making process.

This model is an easy to use tool, and it is intended to overcome the resistance of practitioners, especially owners, to use risk analysis techniques. It is designed to evaluate projects at a high executive level, when risk management is highly effective before the technical challenges arise. Figure 1, presents a flow diagram of the suggested model.

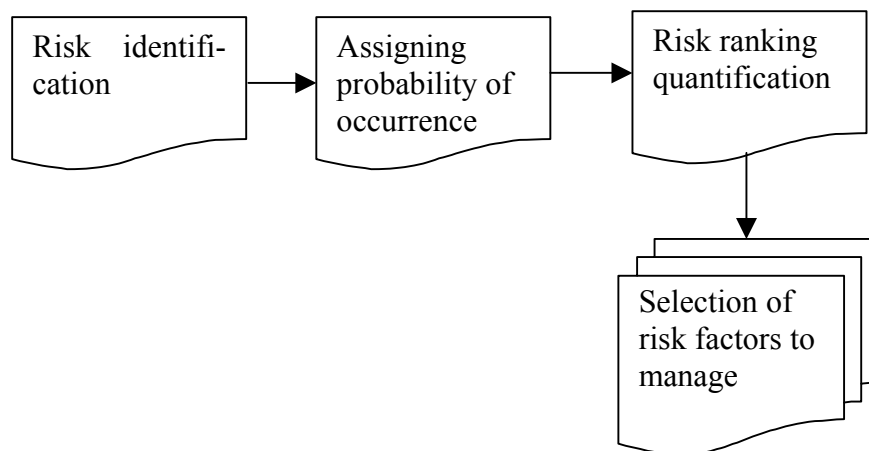


Fig. 1: Risk Management Template - Flow Diagram

The first step in developing a sound risk analysis involves a concise identification of all the possible risk factors that may happen in the project under study. This identification is to be conducted at the early stages of conceptual design, before any technical aspects of the project has been solidified. It concentrates on identifying high level risk factors that may affect the project from an executive and managerial point of view, rather than from a technical standpoint. The proposed model takes into consideration the knowledge acquired from historical data from the past 16 years, and provides as a selection table the risk identification catalog presented in Table 5.

The assignment of a probability of occurrence to a risk factor is not a task that should be taken lightly. It requires a high level of expertise and knowledge of the conditions the project will be exposed to. Only the parties involved in the conceptual phase of the project and with a general knowledge of the externalities that may negatively affect the project would be able to estimate the probability of occurrence of a specific risk factor during the project implementation phase.

Predicting a probability of occurrence may not be easy for all the risk factors identified; some risk factors may be easier to estimate. Historical data from completed projects may provide users with a good reference point to start thinking of the chances a factor has for occurring, when no other information is available (see Table 5). This research espouses the Bayesian School approach in estimating the probability of occurrence of each risk factor. Probability is defined as a degree of confidence that may be different with different persons (Ove Hansson, 2005). Probabilities, for the Bayesian School is a measure of belief that can be either intuitive or calculated. The Bayesian School contends that it is quite difficult to determine if the relative frequency of limited observations is an appropriate estimator of probability of occurrence (Von Winterfeldt and Edwards, 1986).

The objective of the risk quantification phase may not be misinterpreted as a quantification of the effect of each Risk Factor on the project. It is important to clarify that the goal is to provide a reliable ranking system to select the top most influential risk events, rather than calculating their quantitative effect on the project outcome. This concept may be misinterpreted

since the procedure to follow is very similar as the one typically followed by practitioners when quantifying the effect of risk events (Touran 2006). The distribution of impact to be used for each factor is one of the major advantages of this method and presents the most valuable contribution to this method over the conventional ways of selecting risk factors. This distribution of impact per risk factor comes from the study of historical data.

The risk ranking coefficient [Eq.(4)] can be estimated using either a deterministic or probabilistic approach. The deterministic approach is a method that uses the measures of central location (mean) for both impact and the probability of occurrence.

$$\text{Mean ranking coefficient} = \text{Mean impact} \times \text{Probability of occurrence} \quad (4)$$

The main advantages of this method are:

- It does not require much expertise and understanding of probabilistic model
- It is fast and easy to apply
- It does not require any special software package.

The probabilistic approach is the preferred method to be used for the quantification model because it takes into consideration not only the mean, but also the distribution of all possible impact values. However, it is understood that this method may seem unattractive to practitioners since it involves mathematical manipulation of probability distributions.

The probabilistic method uses Monte Carlo simulation to generate numbers based on the statistical distributions of probability of occurrence and impact defined in the risk catalog. There are two steps in the probabilistic calculation of the ranking coefficient. The standard deviations of ranking coefficients can be easily calculated using Monte Carlo simulation.

The advantage of this approach is that it provides a distribution for each risk factor rank that allows the user to determine how likely it is for a factor to become critical. If a critical threshold is defined to select risk factors, one can calculate the probability that a factor is larger than the defined threshold. Additionally, with this approach one can calculate the probability that a certain risk factor can become more critical than any other risk factor. Therefore, it provides more tools for owners to make educated decisions when studying what risk factors should be managed.

8 Selection of Critical Risk Factors

The selection of the risk factors for management action has been divided into two tiers. The first tier contains the most important risk factors to the clear evidence of occurrence and impact. The second tier includes the risk factors that may become critical at some point and even though they may jeopardize the implementation of the project, the evidence of their criticality is not as clear. Therefore the recommendation for the second tier risk factors is

discretionary. They are to be mitigated if the budget allows it to provide owners with an additional level of confidence.

The criterion to define the two tiers and select the corresponding risk factors is adopted from papers published by Al-Bahar et.al. (1990) and Baccarini and Archer (2001). In both sources the severity of the risk factors was defined by iso-risk curves with different constant values. Iso-risk curves are defined as curves that produce a constant value with the product of impact and probability of occurrence.

$$C = Y * X \quad (5)$$

Where,

Y: probability of occurrence

X: impact

C: constant ranking coefficient

Factors with ranking coefficients above the iso-risk curve “1%” are considered critical and are defined as “First tier factors”. The “Second tier risk factors” will be defined taking a more relaxed threshold and containing factors with ranking coefficient between the iso-risk curves of “0.25%” and “1%”. A graphical representation of the risk factors called “Risk management plot” can be prepared to illustrate the concept and show the defined tier areas. The graph will be constructed plotting the mean of each risk’s probability of occurrence on the Y-axis and the mean value of impact on the X-axis. Figure 2 presents an example of the risk management plot.

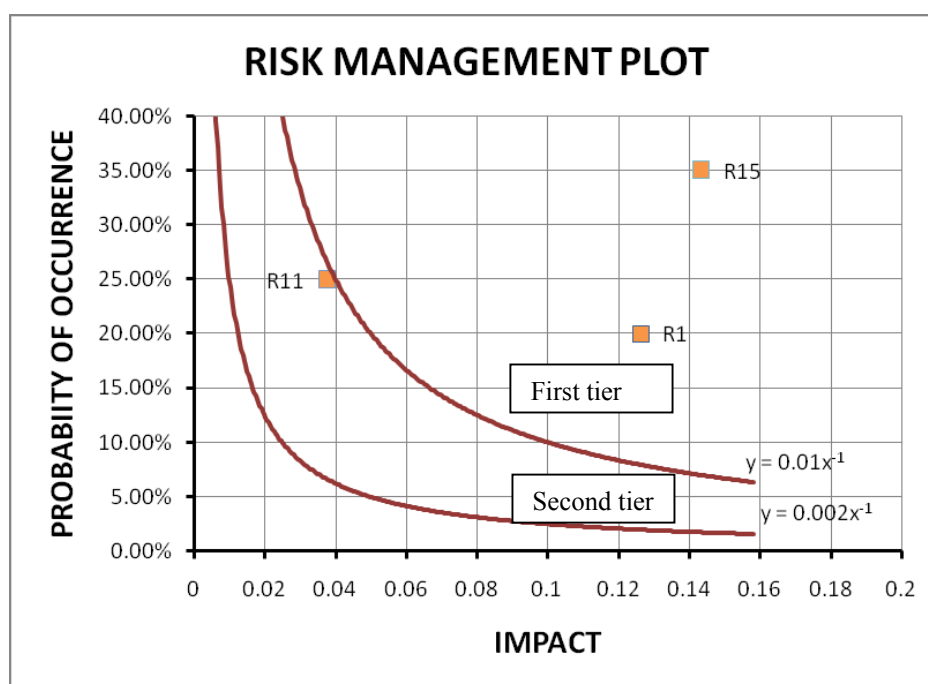


Fig. 2: Risk management plot with iso-risk curves

Ultimately a list of the project risk factors recommended to be managed will be prepared dividing the list into first and second tier risk factors. Note that the ranking groups the risk factors by tier and does not provide a priority of the factors within one tier. This method provides the user with a reasonable roster of the threats the prospect project is predicted to face, and will give them the tools needed to select the risk factors to be managed. The selection of the risk factors to manage is based on the user's criteria and budget. It is understood that the management of a risk factor may impose a significant cost on the project budget; therefore this method allows the owners to use the resources on mitigating the more influential risk factors and document their decision with a consistent and defensible method.

9 Conclusions

Historically, the duration of large scale construction projects has been underestimated. It can be either due to erroneous forecasts (either purposefully or unintentional) or because of weak implementation controls; in either case it is hurting stakeholders that have false expectations based on these poor predictions. This at times has left great infrastructure projects as symbols of failure, while project promoters have overpromised and under-delivered in many cases. This trend has been observed in projects around the world regardless of the level of development of the country, however it is hurting the developing countries that are seeing their scarce resources rapidly eroding.

This paper has presented evidence that transportation infrastructure projects are far from predictable and are not being effectively controlled. Using a sample of 89 transportation projects sponsored by the World Bank, it was observed that in 89% of these projects, a delay occurred and the average delay was 35% of the original duration.

Risk assessment was chosen as the technique to be used to rank the most significant risk factors, in order to improve project performance and predictability. It was shown that the number of major risks affecting these 89 projects was limited to 20 risk factors. This limited number of factors made possible the creation of a risk catalog and a probabilistic risk ranking method. Each risk rank is represented with a probability distribution that will allow the user to assess the risk factor's position within the catalog of the risks identified. Finally a selection criterion has been adapted consisting of the iso-risk curves and a two-tier model is suggested to be used to rank the risk factors by their importance.

10 References

- [1] Al-Bahar, J. and Crandall, K. (1990) "Systematic Risk Management Approach for Construction Projects". *Journal of Const. Engineering and Management*, 116(3), 533-546.

- [2] Allen, Jeffrey and Touran, Ali (2005) "Risk analysis in transit project." Proc., AACE International 49th Annual Meeting, Jun 26-29, New Orleans, LA, United States, Risk.09.1-Risk.09.7
- [3] Ang, A. H-S. and W. H. Tang (1975), Probability Concepts in Engineering Planning & Design, Wiley, Inc. New York, NY.
- [4] Baccarini, D. and Archer, R. (2001) "The risk ranking of projects: a methodology". International Journal of Project Management, 19(3), 139-145.
- [5] Chua, D., Kog, Y. and Loh, P. (1999) "Critical success factors for different project objectives". Journal of Const. Engineering and Management, 125(3), 142-150.
- [6] Devore, J. (2004). Probability and Statistics for engineering and science. Thomson, Belmont, CA. USA
- [7] Flyvbjerg, B. (2002) "Underestimating cost in public works projects: error or lie?" Journal of the American Planning Association, 68(3), 279-295.
- [8] Flyvbjerg, B., Holm, M. and Buhl, S. (2003). "How common and how large are cost overruns in transport infrastructure projects?" Transport Review, 23(1), 71-88.
- [9] Grey, Stephen (1995) Practical risk assessment for project management. Wiley. Chichester, West Sussex, England.
- [10] Jaselskis, E. J. and Talukhaba, A. (1998) "Bidding considerations in developing countries" Journal of Construction Engineering and Management, 124(3), 185-193.
- [11] Kaming, P., Olomolaiye, P. and Holt, G. (1997) "Factors influencing construction time and cost overruns on high-rise projects in Indonesia" Construction Management and Economics. 15(1), 83-94.
- [12] Molenaar, K.R. (2005). "Programmatic Cost Risk Analysis for Highway Mega-Projects," Journal of Construction Engineering and Management, ASCE, 131(3), 343-353.
- [13] Morrow, T.K. (1998) "Effects of selected practices on project cost performance". Dissertation presented to the University of Texas at Austin, Austin, TX, in partial fulfillment of the requirements for the degree of Doctor of Philosophy in Civil Engineering.
- [14] PMI (2004) A Guide to the Project Management Body of Knowledge PMBOK. Third Edition, Project Management Institute Inc. Newtown Square, Pennsylvania.
- [15] @Risk for Excel (2008). Palisade Corporation (version 5.5.0) [Computer Software].
- [16] SPSS 16.0 for Windows (2007). SPSS (version 16.0.1) [Computer Software].
- [17] Tamhane A. and Dunlop D. (2000). Statistics and Data analysis from elementary to intermediate. Prentice Hall, Upper Saddle River, NJ.
- [18] Touran, A., P. Bolster, and S. Thayer. (1994). "Risk Assessment in Fixed Guideway Construction." FTA-MA-26-0022. Washington, DC: U.S. Department of Transportation.

- [19] Touran, A. (2006) "Owners risk reduction techniques using a CM" Report presented to the Construction Management Association of America (CMAA), August.
- [20] Von Winterfeldt, D. and Edwards, W. (1986) "Decision Analysis and Behavioral Research". Cambridge University Press.
- [21] World Bank (n.d.). Harmonized Evaluation Criteria for ICR and OED Evaluations. Washington D.C.
- [22] World Bank (2006). World Bank Annual Report 2006. Washington D.C.
- [23] World Bank (2007). "A Decade of Action in Transport: An evaluation of the World Bank assistance to the transport sector, 1995-2005". Washington D.C
- [24] World Bank (2008) Projects database [Online] Available www.worldbank.org, August 11, 2008

Introducing Nested Sampling

Noel van Erp & Pieter van Gelder
Structural Hydraulic Engineering and Probabilistic Design, TU Delft
Delft, The Netherlands

1 Introduction

Integration of k -variate functions is needed for assessing failure probabilities of systems where multiple load – and resistance variables are present. By reducing any k -variate function f to a corresponding monotonic descending univariate function g , and by using order statistics, the integral of any k -variate function f may be evaluated using a Monte Carlo sampling scheme called Nested Sampling [1]. This paper is organised as follows. First an example of a 2-variate function will be presented to introduce the problem, followed by a presentation of the general philosophy of nest sampling with a stepwise algorithm. Technical details concerning implementation issues are treated in the appendices of this paper.

2 Case study of integrating a bivariate function f with nested sampling

Say we wish to evaluate a bivariate distribution $f(x, y)$ numerically, where

$$f(x, y) = \frac{\sqrt{1-(0.7)^2}}{2\pi} \exp\left[-\frac{1}{2}(x^2 + 1.4xy + y^2)\right] \quad (1)$$

where $-5 \leq x \leq 5$, $-5 < y < 5$.

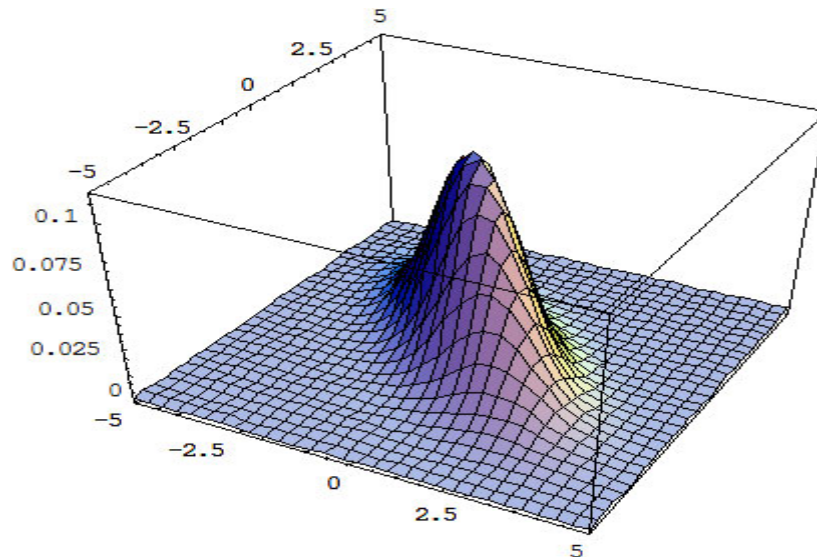


Figure 1: Plot of function f

The total volume under the curve $f(x, y)$ is given by the integral

$$\int_{-5}^5 \int_{-5}^5 \frac{\sqrt{1-(0.7)^2}}{2\pi} \exp\left[-\frac{1}{2}(x^2 + 1.4xy + y^2)\right] dx dy = 0.9993. \quad (2)$$

We may evaluate the integral (2) through brute force. We partition the x, y -plane in little squares with area $dx_j dy_k$, $j = 1, \dots, 20$, $k = 1, \dots, 20$, then define the center of these areas as $(\tilde{x}_j, \tilde{y}_k)$, and compute the strips of volume V_{jk} as

$$V_{jk} = f(\tilde{x}_j, \tilde{y}_k) dx_j dy_k. \quad (3)$$

In Figure 2 we give all the volume elements V_{jk} together:

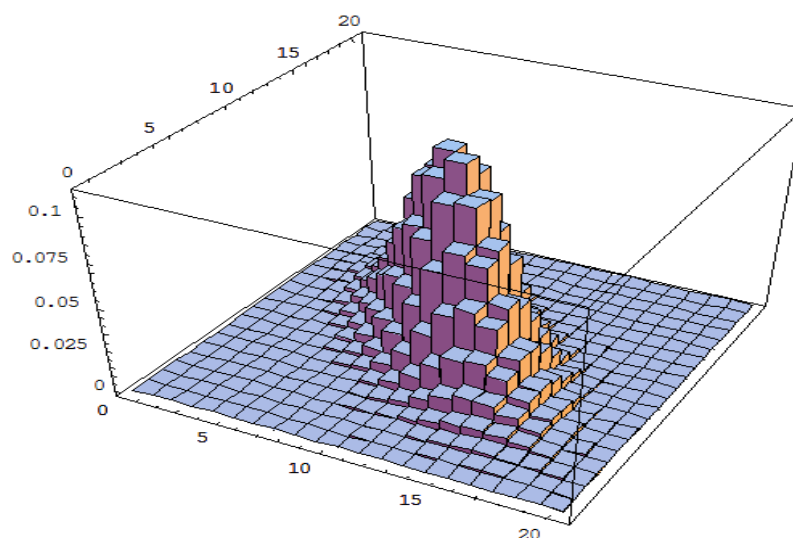


Figure 2: Volume elements of function f

The total volume under the curve $f(x, y)$ may be approximated as

$$volume = \sum_{j=1}^{20} \sum_{k=1}^{20} V_{jk} = 0.9994 \quad (4)$$

Now, we may map these 3-dimensional volume elements V_{jk} to corresponding 2-dimensional area elements A_i . This is easily done by introducing the following notation:

$$dw_i = dx_j dy_k, \quad f[(\tilde{x}, \tilde{y})_i] = f(\tilde{x}_j, \tilde{y}_k), \quad (5)$$

where index i is a function of the indices j and k :

$$i \equiv (j-1)20 + k \quad (6)$$

and $i = 1, \dots, 400$. Using (5), we may rewrite (3) as

$$A_i = f[(\tilde{x}, \tilde{y})_i] dw_i. \quad (7)$$

In Figure 3 we give all the 400 area elements A_i together:

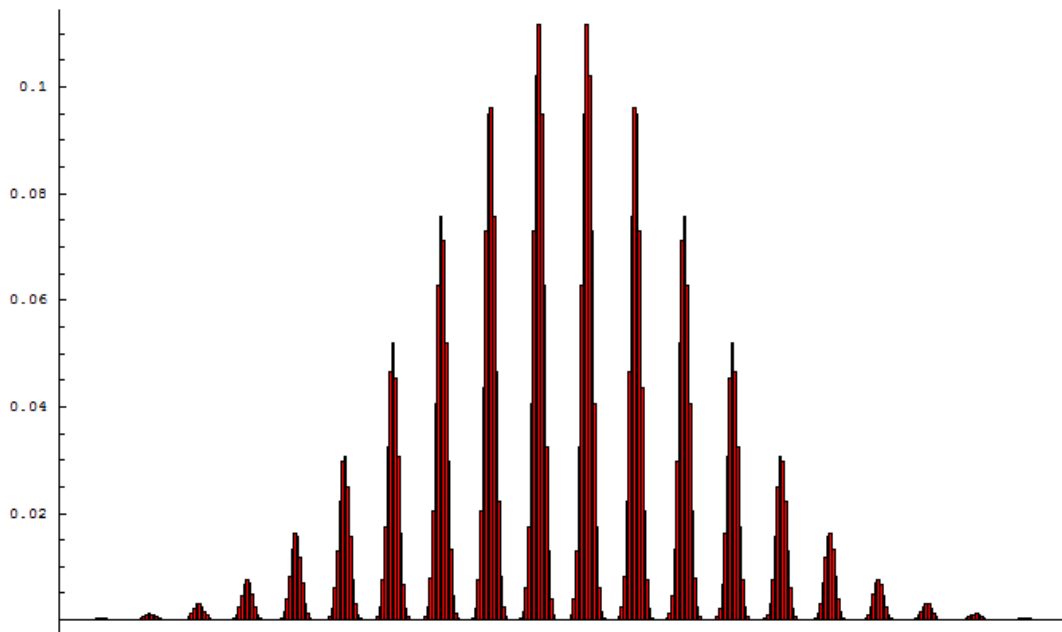


Figure 3: Area elements of function f

Since (7) is equivalent to (3), we have that the mapping of the 3-dimensional volume elements V_{jk} to their corresponding 2-dimensional area elements A_i has not led to any loss of information; that is,

$$area = \sum_{i=1}^{400} A_i = \sum_{j=1}^{20} \sum_{k=1}^{20} V_{jk} = volume. \quad (9)$$

We now may, trivially, rearrange the elements A_i in Figure 2 in descending order:

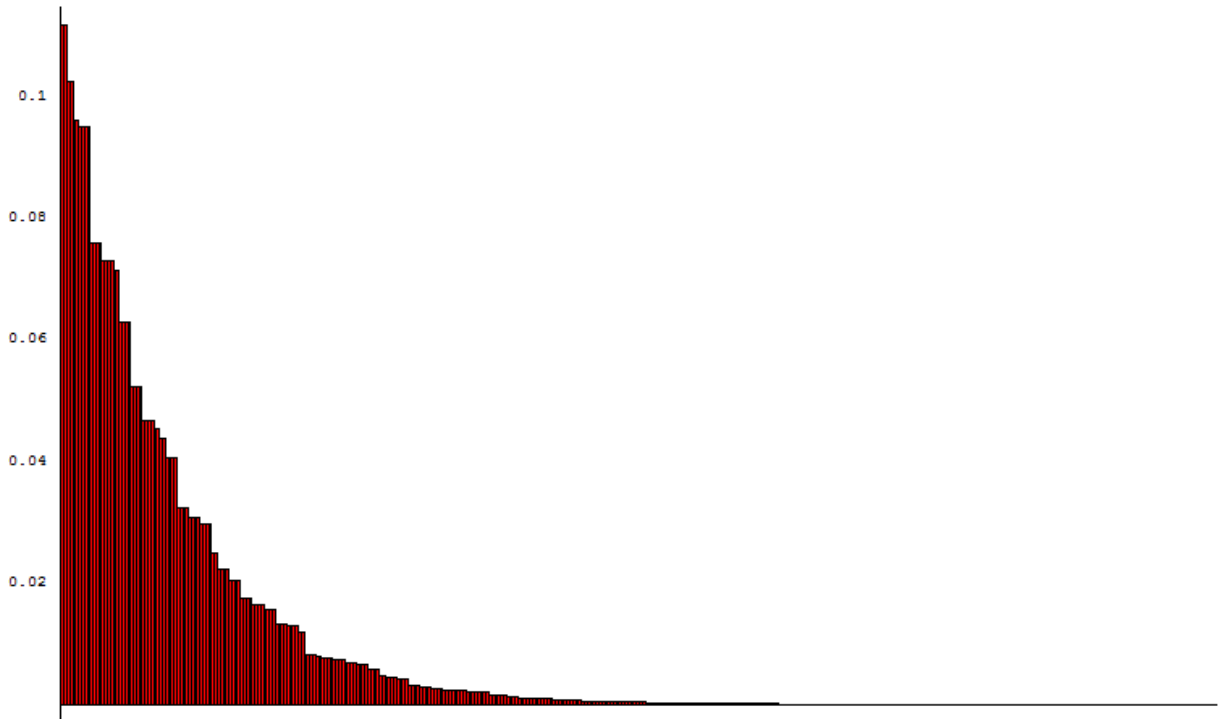


Figure 4: Ordered area elements of function f

Note that the horizontal axis of Figure 4 is non-dimensional. This is because we are looking at an collection of rectangular area elements ordered in one of many possible configurations. Now all these rectangular elements have a base of $dw = dx dy = 0.25$, being that there are 400 area elements we might view Figure 4 as a representation of some monotonic descending function $g(w)$, where $0 \leq w \leq 100$.

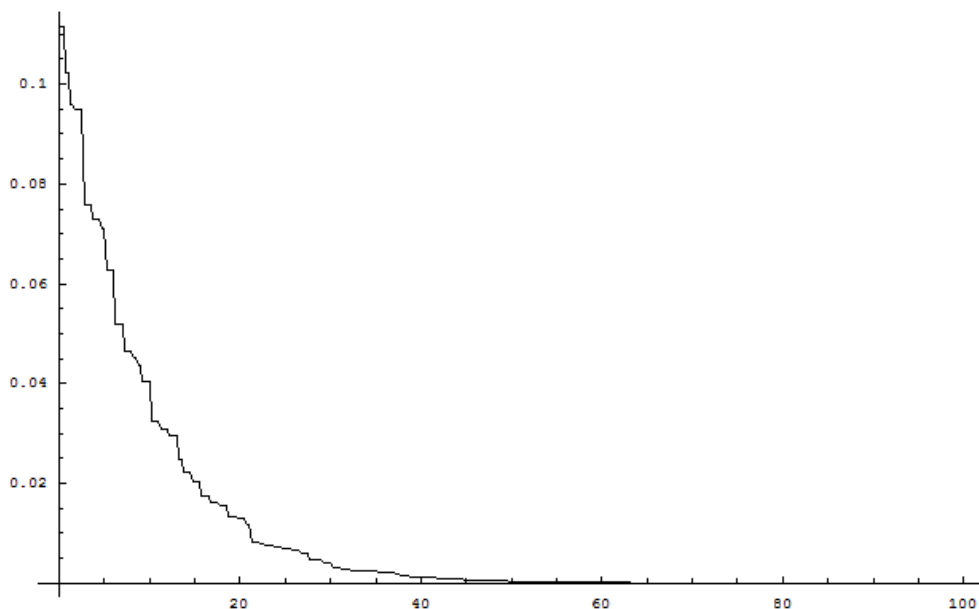


Figure 5: Plot of function g

What we now have accomplished is that we have mapped 3-dimensional volume elements (Figure 2) to 2-dimensional area elements (Figure 3) after which we have rearranged the

area elements (Figure 4) so as to get a monotonic descending ‘function’ $g(w)$ (Figure 5). We now may integrate the univariate function $g(w)$ and, again, get the volume we are looking for. Note that in this manner we may reduce any k -variate function to a corresponding monotonic descending univariate function $g(w)$. We will see that the procedure of Nested Sampling is based upon the equivalence between any k -variate function and its corresponding $g(w)$.

3 Sampling Abcissa’s

Now say, we have a value of $g(w)$, without knowing the value of w . Then the only thing we know about w is that it must lie somewhere in the region $0 \leq w \leq W$, where W is the area for which the k -variate function is defined (see for example, the area for which (1) is defined and the w -axis of Figure 5). So, we have that w is univariately uniformly distributed, $w \sim U(0, W)$, with mean and standard deviation of

$$E(w) = \frac{W}{2}, \quad std(w) = \frac{W}{2\sqrt{3}}. \quad (10)$$

Now, suppose that we sample N values of $g(w)$, that is, we have sampled $g(w_1), \dots, g(w_N)$, and though we still do not know the values of w_1, \dots, w_N , the one thing we now do know is that the smallest realisation of $g(w)$ must correspond with the largest value of w . This is because function $g(w)$ is a monotonic descending function. It follows that we may use an order distribution for the unknown value w_{\max} :

$$p(w_{\max}) = N \left(\frac{w}{W} \right)^{N-1} \frac{1}{W} \quad (11)$$

with mean and standard deviation of

$$E(w_{\max}) = W - \frac{1}{N+1}W, \quad std(w_{\max}) = W \sqrt{\frac{N}{(N+1)^2(N+2)}} \quad (12)$$

and where both the values of N and W are known to us. We have that the standard deviation, that is, our uncertainty regarding the unknown value of w_{\max} , falls off with a factor N . We will see that (12) forms the backbone of the Nested Sampling algorithm.

4 The Basic Nested Sampling Algorithm

In this first version of the Nested Sampling algorithm we will not protect against under- and overflow. We will just focus here on the basic philosophy which underlies Nested Sampling.

Step 1

Find N random values $f(x, y)$ in the x, y -plane. Since we may perform the steps as shown in Figure 1 through 5, it holds trivially that these N values of $f(x, y)$ must correspond with N values of $g(w)$. In the absence of an explicit sorting of the volume/area elements we cannot map the (x, y) -coordinates to the corresponding w -coordinate explicitly. But the thing we can do is use (12) to statistically approximate this corresponding w -coordinate for the smallest sampled value of $f(x, y)$ and thus get our first coordinate (w_1, g_1) of the unknown function $g(w)$, where

$$w_1 = W - \frac{1}{N+1}W, \quad g_1 = [f(x^{(1)}, y^{(1)})]_{\min}, \quad (\text{Alg.1})$$

where the error of our estimated w_1 will fall off with a factor N , as can be seen in (12). We now approximate the integral right of $w_1 = W - W/(N+1)$ as

$$A_1 = \int_{w_1}^W g(w)dw \approx \frac{1}{N+1}W \cdot g_1, \quad (\text{Alg.2})$$

and as a first approximation to the total volume:

$$Z_1 = A_1. \quad (\text{Alg.3})$$

Step 2

We again find N random values $f(x, y)$ in the x, y -plane, but now we constrain these random values to be equal or greater than the value of the minimum of the last iterate, that is, we sample $f(x, y)$ under the constraint

$$f(x, y) \geq g_1 \quad (\text{Alg.4})$$

Now since it holds trivially that the found N values of $f(x, y)$ must correspond with N values of $g(w)$, we may rewrite (Alg.2) as

$$g(w) \geq g_1. \quad (\text{Alg.5})$$

Now, since $g(w)$ is a monotonic descending function and since w_1 is the coordinate that corresponds with the lowerbound g_1 , we may set $0 \leq w \leq w_1$. Using (12) again, but replacing W with w_1 , the second coordinate (w_2, g_2) of the unknown function $g(w)$, where

$$w_2 = w_1 - \frac{1}{N+1}w_1, \quad g_2 = [f(x^{(2)}, y^{(2)})]_{\min}, \quad (\text{Alg.6})$$

We now approximate the integral right of $w_2 = w_1 - w_1/(N+1)$ as

$$A_2 = \int_{w_2}^{w_1} g(w)dw \approx \frac{1}{N+1} w_1 \cdot g_2, \quad (\text{Alg.7})$$

and as a second approximation to the total volume:

$$Z_2 = A_1 + A_2 \quad (\text{Alg.8})$$

Step t

For the t th iterate we find

$$w_t = w_{t-1} - \frac{1}{N+1} w_{t-1}, \quad g_t = [f(x^{(t)}, y^{(t)})]_{\min}, \quad (\text{Alg.9})$$

and

$$A_t = \int_{w_t}^{w_{t-1}} g(w)dw \approx \frac{1}{N+1} w_{t-1} \cdot g_t, \quad (\text{Alg.10})$$

and the estimate of the total volume in the t th iteration becomes:

$$Z_t = \sum_{i=1}^t A_i \quad (\text{Alg.11})$$

Termination Step.

We have that $\lim_{t \rightarrow \infty} w_t = 0$, because of the identity:

$$w_t = \left(1 - \frac{1}{N+1}\right)^t W, \quad (\text{Alg.12})$$

and at the same time we have that g_t cannot be larger than the maximum value of $f(x, y)$. It then follows that $\lim_{t \rightarrow \infty} A_t = 0$. We will take as a stopping criterium the point where A_t does not contribute more than $1/N^2$ part to Z_t , that is,

$$\frac{A_t}{Z_t} > \frac{1}{N^2}. \quad (\text{Alg.13})$$

However, there is of yet no rigorous criterion to ensure the validity of the above terminating condition. Termination remains a matter of user judgement about the problem in hand [1].

Since we are sampling our abscissas some sampling error will occur in our estimate of Z_t , even though this error falls of a factor N . We may record the end points of the likelihood intervals of the areas A_t :

$$A_t^{Left} = \left[\frac{1}{N+1} - \sqrt{\frac{N}{(N+1)^2(N+2)}} \right] w_{t-1} \cdot g_t, \quad (\text{Alg.14a})$$

$$A_t^{Right} = \left[\frac{1}{N+1} + \sqrt{\frac{N}{(N+1)^2(N+2)}} \right] w_{t-1} \cdot g_t, \quad (\text{Alg.14b})$$

in order to compute the end points of the likelihood intervals of total volume Z_t :

$$Z_t^{Left} = \sum_{i=1}^t A_i^{Left}, \quad Z_t^{Right} = \sum_{i=1}^t A_i^{Right}. \quad (\text{Alg.15})$$

This finishes our exposition of the basic idea behind Nested Sampling.

Now if one is to implement the above algorithm one would get an algorithm very differently from the one given by Skilling (2006). These differences are mainly differences of implementation, where the implementations of Skilling are the most efficient ones.

The reason for us to give here the naive algorithm was to point to reader to the elegantly simple idea behind Nested Sampling, without losing ourselves too much in the technicalities of optimal implementations. However, with the core idea behind Nested Sampling demonstrated, we refer the reader to appendices A, B, and C, wherein these points of optimal implementation are treated.

5 Discussion

By reducing any k -variate function f to a corresponding monotonic descending univariate function g , and by using order statistics, the integral of the k -variate function f may be evaluated using Monte Carlo sampling. The procedure by which this done is called Nested Sampling. A special application of Nested Sampling is the case in which the k -variate function f is the product of a prior distribution and a likelihood function. The resulting evaluated integral then equals the evidence value of the corresponding posterior distribution. For the pseudo code of Nested Sampling we refer the interested reader to Skilling (2006).

6 Reference

- [1] Nested Sampling for Bayesian Computations, Skilling, 2006. Proceedings Valencia/ ISBA 8th World Meeting on Bayesian Statistics.

Appendix A: Reduction of Computational Cost

In our algorithm we draw at each iteration N new samples from $f(x, y)$ under the constraint

$$f(x^{(t+1)}, y^{(t+1)}) \geq g_t \quad (\text{A.1})$$

where

$$g_t \equiv [f(x^{(t)}, y^{(t)})]_{\min}. \quad (\text{A.2})$$

Now, we may do this more efficiently by realizing that in iteration $t-1$ we already had $N-1$ objects that satisfied the above constraint. If we keep these $N-1$ objects, then we only need to sample one additional object in order to obtain our needed sample of N objects.

In the words of Skilling (2006): ‘After each iteration t we discard one object from our sample of N objects. This discarded object becomes the lowerbound g_t . The $N-1$ surviving objects are taken to the next iteration and an additional object is sampled under the constraint $f(x^{(t+1)}, y^{(t+1)}) \geq g_t$. This implementation reduces the computational costs with an order of magnitude of N .’

Appendix B: Guarding Against Under- and Overflow

In many problems Z_t may become so large that computational overflow may occur, that is, that Z_t becomes so large that there is no longer a floating number representation possible for its value. To remedy this problem we will have to work with the $\log Z_t$. We also have that certain functions $f(x, y)$ have values so large that computational overflow may also occur. So, in what follows we will sample $\log[f(x, y)]$ instead of $f(x, y)$. Likewise we have that, because of the fact that $\lim_{t \rightarrow \infty} w_t = 0$, for sufficiently large t computational underflow may occur, that is, that w_t becomes so small that there is no longer a floating number representation possible for its value. To remedy the latter situation we will go from the w scale to the $u = \log w$ scale.

To go to the $u = \log w$ scale we will have to make a proper change of variable for the order distribution (11) in order to still be able to sample abscissa values. We have that $du = dw/w$ and $w = \exp u$, so (11) transforms to

$$p(u_{\max}) = \frac{N}{W^N} \exp(Nu), \quad -\infty < u \leq \log W, \quad (\text{B1})$$

with mean and standard deviation

$$E(u_{\max}) = -\frac{1}{N} + \log W, \quad \text{std}(u_{\max}) = \frac{1}{N}. \quad (\text{B2})$$

With a repeated application of (B2) we may find the limits of the u scale after the t th iteration to be

$$u_t = -\frac{t}{N} + \log W \quad (\text{B3})$$

It follows that the width of the t th interval on the original w scale, dw_t , may be written as

$$\begin{aligned} dw_t &= \exp(u_{t-1}) - \exp(u_t) \\ &= \exp\left(-\frac{t-1}{N} + \log W\right) - \exp\left(-\frac{t}{N} + \log W\right) \\ &= W \left[\exp\left(-\frac{t-1}{N}\right) - \exp\left(-\frac{t}{N}\right) \right] \\ &= W \exp\left(-\frac{t-1}{N}\right) \left[1 - \exp\left(-\frac{1}{N}\right) \right] \end{aligned} \quad (\text{B4})$$

It follows that

$$\log(dw_t) = -\frac{t-1}{N} + \log W + \log \left[1 - \exp\left(-\frac{1}{N}\right) \right], \quad (\text{B5})$$

where only the first part is dependent upon the number of iterations. We have that the log of the area element at the t th iteration, $\log A_t$, is the sum

$$\begin{aligned} \log A_t &= \log(dw_t) + \log \left\{ \left[f(x^{(t)}, y^{(t)}) \right]_{\min} \right\} \\ &= -\frac{t-1}{N} + \log W + \log \left[1 - \exp\left(-\frac{1}{N}\right) \right] + \log(g_t) \end{aligned} \quad (\text{B6})$$

Note that (B6) is now sufficiently protected from under- and overflow. We may update $\log Z_{t-1}$ to $\log Z_t$ with $\log A_t$ using the formula for logarithmic addition [1]

$$\begin{aligned} \log[\exp(x) + \exp(y)] &= \log\{ \exp(x) [1 + \exp(y-x)] \} \\ &= x + \log[1 + \exp(y-x)] \end{aligned} \quad (\text{B7})$$

where we set $x \equiv \log Z_{t-1}$ and $y \equiv \log A_t$, so as to get

$$\log Z_t = \log Z_{t-1} + \log[1 + \exp(\log A_t - \log Z_{t-1})] \quad (\text{B8})$$

To summarize, in order to protect the algorithm from under- and overflow, which may easily occur in actual problems, the original algorithm remains unchanged, except that each iteration (B6) is used, instead of (Alg.2), (Alg.7), and (Alg.10), to compute $\log A_t$, while

Z_t is updated using (B8), instead of (Alg.3), (Alg.8), and (Alg.11). Note that the termination condition (Alg.13), may be rewritten as

$$\log A_t - \log Z_t > -2 \log N \quad (\text{B9})$$

Though we remind the reader that of yet there is no rigorous criterion to ensure the validity of the above terminating condition. Termination remains a matter of user judgement about the problem in hand [1].

Appendix C: Restricting Nested Sampling to Posterior Distributions

The log area (18) elements are also used by Skilling in his algorithm. However, Skilling sets $W=1$, because he is concerning himself only with the evaluation of posterior probability distributions; that is,

$$\begin{aligned} f(x^{(t)}, y^{(t)}) &= p(x^{(t)}, y^{(t)} | D) \\ &= p(x^{(t)}, y^{(t)}) L(x^{(t)}, y^{(t)}) \end{aligned} \quad (\text{C1})$$

where $p(x^{(t)}, y^{(t)})$ and $L(x^{(t)}, y^{(t)})$ are the prior and likelihood, respectively. We will now explain.

Say that the area spanned by the likelihood is W , then we know that the uninformative uniform prior $p(x^{(t)}, y^{(t)})$ is equal to W^{-1} , so

$$f(x^{(t)}, y^{(t)}) = W^{-1} L(x^{(t)}, y^{(t)}). \quad (\text{C2})$$

It follows that

$$\log \left\{ \left[f(x^{(t)}, y^{(t)}) \right]_{\min} \right\} = -\log W + \log \left\{ \left[L(x^{(t)}, y^{(t)}) \right]_{\min} \right\} \quad (\text{C3})$$

Substituting (C3) into (B6) we get

$$\begin{aligned} \log A_t &= -\frac{t-1}{N} + \log W + \log \left[1 - \exp\left(-\frac{1}{N}\right) \right] - \log W + \log(L_t) \\ &= -\frac{t-1}{N} + \log \left[1 - \exp\left(-\frac{1}{N}\right) \right] + \log(L_t) \end{aligned} \quad (\text{C4})$$

where L_t is the minimal sampled likelihood at the t th iteration:

$$L_t \equiv \left[L(x^{(t)}, y^{(t)}) \right]_{\min}. \quad (\text{C5})$$

Note that $\log W$ has disappeared, or, equivalently, we may set $W=1$, in the case we are evaluating posterior distributions with uniform priors over the region W .

Appendix D: Generating Monte Carlo Samples

In the case that $f(x, y)$ is a posterior probability distribution, then we may also produce Monte Carlo samples. Every minimum realization $[f(x^{(t)}, y^{(t)})]_{\min}$ corresponds with an area A_t as well with an sample $(x^{(t)}, y^{(t)})$. Now, if we record every $(x^{(t)}, y^{(t)})$ together with the area A_t , then we may assign a weight, that is, probability, to this sample

$$p_t = \frac{A_t}{Z_T}, \quad (\text{D1})$$

where Z_T is the final estimated evidence at the last iteration T . We then may estimate the expectation value of the function $Q(x, y)$ as

$$E(Q) = \sum_{t=1}^T p_t \cdot Q(x^{(t)}, y^{(t)}), \quad (\text{D2})$$

and the a variation of

$$\text{var}(Q) = \sum_{t=1}^T p_t \cdot [Q(x^{(t)}, y^{(t)}) - E(Q)]^2. \quad (\text{D3})$$

Appendix E: Why N^{th} Order Statistics Are Used

Now we may ask ourselves why we take the N th order statistic instead of, say, the 1st order statistic. The reason for this is that, as can be seen in Figure 6 where we have constructed the function $g(w)$ by taking in (1) the limits to be $-50 \leq x \leq 50$ and $-50 \leq y \leq 50$.

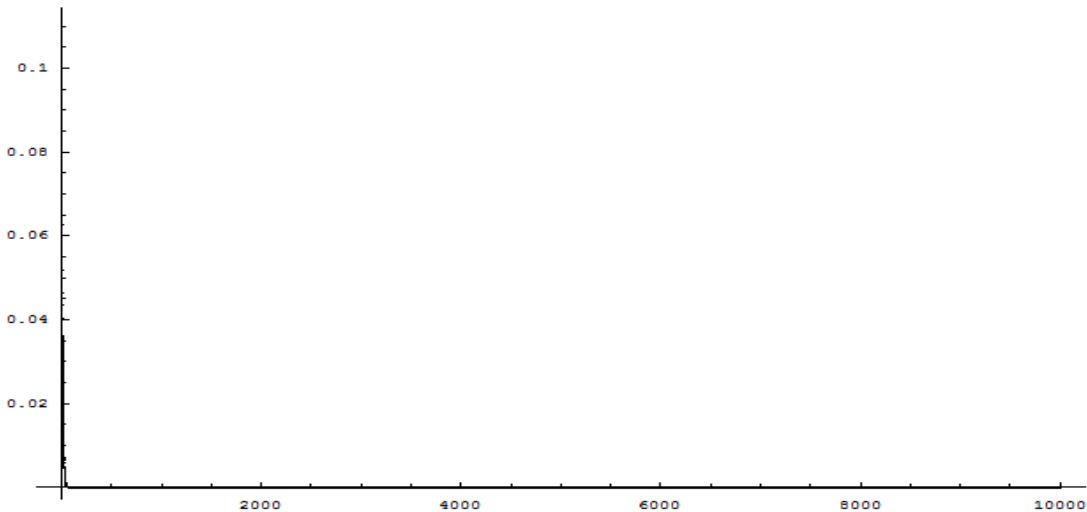


Figure 6: Plot of function g for broader limits of function f

Now we must realise that for limits $-50 \leq x \leq 50$ and $-50 \leq y \leq 50$ the graph for $0 \leq W \leq 100$ in Figure 6 is roughly the same the graph for $0 \leq W \leq 100$ in Figure 5. The reason being that $f(x, y)$ for $-5 > x > 5$ and $-5 > y > 5$ will generally be (much) smaller

than $f(x, y)$ for $-5 \leq x \leq 5$ and $-5 \leq y \leq 5$, combined with the fact that $g(w)$ is constructed by ordering area elements in descending order. We also have that $W = 10000$ which for $N = 100$ leaves us with a mean of about

$$E(w_{\min}) = \frac{1}{N+1} W \approx 100, \quad (\text{E1})$$

and a standard deviation of about

$$\text{std}(w_{\min}) = W \sqrt{\frac{N}{(N+1)^2(N+2)}} \approx 100 \quad (\text{E2})$$

However this means that we leave the informative part $g(w)$, that is, its left-hand side in just one iteration step. However, if we approach the informative part from the right, using the N th order statistic, we have that our intervals fall off with a factor $[N/(N+1)]^t$, because of the identity

$$dw^{(t)} = \frac{w_t}{N+1} \quad (\text{E3})$$

where the limit in the t th iteration w_t is given as:

$$w_t = \left(1 - \frac{1}{N+1}\right)^t W. \quad (\text{E4})$$

So when the informative part of function $g(w)$ is reached, the intervals will in general have shrunk sufficiently to capture all the information in the compressed left-hand part of $g(w)$.

Influence of the Model Creation Methodology on the Failure Probability of Gust Exposed Structures

Emanuel Bombasaro

Research Training Group 1462, Bauhaus Universität, Weimar

Abstract: In this paper the influence of the complexity of the structural model to the failure probability of the structure is investigated. The wind load is applied on the structure following the concept provided by DAVENPORT [1]. But what is missing in this and related concepts is a deep study of the model dimension and the model ability to represent the real structural behaviour under gusty wind load. This paper shows in a first step the solution strategies for different types -different number of considered Eigen modes- of the Davenport model and how they are related to each other. So to be able to give a possibility to estimate a may made error when reducing the model dynamical degree of freedom xor model ability and with the help of this studies to be able to extrapolate the error according to the reality. A simple example is included in the paper showing the problem and the approach of estimating the error resulting out of the model creation methodology.

1 Introduction

Looking at the approach given by DAVENPORT [1] the question of the needed number of considered Eigen modes of the structure arises. In previous paper by BOMBASARO [6] the discretisation and changes in the random field were studied, also some basics for the influence of different number of Eigen modes were given.

In this paper a short introduction to the concept provided by DAVENPORT [1] is given and with the help of a simple example the differences in the result when using a different number of Eigen modes is shown and a simple approach for estimating the may made error is given.

2 Preliminary

2.1 Wind Load Velocity

For the wind load formulation a spectral approach suggested by DAVENPORT [1] is used. The approach it self is nor changed or different possible spectra are use because the main goal of this study is to see if changes in the number of considered Eigen frequencies and variations in the Eigen frequencies of the structure have influence on to the result.

DAVENPORT gives in the paper Gust Loading Factors [3] an approach how wind impacts can be applied to structures using velocity spectrums. Starting from the assumption the mean wind pressure is of the form, see in [3]

$$p(z) = \frac{1}{2} \rho \bar{V}_l^2 C_p(z) \quad (1)$$

in which $p(z)$ = mean pressure at point z above the ground, \bar{V}_l = mean wind velocity at the level of the top of the structure, ρ = air density (1.26 kg/m^3 , varies with the altitude above sea level, in this paper this influence is neglected, which it is generally) and $C_p(z)$ = pressure coefficient of point z . Suitable profiles for the mean wind velocity can be described as logarithmic or power-law profiles. The power-law used by DAVENPORT in [3] is

$$\bar{V}_z = \bar{V}_{10} \left(\frac{z}{10} \right)^\alpha \quad (2)$$

with $\alpha = 0.16$ for countryside and $\alpha = 0.40$ in the city centre. This power-law will be used in this paper to describe the wind altitude velocity profile.

2.2 Wind Spectrum

The computation of the dynamic reaction of buildings under wind load in the frequency domain is suggested by DAVENPORT [2]. Normally the goal of this method is to evaluate the size of a specific or a vary set of structural reaction values and the exceeding probability of the value for dynamic sensitive structures. The probability distribution used in the spectral method is already fixed with the standard Gaussian probability distribution. Initial step of the method is the analytical velocity power spectra suggested by DAVENPORT in [1]

$$S_v(\omega) = \frac{4\kappa\bar{V}_{10}}{\omega} \frac{x^2}{(1+x^2)^{4/3}} \quad (3)$$

in which

$$x = L \frac{\omega}{\bar{V}_{10}} \quad (4)$$

and κ is a drag coefficient of the terrain and has an approximate value of 0.005 in open country and 0.05 in a city complex, \bar{V}_{10} is the mean wind velocity at reference height 10m above the ground and L a length scale of approximately 1200m. This spectrum was found by DAVENPORT by studying a high number of measurements of high wind velocities. The invariant of equation (3) to the evaluation above the ground has to be given a special remark.

2.3 Evaluation

In [4] and a more detailed explanation in [5] is given to the approach to compute wind induced structural reaction with the help of spectral load formulation. The used schema for the spectral wind induced reaction can be found in [4]. With the help of the power spectra velocity function $S_v(w)$ and the aero admittance function $H_{a_i}(\omega)$ the aero force spectrum can be expressed

$$S_p(\omega) = H_{a_i}(\omega) \cdot S_v(w) \quad (5)$$

In [4] for tall cylindrical structures the aero admittance function is given

$$H_{a_i}(\omega) = \rho^2 C_{Di}^2 D_i^2 l_i^2 \bar{V}_i^2 \quad (6)$$

in which ρ is the air density (1.26kg/m³, varies with the altitude above sea level, see note above) and C_{Di} is the pressure coefficient, D_i the dimension of the section, l_i length of the considered beam element and \bar{V}_i is the mean wind velocity. All values are function of the ground distance z_i .

To consider the wind load properly also the effect that the wind load in two different points i and j of the structure are not the same, neither in frequency nor in velocity, this means that a shift in the phase of the stochastic process related to the two points exist. The spectral relation for the same frequency ω and same velocity \bar{V}_i between the two points can be represented with a cross spectral function $S_{V_{i,j}}(\omega)$. This cross spectral function exists of a real part (co spectra) and an imaginary part, which can be neglected respect the real part, see [4]. The cross spectra

$$S_{V_{i,j}}(\omega) = R_{V_{i,j}}(\omega) \sqrt{S_{V_i}(\omega) S_{V_j}(\omega)} \quad (7)$$

with $R_{V_{i,j}}(\omega)$ as cross correlation coefficient, in [1] $R_{V_{i,j}}(\omega)$ is given

$$R_{V_{i,j}}(\omega) = e^{-k \frac{|z_i - z_j| \omega}{\bar{V}_{10}}} \quad (8)$$

in which k is an experimentally determinate value and is suggested to be 7.7, see [1]. Furthermore the cross correlation coefficient can be assumed to be the same vertically and horizontally.

It follows logically that the cross spectral function of the wind load results to

$$S_{P_{i,j}}(\omega) = H_{a_{i,j}}(\omega) \cdot S_{V_{i,j}}(\omega) \quad (9)$$

and the aero admittance function changes to

$$H_{a_{i,j}}(\omega) = \rho^2 C_{D_i} D_i l_i \bar{V}_i C_{D_j} D_j l_j \bar{V}_j \quad (10)$$

Because not all structures can be modelled as a single degree of freedom system this approach has to be expanded for multi degree of freedom systems [4]. For this purpose the equation of motion has to be expressed in matrix form, size of matrix is the number of degree of freedom of the structure. To solve the differential equation the modal analysis is advantageous which is based on the separation of the single equations. With the help of the impulse force in the frequency domain the square of the absolute structural reaction function for every n^{th} natural vibration mode can be expressed, see [5]

$$|H_n(\omega)|^2 = \frac{1}{K_n^2 - [1 + (4\xi_n^2 - 2)(\omega/\omega_n)^2 + (\omega/\omega_n)^4]} \quad (11)$$

In equation (11) ξ_n is the generalized damping coefficient for each mode.

The structure reaction spectral function $S_{Y_r}(\omega)$ for a certain point r is obtained out of the relation

$$S_{Y_r}(\omega) = \sum_n \phi_m^2 |H_n(\omega)|^2 S_{P_n}(\omega) \quad (12)$$

ϕ_m is the n^{th} normalized natural vibration mode vector and $S_{P_n}(\omega)$ is the generalized cross correlation spectral function for the wind load, in case of continuous calculus the sums goes over to integrals.

$$S_{P_n}(\omega) = \sum_i \sum_j \phi_{i_n} \phi_{j_n} S_{P_{i,j}}(\omega) \quad (13)$$

Integrating $S_{Y_r}(\omega)$ gives the variation of the wind-induced deflection of the structure

$$\sigma_{S_{Y_r}}^2 = \int_0^{\infty} S_{Y_r}(\omega) d\omega \quad (14)$$

With this approach the base for solving the problem is given.

2.4 Mode Influence

As addition we need the method of analysing the mode influence showed by BOMBASARO [6]. With this approach we are able to see the influence of every single structural Eigen mode.

With these preliminaries we are able to study the dependency of the concept regarding the number of considered Eigen modes and variations in the Eigen frequencies of the structure.

3 Example

For showing the concept we use a very simple building with the length of 150m and a high of 60m. With the help of structural dynamics the first 10 Eigen modes of the structure were computed and following the approach by DAVENPORT [1] the variation of the deflection for the left upper edge point was computed. We find the used parameters in Tab. 1.

Tab. 1: Parameters used for the example

Wind Properties		
V10	10.0 m/s	Wind velocity
L	1200 m	Gust length
ρ	1.26 kg/m ³	Air density
κ	0.05	Drag coefficient
α	0.30	Power coefficient
k	7.7	Correlation value
Structure Properties		
H	60.0 m	Building high
B	150.0 m	Building dimension
E	5e+8 N/m ²	Young's modulus
m	351000 kg/m	Mass per length
C _D	1.5	Pressure coefficient
ξ	0.01	Damping coefficient

3.1 Result

Fig. 1 shows the reaction spectrum of the structure considering the first 10 Eigen modes, as result we get $\sigma_{S_{Y_r}} = 0.1568m$ and the static deflection $\mu_{S_{Y_r}} = 0.50m$. The strong peak is created by the 7th Eigen mode, which in this case is the dominant one.

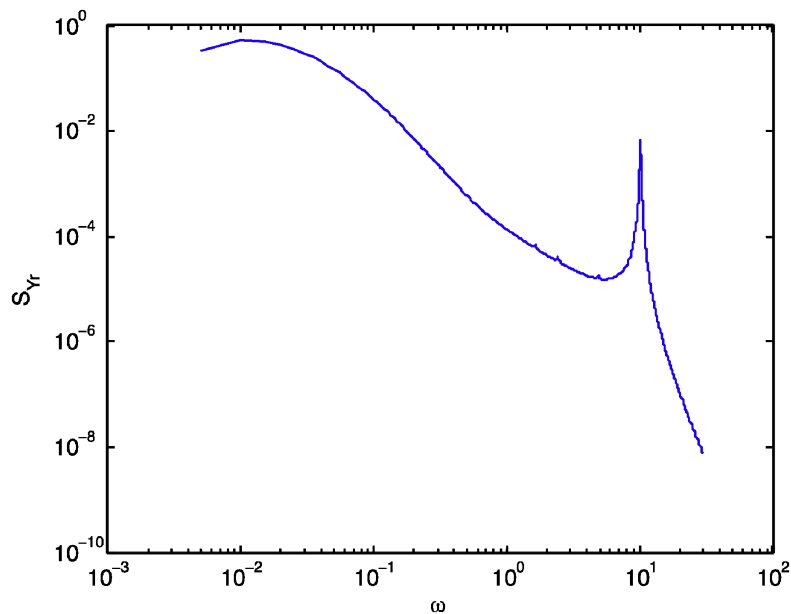


Fig. 1: Structural reaction spectrum considering the first 10 Eigen modes

So now one of the major interests is how many and how strong do the single modes really influence the result. For this purpose we follow the approach given by BOMBASARO [6] for evaluating the influence number ε which is shown in Fig. 2.

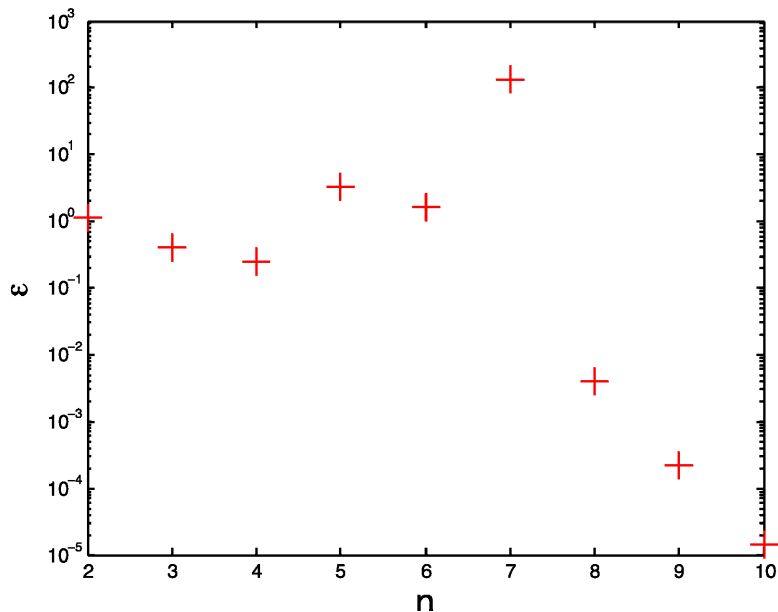


Fig. 2: Influence of considered Eigen mode amount

What we see in Fig. 2 is that the first 7 modes have quite an impact onto the result, the 7th mode has definitely the strongest one. The following higher modes have no influence any more because they are out of the high power region of the wind spectrum.

In Fig. 3 we see the result for $\sigma_{S_{yr}}$ relative to the number of nodes considered, still here of course we see that after the 7th mode the result is not changing significantly.

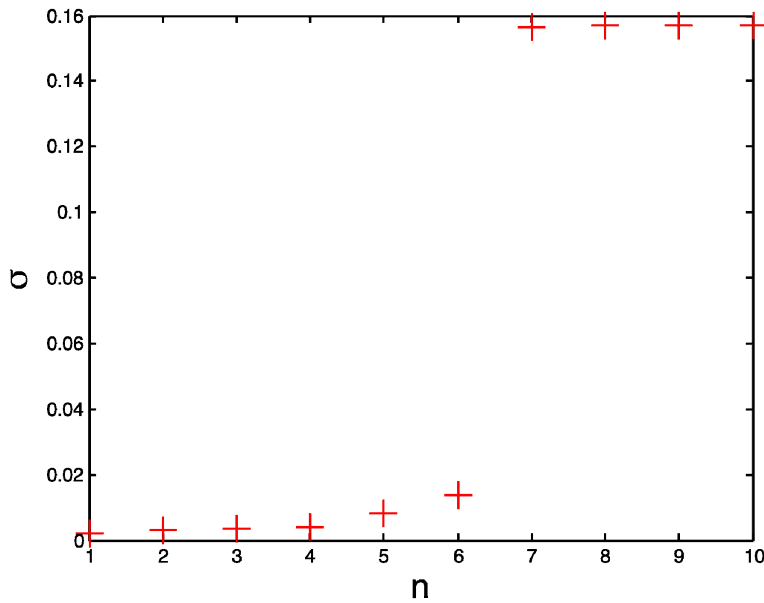


Fig. 3: Result for different Eigen mode amount

3.2 Variation of Eigen frequencies of the structure

Knowing the relevant Eigen frequencies now it is of interest how changes are influencing the result. For this purpose we change the value of ω_2 , ω_5 , ω_6 and ω_7 in the range of $\pm 10\%$. Fig. 4, 5 and 6 shows the obtained results.

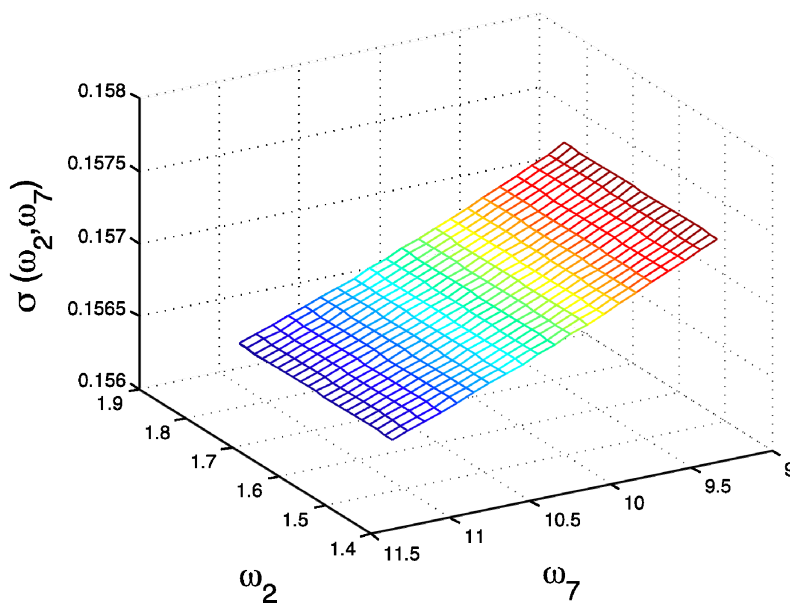


Fig. 4: Influence of different Eigen frequency values ω_2 and ω_7

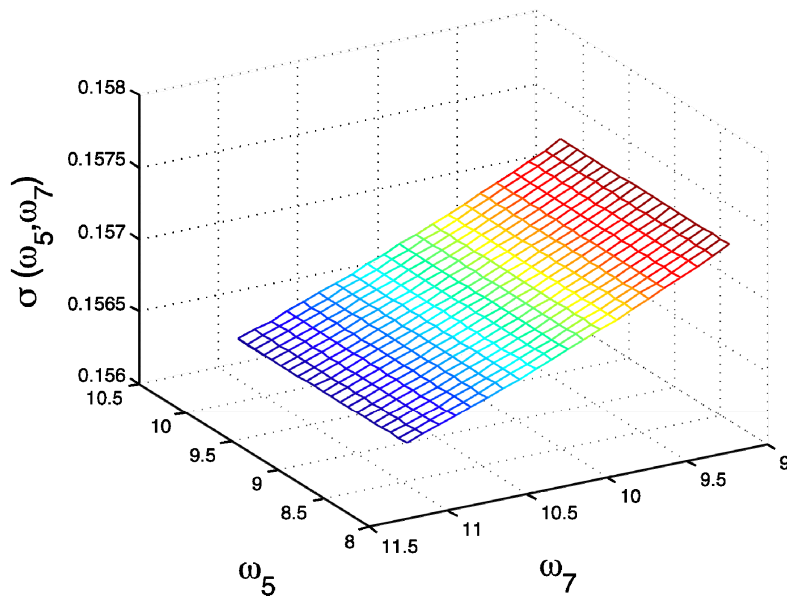


Fig. 5 Influence of different Eigen frequency values ω_5 and ω_7

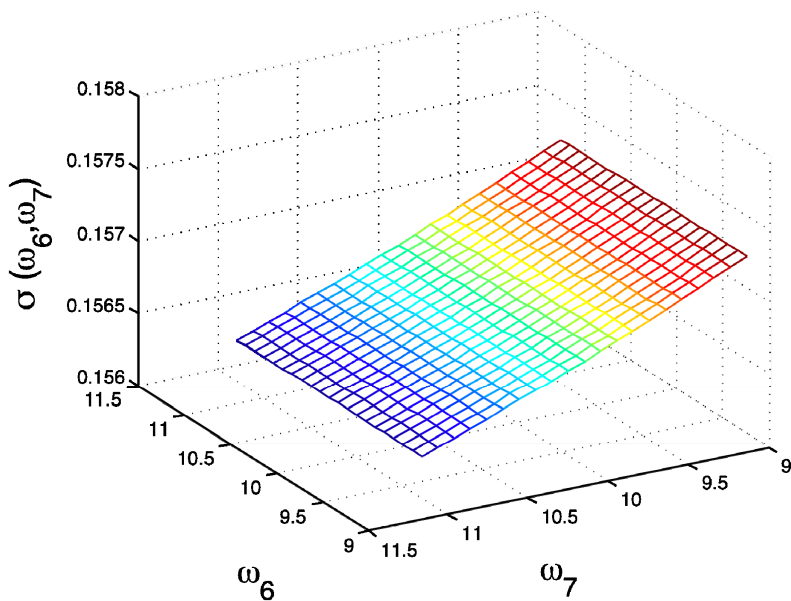


Fig. 6: Influence of different Eigen frequency values ω_6 and ω_7

What we see is, that changes in ω_7 are very sensitive to the result, but still in a range that the exceeding probability stays inside an acceptable range. Changes in the other Eigen frequencies have no influence at all.

4 Conclusion

Looking at the results we see that it is very important to figure out which Eigen frequency is the most dominate and in general it is wrong to say that, which is done in most codes,

the first Eigen frequency is the only one to care about. So one major argument will be to find an appropriate approach to figure out how many or which Eigen frequencies of the structure have to be considered without doing the whole computation. This will be one of the major targets of following research work.

This research has been supported by the German Research Foundation, DFG through Research Training Group 1462, which is gratefully acknowledged by the author.

5 Reference

- [1] Davenport Alan G.: The Spectrum of Horizontal Gustiness Near the Ground in High Winds, *Proc. Inst. Civ. Engrs.* 87 (1961) pp. 194–211
- [2] Davenport Alan G.: The Application of Statistical Concepts to the Wind Load of Structures, *Proc. Instn. Civ. Engrs.* 19 (1961) pp. 449–472
- [3] Davenport Alan G.: Gust Loading Factors, *Journal of the Structural Division* 93 (1967), pp. 11–34
- [4] Schuëller G. I.: Einführung in die Sicherheit und Zuverlässigkeit von Tragwerken Ernst&Sohn, 1981
- [5] Clough R. W., Penzien J.: Dynamics of Structures Computers & Structures, Inc., 3rd Edition, 1995
- [6] Bombasaro E.: Investigation of Modelling Errors of Different Random Field Based Wind Load Formulations. In: Gürlebeck K., Könke C. (eds.) *18th International Conference on the Application of Computer Science and Mathematics in Architecture and Civil Engineering*. Weimar Germany, 2009

Characteristic concrete strength based on compression tests using either vague prior information or using prior information from rebound tests

Raphaël D.J.M. Steenbergen, Adri H.J.M. Vervuurt
TNO Built Environment and Geosciences, Delft, The Netherlands

Abstract: Evaluating and upgrading existing structures becomes more and more important. For a large part of the existing infrastructure in The Netherlands the design life has been reached or will be reached in the near future. These structures need to be reassessed in order to see whether the required safety level is reached. The analysis of the material strength is an important part of that procedure. The characteristic concrete strength can be determined from test methods in two ways. Firstly, the characteristic concrete strength is determined from compression test results, using the statistical theory of Bayes. Starting point is the use of a vague prior distribution for the mean value and the standard deviation. Use can also be made of the fact that it is known from the literature that the concrete compression strength has an approximate constant standard deviation for all concrete types. This fact reduces the statistical uncertainty with respect to the standard deviation and thus again provides higher values for the characteristic concrete strength. It is known that the rebound value may be an indication for the compression strength. For this purpose a calibration graph is made between the compression tests and the rebound tests at the same location. The rebound hammer test values are used in the Bayesian analysis as the prior distribution for the mean. The rebound hammer values can be applied as prior information because they are less vague than the vague prior distributions used in the first method. Concluding remarks are made about the applicability of the three methods.

1 Introduction

For a large part of the existing infrastructure in The Netherlands the design life has been reached or will be reached in the near future. These structures need to be reassessed in order to investigate whether the required safety level is reached. The analysis of the material strength is an important part of that procedure. For this reason, in 2008 and 2009, concrete cores from 83 bridges have been extracted. These have been tested in the laboratory in or-

der to establish the compression strengths. At the same time rebound tests were carried out on these bridges using Schmidt rebound hammers. It is known that there may be a relation between the concrete compressive strength and the rebound hammer value. Because the rebound hammer test is rather cheap and the test is non-destructive, the method may be interesting to use. The question remains whether the results of the rebound hammer test is reliable.

Annex D of EUROCODE EN 1990 'BASIS OF STRUCTURAL DESIGN' [3] provides a method, based on Bayesian theory in order to calculate the characteristic concrete strength from experiments. This method is based on the assumption of having vague prior information for both the mean value and the standard deviation of the concrete strength. However, after the analysis of the bridges as mentioned earlier, the prior information is no longer so vague and more specific knowledge is available concerning the concrete characteristics.

In this paper several methods are presented in order to deal with the more informative prior that could be used in the Bayesian analysis. More specific, the standard deviation of the concrete strength turns out to be less vague and implementing this knowledge in the Bayesian analysis provides higher characteristic strengths. Also the uncertainty concerning the mean value can be reduced by means of implementing the rebound hammer results as prior information for the mean concrete strength in the Bayesian analysis.

2 Test results

In 2008 research has been carried out in order to obtain the characteristic material properties of 19 concrete bridges, viaducts and tunnels in the Dutch infrastructure. For each structure the compressive strength is determined experimentally cores with a diameter of 100mm and a length of 100mm taken from the structure. The compressive strength of these cores equals the cube compressive strength of cubes with dimensions 100x100x100mm. On each of the bridges also rebound hammer tests have been carried out; rebound hammer tests measure the stiffnesses of the concrete skin and these can be translated into a concrete strengths using a calibration graph. In 2009, in a second phase of the research an additional number of 63 bridges has been investigated in the same way. Concrete cores were tested and rebound hammer tests were carried out; however with a different hammer. In both test series some of the rebound hammer tests were carried out on locations where later the concrete cores were taken out.

In this paper first the characteristic concrete strength is derived on the basis of only the strength of the tested cores. Then the empirical relation between the rebound values and the concrete strengths is investigated. Finally the rebound hammer values are used as prior information for the Bayesian analysis in order to determine the characteristic concrete strength from the strengths of the tested cores. In this way conclusions can be drawn which method is preferable.

2.1 Standard deviation concrete compression strength

In this section is studied whether a certain trend can be observed in the standard deviation of the concrete strength. For that purpose the measured standard deviations of the tested

cores of all 82 structures are collected. In the bridges consisting of prefabricated beams combined with in situ cast concrete, a distinction is made between cores coming from the beams and from the concrete in between. Therefore, in total there are 94 bridge (parts) of which the standard deviation is studied. In Fig. 1 the standard deviation per bridge (part) is plotted against the measured value of the compressive strength.

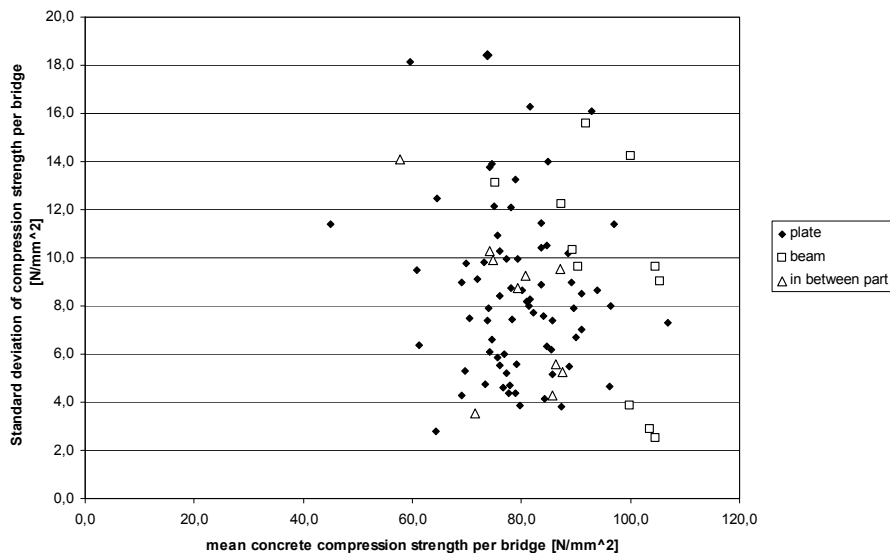


Figure 1: Measured standard deviation as a function of the averaged compression strength.

From Fig. 1 it appears that the standard deviation is varying between 2 N/mm² and 19 N/mm². However from measurements in the past, see WALRAVEN [1] and FABER AND VROUWENVELDER [2], it turns out that the standard deviation of the concrete compression strength is almost constant (5 until 8 N/mm²). However these tests in the past were carried out on large numbers of concrete cubes of 28 days age and coming from only one cast. Here the situation is different. The concrete has strengthened during many years and only a small number of cores has been tested in the laboratory. The measured standard deviation depends highly on the number of tested cores. For that reason, in Fig. 2, the standard deviation is plotted against the number of tested cores.

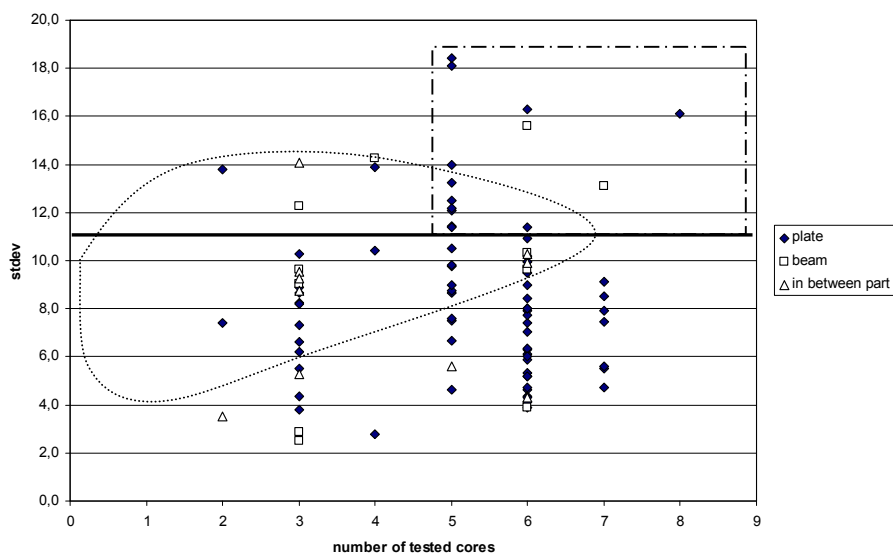


Figure 2: Measured standard deviation as a function of the number of tested cores.

From Fig. 2 it appears that also for higher numbers of test samples (5 until 8 cores) the standard deviation can be large. Consequently, assuming a standard deviation of 8 N/mm^2 in these cases could be unsafe. This is illustrated in Fig. 3, where the standard deviation is shown with the corresponding probability of occurrence.

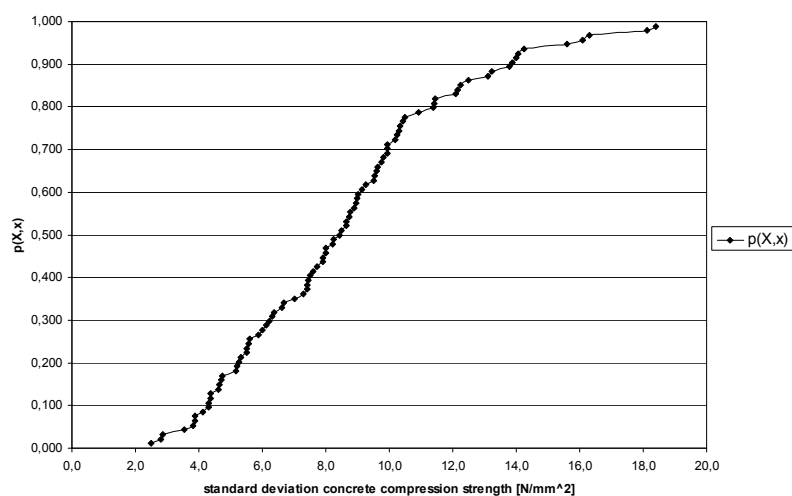


Figure 3: Measured standard deviation with probability of occurrence (cumulative)

From Fig. 3 it follows that for example a standard deviation of 5 N/mm^2 is exceeded in 83% of the cases. 8 N/mm^2 is exceeded in 60% of the cases. Assuming a standard deviation of $5\text{-}8 \text{ N/mm}^2$ would very likely underestimate the actual standard deviation. In order to obtain a conservative approximation dealing with the standard deviation, the following procedure is proposed. At the left hand side of Fig. 2 we find many small standard deviations, based however on a very small number of samples, these value are not trustful. Therefore a reference value for the standard deviation has to be chosen so that safe values for the strength are provided. The point of departure is the use of 11 N/mm^2 for all concrete strengths (probability of exceedence of about 20%). It is noted here that in some cases the use of a standard deviation of 11 N/mm^2 leads to an unsafe or a possibly too conservative approximation. This can be derived from Fig. 2. For the cases in the dotted encircled area in Fig. 5 it may be that the characteristic value of the concrete compression strength determined on the basis of the measured standard deviation including the statistical uncertainty provides a smaller value than the value based on the (as certain considered) standard deviation of 11 N/mm^2 . In that case the smaller characteristic value has to be taken. For larger numbers of samples, the statistical uncertainty is for the greater part reduced to zero. Therefore in the dash dotted encircled area, the characteristic strength on the basis of the measured standard deviation is smaller than the characteristic strength on the basis of the fixed standard deviation of 11 N/mm^2 . In that case the former value has to be taken. Finally the following procedure is used determining the characteristic concrete strength. If the characteristic value of the concrete compression strength on the basis of the measured standard deviation including the statistical uncertainty is small than the value based on the fixed value for the standard deviation of 11 N/mm^2 , then the former, smallest value has to be taken. On the other hand in the case of the bridges with a small standard deviation in the right hand side of Fig. 2 (many samples), the use of the fixed value may be too conservative. In the case that this leads to disapproval of the bridge, a more sophisticated procedure could be used for that field. Instead of the non informative prior from EN 1990, the distribution of the standard deviation as shown in Fig. 3 can be implemented. This is outside the scope of this paper.

2.2 Relation rebound hammer and concrete compression strength

In order to use the rebound hammer values for the structural assesment, the rebound values have to be translated to strength values. For that purpose, in both test series some of the rebound tests were carried out on locations where subsequently the concrete cores were taken out. In the first series a different hammer was used from the one in the second series. In the use of the rebound hammer it is prescribed to use the median of 10 tests in order to avoid sudden stiff locations in the concrete skin. In Fig. 4, for the first 5 bridges from the first series, the median of the rebound hammer values is plotted against the corresponding compression strength. For the other bridges similar graphs are found.

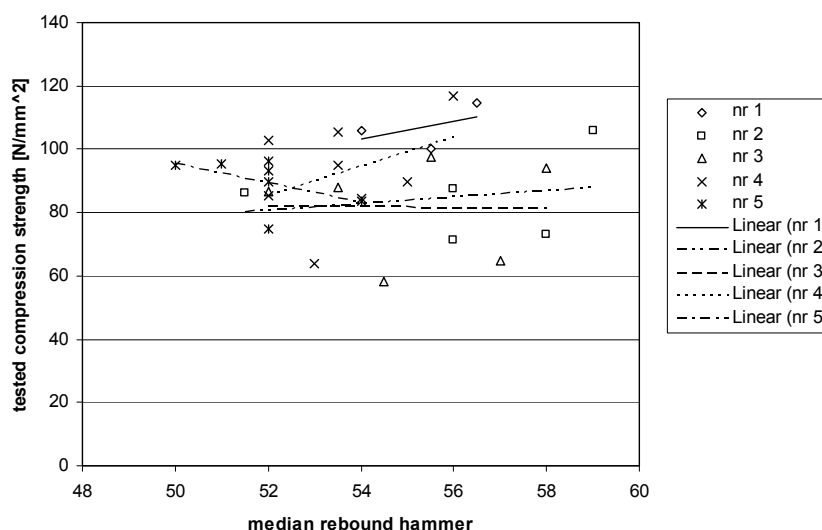


Figure 4: Relation between the median of the rebound hammer values and the tested compression strength for bridge 1-5 out of the first series.

Based on the outcomes in Fig. 4 it is found that no correlation can be found between the individual median values of the rebound hammer and the corresponding concrete compression strength. In Fig. 5, for the first series of 19 bridges, the mean value of the median of the used rebound hammer value per bridge is plotted against the mean value of the tested compression strength per bridge. Here we observe a more clear relation.

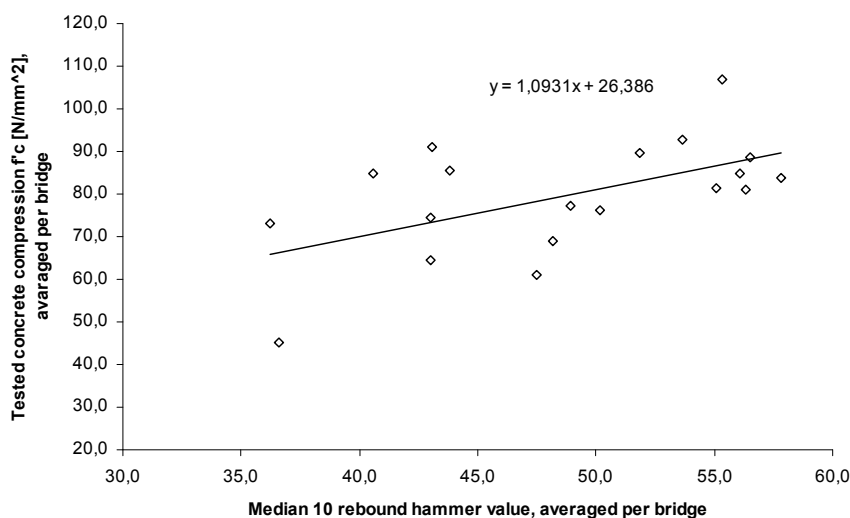


Figure 5: Relation between the per bridge averaged median of the rebound values and the averaged tested compression strength per bridge; series 1.

From Fig. 5 it appears that the per bridge averaged median of the rebound hammer tests can be a measure for the per bridge averaged concrete compression strength. The relation is determined using linear regression (see Fig. 5):

$$f'_{cm} = 1.0931 * \mu (med) + 26.386$$

Where $\mu (med)$ is the per bridge averaged median of 10 rebound hammer values.

The constant standard deviation belonging to this relation is 11.23 N/mm^2 . This value is used in the analysis for determining the compressive strength.

Further it appears that the variation in the rebound hammer values on the various location per bridge is very small (about 4%) compared to the variation in the compression tests. For this reason the rebound hammer values only provide information about the mean value of the concrete compression strength and not about the standard deviation (see also Fig. 4). For this reason the standard deviation as determined in section 2.1 is used.

For the second series of 63 bridges, a different rebound hammer was used. In Fig. 6, for that series, the mean value of the median of the rebound hammer value per bridge is plotted against the mean value of the tested compression strength per bridge. Here we also observe a relation. The relation is:

$$f'_{cm} = 0.4093 * \mu (med) + 58.343$$

where $\mu (med)$ is the per bridge averaged median of 10 rebound hammer values.

The constant standard deviation belonging to this relation is 7.54 N/mm^2 . This value is used in the analysis for determining the compressive strength.

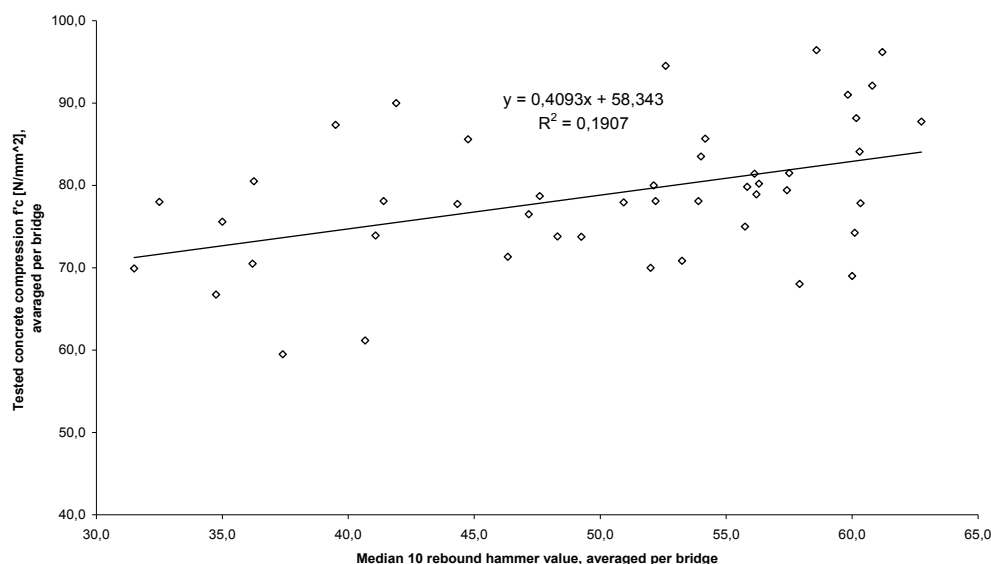


Figure 6: Relation between the per bridge averaged median of the rebound values and the averaged tested compression strength per bridge; series 2.

It is that the correlation in Fig. 6 is weak; for the first series the relation in Fig. 5 was better. In Fig. 6 the regression coefficient R^2 is closer to 0 than to 1: 0.2. So the relation between the rebound hammer values and the concrete strength is weak.

3 Determination of the characteristic concrete compression strength

In this chapter the formulas are presented for calculating the characteristic concrete compression strength.

3.1 Determination of the characteristic concrete compression strength on the basis the results of compression tests

In this section the Bayesian analysis is performed in order to establish the values for the characteristic concrete compression strengths. The analysis is based on the results of the compression tests results and the standard deviation as discussed in section 2.1.

Assuming a normal distribution for f'_{ck} , the characteristic value of the concrete compression strength follows from the smallest value of (1) and (2):

$$f'_{ck} = m - 1.64 \cdot 11 \cdot \sqrt{1 + \frac{1}{n}} \tag{1}$$

$$f'_{ck} = m - s \cdot t_{n-1}(p = 0.05) \cdot \sqrt{1 + \frac{1}{n}} \tag{2}$$

where:

- m = the mean of the measured compression strengths
- s = the standard deviation of the measured compression strengths
- n = the number of tested cores
- t_{n-1} = the value of t_{n-1} according to the student-t distribution

3.2 Determination of the characteristic concrete compression strength on the basis of the combination of compression tests and rebound hammer tests

In this section, the rebound hammer values are used as prior information for the mean value in the Bayesian analysis. From the theory the following formula for the characteristic value of the concrete compression strength can be deduced:

$$R = m'' - t_{v''} \cdot s'' \cdot \sqrt{1 + \frac{1}{n''}}$$

with:

$$\begin{aligned} n'' &= n' + n \\ v'' &= v' + v \\ m'' n'' &= n' m' + n m \\ [v''(s'')^2 + n''(m'')^2] &= [v'(s')^2 + n'(m')^2] + [vs^2 + nm^2] \end{aligned}$$

and m' is the mean value of the compression strength per bridge following from the rebound hammer test and the calibration graph.

s' is the standard deviation of the compression strength as indicated in section 2.2.

n' follows from the following expression where a Bayesian update takes place for the uniform prior distribution for the mean value:

$$V(\mu) = \frac{s'}{m' \sqrt{n'}} \quad V(\mu) = \frac{\sigma}{m'}$$

where σ is equal to the standard deviation belonging to the regression line in Fig. 5 or Fig. 6. v' is equal to a very large number, because it is assumed that the variation coefficient of the standard deviation approaches the value of zero.

Further it holds:

- m = the mean value of the compression tests
- n = the number of compression tests
- v = $n-1$
- s = the standard deviation of the compression tests

4 Results for the characteristic compression strength according to the different methods.

Table 1: Results for the concrete compression strength according to the different methods

Bridge number	f'_{ck} [N/mm ²] compression tests	f'_{ck} [N/mm ²] compression tests + rebound tests	Bridge number	f'_{ck} [N/mm ²] compression tests	f'_{ck} [N/mm ²] compression tests + rebound tests
1	82,2	82,2	42	58,7	60,5
2	52,2	65,7	43	48	53,6
3	46	62,9	44	70	69,5
4	60,6	70,6	45	57,7	59
5	69	69,7	46	55,5	56,2
6	64,6	68,3	47	67,5	67,9
7	53,9	65,2	48	74,6	73
8	41,8	48,7	49	62,5	64,3
9	18,4	31	50	75,4	73,3
10	41,4	58,5	51	47,1	52,1
11	53,2	62,9	52	51,2	53,8
12	70,4	70,7	53	56,1	63
13	60,2	64,6	54	38,1	53,9
14	50,3	54,6	55	49,8	57
15	61,4	64,7	56	48	55,8
16	50,4	55,7	57	66,4	67,7
17	39,9	44,3	58	51,8	57,1
18	56,2	58,4	59	30,8	44,6
19	48,1	51,4	60	60,4	62,1

Bridge number	f_{ck} [N/mm ²] compression tests	f_{ck} [N/mm ²] compression tests + rebound tests	Bridge number	f_{ck} [N/mm ²] compression tests	f_{ck} [N/mm ²] compression tests + rebound tests
20	55,5	58,3	61	63,7	64,3
21	56,7	58,7	62	64,7	65,5
22	17,2	37,8	63	57,3	59
23	59	61,3	64	58,5	58,7
24	58,6	61,1	65	62,6	66,6
25	64,5	63,9	66	71,1	72,3
26	55	57,9	67	72	75,6
27	52,9	55,2	68	45,7	52,7
28	-32,4	47,3	69	40,1	45,9
29	56,5	58,3	70	55,8	58,3
30	48,9	52,6	71	22,7	35,3
31	57,8	60,8	72	66,4	67,2
32	56,9	61,7	73	52,4	55,6
33	35,5	48,4	74	59,2	61,7
34	53,6	62	75	71,7	72,4
35	63,3	61,9	76	63,3	64,3
36	68,4	66,7	77	48,7	53,4
37	51,7	54,8	78	72,3	72,6
38	57,8	60,4	79	54,8	59,9
39	58,4	60,8	80	46,5	55,4
40	54,5	56,5	81	16,5	56,2
41	61,2	60,5	82	64,8	68,4

In Table 1, the results for the characteristic concrete compression strength according to the different methods are displayed. In the second and fifth column the values on the basis of the non-informative prior are displayed. In the third and sixth column the value on the basis of the more informative prior (rebound hammer) are shown.

It appears that the characteristic value of the compression strength, determined on the basis of the more informative prior derived from the rebound hammer tests provides in almost all cases a slightly higher value. However if the characteristic value of the compression strength on the basis of only the compression tests gives a very low value, the combination with the rebound hammer values provides a remarkably higher value. This is the case because the calibration graph of the rebound hammer is not very steep, even more horizontally orientated. The question may arise whether in this case the rebound hammer is still representative for the compression strength. So, if a very small characteristic strength becomes significantly larger when combined with the rebound test values, some prudence is necessary.

In a very few cases (7%) the use of the rebound hammer test value as prior information provides a little smaller value than the use of the value from the compression tests. This is because of the fact that points that are far (large strength) above the regression line in Figs. 5 and 6. are pulled toward that calibration graph which is used to translate the rebound value into compression strengths. So it appears that in some cases the use of the more informative prior is abolished by the fact that that informative prior is located too far left from the distribution of the measured compression strengths.

5 Conclusion

It appears that the characteristic value of the compression strength, determined on the basis of the more informative prior derived from the rebound hammer tests provides in almost all cases a slightly higher value. So rebound hammer test can provide additional information about the shape of the prior distribution. Compression tests are needed in order to establish the characteristic strengths that are used in a structural calculation.

6 Literature

- [1] Walraven, J.C.: *Gewapend Beton*. TU Delft, 1999
- [2] Faber M.; Vrouwenvelder A.C.W.M.: *Probabilistic Model Code*. Joint Committee on Structural Safety (JCSS), 2001.
- [3] Eurocode EN 1990, Basis of Structural Design. 2002.

Assessing the probability of material failure in cantilevered stone stairs

Dermot O'Dwyer, Alan O'Connor and Olwakemi Bashorun
Department of Civil, Structural and Environmental Engineering, Trinity College Dublin,
Ireland

Abstract: Cantilever stone stairs were widely constructed from the 17th to the 20th century. This form of construction has proved to be robust but some recent sudden failures have demonstrated the need to reassess their capacity. The majority of cantilever stone stairs do not cantilever: each tread in a cantilevered stone stairs transfers the loads applied to it to the wall support and to the tread below. The predominant resulting force developed within the tread is a torque. Cantilevered stone stairs are highly statically indeterminate, which complicates their analysis. In addition, the stone used in their construction is a natural and often highly variable material. This paper considers appropriate methodologies for modelling the probability of failure of a natural stone tread under torsion. The paper proposes the use of Weibull's method for calculating the probability of failure for a brittle material. This approach assumes that failure of a stair tread occurs when the applied stresses exceeds the material strength at any location in the tread. The local material strength is assumed to be governed by the presence of microscopic cracks. This paper presents a methodology for developing a probabilistic model for the torsion capacity of a stone tread containing random microscopic irregularities. The complexity of the stress field within the stone tread, the lack of accuracy of the magnitude of the predicted stresses and the difficulties of predicting the failure criteria for a stone tread are all considered. The probability model developed can be used in conjunction with a simple static analysis combined with a detailed torsion analysis to predict the safe load capacity of a complete flight of stairs. The paper also suggests how a comparison of the results of 3-point and 4-point bending test results can be used to identify the key material parameters required to calculate the probability of failure. The paper briefly considers the problem of assessing the probability of failure for inhomogeneous stone, which contains voids or significant fossils.

1 Introduction

Cantilevered stone stairs were one of the predominant forms of stair construction from the 17th to the 19th century. This form of construction was particularly prevalent in substantial masonry buildings. In such buildings the stairs can sometimes be categorised into grand stairs, which are frequently ornate, in the public sections of the buildings, see Figure 1a and simple narrow undecorated stairs in the service areas, see Figure 1b. Both categories of cantilevered stairs function in a similar manner.



Fig. 1. Cantilevered stone stairs (a) Wide decorated staircase (b) Narrow service stairs

Although new cantilevered stone stairs are rarely constructed today a large number of cantilevered stone stairs are still in service. Cantilevered stone stairs often form the fire evacuation routes in older buildings therefore their reliable performance under a full imposed load is of great importance.

In the majority of cases these cantilever stone stairs continue to function well with little or no maintenance but there have been occasional failures. Assessing the load capacity of a cantilever stone stairs can be very difficult and their mode of failure can be very sudden with little or no warning. The failure of masonry walls or masonry arches is principally due to instability: failures of this sort usually give warning in the form of distorted geometry. In contrast, cantilevered stone stairs fail due to overstressing of the tread material and typically give no warning prior to their sudden brittle failure.

2 Structural mechanism

Despite their name, most cantilevered stone stairs do not act as cantilevers. Cantilevered stone stairs comprise a series of solid stone treads that are typically built into their supporting wall by no more than 100mm to 150mm [3, 5]. It is very likely that the masons who constructed these stairs limited the length of the embedded section of the tread to prevent the treads from cantilevering, realising that the treads would not have sufficient strength to support themselves in this way. Instead, cantilever stone stairs support themselves and their imposed loading by developing vertical and torsion reactions at their embedded tread ends.

This paper concentrates on stairs but same structural mechanisms are at play in the stone landings, which are often found at the top of cantilevered stone stairs.

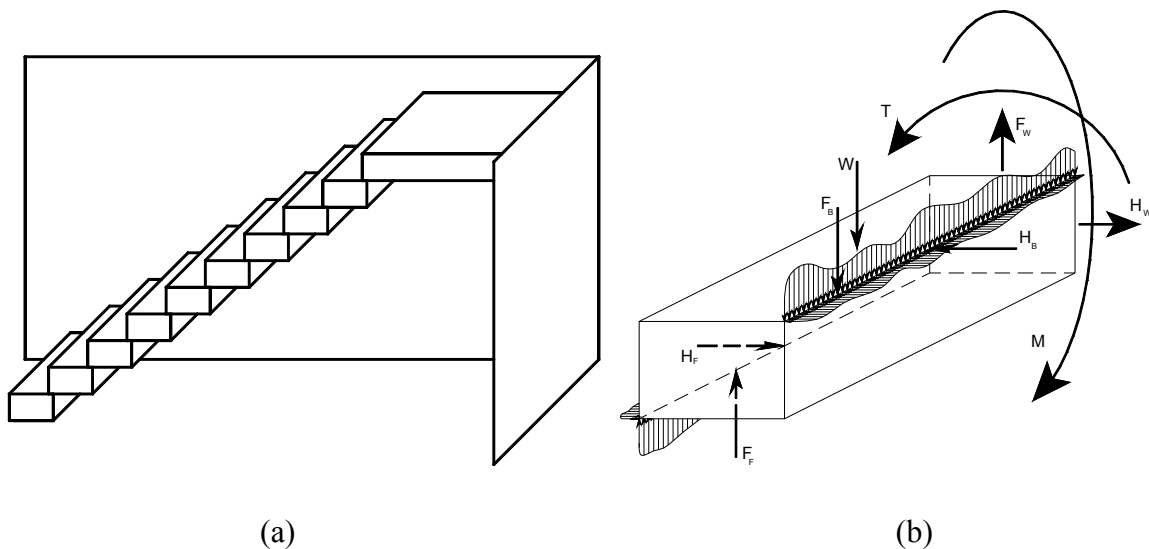


Fig. 2. (a) Schematic of cantilevered stairs and (b) free-body diagram showing forces on a tread

Figure 2(a) shows a single flight of stairs in which each of the stair treads is built into the supporting wall at one end. Figure 2(b) shows a free body diagram of the forces acting on a single tread. This figure indicates a cantilever support reaction applied by the wall to the tread. In general the depth to which the treads were embedded into the wall was limited to prevent the development of this moment. Thus, M , is usually assumed to be zero.

Figure 2(b) indicates the continuous contact forces applied to the tread by the treads above and below, the subscripts F and B are used to indicate the resultant forces acting at the front and back of the tread. The vertical and horizontal resultants of these distributed forces are labelled F and H . The details of the contact forces are complex and the locations of the resultants are not known. Calculating the magnitude of the horizontal resultants H_F and H_B is particularly complex and depends on the connection detail between treads. Figure 3b shows a triangular tread section where there is a substantial connection between the treads. This connection could develop horizontal contact forces. The treads shown in Figure 3a can develop horizontal forces only if there is a hidden rebated connection. Many stairs with rectangular sectioned treads do not allow the development of horizontal contact forces. Figure 3c shows a typical ogee section, widely used on grand stairs. Figure 4 shows the typical hidden rebated interconnection typical of this tread shape. This connection allows horizontal contact forces to develop between treads. If horizontal contact forces can develop, then the torque in the treads is reduced [3,5].

The number of unknowns exceeds the number of static equilibrium equations and therefore cantilevered stone stairs are statically indeterminate structures. These structures can be analysed using the finite element method using solid elements but an adequate analysis can be performed by assuming the locations of the resultants of the contact forces and assuming that the support reactions provided by the wall is limited to a torsional restraint and a vertical restraint.

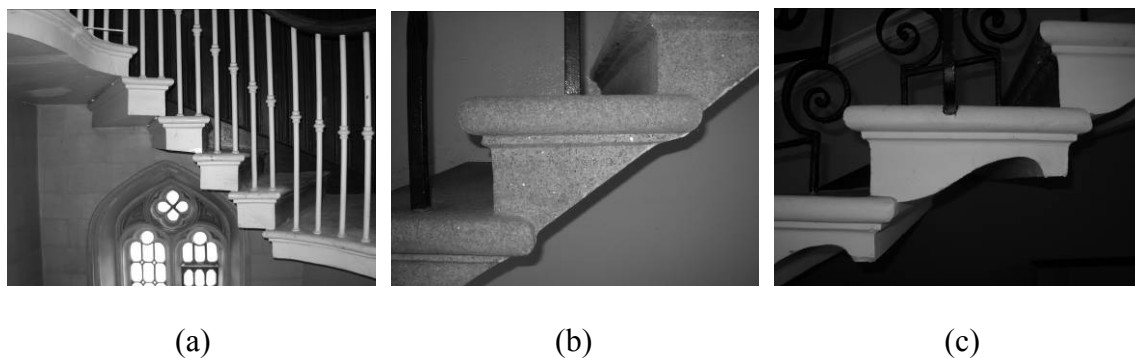


Fig. 3. Various tread sections (a) Nominally square (b) triangular (c) ogee section



Fig. 4. Tread which failed under load – showing rebate between treads

This static analysis is sufficient to determine the probable peak torsion in the tread. Once the peak torsion force is known it is possible to calculate the distribution of torsional shear stresses in the tread. The analysis of solid prismatic sections under torsion is one of the classic problems of solid mechanics. The distribution of stresses is easily determined using the finite difference method.

The problem equates to finding a solution to the equation

$$\frac{\partial^2 \phi}{\partial x^2} + \frac{\partial^2 \phi}{\partial y^2} = -2G\theta \tag{1}$$

Where ϕ is a function of x and y (where z is along the longitudinal axis of the tread, y is the vertical direction and x is in the direction of going) called the *stress function* [7], G is the shear modulus of the tread material and θ is the angle of twist. The torsional shear stresses can be calculated from the stress function

$$\tau_{xz} = \frac{\partial \phi}{\partial y} \text{ and } \tau_{yz} = -\frac{\partial \phi}{\partial x} \quad (2)$$

and T , the total torque in the section, must equal

$$T = 2 \iint \phi \, dx dy \quad (3)$$

The stress function must also satisfy the boundary condition that it is constant along the boundary of the cross section. For solid bars the value of ϕ on the boundary can be taken as 0 [7].

Alternatively, a finite element analysis can be used to generate a three dimensional picture of the state of stress at all points in all treads.

3 Failure criterion

Figure 5 shows the remains of a cantilevered stone stairs that collapsed. The shape of the failure surfaces suggests that the bottom, most heavily loaded steps failed in torsion. This is shown by the helical failure surface. In a prismatic member under torsion a helical failure surface develops as a crack progresses along planes normal to the principal tensile stresses. The near vertical failure surface of the top steps suggests that these treads failed in bending following failure of the lower treads. This failure confirms the structural mechanism outlined in Section 2.

Although the analysis of a cantilevered stone stairs is complex and the exact stresses in a stairs may not be known with precision, it is possible to establish the probable range of stresses within such stairs. In order to assess the safe load capacity of a stairs it is also necessary to calculate the maximum stresses that a tread can carry safely.

3.1 Mohr's failure criterion

Steel and reinforced concrete are the materials of choice for structural engineering because of their desirable structural properties. Structural steel has a relatively moderate yield stress, typically 275-350 N/mm², but is very ductile. Similarly, when concrete is reinforced with steel it behaves in a ductile manner. However, stone is a stiff brittle material that gives little warning of failure [6]. The appropriate failure criterion for stone or concrete is usually assumed to be Mohr's criterion, where failure occurs when the principal tensile stress exceeds the tensile capacity of the stone. This criterion can be modified to take account of tri-axial stress states but in the case of cantilevered stone stairs the principal tensile stresses are much larger than the stresses on the other principal planes.

The Mohr's failure criterion is widely used and in this instance the safety of a tread would be established by comparing the maximum tensile stress with the tensile capacity of the stone.



Fig. 5: A flight of cantilevered stairs which failed

3.2 Ceramic failure criterion

Most modern structural analysis is based on the premise that the load at which a structural member fails is a function of the peak stress developed in the member. The size of the member is irrelevant: it is assumed that there are no size effects [6]. However, brittle ceramics, and this category includes stone and concrete, are influenced by the size of the material. Ceramics are very strong in compression but less strong in tension. Failure in tension occurs by rapid crack development, a failure mechanism first described by Griffith [6]. Griffith identified that for a given level of tensile stress in a material there is a critical size below which a crack will not grow: correspondingly, for a given crack size there is a level of tensile stress at which cracks of this size, or greater, will grow very rapidly. The failure of a ceramic sample when loaded in tension is dependent on the size of micro-cracks within the material. Failure is dependent on the biggest inherent flaw in the material. Para-

doxically, the larger the volume under high tensile stress the lower the stress at which the member is likely to fail.

Weibull [9] was among the first to describe the strength of brittle ceramic members. His approach is sometimes referred to as a weakest link theory because his analysis is similar to the classic probability of calculating the probability of failure of a chain [4]. The failure of a chain in tension is dependent on the strength of the weakest link, in a similar manner Weibull's theory assumes that failure occurs if any small volume of a ceramic has a combination of inherent flaw and applied stress that would cause a crack to develop.

Weibull developed the following formulation to calculate the cumulative probability of failure, P_f , of a part comprising N elements of volume V_i .

$$P_f = 1 - \exp \left[\sum_{i=1}^N \left(\frac{\sigma - \sigma_u}{\sigma_o} \right)^m \frac{V_i}{V_o} \right] \quad (4)$$

σ is the stress in the volume, σ_o is a normalizing material strength and is defined as the characteristic stress at which a reference volume of the material (V_o) would fail in uniaxial tension [4]. Taking a reference volume of material, $V_o = 1$, and replacing the summation over discrete elements to an integral over the volume gives the equation

$$P_f = 1 - \exp \left[- \int_V \left(\frac{\sigma - \sigma_u}{\sigma_o} \right)^m dV \right] \quad (5)$$

m is a coefficient that depends on the material and σ_u is a stress below which the material would never fail. By taking σ_u conservatively as zero the expression for the reliability, R , is

$$R = 1 - P_f = \exp \left[- \int_V \left(\frac{\sigma}{\sigma_o} \right)^m dV \right] \quad (6)$$

Weibull called the integral term of this equation the *risk of rupture*, B , thus

$$B = \int_V \left(\frac{\sigma}{\sigma_o} \right)^m dV \quad (7)$$

and the reliability can be written as

$$R = \exp[-B] \quad (8)$$

If the value of the risk of rupture $B < 0.1$ then the risk of rupture is approximately equal to the probability of failure. The equations given thus far are for uni-axial tension. For a three dimensional stress field where failure is dependent on tensile stresses alone the corresponding equation for probability of failure is,

$$P_f = 1 - \exp \left(- \int_V \left\{ \frac{2m+1}{2\pi\sigma_o^m} \int_0^{2\pi} \int_0^{\pi/2} [\cos^2 \phi (\sigma_1 \cos^2 \psi + \sigma_2 \sin^2 \psi) + \sigma_3 \sin^2 \phi]^m \cos \phi d\phi d\psi \right\} dV \right) \quad (9)$$

This equation comes from integrating the normal component of the principal stresses over a unit sphere, as per Figure 6 [4].

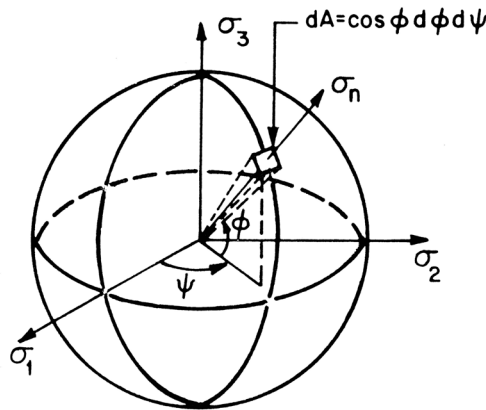


Fig. 6: Component of principal stresses acting normal to dA [4]

Equation 9 gives the theoretical expression for calculating the probability of failure. In practice, a simplified approach may suffice [4].

3.3 Material testing

To evaluate the probability of failure it is necessary to quantify σ_o and m . The standard method of evaluating the tensile capacity of stone is via bending tests in which prismatic test bars are loaded in either 3-point or 4-point bending. Figure 7 [4] shows typical loading arrangements and the corresponding distribution of bending moments in the sample.

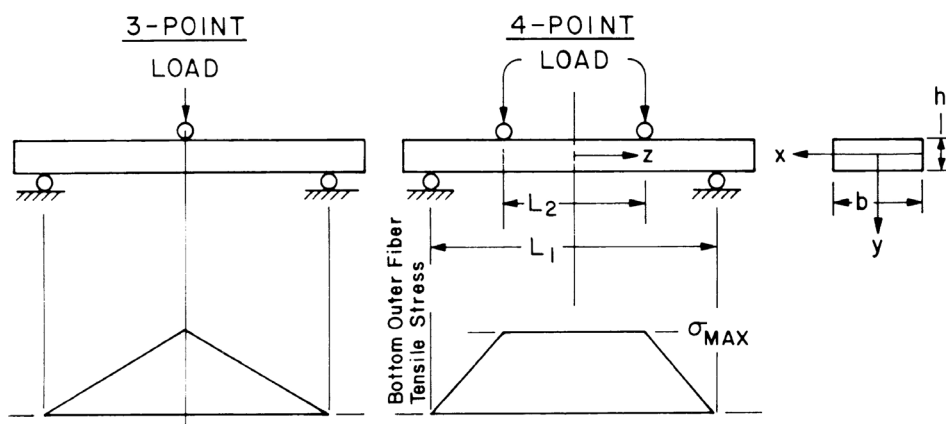


Fig. 7. Loading arrangements and bending moment diagrams for 3-point and 4-point bending tests [4].

Test pieces under 4-point bending will typically fail at a lower load than 3-point bending because the effective volume of material under tensile stress is greater for 4-point bending. The risk of rupture for a test bar in 4-point bending is given by Equation (10) [4]

$$B_{4pb} = \left(\frac{\sigma_{\max}}{\sigma_o} \right)^m \frac{bh}{2} \left[\frac{mL_2 + L_1}{(m+1)^2} \right] \quad (10)$$

Setting L_2 to zero gives the equivalent risk of rupture for 3-point bending

$$B_{3pb} = \left(\frac{\sigma_{\max}}{\sigma_o} \right)^m \frac{bh}{2} \left[\frac{L_1}{(m+1)^2} \right] \quad (11)$$

The ratio of the 4-point bending and 3-point bending risks of rupture is

$$\frac{B_{4pb}}{B_{3pb}} = \frac{mL_2 + L_1}{L_1} \quad (12)$$

Thus a comparison of the results of a series of 3-point bending tests and a series of 4-point bending tests can be used to identify the Weibull parameter m . Once m has been established then the result of either series of bending tests can be used to establish σ_o .

4 Assessing probability of collapse

Once the characteristic strength σ_o of the material used in a stairs has been established then Equation (9), or a simplified version of this equation, can be used to calculate the probability of failure. Because the stresses in a stairs varies from tread to tread the overall probability of failure must consider each tread separately.

The probability of failure for the stairs given by Equation (9) is an over-estimate of the true probability of failure. In most cases where the safety of a cantilevered stone stairs is in question the stairs will be carrying its self-weight successfully. Thus the overall probability of failure is the probability of failure under full imposed loading minus the probability of failure under self-weight.

4.1 Inhomogeneous stone

The analysis of cantilevered stone stairs is complex with many parameters that cannot be determined with complete accuracy. Similarly, identifying the material properties of the stone used in the stairs may be difficult because samples of the stone may be limited. However, these problems are minor compared with the very real problems associated with inhomogeneous materials.

In practice many stairs have been constructed using natural stones that are heavily fossilised and which may also contain voids. Figure 8 below shows a stone sample from a stair tread. This sample shows evidence of both voids and inhomogeneity. The stairs from which this sample came showed very little evidence that the stone used contained irregularities. In contrast there are many stone stairs which show clear evidence that they are constructed using stone that contains multiple large fossils.



Fig. 8: Stone sample showing internal voids.

In cases where the material used in a cantilevered stairs contains voids and is inhomogeneous analysis is potentially difficult. If the irregularities are small then the material tests could overcome take account of their presence. However, the size of the voids and/or fossils would have to be sufficiently small that there would be no size effect. This is certainly not the case in many stairs. In addition, the analysis would only be valid if the distribution of irregularities is random. This is not always the case, indeed there is no reason to suppose that the distribution of either fossils or voids in a stone sample should be random. In these cases applying a full load test to the stairs may be the only sensible approach.

5 Conclusions

Cantilevered stone stairs rarely function as cantilevers. The predominant force applied to each tread in a cantilevered stairs is a torque. Stone is weak in tension and where the applied torque exceeds the capacity of a tread, typically in the bottom tread of a flight, a typical helical failure surface occurs with failure occurring on the plane with the maximum principal tensile stress. Calculating the magnitude of the stresses in a cantilevered stairs is difficult because these structures are highly statically indeterminate. Nevertheless, it is possible to estimate the stresses within a stair tread the reasonable accuracy.

Calculating the tensile strength of the stone in a cantilevered stairs also represents a challenge. Stone is a brittle material and its failure is governed by the presence of microscopic cracks, which, in the absence of macroscopic voids and irregularities, can be assumed to be randomly distributed through the stone. Weibull's probabilistic approach can be used to calculate the probability of failure. This approach requires a number of material parameters. These parameters can be obtained by comparing the results for 3-point and 4-point flexural bending tests.

If the stone in a stairs contains significant voids or fossils, where the fossils are weaker than the parent material or where the fossils present a locus for crack growth, then a full scale load test may be the only appropriate method of establishing the safety of a stairs.

6 References

- [1] Bazant, Z.P.: Scaling of quasibrittle fracture: Asymptotic analysis. *Journal of Fracture*, **83**, 1997, 19–40
- [2] Heyman, J.: *The Masonry Arch*, Ellis Horwood series in engineering Science, Chichester, 1982
- [3] Little, P., Hough, M. & Mullarkey, E.: Stone cantilever stairs - inspection and analysis of cantilever stairs, *The Structural Engineer*, **87**, Issue 8, 21 April 2009, 26 – 33
- [4] McLean, A.F.; Hartsock, D.L.: Design with Structural Ceramics In: Wachtman, J.B. (Editor): *Structural Ceramics: Treatise on Materials Science and Technology Volume 29*. Academic Press, Inc., New York, 1989, 27–97
- [5] Price, S. and Rogers, H.: Stone cantilevered staircases , *The Structural Engineer*, **83**, Issue 2 January 18th 2005, 29 – 36
- [6] RILEM TC QFS: Quasibrittle fracture scaling and size effect – Final report. *Materials and Structures/ Matériaux et Constructions*, **37**, October 2004, 547-568
- [7] Timoshenko, S.P.; Goodier, J.N.: *Theory of Elasticity 3rd Edn*: McGraw-Hill, London, 1970
- [8] Ting, J.: Flexural strength analysis of brittle materials: *Journal of Materials Science*, **38**, 2003, 339 – 341
- [9] Weibull, W.: The phenomenon of rupture in solids, *Proceedings of the Royal Swedish Institute for Engineering Research*, **153**, 1939, 1 – 55

Seismic Risk Assessment of Unreinforced and Prestressed Masonry by Means of Probabilistic Simulations

S.T. Sperbeck¹, H. Budelmann²

¹ Institute of Building Materials, Concrete Construction and Fire Protection and International Graduate College 802, Technische Universität Braunschweig, Braunschweig, Germany

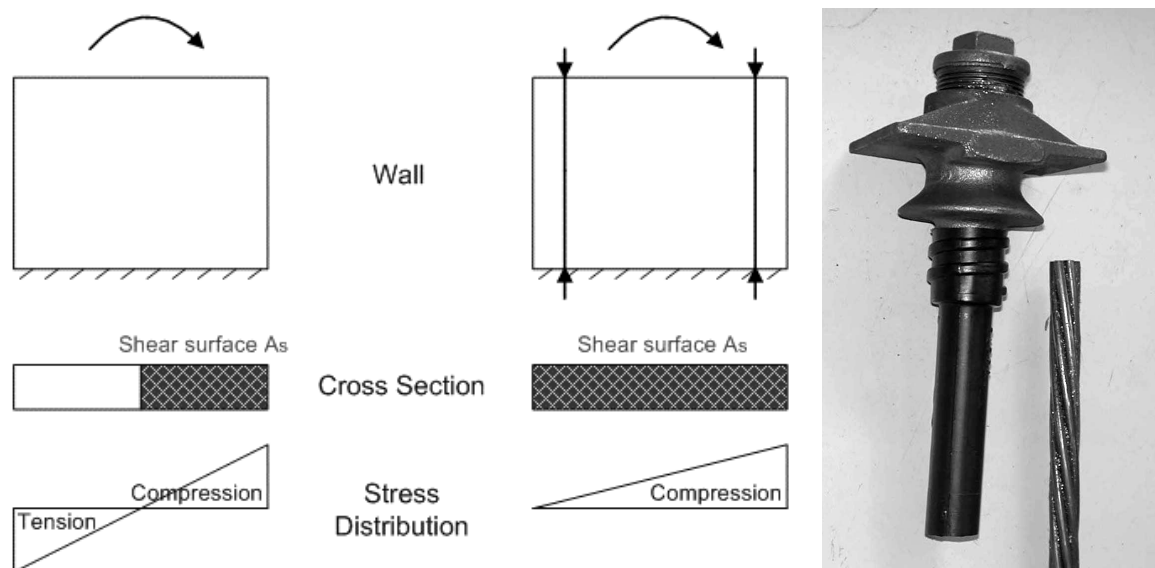
² Institute of Building Materials, Concrete Construction and Fire Protection, Technische Universität Braunschweig, Braunschweig Germany

Abstract: All over the world, a huge amount of masonry structures, which is usually notorious to have a low earthquake resistance, exist. It is limited by low shear strength. Besides, in Eurocode 6 a very small ductility is assumed for unreinforced masonry. Vertical local prestressing is considered in order to improve the shear capacity and the ductility. Static and static cyclic tests have shown the suitability of this method. A detailed investigation of the dynamic behaviour is demandable before using the strengthening method against earthquake action. The large quantity of necessary experimental tests is very expensive, especially with shaking tables to apply dynamic loading. This paper presents a possibility, based on numerical methods, to investigate the usefulness of vertical prestressing with particular emphasis on the dynamic behaviour of prestressed masonry structures as well as to estimate the risk, by means of probabilistic analyses. A risk based design is used, which accounts also for several damage stages, in order to assess the benefit of prestressing more in detail. Therefore, a clear risk management methodology for disaster risk is applied. The focus of this study lies on modern masonry and its in-plane behaviour, since it is very important in case of seismic action. For the transient earthquake simulations a macro modelling method is utilized that allows a prediction of damage via special damage parameters for units and mortar separately. Several detected factors that influence masonry behaviour and numerical results are investigated and discussed. The probabilities of damages are estimated by means of Latin Hypercube sampling with the advanced program optiSLang[®], which is used in combination with ANSYS[®], in order to carry out dynamic probabilistic analyses. The calculated damage probabilities are used to estimate risks and to compare the benefit of vertical prestressing in case of seismic action.

1 Introduction

1.1 Seismic loaded unreinforced and vertical prestressed masonry

The huge amount of masonry structures in seismic areas and the enormous number of damages – as recently occurred during the earthquakes in the region Sichuan, China of 2008 and in L'Aquila, Italy of 2009 – show the necessity to investigate and to improve the load carrying behaviour of masonry. In case of seismic action, bracing walls of houses are mainly loaded in horizontal direction. Thus, the in-plane shear behaviour of masonry walls is of highest interest in this contribution. Detailed descriptions of masonry shear behaviour are given for instance in Van der Pluijm (1993) and Lourenço (1996). Unreinforced masonry has a low resistance against seismic action. On the one hand, this is caused by the limited shear capacity, especially for structures with low vertical loading, and by its low ductility on the other hand. The simple friction law is valid also in masonry walls. While increasing the vertical loading, the horizontal resistance is improved as well. Since, higher masses lead to higher inertia force, vertical prestressing or post-tensioning are good rehabilitation measures. This contribution refers to vertical local prestressing of masonry walls by means of tendons or strands. The following figures present schematically the principle of this method. Tendons are placed in the wall to reduce cracks in the bed joints and to increase the shear capacity. Fig. 1b shows a strand and a prestressing anchor which is used in praxis to fix it on its ends.



(a) Principle of shear surface A_s reduction in the plastic range of a non-prestressed wall in comparison with a prestressed one (Sperbeck 2008) (b) Prestressing anchor and strand (Budelmann et al. 2004)

Fig. 1: Prestressing of masonry walls

In Sperbeck (2008) it is particularly shown in which cases vertical prestressing leads to an increased ductility or not. Internal tendons with bond lead to higher ductility than external tendons, since internal ones tie up the masonry in-between the tendons and prevent so a

brittle collapse which would occur by sliding down of the upper wall triangle. Moreover, it could be shown that the high vertical forces lead to an increased unit failure causing brittle collapse. Experimental tests with internal prestressed masonry walls of Budelmann et al. (2004) have indicated such a ductile behaviour. Four different wall systems have been investigated in static cyclic tests and are used to calibrate the numerical models which are mainly focused on wall 1 and wall 3. The experimental set-up is depicted in Fig. 2.

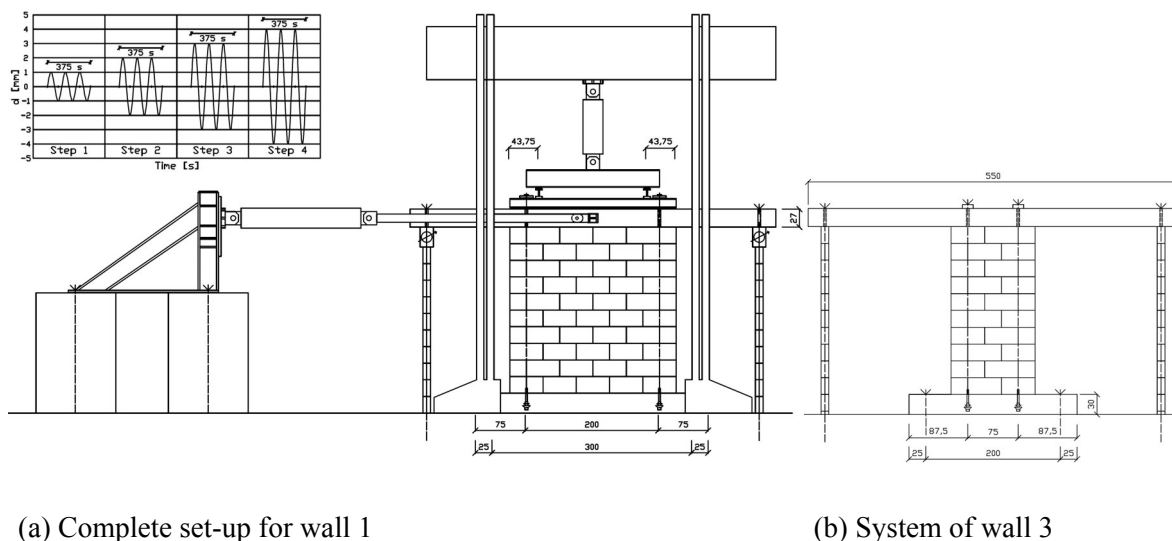


Fig. 2: Experimental set-up (Budelmann et al. 2004)

1.2 Numerical modelling of masonry

A comparison of different possible simulation techniques and materials models is given in Sperbeck (2008). For the probabilistic dynamic simulations the material model of Gambarotta & Lagomarsino (1997) is used. Since, such simulations are very time consuming this efficient constitutive model is chosen. However it is adequate accurate, based on fracture mechanics and macro modelling. Fig. 3 shows the failure domains of bricks and joints of this nonlinear material model that is also able to describe the post-peak behaviour and the degradation of stiffness and strength.

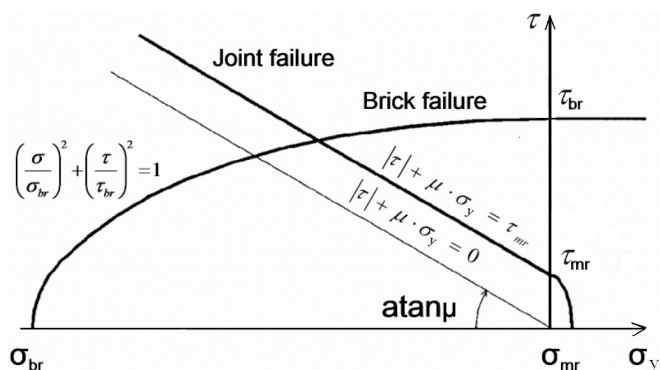


Fig. 3: Mortar joint and brick failure domains (Gambarotta & Lagomarsino 1997)

The last are important in case of static cyclic and dynamic loading. For the damage modelling the inelastic strains are used and two internal damage variables to express the damage

evolution in the bricks and mortar. The damage evolution is defined in accordance to the toughness function or also named R-curve approach, which is used in the theory of fracture mechanics by imposing the damage energy release rate to be less than or equal to the toughness R . These damage variables express the loss of toughness at each node of the element. Loss of toughness might be described as the decrease in energy needed to cause further cracking, expressed as the percentage of the energy needed in the undamaged state.

2 Management of disaster risk

The purpose of the present work is to offer a more detailed insight into the impact of load and material uncertainties with respect to masonry subjected to seismic action. Throughout this study, it is important to realize, that this work is done in the context of giving a prediction of the probability distribution of possible damage states, not to assess the structural safety itself. Therefore, an unified risk management concept is applied (see Fig. 4).

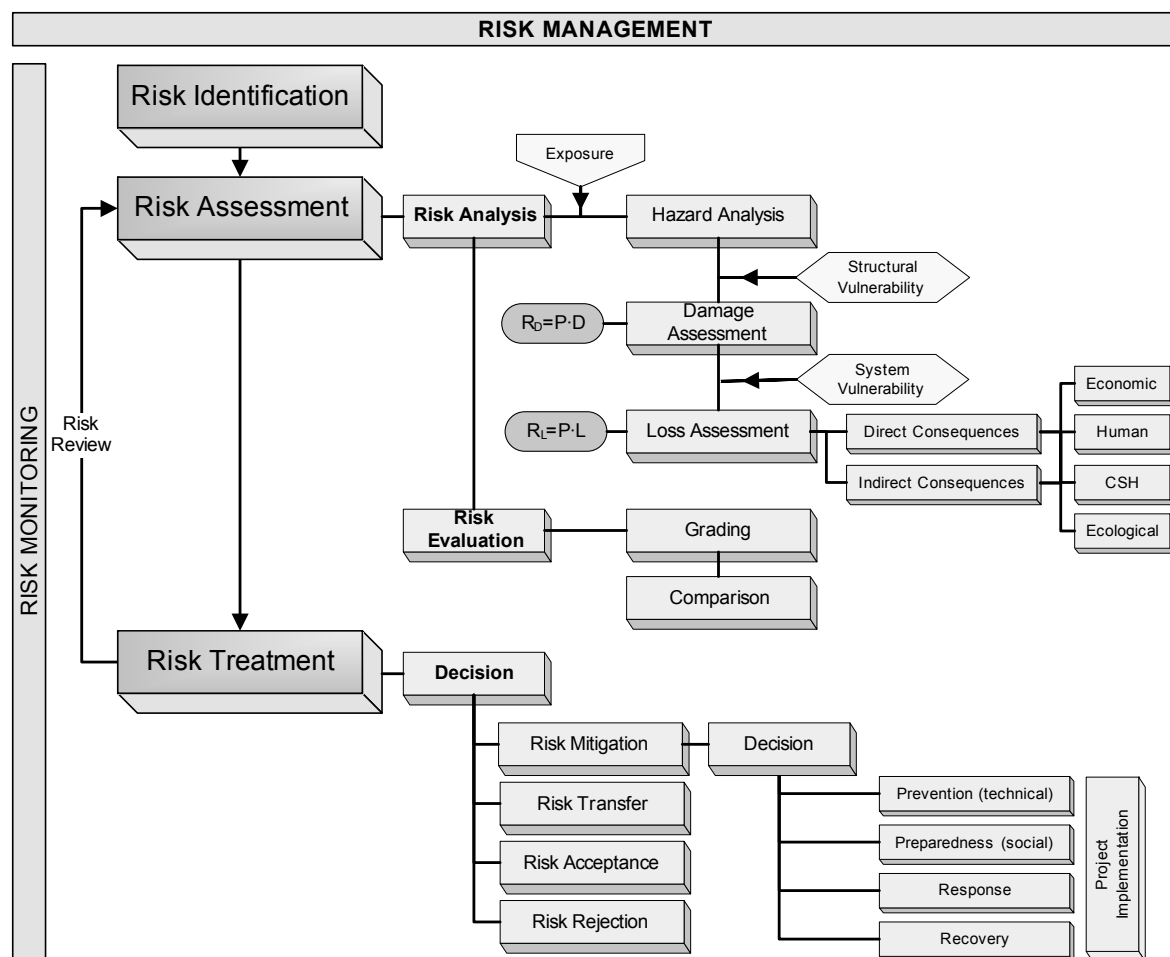


Fig. 4: Overview of the whole risk management process (Pliefke et al. 2007)

The concept results from a long development process for the International Graduate College 802 and is published in Pliefke, Sperbeck, Urban (2006) and Pliefke et al. (2007) to which the interested reader is referred. The approach covers the whole risk management

chain, starting from risk identification over risk assessment up to risk treatment. The methodology is too exhaustive to be applied completely in the framework of this work. The main parts to reach the aim are the hazard analysis of the seismic peril, the damage analysis to estimate the structural damage D and the risk mitigation by means of the technical prevention with prestressed strands. The calculated so-called structural risks R_D are evaluated by a comparison. The total risk R_L – taking also into account further consequences as economic losses L – is not part of this contribution. The risk calculation schemes are integrated in the concept (see Fig. 4). Different definitions as well as ways to estimate and evaluate risk may be found in literature. Here, the definition risk R is equal to damage D times its probability P is used. The different analyses are described in the next subchapters.

2.1 Hazard analysis

The region of Aachen in Germany is assumed as the site for this fictive example. As a base, the results of a probabilistic seismic hazard analysis PSHA carried out by Schmitt (2005) are used. The analysis methodology is resting upon the conception that the seismic hazard at a site is a function of three main components: the space geometry of seismic sources, the characteristics and statistics of their seismicity and the attenuation of intensity. This hazard curve displays the annual probability of the intensity regarding the Medvedev-Spoonheuer-Karnik (MSK) scale which is displayed in Fig. 5 for this region.

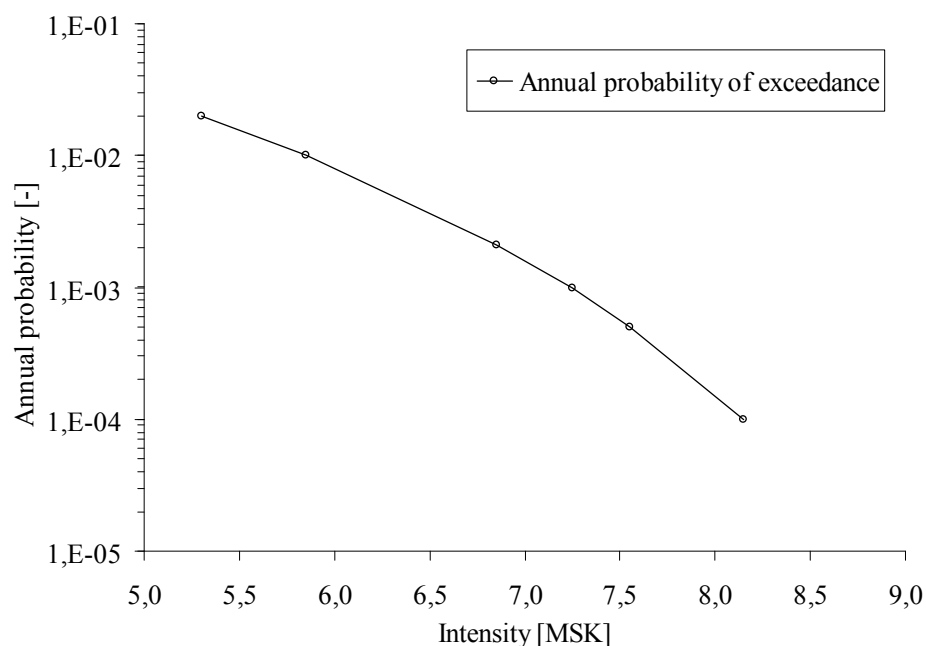


Fig. 5: Seismic hazard curve for Aachen, Germany (Schmitt 2005)

An investigation of the whole range of probabilities (see Fig. 5) is not reasonable in structural analyses by means of probabilistic transient analyses, since many small earthquakes which occur with high probability do not lead to damages. A huge number of transient calculations is redundant, while not leading to damage. Thus, the following new method is suggested and applied in this study. A minimum threshold is selected which is reasonably fitted to the investigated structure. Therefore, the minimum threshold corresponds to a return periods of 475 years in this work, and the maximum to a return period of 10000 years.

Moreover, a return period of 2000 years is used for the subsequent risk based analysis. For the transient simulations, time histories are necessary. The PGAs given in Tab. 1 are used to generate an aim response spectra for each return period of interest.

Tab. 1: Seismic hazard data for the region of Aachen, Germany (Schmitt 2005)

Return period [a]	Annual probability of exceedance [-]	Annual probability of exceedance [%]	Intensity [MSK]	PGA [m/s ²]
50	0.0200	2.00	5.30	0.38
100	0.0100	1.00	5.85	0.52
475	0.0021	0.21	6.85	0.92
1000	0.0010	0.10	7.25	1.15
2000	0.0005	0.05	7.55	1.37
10000	0.0001	0.01	8.15	1.94

Corresponding to each aim response spectra of every investigated return period, four time histories are artificially generated that differ in duration and characteristics. For the return period of 475 years the data are given in a pseudo-velocity diagrams of Fig. 6. Moreover, in the probabilistic transient structural analyses the acceleration scatter by means of a scaling factor, within a range of a lognormal distribution with a standard deviation of 0.6 and a mean value of 1.0 in accordance to Rackwitz (2006) and several other authors.

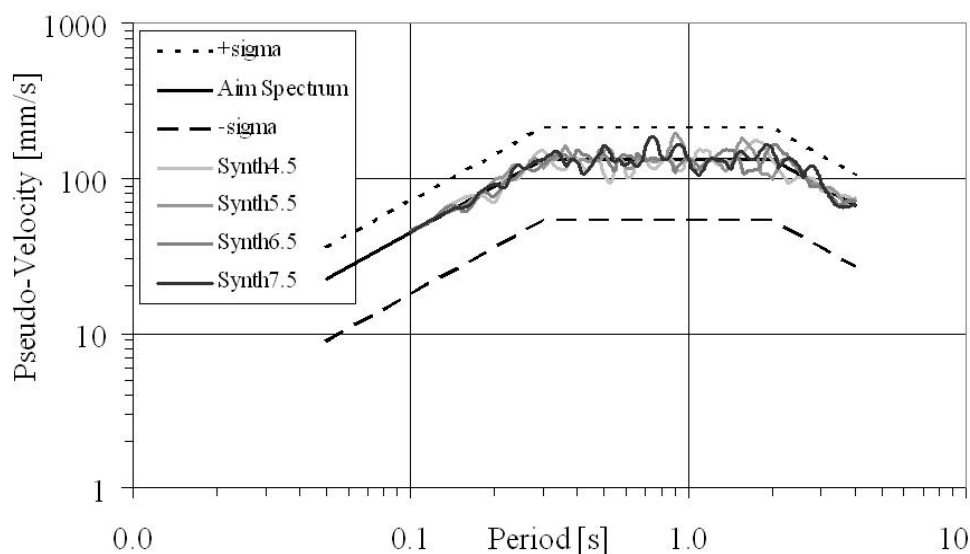
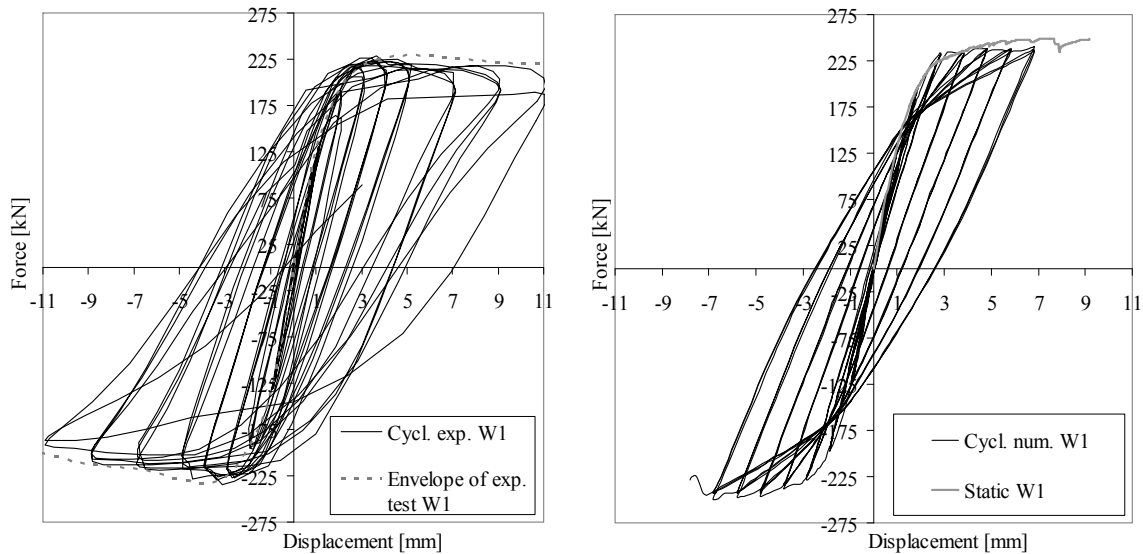


Fig. 6: Pseudo-velocity diagram for the return period of 475 years

2.2 Damage analysis

For the probabilistic dynamic simulations the material input parameters are first of all calibrated on the static cyclic experimental tests of Budelmann et al. (2004). The above explained material model and ANSYS[®] have been used. The results fit well, as shown in Fig. 7. Thereafter, deterministic transient simulations on base of the generated earthquakes

of the hazard analysis are carried out with the mean values on account of plausibility checks. Wall 1 and 3 are modelled in a non-prestressed and a prestressed version in order to analyse the impact of prestressing on damage and its probability. The walls are assumed to be bracing elements of a three storey terraced house in the region of Aachen, Germany.



(a) Experimental results with envelope

(b) Numerical results with static curve

Fig. 7: Horizontal load displacement diagrams of wall 1 – static cyclic curve

Finally, probabilistic analyses are carried out by means of Latin Hypercube sampling with the advanced program optiSLang[®]. An extensive probabilistic damage assessment is carried out for wall 3 in order to estimate risk. In case of this wall, six different probabilistic simulations are carried out for three different seismic load levels regarding the return periods of 475, 2000 and 10000 years. In comparison to wall 3, wall 1 has a much higher resistance. Thus, it is subjected to stronger earthquakes to avoid a loading only in the elastic range, which is not reasonable for the damage assessment. The earthquakes used for wall 1 are stronger than the ones explained in the hazard analysis above and elaborately described in Sperbeck (2008). The damage assessment of wall 3 based on the generated accelerograms of the hazard analysis takes into account the uncertainties of seismic loading in a manner described above. In addition, uncertainties of material resistance, support conditions, vertical loading and the degree of prestress level are included as well. The scatter in terms of probability density functions PDFs, are presented in Tab. 2.

The results of the probabilistic analyses are sensitivities of input and output parameters, as well as PDFs for the predicted damages. A correlation matrix gives an overview of sensitivities via collared illustration of the correlation coefficients. The left matrix misses one line and one row for the variable prestress level. The correlation matrices are very similar for the non-prestressed and for the prestressed wall (see Fig. 8). All output parameters are highly correlated with each other. Not so the mortar damages with the storey drift and the unit damage. This becomes smaller in case of prestressing. The bar charts with linear correlation coefficients as partly given in Fig. 9 show negative correlations of many material parameters with the damage. This means for instance: the higher the strength, the lower the

damage. All damage parameters are mainly influenced by the horizontal excitation (xskal) and the mass of the upper storeys (headmass).

Tab. 2: Varied parameters and applied distributions for wall 3 and a return period of 475 a

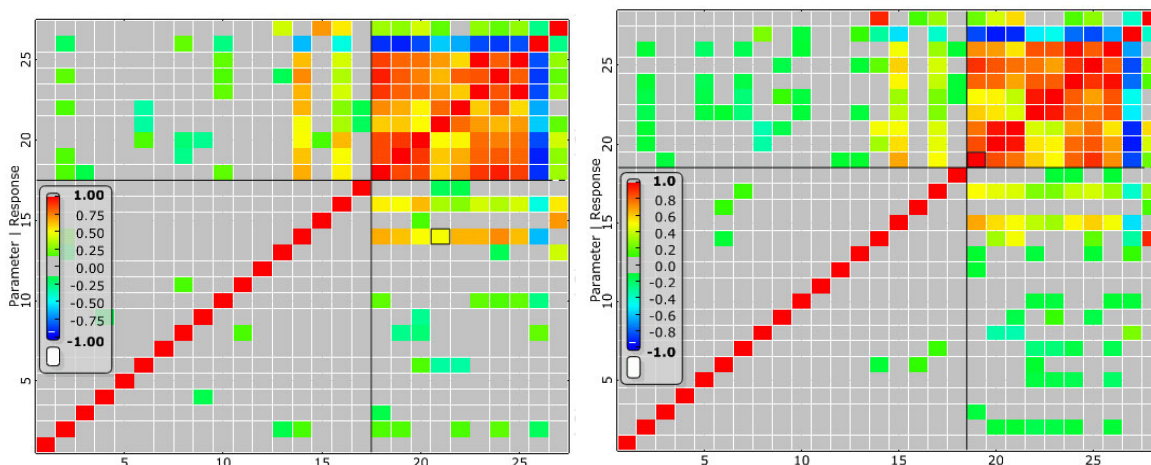
Sym- bol	Abbr. in files	Variable	Distribu- tion	Expected/ mean	Standard deviation	Min.	Max.
Masonry:							
η	nuxy	Poisson ratio	lognormal	0.15	0.0375	-	-
ρ_M	dens	Density of masonry	normal	1.65e-9 to/mm ³	0.12375e-9	-	-
E_M	emod	Young's Modulus of masonry	normal	5800 N/mm ²	580	-	-
μ	fric	Friction coefficient	lognormal	0.436	0.0807	-	-
σ_{mr}	mtens	Tensile strength of mortar joints	lognormal	0.87 N/mm ²	0.3045	-	-
τ_{mr}	mshea	Shear strength of mortar joints	lognormal	0.44 N/mm ²	0.132	-	-
c_{mt}	IDPGm	Inelastic deformation parameter for mortar	uniform	0.95	-	0.5	1.5
σ_{br}	comp	Compressive strength of masonry	lognormal	17.2 N/mm ²	2.924	-	-
τ_{br}	bshea	Shear strength of masonry	lognormal	2.5 N/mm ²	0.375	-	-
c_{bt}	IDPEb	Inelastic deformation parameter for ma- sonry	uniform	1.1	-	0.6	1.55
Support condition - Stiffness of the concrete floor slab:							
E_C	Emod- Con	Young's Modulus of concrete	truncated normal	14000 N/mm ²	5600	0.1	47600
Damping:							
α	adamp	Rayleigh mass damping	uniform	0.62	-	0.4048	0.8352
β	bdamp	Rayleigh stiffness damping	uniform	0.0003	-	0.0001	0.0005
Loading:							
P	PreFo	Sum of prestressing	lognormal	352000 N	123200	-	-
ρ_M	head- mass	Density of mass of upper structure parts	truncated normal	2.29358e-7 to/mm ³	0.91743e-7	1e-10	1.15e-6
D	durat	Earthquake duration of the steady phase	discrete uniform	-	4.5, 5.5, 6.5, 7.5	4.5	7.5

To express the damage, several reasonable damage parameters are used that are summarized in Tab. 3. A detailed descriptions can be found in Sperbeck (2008). The prestressing level (P) correlates very well with the global unit damage and is negatively correlated with the global mortar damage. Consequently, the higher the prestressing, the higher the unit damage, the lower the mortar damage. The damping (adamp and bdamp) has also a small impact on some damage parameters as well as the stiffness of the concrete floor slab

(EmodCon). These trends can be observed also for wall 1 and for the other return periods. Moreover, the stronger the earthquakes, the better the correlations and more significant the impact of xskal and headmass. All these results are very plausible and go in line with deterministic results of previous investigations, experimental tests and the literature.

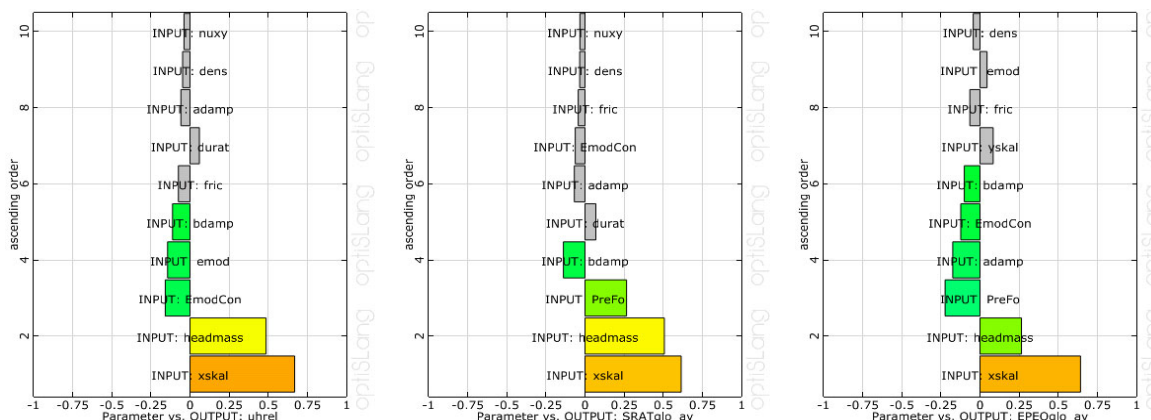
Tab. 3: Notation of the used damage parameters

Symbol	Abbreviation in files	Damage parameter
$\max u_{h,rel} $	uhrel	Absolute maximal horizontal top displacement (storey drift)
$\max \alpha_{b,loc}$	SRATloc	Maximal local brick damage
$\max \alpha_{b,glo}$	SRATglob_av	Maximal average global brick damage
$\max \alpha_{m,loc}$	EPEQloc	Maximal local mortar damage
$\max \alpha_{m,glo}$	EPEQglob_av	Maximal average global mortar damage
$\max \epsilon_{pleq}$	EQV	Maximal plastic equivalent strain
$\max \epsilon_{xy}^{pl}$	EPPLXY	Maximal plastic shear strain
$\max \epsilon_{y,t}^{pl}$	EPPLYtens	Maximal vertical plastic tensile strain
$\max \epsilon_{y,c}^{pl}$	EPPLYcomp	Maximal vertical plastic compression strain



(a) Non-prestressed (17 input parameters) (b) Prestressed (18 input parameters)

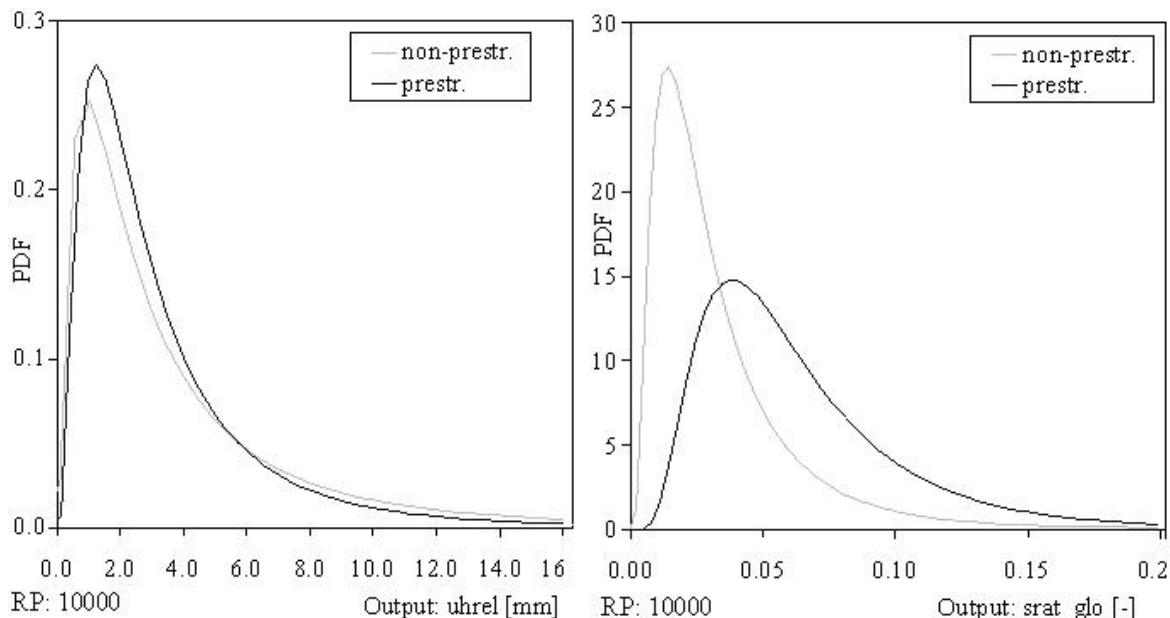
Fig. 8: Correlation matrices of wall 3 for a return period of 475 years



(a) Storey drift (b) Global unit damage (c) Global mortar damage

Fig. 9: Linear correlation coefficients, prestressed wall 3, a return period of 10000 years

Resulting PDFs for the storey drift and the global unit damage are exemplarily depicted in Fig. 10. The deterministic results show a small impact of prestressing on the drift that is confirmed by the PDFs, since there is only a small difference. Not so the unit damage, neither for the deterministic simulation, nor for the probabilistic ones a small impact exists. The probability of great unit damages increases due to prestressing, while the probability for small damages decreases significantly. For mortar damage, it is the opposite.



(a) Horizontal relative displacement

(b) Global unit damage

Fig. 10: Probability density functions for a return period of 10000 years for wall 3

2.3 Risk calculation and risk comparison

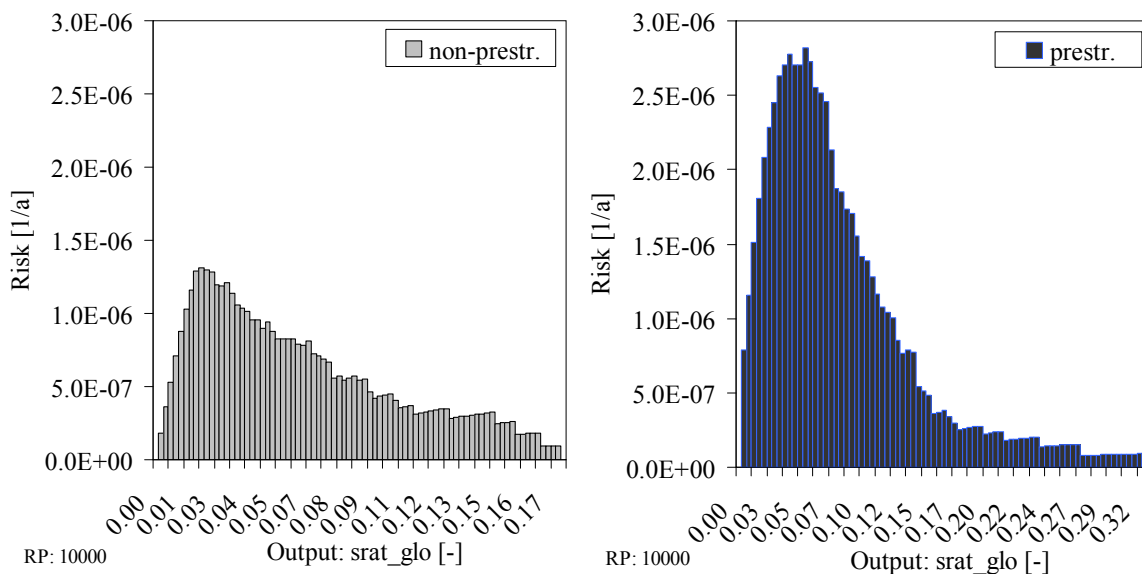
To calculate and compare risks, the focus lies on the structural risk R_D in this work (see Fig. 4). As a result of the hazard analysis, the hazard curve given in Fig. 5 and discrete values in Tab. 1, provides the needed probability of exceedance of the hazard $p_{ex}(H)$ for each of the investigated return periods. The structural risk R_D is calculated by means of $p_{ex}(H)$ and the ‘damage probability’ $p_{ex}(L,R)$ due to resistance and load scatter as a result of the probabilistic damage analysis (see equation (1)).

$$R_D = p_{ex}(H) \cdot p_{ex}(L, R) \cdot D \quad (1)$$

with $p_{ex}(H)$ Probability of exceedance of the hazard
 $p_{ex}(L,R)$ Probability of the damage due to resistance and load scatter
 D Damage degree

On the one hand, load means the level of prestressing and dead load, here in terms of ‘head mass’. On the other hand, the load intensity of an earthquake, which can scatter as well for each return period. The last is considered by means of the scaling factors X_{skal} and Y_{skal} for the horizontal and vertical acceleration histogram and different durations D . Instead of the fitted PDF, the sampled histograms of the probabilistic damage analyses are directly

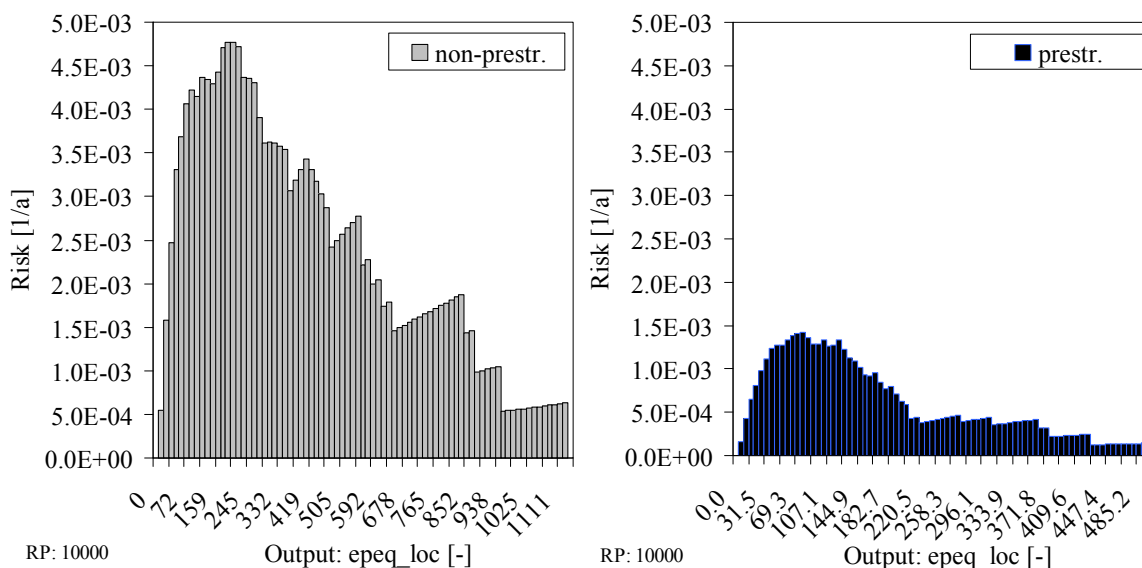
used to avoid inaccuracy and errors. The calculated risks of global unit damage are exemplary presented in Fig. 11. Moreover, the risks for local mortar damage are given in Fig. 12. Also the risk distributions show an increase of the unit damage due to prestressing and a decrease in case of the mortar damage. The trends are confirmed by static and dynamic simulations. In general, the equivalent plastic strain, plastic shear strain and vertical plastic tensile strain are reduced by prestressing as well.



(a) Non-prestressed wall 3

(b) Prestressed wall 3

Fig. 11: Risk distribution of the global unit damage for a return period of 10000 years



(a) Non-prestressed wall 3

(b) Prestressed wall 3

Fig. 12: Risk distribution of the local mortar damage for a return period of 10000 years

3 Conclusion

The probabilistic damage based design of risk management was very helpful to judge on the usefulness of vertical prestressing. The advanced extensive numerical investigation got a deeper insight and exhibited several problems. The question whether the application of prestressing on earthquake loaded masonry is useful cannot be answered generally. It is to distinguish between several cases depending on the structure, degree of seismic excitation, existence and level of other vertical loading as well as means of practical execution. Since, high vertical loading and missing wall tendon interaction lead to brittle collapse, prestressing can be dangerous. Thus, external prestressing especially with high prestressing degrees causes brittle failure, if high earthquake intensities exceed the shear capacity. For regions of high seismicity, a well ductile behaviour has to be ensured by means of further measures, if external prestressing is applied. In regions of low seismicity, the ductility is less important, if a sufficient safety factor guarantees lower horizontal loading than shear resistance. The increased elastic range leads to lower damages up to activation of plasticity. As an advantage, the mortar damage is always decreased by prestressing. However, it is not as important as the unit damage that is in general increased. The same trends are valid for the related risks. For a detailed description the interested reader is referred to Sperbeck (2008).

4 References

- [1] Budelmann, H., Gunkler, E., Husemann, U., Becke, A. (2004): Rationell hergestellte Wände aus vorgespanntem großformatigem MW mit hohem Erdbebenwiderstand, Abschlussbericht, iBMB der TU Braunschweig, Germany.
- [2] Gambarotta, L.; Lagomarsino, S. (1997): Damage models for the seismic response of brick masonry shear walls. Part II: the continuum model and its applications. *Earth. Eng. Struct. Dyn.* 26, pp.441-462.
- [3] Lourenço, P.B. (1996): Computational strategies for masonry structures. Doctoral thesis, Delft University of Technology, Netherlands.
- [4] Pliefke, T.; Sperbeck, S.T.; Urban, M. (2006): The Probabilistic Risk Management Chain - General Concept and Definitions. Internal Discussion Paper, International Graduate College 802, <http://www.grk802.tu-braunschweig.de/Links/>
- [5] Pliefke, T.; Sperbeck, S.T.; Urban, M.; Peil, U.; Budelmann, H. (2007): A standardized methodology for managing disaster risk – An attempt to remove ambiguity. In: Luc Taerwe & Dirk Proske (Eds.), *Proceedings of the 5th IPW*, Ghent, Belgium.
- [6] Rackwitz, R. (2006): Zuverlässigkeit und Lasten im konstruktiven Ingenieurbau. Lecture, Technische Universität München, Munich, Germany.

- [7] Schmitt, T. (2005): Grundlagen der Ingenieurseismologie und Erdbebengefährdungsanalyse. Pub. by: Institute for Geosciences and Natural Resources, Hannover, Germany.
- [8] Sperbeck, S.T. (2008): Seismic Risk Assessment of Masonry Walls and Risk Reduction by Means of Prestressing. Doctoral thesis, Technische Universität Braunschweig.
- [9] Van der Pluijm, R. (1993): Shear behavior of bed joints, in: Proc. 6th North American Masonry Conf., eds. A.A. Hamid and H.G. Harris, Drexel University, Philadelphia, Pennsylvania, USA, pp.125-136.

Modeling of imprecise distribution functions by uncertain stochastic moments within the maximum entropy formulation

T. Most
Research Training Group 1462,
Bauhaus-Universität Weimar, Germany

Abstract: The determination of an exact distribution function of a random phenomena is not possible from a limited number of observations. We assume the stochastic properties of a random variable as uncertain quantities and instead of predefined distribution types we use the maximum entropy distribution. We investigate two methods for the modeling of the required uncertain stochastic moments and the epistemic scatter in the stochastic assumptions is analyzed.

1 Introduction

The estimation of stochastic properties from a limited number of observations causes uncertainties in the statistical measures. Thus the determination of an exact distribution function of a random phenomena is not possible for this case. In this paper we assume the stochastic properties of a random variable as uncertain quantities caused by this so-called epistemic uncertainties. Instead of predefined distribution types we use the maximum entropy distribution [1] which enables the description of a wide range of distribution functions based on the first four stochastic moments. We investigate two methods for the modeling of these uncertain moments, first as random variables and second as fuzzy numbers, which is known as fuzzy randomness [2]. Based on both assumptions the epistemic scatter in the stochastic assumptions is represented. The main focus of this paper is to demonstrate the differences between both approaches and assess them belonging there applicability for complex problems. Based on both uncertainty models we apply standard stochastic analyses on simple examples to demonstrate their differences and limits.

2 Stochastic moments

The absolute moments of a random variable X are given as

$$\mu'_i = E[X^i] = \int_{D_x} x^i f_X(x) dx \quad i = 0, 1, \dots, m, \quad \mu'_0 = 1 \quad (1)$$

where f_X is the probability density function and D_x is the domain of the random variable X . The first absolute moment of X is equivalent to its mean value \bar{X}

$$\bar{X} = E[X] = \int_{D_x} x f_X(x) dx. \quad (2)$$

The central moments are defined as

$$\mu_i = E[(X - \bar{X})^i] = \int_{D_x} (x - \bar{X})^i f_X(x) dx, \quad i = 1, \dots, m, \quad \mu_1 = 0 \quad (3)$$

where the second central moment is the variance σ_X^2

$$\sigma_X^2 = E[(X - \bar{X})^2] = \int_{D_x} (x - \bar{X})^2 f_X(x) dx. \quad (4)$$

Standardized central moment have been introduced

$$k_i = \frac{\mu_i}{\sigma_X^i}, \quad i = 1, \dots, m, \quad k_1 = 0, \quad k_2 = 1, \quad (5)$$

where the third and fourth standardized central moments are the skewness γ_1 and the kurtosis γ_2

$$\gamma_1 = k_3 = \frac{\mu_3}{\sigma_X^3}, \quad \gamma_2 = k_4 = \frac{\mu_4}{\sigma_X^4}. \quad (6)$$

Both describe the shape of a probability density function independent of its variation and mean. For example a normal distribution has always zero skewness due to its symmetry and a kurtosis equal to three.

If we want to estimate these statistical moments from a given set of n observations we can utilize the sample mean

$$\bar{X}_n = \frac{1}{n} \sum_{i=1}^n X_i, \quad (7)$$

the sample variance S^2 and resulting standard deviation S

$$S^2 = \frac{1}{n-1} \sum_{i=1}^n (X_i - \bar{X}_n)^2, \quad S = \sqrt{S^2} \quad (8)$$

the sample skewness

$$G_1 = \frac{n}{(n-1)(n-2)} \frac{\sum_{i=1}^n (X_i - \bar{X}_n)^3}{S^3}, \quad (9)$$

and the sample kurtosis

$$\begin{aligned} G_2 &= \frac{n(n+1) \sum_{i=1}^n (X_i - \bar{X}_n)^4 - 3(n-1) \left(\sum_{i=1}^n (X_i - \bar{X}_n)^2 \right)^2}{(n-1)(n-2)(n-3)S^4} + 3 \\ &= \frac{n(n+1)}{(n-1)(n-2)(n-3)} \frac{\sum_{i=1}^n (X_i - \bar{X}_n)^4}{S^4} - \frac{9n-15}{(n-2)(n-3)}. \end{aligned} \quad (10)$$

For a finite number of observations these estimators give only approximate solutions of the moments of the exact density function. This fact is demonstrated by a simple example: based on an initial normal distribution with zero mean and unit standard deviation we compute a given number of samples by Monte Carlo Simulation and evaluate the statistical moments. This is repeated 100000 times and the variations of the approximated moments are computed. In Table 1 the results are given for several numbers of samples. The table indicates a decreasing variation of the statistical moments with increasing number of samples almost proportional to \sqrt{n} .

With this fact in mind the choice of an exact distribution type with exact variation based on a small number of observations seems to be not sufficient. This is demonstrated by evaluating for each sample set generated from the above investigated standard normal distribution the probability $P[X \geq 3]$. An assumed normal distribution based on the sample mean and sample variance is applied to evaluate the exceedance probability. The resulting variation of this probability is given additionally in Table 1 in terms of the equivalent reliability index $\beta = -\Phi^{-1}(P_F)$ where $\Phi(\cdot)$ denotes the standard normal cumulative distribution function. The results show a variation of the probability similar to the variation of the statistical moments, where again an increasing number of samples decreases this variation proportional to \sqrt{n} . This means the accuracy of the results of probabilistic analyses decreases for small sample estimates of the underlying distribution functions.

3 Bootstrap method

If we estimate a distribution function from the statistical moments of an available set of measurements this results only in approximate results as discussed in the previous section. In our study we want to estimate the approximation errors in these moments based on a single observation set. For this purpose we utilize the bootstrapping approach which was introduced by [3].

Tab. 1: Variation of statistical moments of sample sets generated from a standard normal distribution and resulting variation of a probability of exceedance assuming a normal distribution type in terms of the reliability index $\beta(P) = -\Phi^{-1}(P)$

No. samples	20		100		1000		10000	
	Mean	Stand.	Mean	Stand.	Mean	Stand.	Mean	Stand.
\bar{X}_n	-0.0007	0.2235	-0.0005	0.1003	0.0000	0.0315	0.0000	0.0101
S	0.9873	0.1610	0.9974	0.0709	0.9998	0.0223	1.0000	0.0071
G_1	-0.0004	0.5106	0.0010	0.2416	-0.0001	0.0770	0.0002	0.0248
G_2	2.7131	0.8507	2.9414	0.4672	2.9942	0.1545	2.9991	0.0488
$\beta(P[X \geq 3])$	3.1243	0.5875	3.0237	0.2391	3.0020	0.0742	3.0001	0.0235

Tab. 2: Bootstrap estimates of the variation of the statistical moments based on a single sample set

No.samples	20		100		1000		10000	
Samples	Mean	Stand.	Mean	Stand.	Mean	Stand.	Mean	Stand.
\bar{X}_n	0.1066		-0.0590		0.0460		0.0175	
S	0.8325		1.0420		0.9194		1.0004	
G_1	0.2571		0.4038		-0.0448		0.0010	
G_2	2.8897		3.0796		3.0816		3.0831	
Bootstrap	Mean	Stand.	Mean	Stand.	Mean	Stand.	Mean	Stand.
\bar{X}_n	0.1070	0.1836	-0.0599	0.1027	0.0461	0.0287	0.0175	0.0101
S	0.8020	0.1292	1.0348	0.0746	0.9189	0.0211	1.0004	0.0073
G_1	0.1954	0.4337	0.4028	0.2281	-0.045	0.0766	0.0009	0.0252
G_2	2.8798	0.8271	3.0471	0.4035	3.0754	0.1429	3.0828	0.0492

In the bootstrap method the estimated properties of an estimator are obtained by sampling from an approximate distribution which can be the empirical distribution of the observed data or a parameterized form of this distribution. In our study we use the most common approach the so-called non-parametric bootstrapping where the sampling is done directly from the empirical distribution. This method assumes independent and identically distributed observations and constructs a number of re-samples as follows: from the original set of observations X_1, X_2, \dots, X_n a bootstrap sample set $\mathbf{B}_j = B_{1,j}, B_{2,j}, \dots, B_{n_b,j}$

with n_b samples is chosen by random sampling with replacement from the observation data set. This procedure is repeated many times and the investigated statistical measure e.g. the sample mean value is calculated for each bootstrap sample set \mathbf{B}_j

$$\bar{B}_{n_b,j} = \frac{1}{n_b} \sum_{i=1}^{n_b} B_{i,j}. \quad (11)$$

Based on these results this statistical measure itself can be statistically evaluated e.g. obtaining mean value, standard deviation and histogram. For the sample mean value \bar{X}_n we obtain the bootstrap mean and variance estimates as

$$\begin{aligned} [\bar{X}_n]_{mean} &\approx \frac{1}{n_s} \sum_{j=1}^{n_s} \bar{B}_{n_b,j} \\ \sigma_{\bar{X}_n}^2 &\approx \frac{1}{n_s - 1} \sum_{j=1}^{n_s} \left(\bar{B}_{n_b,j} - \frac{1}{n_s} \sum_{j=1}^{n_s} \bar{B}_{n_b,j} \right)^2 \end{aligned} \quad (12)$$

Generally the number of samples n_b in a single bootstrap sample set is taken equal to the number of observations n and the number of bootstrap sets n_s has to be chosen very large to obtain converged results in the statistical evaluation.

Again we investigate a standardized normal random variable. A single set of observations is generated and the variation of the statistical moments is estimated by the bootstrap method. In Table 2 the results of the example are given. The table clearly indicates a very good agreement of the estimated variations and the variations given in Table 1. Thus the bootstrap method is very suitable to estimate the uncertainties in the statistical moments due to small sample observations.

4 Modeling of uncertainties in stochastic moments

In this section we discuss the topic how we can model the uncertain stochastic moments of a random variable. Two basic approaches are very common for this purpose, whereby we find only formulations for the mean value and standard deviation in literature. Higher order moments are generally not modeled as uncertain properties since a fixed distribution type is mainly assumed. One of these two approaches describes the moments itself as random variables as proposed e.g. in [4, 5] where its statistical properties can be obtained e.g. from the bootstrap results. Another approach models mean value and standard deviation as fuzzy numbers which is proposed as fuzzy randomness in [2]. We will compare both approaches at this point.

If we model the uncertain moments as random variables we have to obtain their mean values and standard deviations, which are a direct outcome of the bootstrap method, and we have to choose suitable distribution types. In the Figures 1 and 3 the bootstrap histograms of the statistical moments of 1000 samples of a normally and log-normally

distributed random variable are shown. The figures indicate that a normal distribution is a good choice for the description of the moments. Similar results have been observed for real measurements of soil properties as shown in [6]. For samples of non-normal distributions and for small numbers of samples some of the resulting bootstrap estimates show significant correlations between each other as shown in Figure 3 and [6]. If we use a random variable description these dependencies can be simply represented by correlated variables.

In the fuzzy randomness approach minimum and maximum values have to be determined for each fuzzy moment. This can be done analogous to [2] by using the 99% confidence intervals obtained from the bootstrap method. Based on these intervals for the statistical moments a probabilistic analysis is carried out whereby the minimum and maximum values of the outcome, e.g. the probability of exceedance of a threshold value, are obtained by an optimization procedure as described in [7]. If no interactions between the fuzzy numbers are considered we obtain a hyper-rectangular parameter space as shown in the scatterplot in the Figure 1 for the mean value and standard deviation of the normal distribution.

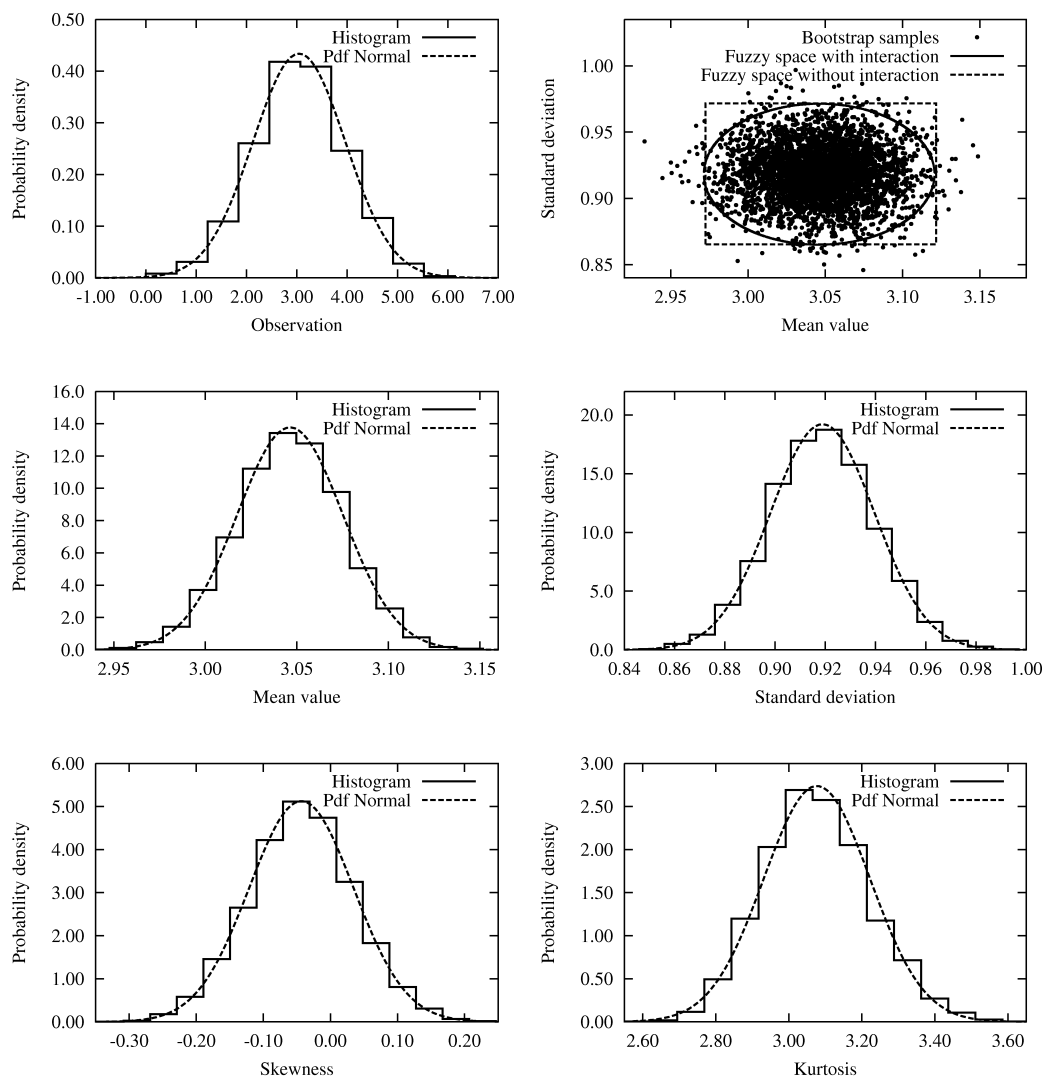


Fig. 1: 1000 observations from a normal random variable (mean value 3, standard deviation 1) with resulting bootstrap distributions of the estimated statistical moments

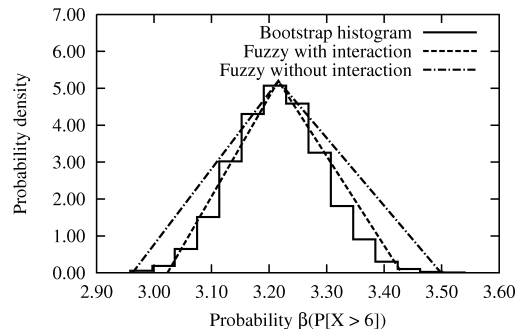


Fig. 2: Resulting bootstrap distribution of the exceedance probability $\beta(P[X \geq 6])$ of a normal distribution compared to fuzzy intervals obtained with and without interaction

Tab. 3: Computed variation of the exceedance probability $\beta(P[X \geq 6])$ from the bootstrap estimates of 1000 samples of a normal and log-normal random variable

Model	Mean value	Stand. dev.	99 % confidence interval
Samples from normal distribution			
Bootstrap samples	3.218	0.079	3.022 - 3.431
Normal pdf	3.218	0.079	3.015 - 3.421
Fuzzy analysis	3.218	-	3.023 - 3.431
Samples from log-normal distribution			
Bootstrap samples	2.423	0.061	2.274 - 2.591
Normal pdf	2.423	0.061	2.267 - 2.580
Fuzzy analysis	2.423	-	2.289 - 2.574

As discussed in [2] even for the uncorrelated case interactions have to be considered which reduces the parameter space to a hyper-ellipse. The results of such an analysis for the 1000 samples of a normal variable where the probability $P[X \geq 6]$ is investigated are given in Figure 2 and in Table 3. The results indicate a very good agreement of the confidence intervals of the probability value obtained from the bootstrap results, the fuzzy randomness analysis with interaction and the assumption of a normally distributed outcome. If the interactions are not considered we obtain a significant larger deviation of the resulting measure. Therefore these interactions have to be considered in order to obtain suitable results. For more complex cases, where the parameter space can not be approximated by such a simple geometry, the automatic determination of the parameter space surface becomes more difficult as discussed in [2]. Due to this reason and due to the coinciding results of both approaches we use the random variable description of the statistical moments. As alternative approach we use the complete bootstrap set of these moments in our analysis as discussed later in this paper.

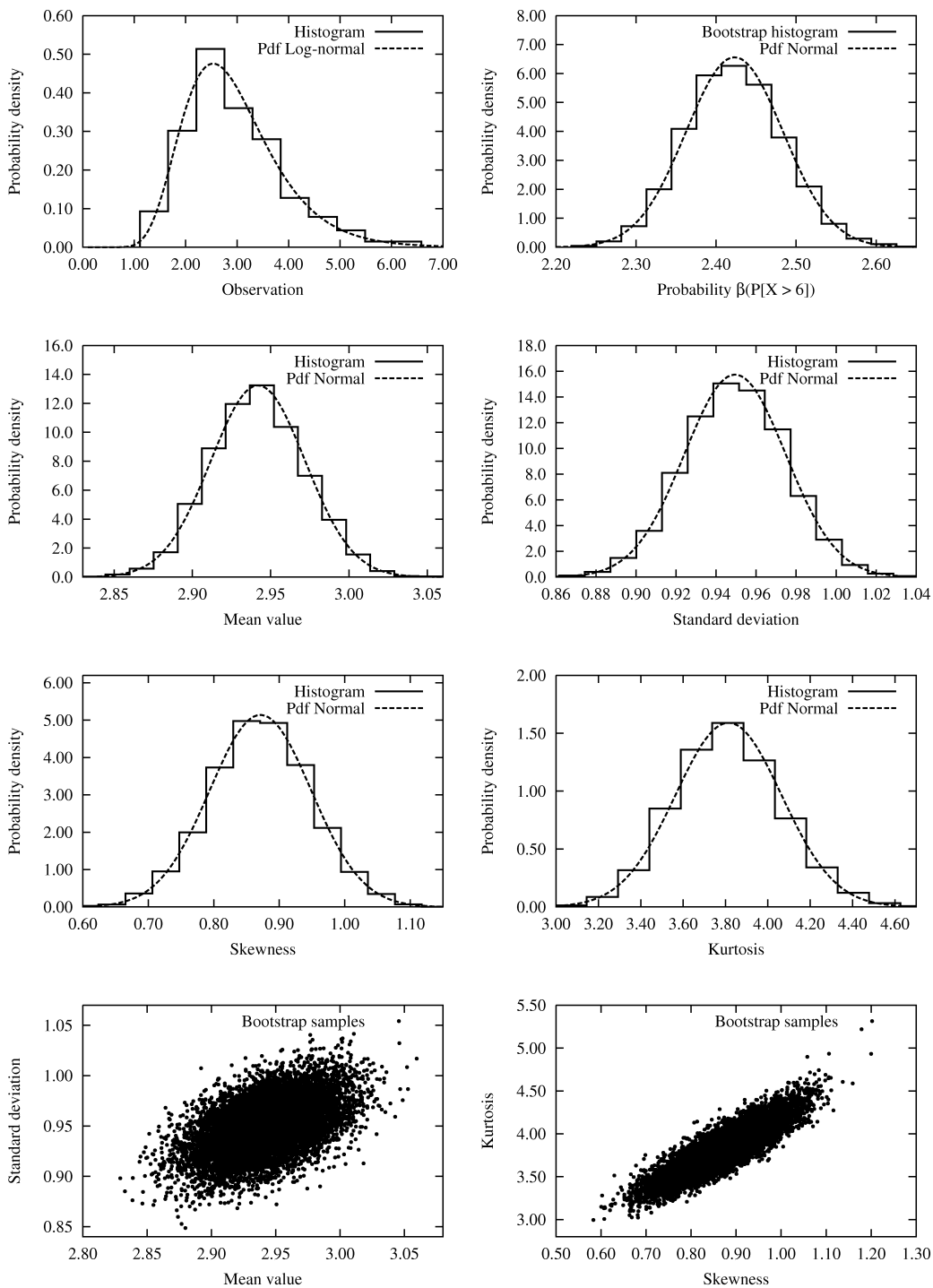


Fig. 3: 1000 observations from a log-normal random variable (mean value 3, standard deviation 1) with resulting bootstrap distributions of the estimated statistical moments and the exceedance probability $\beta(P[X \geq 6])$

5 Maximum entropy distribution

As shown in previous section not only the mean value and the standard deviation have to be modeled as uncertain values but even the distribution function itself. In order to obtain a parameter description of these distribution function higher order moments have to be considered. Thus a flexible distribution function based on these moments is presented in this section.

Based on the entropy principle proposed by [8] entropy distributions are defined to be those which maximize the information entropy measure

$$H = -\int_D f_X(x) \log(f_X(x)) dx. \quad (13)$$

Introducing $m+1$ absolute moment constraints from Eq. (1) the entropy probability density function reads

$$f_X(x) = \exp\left(\lambda_0 + \sum_{i=1}^m \lambda_i x^i\right). \quad (14)$$

In many studies e.g. in [9], [10] and [1] it was shown that the first four moments are sufficient to describe a wide range of distribution types. The formulation using absolute moments in Eq. (1) can be modified for central moments according to [9]

$$f_X(x) = \exp\left(\nu_0 + \sum_{i=1}^m \nu_i (x - \bar{X})^i\right) \quad (15)$$

where $\exp(\nu_0) = 1/c$ is a constant normalizing the area under the density function. If standardized random variables are used an efficient implementation is possible as shown in [1] and [11]. Special types of the maximum entropy distribution are the uniform distribution, the exponential distribution and the normal distribution.

Discrete samples of the above density function are generated in this study by transforming samples from a uniform distribution by the inverse of the cumulative distribution function

$$F_X(x) = \int_{-\infty}^x f_X(\tau) d\tau = \int_{-\infty}^x \frac{1}{c} \cdot \exp\left(\sum_{i=1}^m \nu_i (\tau - \bar{X})^i\right) d\tau, \quad i = 1, 2, 3, 4. \quad (16)$$

For the general case the integral in Eq. (16) can not be solved analytically. Thus we apply a numerical integration. For our purposes we want to model multivariate distribution functions which are constructed in this study by applying the Nataf model [12]. Further details about this procedure can be found in [13].

6 Reliability analysis considering uncertain stochastic parameters

In the reliability analysis the computed failure probability depends on the assumed stochastic distributions of the input variables and the limit state function of the investigated model

$$\hat{P}_F = \hat{P}_F(g(\mathbf{x}), \mathbf{p}). \quad (17)$$

In our study we assume the stochastic parameters \mathbf{p} as uncertain but the limit state function of the structural model $g(\mathbf{x})$ as deterministic. The stochastic model parameters \mathbf{p} are the distribution parameters of each single random variable X_i , in our case the stochastic moments, and the correlation coefficients ρ_{ij} between each pair of variables

$$\mathbf{p} = \begin{bmatrix} p_1, p_2, \dots, p_p \\ \bar{X}_1, \sigma_{X_1}, \gamma_{1_{X_1}}, \gamma_{2_{X_1}}, \dots, \bar{X}_i, \sigma_{X_i}, \gamma_{1_{X_i}}, \gamma_{2_{X_i}}, \dots, \rho_{12}, \dots, \rho_{ij}, \dots \end{bmatrix} \quad (18)$$

Based on the uncertainty of the stochastic parameters observed by the bootstrap method the distribution of the failure probability can be evaluated. In order to avoid a multiple reliability analysis we utilize an approximation technique proposed in [6] which allows a suitable estimation of the distribution of the reliability index $\beta = -\Phi^{-1}(P_F)$ based on a Taylor series expansion. We evaluate this series based on the mean value of the stochastic parameter vector \mathbf{p}_0 only with respect to the parameters \mathbf{p} itself and truncate after the linear term

$$\beta(\mathbf{p}) \approx \beta(\mathbf{p}_0) + (\mathbf{p} - \mathbf{p}_0)^T \nabla \beta(\mathbf{p}_0), \quad \nabla \beta(\mathbf{p}) = \frac{\partial \beta(\mathbf{p})}{\partial \mathbf{p}}. \quad (19)$$

In our study we use the First Order Reliability Method (FORM) proposed by [14] where the joint probability density function of the random variable vector \mathbf{X} is transformed to the uncorrelated standard normal space \mathbf{U}

$$\mathbf{U} = T(\mathbf{X}). \quad (20)$$

This transformation is performed here using the Nataf model [12]. The required derivatives of the reliability index with respect to the stochastic parameters can be computed without additional limit state function evaluations by the FORM sensitivity indices and a numerical derivation of the transformation from the original to the standard normal space. Further details about this are given in [6].

As an alternative approach we use Monte Carlo Simulation in this paper where we propose a novel approach to estimate the influence of the stochastic parameters on the change of the reliability index. The standard Monte Carlo estimate of the failure probability reads

$$P_F = \frac{1}{n} \sum_{i=1}^n I(g(\mathbf{x}_i)) \quad (21)$$

where the indicator function $I(g(\mathbf{x}_i))$ is one if $g(\mathbf{x}_i)$ is negative or zero and zero else. Assuming an initial set of random samples $\mathbf{x}_1, \mathbf{x}_2, \dots, \mathbf{x}_n$ from the random variable vector \mathbf{X} where the indicator function values are already known, we want to estimate the modified failure probability \tilde{P}_F of a modified set of random variables $\tilde{\mathbf{X}}$ without computing new indicator function values. This is realized analogous to the Importance Sampling concept: The initial samples \mathbf{x}_i which can be transformed to standard normal space by the transformation

$$\mathbf{u}_i = T(\mathbf{x}_i), \quad (22)$$

are transformed by the modified transformation

$$\tilde{\mathbf{U}} = \tilde{T}(\tilde{\mathbf{X}}) \quad (23)$$

to the standard normal space of the modified random vector $\tilde{\mathbf{X}}$ as follows

$$\hat{\mathbf{u}}_i = \tilde{T}(\mathbf{x}_i) = \tilde{T}(T^{-1}(\mathbf{u}_i)). \quad (24)$$

The probability density of these transformed samples which is denoted as $f_{\hat{\mathbf{u}}}$ is assumed to be the importance sampling density. The modified failure probability can then be estimated as follows

$$\tilde{P}_F \approx \frac{1}{n} \sum_{i=1}^n w(\hat{\mathbf{u}}_i) I(g(\mathbf{x}_i)), \quad w(\hat{\mathbf{u}}_i) = \frac{f_{\tilde{\mathbf{U}}}(\hat{\mathbf{u}}_i)}{f_{\hat{\mathbf{u}}}(\hat{\mathbf{u}}_i)} \quad (25)$$

where $f_{\tilde{\mathbf{U}}}$ is the probability density of the modified random set $\tilde{\mathbf{X}}$ in its standard normal space. If we assume a multi-dimensional normal probability density for $f_{\hat{\mathbf{u}}}$ we can write

$$f_{\hat{\mathbf{u}}}(\hat{\mathbf{u}}_i) = \frac{1}{(2\pi)^{k/2} \sqrt{\det \mathbf{C}_{\hat{\mathbf{u}}\hat{\mathbf{u}}}}} \exp\left[-\frac{1}{2}(\hat{\mathbf{u}}_i - \hat{\mathbf{u}})^T \mathbf{C}_{\hat{\mathbf{u}}\hat{\mathbf{u}}}^{-1} (\hat{\mathbf{u}}_i - \hat{\mathbf{u}})\right] \quad (26)$$

where k , $\mathbf{C}_{\hat{\mathbf{u}}\hat{\mathbf{u}}}$ and $\hat{\mathbf{u}}$ are the number of random variables, the covariance matrix and the mean value vector of the importance sampling density, respectively. The standard normal density $f_{\tilde{\mathbf{U}}}$ reads

$$f_{\tilde{\mathbf{U}}}(\hat{\mathbf{u}}_i) = \frac{1}{(2\pi)^{k/2}} \exp\left[-\frac{1}{2}\hat{\mathbf{u}}_i^T \hat{\mathbf{u}}_i\right]. \quad (27)$$

Since $f_{\hat{\mathbf{u}}}$ is assumed to be a multivariate normal distribution it holds

$$(\hat{\mathbf{u}}_i - \hat{\mathbf{u}})^T \mathbf{C}_{\hat{\mathbf{u}}\hat{\mathbf{u}}}^{-1} (\hat{\mathbf{u}}_i - \hat{\mathbf{u}}) = \mathbf{u}_i^T \mathbf{u}_i. \quad (28)$$

This leads to the final expression for the weights

$$w(\hat{\mathbf{u}}_i) = \sqrt{\det \mathbf{C}_{\hat{\mathbf{u}}\hat{\mathbf{u}}}} \exp \left[-\frac{1}{2} \hat{\mathbf{u}}_i^T \hat{\mathbf{u}}_i + \frac{1}{2} \mathbf{u}_i^T \mathbf{u}_i \right] \quad (29)$$

which can be directly computed from the original samples by estimating the covariance matrix $\mathbf{C}_{\hat{\mathbf{u}}\hat{\mathbf{u}}}$ from their transformations to the modified standard normal space.

7 Numerical example

In this example we compare the different approximation strategies by means of a two dimensional reliability problem. Assuming two standard normal random variables and a limit state function

$$g(x_1, x_2) = 3 - x_1 - x_2 \quad (30)$$

the theoretical reliability index for the uncorrelated case is $\beta = 3.0$. Now we generate 1000 samples of this 2D random set and perform the bootstrap method to estimate the variation in the statistical moments and of the correlation coefficient $\rho_{x_1 x_2}$. The results of this analysis are given in Table 4.

Based on this results we perform a full FORM analysis for each bootstrap sample by assuming a normal distribution for each variable. Since the limit state function is linear and the variables are normally distributed the FORM results are the exact values for the reliability index. In comparison to this results we compute the reliability indices by FORM using the Taylor series approximation presented in section 6. Additionally we use the Monte-Carlo estimates based on the proposed transformation method using 10^6 samples. Due to the normal original distribution the assumption of a normal distribution in the transformed space is valid and the estimates of the reliability index should agree very well with the exact results. Furthermore a Taylor series approximation with derivatives obtained by using this transformation method is performed. The resulting mean values, standard deviations and confidence intervals of the reliability index are given in Table 5 and the corresponding histograms in Figure 4. The results indicate an excellent agreement of the approximation methods with the exact FORM results. This is also the case if we assume a correlation between both random variables.

In the next step we assume the maximum entropy distribution function for each bootstrap sample set and compute the reliability index again by full FORM analysis and the proposed approximation techniques. Here the FORM approach gives not the exact but a good approximation of the reliability index where an increased variation of the reliability index compared to the results with normal distribution is obtained due to the represented variation in the higher moments. The results are given additionally in Table 5 and Figure 4.

We observe a deviation between the full and approximated FORM analysis whereby the distribution of the reliability index from the full FORM analysis is slightly left-skewed in opposite to the approximated almost normal distribution. Nevertheless the lower bounds of the confidence intervals, which could be a final measure for a reliability based design, coincide very well. This is similar for the results of the MCS approximations. Based on this results we can summarize that an estimation of the accuracy of the reliability index or a corresponding lower bound of the confidence interval can be very good approximated by the proposed methods.

Tab. 4: Bootstrap estimates of the statistical moments of the two random variables and its correlation from a set of 1000 samples

	Uncorrelated				Correlated			
	X_1		X_2		X_1		X_2	
	Mean	Stand.	Mean	Stand.	Mean	Stand.	Mean	Stand.
\bar{X}_n	-0.025	0.033	-0.017	0.032	0.019	0.010	0.014	0.010
S	1.041	0.024	1.014	0.022	1.017	0.007	1.002	0.007
G_1	0.008	0.094	0.008	0.074	-0.041	0.024	-0.028	0.025
G_2	3.116	0.248	2.849	0.139	3.008	0.046	2.971	0.051
		Mean	Stand.			Mean	Stand.	
$\hat{\rho}_{X_1, X_2}$		0.063	0.028			0.491	0.008	

Tab. 5: Computed variation of the reliability index from the bootstrap estimates of 1000 samples of two correlated and uncorrelated normal random variables

Model	Uncorrelated			Correlated		
	Mean	Stand.	90% conf. Int.	Mean	Stand.	90 % conf. Int.
Assuming normal distribution						
FORM full analysis	2.862	0.071	2.749 - 2.981	2.481	0.064	2.379 - 2.589
FORM linear appr.	2.861	0.070	2.747 - 2.977	2.480	0.063	2.377 - 2.585
MCS transformation	2.862	0.071	2.749 - 2.980	2.484	0.064	2.382 - 2.591
MCS linear appr.	2.861	0.070	2.747 - 2.976	2.483	0.063	2.381 - 2.589
Assuming maximum entropy distribution						
FORM full analysis	2.866	0.087	2.729 - 3.013	2.579	0.101	2.422-2.753
FORM linear appr.	2.856	0.081	2.722 - 2.987	2.567	0.095	2.407-2.720
MCS transformation	2.883	0.126	2.692 - 3.104	2.597	0.158	2.338-2.859
MCS linear appr.	2.856	0.120	2.659 - 3.054	2.581	0.155	2.311-2.821

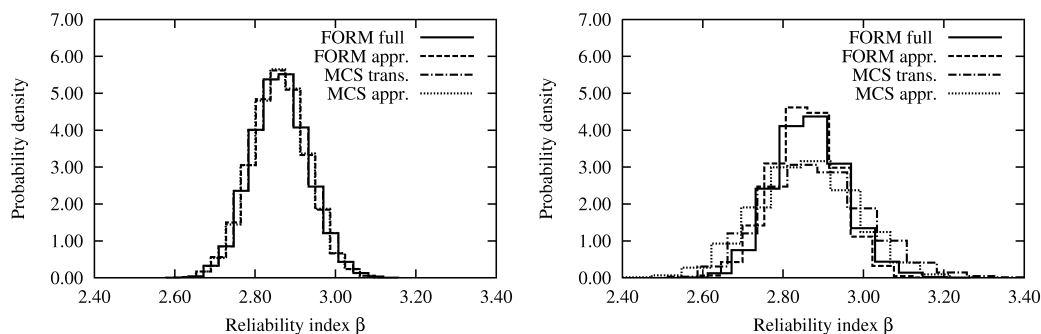


Fig. 4: Computed variation of the reliability index for the 2D example by using normal and maximum entropy distributions and the proposed approximation techniques

8 Conclusion

In this paper we investigated different approaches for the modeling of imprecise distribution functions of random variables caused by small-sample observations. We have shown that a random variable description of the uncertain statistical measures leads to similar results for a computed reliability measure as the application of fuzzy numbers whereby the required representation of interactions between these measures can be modeled more easily with random variables. As flexible model for the distribution function itself we utilized the maximum entropy distribution formulation whereby an extension for multi-variate distribution was proposed based on the Nataf model. With this formulation we can describe the imprecise distribution function very efficiently with the first four in this case also imprecise stochastic moments. Finally we proposed very efficient and sufficiently accurate approximation techniques to estimate the scatter of the reliability index with the same number of limit state function calls as a single reliability analysis.

9 Acknowledgement

This research has been supported by the German Research Council (DFG) through Research Training Group 1462, which gratefully acknowledged by the author

References

- [1] M. Rockinger and E. Jondeau. Entropy densities with an application to autoregressive conditional skewness and kurtosis. *Journal of Econometrics*, 106:119-142, 2002
- [2] B. Möller and M. Beer. *Fuzzy Randomness - Uncertainty in Civil Engineering and Computational Mechanics*. Springer, New York, 2004
- [3] B. Efron. Bootstrap methods: another look at the Jackknife. *The Annals of Statistics*, 7(1):1-26, 1979

- [4] O. Ditlevsen and H. Madsen. *Structural reliability methods*. Wiley, Chichester, New York, 1996
- [5] A. Der Kiureghian. Analysis of structural reliability under parameter uncertainties. *Probabilistic Engineering Mechanics*, 23:351-358, 2008
- [6] T. Most and T. Knabe. Reliability analysis of the bearing failure problem considering uncertain stochastic parameters. *Computers and Geotechnics*, accepted, 2009
- [7] B. Möller, W. Graf, and M. Beer. Fuzzy structural analysis using α -level optimization. *Computational Mechanics*, 26:547-565, 2000.
- [8] C.E. Shannon. The mathematical theory of communication. *Bell Systems Technical Journal*, 27:379-423, 1948
- [9] P.C. Basu and A.B. Templeman. An efficient algorithm to generate maximum entropy distributions. *International Journal for Numerical Methods in Engineering*, 20:1039-1055, 1984.
- [10] A. Zellner and R.A. Highfield. Calculation of maximum entropy distributions and approximation of marginal posterior distributions. *Journal of Econometrics*, 37:195-209, 1988.
- [11] N. van Erp and P. van Gelder. Introducing entropy distributions. In C.-A. Graubner et al., editors, *Proc. 6th Inter. Probabilistic Workshop, November 26-27, 2008, Darmstadt, Germany*
- [12] A. Nataf. Détermination des distributions de probabilités dont les marges sont données. *Comptes Rendus de l'Académie des Sciences*, 225:42-43, 1962.
- [13] T. Most. Estimating uncertainties from inaccurate measurement data using maximum entropy distributions. In K. Gürlebeck and C. Könke, editors, *Proc. 18th Int. Conf. Applications of Computer Science and Mathematics in Architecture and Civil Engineering (IKM), Weimar, Germany, July 7-9, 2009*. Bauhaus-Universität Weimar,
- [14] A.M. Hasofer and N.C. Lind. An exact and invariant first-order reliability format. *Journal of the Engineering Mechanics Division, ASCE*, 100(6):111-121, 1974.

Probabilistic sensitivity of limit states of structures. The Monte Carlo simulation

M. Skowronek

Gdansk University of Technology, Department of Structural Mechanics and Bridge Structures, Gdansk

Abstract: The main issue of the paper is the probabilistic sensitivity of the limit states of structures with respect to selected design variables. Attempt to the problem is done by the dedicated Monte Carlo simulation procedure. Basic design variables are random variables of given probability distributions, presented in the form of random numbers. Featuring is the performance of a single simulation step (realization) of the procedure. The structure is subjected to one-parameter increment of the dominant basic variable (basic variables), finally achieving the structural limit state. The value of the limit multiplier of dominant variable(s) is the output of a single simulation step. The outcome of a problem is a set of multipliers. Statistical analysis leads to the histogram of relative frequencies - the estimate of the probability density function of the limit state. Having the dominant variable(s) assumed the numerical image is presented of the probabilistic sensitivity of the structural limit state. Reliability or the probability of failure are to be estimated, as statistical parameters of the histogram. Numerical examples of engineering structures illustrate the method introduced in the paper, conclusions are formulated eventually.

1 Introduction

Design sensitivity analysis takes into account variations of the design parameters and develops appropriate procedures for calculating a change of structural behaviour that depends implicitly on the design variables (HAUG ET AL, [6]). The theory of structural sensitivity in deterministic description has become an advanced branch of the present-day mechanics (KLEIBER ET AL [10]).

The advent of random philosophy of physical phenomena and eminent progress in applications of probability theory made it possible to make the process of implementing a probabilistic point of view in technical sciences. As far as civil engineering is concerned, a

large group of problems is analysed assuming their random nature. Not only research activity is subject to that tendency, but also building codes of practice are formed in a semi-probabilistic manner. The term sensitivity may therefore be given different meaning than in the deterministic approach, illustrated by a highly state-of-the-art technology.

The term stochastic sensitivity covers the usage of random functions to represent input data and responses of structural systems. Discretized structural models are usually applied to solve the engineering problems, therefore random variables are used instead. Uncertainty analysis can be performed on different levels. The so-called 2nd level probabilistic method means that stress is put only on the first and the second statistical moments of random parameters. In this case perturbation method may be implemented (KLEIBER AND HIEN, [7], [11], GHOSH ET AL. ([5]), In a more advanced, 3rd level, probability density functions are examined of the variables under consideration. Numerical methods are bound to be the most effective for this class of problems. The Monte Carlo simulation method is widely used to estimate numerically probability distributions of random responses.

Reliability sensitivity estimation is developed in a number of papers (MELCHERS AND AHAMED [14], AU [1], RAHMAN AND WEI, [15]). In this approach it is examined how the set of design parameters affects the failure probability, critical loads or critical displacements (IKEDA ET AL, [8]). Local probabilistic sensitivity measures for comparing FORM and Monte Carlo calculations are presented by COOKE AND VAN NOORTWIJK, [4].

The concepts of robust design and reliability-based design were introduced in connection with the optimization and sensitivity analysis of structures (LAGAROS ET AL, [12], BJERAGER AND KRENK, [2]). The joint solution, reliability-based robust design, deals with the random constraints incorporated into the robust design methodology. Another branch to be implemented random methods is material sensitivity. Stochastic sensitivity analysis of random material was presented by KAMINSKI [9]. Time domain stochastic sensitivity, both in Gaussian and non-Gaussian description was presented by BONFRATELLO ET AL. [3].

The paper considers a typical design problem in the probabilistic description, where the structural failure is a very rare event. In the paper an imaginary probabilistic experiment is presented. The basic assumption of this experiment is that the chosen design variable can exceed its design value and the action of this design variable leads the structure to reach its limit state. Making use of this assumption a new notion of the probabilistic sensitivity of the limit state of the structure is proposed with respect to the chosen design variable. The definition and the measure of this probabilistic sensitivity for a simple structural system is presented in an analytical form.

For more complicated engineering structures it is necessary to use the special Monte Carlo Simulation procedure. The attempts to solve the structural reliability sensitivity problems by Monte Carlo simulation method were already made, e.g. LU ET AL [13] used the line sampling technique. In this approach the computational means are transported into the definition to become not only a numerical tool but also part of the methodology. The problem of the probabilistic sensitivity is formulated using the dedicated MCS procedure. Thus it can be regarded as the problem of computational science (THAGARD, [16]).

2 Limit states of engineering structures

Limit state analysis is a branch of mechanics to be performed with a couple of initial assumptions, concerning the failure modes involved. As far as framed structures are concerned, making up the zero-length plastic hinges in critical cross-sections is a widely recognized model of failure, where bending is the dominant action. However, it may be simply generalized, to a limit combination of cross-sectional forces, in planar or three-dimensional problems. Standards often make use of semi-empirical simplified limit state formulae including components of the cross-sectional forces vector. To make an engineer's simplification, the formulae used in codes are often linearised. Serviceability limit states make up another group to be considered. Definition of structural limit state may be otherwise: brittle crack in one or a group of cross-sections, loss of global or local stability, etc.

The general formulation of the limit state problem of a structure does not allow us to provide general analytical solutions. It is required to specify the problem and the relevant failure mode(s). The problem of limit states of structures may be described by a general stochastic operator L to provide a relation between structural input \mathbf{p} and output \mathbf{u} , as follows

$$L_{\omega}(\omega)[\mathbf{u}(s, \omega)] = \mathbf{p}(s, \omega) \quad (1)$$

with ω elementary event
 s position variable

where s is a one-dimensional coordinate on the element axis, ω is an elementary event. Discretization of the problem turns the random vector functions \mathbf{p} and \mathbf{u} into random vectors defined in discretization points. Such a problem cannot be solved analytically, thus the effort has to be concentrated on the development of numerical procedures.

The Monte Carlo simulation algorithm to assess the structural sensitivity of a limit state is based on the designer's decision to choose the dominant input variable or a group of variables. They can be action parameters – loads, temperature increment, restraint forced deflections, or the resistance parameters – dimensions of members or material characteristics, like yield stress of steel or compressive strength of concrete.

Simulation algorithm to assess the structural sensitivity of a structure, with respect to chosen dominant variable(s), consists of several steps. First of all, random structural and action parameters are generated due to the assumed probability distributions, thus every basic variable is represented by a set of random numbers. The general idea lies in the operations of a single simulation step, as follows:

- generation of a structure subjected to external actions – sampling a set of basic variables (loads, dimensions, material properties, imperfections),
- the choice of dominant variable (action or resistance parameter), this variable is subjected to a uni-parametrical deterministic increment, leaving the other sampled

variables constant, until the limit state of a structure is reached, due to the assumed failure mode,

- the dominant variable limit multiplier is the outcome of a single simulation step.

The result of the whole simulation process is the set of limit multipliers. The normalized histogram of relative frequencies is the numerical estimate of the probability distribution of the limit state of the structure with respect to dominant variable(s). Estimators of the distribution parameters can be obtained by statistical analysis: mean, variance, higher order moments and the parameters of engineering importance: reliability or the probability of failure.

3 Numerical examples

3.1 Portal frame under the load combination, ultimate limit state

Let us consider a simple bar structure, a portal frame, made of welded steel I-bars, regarded as a planar system, being subjected to a combination of loads, as shown in Fig. 1. The geometrical imperfection, horizontal displacement v is taken into account.

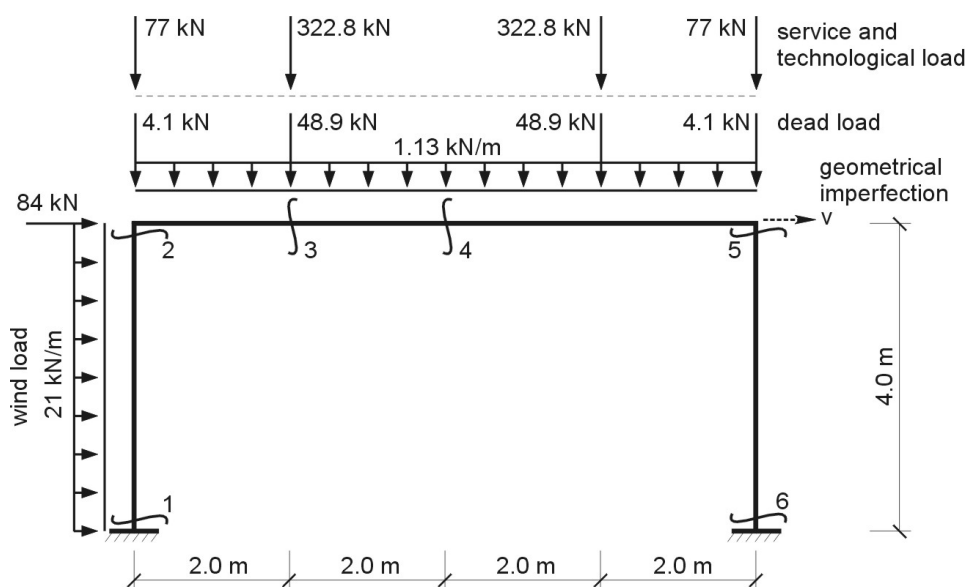


Fig. 1: Model of the structure, deterministic values of the dead load and the mean values of the randomly variable load

The problem is to examine the sensitivity of the structural limit state with respect to selected design variables. Thus, attention is focused on computing the probability distribution of the limit state of the structure in some variants, while different variables are said to be dominant. In the MCS steps use is made of the second – order structural analysis.

The design variables mentioned below are assumed to be deterministic:

- the modulus of elasticity of steel St3S: $\bar{E} = 205 \text{ GPa}$
- the geometrical characteristics of the cross-sections, in particular, total area, web area, moment of inertia and section module of the following structural elements: columns: $A_c = 193 \text{ cm}^2$, $A_{c_w} = 55.5 \text{ cm}^2$, $I_c = 120288 \text{ cm}^4$, $W_c = 4147.9 \text{ cm}^3$ and beam: $A_b = 205 \text{ cm}^2$, $A_{b_w} = 57.5 \text{ cm}^2$, $I_b = 137927 \text{ cm}^4$, $W_b = 4597.6 \text{ cm}^3$
- a set of dead loads, in particular, point forces and uniformly distributed load, shown in Fig. 1

Below are mentioned the design variables which are assumed to be random. Their random variation is depicted in a numerical form and sets of random numbers are generated prior to the following probability distributions:

- service load: Gaussian distribution, within the range $(0.8; 1.2)$, with respect to the mean values given in Fig. 1, parameters of the distribution are: $\mu = 1.0$ $\sigma = 0.0667$,
- wind load (time-invariant problem): Gumbel distribution: $u = 0.2$, $\alpha = 8.0$ for the wind velocity (X), transformed to wind pressure (Y) by the formula $Y = X^2$, bounded by the range $(0.0; 1.3)$, with respect to the mean value given in Fig. 1,
- geometrical imperfection: uniformly distributed in the range of $(0.6, 1.0)$, with respect to the mean value $v_0 = 0.0171 \text{ m}$
- yield stress of steel St3S - uniformly distributed in the range of $(0.9, 1.1)$, with respect to the mean value $\sigma_0 = 235 \text{ MPa}$

Six critical cross-sections are distinguished in the structure. In the incremental procedure, performed in a single simulation step, the dominant variable increases, while the rest of the variables remain constant. Whilst performing this increment, a limit state of a series of critical cross-sections is reached. For all critical cross-sections the linearized limit state formula is applied

$$\frac{N_i(\omega)}{N_{Ri}(\omega)} + \frac{M_i(\omega)}{M_{Ri}(\omega)} + 0.45 \frac{T_i(\omega)}{T_{Ri}(\omega)} = 1, \quad i \in \{1, 2, 3, 4, 5, 6\} \quad (2)$$

where $N_i(\omega)$, $T_i(\omega)$, $M_i(\omega)$ - random axial force, shear force and bending moment, respectively, in critical cross-sections,
 $N_{Ri}(\omega)$, $T_{Ri}(\omega)$, $M_{Ri}(\omega)$ - random load-carrying capacities of critical cross-sections.

A simulation procedure is performed, with reference to the general algorithm presented in section 2. The operations of the single simulation step are listed below:

- the values of the design variables are generated, namely, material and geometrical properties, a set of loadings and the geometrical imperfection – specific structure is formed under a given loading,

- the chosen (dominant) design variable is subjected to one-parametrical increment while the values of other design variables are being fixed. The operation goes on until the limit state is reached, in the course of this procedure the dominant variable multiplier is recorded

Three variants of the problem are performed, the dominant variables are: service load, wind load and yield stress of steel, respectively. The results depict sensitivity of the structural limit state with respect to the dominant variable. Assuming action parameters (loads) as dominant variables, failure probability is estimated form the formula: $p_f = P(\lambda_s < 1.0)$, while the resistance parameter (yield stress of steel) gives another formula: $p_f = P(\lambda_r > 1.0)$. The results – limit state histograms in the three variants of calculations, are shown in Figs. 2 – 4, their statistical parameters are presented in Table 1.

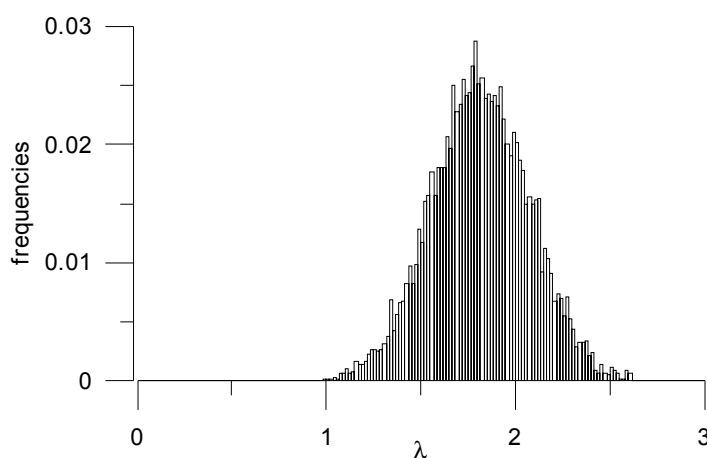


Fig. 2: Histogram – the probability distribution of the limit state, with respect to service loads

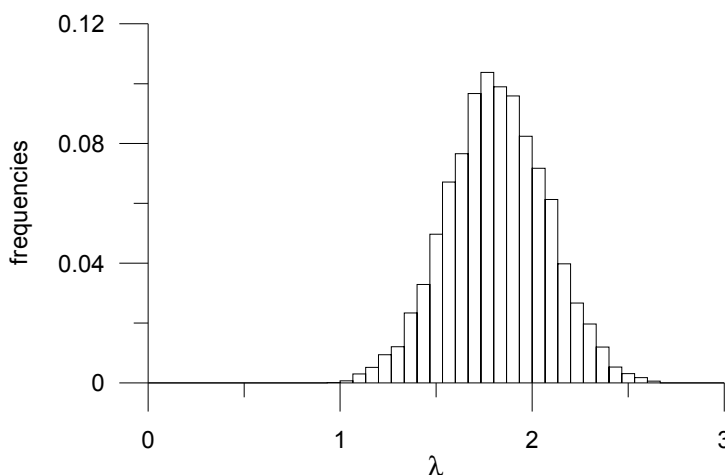


Fig. 3: Histogram of the probability distribution of the limit state involving the wind load

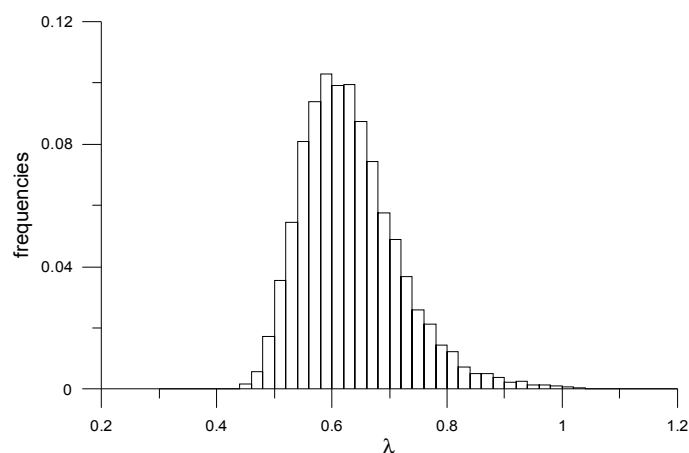


Fig. 4. Histogram – the probability distribution of the limit state with respect to the yield stress of steel

Tab. 1: Comparison of the three variants of calculations

Variant of calculations	a)	b)	c)
Dominant variable	service load	wind load	yield stress
Mean value	1.8187	1.8053	0.5625
Standard deviation	0.2603	0.2470	0.00853
Minimum value λ_{min}	0.9902	0.9921	0.3827
Maximum value λ_{max}	2.7515	2.6127	1.0080
Probability of failure	10^{-4}	10^{-4}	10^{-4}

The histograms in figs 2 – 4 and the Table 1. gives some statistical information about the structural response. The mean live load multiplier to make the structure reach its limit state is 1.82, whereas in the case of wind load the mean multiplier is 1.80. The maximum multiplier in the whole population is greater in the live load case, the general conclusion may be that in the cases mentioned the structure is more sensitive to wind load, but it is only a slight difference in numerical results. It is worthy of noting that the action parameter (load) as dominant variables gives “critical” multipliers greater than unity, whereas the resistance parameter as dominant variable results in the “failed” multipliers less than one.

3.2 Monumental structure – basilica, serviceability limit state

The numerical example concerns the probabilistic serviceability limit state analysis of the monumental structure of the Licheń Basilica. The Basilica was consecrated in the year 2004. Major load-carrying tower part (Fig. 5) consists of the foundation ring, four-column structure supporting the main ring, the two-storey colonnade and the dome. The lower storey of the colonnade consists of two concentric 16-column rings while in the upper storey there are two concentric 16-column rings (Fig. 6). Space frame model of the colonnade is

provided (Fig. 7), consisting of 256 elements. Upper deck deflection of the colonnade is examined.

Main loads acting on the model are: dead load, wind acting on the colonnade walls and the forces on the upper deck of the colonnade, which come from the dome's weight and the wind acting on the dome. The wind direction is shown in Fig. 8. The wind load is assumed as the uniformly distributed load acting on the columns of lower storey middle ring and on the columns of the upper storey outer ring (rigid plates are provided between the columns). Wind load intensity, as the function of the horizontal angle is shown graphically in Fig. 8.

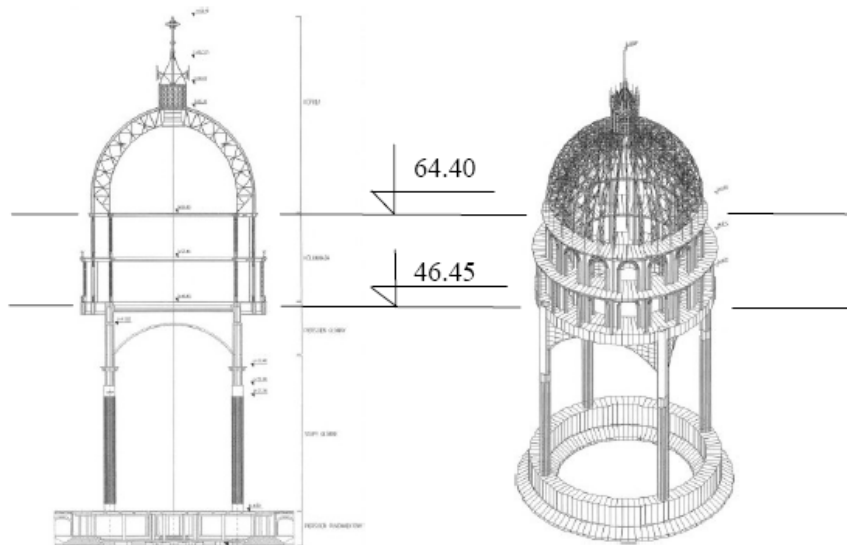


Fig. 5: General view of the tower part of the Basilica, featuring the colonnade

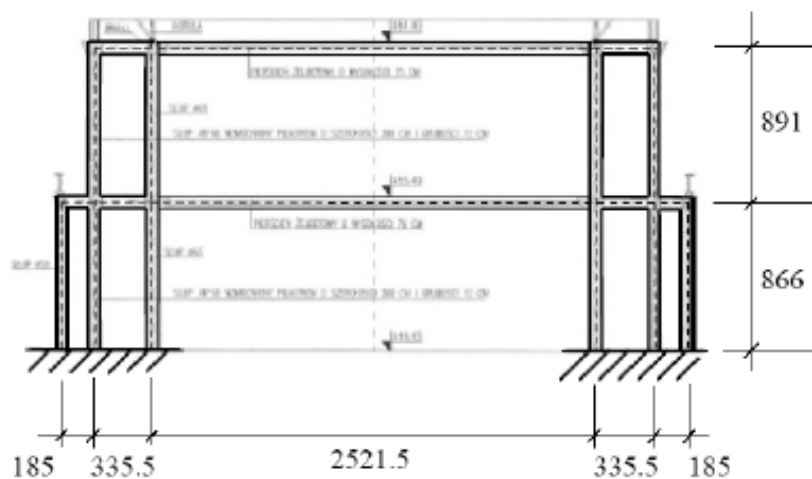


Fig. 6: Cross-section of the colonnade (dimensions in cm)

Basic random variables of the problem were assumed of the following probability distributions (in the form of bounded histograms):

- dead load of colonnade and dome: Gaussian, $N(1.0; 0.0333)$, the range $(0.9, 1.1)$ – variable $D(\omega)$,

- Young's modulus of concrete: uniform, the range (0.8; 1.0) – variable $E(\omega)$
- wind load – the variables: $W_1(\omega)$ referring to the lower storey of the colonnade and $W_2(\omega)$ to the colonnade's upper storey and the dome. Both variables are quadratic transforms of the variables V_1 and V_2 , which depict wind velocities in appropriate intervals. Assumption is made that the two variables V_1 and V_2 are correlated, Gumbel distributed (extreme value, type I).

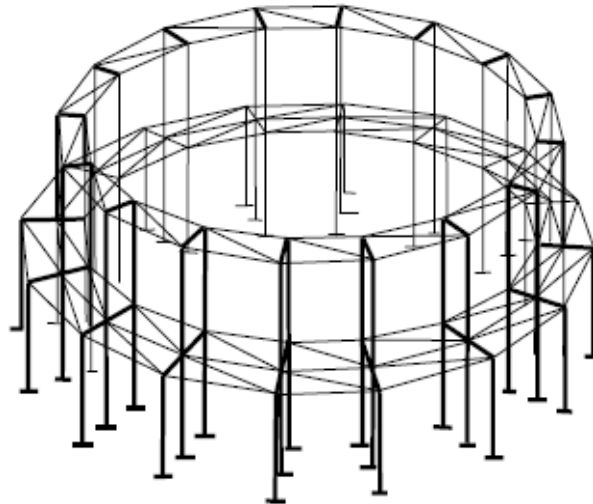


Fig. 7: Space frame model of the Basilica colonnade

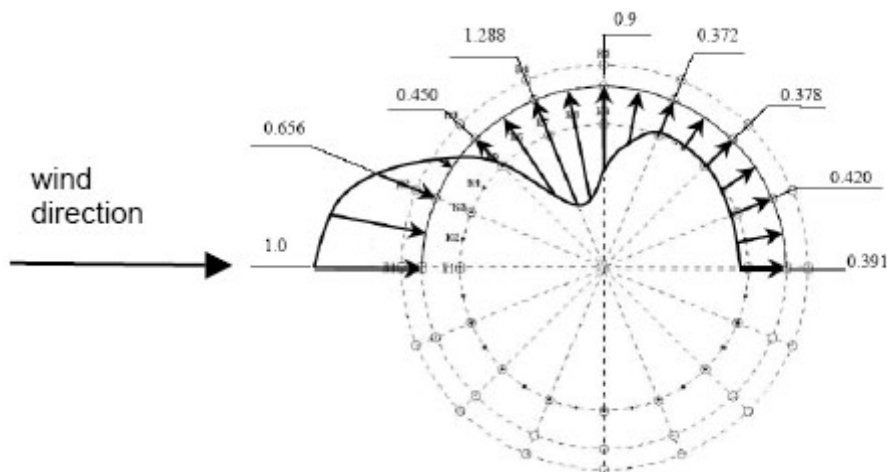


Fig. 8: Situation of the columns of the colonnade on the altitude 46.45 m (three – ring lower colonnade), relative wind load intensities, referring to the maximum value

Assumption is made that the dominant variables are both the wind actions W_1 and W_2 , thus structural sensitivity to wind actions is examined throughout the example.

The following operations make up the single simulation step:

- Analysis of the space framed structure, calculating the initial value of the horizontal upper deck deflection $u(\omega)$ in the wind direction,
- Uni-parametrical load increment, while the structural characteristics are fixed, until the allowable upper deck deflection u_0 is reached. In numerical calculations it was assumed $u_0 = H/400$, where $H = 17.95$ m is the colonnade height.
- The single simulation step produces the limit load multiplier λ_i of this realization – a single value of the variable $A(\omega)$.

Three variants of calculations were provided, with respect to the correlation coefficient ρ of the wind load variables. The following cases were considered:

- variables W_1 and W_2 uncorrelated – the coefficient $\rho = 0$
- variables W_1 and W_2 correlated – the coefficient $\rho = 0.62$
- variables W_1 and W_2 fully correlated – the coefficient $\rho = 1$

The histograms of the serviceability limit state of the structure are presented in Fig. 9 and compared in Table 2.

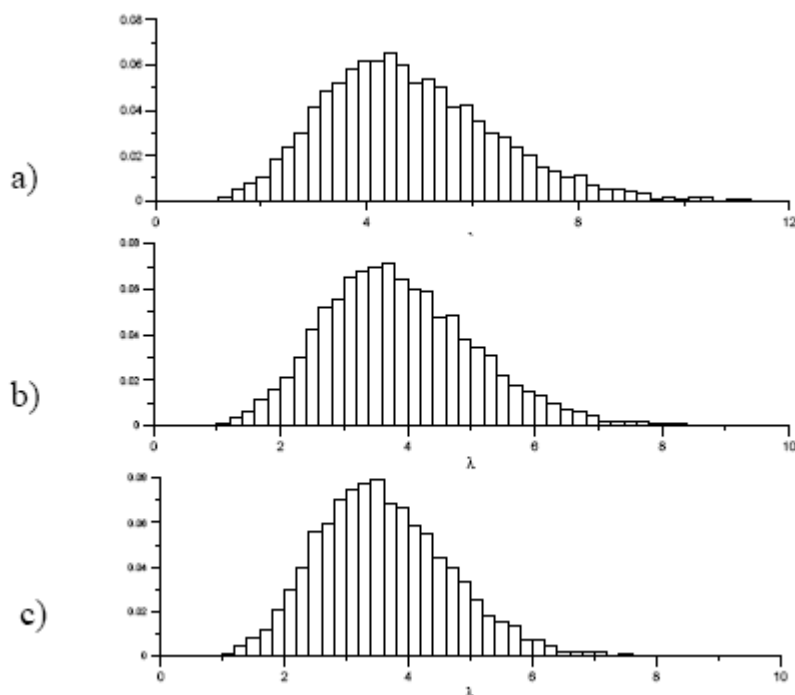


Fig. 9: Relative histograms of the serviceability limit state of the colonnade of the Lichen Basilica, three variants of calculations, with respect to the correlation of the wind load

It is worth pointing out that in the assumed structural and stochastic model each variant of calculation results in the probability of exceeding the allowable deflection lower than the

accuracy of the method (the reciprocal of the number of realizations). On the basis of probabilistic limit state analysis it can be stated that the examined part of the structure is stiff enough to assure the proper structural service.

Tab. 2: Comparison of the three variants of calculations

Variant of calculations	a)	b)	c)
Correlation coefficient of the wind load variables W_1 and W_2 : $r = \rho_{W_1W_2}$	0	0.62	1
Mean value	4.8133	3.8755	3.6128
Standard deviation	1.6106	1.1748	1.0540
Minimum value λ_{min}	1.1804	1.0427	1.0135
Maximum value λ_{max}	11.2338	8.3317	7.5443
Probability of failure	$<10^{-4}$	$<10^{-4}$	$<10^{-4}$

4 Conclusions

Sensitivity analysis of limit states of structures is proposed in the paper, by means of the specific Monte Carlo algorithm. It leads to the third level probabilistic information about the structure, i.e. the limit state histogram. The procedure also enables us to solve the problem limited to the reliability, or the probability of failure estimation.

The technique presented in the paper is alternative to the common variance reduction computational tools. The author does not refer to the abovementioned, making it possible to provide a further development of the methodology.

Simulation-based limit state analysis usually means creating a population of structural states and choosing the failed cases, which determine the failure probability. The procedure proposed is modified and therefore developed. A group of dominant basic variables is chosen, in every simulation step. These variables increase uni-parametrically, to reach finally the structural limit state. Thus every simulated case is led to the limit state. The set of non-dimensional multipliers of dominant variables is the result of simulation. Its histogram serves as the estimator of the PDF of the structural limit state.

5 Literature

[1] Au, S.K.: Reliability-based design sensitivity by efficient simulation. *Computers and Structures* 83 (2005), S. 1048–61.

- [2] Bjerager, P.; Krenk, S.: Parametric sensitivity in first order reliability theory. *Journal of Engineering Mechanics*, 115 (1989), S. 1577-1582
- [3] Bonfratello, S.; Caddemi, S.; Muscolino, G.: Gaussian and non-Gaussian stochastic sensitivity analysis of discrete structural system. *Computers and Structures* 78 (2000), S. 425-434
- [4] Cooke, R.M., van Noortwijk, J.M.: Local probabilistic sensitivity measures for comparing FORM and Monte Carlo calculations illustrated with dike ring reliability calculations. *Computer Physics Communications* 117 (1999), S. 86-98
- [5] Ghosh, R.; Chakraborty, S.; Bhattacharyya, B. (2001) Stochastic sensitivity analysis of structures using first-order perturbation. *Meccanica* 36 (2001), S. 291-296
- [6] Haug, E.J.; Choi K.K.; Komkov V.: *Design sensitivity analysis of structural systems*. Academic Press, Orlando, 1986
- [7] Hien, T.D.; Kleiber, M.: Stochastic structural design sensitivity of static response *Computers and Structures* 38 (1991), S. 659-667
- [8] Ikeda, K.; Oide, K.; Terada, K.: Imperfection sensitive variation of critical loads at hilltop bifurcation point. *International Journal of Engineering Science* 40 (2002), S. 743-772
- [9] Kaminski, M.: Material sensitivity analysis in homogenization of linear elastic composites. *Archive of Applied Mechanics* 71 (2001), S. 679-694
- [10] Kleiber, M.; Antunes, H.; Hien, T.D., Kowalczyk, P.: *Parameter sensitivity in nonlinear mechanics*. John Wiley & Sons, Chichester, 1997
- [11] Kleiber, M.; Hien, T.D.: *The Stochastic Finite Element Method*. Wiley, Chichester, 1992
- [12] Lagaros, N.D.; Plevris, V.; Papadrakakis, M.: Reliability based robust design optimization of steel structures. *International Journal for Simulation and Multidisciplinary Design Optimization* 1 (2007), S. 19-30
- [13] Lu, Z.; Song, S.; Yue, Z.; Wang, J.: Reliability sensitivity method by line sampling. *Structural Safety*, 30 (2008), S. 517-532
- [14] Melchers, R.E.; Ahammed, M.: A fast approximate method for parameter sensitivity estimation in Monte Carlo structural reliability. *Computers and Structures* 82 (2004), S. 55-61.
- [15] Rahman, S.; Wei, D.: Design sensitivity and reliability-based design optimization by univariate decomposition. *Structural and Multidisciplinary Optimization* 35 (2008), S. 245-261
- [16] Thagard, P.: *Computational philosophy of science*. MIT Press, Cambridge, 1993

Part IV

Probabilistic Modelling for Flood Risks

Non-parametric continuous Bayesian belief networks for Earth Dam Safety

Oswaldo Morales-Nápoles¹ and David Joaquín Delgado-Hernández²

¹Netherlands Organization for Applied Scientific Research, Van Mourik Broekmanweg 6,
2628 XE Delft, The Netherlands, Tel:+31 88 8662783,
e-mail: oswaldo.moralesnapoles@tno.nl

²Engineering School, Autonomous University of the State of Mexico, Cerro de Coatepec,
Ciudad Universitaria, Toluca, México, C.P. 50130, Tel: +52-01-722-214-0534 Ext. 1097,
Fax: +52-01-722-214-0534 Ext. 1014 e-mail: david.delgado@fi.uaemex.mx

Abstract: Dams safety is of great importance for authorities around the world. The impacts of a dam failure can be enormous. Models for investigating dam safety are required to help decision makers mitigate the possible adverse consequences of flooding. A model for earth dam safety must specify clearly possible contributing factors, failure modes and possible consequences of dam failure. Probabilistic relations between variables should also be specified. Bayesian belief networks (BBNs) have been identified as tools that would assist dam engineers on assessing risks. BBNs are graphical models that facilitate the construction of a joint probability distribution. Most of the times, the variables included in a model for earth dam risk assessment involve continuous quantities. The presence of continuous random variables makes difficult the implementation of discrete BBNs. An alternative to discrete BBNs is the use of non-parametric continuous BBNs. In this paper non-parametric continuous BBNs will be briefly described. As an example, a model for earth dams safety in the State of Mexico will be discussed. Results regarding the quantification of the model have not been presented before and are introduced here. Because the use of the model has been presented elsewhere, here some results will be shown for demonstration purposes. The methods presented in this paper should be applicable for investigating risks of failure of civil infrastructures other than earth dams. **Keywords:** Bayesian Belief Nets, Dam Safety, Mexico.

1 Introduction

Embankment or earth dams are among the most abundant structures for retaining water. In fact, Donnelly [6] states that embankment dams are the most common type of water retaining structures. It is no surprise that these type of dams fail more frequently than others. Figure 1 shows the number of dams failures per 10 years period from 1891-1990 and the proportion of total number of failures corresponding to embankment dams. Figure 1 was built with data from ICOLD [11, pp.38-45]. It may be seen that for every ten year period, between 50% (1891-1990) and 91.67% (1971-1980) of the failures correspond to embankment dams.

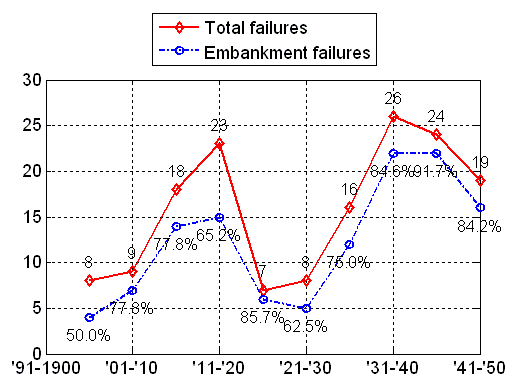


Fig. 1: Number of dams failures per 10 years period from 1891-1990. With data from ICOLD [11, pp.38-45]

The impacts of a dam collapse can be enormous, encompassing the destruction of private housing, transport and public infrastructure, industrial facilities and agricultural land. The losses may also include human harm and serious disruptions in infrastructure operation, leading to significant total economic damages.

A model for earth dam safety must specify clearly possible contributing factors, failure modes and possible consequences of dam failure. Probabilistic relations between variables should also be specified. Literature reports studies within the dam industry. Most are centered on the analysis of specific failure modes, and only few on mathematical models for dam risk assessment (see for example FEMA [7] and FEMA [8]). Bayesian belief networks (BBNs) are graphical models that represent a multivariate distribution.

Through the use of BBNs contributing factors, failure modes and possible consequences of dam failure may be specified in an intuitive and meaningful way. In this paper, we present general concepts regarding BBNs. Special attention is placed in the methodology for model quantification. The use of BBNs for earth dams safety is exemplified using a demonstration model developed for the State of Mexico in central Mexico. The methods described in this paper may be also used for risk assessment of similar civil infrastructure around the globe.

2 Concepts & Definitions

Representing multivariate probability distributions for certain phenomena can be a challenging task. Perhaps the multivariate model which is most widely used is the joint normal distribution. However, many phenomena behave far from normal. This is one of the reasons for researchers to have recourse to alternative models such as copulae.

Copulae are part of the building blocks of the graphical models to be used in this paper and for that reason basic concepts and definitions regarding them are introduced. The book by Nelsen [14] presents an introduction to the subject. Bivariate copulae will be of special interest for us. In this paper by copula (or copulae) we mean a bivariate copula (or bivariate copulae) unless otherwise specified. The *bivariate copula* or simply the *copula* of two random variables X and Y is the function C such that their joint distribution can be written as:

$$F_{X,Y}(x, y) = C(F_X(x), F_Y(y)).$$

Copulae are functions that allow naturally the investigation of association between random variables. Measures of association such as the rank correlation or Kendall's tau may be expressed in terms of copulae [14]. The measures of association to be used in this paper are described next.

2.1 Dependence & Dependence measures.

The product moment correlation of random variables X and Y with finite expectations $E(X)$, $E(Y)$ and finite variances $\text{var}(X)$, $\text{var}(Y)$ is:

$$\rho_{X,Y} = \frac{E(XY) - E(X)E(Y)}{\sqrt{\text{var}(X)\text{var}(Y)}}$$

The rank correlation of random variables X , Y with cumulative distribution functions F_X and F_Y is:

$$r_{X,Y} = \rho_{F_X(x), F_Y(y)} = \frac{E(F_X(x)F_Y(y)) - E(F_X(x))E(F_Y(y))}{\sqrt{\text{var}(F_X(x))\text{var}(F_Y(y))}}$$

The rank correlation is the product moment correlation of the ranks of variables X and Y , and measures the strength of monotonic relationship between variables. The conditional rank correlation of X and Y given Z is:

$$r_{X,Y|Z} = r_{\bar{X},\bar{Y}}$$

where $(\tilde{X}; \tilde{Y})$ has the distribution of $(X; Y)$ given $Z = z$.

The (conditional) rank correlation is the dependence measure of interest because of its close relationship with conditional copulae used in non-parametric continuous BBNs (see section 2.3). One disadvantage of this measure however is that it fails to capture non-monotonic dependencies.

Rank correlations may be realized by copulae, hence the importance of these functions in dependence modeling. Partial correlations are also of interest in this paper. These can be defined in terms of partial regression coefficients. Consider variables X_i with mean zero and standard deviation σ_i for $i = 1, \dots, n$ and let the numbers $b_{1,2;3,\dots,n}, \dots, b_{1,n;2,\dots,n-1}$ minimize:

$$E[(X_1 - b_{1,2;3,\dots,n}X_2 - \dots - b_{1,n;2,\dots,n-1}X_n)^2]$$

The partial correlation of X_1 and X_2 based on X_3, \dots, X_n is:

$$\rho_{1,2;3,\dots,n} = \text{sgn}(b_{1,2;3,\dots,n})(b_{1,2;3,\dots,n}b_{2,1;3,\dots,n})^{1/2}$$

Partial correlations can be computed recursively from correlations (see Yule and Kendall [21]):

$$\rho_{1,2;3,\dots,n} = \frac{\rho_{1,2;3,\dots,n-1} - \rho_{1,n;3,\dots,n-1}\rho_{2,n;3,\dots,n-1}}{((1 - \rho_{1,n;3,\dots,n-1}^2)(1 - \rho_{2,n;3,\dots,n-1}^2))^{1/2}} \tag{1}$$

Denote by Φ_ρ the bivariate standard normal cumulative distribution function with correlation ρ and Φ^{-1} the inverse of the univariate standard normal distribution function then:

$$C_\rho(u, v) = \Phi_\rho(\Phi^{-1}(u), \Phi^{-1}(v)); \quad (u, v) \in [0, 1]^2$$

is called the *normal copula*.

Notice that ρ is a parameter of the normal copula. In the case of a conditional bivariate copula the parameter $\rho_{1,2;3,\dots,n}$ is used instead. The relationship between the correlation of the normal copula r (the rank correlation of the normal variables) and the parameter ρ or $\rho_{1,2;3,\dots,n}$ is known and given by the following formula (Kurowicka and Cooke [12, p.55]):

$$\rho = 2 \sin\left(\frac{\pi}{6} r\right) \tag{2}$$

2.2 Bayesian belief networks

For our purpose *Bayesian Belief Networks (BBNs)* are directed acyclic graphs whose nodes represent univariate random variables and whose arcs represent direct influences between adjacent nodes. These influences may be probabilistic or deterministic¹. The graph of a

¹ When an influence is deterministic, nodes will be called functional. The discussion presented next refers to probabilistic influences unless otherwise specified.

BBN induces a non unique ordering of variables and stipulates that each variable is conditionally independent of its non-descendants given its parents. The parent set of variable X_i will be denoted as $Pa(i)$. Hence, to specify a joint distribution through a BBN the graph must be specified together with conditional probability functions of each variable given its parents (equation 3).

$$f(x_1, x_2, \dots, x_n) = \prod_{i=1}^n f(x_i | x_{Pa(i)}) \quad (3)$$

If $Pa(i) = \emptyset$ then $f(x_i | Pa(i)) = f(x_i)$. A BBN is then a concise and complete representation of the joint distribution. In the case that all nodes in the BBN are discrete then the functions to be specified are conditional probability tables (CPT) of each node given its parents. When variables are continuous, one possibility is to discretize them into a large enough number of states and use discrete BBNs. This approach might however turn out to be infeasible even for a modest sized model mainly because of the number of parameters to be specified. In general, the number of probabilities to be assessed K for a discrete BBN on n nodes with k_i states for each X_i for $i = 1, \dots, n$ is:

$$K = \sum_{j \in S} k_j - |S| + \sum_{l \in C} (k_l - 1) \prod_{m \in Pa(l)} k_m \quad (4)$$

where $S = \{X_j | Pa(j) = \emptyset\}$ and $C = \{X_l | Pa(l) \neq \emptyset\}$ and $|S| + |C| = n$. It is clear from equation (4) that K grows rather quickly as the number of states of each X_i grow. This is one of the main drawbacks of discrete BBNs. Some of the drawbacks of discrete BBNs were discussed in [9] and [5]. We list a summary of them next:

1. K imposes an assessment burden that might lead to informal and indefensible quantification or a drastic discretization or reduction of the model.
2. Marginal distributions are often available from data. Marginal distributions for children nodes is calculated from probability tables and this could impose severe restrictions in a quantification process.
3. Discrete BBNs are flexible with respect to recalculation and updating however they are not flexible with respect to modelling changes. If a parent node is added then the child nodes must be completely re-quantified.

Continuous-discrete non-parametric BBNs ([12], [9]) have been developed to cope with some of the drawbacks that discrete (and discrete-normal) a models impose. These will be discussed next.

2.3 Non-Parametric Continuous BBNs

Another way to deal with continuous nodes in a BBN is with the use of normal [17] or discrete-normal BBNs. For discrete-normal BBNs [5], unconditional means and conditional variances must be assessed for each normal variable. For each arc partial regression coefficients must be assessed. In the absence of data the assessment of partial regression coefficients and conditional variances by experts is difficult if the normality assumption does not

hold². More flexible models will be discussed in this section for dealing with continuous nodes.

Non-parametric BBNs and their relationship to other graphical models were presented in [12] and extended in [9]. A *non-parametric continuous (or continuous-discrete) BBN (NPCDBBN)* is a directed acyclic graph whose nodes represent continuous univariate random variables and whose arcs are associated with parent-child (un)conditional rank correlations. For each variable X_i with parents $X_j, \dots, X_{|Pa(i)|}$ associate the arc $X_{Pa(i)-k} \rightarrow X_i$ with the conditional rank correlation:

$$\begin{cases} r_{i,Pa(i)}, & k = 0 \\ r_{i,Pa(i)-k|Pa(i)-k+1}, & 1 \leq k \leq Pa(i) - 1 \end{cases} \quad (5)$$

The assignment is vacuous if $\{X_j, \dots, X_{Pa(i)}\} = \emptyset$. These assignments together with a copula family indexed by correlation and with conditional independence statements embedded in the graph structure of a BBN are sufficient to construct a unique joint distribution. Moreover, the conditional rank correlations in 5 are algebraically independent, hence any number in $(-1, 1)$ can be attached to the arcs of a NPCDBBN (Hanea et al. [9]).

Any copula with an invertible conditional cumulative distribution function may be used as long as the chosen copula possesses the zero independence property³. Choosing the normal copula presents advantages with respect to other copulae for building the joint distribution. Observe that for the normal copula relation (2) holds and since conditional correlations are equal to partial correlations then formula (1) may be used to compute the correlation matrix corresponding to the graph. Moreover since for the joint normal distribution, conditional distributions are also normal [19, p.33], then analytical updating is possible by this choice [9, p.724].

Figure 2 shows an example of a NPCDBBN on 11 nodes. To illustrate the assignment of rank and conditional rank correlations consider variable X_4 with parents $Pa(4) = \{X_1, X_2, X_3\}$. According to the assignment in (5), the unconditional rank correlations $r_{4,3}$ is used first. Then the conditional rank correlation $r_{4,3-1|3} = r_{4,2|3}$ is assigned. Finally the conditional rank correlation $r_{4,3-2|3,2} = r_{4,1|3,1}$ is assigned. Other (un)conditional rank correlations have been assigned in a similar way. The indices in the assignment (5) refer to the index of the variable in the ordering in the parent set and hence it does not necessarily need to coincide with the variables' original index. However once the correlations have been assigned the variables' original indices are used.

² For a recent discussion about discrete, discrete-normal and non-parametric BBNs see [10].

³ A copula with an analytic form for the conditional and inverse conditional cumulative distribution function accelerates the sampling procedure. One example of such a copula is Frank's copula. See Nelsen [14].

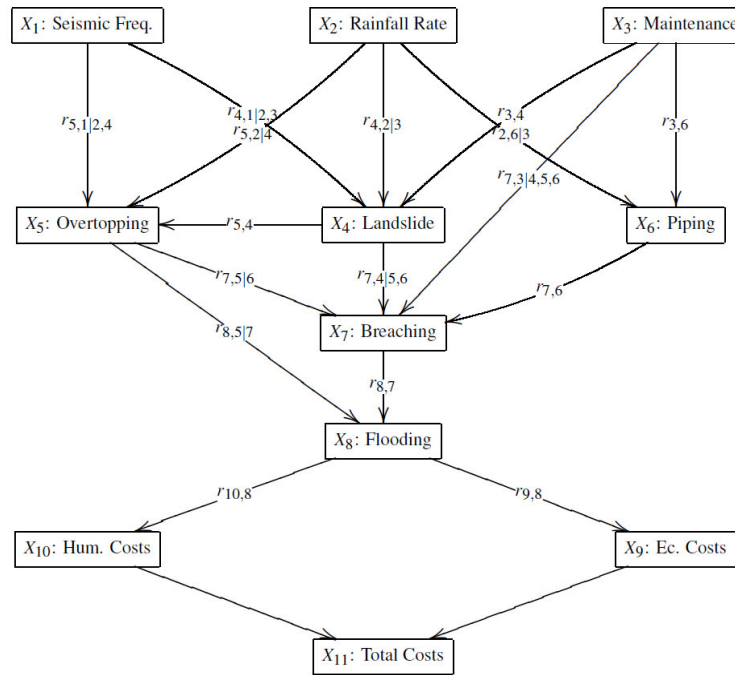


Fig. 2: Example of NPCDDBN on 11 nodes

The structure of the BBN gives information about the dependence structure in the joint distribution. For example variables X_1 , X_2 and X_3 are independent of each other and their dependence with other variables is described in terms of (conditional) rank correlations. In general every variable in the graph is conditionally independent of its ancestors given its parents. For example X_8 is conditionally independent of $\{X_1, X_2, X_3, X_4, X_6\}$ given $\{X_5, X_7\}$. In the same way X_{11} is conditionally independent of X_1, \dots, X_8 given $\{X_9, X_{10}\}$. Observe that arcs between X_{11} and $\{X_9, X_{10}\}$ lack rank correlations because X_{11} is a deterministic function of $\{X_9, X_{10}\}$. For a more complete description of the semantics of a BBN see Pearl [16, ch.3].

3 Non-parametric continuous BBNs in earth dam safety.

Variables involved in the analysis of contributing factors, failure modes and consequences of dam failure are mostly continuous. For example, rainfall rate is measured in mm, the piping of a crest is measured in l/sec or some similar unit and consequences of flooding are measured in monetary or some utility unit such as US dollars, euros or *qalys*. Often, these continuous quantities are discretized to facilitate the calculus of probabilities. Then, variables as the ones described previously are given states such as *low*, *medium* and *high*.

For the modelling of such kind of discrete variables, discrete BBNs are a natural choice. However, when the variables in the model are continuous it is more natural to model them as such. In this section an example of a non-parametric continuous BBN to model earth dam safety will be presented. The quantification techniques discussed as well as the model use may be applied for investigating risks in other civil infrastructure. The model to be

discussed next presents a case study for the State of Mexico in central Mexico. The model may however be quantified with data from other locations.

3.1 Example of NPCBBNs in earth dam safety in Mexico.

The BBN presented in figure 2 represents the model for earth dams safety to be discussed in this paper. Ten variables were identified as most relevant for the study. Their description, units and source of the marginal distributions is detailed next.

- X_1 : Seismic frequency. It refers to the distribution of earthquakes > 5.5 per year, in Richter magnitude scale, between 2000 and 2008 for the locations of interest. Data is available from the Mexican National Seismographic System.
- X_2 : Rainfall rate. It refers to the average value of the seven-basin (i.e. the area of influence of the 7 dams of interest) five-days moving averages in mm/day . Data is available from “ERIC” Mexican database from 1961 to 1998. A short overview of ERIC may be found in Carrera-Hernández and Gaskin [1].
- X_3 : Maintenance. Is the number of years between maintenance activities which would lead the dam to an “as good as new” condition. The marginal distribution comes from structured expert judgment.
- X_4 : Overtopping. Water level from the crest during an event in which such a level may increase beyond the total embankment height (mm). Marginal distribution obtained from expert judgment.
- X_5 : Landslide. Distribution of the security factors (resisting moment/causing moment), for each of the seven dams based on their design geometrical features. The so called “Swedish method” is used for calculating such factors (SRH [18]).
- X_6 : Piping. Distribution of water flowing through the embankment that causes its internal erosion apart from the spillway and outlet pipe torrents (l/sec). Data comes from expert judgment.
- X_7 : Breaching. Refers to the average breach width i.e. the mean of both superior and inferior breach widths, due to embankment’s crest erosion (m). Calculated with the methods reported in Wahl [20] with data from SRH [18].
- X_8 : Flooding. Average water level per day in the downstream flooded area during a dam failure event. Its marginal distribution is built by means of expert judgement (mm/day).
- X_9 : Human costs. Both public and private total costs over a time period equivalent to the maximum human remaining life span, due to all possible damages, health and life losses, caused by a flooding, consequence of a dam failure. It is measured in current USD and obtained through expert judgment.

- X_{10} : Economic cost. Both public and private total costs, due to all possible damages in infrastructures (e.g. schools, hospitals, bridges, roads, transport systems), fields (e.g. farms, crops), housing, supply, commercial and entertainment centers, caused by a flooding, consequence of a dam failure. It is measured in current USD and obtained through expert judgment.

Variables are broadly grouped into three categories: contributing factors (seismic frequency, rainfall rate and maintenance), failure modes (landslide, piping, overtopping and breaching), and consequences (flooding, human and economic cost). The model was built based on such configuration. Observe that as stated previously, arcs between human costs (X_9) and total costs (X_{11}), and economic costs (X_{10}) and total costs (X_{11}) lack a rank correlation because the total costs are simply the sum of human and economic costs and hence the relationship is functional.

From subsection 2.3 it may be seen that in order to specify a joint distribution through a NPCBBN, an undirected graph is required. The nodes of the graph represent univariate random variables with invertible distribution functions and the arcs rank and conditional rank correlations between these nodes.

According to section 3.1, five marginal distributions (X_3 , X_4 , X_6 , X_9 and X_{10}) were elicited from experts and the rest from data. The elicitation of rank and conditional rank correlation was done through structured expert judgment. The classical model of structured expert judgment (Cooke [2]) was used. The elicitation of marginal distributions from experts has been discussed extensively in the past. In 17 years, about 67;000 experts' subjective probability distributions have been elicited from 521 domain experts with the classical model (Cooke and Goossens [3]).

A total of four experts participated in the quantification of the model in figure 2. The elicitation of variables of interest follow the same lines as the elicitation of calibration variables. Calibration variables are those known to the analyst but not to the experts at the moment of the elicitation. These are used to measure experts' performance as uncertainty assessors. One example of a calibration variable for this elicitation is: *Consider the 7 day moving average of the daily average precipitation (mm) from the two stations related to Embajomuy Dam from January 1961 to August 1999 in ERIC II of CONAGUA [1]. What is the maximum moving average for the time period of reference? (please state the 5th, 50th and 95th percentiles of your uncertainty distribution).*

In total three questions about seismicity, four over general characteristics of the sample of 7 dams in the State of Mexico, nine over precipitation and two about water discharge were used as calibration variables. Because the elicitation of marginal distributions has been discussed extensively in the past we do not discuss this issue further the reader may see Cooke [2] for an in depth discussion. Next, we illustrate the elicitation of rank and conditional rank correlations with our example from figure 2.

3.2 Quantification of dependence in the NPCBBNs for earth dam safety in the State of Mexico.

The literature available to guide researchers in the elicitation of a joint distribution is much less than that available for the elicitation of univariate distributions [15]. To elicit the rank correlations in figure 2 a total of 20 questions were asked to each expert following the methods discussed in Morales-N'apoles et al. [13]. For each child node experts were asked to rank parent variables according to the largest unconditional rank correlation with the child in absolute value. This questions were meant to help experts in their next assessments.

Then for unconditional rank correlations experts would assess $P(X_{child} > median | X_{parent} > median)$. This question is translated in our application for **expert A** and the rank correlation $r_{4,3}$ as: *Consider a situation in which the number of years to rebuilt MAINTENANCE action (X_3) is above its median (30 years). What is the probability that the LANDSLIDE measured by the security factor (X_4) is also above its median (1.66)?* Observe that for this question the median value for the security factor is equal for all experts since it comes from data. The number of years to rebuild maintenance actions however comes from expert judgment and is different across experts.

The relationship between $P(X_4 > median | X_3 > median)$ and $r_{4,3}$ under the normal copula assumption is shown in figure 3. The continuous line in figure 3 would be the same for all experts. Once the expert has given a assessment for the probability of exceedence, the analyst then finds the r which satisfies the expert's conditional probability assessment and transforms this to the corresponding rank correlation using the inverse function of equation (2).

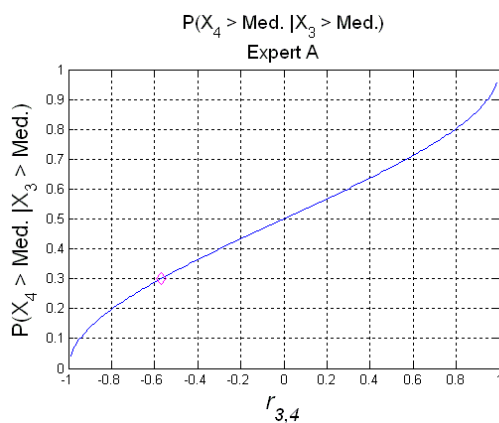


Fig. 3: $P(X_4 > median | X_3 > median)$ vs. $r_{4,3}$ for **expert A** under the normal copula assumption.

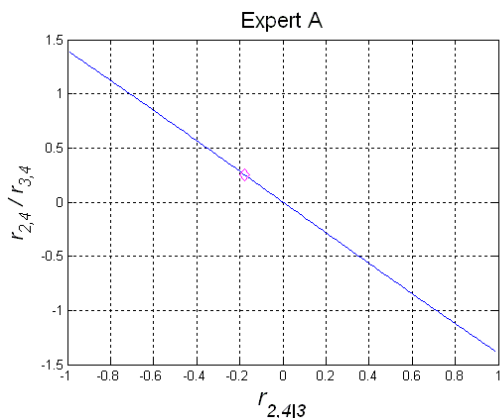


Fig. 4: $r_{4,2}/r_{4,3}$ vs. $r_{4,2|3}$ for **expert A** under the normal copula assumption given $P(X_4 > median|X_3 > median) = 0.3$ and X_2 and X_3 are independent.

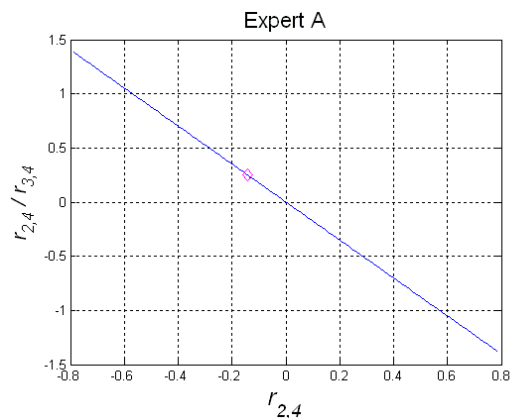


Fig. 5: $r_{4,2}/r_{4,3}$ vs. $r_{4,2}$ for **expert A** under the normal copula assumption given $P(X_4 > median|X_3 > median) = 0.3$ and X_2 and X_3 are independent.

Because of the zero independence property, zero correlation entails that $P(X_4 > median|X_3 > median) = 0.5$. A conditional probability value in the interval $[0, 0.5)$ corresponds to negative correlation. Positive correlation is attained when $P(X_4 > median|X_3 > median) > 0.5$. In our example **expert A** believes that when the number of years between rebuild maintenance are more than 30 for earth dams, then the probability that the security factor is above 1.66 is as low as 0.3. This assessment corresponds to a value of $r_{4,3} = -0.57$.

Once the expert has provided an assessment for the unconditional rank correlation of a given child node to its first parent, ratios of rank correlations of the child with the rest of the parents to the first rank correlation elicited are asked to experts. In our example the question for **expert A** would be: *Given your previous estimates, what is the ratio of $r_{4,2}/r_{4,3}$?*

The answer to this question depends on a number of things. First of all observe that $r_{4,3}$ is negative. Hence if the expert believes that the security factor is positively correlated with rain fall rate then the ratio $r_{4,2}/r_{4,3} < 0$, negative correlation between the security factor and rainfall rate corresponds to $r_{4,2}/r_{4,3} > 0$. Naturally a value of $r_{4,2}/r_{4,3} = 0$ would correspond to zero correlation between rainfall rate and the security factor. Notice that $|r_{4,2}/r_{4,3}| > 1$ corresponds to the expert's belief that $|r_{4,2}| > |r_{4,3}|$ and an analogous situation is observed when $|r_{4,2}/r_{4,3}| < 1$.

Additionally, X_3 has explained already part of the dependence of X_4 on its parents hence X_2 can only explain part of the remaining dependence of X_4 . The structure of the BBN also plays a role at this stage. Observe that in our example X_3 and X_2 are independent. However, if X_3 and X_2 were correlated, additional constraints would be present for the assessment of $r_{4,2}/r_{4,3}$ (see Morales-Nápoles et al. [13]).

Figures 4 and 5 show the relationship of $r_{4,2}/r_{4,3}$ to $r_{4,2|3}$ and $r_{4,2}$ respectively. Observe that the ratio $r_{4,2}/r_{4,3} \in (-1.38, 1.38)$. Because X_2 and X_3 are independent $r_{4,2}/r_{4,3}$ is in a symmetric interval around zero. The assignment of rank correlations in relation (5) entails that $r_{4,2|3}$ can be chosen freely and hence $r_{4,2|3} \in (-1, 1)$. This is shown in figure 4. However, $r_{4,2}$ will be restricted by the expert's previous answer. In this case given the expert's answer that $P(X_4 > median|X_3 > median) > 0.5 \rightarrow r_{4,3} = -0.57, r_{4,2} \in (-0.78, 0.78)$ as observed in figure 5.

In our example **expert A** has stated that $r_{4,2}/r_{4,3} = 0.25$. This entails that our expert believes that the rank correlation between the security factor and rainfall rate is negative and smaller in absolute value than $r_{4,3}$. In particular $r_{4,2} = -0.14$ for **expert A**. Using the dependence statements embedded in the graph and equations (2) and (1) the analyst may compute the value of $r_{4,2|3} = -0.17$ for this expert.

According to figure 2, landslide has one last parent node for which the conditional rank correlation $r_{4,1|2,3}$ needs to be specified. Thus the expert would be confronted with the following question: *Given your previous estimates, what is the ratio of $r_{4,1}/r_{4,3}$?* Again, the possible answers to this question are restricted by the expert's previous answers. The relationship of $r_{4,1}/r_{4,3}$ with $r_{4,1|2,3}$ and $r_{4,1}$ is shown in figures 6 and 7 respectively. The interpretation of $r_{4,1}/r_{4,3}$ follows the same lines as the one described for $r_{4,2}/r_{4,3}$. As before $r_{4,1|2,3}$ may take values in the interval $(-1, 1)$ and given the expert's previous answers $r_{4,1} \in (-0.77, 0.77)$.

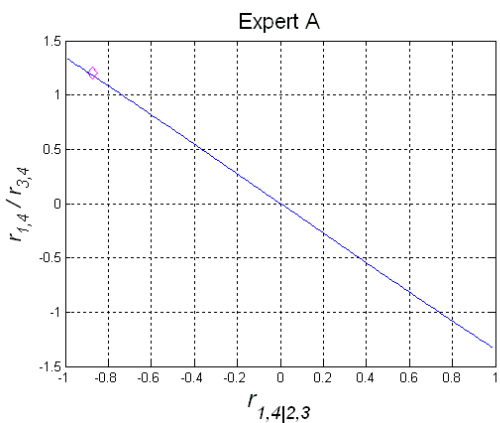


Fig. 6: $r_{4,1}/r_{4,3}$ vs. $r_{4,1|2,3}$ for **expert A** under the normal copula assumption given $P(X_4 > median|X_3 > median) = 0.3, r_{4,2}/r_{4,3} = 0.25$ and X_2 and X_3 are independent.

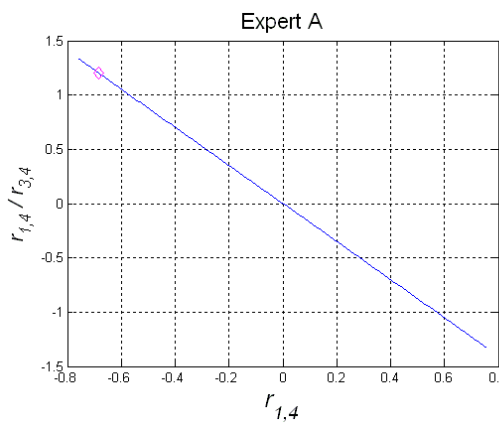


Fig. 7: $r_{4,1}/r_{4,3}$ vs. $r_{4,1}$ for **expert A** under the normal copula assumption given $P(X_4 > median|X_3 > median) = 0.3, r_{4,2}/r_{4,3} = 0.25$ and X_2 and X_3 are independent.

In our example **expert A** believes that there is a negative correlation between seismic frequency and the security factor. The expert also believes that the correlation between the security factor and the years until rebuild maintenance is smaller than the correlation between the security factor and the seismic frequency. The value for the ratio stated by ex-

expert A is $r_{4,1}/r_{4,3} = 1.2$. This value corresponds to $r_{4,1} = -0.68$. Again by using the dependence statements embedded in the graph and equations (2) and (1), $r_{4,1} = -0.68$ is translated to a conditional rank correlation $r_{4,1|2,3} = -0.87$.

The full quantification of rank correlations in the BBN in figure 2 follows the same procedure as the one described for the elicitation of $r_{4,3}$, $r_{4,2|3}$ and $r_{4,1|2,3}$. For each expert a BBN is obtained. Once a joint distribution is available for each expert these may be combined via the weight derived from the calibration and information scores in the classical model.

The linear combination of experts' individual densities might be tempting. However, in general the resulting distribution will not preserve the conditional independence statements required by the graph. Instead of combining linearly experts' joint distributions, a linear pooling of exceedence estimates such as $P(X > median | Y > median)$ is done.

One disadvantage of this approach is that the medians of X and Y could be different. This is usually the case when the distributions of X and/or Y are retrieved from experts. In this case the idea is to compute the probabilities that each expert "would have stated" if he/she had been asked probabilistic statements regarding the chosen quantile (median in this case) of the combined opinion such that his/her estimates for the rank correlations remain unchanged. Details about the combination of expert judgments may be found in Morales-Nápoles et al. [13].

3.3 Elicitation results for the BBN for earth dam safety in the State of Mexico.

In total four experts (A,B, C and D) participated in the elicitation. Three of the experts hold positions at the National Water Commission (CONAGUA) in the State of Mexico. The other expert holds a position in the Municipality of Zinacantepec as water manager. Two of the experts are lecturers in civil engineering at the Autonomous University of the State of Mexico (UAEM). A workshop was held on July 18 2008 in the faculty of engineering of UAEM. Individual interviews were held with each expert during the months of July and August according to experts' availability. The questionnaire included 6 questions to elicit marginal distributions, 20 to elicit the rank and conditional rank correlations from figure 2 and 20 calibration variables.

After processing the results of the elicitation, no individual expert had a calibration score corresponding to a p-value above 5%. Information scores were within a factor 2.5 for the four experts. **Expert B** had the lowest calibration score, however was also the most informative. In contrast, **expert A** had the largest calibration score and is the least informative. This is a recurrent pattern, however low informativeness does not translate automatically into better calibration [3, p.669]. In the classical model, experts' scores are the product of calibration and information scores. Experts with a calibration score less than the significance level are weighted with zero. The global weight decision maker (GWDM) uses the information score per variable while the item weight decision maker (IWDM) uses the average information score. In our example the IWDM and GWDM were equal, hence in the future we refer to the former exclusively. In this elicitation the GWDM is better cali-

brated than each expert individually, however its information scores are lower than the information scores of each expert individually. The calibration score of the GWDM is still lower than 5% which fails to confer the requisite level of confidence for the study.

The equal weight decision maker (EWDM) does not take into account experts' performance on calibration variables and gives equal weight to all experts. In our application this was the only expert with a p-value above 5%. For this reason the EWDM is the recommended choice and further analysis will be conducted with this combination. The cost of this choice is in the information scores (about 3 times smaller than the GWDM). The results of the combination scheme are presented in table 1.

(Un)Conditional Rank Correlation	(Un)Conditional Rank Correlation
$r_{3,6}$	0.1799
$r_{2,6 3}$	0.1067
$r_{4,3}$	-0.3996
$r_{4,2 3}$	-0.3164
$r_{4,1 2,3}$	-0.4307
$r_{5,4}$	-0.1278
$r_{5,2 4}$	0.1711
$r_{5,1 2,4}$	0.3025

Tab. 1: EWDM Dependence estimates for the dam safety model from figure 2

One of the advantages of BBNs is that once the model has been fully quantified, whenever evidence becomes available the joint distribution may be updated accordingly. In the case of NPCBBNs one may exploit the fact that the normal copula is used to build the joint distribution. In this case as stated before the conditional distributions will also be normal. In general other copulae may be used to build the joint distribution, the cost would be greater computational effort during the quantification and updating phase. Next we illustrate the use of NPCBBNs in earth dam safety with the model from figure 2.

3.4 Model use.

One of the objectives of the model is to update the joint distribution whenever evidence becomes available. Figure 8 shows the model from figure 2 in UNINET. UNINET is a stand alone application developed at the TU Delft for NPCBBNs (see Cooke et al. [4]). Marginal distributions are represented by histograms. Means and standard deviations (after the \pm sign) are shown. Figure 9 presents the model when 21.3 earthquakes per year, 16.159 $\frac{mm}{day}$ in a 5 day moving average and 66.57 years without rebuilt maintenance are observed.

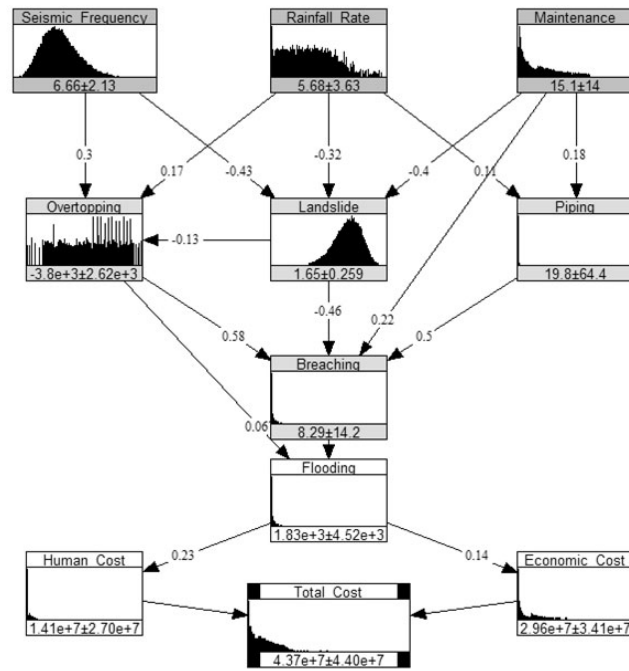


Fig. 8: Unconditional dam safety model.

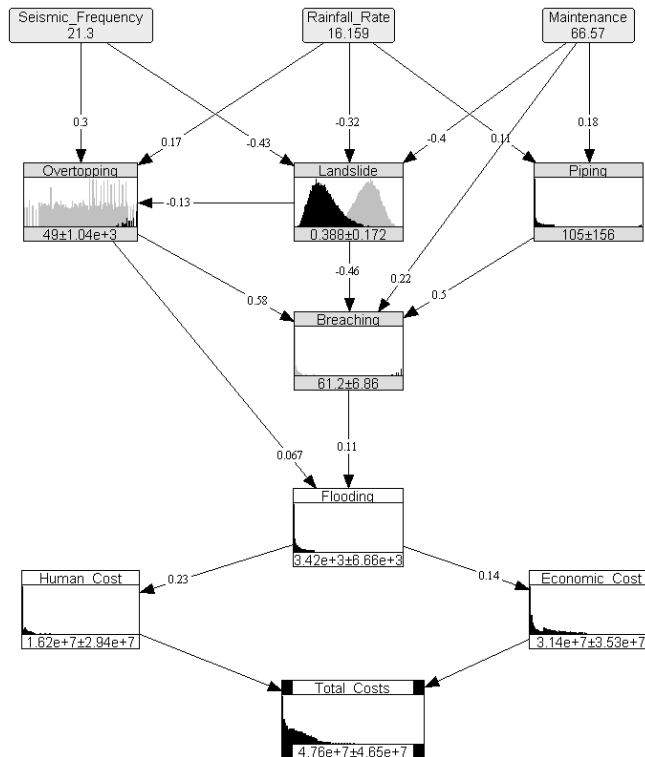


Fig. 9: Dam safety model given seismic frequency is 21.3, rainfall rate is 16.159 and maintenance is 66.57.

The original marginal distributions are shown in figure 9 in grey while the updated belief is shown in black. The reader may observe that the possible failure modes (*overtopping, landslide, piping* and *Breaching*) present larger changes than the possible consequences (*flooding* and *costs*). This is because the experts' combined opinion says that given a dam failure in the State of Mexico the consequences are almost the same regardless of the size of the failure.

Samples may be retrieved from either the unconditional distribution (figure 8) or any conditional distribution as the one shown in figure 9. For example the exceedence probability of *Flooding* is presented in figure 10. Observe that the largest differences are in the tail of the distribution. The 5%, expectation and 95% percentiles of the distributions from figure 10 are presented in figure 11. The expectation of flooding in the case of a failure in the baseline case is 1.6 times higher than in the case when low seismicity, low levels of rainfall rate and periodic maintenance is expected. The uncertainty in both cases is comparable (0 to 4.9E3) in the 'less risky' case vs. (0 to 6.4E3) in the baseline case.

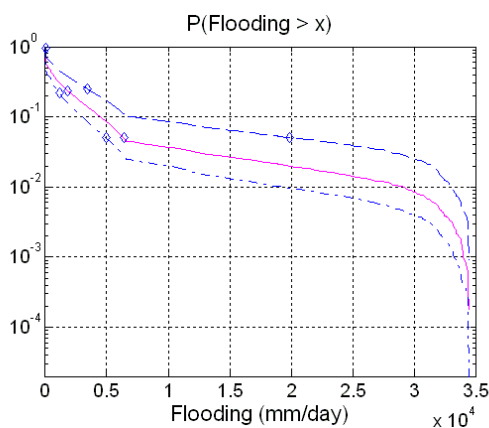


Fig. 10: Unconditional and different conditional distributions of flooding [$P(X_8 > x)$]

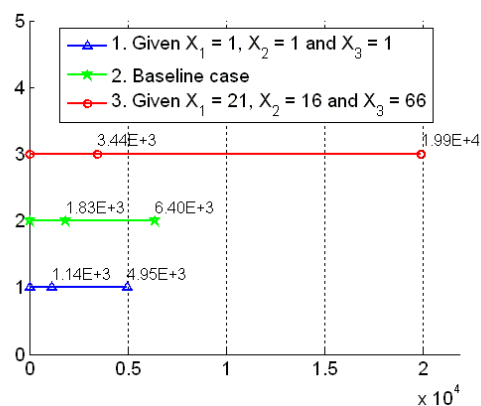


Fig. 11: 5%, $E[X_8]$ and 95% percentiles of flooding

On the other hand, in a situation where a high amount of earthquakes per year, high value for the 5 day moving average of rainfall rate and no maintenance is observed (such as the one in figure 9). The expectation of flooding in the case of a failure is about 1.9 times higher than in the baseline case and 3 times higher than in a 'safer' scenario. However, the 95th percentile in this case is about 3 times larger than the 95th percentile in the baseline case and about 4 times larger than the 'low risk' scenario. Similar kind of analyzes as the one presented in this section may be carried out with other variables in the model. For example in the failure mode variables where larger changes are expected to happen. Similarly, other variables may be conditionalized in order to observe the experts' combined believe regarding the probabilistic relations between variables.

4 Conclusions and final comments.

This paper shows a model for possible consequences of earth dam failure, and their failure modes emphasizing risk assessment in a dams within the State of Mexico. The combination of BBNs and expert judgment stemmed from the recognition that dam managers need intuitive, useful and practical tools for carrying out quantitative risk assessment, based on a solid theoretical foundation.

The availability of experts with was one of the main difficulties encountered during the quantification of the model. This step is critical in future refinements of the model. The inclusion of more variables in the model should be considered. This is particularly relevant if some local cases have shown that other variables are important in the risk evaluation apart from those reported in international statistics.

The equal weight combination was proposed as the preferred choice for the decision maker. The choice was motivated mainly because of suboptimal performance of each individual expert. This in turn led to a suboptimal performance of the optimized decision makers. The training of experts in probabilistic assessments is fundamental for the classical method for structure expert judgment. Results from this study suggest that better training or a selection of seed variables that characterizes better the expertise in the expert panel is desired for the follow up of the project.

In spite of these observations, it is strongly believed that the methodology utilized to build the model can be applied to carry out similar exercises in different locations. Overall this research has demonstrated that the use of NPCBBN in Mexican dams' risk assessment is not only feasible but also beneficial. Finally, it should be emphasized that this research is hoped to be the starting point of a bigger project aimed at developing a more comprehensive model applicable to different types of dams.

References and Bibliography

- [1] Carrera-Hernández, J.J. and Gaskin, S.J. (2008), "The basin of Mexico hydrogeological database (bmhdb): Implementation, queries and interaction with open source software." *Environmental Modelling & Software*, 23, 1271–1279.
- [2] Cooke, R.M. (1991), *Experts in uncertainty*. Oxford University Press.
- [3] Cooke, R.M. and Goossens, L.H.J. (2008), "TU Delft expert judgment data base." *Reliability Engineering & System Safety*, 93, 657–674.
- [4] Cooke, R.M., Kurowicka, D., Hanea, A.M., Morales, O. Ababei, D., Ale, B. and Roelen, A. (2007), "Continuous/discrete non parametric bayesian belief nets with unicorn and uninet." In *Proceedings of the Mathematical Methods for Reliability conference* (T Bedford, J. Quigley, L. Walls, and A. Babakalli, eds.).
- [5] Cowell, R.G., Dawid, A.P., Lauritzen, S.L. and Spiegelhalter D.J. (1999), *Probabilistic Networks and Expert Systems*. Statistics for Engineering and Information Science, Springer.

- [6] Donnelly, R. (2006), "Safe and secure: risk-based techniques for dam safety." *International Water Power and Dam Construction*. [Http://www.waterpowermagazine.com/story.asp?storyCode=2040340](http://www.waterpowermagazine.com/story.asp?storyCode=2040340).
- [7] FEMA (2007), "The national dam safety program final report on coordination and cooperation with the european union on embankment failure analysis." REPORT FEMA 602, Federal Emergency Management Agency (FEMA).
- [8] FEMA (2008), "Risk prioritization tool for dams users manual." Manual FEMA P713CD, Federal Emergency Management Agency (FEMA).
- [9] Hanea, A., Kurowicka, D. and Cooke, R.M. (2006), "Hybrid method for quantifying and analyzing bayesian belief nets." *Quality and reliability Engineering International*, 22, 709–729.
- [10] Hanea, A.M. (2008), Algorithms for Non-parametric Bayesian belief nets. Ph.D. thesis, TU Delft, Delft, the Netherlands.
- [11] ICOLD (1995), "Dam failure statistical analysis." Bulletin 99.
- [12] Kurowicka, D. and R.M. Cooke (2005), "Distribution-free continuous bayesian belief nets." In *Modern Statistical and mathematical Methods in Reliability* (Keller- McNulty S. Wilson A., Limnios N. and Armijo Y., eds.), 309–323.
- [13] Morales-Nápoles, O., Kurowicka, D. Cooke, R.M. and van Baren, G. (2009), "Expert elicitation methods of rank and conditional rank correlations: An example with human reliability models in the aviation industry." *Submitted to RE&SS*.
- [14] Nelsen, Roger B. (1998), *An Introduction to Copulas* (Lecture Notes in Statistics). Springer.
- [15] O'Hagan, A. (2005), "Research in elicitation." In *Bayesian Statistics and its applications* (U. Singh and D.K. Dey, eds.), 375–382, Anamaya, New Delhi.
- [16] Pearl, J. (1988), *Probabilistic Reasoning in Intelligent Systems : Networks of Plausible Inference*. Morgan Kaufmann.
- [17] Schachter, R.D. and C.R. Kenley (1989), "Gaussian influence diagrams." *Management Science*, 35, 527–550.
- [18] SRH (1976), *Dams built in Mexico (In Spanish: Presas Construidas en México)*. México.
- [19] Tong, Y.L. (1990), *The multivariate Normal Distribution*. Series in Statistics, Springer.
- [20] Wahl, T.L. (1998), "Prediction of embankment dam breach parameters." Report DSO-98-004, Dam Safety Office, US.
- [21] Yule, G. and M. Kendall (1965.), *An introduction to the theory of statistics*, 14th edition. Charles Griffin & Co., Belmont, California.

Extension of the probabilistic evacuation decision model

Karolina Wojciechowska
HKV CONSULTANTS, the Netherlands

Abstract: In 1995, due to danger of flooding, a massive evacuation in the province of Gelderland in the Netherlands took place. The decision about the evacuation was mainly a consequence of a presumption the dikes would not be able to withstand the forces of nature. The process of the evacuation went well, but life-threatening flooding did not occur. In the decision uncertainty in the load and uncertainty in the condition of the flood defences played a role. In general, such uncertainties are taken into consideration during operational flood management; however, not explicitly. There are several methods in decision theory, which can be used to include uncertainty in decision-making in an explicit way, for example the decision tree approach. This method can support decision-making when high costs and probabilities of undesirable events are involved. In this paper, we present an evacuation decision model, based on the decision tree theory and developed in FRIESER [4]. We present application of this model for three dike failure mechanisms, namely overflow, overflow/wave overtopping and uplifting/piping, what is an extension comparing to FRIESER [4]. The model requires specification of dike failure probabilities. Here we emphasize that operational decisions, like evacuation, require *operational* probabilities. These probabilities can be calculated using the concept of *fragility curves* and *short-term* water level density function. At the end, we shortly discuss usefulness the model in a real-life situation.

1 Introduction

The Netherlands is a country located in the delta of three European rivers, namely the Rhine, the Meuse and the Scheldt. Nearly 65% of the country is situated below sea level and/or is threatened by floods from the rivers (and tributaries). Natural barriers like dunes and high grounds, and man-made constructions like dikes and storm surge barriers protect the area from flooding. Despite the flood protection a flood danger remains; the flood (danger) in 1995 is a quite recent example.

At the beginning of 1995, heavy rainfalls in France and the Ardennes led to increase of water levels on the rivers Meuse, Rhine and Waal. In the Dutch province of Gelderland, the waters reached a level of serious concern. The regional management team decided to evacuate a part of the area. That was a large scale evacuation; nearly 250,000 people left their homes. The process of the evacuation went well; however, life-threatening flooding did not occur. For more information see BEZUYEN et al. [1], INT [6] and INT [7].

A primary goal of an evacuation is to save human lives. However, every evacuation, even an unnecessary one, has an great influence on the society, economy and animals. People are under a lot of stress; there are losses in income and production; there is a negative influence on livestock, horticulture and agriculture. Besides these, the costs of the operation and care for the evacuated people should be taken into account (see BEZUYEN et al. [1]). Because of these arguments every decision about an evacuation should be very carefully considered.

In 1995, the evacuation decision was mainly based on the opinion that the dikes would not be able to guarantee the safety in the region. In general, experience and experts' judgement had an influence on the evacuation decision. Because the flooding did not happen some question the evacuation (see FRIESER [4]). In the decision uncertainties in the coming water load and condition of the dikes played a role; these uncertainties were included into the decision-making process by means of experience and expertise (see BEZUYEN et al. [1]).

In FRIESER [4] a probabilistic evacuation decision model is developed. The model is based on the decision tree theory and aims to give a rational support to a decision-maker; in the model some of the uncertainties are explicitly (mathematically) included. According to the model, decision (evacuate yes or no) is based on a combination of costs and probabilities of a dike failure. The probabilities are *operational*, since the decision has to be taken in operational time. In FRIESER [4] a method is developed to calculate such probabilities for one dike failure mechanism, namely overflow. In this article we extend the model concept by implementing a wider approach to the calculation of the operational probabilities of a dike failure. We aim to compute the operational probabilities for two dike failure mechanisms, overflow/wave overtopping and uplifting/piping, using *fragility curves* and *short-term* water level density function. In the following sections we give a definition of the operational probabilities of a dike failure, present the concept of the probabilistic evacuation decision model and, by means of a case study, incorporate the extended approach for calculation of the probabilities into the decision model.

2 Dealing with uncertainties

2.1 Operational probability of a dike failure

Failure of a dike (a dike does not fulfil some of its functions, a lack of water retaining capacity) is governed by the strength, represented by geometry and material characteristics of the dike, and by the threats e.g. occurring hydraulic load. High water levels and waves usually constitute the most dominant danger to flood defences. Nevertheless, the failure can also be

caused by a number of other physical, biological and human factors (see TAW [12]). There are several *failure mechanisms*, which can be distinguished in the context of a dike failure. Most of the mechanisms are presented in Fig. 1.

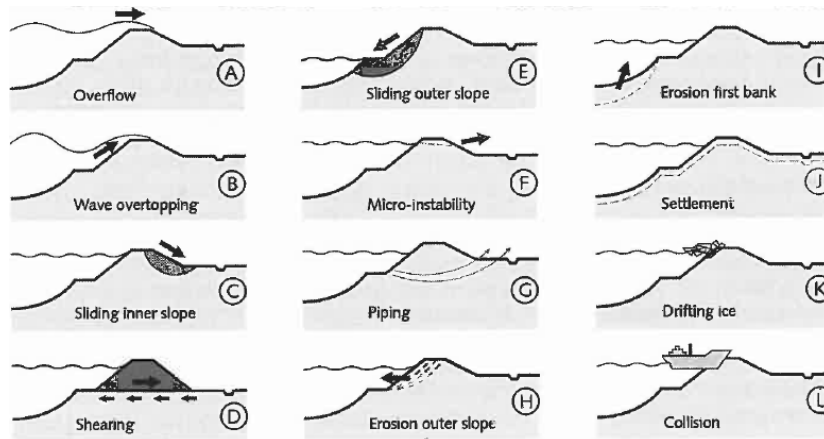


Fig. 1: Dike failure mechanisms (TAW [12]).

In this article, three dike failure mechanisms are considered more closely: overflow, overflow/wave overtopping and uplifting/piping. In case of overflow, the local water level is higher than the crest level of a dike causing erosion of the inner slope of the dike and entering of water in the area behind the dike. In case of overflow/wave overtopping also waves can lead to the failure (see TER HORST [5] and STEENBERGEN & VROUWENVELDER [11]). In case of the uplifting/piping failure mechanism, water seeps locally under a dike leading to the formation of channels (pipes), which weaken the dike. Pipes start to develop if the clay layer under the dike lifts up and cracks appear (see TER HORST [5]). A dike failure mechanism can be expressed by a model, which has an empirical or mathematical character. Usually, the model is formulated in terms of a limit state function Z , where strength of a dike is compared with the load imposed upon the dike. When $Z < 0$ failure of the dike occurs. Examples of the limit state functions for overflow and overflow/wave overtopping are given in Tab. 1.

Tab. 1: Limit state functions for overflow, overflow/wave overtopping and uplifting/piping.

Failure mechanism	Limit state function	Parameters
Overflow	$Z = h_d - h$	h_d = the crest level of a dike, h = local water level,
Overflow/wave overtopping	$Z = h_d - h$ or $Z = q_c - q$	q_c = critical overtopping discharge, q = occurring overtopping discharge

The limit state functions depend on the local water level. Moreover, several other (random) variables and parameters are contained in Z . Keeping the above in mind, the general description of the probability of a dike (section) failure is:

$$P_f = P\{Z < 0\} = P\{R < S\} \tag{1}$$

where $Z = R - S$, P_f stands for the probability of a dike failure, Z stands for the limit state function, R stands for the strength of the dike and S stands for the load imposed upon the

dike. R and S are assumed to be independent. Clearly, the probability of a dike failure is equal to the probability that the load imposed upon the dike exceeds the strength of the dike.

When the local water level is the dominant load, as is often the case with fluvial dikes (TAW [12]), it is useful to write the probability (1) as:

$$P_f = \int_{-\infty}^{\infty} P\{Z < 0 | H = h\} f_H(h) dh \quad (2)$$

where H stands for the local water level and f_H denotes the probability density function of H. The component $P\{Z < 0 | H = h\}$ represents the probability of a dike failure given a specific local water level. The function $h \rightarrow P\{Z < 0 | H = h\}$, in this context, is called a *fragility curve* (see BUIJS et al. [2] & [3] and VAN DER MEER et al. [8]). The component f_H is a long-term local water level density function. From now on, the term *local* will be omitted.

Keeping the above information in mind, we define the *operational* probability of a dike (section) failure, $P_{f|pred}$, as:

$$P_{f|pred} = \int_{-\infty}^{\infty} P\{Z < 0 | H = h\} g_H(h | h_p) dh \quad (3)$$

where g_H is a *short-term* water level density function and h_p is a forecasted water level. The operational probability of a dike failure is needed in operational decision-making (it incorporates present information concerning water levels).

The only difference between the equations (2) and (3) occurs in the formulation of the water level density function. The function f_H can be derived on the basis of distribution of annual river discharge maxima and relations between the discharge and water level (see TER HORST [5]), whereas the function g_H can be based on actual (operational) information concerning future water levels. The last function is more extensively considered in the following section.

2.2 Short-term water level density function

In our study, the short-term water level density function is assumed to be normal with mean μ , equal to the forecasted water level h_p and standard deviation $\sigma > 0$, which represents accuracy of the forecast. Having a dataset of observed and corresponding forecasted water levels, the standard deviation can be estimated as:

$$\hat{\sigma} = \sqrt{\frac{1}{N} \sum_{i=1}^N \varepsilon_i^2} \quad (4)$$

where ε is a historical forecast error (i.e. a difference between an observed water level and its forecast) and N denotes the size of the ensemble of the historical forecast errors. The right-hand side of (4) is the RMSE (Root Mean Squared Error), a measure often used to assess accuracy of a forecast model. It is important to emphasize that σ depends on a lead time of a

forecast – indeed, the further in time a forecast is made, the less accurate it is. Therefore, the estimation should be made with respect to lead times.

It is used to say that the Rhine enters the Netherlands at Lobith. In FRIESER [4] the parameter σ is estimated for this location according to (4). The estimations are derived using a dataset of observed and corresponding forecasted water levels (high water periods in 1998-1999). In the analysis two water level forecast models are considered, namely model LOBITH and FloRIJN. The estimations are presented in Tab. 2.

Tab. 2: RMSE for two water level forecast models, location Lobith in the Netherlands, (round 30 observations per combination: model x lead time), FRIESER [4].

Forecasting model	RMSE 4 days ahead [m]	RMSE 3 days ahead [m]	RMSE 2 days ahead [m]	RMSE 1 day ahead [m]
LOBITH	0.49	0.30	0.31	0.07
FloRIJN	0.37	0.21	0.13	0.11

In general, the estimations decreases together with decrease of a lead time in case of both forecast models. Differences in the estimations follow from characters of the models. The model LOBITH is a multi-linear regression model (a statistical model), whereas a one-dimensional hydrodynamic model SOBEEK constitutes the core of the model FloRIJN. For more information about the models see SPROKKEREEF [10].

As an example, consider forecasted water levels for the location Lobith: 14.24, 14.96, 15.28 and 15.44 m+NAP. These are 1, 2, 3 and 4 days ahead forecasts derived with model FloRIJN. On the basis of these values and estimations from Tab. 2, 5% and 95% quantiles of the normal distribution can be derived for the considered lead times and the forecast model. Fig. 2 presents the results.

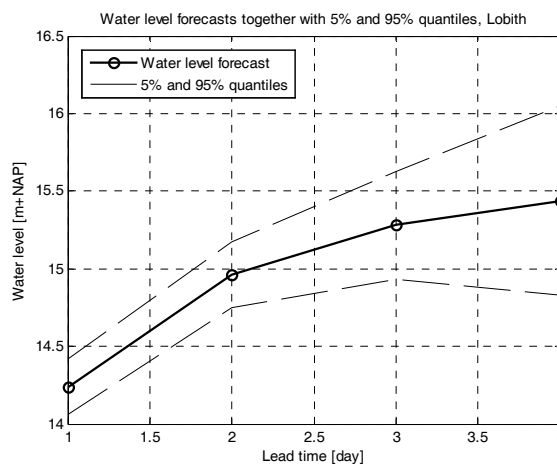


Fig. 2: Water level forecasts for four days ahead together with 5% and 95% quantiles, location Lobith, forecast model FloRIJN.

In the following section, the probabilistic evacuation decision model will be presented. The concept of operational probability of a dike (section) failure is used in the model.

3 Decision-tree for evacuation

Decision about evacuation of inhabitants of an area *endangered* by flooding is very difficult, mainly because the flood event is uncertain. The decision maker is concerned about consequences of an unnecessary evacuation on the one hand, and consequences (fatalities) if no evacuation decision is taken and the flood occurs on the other hand. An example is the evacuation in the province of Gelderland in 1995; despite expectations, flooding did not happen then. The decision about the evacuation was taken on the basis of deterministic information (like forecasted high water levels, see FRIESER [4]), experience and expertise; no robust technique, where uncertainties are explicitly incorporated, was used (see FRIESER [4]).

In FRIESER [4] a decision model for evacuation is developed. The aim of this model is to give a rational support to a decision maker, in case of a flooding danger. In the model uncertainties are explicitly (mathematically) included; the model uses the concept of a decision tree. This method can support decision-making process involving high costs and probabilities of undesirable events. Clearly, these factors are present in case of a decision about evacuation: costs of evacuation and flood damage and probability of a dike failure. The decision tree method applies a graphical approach to compare competing alternatives (decisions) and to assign values to those alternatives by combining probabilities and costs into expected values. Consequently, an alternative with the lowest expected value is indicated as the optimal. The decision model for evacuation is presented in Fig. 3.

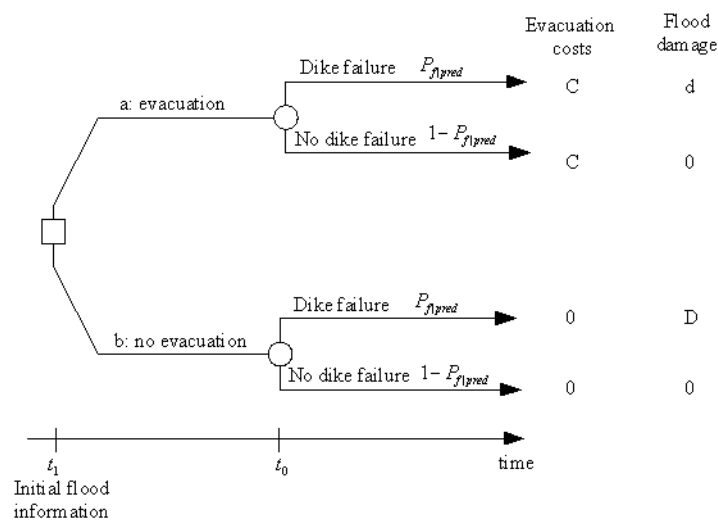


Fig. 3: Evacuation decision model.

The model describes four scenarios, which occur during evacuation decision-making. One of the scenarios is evacuation decision at time t_1 and a dike failure at time t_0 (the most upper branch in Fig. 3). Consequently, there is approximately $|t_1 - t_0|$ time available for the evacuation. Costs of evacuation and flood damage are assigned to every scenario. The costs of evacuation is equal to C ; if flooding occurs and evacuation did not take place then the flood damage is equal to D ; if flooding occurs and evacuation took place then the flood damage equals d , where $d < D$. The last observation is connected with reduction of flood damage

caused by the evacuation performed in the available time. Note that one of the model assumptions is equality of flooding with dike failure (this is not always the case, see FRIESER [4]). The model contains information about probability of a dike (section) failure, this is a probability that a dike fails at time t_0 , given forecasted water level. The forecast is derived at time t_1 and attempts to estimate water level at time t_0 . The probability can be derived for different dike failure mechanisms and can be expressed with the formula (3).

According to the model, the optimal decision is chosen on the basis of the minimum expected cost criterion:

$$Opt.decision = \arg \min_{\{a,b\}} \{EV(a), EV(b)\} \quad (5)$$

where EV stands for expected value of decision (combination of total costs and probability of a dike failure), a and b are possible decisions as defined in Fig. 3.

In the following section a case study is given, where application of the model is presented.

4 Case study

4.1 Introduction

Consider a fictive (although representative for the Netherlands) dike-ring area, situated along the river Rhine. It is assumed that 250,000 people inhabit the area; also several economic branches are present in the region. Suppose that a decision maker receives information about a danger of flooding in the area. The information is given in a form a forecasted water level for a location along the dike-ring. The forecast is 15.52 m+NAP on the third day from *now*. The crest level of a dike at the location is equal to 15.90 m+NAP; tangent of the slope angle of the dike is equal to 1/3.

The decision maker, concerned about condition of the dike and uncertainty in the load, considers evacuation of the area. It is assumed that the decision must be taken now using the given information. In order to support the decision, the decision maker uses the evacuation decision model. The model requires specification of costs and operational probability of a dike failure as input; these are considered in the following sections. These parameters depend on the lead time of the forecast (under the above assumptions there are approximately 3 days available for the evacuation).

4.2 Costs

In order to apply the evacuation decision model, costs of the evacuation (C) and flood damage (d or D, assuming that flood occurs) have to be estimated. It is assumed that the cost of evacuation emerges as the sum of initial evacuation cost and direct, and indirect economic damage. The last two arise as a consequence of evacuation. In this study, the initial

evacuation cost is equal to an amount of compensations paid out to the evacuated people and expenses incurred by the police. The direct economic damage arises as a result of suspension of production and depends on the type of economic branch (e.g. minerals extraction, banks/insurance companies) and duration of the suspension. Indirect economic damage consists of losses to supply companies and customers, and losses caused by difficulties in traffic in the regions outside of the endangered area. Furthermore, it is assumed that the flood damage is equal to the sum of economic value of loss of human life and economic value of loss of replaceable moveable goods (e.g. television-set). The loss of human life is estimated using present value of the Net National Product per head of the country; obviously the loss decreases if an evacuation is carried out. Note that the flood damage does not contain cost of damage to e.g. buildings – since evacuation does not have any influence on such damage, it will not be considered here. The costs are estimated for the representative dike-ring area using data and models given in FRIESER [4]; the results are shown in Tab. 3.

Tab. 3: Costs of the evacuation and flood damage (in case of evacuation and no evacuation) for a representative dike-ring area; approximately 3 days available for the evacuation.

Costs	Value [mln]
Costs of evacuation (C)	107.5
Flood damage in case of no evacuation (D)	4430
Flood damage in case of evacuation (d)	85

4.3 Operational probability of a dike failure

The evacuation decision model requires specification of operational dike failure probability, $P_{f|pred}$. In FRIESER [4] this probability is estimated for one dike failure mechanism, namely overflow. Other mechanisms were not considered, due to study assumptions. In our research we extend the model concept by calculation of $P_{f|pred}$ for two dike failure mechanisms: overflow/wave overtopping and uplifting/piping. At the same time, we will give comparison with the overflow failure mechanism approach.

According to equation (3), the operational probability of dike failure can be computed as an integration of a fragility curve for a particular failure mechanism and short-term water level density function. In order to derive a fragility curve, a limit state function has to be specified. For the considered failure mechanisms, limit state functions are implemented according to STEENBERGEN & VROUWENVELDER [11] and TAW [12]. Every limit state function contains random variables e.g. crest height of a dike, significant wave height, etc.; usually experts determine types of probability distributions of the variables. Some of the most essential random variables, used in our study, are presented in Tab. 4. The mean values and standard deviations of the variables are realistic for a dike.

Tab. 4: Examples of random variables in the limit state functions.

Variable	Type	Mean	Standard deviation/coefficient of variation
Crest height	Normal	15.90 m+NAP	(s.d.) 0.1 m
Significant wave height	Gumbel	0.2 m	(s.d.) 0.13 m
Critical overtopping discharge	Log normal	10 l/s/m	(s.d.) 10 l/s/m
Length of seepage path	Log normal	100.4 m	(v.) 0.1
Thickness of a sand layer	Log normal	25 m	(v.) 0.1
Impervious covering layer	Log normal	2 m	(v.) 0.30
Inside water level	Normal	7 m+NAP	(s.d.) 0.1 m

Fragility curves for the considered location are presented in Fig. 4. Every fragility curve was derived using Monte Carlo simulations: for a given water level, variables in the limit state function(s) Z were sampled 30,000 times; since failure arises when Z is less than zero, the probability of a failure given the load was estimated as a number of times Z is less than zero divided by the number of the Monte Carlo runs (see BUIJS et al. [2]). The simulations were done under assumption of mutual independence of all random variables.

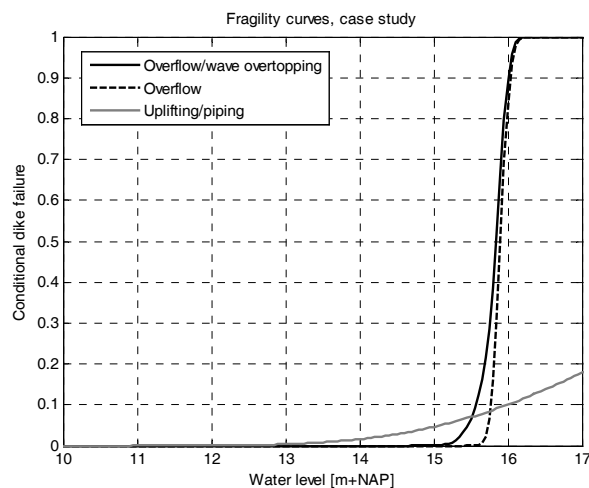


Fig. 4: Fragility curves for overflow/wave overtopping, overflow and uplifting/piping.

A few conclusions can be drawn from Fig. 4. First of all, it can be observed that uplifting/piping is a governing failure mechanism, for water levels lower than approximately 15.50 m+NAP. For higher water levels, the probability of dike failure due to overflow or overflow/wave overtopping is significantly higher than the probability of a dike failure due to uplifting/piping. Second of all, the probability of dike failure due to overflow or overflow/wave overtopping reaches critical values for water levels close to the crest level of the dike; this does not occur for uplifting/piping, since this mechanism does not depend on the height of a dike. Finally, the conditional probability of a dike failure due to overflow/wave overtopping is higher than due to (only) overflow – in case of overflow/wave overtopping, additionally, waves contribute to dike failure.

The next step in the calculation of the operational probability of a dike failure is derivation of the short-term water level density function. Recall that the decision maker is informed about the forecasted water level on the third day from now. As a result, the short-term water level density function is assumed to be normal with a mean equal to the forecasted water level 15.52 m+NAP and a standard deviation 0.30 m. The standard deviation is roughly chosen on the basis of Tab. 2.

For a given dike failure mechanism, integration of the corresponding fragility curve and short-term water level density function leads to the operational dike failure probability (see equation (3)). The probabilities, with respect to dike failure mechanisms, are presented in Tab. 5.

Tab. 5: Operational probability of dike failure for three failure mechanisms.

Failure mechanism	Operational probability of dike failure
Overflow/wave overflow	0.20
Overflow	0.12
Uplifting/piping	0.07

The operational probability of dike failure due to overflow/wave overtopping is the highest. Because of the form of the fragility curves, the probability of dike failure due to overflow/wave overtopping is higher than due to (only) overflow.

4.4 Optimal rational decision

In the evacuation decision model, the optimal decision is determined by the minimum expected cost criterion. Using the estimated costs (Tab. 3) and operational probabilities of dike failure (Tab. 5), the expected values of *a: evacuation* and *b: no evacuation* are derived, and shown in Tab. 6.

Tab. 6: Optimal decision according to the evacuation decision model for three dike failure mechanism; a: evacuation, b: no evacuation; 3 days available for the evacuation.

Failure mechanism	EV(a) [mln]	EV(b) [mln]	Decision
Overflow/wave overflow	124.3	874.5	a: evacuation
Overflow	117.2	507.7	a: evacuation
Uplifting/piping	113.7	321.2	a: evacuation

Since for every considered failure mechanism the expected value of evacuation is smaller than the expected value of no evacuation, the decision *a: evacuation* is indicated as optimal by the model. Thus, on the basis of this rational approach, the decision maker should evacuate the area.

5 Conclusions, remarks and discussion

In many situations, computation of operational probability of a dike failure cannot be only restricted to the overflow failure mechanism; a dike can fail due to other failure mechanisms. Indeed, in the case study the probability of a dike failure due to overflow/wave overtopping is higher than due to the other mechanisms. Application of the operational probabilities of dike failure, according to the formula (3), leads to improvement of the probabilistic evacuation decision model.

Other conclusions, remarks and discussion points following from our study are:

- In FRIESER [4] some variations of the probabilistic evacuation model (delay of evacuation is taken into account) are given. Application of such an approach can lead to other decision.
- In our study, the evacuation decision model was implemented for three dike failure mechanisms (three probabilities). The indicated optimal decision was the same in every situation; however, this is not always the case. In general, the probability of occurrence of single failure mechanisms and relations between them lead to the probability of the main event, i.e. a dike failure. A future work will consider implementation of a total dike failure probability in the evacuation decision model. Moreover, in the case study, we assume that the random variables are independent, what leads to *basic* Monte Carlo simulations. If dependence is of importance, other calculation routines (like e.g. FORM, see TAW [13]) are used.
- The presented model does not take into account possible changes in the decision caused by trend of water level forecast. More precisely, if the model (based on a point water level forecast) indicates evacuation and the trend of the water level forecast decreases, then *no evacuation* decision may be more reasonable. Consideration of the trend influence is a subject of future work.
- The short-term water level density function is assumed to be normal. In VAN SCHROJENSTEIN LANTMAN [9] the normality has been proven for a dataset of observed and corresponding forecasted water levels (forecast model FloMaas for the river Meuse). However, the assumption of normality is debatable. In fact, the type of the density function changes with actual circumstances. Here, an example of an ensemble forecasting approach (used for generation of probability forecast) can be given; usually the quantiles of the probability forecast do not correspond with the quantiles of a normal distribution.
- The historical forecast errors provide information about accuracy of a forecast model. Moreover, the errors can be used to estimate bias in the forecast model; e.g. the model can on the average forecasts 4 cm too low water levels 2 days ahead. The bias is not included in the considered definition of the short-term water level density function.
- The presented evacuation decision model constitutes a rational tool, which can assist in

operational decision-making. An advantage of the model is that uncertainties (in dike failure) are mathematically included in it. It is important to say that the model can be applied as a support (source of additional information) in a real-life situation. However, the model cannot replace the usual decision-making, where often intuition is taken into account. In VAN SCHROJENSTEIN LANTMAN [9] a study is carried out, which shows that adjusting of a forecast model outcome by experts leads usually to improvements. This shows that expertise can indeed have a positive influence.

6 Acknowledgement

This research is part of the Flood Control 2015 program. The program is partly funded by the Dutch Ministry of Transport, Public Works and Water Management. For more information please visit <<http://www.floodcontrol2015.com>>.

Literature

- [1] Bezuyen, M.J.; van Duin, M.J.; Leenders, P.H.J.A.: Flood Management in The Netherlands, *Australian Journal of Emergency Management*, winter 1998
- [2] Buijs, F.; Simm, J.; Wallis, M.; Sayers, P.: *Performance and Reliability of Flood and Coastal Defences*, Joint Defra/EA Flood and Coastal Erosion Risk Management R&D Programme, R&D Technical Report FD2318/TR1, August 2007
- [3] Buijs, F.; Simm, J.; Wallis, M.; Sayers, P.: *Performance and Reliability of Flood and Coastal Defences*, Joint Defra/EA Flood and Coastal Erosion Risk Management R&D Programme, R&D Technical Report FD2318/TR2, August 2007
- [4] Frieser, B.I.: *Probabilistic Evacuation Decision Model for River Floods in the Netherlands*, Master's thesis, Delft University of Technology & Ministerie van Verkeer en Waterstaat Rijkswaterstaat, Delft, June 2004
- [5] ter Horst, W.L.A.: *The Safety of Dikes during Flood Wave, Analysis of the Failure Probability of Dike Ring Areas in Flood Wave Situations*, Master's thesis, Delft University of Technology & Ministerie van Verkeer en Waterstaat Rijkswaterstaat, Delft, February 2005
- [6] INT: *Interview with Mieke Bloemendaal*, mayor of Culemborg in 1995 (in Dutch), <http://www.burgemeesters.nl/bloemendaal>
- [7] INT: *Interview with Ed van Tellingen*, mayor of Tiel in 1995 (in Dutch), <http://www.burgemeesters.nl/vantellingen>
- [8] van der Meer, J.W.; ter Horst W.L.A.; van Velzen, E.H.: Calculation of fragility curves for flood defence assets, *Flood Risk Management: Research and Practice* – Samuels et al. (eds), © 2009 Taylor & Francis Group, London, ISBN 987-0-415-48507-4

- [9] van Schroyen Lantman, J.: *Hoogwatervoorspellingen op de Maas in crisissituaties* (in Dutch), Master's thesis, Twente University of Technology, Enschede, February 2004
- [10] Sprokkereef, E.: *FloRIJN 2000* (in Dutch), report no. 2001.060, RIZA, 2001 Lelystad
- [11] Steenbergen, H.M.G.M.; Vrouwenvelder A.C.W.M.: *Theoriehandleiding PC-Ring, Versie 4.0, Deel A: Mechanismenbeschrijving* (in Dutch), TNO Bouw, DG Rijkswaterstaat, projectnummer 006.11831, April 2003
- [12] TAW: *Fundamentals on Water Defences*, Technical advisory committee on water defences, January 1998
- [13] TAW: *Probabilistic design of flood defences*, Technical advisory committee on water defences, report 141, June 1990

Determination of safety levels for quay wall structures

J. Böckmann¹, J. Grünberg¹

¹ Institute of Concrete Construction, Leibniz Universität Hannover, Germany

Abstract: Construction types of quay walls all over the world depend on the location of the port, the dimensions of the ships and the soil conditions in the harbour. With the ongoing progress of trade and the simultaneous increase of the ship dimensions, engineers have to realise the changing conditions for quay wall structures using new innovative design approaches.

The safety requirements are achieved by safety factors regulated in codes and recommendations. The safety factors in codes are mostly determined by experiences. A verification of the safety factors is possible using probabilistic analyses.

The limit state of bending of anchored diaphragm walls is examined in a probabilistic analysis. The results for the reliability index are compared with the target value of the safety category.

High investment costs will be required for the construction of quay walls also in future. An adjusted safety concept for quay walls offers the basis for a construction method as efficient as possible complying with the required safety standards.

1 Introduction

1.1 Current state

The aim of the new design concepts is to offer a design basis satisfying the safety requirements. Traditional design was based on deterministic design approaches. The application of full probabilistic approaches for the design of structures is very complicated and involves a great effort for the planning civil engineers. For this reason the new national and European standards are based on semi-probabilistic approaches. In 1988, the Construction Products Directive [9] was published. Based on this directive, the European Codes for Structural Engineering have been developed under the leadership of the European Committee for Standardization (CEN). The European Commission has produced strong recommendations to Member States regarding the implementation of Eurocodes [8]

[10]. Each Member State shall implement ENs as National Standards by publication of equivalent texts. Each National standard will be composed of the EN Eurocode text, generally followed by a National Annex. The National Annex may contain information on those parameters which are left open in the Eurocodes for national choice, the Nationally Determined Parameters (NDPs), to be used for the design of buildings and civil engineering works to be constructed in the country concerned.

For the design of quay wall structures the following European standards are relevant. In Eurocode 2 [3] the design of concrete structures and in Eurocode 7 [5] the geotechnical design is regulated. For Eurocodes 2 and 7 the national German annexes are available as draft standards [4] [6]. The safety concept of the current German standards for the geotechnical design (DIN 1054) and for the design of concrete structures (DIN 1045-1) is adjusted to the new European standards (Eurocodes 7 and 2). For the specific design of quay walls further recommendations are available in Germany. Most important is the recommendation called EAU [12] which is edited by the German Port Construction Association (Hafenbau Technische Gesellschaft). The specifications for calculation and design regulations in EAU [12] significantly are the results of years of experience in foundation and harbour engineering. The last version of the EAU [12] was published in 2004, and best fit with European standards was aimed. In the current German standards (DIN 1054, DIN 1045-1), partial factors are applied to the action effects and to the resistances. The partial factors should be based on probabilistic analysis, but probabilistic verifications of the partial safety factors for the dimensioning of quay walls are rare. Therefore, partial factors for the design of quay walls are based on experience.

For this reason, an examination should be carried out whether the applied safety factors satisfy the safety requirements. The new national and European semi-probabilistic design is based on the approach that a design must satisfy a defined minimum probability of failure. For the probabilistic design all input parameters are considered stochastic. Adjusted and assured partial safety factors for semi-probabilistic design concepts can be derived by the probabilistic analysis of quay walls. The safety requirements are presented by safety levels that are expressed in a reliability index. These safety levels are defined for example in EN 1990 [7]. The acceptable probability of failure decreases with the raising consequences of failure. The selection of the target safety index for quay walls is described in chapter 2.4.

The results presented in this paper relate to the structural analysis of a diaphragm wall construction. The ultimate limit state of the bending load capacity is investigated. The influence of the incoming stochastic variables is studied with regard to the safety level.

2 RELIABILITY THEORY

2.1 Basic principles

The probability of failure can be calculated for each limit state by means of a probabilistic analysis in which the input parameters are considered stochastic. The stochastic modeling of the input parameters, their distributions and characteristic values are chosen on the basis of data determined from laboratory experiments or from in-situ measurements. The realistic estimation of the statistical input parameters and the choice of their distribution influence the calculation of probability significantly.

The basic principles of the reliability theory are available in numerous publications, for example Faber [14]. The probability of failure is determined for several variables through the following n-dimensional integral (1).

$$P_F = \int \dots \int f_x(x_1, \dots, x_n) dx_1 dx_2 \dots dx_n \tag{1}$$

with $f_x(x_1, \dots, x_n)$ probability density function of the vector of basic random variables

2.2 Solution procedures in the reliability theory

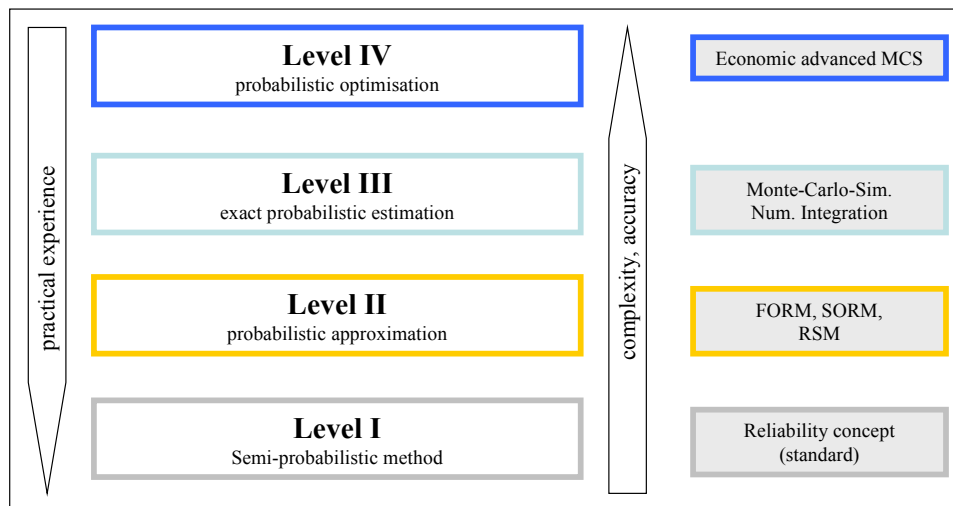


Fig. 1: Level of sophistication (Hansen [17]).

Generally, there is no analytic solution of the multi-dimensional integral shown in equation (1). Therefore, approximate solutions and simulation solutions shall be used. Solution procedures in the reliability theory may be classified according to their accuracy and complexity, figure 1. A detailed description of the procedures with their advantages and disadvantages is given in Hansen [18].

The First Order Reliability Method (FORM) and Second Order Reliability Method (SORM) allow for deriving values for the partial safety factors. FORM and SORM are used in the scope of this study. The results were verified by the Monte Carlo method with Importance Sampling (MCMIS). A comparison of the results is presented in chapter 4.3. The Variables Processor (VaP 2.3) [11] is used for the probabilistic analyses.

2.3 Derivation of safety elements

Partial safety factors are calculated according to the following approach (3) with regard to the coefficients of variation (V_i). Furthermore, the sensitivity factors α_i and the reliability index β are required. FORM and SORM enable the calculation of the probability of failure p_f , of the reliability index β and of the sensitivity factors for actions α_E and for resistances α_R .

$$k_E = -\Phi^{-1}(q) \qquad k_R = -\Phi^{-1}(q) \qquad (2)$$

$$\gamma_E = \frac{1 + \beta \cdot \alpha_E \cdot v_E}{1 + k_E \cdot v_E} \qquad \gamma_R = \frac{1 - k_R \cdot v_R}{1 - \beta \cdot \alpha_R \cdot v_R} \quad (\text{normal distributed}) \qquad (3)$$

$$\gamma_E \cdot E \leq \frac{R}{\gamma_R} \qquad (4)$$

2.4 Target reliability and margin of safety

The target safety index shall represent the failure probability with an optimum relation between the consequences to be expected with a failure of the building and the relative cost of structural safety.

Basic criteria for the selection of the target reliability, which are also adopted in actual design standards and recommendations are summarised in figure 2. Different methods are used for the choice of target value of the reliability index according to Oumeraci et al. [19].

- Agreement on "reasonable value"
- Code Calibration (documentation of accepted practice)
- Cost Optimization over structure life time

Different target reliability indexes are derived from examinations and published in codes and recommendations. The target values of the reliability index presented in [7] [15] depend on consequences of the construction failure, therefore three consequence classes are defined, table 1.

For the quay walls examined in the scope of this study we act on the assumption that high economic damage will result from failure, but only little to medium risk for human life. Therefore, a classification into the consequence class 2 according to EN 1990 [7] [15] with a medium risk for loss of life and considerable economic, social or environmental harmful

consequences does make sense. For the quay walls examined in this study a target value of the safety index of $\beta = 3.8$ is used for a reference period of 50 years according to EN 1990 (consequence class 2) [7] [15].

This assumption is in accordance with the Dutch code NEN-6700. The safety categories 1 to 3 in NEN-6700 are almost similar to the consequence classes defined in EN 1990 [7], table 1. In [16] is assumed, that failure of larger quay structures will cause considerable economic damage, but risk to human life will remain low. This results in a placement of this type of structure in safety category 2 (reliability index $\beta = 3.4$, reference period of 50 years, NEN-6700). Under unusual circumstances the quay is placed in safety category 3, for example if it forms part of a flood defence. For Safety category 3, Rijkswaterstaat takes a β -value of 4.5 in the Netherlands [16].

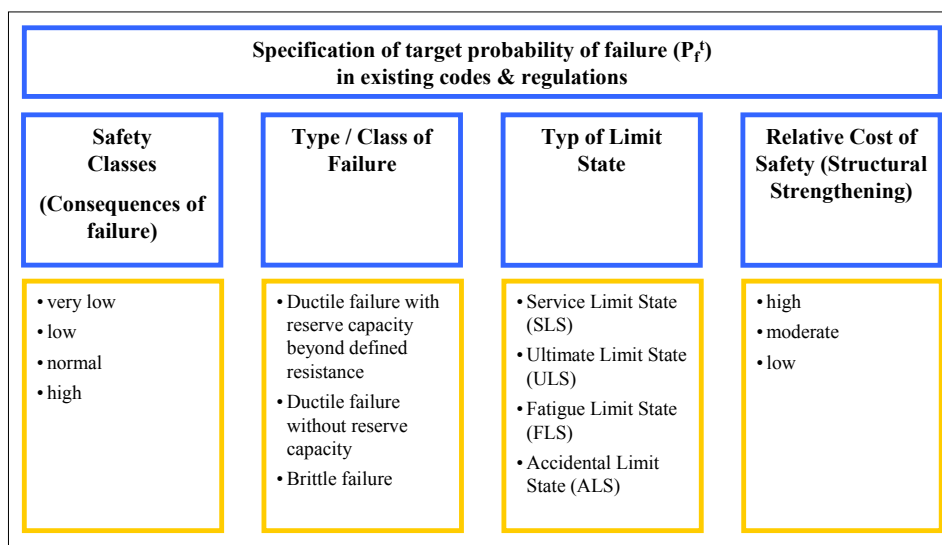


Fig. 2: Criteria for adopting target probabilities of failure in existing codes and regulations, Oumeraci et al. [19].

Tab. 1: Consequence classes, EN 1990 [7].

Consequence class	Characteristics	Examples
CC 3	high risk to human life <u>or</u> large economic, social or environmental consequences	tribune, public buildings with high consequences of failure (for example concert hall)
CC 2	medium risk for human life, considerable economic, social or environmental consequences	office and apartment buildings, public buildings with medium consequences of failure
CC 1	small risk for human life <u>and</u> small or negligible economic, social or environmental consequences	agricultural structures without regular presence of persons (for example barn, greenhouse)

2.5 Limit States for the Diaphragm Wall

The essential limit states for structural and geotechnical failure of diaphragm walls are presented in figure 3. The examination in this article refers to the ultimate limit state of the bending load capacity.

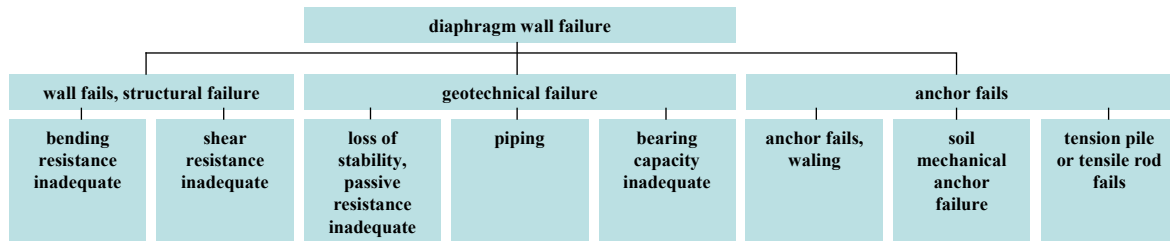


Fig. 3: Limit states for structural and geotechnical failure of the diaphragm wall.

3 MODELLING

3.1 Mechanic model – diaphragm wall

The results for the diaphragm wall are presented for the ultimate limit state of the bending load capacity. The system and material parameters were also used in [13] for a probabilistic analysis of the limit state of bending. The diaphragm wall was designed according to DIN 1045-1 [1], the internal forces were calculated by a girder model with fixed supports [22], see figure 4. The embedment depth d is varied, so that different degrees of restraint of 25%, 50% and 75% exist. Due to the high bending stiffness of the wall, full restraint cannot be achieved for a system with upper anchorage. A homogenous soil is assumed with varying material properties, table 2.

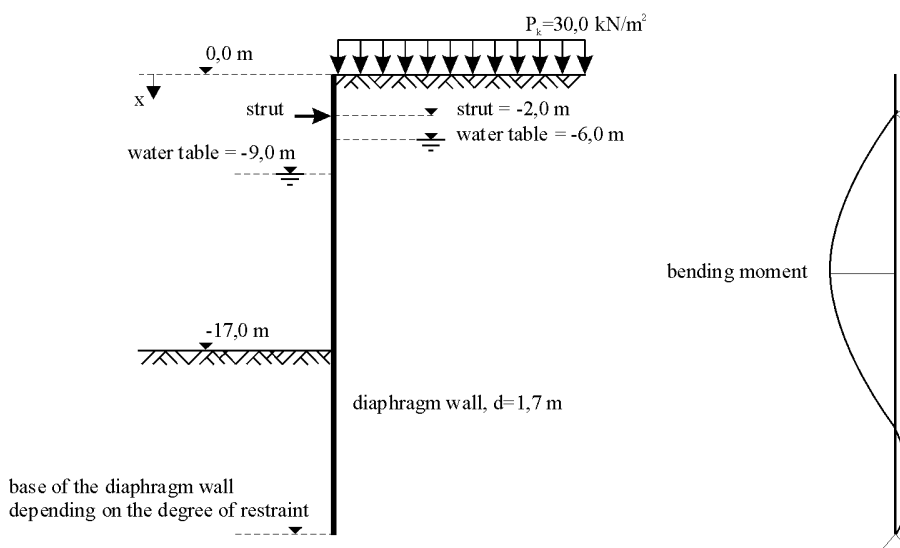


Fig. 4: Geometry of the diaphragm wall.

3.2 Stochastic model - diaphragm wall

The basic variables presented in table 3 are assumed for the probabilistic analysis. Several types of distribution were examined for the surface load P, and a logarithmic formula was used here. The basic variables are the same variables chosen in [13] for the probabilistic analysis.

Two different equations for describing the limit state of the capacity of bending are used in [13]. The first approach (action effect (6) and resistance (10)) does not consider a normal force. The normal force is neglected. In the second approach (action effect (7) and resistance (11)) the limit state equation was derived such, that a normal force is included for the probabilistic calculation. For simplification, the imposed load N_E is taken from the structural design and the design value of N_E is assumed as a deterministic variable in the probabilistic analysis in [13]. Additionally, the results for the limit state (5) are calculated under consideration of the normal force depending on its basic variables (action effect (8) and resistance (12)). The results of the reliability index according to the resistances (6), (7) and (8) and the action effects (10), (11) and (12) are compared. The derivation of the resistance for the limit state (5) under consideration of the normal force is given in equation (13) to (18). Note: Action effects and resistances are expressed for slab sections of unit width $b = 1.0$.

$$G(R, E) = R - E \quad (5)$$

action effect:

model neglecting normal force:

$$E = m_e \cdot (M_E(\gamma, \gamma', P, \varphi, c, \Delta h)) \quad (6)$$

model including normal force
(deterministic variable N_E , simplified approach):

$$E = m_e \cdot (M_E(\gamma, \gamma', P, \varphi, c, \Delta h) - N_E \cdot (h/2 - d_1)) \quad (7)$$

model including normal force
(variable N_E depending on the basic variables, exact approach):

$$E = m_e \cdot (M_E(\gamma, \gamma', P, \varphi, c, \Delta h) - N_E(\gamma_B, \gamma, \gamma', P, \varphi, c, \Delta h) \cdot (h/2 - d_1)) \quad (8)$$

resistance: $R = m_r \cdot (M_{R1} + M_{R2}(\gamma', \varphi, c)) \quad (9)$

model neglecting normal force:

$$M_{R1}(A_s, f_y, d, k_a, \alpha_R, f_c, b) = (A_s \cdot f_y) \cdot d \cdot \left[1 - k_a \cdot \frac{(A_s \cdot f_y)}{\alpha_R \cdot f_c \cdot b \cdot d} \right] \quad (10)$$

model including normal force
(deterministic variable N_E , simplified approach):

$$M_{R1}(A_S, f_y, d, k_a, \alpha_R, f_c, b, N_E) = (A_S \cdot f_y - N_E) \cdot d \cdot \left[1 - k_a \cdot \frac{(A_S \cdot f_y - N_E)}{\alpha_R \cdot f_c \cdot b \cdot d} \right] \quad (11)$$

model including normal force
(variable N_E depending on the basic variables, exact approach): (12)

$$\begin{aligned} & M_{R1}(A_S, f_y, d, k_a, \alpha_R, f_c, b, \gamma_B, \gamma, \gamma', P, \varphi, c, \Delta h) \\ &= (A_S \cdot f_y - N_E(\gamma_B, \gamma, \gamma', P, \varphi, c, \Delta h)) \cdot d \cdot \left[1 - k_a \cdot \frac{(A_S \cdot f_y - N_E(\gamma_B, \gamma, \gamma', P, \varphi, c, \Delta h))}{\alpha_R \cdot f_c \cdot b \cdot d} \right] \end{aligned}$$

with M_{R1} internal resistance moment
 M_{R2} : resistance moment M_R considering the ground resistance, calculated according to [22]
 M_E : action moment M_E considering the ground actions and surface loads, calculated according to [22]
 N_E : normal force

Derivation of equation (11) and (12):

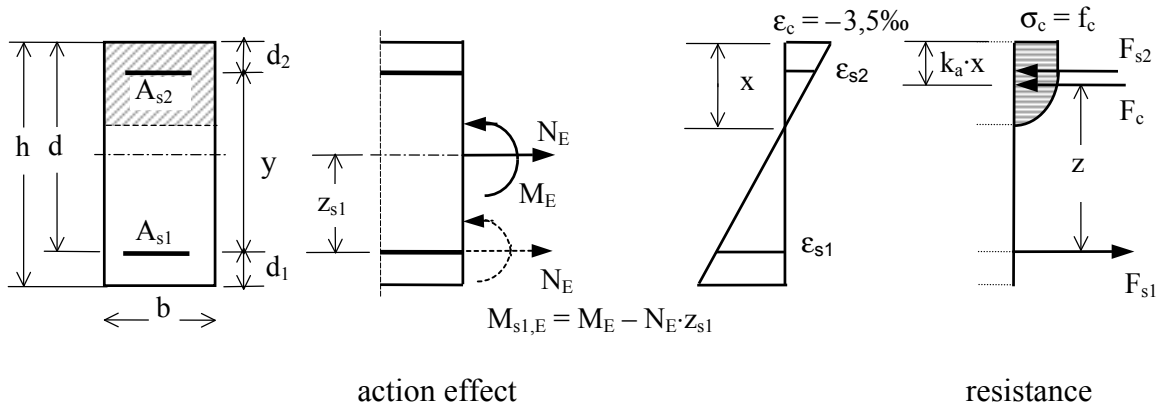


Fig. 5: Equilibrium for the bending capacity.

$$M_{R1} = M_{s1,E} = F_c \cdot z + F_{s2} \cdot (d - d_2) \quad (13[M1])$$

$$= \alpha_R \cdot b \cdot x \cdot f_{cd} \cdot z + A_{s2} \cdot f_y \cdot (d - d_2)$$

$$N_E = -F_c - F_{s2} + F_{s1} \quad (14[M2])$$

$$= -\alpha_R \cdot b \cdot x \cdot f_c - A_{s2} \cdot f_y + A_{s1} \cdot f_y$$

$$x = \frac{-N_E - A_{s2} \cdot f_y + A_{s1} \cdot f_y}{\alpha_R \cdot b \cdot f_c} \quad (15)$$

$$\text{assumption: } z \approx d - k_a \cdot x \quad (16_{[M3]})$$

$$y = (d - d_2) \approx 0,75 \cdot d$$

$$\begin{aligned} M_{s1,E} &= \alpha_R \cdot b \cdot x \cdot f_c \cdot z + A_{s2} \cdot f_y \cdot (d - d_2) \\ &= \alpha_R \cdot b \cdot x \cdot f_c \cdot (d - k_a \cdot x) + A_{s2} \cdot f_y \cdot 0,75d \end{aligned} \quad (17)$$

$$\begin{aligned} M_{s1,E} &= \alpha_R \cdot b \cdot \left(\frac{-N_E - A_{s2} \cdot f_y + A_{s1} \cdot f_y}{\alpha_R \cdot b \cdot f_c} \right) \cdot f_c \cdot \left(d - k_a \cdot \left(\frac{-N_E - A_{s2} \cdot f_y + A_{s1} \cdot f_y}{\alpha_R \cdot b \cdot f_c} \right) \right) \\ &\quad + A_{s2} \cdot f_y \cdot 0,75d \end{aligned} \quad (18)$$

without compressive reinforcement:

$$M_{s1,E} = (-N_E + A_{s1} \cdot f_y) \cdot d \cdot \left(1 - k_a \cdot \left(\frac{-N_E + A_{s1} \cdot f_y}{\alpha_R \cdot b \cdot f_c \cdot d} \right) \right)$$

Tab. 2: Soil parameters

		soil 1	soil 2	soil 3
friction angle	φ	32,5	30	27,5
cohesion	c	0	5	10

Tab. 3: Probabilistic models for basic variables.

Basic variable	Symbol	Distr.	Mean	CoV
Model action factor	m_e (me)	N	1,0	0,1
Model resistance factor	m_r (mr)	N	1,0	0,08
Specific weight concrete	γ_B (gammaB)	N	24 kN/m ³	0,04
Surface load	P (P)	LN	*)	0,4
Specific soil weight (dry)	γ (gamma2)	N	20 kN/m ³	0,05
Specific soil weight (saturated)	γ' (gamma2a)	N	12 kN/m ³	0,05
Angle of friction	φ (phi)	LN0	see table 2	0,075
Cohesion	c (c)	LN	see table 2	0,25
Difference of water level	Δh (deltah)	N	3 m	0,12
Concrete strength	f_c (fc)	LN	fck+8 N/mm ²	0,13
Steel yield stress	f_y (fy)	LN	560 N/mm ²	0,053
coefficient ¹	α_R (alphar)	N	0,8095	0,1
coefficient ²	k_a (ka)	N	0,416	0,1
Reinforcement	A_s (As)	N	$A_{s,nom}$	0,025

N –normal distribution; LN0 –lognormal distribution with the lower bound at the origin;

LN –lognormal distribution

1 coefficient describing the form of the parabola-rectangle diagram for concrete

2 coefficient for the contact point of the compressive force

*) see equation (19)

Mean value of the surface load, table 3:

$$m_Q = \frac{Q_k}{\exp\left(-0,5 \cdot \ln(1+v^2) + \Phi^{-1}(q) \cdot \sqrt{\ln(1+v^2)}\right)} \quad \text{with } q = 0,98 \quad (19_{[M4]})$$

4 Results

4.1 Reliability index for the limit state of bending

In figure 6 the reliability indices are shown depending on the distance from the top of the diaphragm wall. The lowest β -values result at the level of the diaphragm wall with the decisive design moment.

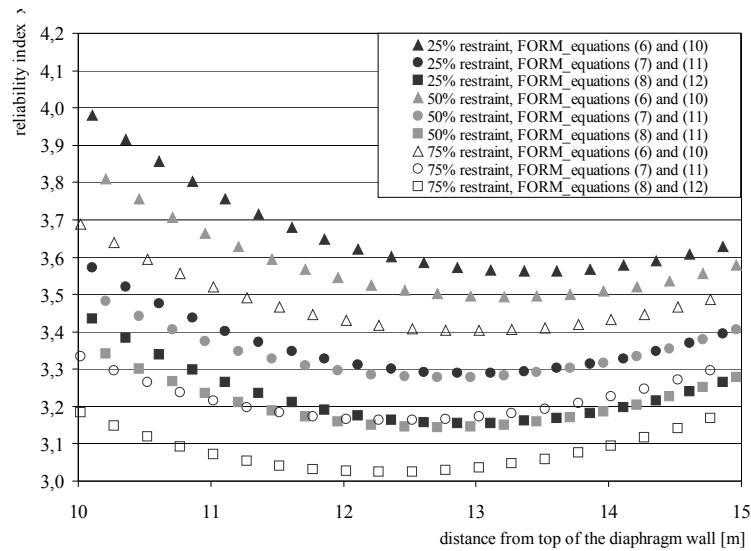
Generally, the results of the reliability index calculated with the approach neglecting normal force (equations (6) and (10)) are higher than the results calculated with the approaches including the normal force, figure 6. In case of normal forces included, β -values calculated with the simplified approach (equations (7) and (11)) exceed the results calculated with the exact approach (equations (8) and (12)), figure 6. These trends are independent of the chosen soil parameters and the embedment depth.

Comparing the approaches including the normal forces, the differences between the reliability indices obviously are caused by the additional influence of the corresponding stochastic basic variables in case of the exact approach (equations (8) and (12)).

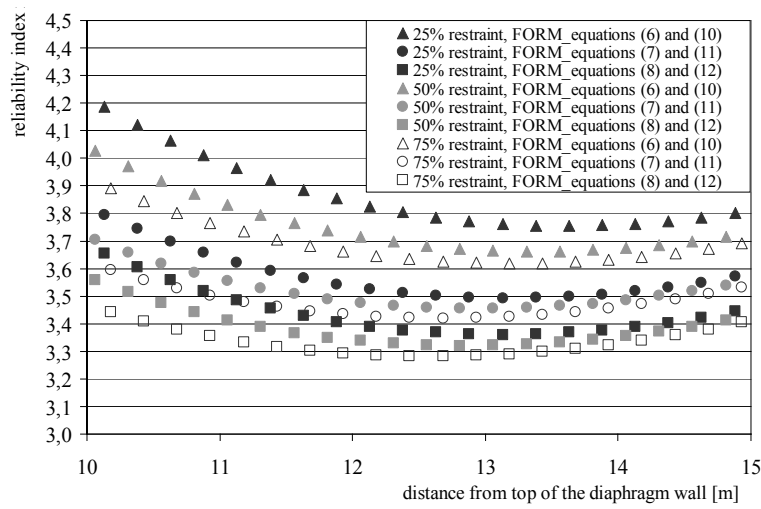
The high β -values calculated with the approach neglecting normal forces depend on the mean value of the basic variable A_s . For the reinforcement A_s , the design value calculated with DIN 1045-1 is used as mean value in the probabilistic analysis. The design leads to higher values for A_s if the normal forces are neglected. In the probabilistic analysis with equations (6) and (10) the mean value of A_s is assumed higher than in the calculation according to (7), (8), (11) and (12). For this reason, the β -values of the calculation neglecting normal forces exceed the other results, figure 6.

Figure 7 shows the results of the probabilistic analysis assuming an uniform mean value of A_s for all three approaches. In contrast to the results presented in figure 6, the calculation with an uniform value A_s yields the lowest β -values with equation (6) and (10). This is due to the fact, that a compressive normal force leads to a decrease of the required reinforcement and therefore to a safety level.

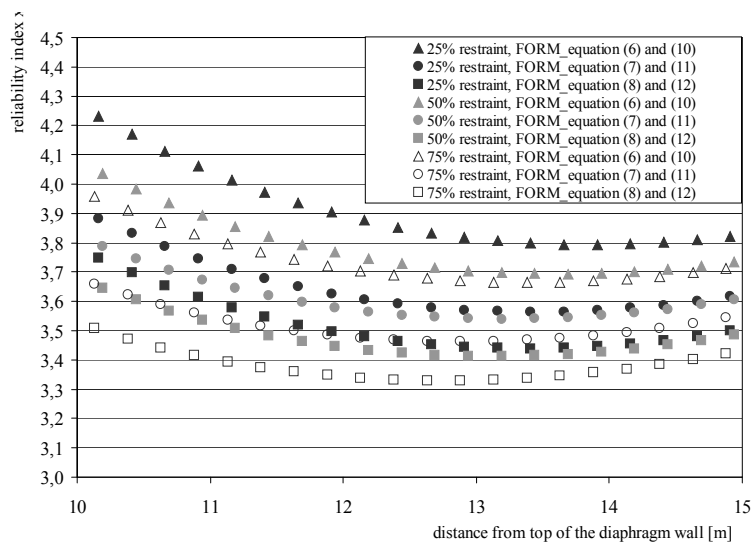
In dependence on the degree of restraint and the chosen soil parameters a minimal reliability index of among ~ 3.0 to ~ 3.5 is calculated using the exact approach. This result is less than the target value of the reliability index ($\beta = 3.8$) determined in chapter 2.4.



A: soil 1



B: soil 2



C: soil 3

Fig. 6: Reliability index calculated with different equations for the limit state depending on the consideration of normal force (A: soil 1, B: soil 2, C: soil 3, see table 2).

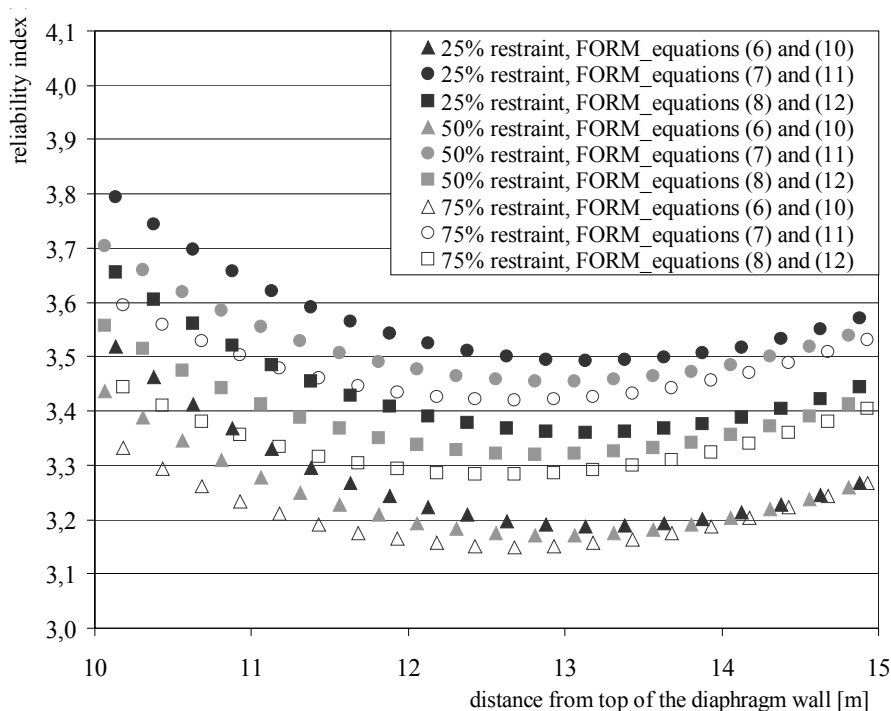


Fig. 7: Reliability index calculated depending on the consideration of normal force and the parameters of the basic variable A_s (soil 2).

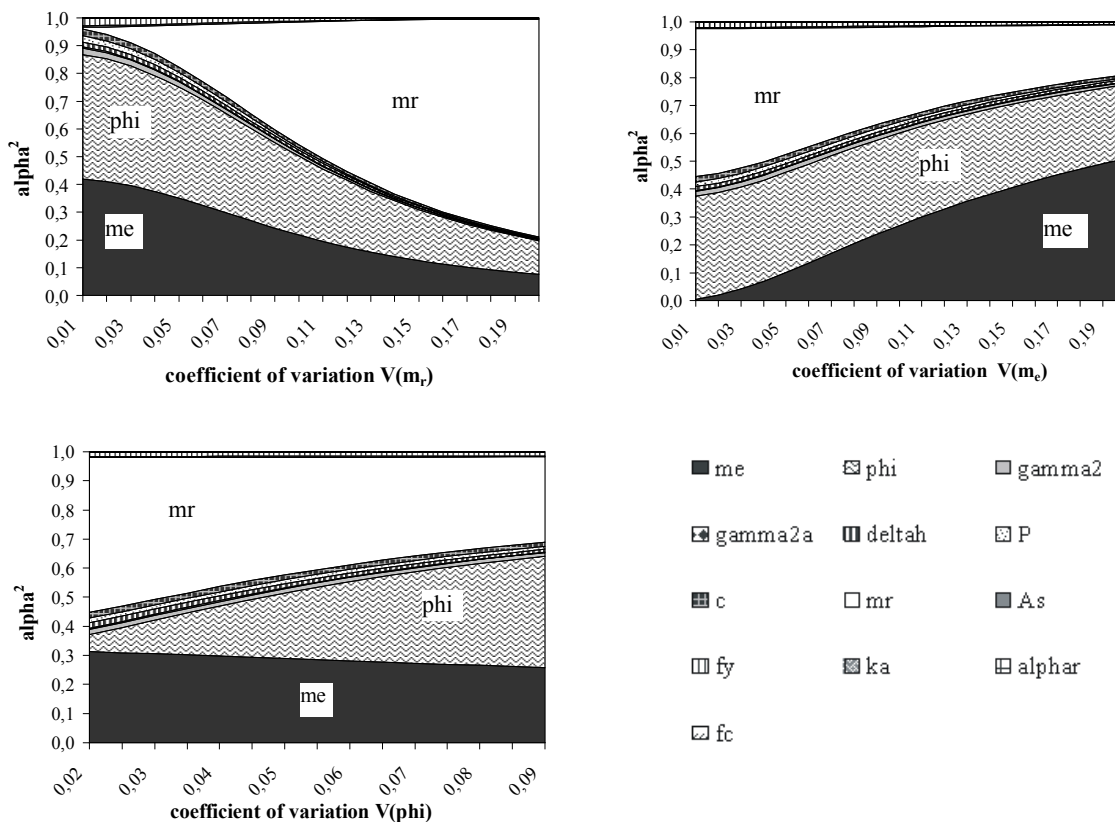


Fig. 8: Weighting factors against the variation coefficients of model factors m_e , m_r and ϕ (soil 2, 50% restraint $_{[M5]}$).

4.2 Influence of the basic variables

The influence of the basic variables is depicted by weighting factors α_i . The variables φ (angle of friction), m_r (model resistance factor) and m_e (model action factor) are the variables with the largest weighting factors for the probabilistic analysis analysing the limit state of bending. The weightings of the basic variables depending on the change of the variation coefficients of the basic variables $V(\varphi)$, $V(m_r)$ and $V(m_e)$ are shown in figure 8. Any change of the variation coefficients of the basic variables $V(\varphi)$, $V(m_r)$ and $V(m_e)$ clearly influences the failure probability.

4.3 Comparison of different solution procedures

The solution procedures FORM, SORM and MCMIS are used for the calculation of probabilities of failure for the bending load capacity, see 2.2. While the results calculated with FORM and SORM are almost the same, the results for the probability of failure p_f and the reliability index β applying to MCMIS differ from FORM/SORM, figure 9. The deviation of the reliability index β by approximately ~ 0.07 is very small. Therefore, the agreement of the three different solution methods FORM, SORM and MCMIS is acceptably.

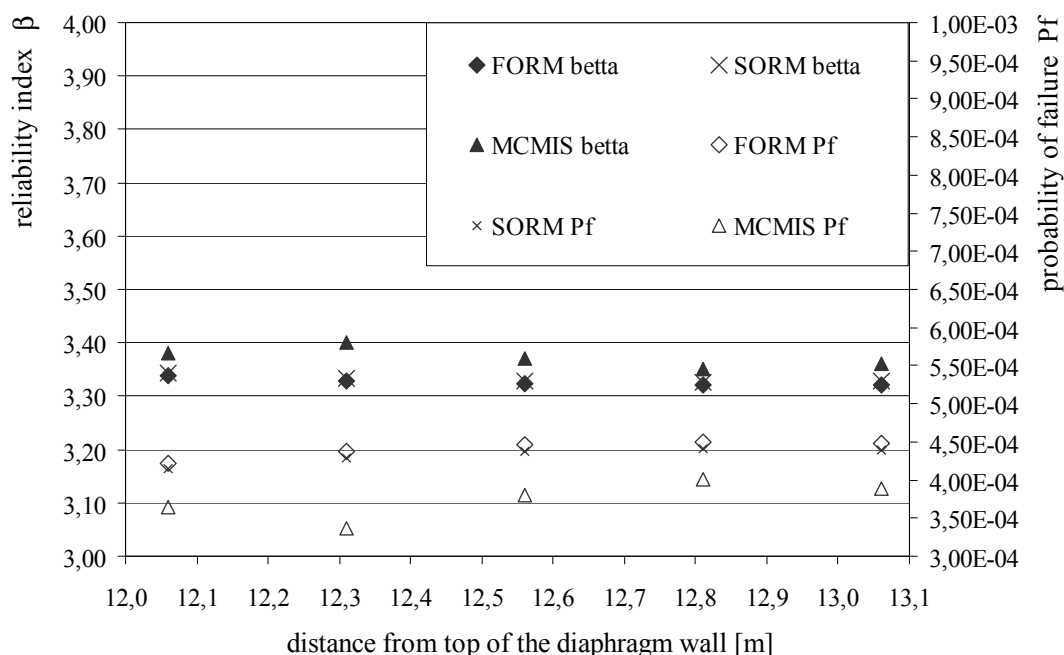


Fig. 9: Comparison of the reliability indices β and the probabilities of failure p_f calculated with three solution procedures FORM, SORM and MCMIS (soil 2, 50% restraint).

5 Conclusions and recommendations

- The achieved safety level for the limit state of bending load capacity significantly depends on the selection of the distribution of the basic variables and their stochastic parameters for a quay wall constructed as diaphragm wall. The failure probability reacts in a very sensitive way particularly to the change of the variation coefficients $V(\varphi)$, $V(m_r)$ and $V(m_e)$.
- The reliability index changes depending on the assessed type of ground, particularly characterized by the existing friction angle and the cohesion.
- The influence of the normal force on the limit state of the load bearing capacity for bending is examined applying a probabilistic analysis. Overall, a reliability index of 3.8, which was required as target value, cannot be verified for the exact approach. As the safety factors published in actual codes are based on years of experience the calculated safety level seems to be satisfactory. Quay walls do not fit in the available consequence classes presented for example in [7], table 1. Further studies of variables and analyses of different limit modes are necessary to fix the target value of the reliability index for quay walls.

6 References

- [1] DIN 1045/1-08: *Tragwerke aus Beton, Stahlbeton und Spannbeton – Teil 1: Bemessung und Konstruktion*. Deutsches Institut für Normung (Hrsg.). Berlin, Köln: Beuth, August 2008.
- [2] DIN 1054/1-05: *Baugrund – Sicherheitsnachweise im Erd- und Grundbau*. Deutsches Institut für Normung (Hrsg.). Berlin, Köln: Beuth, Januar 2005.
- [3] DIN EN 1992-1-1 – *Eurocode 2: Bemessung und Konstruktion von Stahlbeton- und Spannbetontragwerken – Teil 1-1: Allgemeine Bemessungsgrundlagen und Regeln für den Hochbau*. Ausgabe 10.05
- [4] DIN EN 1992-1-1/NA – *Eurocode 2: Bemessung und Konstruktion von Stahlbeton- und Spannbetontragwerken – Teil 1-1: Allgemeine Bemessungsgrundlagen und Regeln für den Hochbau*. Nationaler Anhang (Deutschland), Entwurf, Ausgabe 09.08
- [5] DIN EN 1997-1 – *Eurocode 7: Entwurf, Berechnung und Bemessung in der Geotechnik – Teil 1: Allgemeine Regeln*. Ausgabe 10.05
- [6] DIN EN 1997-1/NA – *Eurocode 7: Entwurf, Berechnung und Bemessung in der Geotechnik – Teil 1: Allgemeine Regeln*. Nationaler Anhang (Deutschland), Entwurf, Ausgabe 02.09
- [7] EN 1990: *Eurocode: Grundlagen der Tragwerksplanung*. Deutsche Fassung EN 1990:2002. Deutsches Institut für Normung (Hrsg.). Berlin, Köln: Beuth, Oktober 2002.

- [8] Commission Recommendation of 11 December 2003 on the implementation and use of Eurocodes for Construction Works and Construction products. Office of the European Union pp L 332/62 – 63.
- [9] Council Directive of 21 December 1988 on the approximation of laws, regulations and administrative provisions of the Member States (89/106/EEC). Official Journal of the European Communities, L40 of 11 February 1989, pp 12–26.
- [10] Guidance Paper L (concerning the Construction Products Directive – 89/106/EEC) – Application and Use of Eurocodes. European Commission, Enterprise Directorate-General, 2004.
- [11] PSP - Petschacher Software und Projektentwicklungs GmbH, Variables Processor (VaP 2.3), Feldkirchen, Österreich.
- [12] *Recommendations of the Committee for Waterfront Structures, Harbours and Waterways* - EAU 2004 / issued by the Committee for Waterfront Structures of the Society for Harbour Engineering and the German Society for Soil Mechanics and Foundation Engineering, 2005.
- [13] Böckmann, J.; Grünberg, J.: *Reliability for quay wall structures*. IABSE-fib Conference, Dubrovnik, Croatia, May 3-5, 2010 (submitted for full-paper acceptance).
- [14] Faber, M. H.: *Risk and Safety in Civil, Environmental and Geomatic Engineering*. Eidgenössische Technische Hochschule Zürich, 2008.
- [15] Grünberg, J.: *Comments on EN 1990 „Basis of Structural Design“*, Guidelines for implementation and application. Beuth Verlag, Berlin 2007
- [16] Handbook Quay Walls. Centre for Civil Engineering Research and Codes (CUR), Taylor and Francis, 2005.
- [17] Hansen, M.; Grünberg, J.: *Risk-based design approach for Offshore Wind Turbines*. Proceedings of the 6th International Probabilistic Workshop, Darmstadt, 2008.
- [18] Hansen, M.: *Zur Auswirkung von Überwachungsmaßnahmen auf die Zuverlässigkeit von Betonbauteilen*. Dissertation, Institut für Massivbau, Universität Hannover, 2004.
- [19] Oumeraci, H.; Kortenhaus, A.; Allsop, N. W. H.; De Groot, M. B.; Crouch, R. S.; Vrijling, J. K.; Voortman, H. G.: Probabilistic design tools for vertical breakwaters. Final Report, MAST III / Proverbs, 1999.
- [20] Pottharst, R.: Versagenswahrscheinlichkeit und Sicherheit von Flachgründungen als Grundlage für Bauvorschriften. Abschlussbericht T960/2, 1980.
- [21] Thurner, R.: *Probabilistische Untersuchungen in der Geotechnik mittels deterministischer Finite Elemente-Methode*. Graz, 2001.
- [22] ThyssenKrupp GfT Bautechnik, *Spundwandhandbuch Berechnung*, 2007.

A qualitative approach to assess flood risk associated with landfills

Clemens Neuhold, Hans-Peter Nachtnebel

Institute of Water Management, Hydrology and Hydraulic Engineering,
University of Natural Resources and Applied Life Sciences, Vienna

Abstract: Landfills induce a long term risk by means of potential environmental contamination due to flooding. In consequence of the complex composition of deposits as well as temporal and spatial flood characteristics there is yet no assessment standard available. This paper aims to develop a qualitative approach to assess flood risk associated with flood prone landfills at the basis of Austrian case studies. The inventory of controlled landfills and documented old waste deposits was evaluated for the federal territory of Austria. The collected data set was subsequently compared with flood risk zones. Out of 1064 screened landfills, roughly 30 % are located within or close to flood risk zones. Three representative case study areas were investigated in detail by applying a 2D hydrodynamic model to simulate flow depths and shear stress as well as by developing four chemical emission scenarios. The landfill leaching scenarios ranged from minor emissions up to total erosion of the landfill. The hydrodynamic modelling covered three hydrologic scenarios in the range of a 30-year up to a 300-year flood event. Based on four parameters representing the flood characteristics, the susceptibility to erosion (flow velocity and shear stress) as well as the estimated leaching behaviour of a saturated landfill a flood risk evaluation matrix (FREM) was elaborated to assess the ecologic risk associated with landfills qualitatively. The study outlines that in case of flooding or erosion of landfills the hazardous waste released to the environment could lead to partly tremendous ecologic damages. Further, the uncertainties associated to the considered processes were considerably high hence the derivation of a quantitative risk assessment approach would not yet lead to feasible results. However, the developed qualitative approach provides a decision support aid to identify landfills with imminent risk for humans and the environment.

1 Introduction and objectives

This paper discusses a qualitative approach to assess flood risk associated with landfills. Risk assessment aims to provide an answer to the question “what can possibly happen?” (BUWAL, 1999a). Risk is investigated as a function of the probability of an event and the consequences of that event (EU, 2007). Risk identifies the extent of a hazard and therefore, provides the basis for determining the need for action (BUWAL, 1999a).

Flood risk can be classified into (1) risk for individuals, (2) risk for property and (3) consequential risk, arising as a subsequent process (EGLI, 1996; EU, 2007; BUWAL, 1999a, b; WBGU, 1999; MERZ, 2006). This study focuses on consequential risks related to the environment. Special attention was drawn on municipal solid waste (MSW) landfills which pose a tremendous and permanent risk potential for humans and the environment (LANER et al. 2009, NACHTNEBEL et al., 2009). Due to assessed maintenance durations of 200 to 500 years depending on waste composition, climatic conditions and applied methodologies (EHRING & KRÜMPPELBECK 2001, STEGMANN & HEYER 1995, BELEVI & BACCINI 1989) even sites showing flood mitigation measures are highly likely to be inundated.

During a flood event it has to be assumed that an inundated landfill body becomes water saturated which leads to a substantial mobilisation of pollutants, since the presence of water enhances decomposition and transport processes (KLINK & HAM, 1982; BOGNER & SPOKAS, 1993; CHRISTENSEN et al., 1996). Additionally, water saturation of landfilled waste may lead to mechanical stability loss, which cause shear and sliding fractures (BLIGHT & FOURIE, 2005).

In the recent past the erosion of landfilled material and therefore the release of pollutants were monitored (HABERSACK & MOSER 2003; YOUNG et al., 2004). For instance GELLER et al. 2004 observed increased inputs of pollutants into floodplain soils and river sediments during the 2002 Elbe River flood emerging from inundated landfills. BLIGHT & FOURIE 2005 provide a review of catastrophic failures of waste landfills, highlighting the impact of such disasters on both, the environment and the population.

Hence, the objectives of this paper were:

- the collection of the inventory of controlled landfills and documented old waste deposits for the federal territory of Austria
- the evaluation of the exposure to floods
- the definition of landfill leaching scenarios as well as the analyses of release mechanisms
- the derivation of case study sites to enable the analyses on a micro scale level
- the analysis of hydrological scenarios including 2D hydrodynamic simulation runs to assess the impacts on landfills

- the interpretation of consequences on protected properties (ground water bodies, nature reserves, protected landscape, settlements, ...) due to flooding of landfills
- the assessment of the overall resulting risk for ecological goods

Consequential, a flood risk evaluation matrix (FREM) was elaborated to assess the ecological risk associated with landfills based on parameters representing the flood characteristics, the susceptibility to erosion as well as the estimated leaching behaviour of a saturated landfill.

2 Methodology

This section discusses the available database and a qualitative approach to assess flood risk related to landfills for the federal territory of Austria. Sub-steps as well as associated uncertainties are documented to allow a feasible conclusion of the significance of the derived risk assessment procedure.

2.1 Inventory of landfills and their exposure to floods

Section 2.1 describes the determination of the inventory of flood prone landfills in Austria by assessing their exposure to floods. The compilation of data sets related to landfill sites in Austria is based on information provided by the Austrian Federal Waste Management Plan (KRAMMER et al., 1992; BMFLUW, 2006a) and several waste management reports published by federal as well as local authorities (LUNZER et al., 1998; KÄRNTEN, 2000; FLÖGEL, 2002; TIROL, 2002; ROLLAND and OLIVA, 2004; BURGENLAND, 2005; NIEDERÖSTERREICH, 2005; VORARLBERG, 2005) and the collaboration with the Austrian Federal Environment Agency (AFEA, 2008).

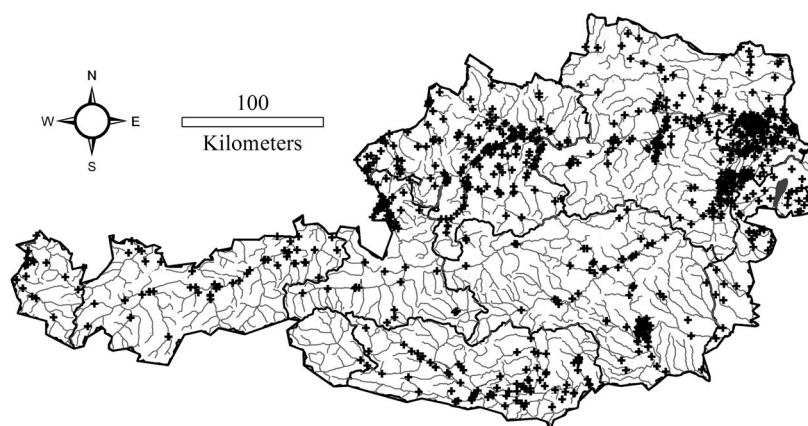


Fig. 1: Reported sites of MSW landfills in Austria (BMFLUW, 2007)

The elaborated data set of landfills in Austria comprises of 1064 locations (Fig. 1), whereas 103 sites are characterised as controlled landfills and 961 sites are identified as old deposits with overall volumes of more than 25000 m³ (AFEA, 2008).

Although the list of landfills is clearly not comprehensive – the degree of data ascertainment for old waste deposits in the AFEA database is supposed to be less than 70% (SKALA et al., 2007 – it represents an unbiased sample for the estimation of flood risk related to MSW landfills in Austria (LANER et al., 2009).

The evaluation of flood exposure is based on the HORA data set provided by the Federal Ministry of Agriculture, Forestry, Environment and Water Management (BMFLUW, 2006b; MERZ et al., 2006). This data delineates potential flood inundation zones along rivers for discharges with statistical return periods of 30, 100 and 200 years (Fig. 2). Substantial uncertainties arise due to disregarded technical flood mitigation measures and neglected processes like sediment transport, rock jam and log jam (NEUHOLD et al., 2009). The queries can therefore be characterised as an indicator for risk potentials, considering residual risk by means of failure of structural mitigation measures.

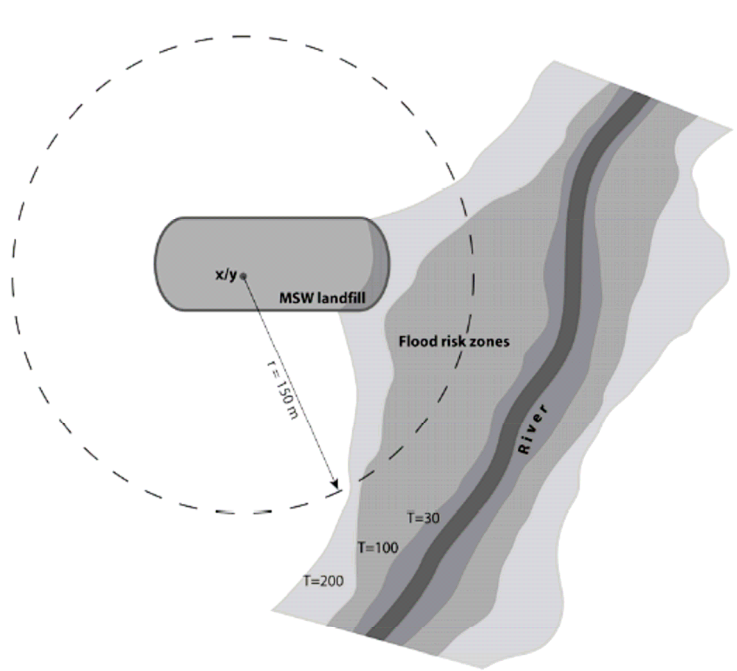


Fig. 2: Schematic illustration of the procedure to evaluate the flood risk probability landfills in Austria, based on the HORA data set (LANER et al., 2009)

The proximity of landfills, represented by a pair of x/y point coordinates, to inundation lines was evaluated under aid of a geographic information system (GIS) whereby the individual landfill geometries could not be taken into consideration by this procedure. Therefore, buffers of various radii were defined to assess risk categories from low to high probabilities (Fig. 2). Landfills showing high probabilities of flooding (the site is situated within or near – 150 m – a flood risk zone with a recurrence interval of 200 years or less) were considered for further investigations and analyses.

The disadvantage of this procedure and hence, substantial uncertainties were identified in the representation of landfills by point coordinates extended by 150 m Buffers (Fig. 2). In reality the landfill geometry is generally not circular and site coordinates are not located necessarily in the centre of the landfill body (LANER et al., 2009).

In order to verify the results, a visual assessment was conducted using the online HORA tool (BMFLUW, 2006b), with imbedded areal photographs, which proofed that the approximation to represent an average landfill topology by a circle of 150 m is sufficient. Nevertheless, for an individual, site-specific analysis of flood risk exposure, the individual geometry of landfill bodies and the existence of technical flood protection measures have to be taken into account (LANER et al., 2009).

2.2 Landfill leaching scenarios

For landfills identified as flood exposed (see section 2.1), emission potentials and substance releases during flood events were estimated whereas the metabolism of flooded MSW deposits is widely unknown. Therefore, the emissions during flood events were based on the estimation of four substance release scenarios. The scenarios I-III assume an increased discharge of soluble substances as a consequence of water saturation of previously dry waste zones with the intensities from (I) low to (II) medium and (III) high. Scenario IV considers a loss of stability of the waste body due to erosion and therefore, the full emission potential of deposited waste.

Zones of low water contents within landfills are reported by various investigations (MALOSZEWSKI et al., 1995; BENDZ & SINGH, 1999; ROSQVIST & DESTOUNI, 2000; FELLNER et al., 2003). They are the result of preferential flow paths that shortcut water flow in landfills. Since the presence of water (POHLAND, 1975; LECKIE et al., 1979; KLINK & HAM, 1982; BOGNER & SPOKAS, 1993) and its redistribution (CHRISTENSEN et al., 1996) are essential for leaching and biochemical degradation processes, the initial pollution load of mostly dry waste zones remains unaltered over long time. However, during flooding it has to be assumed that the whole landfill body gets saturated with water. Consequently, biochemical processes in previously dry zones are restored, resulting in intensified generation of leachate and landfill gas.

The soluble content of substances during water saturation of the waste (scenarios I-III) was roughly estimated using data of BELEVI and BACCINI (1989), who performed leaching experiments on waste samples taken from MSW landfill sites. The available pollution potential of single substances for scenario IV was assessed according to investigations of BACCINI et al. (1987) and DÖBERL et al. (2002), who determined transfer coefficients for C, N, P, Cl, Fe, Pb, Cu, Zn and Cd in dependence to landfill age.

Basically, it is assumed that approximately 70 % of the deposited waste releases its soluble substances during a flood (scenarios I-III). Obviously, this is a rough estimate representing rather upper limits of substance releases than real conditions in case of flooding. However, with respect to the large uncertainties regarding the metabolism of flooded MSW bodies, and as emission scenarios are aimed to illustrate potential emission loads, the selected approach seems to be justified (LANER et al., 2009).

2.3 Derivation of case study sites

Supporting the derivation of a qualitative risk assessment approach three case studies were conducted. Therefore, particularly endangered sites were identified under aid of the inventory of landfills, the HORA data set as well as an online platform accounting for ecological goods (GEOLAND, 2009). Criteria were defined to rank the significance of landfill sites by means of exposure, composition and size. Following attributes were considered as relevant:

1. Immediate vicinity to ecological goods
2. Municipal solid waste composition
3. A volume of at least 100.000 m³
4. Landfilling after 1980
5. No sufficient flood protection measures
6. Data availability

The queries yielded one controlled landfill site and two old waste deposits which were investigated in detail (NACHTNEBEL et al., 2009).

2.4 Hydrologic scenarios and hydrodynamic modelling

It was contemplated to consider climate change influences on hydrologic scenarios but numerous surveys outlined that no significant trend, neither for increase nor for decrease of flood peaks, was identified for the overall federal territory of Austria (BMFLUW, 2009; NACHTNEBEL et al., 2001). Therefore, three hydrologic scenarios following national and international guidelines for flood risk assessment (BMFLUW, 2008; EU, 2007; MESSNER et al, 2007,) were considered: HQ₃₀, HQ₁₀₀ and HQ₃₀₀. Hydrologic scenarios were simulated under aid of hydrodynamic 2-dimensional models to assess the impacts on landfills for three case study sites (Fig. 3).

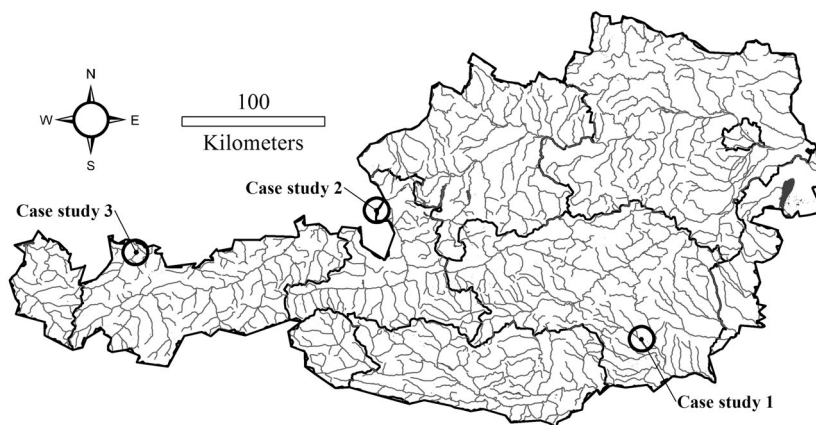


Fig. 3: Case study sites: (1) Kainach, (2) Salzach, (3) Lech (BMFLUW, 2007)

Due to the large variety of the case study sites:

1. Kainach River: lowland river morphology
2. Salzach River: Alpine/Alpine foreland River morphology, heavily modified by river engineering works
3. Lech River: Alpine River morphology

three different models based on the depth-averaged Navier-Stokes equation have been applied. The three model developers followed different philosophies:

- CCHE-2D (ZHANG, 2006; JHANG & JIA, 2007) – applied on the lowland river
 - Developed to simulate flow and sediment transport
 - Finite-Element-Method
 - Mesh-Generator and Graphical user interface
- Hydro_AS-2D (HYDROTEC, 2008) – applied on the Alpine foreland river
 - Developed to simulate dyke breach and flood wave propagation
 - Finite-Volume-Method
 - Mesh generation and post processing by SMS (SSG, 2008)
- River2D (BLACKBURN & STEFFLER, 2002) – applied on the Alpine river
 - Developed to simulate flow and fish habitat availability (WADDLE, 2001)
 - Finite-Element-Method
 - Modular composition (river morphology, ice cover, mesh generation, calculation)

2.5 Flood risk evaluation matrix (FREM)

Based on information on the flood characteristics, the susceptibility to erosion and the landfill's leaching behaviour a flood risk evaluation matrix (FREM) including a grey scale scheme (the higher the risk – the darker the shade of grey) was developed (Fig. 4). Three basic categories were chosen to express the consequential risk emanating from flooded landfills: “minor risk”, “moderate risk” and “serious risk”. The category “no risk” was knowingly avoided due to residual risk such as unexpected failure scenarios, wrong flood risk management decisions, exceedance of calculation parameters, etc.

The first input parameter to the FREM represents the flood characteristics based on the percentage of inundated landfill area for all considered scenarios (HQ₃₀, HQ₁₀₀ and HQ₃₀₀) represented by single columns. Moreover, the inundation depth is calculated representing a decision aid if the overall risk is in between two categories (widely high inundation depth > 1 m leads to the selection of the higher risk category). Minor risk has been defined for landfill sites whereas boundary areas are inundated. Moderate risk (inundation up to 50 %) and serious risk (50 % to 100 % inundated) has been defined for directly affected MSW deposits. The susceptibility to erosion has been assessed by the parameters flow velocity and shear stress whereas the impact on two separate areas was estimated: (1) boundary and

flood mitigation measures and (2) landfill body. The definition of risk categories was based on critical shear stress values calculated by LANGE & LECHNER (1993).

The assessment of susceptibility to erosion for boundary areas and flood mitigation measures was based on values for lawn. Values for medium to coarse gravel built the basis for the estimation of critical conditions for the landfill body itself. The fourth parameter is defined by the overall evaluation of emissions due to leaching processes within the MSW landfill body. Therefore, a water volume has to be calculated which is able to dissolve substances during a flood event (NACHTNEBEL et al., 2009):

$$V_d = \left(\frac{A_v}{A_\tau} * v_{mean} \right) * b_A * h_{mean} * t \tag{1}$$

- V_d Water volume available for dissolving substances [m^3/s]
- A_v Area of landfill where flow velocities > 0 [m^2]
- A_τ Area of landfill where shear stress is > 0 [m^2]
- v_{mean} mean flow velocity [m/s]
- b_A wetted width of landfill [m]
- h_{mean} mean water depth [m]
- t time [s]

The water volume available for dissolving substances (V_d) was subsequently multiplied by the values of landfill leaching scenarios (sec. 2.2) and compared to thresholds defined for controlled landfill conditions related to the general emission act (BMFLUW, 1996). Moderate and even serious risk categories have to be assumed for emissions within threshold levels because values of V_d are extensively higher than emission volumes of controlled landfills. The overall risk is derived from the mean grey scale and demands additional expert judgment for results in between two categories by means of weighting the significance of single FREM parameters and their impact on the consequential risk.

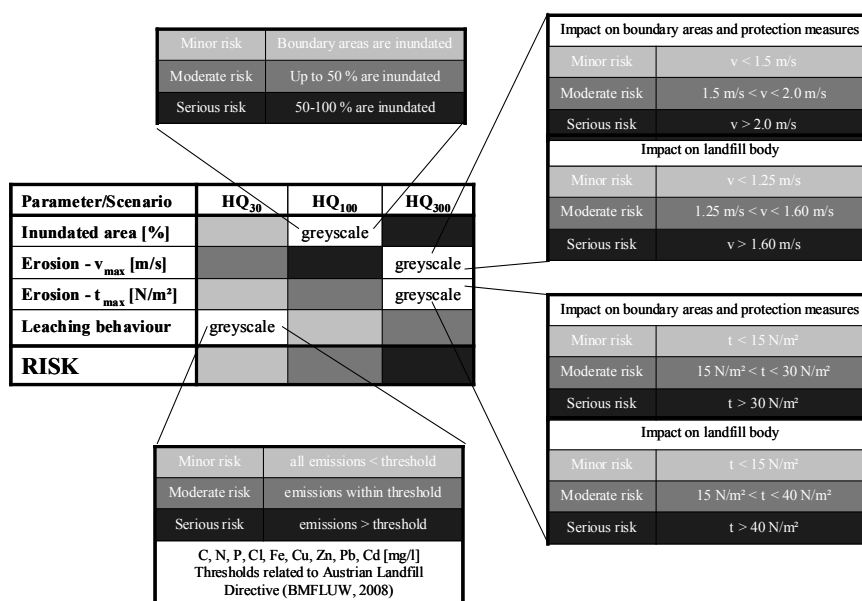


Fig. 4 Description of input parameters and thresholds to the flood risk evaluation matrix

3 Results and discussion

3.1 Exposure to floods

The results on flood risk exposure are based on a sample of 103 controlled MSW landfills and 961 old waste deposits with at least 25000 m³ of volume. The point coordinate based site information was intersected with a nationwide dataset of flood risk zones – the HORA data base (BMFLUW, 2006). With respect to the MSW landfill sites, one third (34) of controlled landfills were highly probable to be inundated by floods. 26 % of these sites are directly located within an inundation area with a recurrence interval of 200 years or less. Roughly 30 % of old waste deposits were identified as highly endangered by floods. The data set of 1064 considered landfills indicates that one third is highly vulnerable to floods, when technical flood mitigation measures are neglected.

Information about flood protection measures was collected from landfill operators. The analysis of the data shows that the majority (60 %) of active controlled landfills are protected by technical measures like dykes as it is required by the Austrian Landfill Directive (BMFLUW, 2008). In particular, large landfills in flood prone areas that are still operated are protected against flood events with a statistical recurrence interval of 100 years or higher. Nevertheless, the majority (70 %) of closed sites has no flood protection at all.

Altogether flood protection measures are reported for roughly 40 % of controlled MSW landfills. For old waste deposits this information was not available, as they have been operated on an informal basis. In general it has to be assumed that these sites are not protected at all (LANER et al., 2009).

3.2 Landfill leaching scenarios

For landfill sites which proofed to be vulnerable to floods (they were identified as near to or within flood inundation lines) four emission potentials of pollutants (scenario I-III: emission of potentially mobile substances during an event; scenario IV: loss of landfill stability and erosion of landfill body) during flood events were estimated (LANER et al., 2008a, b; LANER et al., 2009; NACHTNEBEL et al., 2009).

Compared to conventional landfill conditions, emissions during a flood event might increase by three (e.g. Cl) to six orders of magnitude (e.g. Cd, Cu, Fe, Pb, Zn) for scenario IV. For the scenarios I-III emissions are estimated smaller, but they still exceed ordinary emissions by two (e.g. P, Cl) to four orders of magnitude (e.g. Zn).

3.3 Case study findings, uncertainties and conclusion

This section serves to outline deficits in the frame of applying the qualitative approach to assess flood risk associated with landfills. Sect. 3.3 discusses problems arising on examining three case studies (NACHTNEBEL et al., 2009). Hence, an overview with respect to lack of knowledge, lack of data and data uncertainty can be provided.

Flooding of MSW landfills has been observed during major flood events, resulting in the contamination of surface water, groundwater and soil. In the frame of evaluating the inventory of landfills and their exposure to floods roughly 30 % were identified as highly vulnerable. Hence, numerous landfills pose imminent risk for individuals, ecologic and economic goods. Three case studies were derived under special consideration of the vicinity to ecological goods, the waste composition, the volume of the waste body and the land-filling period. Within this query two considerable sources of uncertainty had been identified.

First of all the representation of partly large MSW landfills by one pair of x/y coordinates is not sufficient due to the disregard of site attributes. Moreover, case study 3 outlined that the accuracy of denoted coordinates are by no means exact. Subsequently to the choice of case study 3 – an area defined as waste deposit according to available data sets (AFEA, 2008) – a single document reported the falseness of coordinates and the category (old waste deposit) without being implemented to the GIS database used. The limping update of the GIS based data collection with single reports lead to a serious misinterpretation and the analyses of a wrong site.

Secondly, the neglect of mitigation measures within the HORA data set (BMFLUW, 2006) leads to an overestimation of exposed landfills. Case study 2, chosen based on HORA, showed a protection level up to a recurrence interval of 300 years within the simulation runs. HORA therefore, can only be utilised as rough decision aid to identify sites that might possibly be affected. For in-depth analyses hydrodynamic modelling including numerous simulation runs is by all means necessary to gain feasible results. Therefore, the datasets describing waste deposits and controlled landfills have to be validated, enhanced and corrected.

For case study 1 the selection criteria were verified – the waste deposit proofed to be within flood risk zones referring to the HORA data set and the coordinates to identify the landfill site were correct. In the frame of the model development the scarce data availability lead to uncertain results because no actual measurement or airborne laser scan was available. Therefore, a digital elevation model (Digitales Höhenmodell, BEV, 2008) was used (knowing that the z-coordinates vary up to ± 6 m) and cross section information based on measurements were imbedded. The information provided by the BEV was validated by some available point informations of measurements and proofed to vary in between some mm up to several dm. Further, a lack of documented historical flood events was identified whereas calibration and validation of simulated extreme events seems to be impossible.

Due to a lack of information related to possible emissions from landfills during flood events four leaching scenarios were investigated. The results illustrate that compared to controlled landfill conditions, the load of pollutants from flooded landfills might increase by up to six orders of magnitude, depending on the substance and the underlying assumption of the scenarios. Thus, the flows of substances from flooded MSW landfills to the environment and therefore, the ecological risk are potentially high. Despite of the high dilution potential during a flood event the Austrian Water Quality Standards for discharge into rivers are highly likely to be exceeded.

The paper clearly highlighted considerable uncertainties related to each sub-step of the presented qualitative approach to assess flood risk related to landfills. Hence, the derivation of a quantitative approach would not yet lead to feasible results. The evaluation of the inventory of potentially affected old waste deposits and controlled landfills outlined that a judgment, based on point coordinate and not yet updated data sets leads to misinterpretations. Moreover, the neglect of flood mitigation measures within the HORA database leads to an overestimation of flood exposed sites. A lack of methodologies regarding the evaluation of emissions due to saturated conditions has been identified which leads to uncertain quantification of impacts on ecological goods.

Nevertheless, the study outlines that in case of flooding or erosion of landfills the hazardous waste released to the environment could lead to partly tremendous ecologic damages. The developed methodology enables a qualitative assessment by means of categories like “minor risk”, “moderate risk” and “serious risk” providing a decision support aid to identify landfills with imminent risk for humans and the environment.

4 References

- [1] AFEA, Austrian Federal Environment Agency – Umweltbundesamt, GIS data supply <http://www.umweltbundesamt.at/umweltschutz/altlasten/>, 2008.
- [2] Baccini, P.; Henseler, G.; Figi, R.; Belevi, H.: Water and Element Balances of Municipal Solid Waste Landfills. *Waste Manage Res* 1987; 5: 483-499.
- [3] Belevi, H.; Baccini, P.: Long-Term Behaviour of Municipal Solid Waste Landfills. *Waste Manage Res* 1989; 7: 43-56.
- [4] Bendz, D.; Singh V.P.: Solute transport under steady and transient conditions in municipal solid waste. *Water Resour Res* 1999; 35: 2333-2345.
- [5] BEV: Bundesamt für Eich- und Vermessungswesen, GIS data supply digital elevation model, <http://www.bev.gv.at>, 2008.
- [6] Blackburn, J.; Steffler, P.: River2D, Two-Dimensional Depth Averaged Model of River Hydrodynamics and Fish Habitat, Introduction to Depth Averaged Modelling and User’s Manual, University of Alberta, <http://www.river2d.ualberta.ca/> 2002.
- [7] Blight, G.E.; Fourie, A.: Catastrophe revisited – disastrous flow failures of mine and municipal solid waste. *Geotechnical and Geological Engineering* 2005; 23: 219-248.
- [8] BMFLUW: Flood Risk II, Vertiefung und Vernetzung zukunftsweisender Umsetzungsstrategien zum integrierten Hochwassermanagement, Synthesebericht, 2009.
- [9] BMFLUW: Austrian Landfill Directive. Verordnung über die Ablagerung von Abfällen, <http://www.lebensministerium.at/article/articleview/26629/1/6969/>, 2008a.

- [10] BMFLUW: Kosten-Nutzen-Untersuchung im Schutzwasserbau: Richtlinie, impresum.lebensministerium.at/filemanager/download/26589/, 2008b.
- [11] BMFLUW: Digital Hydrologic Atlas Austria <http://www.boku.ac.at/iwhw/hao/>, 2007.
- [12] BMFLUW. Federal Waste Management Plan 2006. Federal Ministry of Agriculture and Forestry, Environment and Water Management, Vienna, 2006a, pp. 320.
- [13] BMFLUW. Hochwasserrisiko zonierung Austria – HORA, Bundesministerium für Land- und Forstwirtschaft, Umwelt und Wasserwirtschaft, www.hochwasserrisiko.at, 2006b.
- [14] BMFLUW: Bundesgesetzblatt für die Republik Österreich, 186. Verordnung: Allgemeine Begrenzung von Abwasseremissionen in Fließgewässer und öffentliche Kanalisationen (AAEV). Wien, 1996.
- [15] Bogner, J.; Spokas, K.: Landfill CH₄: Rates, fates, and role in global carbon cycle. *Chemosphere* 1993; 26: 369-386.
- [16] Burgenland: Umwelterklärung des Burgenländischen Müllverbandes, Oberpullendorf., 2005.
- [17] BUWAL: Risikoanalyse bei gravitativen Naturgefahren – Methode. Umwelt-Materialien Nr. 107/I, Naturgefahren: Bern: Bundesamt für Umwelt, Wald und Landschaft, 1999 a.
- [18] BUWAL: Risikoanalyse bei gravitativen Naturgefahren – Fallbeispiele und Daten. Umwelt-Materialien Nr. 107/II, Naturgefahren: Bern: Bundesamt für Umwelt, Wald und Landschaft, 1999 b.
- [19] Christensen, T.H.; Kjeldsen, P.; Lindhardt, B.: Gas-generating processes in landfills. In: Christensen, T.H.: editor. *Landfilling of waste: biogas*. 27-44. E&FN Spon, London, 1996.
- [20] Döberl, G.; Huber, R.; Fellner, J.; Cencic, O.; Brunner, P.H.: Neue Strategien zur Nachsorge von Deponien und zur Sanierung von Altlasten (Projekt STRANDEZA). Abteilung Abfallwirtschaft und Stoffhaushalt, Technische Universität Wien, 2002, pp. 267.
- [21] EU: Richtlinie 2007/60/EG des europäischen Parlaments und des Rates über die Bewertung und das Management von Hochwasserrisiken, 2007.
- [22] Egli, T.: Hochwasserschutz und Raumplanung. Schutz vor Naturgefahren mit Instrumenten der Raumplanung – dargestellt am Beispiel vom Hochwasser und Murgängen. ORL-Bericht 100/1996, ETH Zürich, 1996, 165 pp.
- [23] Ehrig, H.J.; Krümpelbeck, I.: The Emission Behaviour of Old Landfills in the After-care Phase. In: Christensen TH, Cossu, R. & Stegmann, R., editor. *Proceedings Sar-*

- dinia 2001, Eighth International Waste Management and Landfill Symposium. IV. CISA, S. Margherita di Pula, 2001, pp. 313-323.
- [24] Fellner, J.; Huber, R.; Döberl, G.; Brunner, P.H.: Hydraulics of MSW landfills and its Implications for Water Flow Modelling. In: Christensen, T.H.; Cossu, R.; Stegmann, R.: editor. Proceedings Sardinia 2003, Ninth International Waste Management and Landfill Symposium. CISA, S. Margherita di Pula, 2003.
- [25] Flögl, W.: Klimarelevanz der Deponien in Oberösterreich. Dr. Flögl Hydro Consulting Engineers, Linz, 2002.
- [26] Geller, W.; Ockenfeld, K.; Böhme, M.; Knöchel, A.: Schadstoffbelastung nach dem Elbe-Hochwasser 2002. Final report of the ad-hoc-project 'Schadstoffuntersuchungen nach dem Hochwasser vom August 2002 - Ermittlung der Gefährdungspotentiale an Elbe und Mulde'. UFZ - Umweltforschungszentrum Leipzig-Halle GmbH., Magdeburg, 2004.
- [27] Geoland: Geodatenbank der österreichischen Länder, www.geoland.at, 2009.
- [28] Habersack, H.; Moser, A.: Ereignisdokumentation - Hochwasser August 2002, Final Report. University of Natural Resources and Applied Life Sciences, Vienna, 2003, pp. 184.
- [29] Hydrotec: Das 2D Strömungsmodell HYDRO_AS-2D, Hydrotec Ingenieurgesellschaft <http://www2.hydrotec.de/unternehmen/hydrothemen/hydrothemen07/hydro-as-2d/>, 2009
- [30] Kärnten: Kärntner Abfallbericht und Abfallwirtschaftskonzept. Amt der Kärntner Landesregierung, Abteilung 15 - Umweltschutz und Technik, Klagenfurt., 2000.
- [31] Klink, R.E.; Ham, R.K.: Effects of moisture movement on methane production in solid waste landfill samples. Resources and Conservation 1982; 8: 29-41.
- [32] Krammer, H.J.; Domenig, M.; Striedner, J.; Vogel, G.: Materialien zum Bundesabfallwirtschaftsplan (BAWP), Band 3: Kommunale Abfälle. Bundesministerium für Umwelt, Jugend und Familie, Wien, 1992, pp. 180.
- [33] Laner, D.; Fellner, J.; Brunner, P.H.: Flooding of municipal solid waste landfills – a long-term environmental hazard? Science of the total environment, 407 (12), 2009, pp 3674-3680.
- [34] Laner, D.; Fellner, L.; Brunner P.H.: Gefährdung durch Deponien und Altablagerungen im Hochwasserfall – Risiko und Analyse (GEDES), Dokumentation zum Arbeitspaket 1, Zwischenbericht, TU-Wien IWA, 2008a, pp. 54.
- [35] Laner, D.; Fellner, J.; Brunner, P.H.; Neuhold, C.; Kolesar, C.: Environmental Relevance of Flooded MSW Landfills in Austria, In: ISWA/WMRAS, ISWA/WMRAS World Congress 2008 - East meets Waste, Singapore Nov 3-6, 2008b.

- [36] Lange, G.; Lechner, K.: Gewässerregelung & Gewässerpflege – Naturnahe Ausbau und Unterhaltung von Fließgewässern. Verlag Paul Parey, 3.Auflage, Hamburg/Berlin, 1993.
- [37] Leckie, J.O.; Halvadakis, C.; Pacey, J.G.: Landfill Management with Moisture Control. *J Environ Eng* 1979; 105: 337-355.
- [38] Lunzer, H.; Domenig, M.; Rosian, J.; Mostbauer, P.; Häusler, G.: Hausmülldeponien in Österreich. Umweltbundesamt, Wien, 1998.
- [39] Maloszewski, P.; Moser, H.; Stichler, W.; Trimborn, P.: Isotope hydrology investigations in large refuse lysimeters. *J Hydrol* 1995; 167: 149-166.
- [40] Merz, B.: Hochwasserrisiken – Grenzen und Möglichkeiten der Risikoabschätzung, E. Schweizerbart'sche Verlagsbuchhandlung (Nägele u. Obermiller), Stuttgart, 2006.
- [41] Merz, R.; Blöschl, G.; Humer, G.; Hofer, M.; Hochhold, A.; Wührer, W.: Hochwasserrisikoflächen Österreich (HORA) – Hydrologische Arbeiten (Technical Report). Institut für Wasserbau und Ingenieurhydrologie, TU Wien, Wien, 2006.
- [42] Messner, F.; Penning-Rowsell, E.; Green, C.; Meyer, V.; Tunsall, S.; van der Veen, A.: Evaluating flood damages: guidance and recommendations on principles and methods, report number T09-06-01, www.floodsite.net, 2007.
- [43] Nachtnebel, H.P.; Fuchs, M.; Schober, S.; Hebenstreit, K.; Diernhofer, W.; Blum, M.: Die Hydrologie Österreichs unter dem Einfluß von Szenarien einer möglichen Klimaänderung. Endbericht Teil I-III, Universität für Bodenkultur, IWHW, Wien, 2001.
- [44] Nachtnebel, H.P.; Holzmann, H.; Neuhold, C.; Haberl, U.; Kahl, B.; Bichler, A.: GEDES: Gefährdung durch Deponien und Altablagerungen im Hochwasserfall - Risikoanalyse und Minimierung - Teilbericht 2, Wien, 2009.
- [45] Neuhold, C.; Stanzel, P.; Nachtnebel H.P.: Incorporation river morphological changes to flood risk assessment: uncertainties, methodology and application, *Natural Hazards and Earth System Sciences*, 2009, 9, pp. 789-799.
- [46] Niederösterreich: Niederösterreichischer Abfallwirtschaftsbericht 2005. Amt der NÖ Landesregierung, Gruppe Raumordnung, Umwelt und Verkehr, St. Pölten, 2005.
- [47] Pohland, F.G.: Sanitary landfill stabilization with leachate recycle and residual treatment. USEPA, Cincinnati, OH, 1975.
- [48] Rolland, C.; Oliva, J.: Erfassung von Deponiegas - Statusbericht Österreichischer Deponien. Umweltbundesamt, Wien, 2004.
- [49] Rosqvist, H.; Destouni, G.: Solute transport through preferential pathways in municipal solid waste. *J Contam Hydrol* 2000; 46: 39-60.

- [50] Skala, C.; Kanovsky, A.; Ortmann, M.; Schamann, M.; Weihs, S.; Jobstmann, H.: Altlastensanierung in Österreich - Effekte und Ausblick. Bundesministeriums für Land- und Forstwirtschaft, Umwelt und Wasserwirtschaft, Wien, 2007, pp. 191.
- [51] SSG: Scientific Software Group, SMS-Surface Water Modelling System, current version 10.0, <http://www.scientificsoftwaregroup.com/>, 2008
- [52] Stegmann, R.; Heyer, K.U.: Langfristiges Gefährdungspotential und Deponieverhalten von Ablagerungen. Statusseminar Deponiekörper. BMBF, Wuppertal, 1995.
- [53] Tirol: Abfallbewirtschaftung in Tirol. Tiroler Landesrechnungshof, Innsbruck, 2002.
- [54] Vorarlberg: Abfallwirtschaftsdaten Vorarlberg 2005. Amt der Vorarlberger Landesregierung, Abteilung Abfallwirtschaft., Bregenz, 2005.
- [55] Waddle, T.J.: PHABSIM for Windows: user's manual and exercises: U.S. Geological Survey Open-File Report 01-340, 2001, 288 p.
- [56] WBGU: Wissenschaftlicher Beirat Globale Umweltveränderungen, Welt im Wandel: Wege zu einem nachhaltigen Umgang mit Süßwasser, Jahresgutachten 1997, Springer-Verlag, Berlin, 1999, 419 pp.
- [57] Young, S.; Balluz, L.; Malilay, J.: Natural and technologic hazardous material releases during and after natural disasters: a review. *Sci Total Environ* 2004; 322: 3-20.
- [58] Zhang, Y.: Technical Report No. NCCHE-TR-2006-03, CCHE-GUI – Graphical Users Interface for NCCH Model, User's Manual – Version 3.0, NCCHE, The University of Mississippi, 2006.
- [59] Zhang, Y.; Jia, Y.: Technical Report No. NCCHE-TR-2007-01, CCHE-Mesh: 2D Structured Generator, User's Manual – Version 3.0, NCCHE, The University of Mississippi, 2007.

Risk management of concrete flood protection walls by application of Bayesian networks

J Marengwa¹ and JV Retief²

¹Agency for Roads, Bridges and Water (LSBG), Free and Hanseatic City of Hamburg, Germany

²Department of Civil Engineering, University of Stellenbosch, South Africa

Abstract: Flood protection structures are exposed to unique operation conditions of being required to perform their protection function under rare and exceptional conditions, whilst they are continuously exposed to deteriorating processes. The technical demands on such structures are compounded by economic pressures and constraints on their maintenance. Since their proper functioning is not directly related to operational requirements the allocation of sufficient budgets and resources for maintenance is problematical.

This can effectively be rectified by the implementation of rational measures to obtain allocation of resources and procedures for structural maintenance. In this paper, an example of an updating process of concrete compressive strength and a proposed process of updating based on a Bayesian network, is presented and applied on the corrosion risk of a flood protection wall.

1 Introduction:

1.1 Current Situation

Flood protection walls (FPW) are exposed to unique operation conditions of being required to perform their protection function under rare and exceptional conditions, whilst they are continuously exposed to deterioration processes. In this context it is very useful to assess risks to these aging infrastructures. This allows using inspection data to optimize maintenance strategies. The benefits are a defined risk management and lower maintenance costs. To achieve these goals it is necessary to have representative deterioration models and the most reliable input data as possible.

FPW are subjected to time dependant effects. Corrosion is one main effect of degradation. The process evolution can be forecasted by using physical models leading to an estimation of the rate of ageing and the risk of failure.

Based on a few samples the compressive strength of concrete R_c and chloride concentration in the depth X will be determined. This data will be collected and will be used to calibrate the model. Beside the material properties other uncertain parameters can be identified (i.e. concrete cover thickness). On site measurements will also be taken into account where available.

1.2 Structural Performance of Flood Protection Walls

The maintenance planning of existing deteriorating concrete structures like flood protection walls is considered by taking the general approach to the probabilistic prediction of the structural service life. Any structure is undergoing some degree of deterioration with time, due to its exposure to the environment. The effects of deterioration are structure and site specific. Concerning structural strength, corrosion and fatigue are the main deterioration processes. Typical indications of deterioration are spalling, cracking, and degraded surface conditions.

The majority of concrete structures in the marine environment under hydraulic loads show signs of degradation due to corrosion of the reinforcement. Beside the influence of the marine environment other factors are responsible for the corrosion, such as: poor construction quality, non-rational standards based on prescriptive measures; and poor design as a result of insufficient information about the most important parameters that influence the degradation process.

While standards are gradually improving, with the tendency to become rational and performance based in future, the existing structures are based on the previous generation of standards. This paper describes the planning of research that is aimed at providing maintenance engineers with adequate means for probability-based durability analysis of existing concrete structures in marine or coastal environment.

The level of safety of many existing structures can be inadequate, or at least unknown, compared to current design requirements. That leads to problems for owners and maintenance personnel, because the public safety is very important and consequences of failure are high. The customary strategy and commonly applied concept of maintenance includes periodical inspection, which usually starts with a visual inspection. This may yield invaluable information affecting the choice of methods and location of test points. Experience in the knowledge of the processes in question and expertise with the various tools and means of investigation and analysis are essential if a correct investigation is going to be made and accurate interpretation placed on the received data.

In order to make the step from knowing the deteriorating processes of concrete, to selecting the best methods of inspection for repair, engineers require guidance on techniques available both for condition assessment and for interpretation of the data.

Uncertainties associated with modelling of deteriorating structures strongly affect management decisions, such as inspection, maintenance and repair actions. The objective of the study is to find a methodology for performance updating of deteriorating concrete flood protection walls. This methodology is going to be illustrated with one simple example of a flood wall. The results will show the benefits from introducing reliability based technology in managing concrete structures subject to deterioration, and quantify the reduction in uncertainties and their subsequent effect on predictions of the performance of future concrete structures.

The selection of cost effective preventive and essential maintenance measures is normally based on condition assessments achieved through inspections, tests and monitoring. Such condition assessments are subject to significant uncertainties.

Deterioration of concrete structures is going on in a number of phases with different consequences. The inspection may observe this deterioration processes. The cost effectiveness of maintenance and repair activities is depending on when and how these activities are implemented.

This project proposes on the use of a Bayesian approach in inspection and maintenance planning of concrete structures based on condition indicators. Concrete characteristics (e.g. concrete strength, concrete cover, critical chloride concentration, etc.) are highly variable due to the variability of fabrication and workmanship during the construction of a structure. Therefore corrosion initiation and propagation are variable and thus the structural and serviceability performance of the structure are accordingly influenced.

The assessment of an existing structure differs very much from the design of a new one. Due to deterioration and damage it is general practice to inspect existing structures and if necessary to repair and/or strengthen them. While, initially, the various uncertainties related to loads and resistance parameters must be assessed a priori resulting in appropriate safe codified design provisions, actual observations update the prior assessment. Consequently, regarding the state of information the situation in assessing existing structures is completely different from that during design. In addition, special attention is paid to specific parts of the existing structure and to a probably limited part of items with a real risk of damage according to the observed behaviour of the structure.

1.3 Inspection, Monitoring and Maintenance

The objective of structural assessment is to provide information about the structural state for optimisation of the point in time and the extent of inspection, maintenance and repair work. That means maximum operation effect at minimum costs. It is also important for prioritisation of maintenance and repair work.

In most cases of assessment it is necessary to gather information about material and structural properties and dimensions as well as about the loading on the structure (previous, current and/or future). Environmental conditions are of physical, chemical or biological nature and can have an effect on material properties. That's a very important fact when talking about the marine environment.

Carbonation-based corrosion is of great importance because it can lead to a decrease of mechanical performance of a structure. Material properties like concrete strength or the depth of carbonation are not the only uncertain parameters. During the building process of the concrete structures, concrete cover thickness is also a parameter subjected to random variations.

The main difference between design and assessment of an existing structure is that uncertainties can be reduced significantly by site specific data from the real and existing structure. There is a wide range of methods of data acquisition. The choice depends on the assessment objective and with that on the assessment procedure. The methods are varying in expenses and accuracy. Usually one will start in the beginning with a simple method like the study of documents. To reduce uncertainty within higher assessment levels more improved test methods need to be applied. Whenever it is possible non-destructive methods should be

used. Beside the provision of data which describes the current state of the structure, also information about time depending processes like deterioration need to be acquired.

Reviewing documents from design and construction process and studying inspection and maintenance reports is the easiest way of gathering data about the existing structure to be assessed. Loads can be usually determined from current loading codes. Environmental conditions may be investigated from inspection reports.

Resistance properties can be obtained from codes, drawings and other design specifications (e.g. material and structural properties and dimension).

It is very important to reduce uncertainties about load and resistance where possible. Helpful can be site specific data which should be used within the assessment process. There exists a large variety of inspection and testing methods. It starts with simple visual inspection and ends up with high-end non-destructive techniques. Inspections are especially for detection and investigation of deterioration processes like corrosion and fatigue. That helps to detect changes in the structural systems.

Maintenance of civil infrastructure systems at acceptable performance levels requires timely maintenance, repair and rehabilitation actions (MRR).

Generally, MRR actions in civil infrastructure are reactive rather than proactive. In practice, the condition of a structure or group of structures is monitored at periodic intervals and when significant structural damage is observed measures are initiated. Structural performance is monitored with the following methods:

1. Visual inspection and condition ratings
2. Health monitoring of structures
 - a. Continuous monitoring systems
 - b. Periodic monitoring
3. Testing techniques
 - a. Non-destructive methods
 - b. Destructive methods

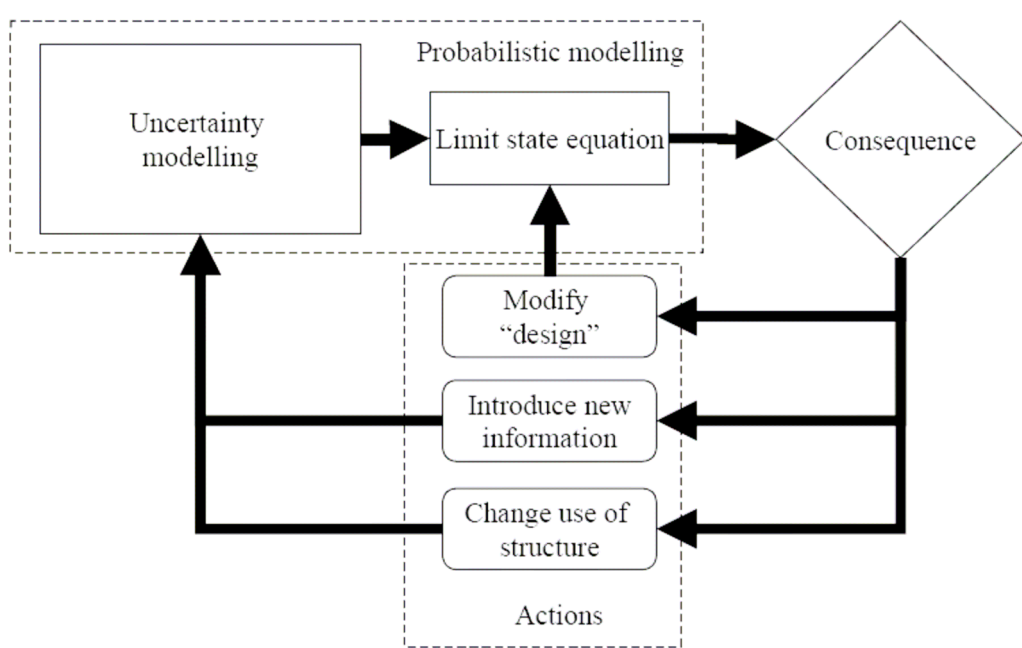
In probability terms of assessment of existing structures there is a direct correlation between the structural risk acceptance and the required minimum structural reliability or so-called target reliability. The requirements are formulated in terms of the accepted minimum reliability index β or the accepted maximum failure probability P_f . The target reliability level can be determined on existing practice or existing codes. Determining the target reliability level should take into account the type of structure and its vital role. It is important to consider possible consequences and socio-economic-criteria.

1.4 Updating of Existing Structures

When carrying out assessment basing on documents and visual inspection the structural analysis is using knowledge from the design process. The main target of investigating existing structures is to update measured quantities and to get new information about the structural resistance. The estimation of the prior distribution functions can be updated using the new data. With that the characteristic and / or design values can also be updated. With new information gathered through inspection it is possible to improve any previous estimate of the structural reliability of that structure. The updated failure probability P_f is then given by Bayes' theorem.

There are several procedures for updating the failure probability. These updating procedures can be used to derive updated probabilities of failure or characteristics and representative values of basic variables. These probabilities can then be used in probability based assessment. Assessment of existing structures using such methods of modern reliability theory are a successive process of modelling, consequence evaluation and model updating by introduction of new information, by modification of the structure or by changing the use of the structure. The process is shown in Figure 1.

Fig. 1: Bayesian probabilistic assessment of structures (Diamantidis, 2001)



There are various steps in the assessment (Diamantidis 2001):

1. Formulation of prior uncertainty models
2. Formulation of limit state functions
3. Establishing posterior probabilistic models
4. Performing prior, posterior and pre-posterior decision analysis
5. Setting acceptable levels for the probability of failure.

When new information becomes available the probability model formulating the decision problem can be updated. If the probability structure is updated the reassessment decision analysis is unchanged to the situation with given prior information. With an observation or a test result z_k , the updated probability structure or the posterior probability is $P''(\theta|z_k)$ and may be found by use of Bayes rule.

$$P''(\theta) = \frac{P[z_k|\theta_i]P'[\theta_i]}{\sum_j P[z_k|\theta_j]P'[\theta_j]} = \frac{1}{\sum_j P[z_k|\theta_j]P'[\theta_j]} \cdot P[z_k|\theta_i] \cdot P'[\theta_i] \quad (1)$$

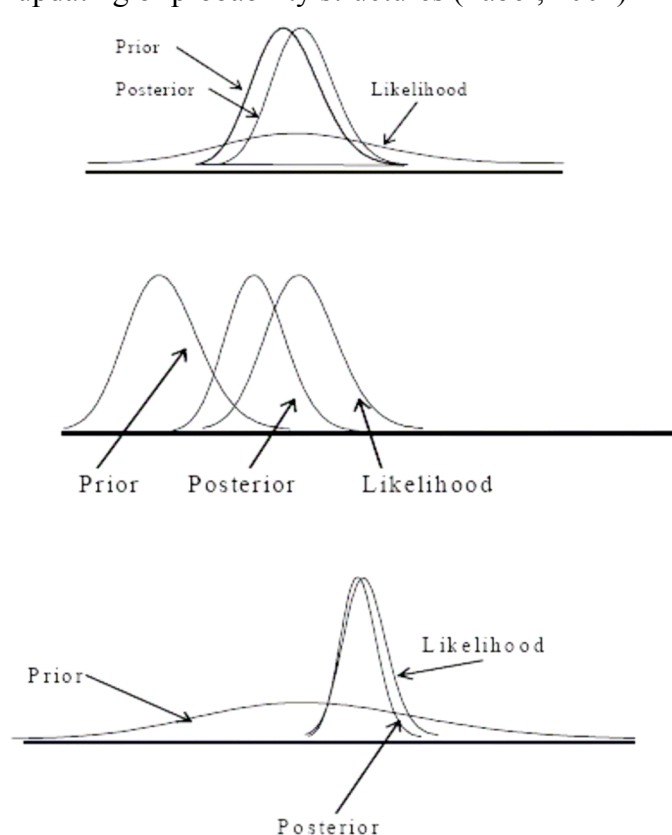
That can be explained in the following way:

$$\left(\begin{array}{l} \text{Posterior probability of } \theta_i \\ \text{with given sample outcome} \end{array} \right) = \left(\begin{array}{l} \text{Normalising} \\ \text{constant} \end{array} \right) \left(\begin{array}{l} \text{Sample likelihood} \\ \text{given } \theta \end{array} \right) \left(\begin{array}{l} \text{prior probability} \\ \text{of } \theta \end{array} \right) \quad (2)$$

The mixing of new and old information appears through the sample likelihood

$P''(z_k|\theta_i)$ and the prior probability $P''(\theta_i)$. The likelihood is the probability of obtaining the observation z_k given the true state of nature θ_i (Faber, 2001). Figure 2 shows an illustration of corresponding prior and posterior probability density functions together with likelihood functions.

Fig. 2: Illustration of updating of probability structures (Faber, 2001)



In the first case the prior information is strong and the likelihood is weak (small sample size). In the second case the prior information and the likelihood are of comparable strength. In the last case the prior information is relatively weak in comparison to the likelihood.

Degradation models of concrete structures are using uncertain variables. Using reliability assessment, they are leading to time dependant evolution of failure probabilities. In general, only few observations or measurements are available. This leads to two types of uncertainties. There is a basic uncertainty, depending on the modelled problem. And there is another one related to the precision of the measurements. Each new observation that becomes available is a piece of information which allows updating the initial prediction, whereas classical probability theory allows the treatment of one type of uncertainty only.

Therefore Bayesian networks offer great possibilities: Uncertain or indirect measures can be used for updating. Good control of uncertainty is allowed through the combination of heterogeneous information like expert statements and other uncertain measures. If only a few measurements are available, the method is particularly advantageous.

1.5 Example of updating concrete strength

When non-destructive or destructive test are performed, new information becomes available. This new information can be used in durability assessment of structures to reduce the uncertainty on the assessment. In the current practice, this data is directly included in the assessment process.

When using the Schmidt-Hammer test for analysing the compressive concrete strength of an existing structure in most cases, for several tests performed, the results will differ significantly. This is for two main reasons.

1. The properties of concrete change from one element or the other within the same structure.
2. Even if the test is repeated at the same point, the results will differ due to little changes in the execution of the test.

The uncertainty arises from uncertainty in the material properties and from bad accuracy of the test. In Bayesian updating framework this sources of uncertainty are considered in a consistent way. That leads to a more reliable indication of the real properties of materials and a more accurate assessment of a structure.

As destructive and even non-destructive test are highly cost effective, the engineer will pre-estimate the most significant parameter for the analysis of the structure. This initial data will be denoted as prior. This information is based on experience and pervious analysis of this structure. Therefore the information has different levels of confidence and is associated with large uncertainty. The main reason for performing tests (destructive or non-destructive) is to reduce these uncertainties and to adjust the data obtained.

Defining the concrete compressive strength by θ , the probability density function is:

$$\theta \sim f_{\theta}(\theta) \tag{3}$$

If there is no information of the property available a so-called non-informative prior can be used. This is simply a function that is constant for all possible values of the property θ .

The prior model represents the information which is available concerning the parameter vector θ prior to the observation of the data x . The posterior model gives back what is known about θ given knowledge of the data x . If the sample data support the subjective opinion about θ , then the posterior model should reflect increased confidence in the subjective notions in the prior model. If the sample data do not support the subjective information, the posterior model should reflect a weighted consideration of both assessments. This is the way Bayes' theorem can be used to calculate the posterior model.

The posterior distribution of the unknown variable θ can be found through:

$$f'_{\theta}(\theta) \propto f_{\theta}(\theta) \prod_{i=1}^n f_{x_i|\theta}(x_i|\theta) \quad (4)$$

The first term refers to the prior distribution probability. The second one describes the likelihood of a certain value of x being output from a test, for a certain value of θ . The likelihood function is important in Bayes' theorem. It can be regarded as the function that represents the information about θ .

A lot of structural parameters are represented with a Gaussian distribution. In this case the characteristic values of this parameter can be formulated with the following expression:

$$X_k = m - t_{vd} \cdot s \sqrt{(1+1/n)} \quad (5)$$

With: n number of samples/tests
 m mean value from tests and prior knowledge
 s standard deviation from tests and prior knowledge
 t_{vd} coefficient

In the case where no prior information is available, the standard deviation and the mean are given by the sample mean and the standard deviation:

$$m = \sum x_i / n \quad (6)$$

$$s = \sqrt{1/n \sum (x_i - m)^2} \quad (7)$$

Prior information gives a belief on the mean and standard deviation in terms of expected values and uncertainty. This is not based on absolute certainty. This is the reason why this belief is defined in a probabilistic way with the expected value and the coefficient of variation of the prior mean $m(\mu')$ and $V(\mu')$. In this case the expected value and the coefficient of variation of the prior standard deviation are given by $m(\sigma')$ and $V(\sigma')$. The prior is equivalent to n' together with parameter v' (Rücker et al., 2006):

$$n' = [(m(\sigma') / m(\mu')) (1 / V(\mu'))]^2 \quad (8)$$

$$v' = 0,5 \cdot 1 / [V(\sigma')]^2 \quad (9)$$

In the following example the results of a non-destructive test on the material properties of concrete are used for an assessment.

In this example the concrete strength based on the Schmidt Hammer test is analysed. A set of 4 tests are representing the whole length of the flood protection structure. The total concrete strength will be calculated based on the arithmetic mean rebound value R_m . The tests yields the following results: 53,2, 53,3, 52,5 and 55,0.

The mean and standard deviation of the observed values are:

$$m = \sum x_i / n = 53,5 \quad (10)$$

$$s = \sqrt{1/n \sum (x_i - m)^2} = 1.061 \quad (11)$$

If no prior information is available, the rebound value R is calculated with t_{vd} which is derived from a table of the Student distribution¹.

For a percentile of 5 %, t_{vd} is 2,92 for $v=n-1=2$.

$$X_k = m - t_{vd} \cdot s \cdot \sqrt{(1+1/n)} = 53,5 - 2,92 \cdot 1.061 \cdot \sqrt{(1+1/4)} = 50,04 \text{ (R}_m\text{)} \quad (12)$$

With $R_m = 50,04$ the concrete compressive strength is 550 kg/cm^2 which is $53,95 \text{ N/mm}^2$ or $53,95 \text{ MPa}$.

According to DIN 1048 Part 2 (1991) for a concrete B45 the min R'_m for an area is 47. With $53,95 \geq 47$ the concrete class is a B 45 (DIN 1045 old) or a C 35/45 (DIN 1045-2 new).

The Bayesian approach is another possibility to face this problem. It can be considered that the resistance of concrete is represented by a normal distribution with an unknown standard and mean deviation, which than can be treated as random variables. In the case that no prior information about the concrete used exists, the standard deviation of the concrete strength can be assumed with round about 3 Mpa, so the standard deviation of the resistance is a random variable with a mean of 3 Mpa. If the coefficient of variation is assumed to be 10% and the mean of the resistance is defined by a normal variable with mean equal to 45 MPa. The deviation is assumed to be a normal distribution.

The prior information can be added to the test results. Following Bayesian concept, the unknown value n' and a corresponding degree of the freedom v' may be assessed using the relations for the coefficients of variation of the mean ($w(\mu')$) and $w(\sigma')$, (the parameters μ' and σ' are considered as random variables in Bayes' concept) for which it holds

$$n' = [(m(\sigma') / m(\mu'))(1/ V(\mu'))]^2 = [(3/10) (1/10)]^2 \sim 0 \quad (13)$$

$$v' = 0,5 \cdot 1 / [V(\sigma')]^2 = 0,5 \cdot 1 / [0,1]^2 = 50 \quad (14)$$

With no information on the mean, the prior is equivalent to zero tests. The degree of freedom is 50, since the standard deviation is quite well known.

¹ Table in Martz, H., Waller, R., 1991

The prior information is now combined with the tests.

$$n' = n + n' = 4 + 0 = 4 \quad (15)$$

The updated value of the mean is based on the prior knowledge and real tests.

$$m(\mu') = (n \cdot m + n' \cdot m(\mu')) / n'' = (4 \cdot 53,5 + 0 \cdot 45) / 4 = 53,5 \quad (16)$$

Since there was no prior information on the mean value, the updated mean is based on the tests alone.

With

$$v = n - 1 = 4 - 1 = 3 \quad (17)$$

the updated degrees of freedom are:

$$v'' = v + v' \text{ if } n' = 0 \rightarrow v'' = 3 + 50 = 53 \quad (18)$$

The updated value of the standard deviation is:

$$\begin{aligned} m(\sigma') &= \sqrt{[(v' \cdot m(\sigma')^2 + n' \cdot m(\mu')^2) + [v \cdot s^2 + n \cdot m^2] - n'' \cdot m(\mu')^2] / v''} \\ &= \sqrt{[50 \cdot 3^2 + 0 \cdot 45^2] + [4 \cdot 1,061^2 + 4 \cdot 53,5^2] - 4 \cdot 53,5^2} / 53 = 1,72 \end{aligned} \quad (19)$$

The new characteristic value is:

$$X_k = m - t_{vd} \cdot s \sqrt{(1 + 1/n)} = 53,5 - 1,68 \cdot 1,72 \cdot \sqrt{(1 + 1/4)} = 50,27 \text{ (R}_m\text{)} \quad (20)$$

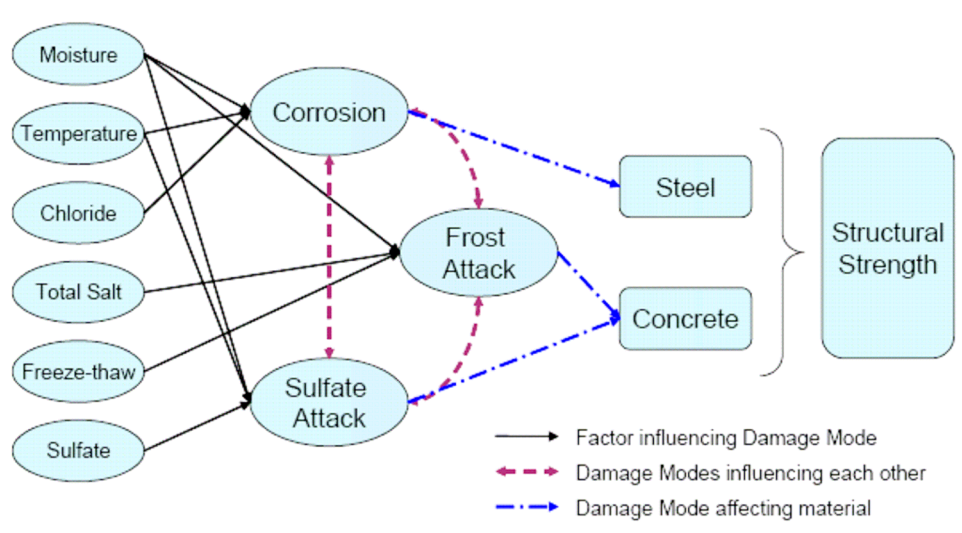
As this short example shows, also very limited information like the expected standard deviation of a certain value can be used to update the information.

Even if the mean value is not changed, a reduction in the standard deviation can be observed. This leads to a significant lower value. It is shown that Bayesian updating is very useful in the assessment of existing concrete structures, to upgrade the models, when some data due to tests are available. Also engineer judgement can then be combined with test results.

2 Degradation

The main degradation process for durability of reinforced concrete structures is the corrosion of the concrete reinforcement. In marine environment the corrosion occurs almost entirely due to the presence of chlorides in the sea water. The main mechanisms responsible for the transport of chlorides into the concrete are known and a lot of literature about this topic is available.

Fig. 3: Influence pattern for reinforced concrete component (Richard, 2003)

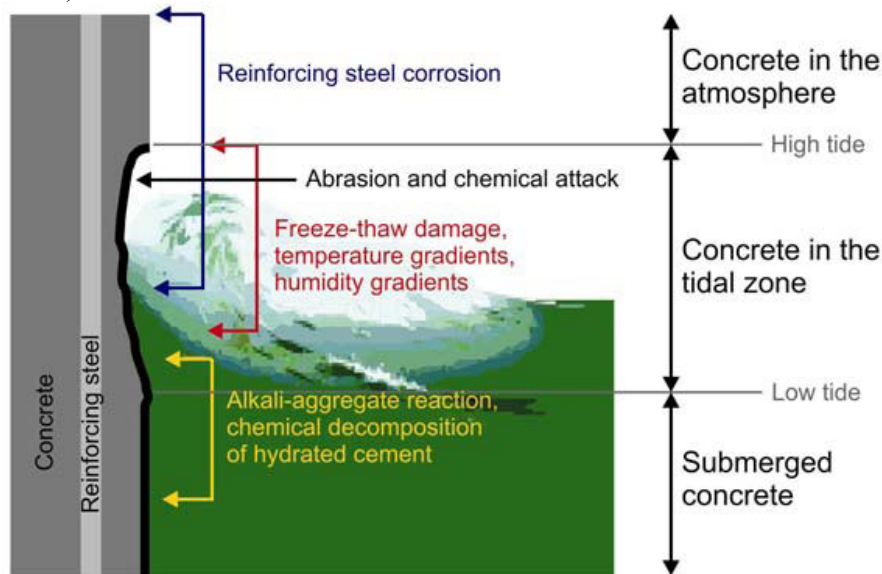


Reinforced concrete is a versatile and widely used construction material. Usually it is durable and strong, performing well throughout its service life. If there exist performance problems one or a combination of the following factors are part of the problem: poor design, poor construction, inadequate materials selection, exposed to a more severe environment than anticipated.

There are a number of contributing factors which affect the durability of concrete. Several degradation mechanisms can act simultaneously with possible synergistic effects.

The figure 4 shows how different degradation mechanisms can act on concrete exposed to sea water.

Fig. 4: Possible degradation mechanisms acting on concrete exposed to sea water (Malhorta, 2000)



2.1 Degradation Model

In concrete structures exposed to normal conditions (outdoor) and in the marine environment the effects of degradation mechanisms can be classified into the following structural deterioration mechanisms:

- Corrosion of reinforcement at cracks in the concrete, causing a reduction in the cross-sectional area of steel bars.
- Surface deterioration or frost attack, causing a reduction in the cross-sectional area of concrete.
- Alkali-Aggregate Reactions, they are chemical processes where alkali from the binders reacts with silica from the aggregates under the influence of calcium and water.

The degradation can be modelled as one or a combination of the three processes. The process of reinforcement corrosion is best known. The frost attack process and the alkali-aggregate reactions are not well researched so far and a proper mathematical model does not exist (Lindvall, 2000).

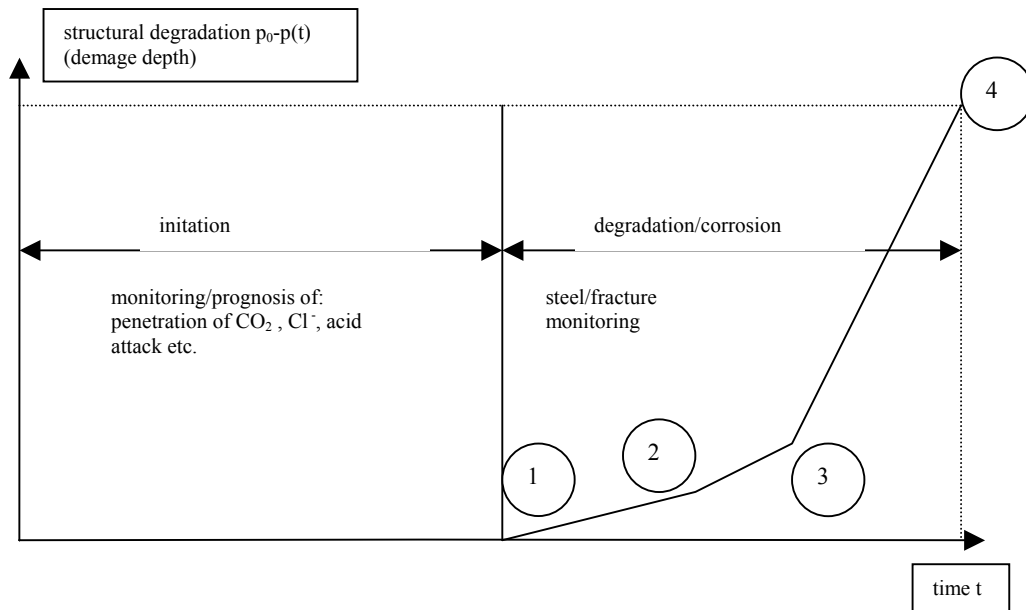
The corrosion process consists of a number of sequential phases. The generally accepted model is talking of an initiation and a propagation phase (See fig. 5). The initiation phase describes the permeation of aggressive agents through the concrete cover until they reach the reinforcement. The propagation phase describes the development of rust products that induce cracking and spalling of the concrete cover.

Models that include the propagation stage generally states that the service life of the structure formally ends after a critical crack width has been developed. The service life of a concrete structure is based on the following value:

$$t_{\text{service}} = t_{\text{corr}} + \Delta t_{\text{crack}} \quad (21)$$

Where: t_{service} = service life, t_{corr} = time of initiation of corrosion, Δt_{crack} = time from corrosion initiation to cracking of the concrete cover.

Fig. 5: Structural degradation and limit states



Limit States:	1	steel passivation (SLS)
	2	crack development
	3	concrete spalling
	4	failure of member (ULS)

Numerical models allow approximate prediction of the initiation phase for rebar corrosion and cracking of concrete elements. These models are reliable tools to evaluate time dependent issues of concrete structures.

The depassivation of the reinforcement due to carbonation is the relevant limit state. As the depassivation does not lead to severe consequences the limit state can be allocated as a serviceability limit state (SLS). The variable describing the resistance is being compared with the variable describing the load. By considering the depassivation of the reinforcement due to carbonation, the concrete cover is defined as the resistance and the carbonation depth as the load. As the carbonation depth is increasing with time, this load variable has to be defined as time dependent.

A number of numerical models are available to model the corrosion process. These are for example:

- Duracrete Model
- Mejelbro-Paulsen Model
- ClinCon Model
- Colleparidi Model
- Visser Model

It is shown that ingress of chlorides can best be modelled by a diffusion process.

Diffusion is the movement of a chemical species from an area of high concentration to an area of lower concentration. The controlled diffusion of particles into silicon to alter the type and level of conductivity of semiconductor materials is the foundation of forming a p-n junction and formation of devices during wafer fabrication. The mathematics that govern the mass transport phenomena of diffusion are based on Fick's laws. The application of Fick's laws of diffusion to describe the transport processes in concrete is based on the simplified assumption that concrete is homogeneous, isotropic and inert.

Whenever an concentration gradient, $\partial C/\partial x$, exists in a finite volume of a matrix substance the impurity material will have the natural tendency to move in order to distribute itself more evenly within the matrix and decrease the gradient. Given enough time, this flow of impurities will eventually result in homogeneity within the matrix, causing the net flow of impurities to stop. The mathematics of this transport mechanism was formalized in 1855 by Fick, who postulated that the flux of material across a given plane is proportional to the concentration gradient across the plane. Fick's First Law states:

$$J = -D (\partial C(x, t)/\partial x) \tag{22}$$

where J is the flux, D is the diffusion constant for the material that is diffusing in the specific solvent, and $\partial C(x,t)/\partial x$ is the concentration gradient. The diffusion constant of a material is also referred to as "diffusion coefficient" or simply "diffusivity". It is expressed in units of length²/time, such as $\mu\text{m}^2/\text{hour}$. The negative sign of the right side of the equation indicates that the impurities are flowing in the direction of lower concentration.

Fick's First Law does not consider the fact that the gradient and local concentration of the impurities in a material decreases with an increase in time, an aspect that's important to diffusion processes.

The flux J1 of impurities entering a section of a bar with a concentration gradient is different from the flux J2 of impurities leaving the same section. From the law of conservation of matter, the difference between J1 and J2 must result in a change in the concentration of impurities within the section (assuming that no impurities are formed or consumed in the section).

This is Fick's Second Law, which states that the change in impurity concentration over time is equal to the change in local diffusion flux, or

$$\partial C(x,t)/\partial t = - \partial J/\partial x \quad (23)$$

or, from Fick's First Law,

$$\partial C(x,t)/\partial t = \partial(D\partial C(x,t)/\partial x)/\partial x. \quad (24)$$

If the diffusion coefficient is independent of position, such as when the impurity concentration is low, then Fick's Second Law may be further simplified into the following equation:

$$\partial C(x,t)/\partial t = D \partial^2 C(x,t)/\partial x^2. \quad (25)$$

The main problem with using Fick's second law is that the chloride ions interact with the concrete and that diffusion is not the only transport mechanism working.

Takewaka and Matsumoto presented a Fickian chloride ingress model for marine environment. Since then many researchers have tried modifications. In most studies, model parameters, typically diffusion coefficients and initial surface concentration are measured and calibrated in-situ or in laboratory. It is consensual that testing is needed to calibrate any model which is used.

Probabilistic methods became more interesting due to the random and systematic variability's in deterioration models. Thoft-Christensen et al. (1996) and Sorensen et al. (1996) introduced a probabilistic framework for corrosion initiation and propagation at rebar level. Besides others Frangopol et al. (1997), Stewart and Rosowsky (1998), and Vu and Stewart (2000) are have further developed and used probabilistic models to predict time-varying performance of concrete bridges under chloride attack.

Corrosion is initiated when the chloride concentration at the bar surface exceeds a threshold level (C_{cr}). The chloride content [$C_{(x,t)}$] at a distance x from the concrete surface at time t is calculated from Fick's second law

$$C_{(x,t)} = C_0 [1 - \text{erf}(x/2\sqrt{tD})] \quad (26)$$

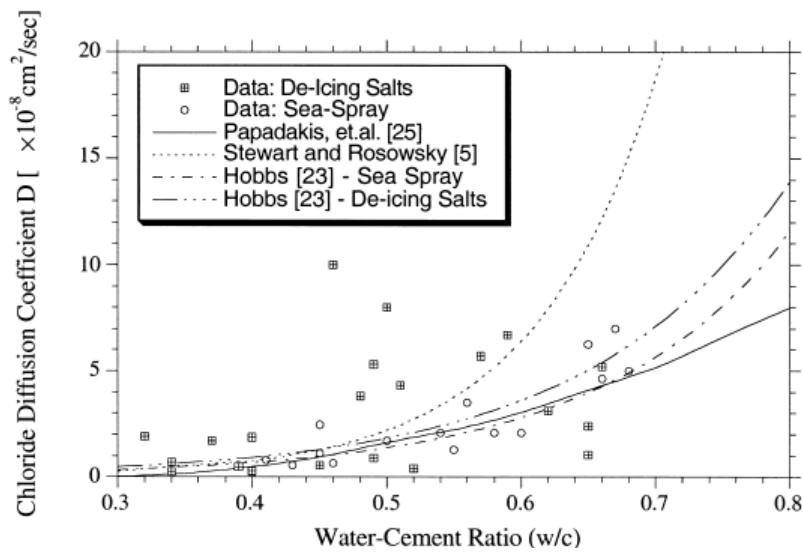
where C_0 is the surface chloride content (kg/m³ of concrete), D is the apparent diffusion coefficient (cm²/s) and erf is the error function. Corrosion initiation occurs if the chloride concentration $C_{(x,t)}$ exceeds the threshold chloride concentration (C_r).

The chloride surface concentration C_0 , and the chloride concentration $C_{(x,t)}$ in the depth X , are parameters depending on the concrete composition and on the environmental conditions.

The most important environmental variables influencing the chloride surface concentrations are the equivalent chloride concentration of the chloride source and the distance of the concrete surface from this chloride source.

There has been developed quite a number of models which consider the influence of mix proportions on chloride diffusion coefficient. All models exhibit similar trends and for w/c ratios typical for most RC structures differences between models are not significant.

Fig. 6: Influence of water/cement ratio on diffusion coefficient (Vu and Stewart, 2000)



Vu and Stewart (2000) presented a model, based on the model of Papadakis in 1996, in which the diffusion coefficient is considered as a parameter, dependent on water to cement ratio, aggregate to cement ratio, mass densities of cement and aggregates. The model developed by Papadakis et al. seems to be the best fit to the available literature, and is represented as

$$D = D_{H_2O} 0.15 \frac{1 + \rho_c \frac{c}{w}}{1 + \rho_c \frac{w}{c} + \frac{\rho_c a}{\rho_a c}} \left(\frac{\rho_c \frac{w}{c} - 0.85}{1 + \rho_c \frac{w}{c}} \right)^3 \quad (27)$$

where a/c is the aggregate-to-cement ratio, p_c and p_a are the mass densities of cement and aggregates and D_{H_2O} is the chloride diffusion coefficient in an infinite solution for NaCl. This model requires w/c ratio as an input parameter, which is estimated from concrete compressive strength using Bolomey's formula.

$$w/c = 27/(f_{cyl} + 13,5) \quad (28)$$

where f_{cyl} is the concrete compressive strength of a standard test cylinder in MPa (Vu and Stewart, 2000).

If the characteristic compressive strength ($F'c$) is specified by the designer (i.e. $F'c$ is known), then f_{cyl} , w/c and D [Eq. (27)] are dependent variables. Field-studies have shown coefficients of variation of 0.5 for coastal structures, 0.69 for coastal structures (Vu and Stewart, 2000). The model from Papadakis et al. seems to fit to the data quite well and it can be expected that the error is quite low. It is not possible to calculate statistical parameters for the model error because important details are missing (e.g. a/c , p_c , p_a).

If $[Cl^- (aq)]_{cr}$ indicates the diffusion coefficient of Cl^- in the aqueous phase (mol/m^3) required for the depassivation of steel bars, and with the the concrete cover c_c (mm), then time t_{cr} (years) to depassivation is given by (Teply B, 2002):

$$t_{cr} = \frac{[Cl^- (solid)]_{sat} (c_c/1000)^2}{3.1536 \cdot 10^7 \cdot 2D_{e,Cl^-} [Cl^- (aq)]_0 \left(1 - \frac{[Cl^- (aq)]_{cr}}{[Cl^- (aq)]_0}\right)^2} \quad (29)$$

It has been assumed that the diffusion coefficient and surface chloride concentration are independently derived variables. Literature shows that diffusion coefficients and surface chloride concentrations are not obtained by physical measurements. However, there appears to be no correlation between these two parameters but a good fit to Fick's law.

Usually corrosion rate is time-variant as the corrosion products reduce diffusion of the chloride ions away from the steel surface. The corrosion rate can be expressed as a time-dependent variable (Vu and Stewart, 2000):

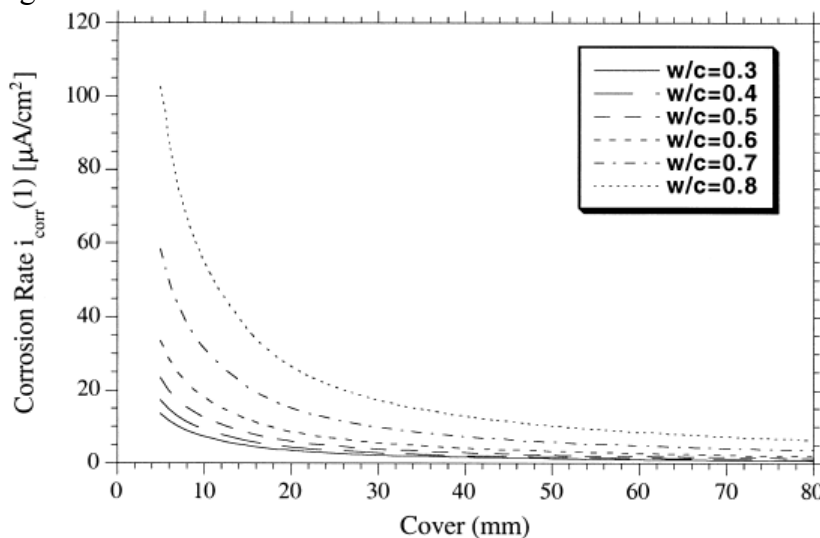
$$i_{corr}(t_p) = i_{corr}(1) \cdot 0,85t_p^{-0,29} \quad (30)$$

with t_p corrosion initiation $i_{corr}(1)$ is given by

$$i_{corr}(1) = [37,8 (1 - w/c)^{-1,64}]/cover \ (\mu A/cm^2) \quad (31)$$

Figure 7 shows the effect of concrete quality and cover on the corrosion rate, for a relative humidity of 75% and temperature of 20 C. In real assessment i_{corr} can only be obtained from site measurement and is a value of high uncertainty (Li et al, 2008).

Fig. 7: Influence of water/cement ratio and cover on corrosion rate (Vu and Stewart, 2000)



Vu and Stewart (2000) suggest that corrosion rate is slowed by the formation of rust products which impedes the access of reactive products to the steel surface and suggest that $\alpha = 0.85$ and $\beta = -0.3$. If the amount of corrosion product to produce cracking is the same for both time

variant and time invariant corrosion rates, then Vu et al. (2005) propose that the time to excessive cracking for a time variant corrosion rate T_{sp} (years) is

$$T_{SP} = [\beta + 1/\alpha(t_{sp} - 1 + \alpha/(\beta + 1))]^{1/(\beta + 1)} \quad t_{sp} > 1 \text{ year and } w_{lim} < 1\text{mm} \quad (32)$$

The main basic variables for steel corrosion and surface cracking are concrete cover, concrete strength and surface chloride concentration. The basic variables are modelled over time and space as spatial variables across the concrete surface. Corrosion initiation, corrosion rate, crack initiation and occurrence of severe cracking are dependent spatial variables. Table 1 shows the different stages of chloride induced corrosion:

Tab. 1: Definition of stages in the deterioration process and primary factors (Takewaka, 2005)

Stage No.	Definition of period	Primary factors characterizing the deterioration
1	Chloride penetration until the chloride concentration is up to the threshold value (around rebars)	<ul style="list-style-type: none"> • Chloride diffusion rate • Cover thickness
2	Progress of corrosion on rebar until concrete cracks due to corrosion	<ul style="list-style-type: none"> • Rebar corrosion rate • Resistance against concrete cracking
3	Corrosion on rebar after the appearance of concrete cracks	<ul style="list-style-type: none"> • Rebar corrosion rate • Crack width due to rebar corrosion
4	Degradation of structural performance due corrosion of rebar and cracking of concrete	

The Gaussian correlation is often used for spatial modelling of RC structures. The squared exponential function is defined for a stochastic two-dimensional random field. Monte-Carlo simulation is used to generate random variables for each element. Monte-Carlo simulation is a process which allows predicting the state of deterioration of each element at every time interval (Qinghui and Stewart, 2009).

A physical model would provide a more robust solution but the process of cover cracking is complex and dependent on a large number of variables. A physical model would require a large number of assumptions and/or data collecting which introduces scope for errors or inaccuracies in prediction. Physical models which are using finite elements analysis techniques may cause problems if Monte Carlo models are used because a very large number of simulations are required. The use of an empirical model provides a computationally fast, relatively accurate prediction for cracking times based on input parameters that are readily available and is therefore a suitable for use in reliability based analyses which is a motivation for the predictive model developed herein (Mullard, J.A., Stewart, M.G., 2009).

2.2 Application of Bayesian networks

2.2.1 Introduction

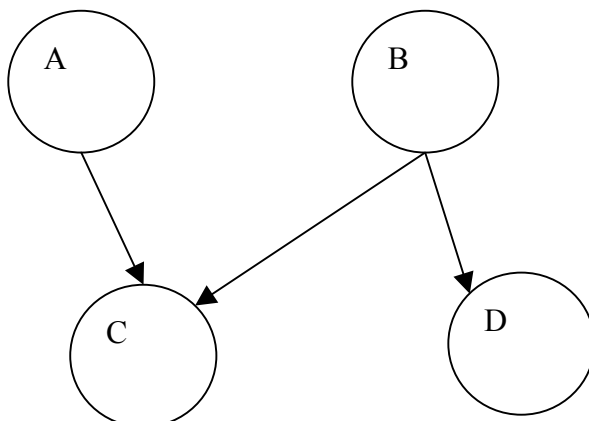
Flood protection concrete structures can be considered as large parts of engineering systems. Deterioration of concrete structures in the context of inspection and maintenance planning has become increasingly recognized by engineers and decision makers as being important. This paper is proposing to establish a probabilistic model of the performance and risk of large-scale concrete structures. One main problem herein is how to consistently integrate the experience and expertise of the inspection personnel and the collection of information into a model. One possible solution is the adaptation of Bayesian Probabilistic Networks (BPN) or Bayesian Belief Networks (BBN), which provide the rationale for combining the prior knowledge with the statistical data and give a representation between the variables relevant for assessment of concrete structures. BBN are a modelling probabilistic formalism that allows a robust and efficient framework for reasoning with uncertain knowledge. The development of the theory and application areas for Bayesian probabilistic nets has been and is still evolving rapidly. It is at present possible to utilise the techniques for almost any aspect of probabilistic modelling and decision making, ranging from inference problems, model building and data mining over to pre-posterior decision analysis.

A BPN is a directed acyclic graph (DAG) in which the nodes represent the system variables and the arcs symbolize the dependencies or the cause-effect relationships among the variables. BPN perform the variables joint distribution factorization based on the conditional dependencies. The main objective of BPN is to calculate the distribution probabilities in a group of variables (Capra, B., Le Drogo, 2007).

Formally a Bayesian network is composed of

- A set of variables and a set of directed edges (or connections) between the variables.
- Each variable may have a countable or uncountable set of mutually exclusive states.
- The variables together with the directed edges form a directed acyclic graph (DAG)
- To each variable A with parents B, C, D, \dots there is assigned a conditional probability structure $P(A|B,C,D,\dots)$

Figure 8: Bayesian Network



A Bayesian network is a representation of the joint distribution over all the variables represented by nodes in the graph. The network of figure 9 can be described as:

$$P(A, B, C, D) = P(A).P(B).P(C|A, B).P(D|B) \quad (33)$$

When an observation, or evidence, is put on one node, inference algorithm produces a conditional distribution of the variables given the evidence: the posterior distribution. This is based on Bayes' theorem. In a Bayesian network, conditional law parameters can also be random variables. These parameters will be updated when adding observations on the other nodes of the network.

As mentioned before, the main concept is to make use of the Bayes' theorem. With n numbers of hypotheses H_j and a given evidence E, the updated probability is

$$p(H_j|E) = \frac{p(E|H_j) \times p(H_j)}{\sum_{i=1}^n p(E|H_i) \times p(H_i)} \quad (34)$$

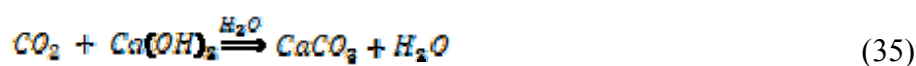
The expression $p(H_j|E)$ is the belief of hypothesis H on observing the evidence E. The term $p(E|H)$ is the likelihood that the evidence E is observed, assuming that H is true. $p(H)$ is the probability of trueness of the hypothesis and $p(E)$ is the probability that the evidence E will happen. With a BBN it is possible to update probabilities in the moment new information is available.

In general the advantages of BBN in Risk assessment are as follows (Friis-Hansen, A., 2000):

- Qualitative and quantitative variables can easily be combined in the same model
- Consistent dependence/independence statements
- Nods are not restricted to binary states as in the case for fault trees
- Compact representation
- Insertion of evidence and subsequent updating of the model
- Identification of requisite and irrelevant information
- Dynamic model.

2.2.2 Bayesian-Belief-Network-Model for Carbonation-Induced Corrosion

The carbonation induced corrosion of reinforced concrete is typically defined as the chemical reaction between atmospheric carbon dioxide and the product of hydration, mainly calcium hydroxide reducing the pH of concrete and destroying the passive layer on steel rebars which gives start to corrosion.



The carbonation process requires the presence of a certain amount of water. If the concrete is too dry (RH <40%) CO_2 cannot dissolve and no carbonation occurs. In the case that the concrete is too wet (RH >90%) CO_2 cannot enter the concrete and the concrete will not carbonate. Optimal conditions for carbonation occur at a RH of 50% (range 40 to 90%).

Moisture is a very important factor for the rate of carbonation. Carbonation only occurs in presence of water (see Eq. 35).

The mathematical function normally used for a first approximation of the rate that concrete carbonation penetrates inward to a depth x proportional to the square root of the exposure time t is

$$x = k t^{1/m} \quad (36)$$

As mentioned before the concrete quality has a major effect on the carbonation process. The w/c determines the porosity and permeability of the concrete. The lower the water-cement-ratio of concrete is the lower is the porosity. With a lower porosity the carbon dioxide diffusivity also turns lower. Carbonation occurs progressively from the outside surface of the concrete exposed to atmospheric CO_2 , but does so at a decreasing rate because the CO_2 has to diffuse through the pore system, including the already carbonated surface zone of concrete. If the pores of the hydrated cement paste are filled with water, the diffusion of CO_2 is further slowed because its diffusion through water is time four slower than in air.

Equation 36 is valid only under steady-state environmental conditions that supplies steadily CO_2 and uniform concrete properties that allow steady diffusion of CO_2 . These conditions, however, are usually not attained in field exposures. Field environments vary as temperature, relative humidity, and CO_2 concentration fluctuate, and diffusion properties vary with variations in concrete properties.

The carbonation coefficient k is a variable which can change over time and also within one structure. The coefficient depends on the effective diffusion of CO_2 through the concrete and on the environment and in-depth concentrations of CO_2 .

The BBN will be established by using the carbonation coefficient k under different exposure conditions. Richardson (1988) developed a formula to calculate k which takes the different influencing parameters into account (Richardson, 1988):

- CO_2 concentration
- Surface inclination
- Carbonation profile
- Moisture condition
- Concrete quality

Additionally a special correlation factor k_{av} is introduced by Richardson (1988) by a value of 1.5 to 2.0.

By making use of Eq. 36 the carbonation depth can be calculated. The carbonation depth x node strongly relates to the carbonation coefficient k and the time nodes t .

The depassivation (SLS) takes place at the end of the initiation phase and is the beginning of the destruction phase (see Fig. 5).

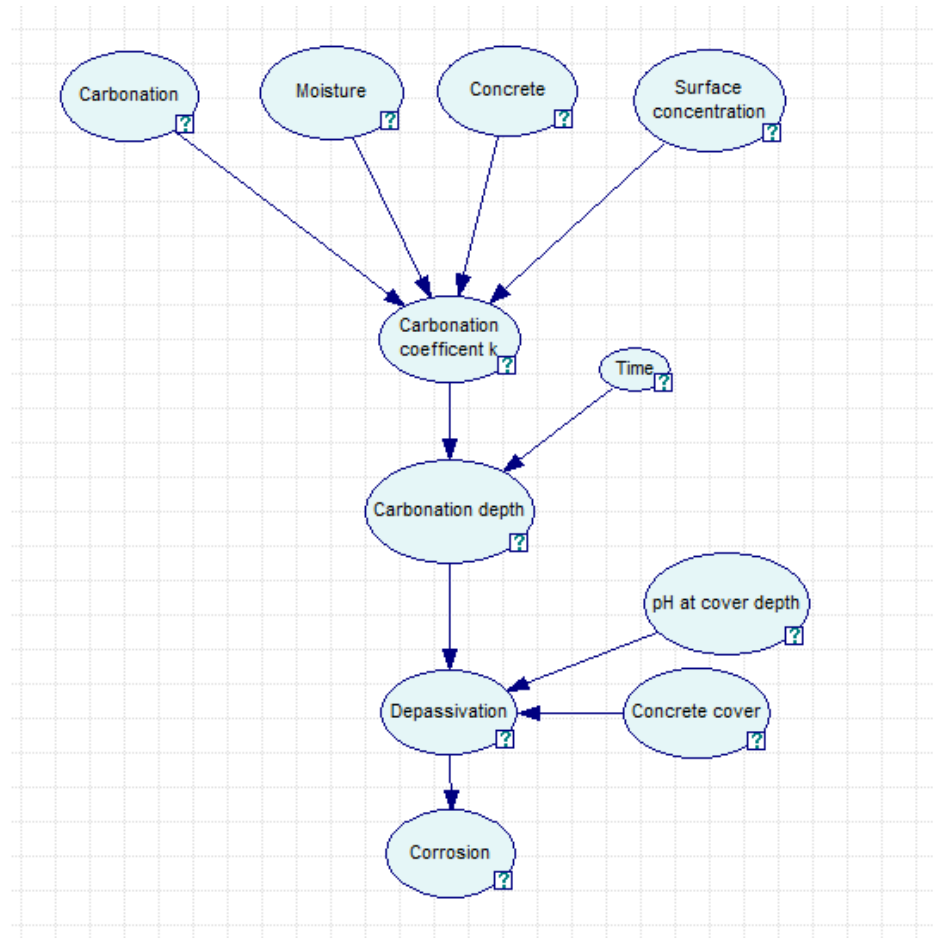
In the Bayesian probabilistic approach “depassivation” is the evidence E. That means that when the evidence turns true the depassivation node turns also “true”. That happens when the carbonation front has reached the steel or when

$$x \geq c \tag{37}$$

With x : carbonation depth
 c : concrete cover

The carbonation depth can be measured by the use of the coloured indicator phenolphthalein. Phenolphthalein is a pH indicator at cover depth. That is why the pH indicator is coupled with the depassivation node.

Figure 9: Bayesian-Belief-Network-Model for Carbonation-Induced Corrosion



Because the choice of the prior probabilities is not based on sharp evidence, a sensitivity study is needed to check the influence of the prior probabilities on the final results. The structure of a probabilistic graphical model represents qualitative dependencies among

situation attributes, and its parameters (probabilities) represent a quantification of these dependencies. Model parameters represent both the strongest and weakest aspect of probabilistic graphical models. In this context, it is useful to determine which variables have the largest impact on the uncertainty in the model (Grete-Regamey, A., Straub, D. (2006). The sensitivity analysis in this case will be conducted on carbonation coefficient, carbonation depth and depassivation.

2.2.3 Proposed study

This project is part of research of Risk Based Maintenance Planning of FPW. The Bayesian probabilistic network can help to reach this goal by providing the rationale for combining prior knowledge with statistical data. It represents the coherence between the variables which are relevant for assessment of existing structures.

The presented Bayesian network (Fig. 9) will be applied on a concrete FPW in Hamburg.

For this case data on carbonation will be generated from literature studies because there is no measured data available and destructive test are not eligible in the case of flood protection structures in use.

As mentioned before some Schmidt-Hammer tests are a basis to determine the compressive strength of the concrete R_c of the flood protection structure. This test is an indirect test which leads to indirect measures to be used to update the model.

The use of available on site measurements will lead to a probability density function of concrete cover c . The relative humidity of concrete in such a structure is strongly related to environmental conditions. One assumption is that the humidity is constant with a representative mean value of 75% for the coastal environment.

The plausibility of each structural model within a set of possible models, given the measured data, is quantified by the joint posterior probability density function of the model parameters. This Bayesian approach requires the evaluation of multidimensional integrals. Markov chain Monte Carlo simulation methods have been developed to solve the Bayesian model updating problem (Cheung, S.H., Beck, J.L., 2009).

There is software available for the simulation of Bayesian networks, SIMEO MC², developed by Oxand^R. This software is using a Gibbs Sampling algorithm which belongs to the family of Markov Chain Monte Carlo (MCMC) algorithms. The Gibbs sampler is an algorithm to generate a sequence of samples from the joint probability distribution of random variables. It is used to compute an integral (Capra, B., Le Drogo, 2007).

With such software the convergence of the algorithm will be checked by making use of convergence curves of multiple simulations.

Based on this study condition indicators can be identified for the assessment whether they are directly or indirectly measured.

The main target is to establish a probabilistic model of deterioration due to carbonation for planning of inspection and maintenance.

3 Conclusion

The first example shows that also very limited information like the expected standard deviation of a certain value can be used to update the information.

Even if the mean value is not changed, a reduction in the standard deviation can be observed. This leads to a significant lower value. It is shown that Bayesian updating is very useful in the assessment of existing concrete structures, to upgrade the models, when some data due to tests are available. Also engineer judgement can then be combined with test results.

Concerning deterioration processes it must be stated that predictive models of structural systems can reveal inaccurate when the physics is grossly described by the models and when the model parameters are not well known.

The proposed approach in this paper is based on the Bayesian updating of the prior densities of the input parameters using measures of response quantities. Within the classical probabilistic study, it is just possible to use one type of the measures available (X calculated by measures on R_c or X measured directly).

The problem is that usually not the two types of measures can be used together because that will lead to a loss of information. The reason for that is, that not all the data available is used.

The proposed application of Bayesian Networks seems to have great potential in the risk management of concrete flood protection walls. Bayesian networks will allow a better control of uncertainty combining heterogeneous information like expert statements and uncertain ground measures. If only few measures are available, the utility of such a method is undeniable. Bayesian networks make it possible for the engineer to balance relative confidences between expert opinion and measurements.

4 References

- Capra, B., Le Drogo, (2007) J., Reinforced concrete corrosion: application of Bayesian networks to the risk management of cooling towers in nuclear plants
- Cheung, S.H., Beck, J.L. (2009), Bayesian Model Updating Using Hybrid Monte Carlo Simulation with Application to Structural Dynamic Models with Many Uncertain Parameters In: Journal of Engineering Mechanics, ASCE, April 2009, pp. 243-255
- Diamantidis, D. (2001), Probabilistic Assessment of Existing Structures – JCSS Report
- Faber, M.H. (2001), Risk and Safety in Civil, Surveying and Environmental Engineering, Lecture Notes, Zürich
- Friis-Hansen, A. (2000), Bayesian Network as a Decision Support Tool in Marine Applications, PhD-Thesis, Internet: <http://www.skk.mek.dtu.dk/>
- Grete-Regamey, A., Straub, D. (2006), Spatially explicit avalanche risk assessment linking Bayesian networks to a GIS, Nat. Hazards Earth Syst. Sci., 6, 911–926
- Li, C. Q., et al (2008), Prediction of Reinforcement Corrosion in Concrete and Its Effects on Concrete Cracking and Strength Reduction, In: ACI Materials Journal, V. 105, No 1

- Lindvall, A. (2000), Probabilistic Performance Based Service Life Design of Concrete Structures – Environmental Actions and Response
- Malhorta, V.M. (2000), Durability of Concrete, Corrosion Handbook Second Edition, R.W. Revie Ed., Wiley
- Martz, H. F. (1991), Bayesian Reliability Analysis, Krieger Publishing Company, Florida
- Mullard, J.A., Stewart, M.G., (2009), Corrosion-Induced Cover Cracking of RC Structures: New Experimental Data and Predictive Models, Research Report No. 275.05.2009
- Qinghui, S., Stewart, M.G., (2009), Corrosion cracking prediction updating of deteriorating RC structures using inspection information. In: Reliability Engineering and System Safety 94 pp. 1340 - 1348
- Rafiq, M. I. et al. (2004), Performance updating of concrete bridges using proactive health monitoring methods. In: Reliability Engineering and System Safety 86 pp.247–256
- Richard, D., (2003) Lifecycle Performance Model For Composite Materials In Civil Engineering, Master-Thesis, University of Cincinnati
- Richardson, M.G. (1988), Fundamentals of durable reinforced concrete, E&FN Spon Press, New York
- Thoft-Christensen, et al (1996), Assessment of the reliability of concrete slab bridges. In: Frangopol DM, Corotis RB, Rackwitz R, editors., Proceedings of the Seventh IFIP WG 7.5 Working Conference on Reliability and Optimization of Structural Systems. 1996. pp. 323–328.
- Vu, K., Stewart, M., (2000), Structural reliability of concrete bridges including improved chloride-induced corrosion models. In: Structural Safety 22 (2000) pp. 313-333

Probabilistic service life prediction of hydraulic structures under abrasion loads

M. Vogel, H. S. Müller
Institute of Concrete Structures and Building Materials,
University of Karlsruhe (TH), Germany

Abstract: Regarding the durability of hydraulic structures, the mechanical wear of the concrete surface zones represents a key exposure. Abrasive wear of concrete in hydraulic structures generally causes a reduction in service life as well as high costs due to necessary repair work and corresponding production downtimes. The knowledge about abrasive mechanisms is still insufficient. Furthermore no standardized test method for the realistic verification of the abrasion resistance of concrete exists so far. On this background an advanced test apparatus for the simulation of the abrasive wear of concrete is presented in this paper. Using this test method, the relevant material parameters, which affect the abrasion resistance of concrete, could be identified. Furthermore, the development of an empirical degradation model by means of statistical methods is shown. The main focus of this paper is on the probabilistic service life prediction of hydraulic structures under abrasion load.

1 Introduction

Abrasive damages at hydraulic structures primarily result from waterborne sand, gravel, rocks and other debris which circulate over concrete surfaces. This exposure causes a progressive degradation of the concrete by a continuous material removal, see Figure 1. Abrasive damages on hydraulic concrete structures range from a few centimetres to several decimetres [1, 2, 3, 4].

The rate of abrasion wear depends on the kind of exposure and on the durability of concrete. The main factors regarding the exposure are quantity, hardness, shape and size of the rubble as well as the velocity of the water. The concrete durability is influenced by the hardness, shape and size of the aggregates, the aggregate/paste bond and the content, hardness and elasticity of the paste [4, 5, 6].

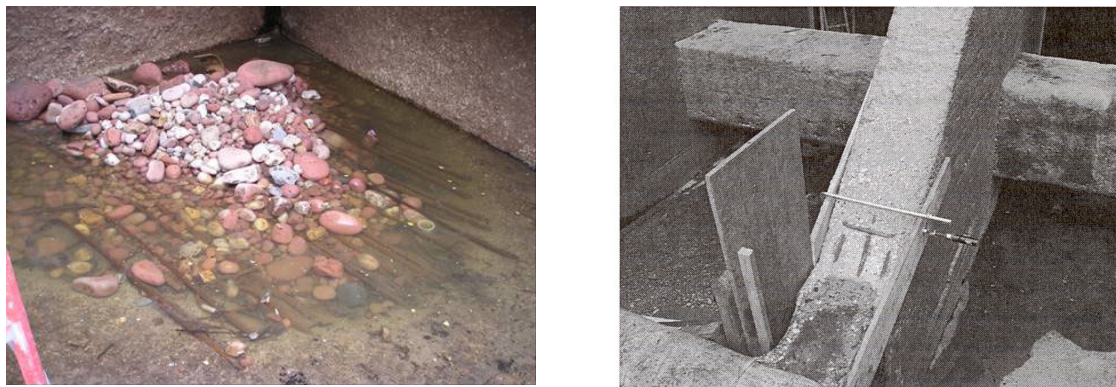


Fig. 1: Examples of abrasive wear damages on hydraulic structures (left: base of a stilling basin; right: dam pillar)

As the abrasive wear of concrete is a very complex process, i. e. a combination of rubbing and impact action, so far there is no standard test procedure which can completely reproduce the natural conditions on hydraulic structures. For example, the standard abrasive wear test methods [7, 8, 9] simulate mainly either the rubbing or the impact action. Bania [10] realised this problem and developed an abrasion test machine for simulating the abrasive wear in a more realistic way.

The characteristic values of hardened concrete, which mainly affect the abrasion resistance, have not yet been identified so far. Besides the compressive strength, the flexural tensile strength, the tensile splitting strength, the modulus of elasticity and the porosity are mentioned in the literature as influencing factors [1, 4, 11, 12, 13, 14].

The modelling of abrasion wear of concrete is a complex problem because the abrasive wear is inherent in the hydraulic system. Bania [10], Atiş [12], Pat & Reinhardt [15], Hu et al. [16] and Horszczaruk [17] modelled the abrasive wear of concrete surfaces under laboratory conditions. Particularly the model by Bania seems suitable for the prediction of the abrasion damaged in hydraulic structures. The comparison of field tests by Jacobs [4] showed in a first approximation a consensus between the calculations using the model by Bania and the in situ measurements.

An established method in order to predict realistically the durability of concrete is based on the probabilistic service life design of concrete [18]. The well-known models to describe the ingress of chloride ions into concrete or the process of carbonation are applied in order to estimate the time-dependent concrete durability. Regarding the abrasive wear, no such approaches have been shown in the literature.

2 Abrasion test

Within the own experimental studies an innovative abrasive wear test apparatus was developed and applied [10]. The effectiveness and functional capability of this apparatus was verified in detail by the application of statistical methods.

2.1 Abrasive wear test apparatus

The test apparatus consists of a steel cylinder with an internal hollow shaft. The shaft is powered via a chain drive with a gear motor, see Figure 2. On the shaft up to 18 concrete samples can be fixed on mountings. The rotation speed of the hollow shaft can be steplessly increased from 10 to 70 rpm. Hence, the load energy ranges from 900 to 6000 J/m³. With the help of 24 steel paddles the solid-water-composite – the rubble – is agitated. The solid-water-composite contains basalt/water and river-gravel/water at a ratio of 1:1 by mass. The fill factor in the steel cylinder is about 14 Vol.-%.

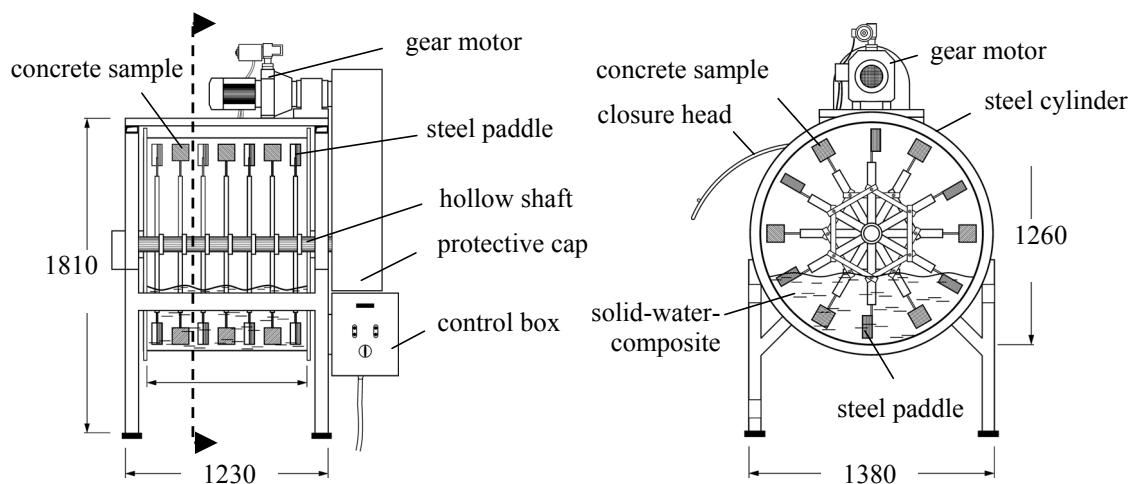


Fig. 2: Abrasive wear test apparatus; dimensions in [mm]

2.2 Experimental investigations with respect to the test apparatus

To prove the efficiency of the test apparatus the solid-water-mixture, the concrete samples as well as the reproducibility and the adjustment of the specimens in the steel cylinder have to be considered, see Table 1.

Tab. 1: Overview on the test program

test no.	designation	solid-water-mixture	geometry	number	test duration
1	"basalt 16"	basalt-water mix gravel 2/16 mm	cube	6 pieces	22 hours
2			cylinder		
3	"quartz 16"	quartz-water mix gravel 2/16 mm	cube		
4			cylinder		
5	"quartz 32"	quartz-water mix gravel 2/32 mm	cube		
6			cylinder		
7	"quartz 16 w"	quartz-water mix gravel 2/16 mm	cube		
8					
9					
10	"quartz 16 l"		cylinder		

For the test series according to Table 1 the abrasion energy was adjusted to approximately 3900 J/m^3 and the test duration was set to 22 hours. After each test, the rubble was changed. The portland cement concrete used in this program was designed to have a target compressive strength $f_{cm} = 40 \text{ MPa}$ with a w/c ratio of 0.56. The applied natural aggregates were composed of river sand and gravel and had a grading curve of A/B 16 according to DIN 1045-2 [19]. The curing and storing were arranged according to DIN EN 12390-2 [20]. The dimensions of the specimens were 100 mm edge length for the concrete cubes and 100 mm height and 100 mm diameter for the concrete cylinders. The measurement of the abrasive wear was carried out with a focus on the mass loss. The time dependent process of the abrasive wear is shown in Figure 3.

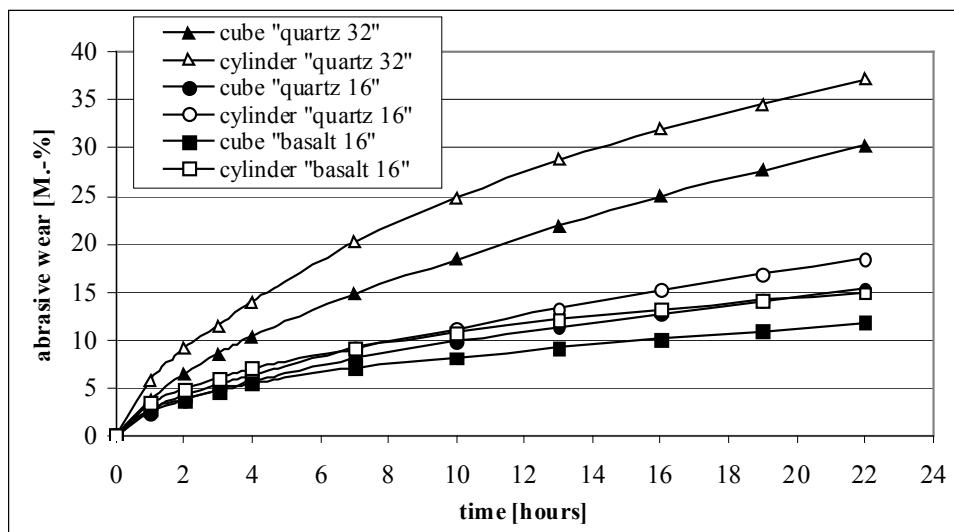


Fig. 3: Abrasive wear-time sequence plots for the different tests

The tests No. 1 to 6 in Table 1 were designed to identify the optimal test conditions (variability investigations), whereas tests No. 7 to 10 were conducted to specify potential undesired effects (hypothesis testing). For the last test – No. 10 – 18 specimens were mounted in the steel cylinder for testing the adjustment of the specimens in the cylinder. The working hypothesis for the tests No. 7 to 9 is whether test repetition significantly affects the abrasion. For the test No. 10 the hypothesis is whether the adjustment of specimens (six specimens each alignment) in the test apparatus affects the abrasion significantly. One-way analysis of variance was used to test the above stated hypotheses [21]. The tests were conducted on a level of significance of 5 %.

2.3 Results

The results of the analytical investigations according to tests No. 1 to 6 showed that the optimal test conditions include cylindrical concrete samples in conjunction with solid-water-mixture composed of quartz with 16 mm maximum aggregate size. Hereby, a visible and measurable abrasive wear under controlled terms with low deviations could be realized. The one-way analysis of variance tests showed that the factors “experimental repetition” and “adjustment of the specimens” are not significant. Therefore the differences between the mean values depend on natural scatter.

3 Identification of the relevant material parameters

3.1 Concrete mixtures

Ordinary Portland cement (CEM I 32.5 R) and blast furnace cement (CEM III/B 32.5 R) were used for the subsequent investigations. Furthermore, four w/c-ratios of 0.35, 0.45, 0.55 and 0.65 as well as four grading curves of A16, A32, B16 and A16SP (SP = crushed aggregates) were selected. The different concretes were either prepared using a constant amount of cement paste contents (31 Vol.-%) or with various contents of cement paste (25, 28, 34 and 37 Vol.-%). For each concrete mix specimens were casted for the abrasion tests as well as for parallel conducted investigations on material properties.

3.2 Test program

At an age of 28 days the different concretes were tested for 22 hours under the conditions specified in chapter 2. Before and after the abrasive wear test the mass of the specimens was measured. Extensive material testing was conducted on separate samples in order to identify the key material constants, which significantly affect the abrasive wear resistance of the different concretes. These tests included the compressive strength, the flexural strength, the splitting tensile strength, the adhesive tensile strength, the rebound hammer test, the static and dynamic modulus of elasticity, the true porosity, the water absorption coefficient, the pore size distribution and the fracture energy.

3.3 Statistical analysis

The results of the test procedure provided the basis for the application of multivariate statistical analysis methods. These methods are regression and correlation analyses as well as analysis of covariance [21].

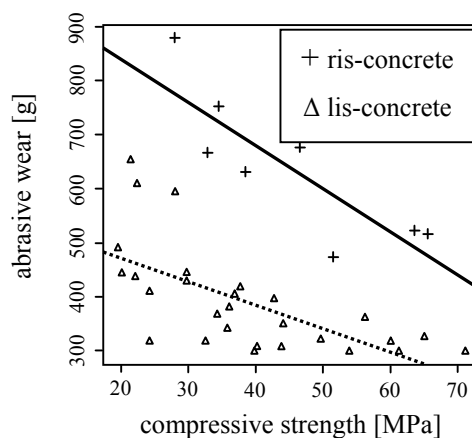


Fig. 4: Model fit of the data according to the abrasive wear and the compressive strength

With the analyses of covariance it is possible to combine explanatory variables like compressive strength with categorical variables, like cement type. Figure 4 shows the model-

ling of the test data affected by the compressive strength and the factor “graining” (ris = high amount of sand, lis = low amount of sand). The effect of the factor “graining” and “cement type” was confirmed by a (Welch-modified) t-test on the 5 % level of significance. The variable selection for the identification of the statistical model was made with the testing-based procedures.

3.4 Results

The compressive strength combined with the dynamic modulus of elasticity present the two main factors that affect the abrasion wear significantly. The new defined material constant, which is a multiplicative junction of the above described constants is named M, see equation (1). The average material constant M ranges from 0.7 to 2.6 [MN²/mm⁴].

$$M = f_{cm, cyl} \cdot E_{c, dyn} \quad (1)$$

4 Modelling the abrasive wear

To model the time dependent processes of abrasive wear an empirical model was developed for concretes that are commonly used in hydraulic structures. The basis of the model is a power function, which contains the load duration, the load energy and the material properties.

4.1 Concrete mixtures

Concrete specimens were made with natural aggregate river sand, gravel and ordinary Portland cement (CEM I 32.5 R). The continuous grading curve according to DIN 1045-2 [19] was set to be between A and B, close to A. The range of the w/c-ratio is between 0.35 and 0.80. The cement content was varied from 210 kg/m³ to 500 kg/m³. A plastic consistency of the concrete mix was projected.

4.2 Test program

All specimens were tested for 100 hours starting at the age of 28 days according to chapter 2. The mass loss of the specimens was measured after 1, 2, 4, 7, 12, 20, 28, 38, 48, 60, 72, 86 and 100 hours. Six different load energies 981, 1607, 2387, 3321, 4409 and 5650 J/m³ were applied. The chosen energy was kept constant over the test duration. Applying test results on parallel samples the material constants M were calculated.

4.3 Empirical model

The experimental investigations delivered 36 different temporal developments for the abrasive wear of concrete. These time paths are dependent on the load duration, the load energy

and the material behaviour. On the basis of the database an empirical model for the abrasive wear was developed, see equation (2) to (7).

$$S(t, M, E, \alpha) = \frac{A \cdot M^B \cdot t_a^{0.4161}}{\rho_B} \cdot \eta_\alpha \quad (2)$$

$$S(t, M, E, \alpha) = \text{abrasive wear [mm]}$$

$$A(E) = 0.2680 \cdot E^3 - 3.6913 \cdot E^2 + 32.5290 \cdot E \quad (3)$$

$$B(E) = -5.925 \cdot 10^{-3} \cdot E^3 + 5.6011 \cdot 10^{-2} \cdot E^2 - 0.2576 \cdot E \quad (4)$$

$$E(v, q) = \frac{q \cdot v^2}{2} \quad (5)$$

$$q = \text{total solid [kg/m}^3\text{]}$$

$$v = \text{flow velocity [m/s]}$$

$$\rho_B = \text{concrete bulk density [kg/m}^3\text{]}$$

$$t_a(a, d) = a \cdot 8766 \cdot \left(\frac{d}{365.25} \right) \quad (6)$$

$$t(a, d) = \text{load duration in hours [h]}$$

$$a = \text{load duration in years [a]}$$

$$d = \text{days of load duration per year [d]}$$

$$\eta_\alpha(\alpha) = \frac{\left(-1.4808 \cdot \left(\frac{\alpha}{90^\circ} \right)^2 + 1.6381 \cdot \left(\frac{\alpha}{90^\circ} \right) + 0.9684 \right)}{1.2939} \quad (7)$$

$$\eta_\alpha(\alpha) = \text{angle coefficient [-]}$$

$$\alpha = \text{angle of attack [}^\circ\text{]}$$

A fitting of the model was carried out with a nonlinear regression analysis based on the experimental data using the Gauss-Newton method for iterative model estimation [22]. The calculations were done with the statistic program ‘‘R’’ [23].

5 Probabilistic service life prediction

The use of statistical methods combined with the developed empirical model for service life prediction is based on essential design steps which are briefly described below.

5.1 Statistical quantification of the model parameters

The model parameters load energy and material constant are afflicted with a certain statistical variance. Therefore, these parameters are random variables, so called basic variables. For these values, the mean and the coefficient of variation must be declared by means of statistical calculations.

5.2 Damage processes and limit states

During the damage process of a concrete structure several limit states are reached. A limit state is a condition, at which the hydraulic structure component does not satisfy its planned serviceability anymore, i. e. the predefined limit state is reached after a certain period of time. In the following, the limit state is defined by the condition in which the abrasion wear has destroyed 80 % of the concrete cover. Moreover it is important to notice that economic maintenance at hydraulic structures is only possible if the reinforcement in the concrete component is not affected by the abrasion wear.

5.3 Service life of hydraulic structures

The service life of a hydraulic structure is a parameter to be defined when planning the structure. Reference values of the service life of buildings and structures are listed in relevant standards and guidelines. As an example, the service life of residential buildings and other simple engineering structures is 50 years, for hydraulic structures and complex engineering structures it is 100 years [24].

5.4 Failure probability and limit state function

Service life prediction or durability design can be achieved in the context of a failure probability. The failure probability P_f is defined as the probability for exceeding a limit state within a defined reference time period. The limit state can be expressed by correlating the resistance R and action E , see equation (8).

$$G = R - E \tag{8}$$

If the value of G turns to zero, the limit state is reached. The statistical properties of the limit state function G can be expressed by means of a distribution function, if the limit state function is considered to be normal-distributed and the resistance R as well as the action E are expressed using related mean values μ and standard deviations σ , see Figure 5.

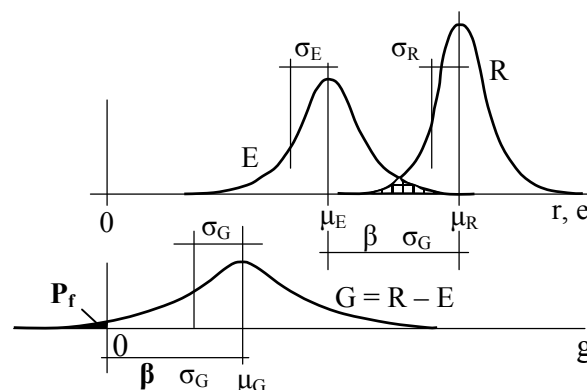


Fig. 5: Failure probability P_f and reliability index β

In case of a normal distributed limit state function G , the failure probability P_f can be determined directly by equation (9).

$$P_f = P(G \leq 0) = \Phi(-\beta) \tag{9}$$

Here, the variable Φ is the distribution function of the standardized normal distribution. The correlation between the reliability index β and the failure probability P_f is given in Table 2.

Tab. 2: Correlation between reliability index β and failure probability P_f [24]

P_f	10^{-1}	10^{-2}	10^{-3}	10^{-4}	10^{-5}
β	1.28	2.32	3.09	3.72	4.27

Problems with the durability of concrete structures are generally connected to time dependent deterioration processes. Therefore, a reference period has to be given to make the assessment of the structure’s reliability possible. Table 3 contains target values of the reliability index for building components in the serviceability limit state (SLS).

Tab. 3: Target values of the reliability index β [25]

relative cost of safety measures	reliability index β
high	1.3
moderate	1.7
low	2.3

The calculation of the failure probability for a hydraulic structure component in the unintentional condition “abrasive wear depth reaches the reinforcement” can be performed by the use of the following equation (10). The parameter c is the concrete cover and $P_{f, \max}$ is the maximum permissible failure probability.

$$P_f = P\{0.8c - S(t, M, E, \alpha) \leq 0\} \leq P_{f, \max} \tag{10}$$

The limit state is reached when 80 % of the concrete cover is destroyed.

5.5 Prediction of the abrasive wear of concrete in hydraulic structures

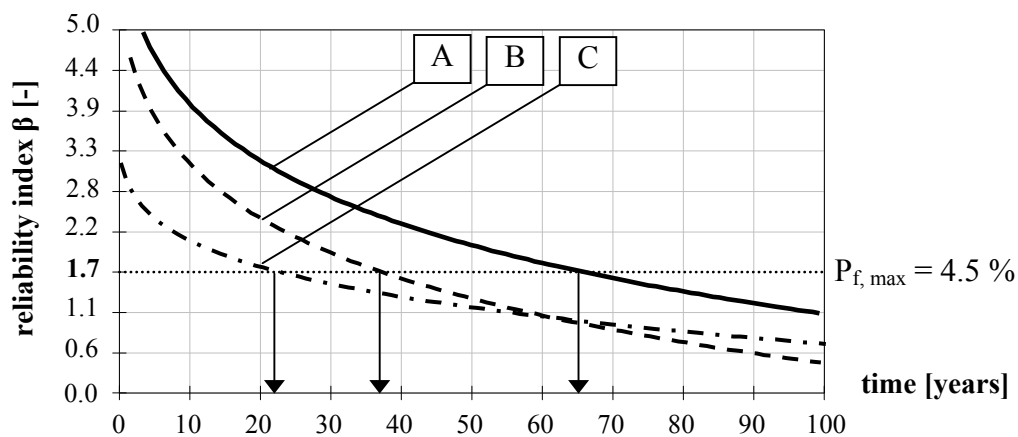
For predicting the durability of a hydraulic structure, the above mentioned parameters need to be defined. In the field test by Jacobs [4] the concrete of a bottom plate in a diversion tunnel was considered. The parameters for the probabilistic service life design have to be statistical quantified, see Table 4.

The prediction of the durability of the bottom plate was performed for a reference period of 100 years. The target value of the reliability index was set to be 1.7 and corresponds to a failure probability $P_{f, \max}$ of about 4.5 %, see Table 3. The determination of the time-dependent reliability index β was calculated with the FORM-method using the software STRUREL [26], see Figure 6.

Tab. 4: Statistical parameters for the durability design

parameter	dimension	distribution	par. a	par. b	par. c	par. d
duration of loading t	[a]	-	100	-	-	-
exposure days per year d	[d]	-	80	-	-	-
material constant M	[N ² /mm ⁴]	normal	2.636	0.30	-	-
concrete bulk density ρ_B	[kg/m ³]	lognormal	2568	50	-	-
flow velocity v of water	[m/s]	lognormal	12.9	1.3	-	-
total solid q content in water	[kg/m ³]	normal	3.1	0.60	-	-
angle of attack α	[°]	-	0	-	-	-
concrete cover c	[mm]	beta	60	9	0	100

The calculated probability of abrasive wear damage for the above mentioned conditions after a service life of 100 years is $P_f = 14\%$. The limit state is reached after 65 years of service life, see curve A.


 Fig. 6: Reliability index β vs time t for various concrete covers c, see Table 5

Based on this analytical investigation a deliberate sensitivity analysis according to the relevant model parameter was performed, see Figure 6 and Table 5. For example, if the concrete cover is reduced to $c = 50$ mm – at constant scatter – the remaining service life is only 37 years, see curve B. For this study after a service life of 100 years the failure probability is $P_f = 33\%$. On the other hand, if the scatter of the concrete is twice as at the initial state A the calculated remaining service life is about 22 years, see curve C. In this case however, after 100 years of service life the calculated failure probability is $P_f = 24\%$.

Tab. 5: Parameter study according to the concrete cover

study	mean a [mm]	standard deviation b [mm]	par. c [mm]	par. d [mm]	reliability index β [-]	failure probability P_f [%]
A	60	9	0	100	1.1	14
B	50	9	0	100	0.4	33
C	60	19	0	100	0.7	24

This brief study shows the relative influence of the statistical parameters describing the service life of a hydraulic structure component subjected to abrasive wear conditions. The obtained results show clearly that an exact quantification of the statistical parameters is an important task within the framework of the service life prediction.

6 Conclusions

The presented test apparatus applied in this study is appropriate to simulate the abrasive wear in a realistic and effective way. On the basis of the gathered data the relevant material parameters, that affect the abrasion resistance of concrete, were identified, see chapter 3.4. With the developed abrasion wear model in a first approach the service life prediction of hydraulic structures under abrasion loads is possible. Further investigations are required e. g. to calibrate the model by results of field studies on hydraulic structures.

7 Literature

- [1] ACI Committee 210: Erosion of Concrete in Hydraulic Structures. ACI 210R-87, ACI Materials Journal, March - April 1987
- [2] McDonald, James E.: Maintenance and Preservation of Concrete Structures: Report 2, Repair of Erosion-Damaged Structures, Technical Report No. C-78-4 U.S. Army Engineer Waterways Experiment Station, Vicksburg, Apr. 1980
- [3] Hallauer, O.: Die Abriebbeanspruchung von Tosbecken. Mitteilungen der Versuchsanstalt für Wasserbau, Hydrologie und Glaziologie, Internationales Symposium über Erosion, Abrasion und Kavitation im Wasserbau, Zürich, (1988), Nr.99, 63-93
- [4] Jacobs, F., Winkler, K., Hunkeler, F., Volkart, P.: Betonabrasion im Wasserbau - Grundlagen/Feldversuche/Empfehlungen. Mitteilungen der Versuchsanstalt für Wasserbau Hydrologie und Glaziologie der Eidgenössischen Hochschule Zürich, Zürich, 2001
- [5] Papenfus, N.: Applying Concrete Technology to Abrasion Resistance. Proceedings of the 7th International Conference on Concrete Block Paving (Pave Africa 2003), Sun City, South Africa, 2003
- [6] Haroske, G.: Hydroabrasionsverschleiß von Betonoberflächen. Deutscher Ausschuss für Stahlbeton, Heft 511, Beuth Verlag GmbH, 2000
- [7] ASTM 799/C 779M – 00: Standard Test Method for Abrasion Resistance of Horizontal Concrete Surfaces, 2000
- [8] ASTM C 418-98: Standard Test Method for Abrasion Resistance of Concrete by Sandblasting, 1998
- [9] ASTM C 1138-89: Standard Test Method for Abrasion Resistance of Concrete (Underwater Method), 1989

- [10] Bania, A.: Bestimmung des Abriebs und der Erosion von Betonen mittels eines Gesteinstoff-Wassergemisches. Wismar, Dissertation, 1989
- [11] Dhir, R. K., Hewlett, P. C., Chan, Y. N.: Near-surface characteristics of concrete: abrasion resistance. In: *Materials and Structures*, 24 (1991), 122-128
- [12] Atiş, C. D.: Abrasion-Porosity-Strength Model for Fly Ash Concrete. In: *Journal of Materials in Civil Engineering*, ASCE, 15 (2003), Nr. 4, 408-410
- [13] Liu, Y.-W., Yen, T., Hsu, T.-H.: Abrasion erosion of concrete by water-borne sand. In: *Cement and Concrete Research* 36 (2006), 1814-1820
- [14] Sadegzadeh, M.: Abrasion Resistance of Concrete. Thesis submitted for the degree of Doctor of Philosophy, University of Aston in Birmingham, 1985
- [15] Pat, M. G. M., Reinhardt, H. W.: Erosion of Concrete. In: *Heron* 24 (1979), Nr. 3, 3-24
- [16] Hu, X., Momber, A. W., Yin, Y.: Flüssigkeitserosion und Hydroabrasivverschleiß von Stahl-faserbeton. In: *Beton- und Stahlbetonbau*, 98 (2003), Nr. 12, 764-772
- [17] Horszczaruk, E.: The model of abrasive wear in hydraulic structures. In: *Wear* 256 (2004), 787-796
- [18] Model Code for Service Life Design. CEB-FIB, Bulletin 34, 2006
- [19] DIN 1045-2: Tragwerke aus Beton, Stahlbeton und Spannbeton – Teil 2: Festlegungen Eigenschaften, Herstellung und Konformität – Anwendungsregeln zu DIN EN 206-1. Beuth Verlag, Berlin, August 2008
- [20] DIN EN 12390-2: Prüfung von Festbeton. Teil 2: Herstellung und Lagerung von Probekörpern für Festigkeitsprüfungen, Beuth Verlag, Berlin, Juni 2001
- [21] Faraway, J. J.: *Linear Models with R*, Texts in Statistical Science, Chapman & Hall/CRC, 2005
- [22] Douglas, M. B., Watts, D. G.: *Nonlinear Regression Analysis and Its Applications*, John Wiley & Sons, 1988
- [23] R Development Core Team (2007), 'R, A language and environment for statistical computing', R Foundation for Statistical Computing, Vienna, Austria. ISBN 3-900051-07-0, URL <http://www.R-project.org>.
- [24] DIN EN 1990: Eurocode: Grundlagen der Tragwerksplanung. Deutsche Fassung EN 1990: 2002, Oktober 2002
- [25] Joint Committee on Structural Safety (JCSS). Probabilistic Model Code, Part I: Basis of Design, 2001
- [26] RCP GmbH: STRUREL, 'A Structural Reliability Analysis Program System', (STATREL Manual 1999; COMREL & SYSREL Manual, 2003) RCP Consulting GmbH München

Probabilistic method of minimal safety depth evaluation for maximal ferries approaching to Ystad port

Lucjan Gućma, Maciej Gućma
Maritime University of Szczecin, Poland

Abstract: Paper presents method of safety water depth evaluation for ship approaching to ports. The method utilizes two models: real time simulation model used for determination of ships speed approaching to given port, and Monte Carlo model for determination of probability of accidental collision with the bottom. Minimal safety depth has been calculated with use of probabilistic acceptance criteria presented in the paper.

1 Introduction

Marine Traffic Engineering (MTE) research team of Maritime University of Szczecin since 70-ties is engaged in research works concerned with evaluation of navigation safety for port design and optimization of water areas. In this paper Authors intention is to present complex researches for determination of safety waterway depth for approach ships. It is widely known that squat of ships is most important factor affecting underkeel clearance (UKC). Unfortunately the major factor of squat – ship's speed, cannot be reduced especially in difficult navigational conditions. This happens because it is necessary to maintain high speed to keep proper manoeuvrability. Only one way to determine ships speed during approach especially in non existing solutions is to use simulation models (real time simulators) where navigators can freely adjust speed of ships to given conditions.

From the other side speed is not the only one factor of underkeel clearance (UKC). To deal with such complex phenomenon as underkeel clearance, Monte Carlo method is most suitable in Authors opinion and is applied in presented researches.

With use of probabilistic acceptable risk criteria it is possible to achieve the results of presented method: the minimal required depth for approaching ships in given area.

2 Modernisation of Ystad Port by simulation researches

The researches described in this paper are focused on Ystad port modernisation which is one of the latest research studies of MTE team. The main aim of researches has been focused on [Computer simulation 2008]:

1. Determination of optimal parameters of:
 - approach channels to reconstructed port of Ystad with respect to shape, width and depth,
 - inner and outer port breakwaters with respect to its shape with respect to waving in port;
 - turning places with respect to its shape and optimal depth;
 - two new berthing places in inner port in respect to its shape, length, depth, maximal energy of ships contact, maximal speed of ships propeller and bowthruster streams on the bottom.
2. Determination of safety conditions of port operation in respect to:
 - admissible meteorological conditions for given kind of ships and manoeuvres;
 - other navigational conditions and limitations like presence of other ships on berths, use of position fixing systems on approach, navigational markings, vessel traffic service.
3. Determination of manoeuvring procedures during berthing and unberthing for different kind of ships and propulsion systems.
4. Determination of underkeel clearance by Monte Carlo method.
5. Determination of usage of main engine during entrance.
6. Determination of ferry distances to the most dangerous objects.
7. Carrying out most typical emergency runs and describe necessary emergency action for the captains.

Two characteristic Ro-Pax ship has been chosen as typical for development of Ystad port. M/f *Wolin* is midi size ferry originally built as train ferry. The second ship m/f *Piast* is newly designed ferry build for Unity Line by Stocznia Szczecinska Shipyard. Most important parameters of ferries are presented in the Table 1.

Tab. 1: Main parameters of *Wolin* and *Piast* as typical ferries operated on the Baltic Sea area

Parameter	<i>PIAST</i>	<i>WOLIN</i>
Operator (route)	Unity Line (Swinoujscie-Trellborg)	Unity Line
Building year	1986 / 2002 rebuild	expected 2009
Length - LOA	207 m	188.9 m
Breadth	27 m	23.7 m
Draft	6.3 m	5.9 m
DWT	8000 t	5143 t
Machinery	total 21.600kW at 500rpm.	total 13.200kW at 600 rpm.
Propeller	2 variable pitch propellers turning inside at 145 rpm	2 variable pitch propellers turning inside at 150 rpm
Speed	approx. 21 kn.	18 kn.
Rudder	2x70 deg. active	2x70 deg. active
Bowthrusters	2x2.300kW	2x1100 kW
Sternthruster	1x1.200kW	1x736 kW

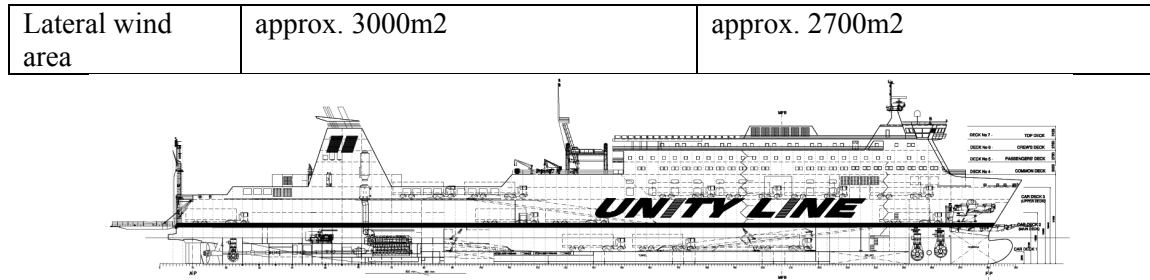


Fig.1. General arrangement of m/f *Piast*



Fig. 2. Photo of m/f *Wolin* ferry

The most important aim of Ystad port modernisation is to provide access to the port by ferries up to 210m length and enable future port development in the future to serve ships of 240m length [Computer simulation 2008]. Three most important changes are planned (Fig.3):

1. building two instead of three ferry quays in inner port,
2. design of new turning place in outside port,
3. shortening of inner western breakwater,
4. lengthening of outer breakwater to provide shelter in western winds of turning place.

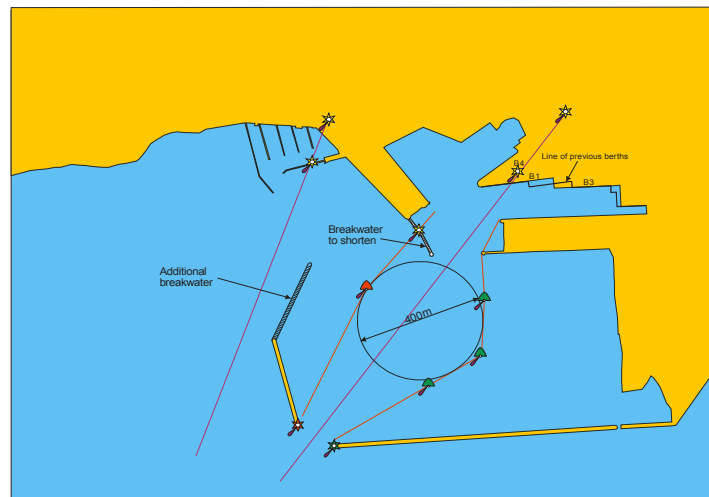


Fig. 3. Proposed changes in berths, turning place and breakwaters arrangements in Port of Ystad

3 Real time simulation methods applied

Real time simulation the interactive method with captains and pilots engaged in ships manoeuvring trials have been applied. This method is assumed as most reliable and suitable in this kind of research studies [Gucma 2005]. MTE research team possesses several kinds of manoeuvring simulators: from self made limited task with 2D display to modern commercial full mission simulator with 3D and real control systems. Both simulators have been applied in presented researches.

3.1 Real time simulation method – limited task simulator

Two classes of hydrodynamic models in MTE team own limited tasks simulators are utilized. First class of models are used when only limited parameters are known (usually when non existing ships or general class of ships are modelled) the second class models are used when detailed and exact characteristics of hulls, propellers and steering devices are known. Additionally real manoeuvring characteristics are used for validation of models. In present researches the second model has been used (m/f *Wolin* exists and sea trials are available *Piast* trial parameters has been extrapolated).

The model used in researches is based on modular methodology where all influences like hull hydrodynamic forces, propeller drag and steering equipment forces and given external influences are modelled as separate forces and at the end summed as perpendicular, parallel and rotational ones.

The model is operating in the loop where the input variables are calculated instantly (settings and disturbances) as the forces and moments acting on the hull and momentary accelerations are evaluated and speeds of movement surge, sway and yaw. The most important forces acting on the model are:

1. thrust of propellers
2. side force of propellers;
3. sway and resistant force of propellers;
4. bow and stern thrusters forces;
5. current;
6. wind;
7. ice effects;
8. moment and force of bank effect;
9. shallow water forces;
10. mooring and anchor forces;
11. reaction of the fenders and friction between fender and ships hull;
12. tugs forces;
13. other depending of special characteristics of power and steering ships equipment.

The functional idea of the ship manoeuvring simulation model is presented in Fig. 4.

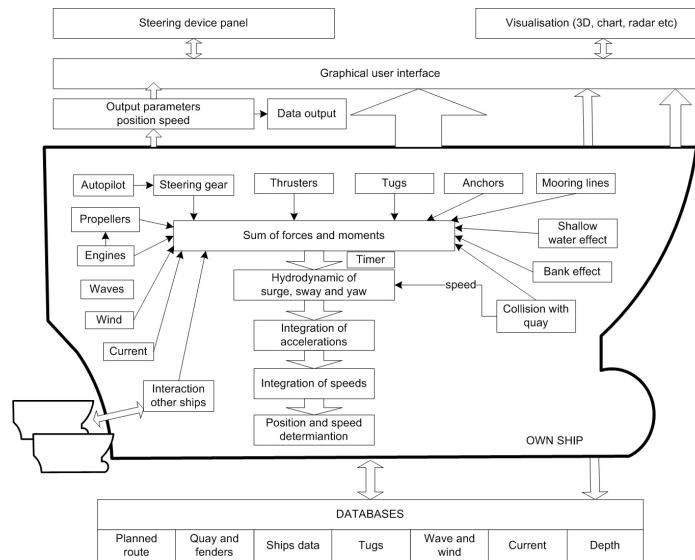


Fig. 4. The main diagram of simulation model

Interface of model is typical 2D chart interface (Fig.5). The interface covers information of ships state (position, course speed, yaw etc), quay and shore line location, navigational markings, soundings, external conditions, tug and line control and control elements of the model. The model is implemented in Object Pascal with use of Delphi™ environment and Visual C™ with use of C++ language.

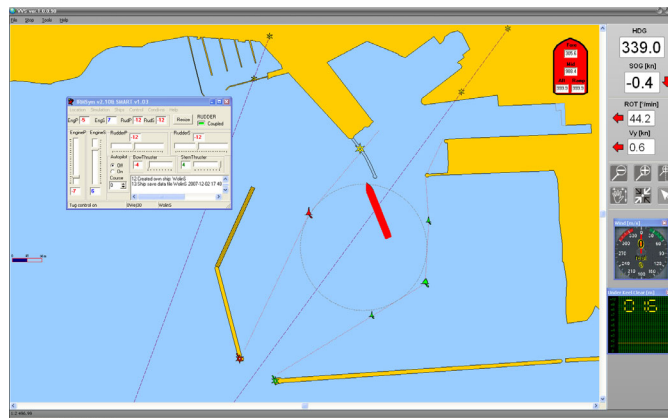


Fig. 5. Interface of simulation model ferry *Wolin* turning at outer turning place of Ystad Port (limited task simulator)

3.2 Real time simulation method – full mission simulator

Kongsberg Polaris™ simulator located at Marine Traffic Engineering Centre (MTEC) premises in Maritime University of Szczecin comprises (Fig. 6):

- one full mission navigation bridge simulator with 270° visual projection and live marine ship equipment (DNV class A),
- two part task navigation bridges with 120° visual projection and mix of real and screen-simulated ship-like equipment including one Voith-Schneider tug console (DNV class B),

- two desktop PC simulators with one monitor visual projection and one monitor screen-simulated ship-like equipment.



Fig. 6. Bridge A at MTEC (with 270° visual projection) and captain “at work”.

All hardware and software forming the Polaris ship manoeuvring simulator has been granted DNV certificate for compliance or exceeding the training regulations set forward in STCW'95 (section A-I/12, section B-I/12, table A-II/1, table A-II/2 and table A-II/3).

In order to create own ship models a hydrodynamic ship-modelling tool is available. This tool enables creating almost any ship type (controls for at least two engines with propellers' controls for fixed propeller, adjustable pitch propeller and azimuth; rudder controls adequate for various types of conventional rudders, active rudders, Z-drive/azimuth and thrusters) with very high fidelity hydrodynamics in 6 DOF (surge, sway, heave, yaw, roll, pitch). The hydrodynamics comprise all known to state of the art external effects like squat, bank and channel effects.

4 Assumptions to safety depth evaluation

The main aim of this part is to determine safety depth of Ystad waterway. The probabilistic criteria of acceptable risk is applied and together with simulation results (real time ships manoeuvring) used to obtain minimal acceptable (under given safety conditions) depth of waterway (Fig. 7).

The minimal depth on approach to sea ports is very important factor which influence safety of navigation in respect to underkeel clearance which is together with horizontal area the most important factor of navigational safety.

Following assumptions have been taken into consideration:

1. Swedish water levels for design:

HHW +1.65

MHW +0.87

MW +0.03

MLW -0.97

LLW -1.47

2. Water level for calculations = MLW
3. Ship lifetime = 15 years
4. Waterway lifetime = 50 years
5. Ships draught = 6.3m
6. Ships speed = variable according to simulations results
7. Wave = 0.4m – 0m.

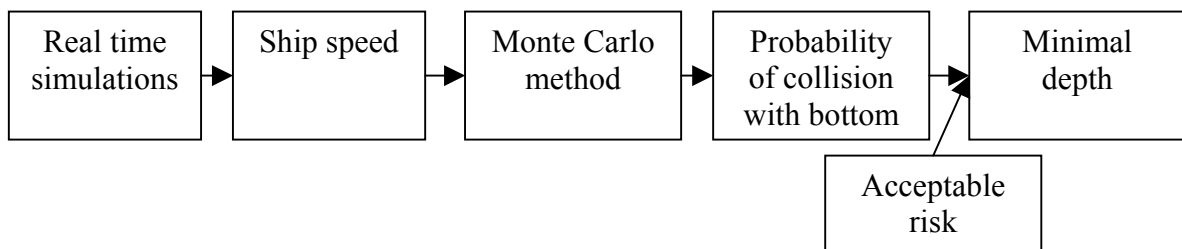


Fig. 7. Method of safety depth evaluation

5 Navigational risk

The navigational risk can be defined as probability of certain losses during expected period of time (one year/ lifetime of ships or waterway):

$$R = P_A C$$

where:

- P_A – probability of serious grounding accident
- C – consequences of accident

With assumption that accidents consequences are similar (grounding of passenger ship without losses) we can express risk as probability of accident only.

6 Acceptable risk criterion

Probabilistic acceptance criterion is proposed in this study. Such criteria are widely used in Marine Traffic Engineering (Dutch, England, Denmark, and Poland).

Monte Carlo simulations performed in stage II of researches enabled to find probability of accident in single passage assumed when $UKC < 0$ is expressed as $P_{UKC < 0}$.

Most of the accidents are not serious. Probability of serious accident can be calculated with assumption that serious accidents are 10% of all of total number of accidents: $P_{SA} = 0.1$ (so called Heinrich factor usual assumption in restricted water areas validated by real accidents statistics see [Savenije 96]). Under above assumptions probability of serious accident P_{AS} can be calculated as:

$$P_A = P_{SA} P_{UKC < 0}$$

Intensity of all accidents in given time (ex. one year) can be calculated as:

$$\lambda = NP_A$$

where:

N – ship movement intensity per 1 year.

Typical probabilistic criterion for risk of collision with the bottom is based on Poisson process the collisions with the bottom are random with intensity λ [collision/time] and expected number n during given time t :

$$P(n) = \frac{(\lambda t)^n e^{-\lambda t}}{n!}$$

where:

n – expected number of collision with bottom in given time period,

λ – intensity in given time.

No accident probability in given time period t can be calculated with assumption that $n=0$ as:

$$P(n=0) = e^{-\lambda t}$$

The opposite to above safety factor can be expressed as occurrence at least of one accident in given time t and expressed as:

$$P(n \geq 1) = 1 - e^{-\lambda t}$$

Typical probabilistic safety criterion is probability of no accident in given time. For example Dutch criterion on approach to Rotterdam (with tides consideration) is 10% probability of more then one accident in 25 years of waterway operation which is expressed as:

$$P(n \geq 1) = 1 - e^{-\lambda t} = 0.1$$

(where $t=25$ years) which gives $\lambda t = 0.105$. Assuming that $t=25$ years of operation we obtain $\lambda = 0.0042$ of all accidents per year which lead to following criterion: one accident in 238 years period ($=1/\lambda$). The criterion comprise all accidents so with assumption that se-

rious accidents are 10% of all accidents we can calculate criteria value of yearly intensity of serious accident as:

$$\lambda_s = 0.1\lambda = 0.00042 .$$

Polish criterion that is used in Marine Traffic Engineering is slightly less restrictive due to low traffic intensity, and nature of the bottom in ports (sand, mud). In Poland it is assumed limit accident rate per year at the level $\lambda = 0.007$ of all accidents or $\lambda = 0.0007$ for serious accidents (serious accident is such accident where special rescue action should be undertaken) as criterion value (the criterion is based on acceptance of one serious accident per ships lifetime which equals 15 years, because ships during this time are not likely to be rebuild in opposite to waterway which during 50 years of operation will be rebuild few times most likely).

In further step taking into consideration the passages of ferries which is around 10 per day in Ystad Port ($N=10*365=3650$ passages/year) it is possible to calculate limited probability of collision with the bottom (accident) in single passage as:

$$P_{A-accept} = \lambda / N = 0.0042 / 3650 = 1.15 * 10^{-6}$$

7 Monte Carlo method of under keel clearance on ferry approach

The stochastic model of under keel clearance evaluation has been presented in [Gucma 2005]. It is based on Monte Carlo methodology where overall ships underkeel clearance is described by following mathematical model (Fig. 8):

$$UKC = (H_0 + \sum \delta_{Hoi}) - (T + \sum \delta_{Ti}) + (\Delta_{Swa} + \sum \delta_{Swi}) + \delta_N$$

where:

- δ_{Hoi} – the uncertainties concerned with depth and its determination,
- δ_{Ti} – the uncertainties concerned with draught and its determination,
- δ_{Swi} – the uncertainties concerned with water level and its determination.
- δ_N – navigational and manoeuvring clearance.

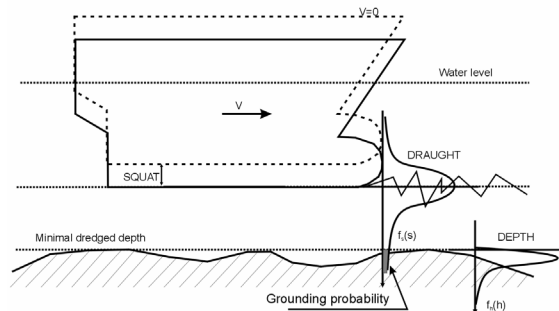


Fig. 8. Concept of probabilistic underkeel clearance of ships determination

The final model takes into account depth measurement uncertainty, uncertainty of draught determination in port, error of squat determination, bottom irregularity, tides and waves influence are deciding factors for underkeel clearance of ships. Program is capable to consider above mentioned uncertainties using distributions and their parameters. The following parameters are randomly selected from their distributions:

1. depth - h_i (averaged in following sections -100m, 0m, +100m, 200m, 300m from the breakwater),
2. sounding error- δ_{BS_i} ,
3. mudding component clearance - δ_{Z_i} ,
4. draught determination error - δ_{T_i} ,
5. ship's heel error - δ_{P_i} .

Random draught module. User-entered draught is corrected for draught determination error value and ship's heel error. Iterated draught (T_i) is calculated as follows:

$$T_i = T + \delta_{T_i} + \delta_{P_i}$$

where:

- T - ships draught [m] assumed as 6.3m,
- δ_{T_i} - draught determination error (assumed as +/-0.05m),
- δ_{P_i} - ships heel error (assumed as +/-3 degrees).

Water level module. Water level PW_i can be automatically load from online automatic gauges if such exists (Szczecin solution). In these researches the level has been modelled as normal cut distribution with parameters (0, +/-0.1m).

Depth module. Depth h_i has been assumed as constant in given sections (it varies from 9 before and near breakwater to 8.5m inside the port see figure).

Squat module. Squat (ship sinkage due to decrease of water pressure during movement) is calculated in three stages. First module calculates squat with analytical methods used to obtain moving vessel squat (Huusk, Milword 2, Turner, Hooft, Barrass 1, Barrass 2). Next standard errors of each method are applied. Squat model selection and their standard errors have been verified by GPS-RTK experimental research [Determination of squat of m/f Sniadecki by RTK method in Swinoujscie Port. MUS Research work 2006]. As a result of the experiment uncertainty of each model has been assessed and each squat method assigned weight factor. Method's weights and statistical resampling bootstrap method are used later on to calculate final ship's squat.

Underkeel clearance module. Underkeel clearance Z_i is determined by using draught, depth, water level and squat results which have been calculated before. Underkeel clearance is defined as:

$$Z_i = (h_i + \delta_{Z_i} + \delta_{BS_i}) - (T_i + O_i + \delta_N + \delta_{WP_i} + \delta_F)$$

where:

- h_i – up-to-date depth in each iteration in sections (sounding from October 2007),
- δ_{Z_i} – mudding component clearance (normal cut distribution with 0 and +/-0.1m),
- δ_{BS_i} – sounding error (normal cut distribution with 0 and +/- 0.1m),
- T_i – ships draught with its uncertainty (0, +/-0.05m),
- O_i – iterated squat (bootstrap model),
- δ_N – navigational clearance (0m),
- δ_{WP_i} – height of tide error (0m),
- δ_F – wave clearance (wave height assumed as h=0.4m before breakwater, h=0.2m in the breakwater and h=0m inside, direction from ferry traverse).

8 Results

As the result of combined method Monte Carlo with simulations results in sections of waterway (breakwater=0m) we obtain parameters of distributions of *UKC* in distance from breakwater for real mean depth existing in Ystad port (Fig.9).

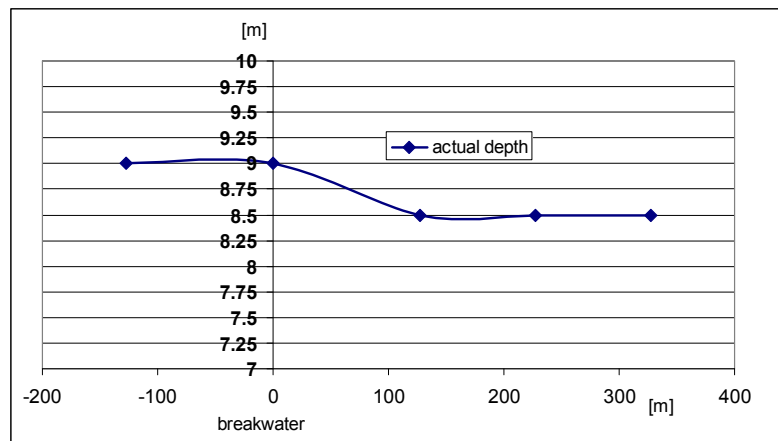


Fig. 9. Mean actual depth in given sections (sounding from fall 2007)

Speed of approaching ships has been determined from real time simulations (extreme conditions E20 m/s wind) have been applied (Fig. 10). Speed applied in Monte Carlo model has been calculated with 95% probability level.

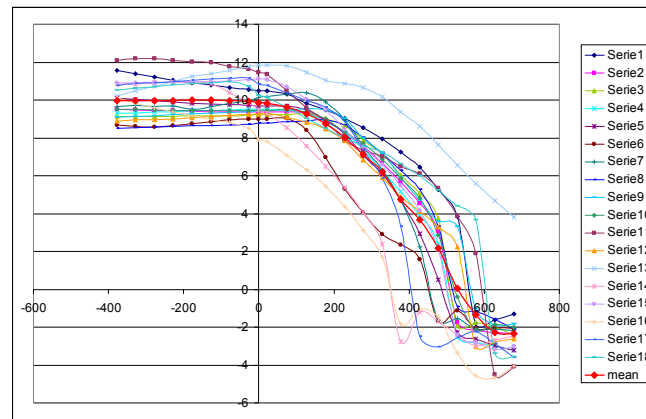


Fig. 10. Speed of ferry Piast in knots on approach with E20m/s wind (x=0 outer breakwater) obtained by mean of real time researches

In next step Monte Carlo model described in Ystad development study has been applied to determine histograms and parameters of distributions of UKC (Fig. 11) in function of ships position on the waterway. Wave influence has been taken into account.

In the further step on the basis of Monte Carlo results the UKC on 95% and squat has been calculated (Fig. 12). Important for the probability calculations is mean UKC and standard deviation of UKC presented in Fig. 13. Due to lack of distribution or probabilities of given water levels the water level assumed in this study is equal to MLW= -0.97m.

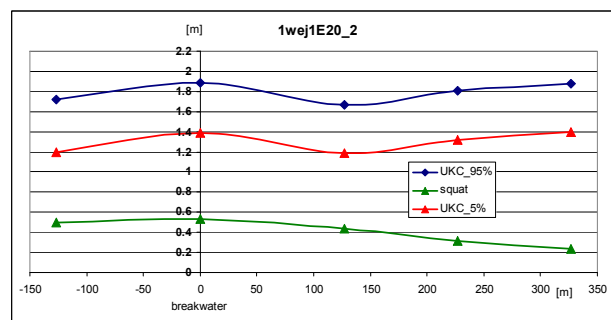


Fig. 12. UKC on 95% and 5% level of confidence of m/f Piast approaching with E20m/s wind (x=0 outer breakwater)

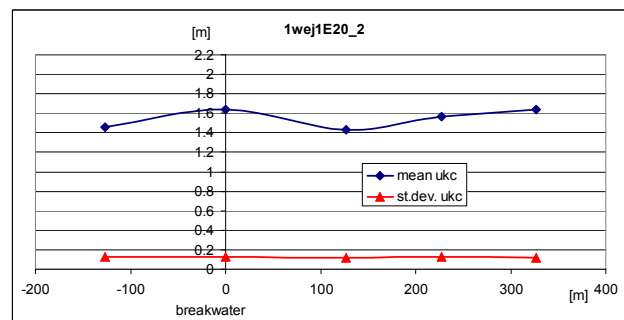


Fig. 13. Mean UKC and standard deviation of UKC of Piast ferry (T=6.3m) entering to Ystad Port

Final calculation of required depth (H) for distribution with parameters m and σ to fulfill assumed Dutch criterion is based on following formula:

$$P_A = 1 - \int_H^{-\infty} f_{(m,\sigma)}(x)dx \leq P_{A-accept} = 1.15 * 10^{-6}$$

The results as required depth on approach to Ystad Port are presented in Fig.14.

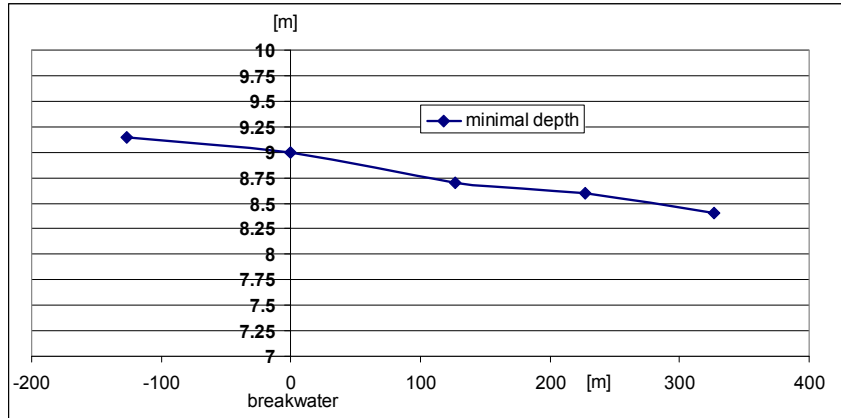


Fig. 14. Minimal depth in Ystad port with criterion $P_A \leq P_{A-accept} = 1.15 * 10^{-6}$

9 Conclusions

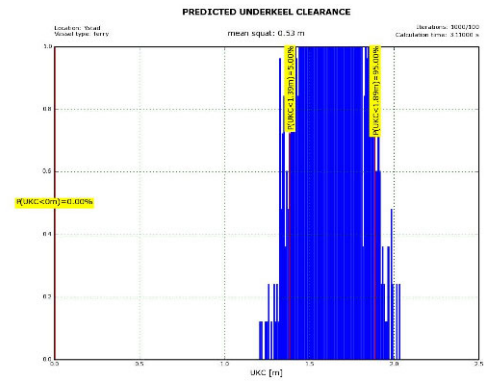
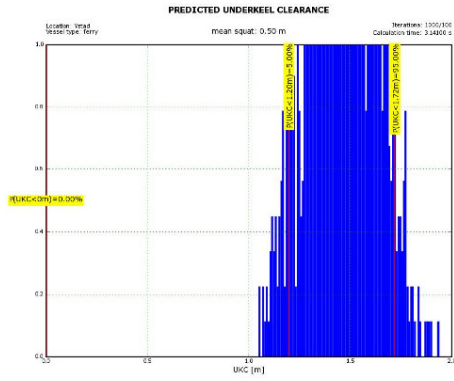
Minimal depths for ferry *Piast* ($T=6.3m$) in function of distance to outside breakwater heads are presented in Fig 14. Minimal safety depths to fulfil criterion are varied from 9.2m before breakwater heads to 8.3m inside the avanport.

Probabilistic safety criterion (so called Dutch criterion used in Rotterdam Port) has been applied (acceptable level of 0.0042 accidents per year). On the basis of this the limited probability of hitting the bottom accident have been evaluated and used for minimal depth in Ystad Port.

References

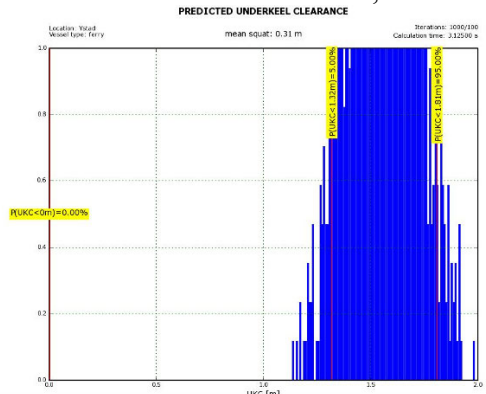
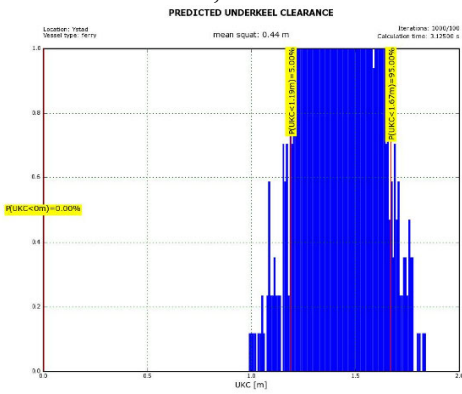
- [1] Artyszuk J. 2005. Towards a Scaled Manoeuvring Mathematical Model for a Ship of Arbitrary Size. Scientific Bulletin, Maritime University of Szczecin.
- [2] Computer Simulation (2008) for Port Design and Safe Manoeuvring of ships Simulation researches of m/f *Piast* conducted by means of PC Ship Manoeuvring Simulator and Full Mission Simulator. Stage I and II. Research Work Maritime University of Szczecin 2008.
- [3] Guema L, Risk Modelling of Ship Collisions Factors with Fixed Port and Offshore Structures. Maritime University of Szczecin 2005.

- [4] Gućma L., Gućma M., Tomczak A., Przywarty M., Experimental determination of squat and trim of sea ferry *Jan Śniedeki* on approach to Swinoujście port by means of RTK method (in polish) Proc. of XV Nav-Sup Conference. Gdynia 2006.
- [5] Gućma L., Jankowski S. 2001. Method of determining probabilistic models of propeller streams speed at the bottom of manoeuvring ships. Proceedings of the IX International Scientific and Technical Conference on Marine Traffic Engineering, Szczecin.
- [6] Gućma L., Schoeneich M. 2007. Probabilistic model of underkeel clearance in decision making process of port captain. Proc of Trans-Nav Conference Gdynia.
- [7] Iribarren J.R. 1999. Determining the horizontal dimensions of ship manoeuvring areas. PIANC Bulletin No 100, Bruxelles.
- [8] Savenije R.Ph. *Probabilistic Admittance Policy*, PIANC Bulletin No 91. Bruxelles 1996.
- [9] Vasco Costa, F. 1969. Berthing manoeuvres of large ships. The Dock and Harbour Authority. March



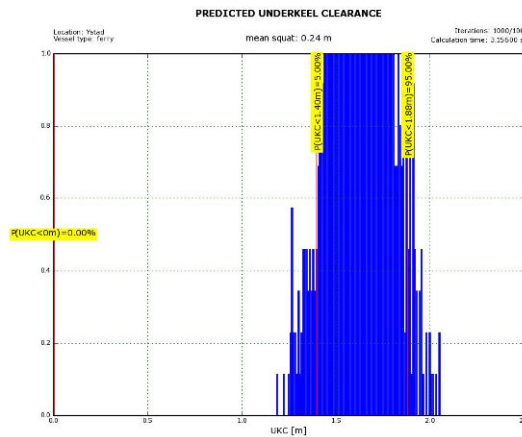
Histogram of UKC and squat value 130m before heads /traverse sea wave =0,4 m/

Heads: Histogram of UKC and squat value 130m /traverse sea wave =0,2 m/



Histogram of UKC and squat value 130m behind heads /sea wave =0m/

Histogram of UKC and squat value 230m behind heads /sea wave =0m/



Histogram of UKC and squat value 330m behind heads /sea wave =0m/

Fig. 11. UKC of Piast ferry and squat in meters on approach with E20m/s wind (x=0 outer breakwater)

Part V

Probabilistic Modelling
of
Infrastructure

A Probabilistic Framework to Determine the Probability of Collapse for Bridges Subject to Vessel Collision

M. Davidson¹ and G. Consolazio¹

¹University of Florida, Gainesville FL, USA

Abstract: Accounting for waterway vessel collision is an integral component of structural design for any bridge crossing a navigable waterway. Each time a vessel traverses a given waterway, there exists an associated risk that the vessel will become aberrant from the intended transit path, and once aberrant, will strike a nearby bridge structural component. During collision events, massive waterway vessel groups, such as barge flotillas, are capable of dynamically transmitting horizontal forces to impacted bridge components such as piers. Furthermore, such collision-induced forces can be sufficient to cause collapse of a pier or roadway spans in the vicinity of the impact location. If collapse takes place, economic loss is suffered due to subsequent traffic rerouting and bridge replacement costs. Additionally, fatalities may occur if the roadway is occupied during or shortly after the collapse event. The research presented here focuses on the development of a probabilistic framework for determining the probability of bridge collapse (failure) in the event of barge-bridge collision. This framework is developed in a rational manner with reliance on nonlinear dynamic structural analysis and probabilistic descriptions of a multitude of pertinent random variables. As a demonstration, the probability of collapse for an existing bridge is assessed and comparisons are made between the probabilistically determined value and that obtained from current bridge design provisions.

1 Introduction

From 1960-2002, a total of 31 bridge collapses occurred worldwide as a result of vessel collision [2]. These events have resulted in 342 fatalities and substantial economic losses. Since 1991, the American Association of State Highway and Transportation Officials (AASHTO) *Guide Specification and Commentary for Vessel Collision Design of Highway Bridges* [1] has provided a means for bridge designers to assess the risk associated with collision events for a given waterway and bridge. As part of the risk assessment, the probability of collapse for each pier in a waterway of interest is determined under the condi-

tional probability that vessel impact is imminent. However, the expression used to determine the probability of collapse was adapted from a study of *ship-ship* (i.e., not ship-bridge) collisions. Very little prior research has been devoted to establishing a rational basis for determining the probability of bridge collapse as it relates to *barge-bridge* collision. MANUEL et al. [17] recognized that probabilistic descriptions of barge and bridge structural parameters facilitate alternate means of assessing bridge collapse rates, however, the framework proposed in that study was formed within the confines of the existing AASHTO [1] provisions. In the present paper, a rational, independent framework for determining the probability of collapse is defined for bridges subject to barge impact. Also, in this paper, a probability of collapse estimate obtained from the current AASHTO formulation is compared to that determined using the newly proposed probabilistic (i.e., simulation-based) framework for a selected case. Such comparisons highlight the need to revise the current AASHTO approach for determining collapse rates.

2 AASHTO vessel collision risk assessment

The intent of the current AASHTO guide specification is to establish analysis and design provisions to minimize susceptibility to catastrophic collapse for bridges that are at risk for vessel collision [2]. This intent is manifested through a risk assessment that culminates in an annual frequency of collapse expression:

$$AF = (N)(PA)(PG)(PC)(PF) \quad (1)$$

where AF is the annual frequency of bridge collapse. In determining AF from equation (1), vessels that traverse a given navigable waterway are divided into groups based on type, length, dead weight tonnage (DWT), etc. and each group is assigned a vessel trip frequency value (N). The remaining terms in equation (1)—the probability of vessel aberrancy (PA); the geometric probability (PG), or the probability that a given pier will be struck by an aberrant vessel; the probability of collapse (PC); and the protection factor (PF), which accounts for the presence of impact protection external to the bridge—are all determined for each pier, and in turn, for each vessel group. The annual frequency of collapse for a bridge of interest is then determined by computing the products of the above terms and summing them over all vessel groups and piers.

2.1 AASHTO probability of collapse (PC) expression

The AASHTO PC expression—which is used in risk assessments involving barge collision—was derived from a study of ship-ship collision damage rates (AASHTO [2], FUJII AND SHIOBARA [11]). In this derivation, a correlation was made between monetary ship damage rates and capacity-demand ratios of bridge resistance relative to impact force, which led to the following expressions:

$$PC = 0.1 + 9 \left(0.1 - \frac{H}{P_B} \right), 0 \leq H/P_B < 0.1 \quad (2a)$$

$$PC = \left(1 - \frac{H}{P_B}\right), 0.1 \leq H/P_B \leq 1 \quad (2b)$$

$$PC = 0, H/P_B > 1 \quad (2c)$$

Equation (2) requires input of *static* pier (pushover) capacity (H) and *static* impact load (P_B). However, recent studies have shown that significant *dynamic* forces can develop in bridges during barge-bridge collision (CONSOLAZIO et al. [5], CONSOLAZIO et al. [9]). Furthermore, no means currently exist for obtaining equation (2) input parameters from analyses that incorporate dynamic effects. This shortcoming alone (regardless of the basis for the current AASHTO PC expression) warrants the formulation of a revised PC framework.

3 Proposed PC framework

Recently developed vessel collision simulation and bridge modeling techniques enable rapid, yet accurate assessment of dynamic bridge response. These analytical techniques can be used in conjunction with statistical descriptions (discussed later) of relevant barge and bridge parameters to form a probabilistic PC framework. The use of dynamic barge-bridge collision analysis—as opposed to structural damage cost estimates from ship-ship collisions—constitutes a rational platform for assessing bridge collapse rates.

3.1 Coupled vessel impact analysis (CVIA)

Dynamic barge-bridge interaction limits the use of prescribed barge impact load-histories for barge-bridge collision analysis. However, a dynamic (time-history) vessel collision analysis technique has been developed that eliminates the need for prescribed impact load-histories (CONSOLAZIO AND COWAN [6]). Namely, coupled vessel impact analysis (CVIA), utilizes a shared contact force (F) to computationally link single-degree-of-freedom (SDF) vessel models—with specified mass, initial velocity, and crushing characteristics—to multiple-degree-of-freedom (MDF) bridge models (Fig. 1). Upon impact, the vessel generates a time-varying force and the MDF bridge-soil model displaces and develops internal forces in reaction to the imparted load. Hence, the impact load-history and bridge response-histories are calculated simultaneously. The CVIA procedure has been validated using data measured from full-scale barge impact experiments (CONSOLAZIO AND DAVIDSON [7]). Additionally, nonlinear barge crushing characteristics (i.e., force-deformation relationships) are available (e.g., CONSOLAZIO et al. [8], YUAN et al. [22]) for multiple barge structural configurations and a wide array of impacted pier geometries (widths, shapes, orientations). Given the availability of these barge descriptors, the CVIA procedure can be used to accurately assess dynamic bridge response for many impact scenarios and bridge configurations.

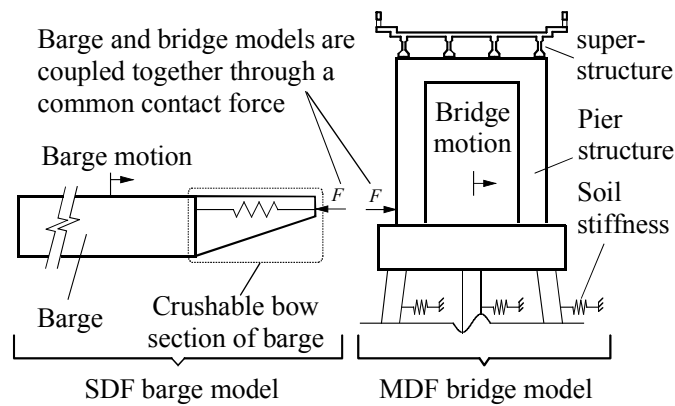


Fig. 1: Coupling between barge and bridge (after CONSOLAZIO AND COWAN [6]).

3.2 One-pier two-span (OPTS) bridge modeling

For full bridge models, the use of CVIA can become computationally expensive. As mitigation to this expense, collision analysis can be conducted using an equivalent one-pier two-span (OPTS) bridge model (Fig. 2). The OPTS modeling procedure involves reducing a multiple-pier, multiple-span bridge model to an equivalent model with condensed stiffnesses and masses connected at the distant ends of each of the two retained spans. See CONSOLAZIO AND DAVIDSON [7] for descriptions of OPTS stiffness and mass formulations. The OPTS modeling technique has been shown to greatly reduce computational expense while retaining accuracy relative to corresponding full bridge model analyses for a wide array of bridge configurations (CONSOLAZIO et al. [9]).

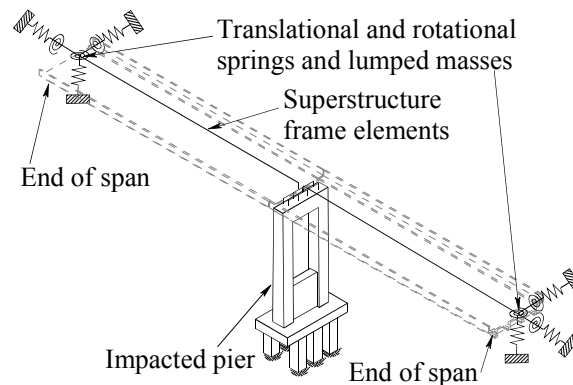


Fig. 2: OPTS numerical model (after CONSOLAZIO AND DAVIDSON [7]).

3.3 OPTS-CVIA implementation in finite element analysis software

Both CVIA and OPTS have been implemented in an experimental version of the bridge finite element analysis (FEA) program FB-MultiPier [3]. FB-MultiPier possesses nonlinear (constitutive and kinematic) analysis capabilities and employs nonlinear fiber-based frame elements for piles, pier columns, and pier caps; flat shell elements for pile caps; discrete

stiffnesses for bearings; and resultant frame elements for superstructure spans. Also, in FB-MultiPier, soil-structure interaction is modeled using distributed nonlinear soil springs.

3.4 Random variables

Statistical descriptions of random variables for probabilistic simulation (using OPTS-CVIA) are taken from the literature. Given that a version of the FEA program FB-MultiPier contains OPTS-CVIA features, random variables are discussed in relation to FB-MultiPier bridge model input.

3.4.1 Resistance

Statistical parameters were derived by NOWAK AND COLLINS [20] for shear and moment resistances of several girder types based on discrepancies between analytical prediction and physical measurement (Tab. 1). These parameters are not directly compatible with FB-MultiPier, where stiffness for resultant-frame span elements is largely dependent on material moduli. However, by assuming that moment and shear capacity parameters in Tab. 1 approximately correspond to bending stiffness and shear stiffness, respectively, statistical parameters of resistance are formed for all superstructure elements.

Tab. 1: Statistical parameters for bridge girder resistance (NOWAK AND COLLINS [20])

Type of girder	Distribution	Moment capacity factor		Shear capacity factor	
		Bias	COV	Bias	COV
Composite / Non-composite steel	Lognormal	1.12	0.10	1.14	0.105
Reinforced concrete	Lognormal	1.14	0.13	1.20	0.155
Prestressed concrete	Lognormal	1.05	0.075	1.15	0.14

Discrete cross-section descriptions are employed in FB-MultiPier for pile, pier column, and pier cap members, enabling a probabilistic treatment of member dimensions and reinforcement layouts. However, NOWAK AND COLLINS [20] state that cross-section dimension error (pertaining primarily to reinforced concrete beams) is roughly independent of member size. For typical dimensions of concrete members within pier structures (where dimensions commonly exceed 1 m), only a nominal benefit is gained by incorporating variability into member cross-section dimensions. Additionally, size variations are considered to be small for reinforcing bars of concrete members and hot rolled steel shapes [18]. Pier member dimensions (including size and placement of reinforcement) are therefore treated in a deterministic manner.

The strength of constituent materials in pier structural members (in contrast to member dimensions) can vary widely enough to affect internal force distributions throughout an impacted pier. The statistical parameters given in Tab. 2 are all that is required by FB-MultiPier to form nonlinear constitutive relationships for concrete, mild steel, and prestressed steel. Due to a lack of available statistical data, the material stiffness of non-rigid substructure-superstructure load transfer devices (e.g., elastomeric bearings) and the level of prestress loss in prestressed concrete piles are modeled deterministically.

Tab. 2: Statistical parameters for pier structural materials

Variable	Applicability	Distribution	Bias	COV	Source
Elastic modulus	Steel reinforcement	Lognormal	1.00	0.033	[18]
Yield stress	Steel reinforcement	Lognormal	1.00	0.098	[20]
Ultimate stress	Prestressed strands	Lognormal	1.00	0.025	[20]
Compressive strength	Concrete	Normal	Varies		[16]

Soil resistance is represented in FB-MultiPier (2008) by distributed nonlinear springs along each below-soil pile (or drilled shaft) node. For a given soil type, soil boring data (i.e., standard penetration test, or SPT, blow counts) are used in empirical equations to form applicable soil strength parameters. The parameters are, in turn, specified in FB-MultiPier and used to form soil load-deformation curves (soil springs). A lognormal distribution (with COV of 0.5)—as given in BARKER et al. [4]—is used for all SPT to soil-strength correlations.

3.4.2 Non-collision load

Statistical descriptions corresponding to all non-collision load types considered are given in Tab. 3. Bridge member permanent (dead) loads are varied according to a normally distributed unit weight factor. Water elevation (which is specified directly in FB-MultiPier) is varied according to waterway elevation data that are available from government agency databases (e.g., NOAA [19]). Soil scour depths are modeled in FB-MultiPier by lowering the top soil layer elevation to match the given (normally distributed) scour elevation.

Tab. 3: Statistical parameters for pier structural materials

Variable	Applicability	Distribution	Bias	COV	Source
Unit weight factor	All members	Normal	1.05	0.10	[20]
Water level	Waterline elevation	Varies	Varies		[19]
Scour depth factor	Top soil elevation	Normal	0.55	0.52	[14]

3.4.3 Barge collision load

Vessel traffic data for a waterway of interest provide a platform for the statistical description of barge collision loading. As illustration, consider the vessel traffic that passes under the New St. George Island Bridge located in Florida, USA (Tab. 4). The traffic is categorized (by draft) into eight vessel groups where data are expressed in one-year intervals (WANG AND LIU [21]). In Tab. 4, N is the vessel group trip frequency (the average number of annual passages under the bridge); B_{barge} and L_{barge} are the width and length of individual barges (m), respectively within the vessel group; LOA is the overall flotilla length (m); W is the flotilla, or vessel group, weight (kN); and, V is the flotilla velocity (m/s). Given the vessel traffic data in Tab. 4, a discrete probability density function (DPF) that governs vessel group selection (and all pertinent vessel parameters) is formed by normalizing trip frequencies for each vessel group by the total number of vessel trips. This yields weighted vessel trip frequencies (or trip weights) for each vessel group. Vessel group characteristics (e.g., W , V , LOA) are then selected in proportion to respective vessel trip weights per the

DPF. For example, characteristics for vessel group 1 (Tab. 4) are selected at a rate of 16% (85 trips out of 522.5 total trips).

Tab. 4: Annually averaged vessel traffic data

Vessel group	Direction	N	Draft (m)	No. barges	B _{barge} (m)	L _{barge} (m)	LOA (m)	W (kN)	V (m/s)
1	up	85	0.6	1	15.5	65.9	88.8	9520	2.9
2	up	24.6	1.7	1	17.9	96.4	119	32240	2.4
3	up	117	2.5	1	15.4	75.0	97.9	31960	2.4
4	up	92.2	3.4	1	16.5	97.3	133	57930	2.4
5	down	135	0.6	1.9	15.5	81.4	178	17430	3.3
6	down	21.6	1.5	1.9	19.0	100	213	59100	2.8
7	down	19.4	2.5	1.9	13.8	76.6	168	58300	2.8
8	down	27.7	3.6	1.9	22.1	78.1	185	121080	2.8

For each vessel group selected from the DPF, the flotilla weight (W) is subsequently varied using a normal distribution with a COV of 0.10 (GHOSN et al. [12]). Draft associated with this weight (W_{rand}) is then determined using weight-draft relationships in AASHTO [2]. Draft is then related to hydrodynamic mass coefficient (C_H), which accounts for the mass of water surrounding and moving with the flotilla (see AASHTO [2] for details). Given W_{rand} and C_H , flotilla impact weight (W_{impact}) is expressed as:

$$W_{impact} = C_H \cdot W_{rand} \quad (3)$$

In contrast to impact weight, flotilla impact velocity (V_{impact}) is dependent not only on vessel group data, but also on flotilla orientation and flotilla distance (relative to the flotilla centerline) from the intended transit path. The process of deriving V_{impact} from V is summarized in Fig. 3. The first step in this process is selection of the vessel group—from Tab. 4—to obtain values of V , LOA, and B_{barge} (Fig. 3, top left). Flotilla orientation (or impact angle, ϕ) is determined using a bounded (with 2% and 98% bounds) normal distribution with COV of 10°, as proposed by KUNZ [15], where the deterministic angle of vessel transit is taken as the mean (Fig. 3, top right). The impact angle (ϕ) orients an axis used to measure the distance from channel centerline to flotilla centerline for aberrant flotillas (Fig. 3, center). A normal distribution (with standard deviation equal to LOA) that governs this distance—the flotilla centerline offset (x_{LOA})—is taken from AASHTO [2]. Using V and x_{LOA} , an adjusted velocity (V_{adj}) is then determined (Fig. 3, bottom left) based on the distance, x_{LOA} , relative to channel edge distance and $3 \cdot LOA$ (per AASHTO [2]). For x_{LOA} distances greater than $3 \cdot LOA$, the adjusted velocity, V_{adj} , is reduced to the velocity of a drifting (non-propelled) vessel (0.5 m/s is commonly used in design). Finally, a lognormal distribution with a mean of V_{adj} and COV of 0.33 (consistent with JCSS [13]) is used to determine V_{impact} .

The CVIA vessel model, as implemented in FB-MultiPier, requires specification of an impact node on the bridge structure as well as barge crushing characteristics (in addition to W_{impact} and V_{impact}). As a consequence of determining V_{impact} , however, all barge parameters necessary to specify the impact location are determined. Furthermore, impacted pier

surface geometry in the vicinity of impact—dictated by the pier structural configuration and known barge-pier orientation—can be determined, and hence, barge crushing characteristics are readily identified (e.g., using CONSOLAZIO et al. [8]).

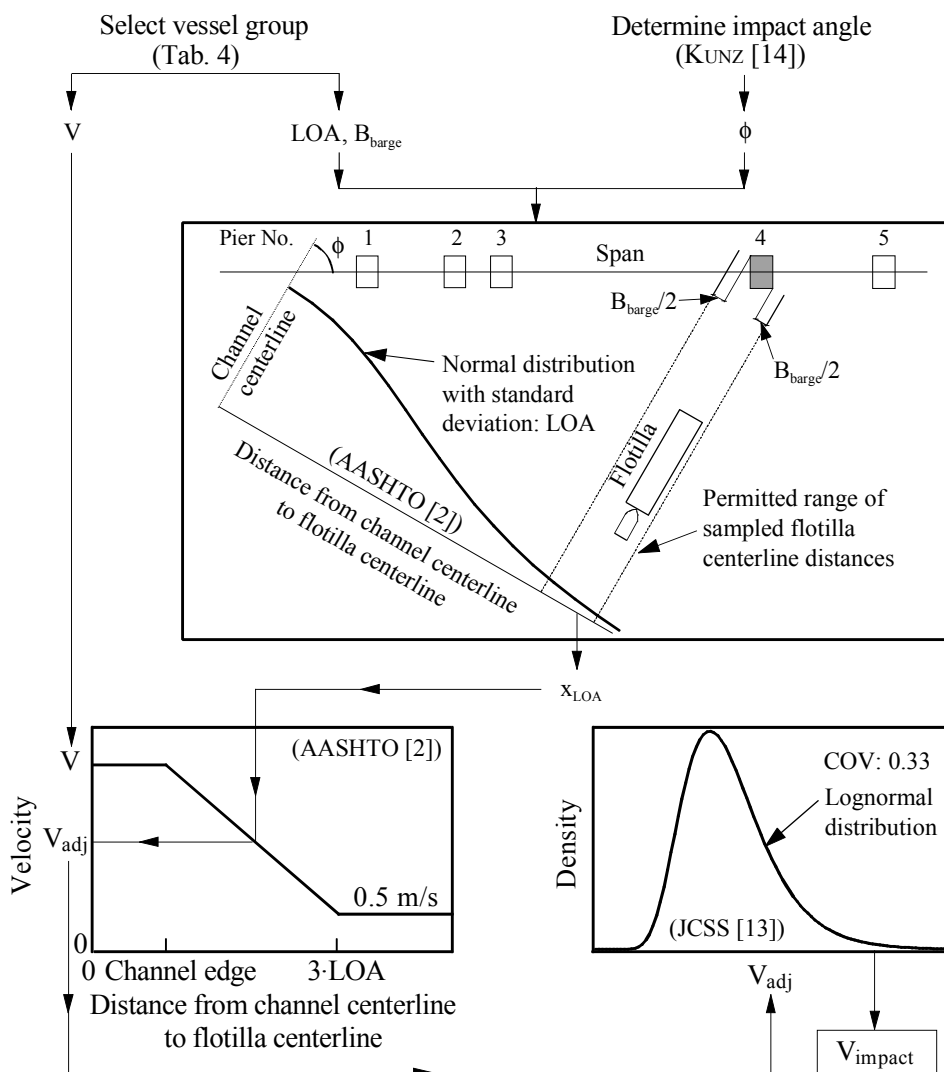


Fig. 3: Impact velocity (V_{impact}) flowchart.

3.5 Definition of bridge collapse (failure)

In the US, bridge owners are responsible for approving the degree of damage that bridge components are allowed to sustain during impact events (AASHTO [2]). State departments of transportation typically hold ownership of bridges spanning navigable waterways and are responsible for defining bridge collapse (failure) as a result of vessel collision. For example, the Florida Department of Transportation (FDOT) defines the following limit states for vessel collision design: load transferred to the superstructure must not exceed the capacity of load transfer devices (e.g., shear pins) at the substructure-superstructure interface; load redistribution must not be permitted when the ultimate bearing capacity (UBC) of axially loaded piles is reached; and, the superstructure must not collapse [10]. Limit states are incorporated into the proposed PC framework by quantifying the pertinent capacity

(e.g., pile axial capacity) and monitoring the pertinent demand (e.g., pile-soil axial load) throughout each probabilistic simulation. If any of the limit states are reached, then the bridge is considered to have collapsed (structurally failed).

3.6 Framework summary

The proposed framework (summarized in Fig. 4) requires, for a bridge of interest, the identification of owner-defined limit states; the selection of a pier of interest; the development of a corresponding OPTS model; and collection of vessel traffic data. Using bridge and vessel traffic data, statistical descriptions of barge and bridge parameters—including limit state capacities—are formed. Subsequently, n simulations (standard Monte Carlo simulations) are conducted. Finally, PC is estimated based on the ratio between the total number of failures (the number of individual simulations where one or more limit states are reached), NF, and the total number of simulations conducted (n).

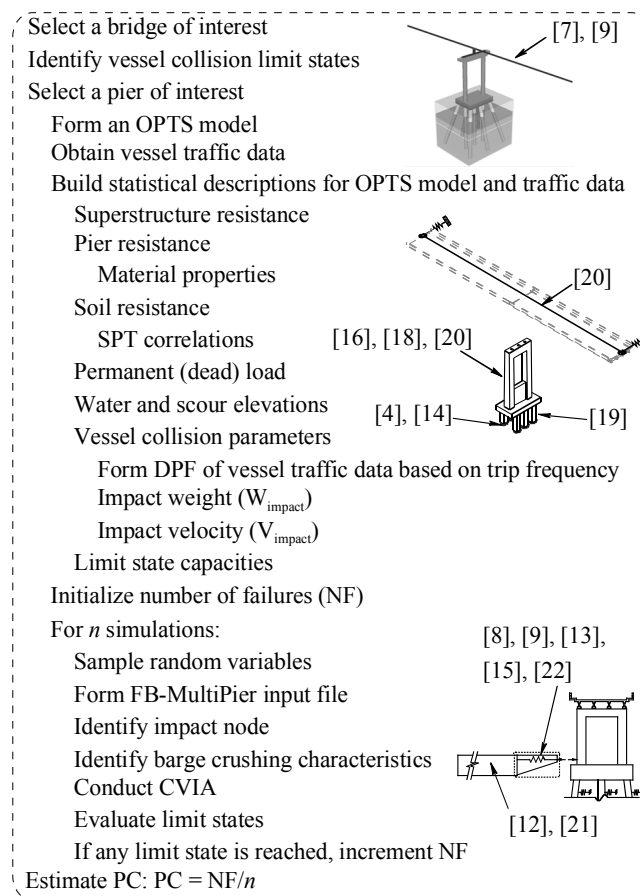


Fig. 4: Summary of proposed PC framework.

4 Comparative demonstration

An OPTS model of Pier 53 from the New St. George Island Bridge (Fig. 5a), located in Florida, USA, was selected for PC assessment using both the current AASHTO procedure

and the proposed framework. Pier 53, positioned several spans away from the navigation channel, supports five prestressed girders (2 m deep) that span 43 m to each side. Although girders atop Pier 53 are separated by an expansion joint across the pier cap, the superstructure deck is continuous. Two elastomeric bearings and a cast-in-place shear pin are provided at each of five evenly spaced bearing locations. Below the pier cap, Pier 53 contains two round (1.7 m diameter) pier columns and a 2 m thick waterline pile cap foundation. The underlying concrete piles consist of six battered and three plumb 1.4 m diameter prestressed cylinder piles. Construction drawings specify a 10.2 MN static impact design load for Pier 53, and the corresponding OPTS model was verified to reach collapse (failure) at a similar static load level before any probabilistic simulations were carried out.

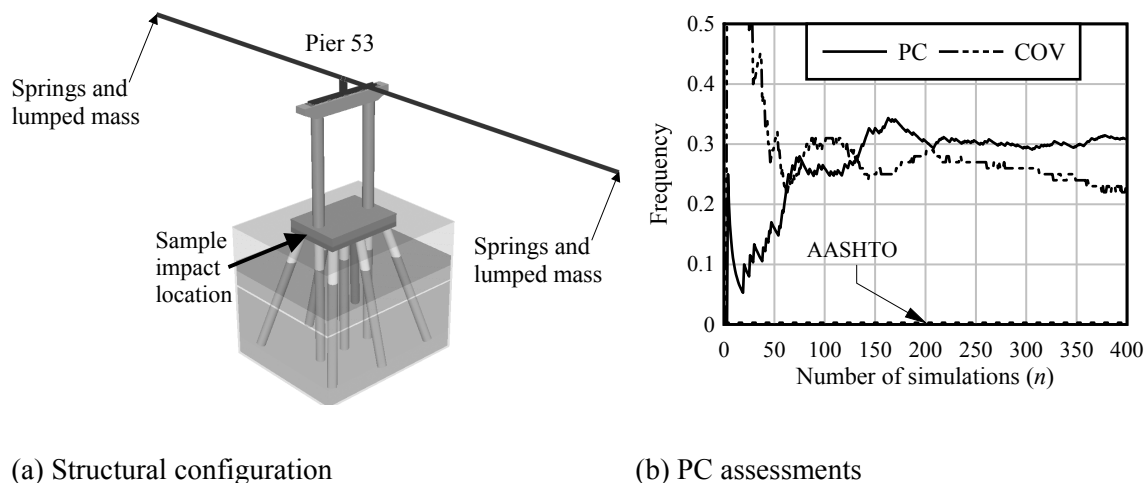


Fig. 5: New St. George Island Bridge Pier 53 OPTS model.

The AASHTO PC estimate for Pier 53—expressed as a weighted average relative to vessel trip frequencies from Tab. 4—is 0.0029 (Fig. 5b). This estimate was calculated using FDOT vessel collision risk assessment software, as referenced in [10]. In sharp contrast, the proposed framework produces a PC estimate of 0.31 for Pier 53 when determined using 400 simulations (Fig. 5b) and the FDOT vessel collision limit states [10]. It can be confidently stated that the AASHTO PC estimate is extremely small relative to that obtained using the proposed probabilistic framework, regardless of the limited reliability associated with the latter estimate (the corresponding COV is 0.23). This discrepancy demonstrates the potential for the current AASHTO PC formulation to produce unconservative bridge collapse estimates.

5 Concluding remarks

A rational framework for determining the probability of bridge collapse (failure) in the event of barge-bridge collision has been presented in this paper. The proposed framework employs efficient, yet accurate nonlinear dynamic collision analysis and bridge modeling techniques. Statistical descriptions of pertinent barge and bridge parameters are used in conjunction with these techniques to assess bridge collapse rates through probabilistic simulation. Furthermore, the proposed framework is highly modular; substantial alterations to framework components (e.g., the implementation of a relatively more efficacious prob-

abilistic simulation technique) can be incorporated in a robust manner as part of future efforts. The proposed framework has been used to estimate the probability of collapse for a selected case. Significant discrepancies between this estimate and that obtained using current bridge design provisions suggest the need for revisions in the existing vessel collision risk assessment. Namely, the incorporation of a rational probability of collapse framework will undoubtedly enable designers to more accurately plan and assess bridge structural safety.

6 References

- [1] AASHTO: *Guide Specification and Commentary for Vessel Collision Design of Highway Bridges*, 1st Edition, AASHTO, Washington D.C., USA, 1991
- [2] AASHTO: *Guide Specification and Commentary for Vessel Collision Design of Highway Bridges*, 2nd Edition, AASHTO, Washington D.C., USA, 2009
- [3] Bridge Software Institute (BSI): *FB-MultiPier User's Manual*. BSI, University of Florida, Gainesville, FL, USA, 2009
- [4] Barker, R.M.; Duncan, J.M.; Rojiani, K.B.; Ooi, P.; Tan, C.K.; Kim, S.G.: *Manuals for the Design of Bridge Foundations*, National Cooperative Highway Research Program (NCHRP), Report 343, NCHRP, Washington D.C., USA, 1991
- [5] Consolazio, G.R.; Cook, R.A.; McVay, M.C.; Cowan, D.R.; Biggs, A.E.; Bui, L.: *Barge Impact Testing of the St. George Island Causeway Bridge*, Structures Research Report No. 26868, University of Florida Engineering and Industrial Experiment Station, University of Florida, Gainesville, FL, USA, 2006
- [6] Consolazio, G.R.; Cowan, D.R.: Numerically Efficient Dynamic Analysis of Barge Collisions with Bridge Piers, *ASCE Journal of Structural Engineering*, Vol. 131, No 8, 2005, pp. 1256-1266
- [7] Consolazio, G.R.; Davidson, M.T.: Simplified Dynamic Barge Collision Analysis for Bridge Design, *Journal of the Transportation Research Board*. No 2050, 2008, pp. 13-25
- [8] Consolazio, G.R.; Davidson, M.T.; Cowan, D.R.: Barge Bow Force-Deformation Relationships for Barge-Bridge Collision Analysis, *Journal of the Transportation Research Board*, 2009, (in press)
- [9] Consolazio, G.R.; McVay, M.C.; Cowan D.R.; Davidson, M.T.; Getter, G.J.: *Development of Improved Bridge Design Provisions for Barge Impact Loading*. Structures Research Report No. 2008/51117, Engineering and Industrial Experiment Station, University of Florida, Gainesville, FL, USA, 2008
- [10] FDOT: *Structures Design Guidelines*, FDOT, Tallahassee, FL, USA, 2009

- [11] Fujii, Y.; Shiobara, R.: "The Estimation of Losses Resulting from Marine Accidents," *Royal Institute of Navigation*, Cambridge University Press, UK, 1978
- [12] Ghosn, M.; Moses, F.; Wang, J.: *Design of Highway Bridges for Extreme Events*, NCHRP Report 489, NCHRP, Washington D.C., USA, 2003
- [13] Joint Committee on Structural Safety (JCSS), *Probabilistic Model Code*, ISBN 978-3-909386-79-6, 2006
- [14] Johnson, P.A.: Comparison of Pier Scour Equations Using Field Data, *ASCE Journal of Hydraulic Engineering*, Vol. 121, No. 8, 1995, pp. 626-629
- [15] Kunz, C.U.: Ship Bridge Collision in River Traffic, Analysis and Design Practice, *Ship Collision Analysis*, Gluver and Olsen (eds.), Balkema, Rotterdam, 1998
- [16] MacGregor, J.G.; Wight, J.K.: *Reinforced Concrete: Mechanics and Design (4th Edition)*, Pearson Prentice Hall, Upper Saddle River, NJ, USA, 2005
- [17] Manuel, L.; Kallivokas, L.; Williamson, E.; Bomba, M.; Berlin, K.; Cryer, A.; Henderson, W.: *A Probabilistic Analysis of the Frequency of Bridge Collapses due to Vessel Impact*, Center for Transportation Research, University of Texas at Austin, TX, USA, FHWA/TX07/0-4650-1, 2006
- [18] Melchers, R.E.: *Structural Reliability Analysis and Prediction (2nd Edition)*, Wiley, NY, USA, 1999
- [19] National Oceanic and Atmospheric Administration (NOAA): *Tides & Currents*, tide-sandcurrents.noaa.gov, 2009
- [20] Nowak, A.S.; Collins, K.: *Reliability of Structures (1st Edition)*, McGraw-Hill, NY, USA, 2000
- [21] Wang, T.L.; Liu, C.: *Synthesizing Commercial Shipping (Barge/Tug Trains) From Available Data For Vessel Collision Design*, HPR Study No. 0510841, Florida International University, Miami, FL, USA, 1999
- [22] Yuan, P.; Harik, I.E.; Davidson, M.T.: *Multi-Barge Flotilla Impact Forces on Bridges*, Kentucky Transportation Center, University of Kentucky, Lexington, KY, USA, Research Report No. KTC-05 /SPR261-03-1F, 2008

Scenario characteristics affect the risk of fatalities after accidents with chlorine and ammonia at a category III of evidence

Frank van Boven
Rotterdam, The Netherlands

Abstract: Production, storage and transportation of hazardous materials is a threat to human population. Various studies have been done on predicting consequences of accidents with hazardous materials. However, findings of these studies have to be considered as low strength of evidence (category IV of evidence), as statistical inferences were absent. The aim of the present study is to investigate the possible relationship between the risk for fatalities and specific characteristics of accidents with hazardous materials at a category III of empirical evidence. Brockhoff et al. (J. Hazardous Mater., 29 (1992) 405-425) presented data on the risk of hazardous materials in the United States during the period 1914 - 1986. Two sub-sets were selected from the data presented by Brockhoff et al. The first sub-set of 28 accidents reports the hazardous material, the estimated released mass, the estimated number of fatalities and a characteristic for the population density. The second sub-set of 36 accidents reports the released mass and number of fatalities. In order to uniform the first sub-set the released mass was multiplied by a toxicological index for lethality by chlorine and ammonia. Prior to statistical analysis, the results were classified to present the data using frequency tables. Exact goodness-of-fit tests with respect to four log-linear models were performed with the R package exactLoglinTest (R version 2.6.1). Tests of goodness-of-fit for the first sub-set regarding the statistical log-linear models indicated an association between population density and scenario related number of fatalities but independent from released toxicological mass. In the second sub-set an association between variables was found between released toxicological mass and scenario related fatalities for 36 incidents involving chlorine. Various factors influence the consequences of accidents with hazardous materials. Statistical analysis on accidents with chlorine and ammonia in the United States that took place between 1914 - 1986 indicates that the released toxicological mass and the population density class affected the scenario related number of fatalities at a category III of evidence. Further research is recommended on estimating fatalities at a higher strength of evidence.

1 Introduction

Production, storage and transportation of hazardous materials is a threat to human population. During the 20th century, the frequency of technological disasters increased exponentially, primarily due to fires and explosions. However, the mean number of fatalities per incident declined (Coleman, 2006).

Probabilistic risk analysis has been developed to assess the risks of these seldom occurring events which have large consequences (Bedford and Cooke, 2001). Several investigators presented empirical approaches on estimating fatalities (Marshall, 1977; De Weger et al., 1991; Brockhoff et al., 1992; Rocard and Smets, 1992; Carol et al., 2001). Marshall (1977) called for a correction of his statistical estimations. Statistical evaluations reflect the strength of evidence of the predictions. Strength of evidence of the prediction of consequences can be categorised to reflect its susceptibility to bias (Shekelle et al., 1999): I. Meta-analysis and randomized controlled trials; II. Controlled and experimental studies; III. Comparative and correlation studies; IV. Expert opinions and case-studies. With regards to methods of presented empirical approaches, earlier findings on estimating fatalities have to be considered as low strength of evidence (category IV of evidence), as statistical inferences and goodness-of-fit were absent.

The aim of the present study is to investigate the possible relationship between the risk for fatalities and specific characteristics of accidents with hazardous materials at a category III of empirical evidence. The study is limited to accidents with chlorine and ammonia as reported previously (Brockhoff et al., 1992).

2 Material and methods

2.1 On the definition of risk

Several possible interpretations of the definition of risk have been presented and discussed (Gratt, 1987). Kaplan and Garrick (1981) defined risk as either of three possible set of triplets:

$$R = \{ \langle s_i, p_i(\phi_i), x_i \rangle \} \tag{1}$$

$$R = \{ \langle s_i, p_i(\phi_i), \xi_i(x_i) \rangle \} \tag{2}$$

$$R = \{ \langle s_i, p_i(\phi_i, x_i) \rangle \} \tag{3}$$

with R risk of a disaster (or the expected number of fatalities per year)

s_i scenario of the undesired event

p_i probability of the scenario per year

ϕ_i frequency of the i^{th} scenario

x_i effect when scenario takes place (actual number of fatalities)

ξ_i probability of the effect of the i^{th} scenario

This definition is often simplified to:

$$R = p_i * x_i \tag{4}$$

The aim of a risk assessment is to quantify the probability p_i and the effect x_i . The probability factor has a stochastic character by definition. Probability p_i is a statistical parameter of the random variable scenario s_i . The effect is assessed as a function of its cause(s). The cause is represented by the scenario. Kaplan and Garrick (1981) define scenario as a description of the event, “What can happen” or “What can go wrong”. However, definitions of various scenario can differ. In this study the variable scenario is a description of a hazardous event. Hazard is, in this case, defined as “the intrinsic property of a physical situation, with a potential for creating damage to human health or the environment” (according to Ale, 2002). Scenario is considered a random variable. It can be described by statistical parameters such as intensity or strength, domino effects, frequency, space of time, location, population density threatened by the scenario. The frequency of the scenario is assumed to be collinear with intensity and is therefore not further discussed in this study.

For the variable effect in this study, only fatalities are taken into account. Injury and economic damage are not taken into account. Fatalities can be defined in different ways. An important consideration is whether fatalities are related directly to the accident, or they are caused by an indirect result of a primary event. In this study, no specified information is available about the definitions used for fatalities, thus fatalities are defined as scenario-related.

The thesis of this study is whether the two variables, that of scenario and effect, are in fact independent. If not, scenario and effect must be dependent. In that case, knowledge of the value of the first random variable would provide us some insight into the probable behaviour of the second variable (Larsen and Marx, 1986). This insight provides a basis when specifying probabilistic models for the sake of the risk assessment.

2.2 Observations

Brockhoff et al. (1992) presented data on the risk of hazardous materials in the United States during the period 1914 – 1986. One sub-set A of this data consists of 13 accidents involving chlorine and 15 accidents involving ammonia (see appendix A). For each accident the estimated released mass, estimated number of fatalities and a characteristic for the population density is given. Another sub-set B consists of 36 accidents involving release of chlorine with incomplete data on population density. In order to uniform the first sub-set the released mass was multiplied by a toxicological index for lethality by chlorine and ammonia (toxic index chlorine versus ammonia 10:1, based on the immediate lethal concentration in parts per million (as presented by Brockhoff et al.)). The product was defined as released toxicological mass with unit toxic megagram. Prior to statistical analysis, the results were classified to present the data using frequency tables. The classification yields the partitioning of the scenario related number of fatalities around the rounded median (variable x_i), partitioning of the estimated released toxicological mass around the rounded median (variable s_{1j}) and the categorisation of the estimated population density class into two options: urban area or not (variable s_{2k}). The variables s_{1j} and s_{2k} represent the scenario.

2.3 Statistical analysis

Exact goodness-of-fit tests (Caffo, 2006) with respect to four log-linear models without interactions were applied on the two sub-sets:

$$\log E(Y_{ijk}) = \mu + s_{1j} + s_{2k} \quad (5)$$

$$\log E(Y_{ijk}) = \mu + x_i + s_{1j} \quad (6)$$

$$\log E(Y_{ijk}) = \mu + x_i + s_{2k} \quad (7)$$

$$\log E(Y_{ijk}) = \mu + x_i + s_{1j} + s_{2k} \quad (8)$$

with x_i scenario related number of fatalities

s_{1j} estimated released toxicological mass in toxic Mg

s_{2k} estimated population density class

Calculations were performed with the package exactLoglinTest in R version 2.6.1 (Ihaka and Gentleman, 1996) – see appendix B. Log-linear models were selected by use of hierarchical elimination. The first sub-set A was analysed for independence between released toxicological mass, population density class and scenario related number of fatalities. The second data sub-set B was analysed for independence between released toxicological mass and scenario related number of fatalities only (limited to equation 6). The level of significance is taken as $\alpha = 0.05$.

2.4 Sensitivity

In order to examine the robustness of statistical analysis, different classifications and specifications on toxicological index for lethality by chlorine and ammonia has been tested. These alternative tests include partitioning around three differing parameters (see table 1 and 2), additional categorisation of the estimated population density class into two options: urban and industrial area or not (variable s_{2k}) and additional testing of a toxic index chlorine versus ammonia 5:1 and a toxic index chlorine versus ammonia 20:1.

Tab. 1: Classifications for x_i and $s_{1,j}$ for sub-set A

Alternative	x_i	$s_{1,j}$
Lower percentile	$0 \text{ or } \geq 1$	$\leq 10 \text{ or } > 10$
Rounded median	$0 \text{ or } \geq 1$	$\leq 100 \text{ or } > 100$
Upper percentile	$< 10 \text{ or } \geq 10$	$\leq 500 \text{ or } > 500$

Tab. 2: Classifications for x_i and $s_{1,j}$ for sub-set B

Alternative	x_i	$s_{1,j}$
Lower percentile	$0, 1-4, \geq 5$	$\leq 25 \text{ or } > 25$
Rounded median	$0, 1-9, \geq 10$	$\leq 100 \text{ or } > 100$
Upper percentile	$0, 1-14, \geq 15$	$\leq 250 \text{ or } > 250$

3 Results

11 of 28 incidents (sub-set A), of which 14 took place in an urban environment, resulted in fatalities (median value 0 scenario related fatalities). The released toxicological mass varied from 0.5 to 950 toxic Mg (median value 118 toxic Mg). 14 of 36 incidents involving chlorine (sub-set B) resulted in fatalities (median value 0 scenario related fatalities). The released toxicological mass from 36 incidents varied from 0.5 to 950 toxic Mg (median value 98 toxic Mg). Tests of goodness-of-fit regarding the statistical log-linear models indicated an association between variables with regards to the chosen toxicological index for lethality by chlorine and ammonia (table 3). Alternative tests on goodness-of-fit indicated grosso modo, an association between population density and scenario related fatalities but independent from released toxicological mass (table 4-6). For the second sub-set B of 36 incidents involving chlorine an association was found between released toxicological mass and scenario related fatalities (table 7).

Tab. 3: Association between risk for fatalities and scenario characteristics for sub-set A with different toxicological index for lethality by chlorine and ammonia when x_i and $s_{1,j}$ partitioned around the median

Model	Hypothesis	Toxic index 5:1	Toxic index 10:1	Toxic index 20:1
(5)	Mutual independence $s_{1,j}$ and $s_{2,k}$	0.03	0.10	0.08
(6)	Mutual independence x_i and $s_{1,j}$	0.05	0.15	0.12
(7)	Mutual independence x_i and $s_{2,k}$	0.04	0.15	0.12
(8)	Mutual independence x_i , $s_{1,j}$ and $s_{2,k}$	0.03	-	-

Significant values in bold.

Tab. 4: Association between risk for fatalities and scenario characteristics for sub-set A with different classifications for x_i and $s_{1,j}$ for a toxicological index of 5:1

Model	Hypothesis	Partitioned around lower percentile	Partitioned around rounded median	Partitioned around upper percentile
(5)	Mutual independence $s_{1,j}$ and $s_{2,k}$	0.08	0.03	< 0.001
(6)	Mutual independence x_i and $s_{1,j}$	0.13	0.05	1.0
(7)	Mutual independence x_i and $s_{2,k}$	< 0.001	0.04	< 0.001
(8)	Mutual independence x_i , $s_{1,j}$ and $s_{2,k}$	-	0.03	-

Significant values in bold.

Tab. 5: Association between risk for fatalities and scenario characteristics for sub-set A with different classifications for x_i and $s_{1,j}$ for a toxicological index of 10:1

Model	Hypothesis	Partitioned around lower percentile	Partitioned around rounded median	Partitioned around upper percentile
(5)	Mutual independence $s_{1,j}$ and $s_{2,k}$	0.09	0.10	< 0.001
(6)	Mutual independence x_i and $s_{1,j}$	0.17	0.15	0.73
(7)	Mutual independence x_i and $s_{2,k}$	0.003	0.15	< 0.001
(8)	Mutual independence x_i , $s_{1,j}$ and $s_{2,k}$	-	-	-

Significant values in bold.

Tab. 6: Association between risk for fatalities and scenario characteristics for sub-set A with different classifications for $s_{2,k}$ when x_i and $s_{1,j}$ partitioned around the median and for a toxicological index of 10:1

Model	Hypothesis	Population den- sity: urban area or not	Population den- sity: urban and industrial com- bined
(5)	Mutual independence $s_{1,j}$ and $s_{2,k}$	0.10	0.15
(6)	Mutual independence x_i and $s_{1,j}$	0.15	0.07
(7)	Mutual independence x_i and $s_{2,k}$	0.15	0.24
(8)	Mutual independence x_i , $s_{1,j}$ and $s_{2,k}$	-	-

Significant values in bold.

Tab. 7: Association between risk for fatalities and scenario characteristics for sub-set B with different classifications for x_i and $s_{1,j}$

Model	Hypothesis	Partitioned around lower percentile	Partitioned around rounded median	Partitioned around upper percentile
(6)	Mutual independence x_i and $s_{1,j}$	< 0.001	0.02	0.91

Significant values in bold.

4 Discussion

Presented here is an empirical study of the relationship between scenario and effect using data on accidents with chlorine and ammonia in the United States. The study involves testing whether there is independence between scenario and effect. Starting point of this study is the first set of risk triplets: $R = \{< s_i, p_i(\phi_i), x_i >\}$ as defined by Kaplan and Garrick (1981).

When observing accident characteristics of all fifty-one accidents with chlorine and ammonia in the United States that took place between 1914 – 1986, dependence was found between the released toxicological mass $s_{1,j}$, respectively the population density class $s_{2,k}$ and the scenario related number of fatalities x_i . The dependence is limited to the used subsets of the data.

When combining chlorine and ammonia the majority of tests on independence between the population density class $s_{2,k}$ and the scenario related number of fatalities x_i were rejected. Dependence on the released toxicological mass $s_{1,j}$ was only measured when partitioning around rounded medians for a toxicological index of 5:1. Industrial areas did not appear to affect scenario related number of fatalities. In the case of partitioning around upper percentiles of the released toxicological mass both as larger numbers of fatalities all extreme accidents become rare. In that case, no dependence can be discriminated between the released toxicological mass and scenario related number of fatalities.

Classical goodness-of-fit requires minimum expected values in classes ($n\hat{p}_i > 5$ for all classes), which was not met in this study. However, the use of an exact procedure corrected this problem. The log-linear models used in this study were defined without interactions. Testing of log-linear models, with interactions, calls for a larger dataset with approximately sample size of one hundred accidents. Depending on the number of predictors used, a prediction model calls for an even larger sample size of accidents.

In earlier research, Marshall (1977) assessed mortality of toxic releases by empirical basis. His assessment was based on limited data sources. Mortality was calculated by dividing the sum total of the fatalities by the sum total of the quantity of toxic material released from a total of 36 incidents. Marshall recommended a more extensive statistical evaluation of his own results. De Weger et al. (1991) derived probit constants for human exposure to toxic gases from animal data. Brockhoff et al. (1992) assessed mortality from toxic releases by a simple regression through the origin, differentiated to three population density classes. Ro-

card and Smets (1992) analysed six accidents in France by use of the Pareto distribution. Parameters were estimated and extrapolated to severe accidents, and then compared with Pareto analysis on larger samples. Carol et al. (2001) estimated consequences of accidental explosions using applied regression. The approach of Carol et al. can be considered a statistical confidence interval for the approach of Marshall with α ranging from 0 to 1. All investigators reported their findings without statistical evaluation or goodness-of-fit. However, all findings are based on relating effects to the physical situation (released mass or explosive mass), with an exception of Rocard and Smets who related fatalities to the frequency per year. Only Brockhoff et al. related effects to population density. However, they did not report on significance of the population density. Results of Marshall and Brockhoff et al. are comparable. With a release of 10 tonnes chlorine, Marshall predicts 5 fatalities. Depending on population density and with a release of 10 tonnes chlorine, Brockhoff et al. predict 0 – 22 fatalities. The mean value of Brockhoff et al. is 8 fatalities. In general, the associations found in this study statistically confirm the earlier findings of Marshall and Brockhoff et al., which have to be considered as low strength of evidence (category IV of evidence), as statistical inferences and goodness-of-fit were absent.

Fairhurst and Turner (1993) introduced a concept of “toxic load”, comprising exposure concentration and exposure duration. The latter is not involved in this study, since the data did not contain information on exposure duration. Considering the definition of scenario used in this study, exposure duration (or space of time) could also be of importance. The question of interest is, there for, whether toxic load is a more appropriate characteristic than released mass as used in this study. Both variables, the released mass and toxic load support the opportunity to combine different types of hazardous materials.

Two specifications on the toxicological index were tested in this study, a fatality ratio between chlorine and ammonia of 5:1 and 10:1. Brockhoff et al. (1992) estimated this ratio to be 15, ranging a factor 1-3. De Weger et al. (1991) presented a ratio of approximately 6:1 for 30 minutes exposure with 50 % mortality. Results of Brockhoff et al. refer to overall mortality. Results found in this study on ratios 5:1 and 10:1 supported previous studies.

The associations found in this study are at level of category III of evidence. Study designs of the highest category of evidence, meta-analysis and randomised controlled trials are commonly used in health sciences, but not in safety sciences. From the domain of health sciences it can be concluded that meta-analysis do not obviously support health interventions however, correlation studies suggest clinical effects (Gøtzsche and Johansen, 2008).

In summary, statistical analysis on accidents with chlorine and ammonia in the United States that took place between 1914 - 1986 indicates that the released toxicological mass and the population density class affected the scenario related number of fatalities at a category III of evidence. The associations suggest for a validation in a larger-scale study. Further research is recommended on estimating fatalities at a higher strength of evidence.

5 Acknowledgements

Prof. dr. B.J.M. Ale is thanked for interesting discussion on an earlier draft of this paper. The Municipal of Capelle aan den IJssel is thanked for financial support.

6 References

- [1] Ale, B.J.M.: Risk assessments practices in The Netherlands. *Safety science*, vol. 40 (2002), p. 105-26
- [2] Bedford, T; Cooke, R.M.: *Probabilistic risk analysis: Foundations and methods*, Cambridge, 2001 (Cambridge University Press)
- [3] Brockhoff, L.; Styhr Petersen, H.J.; Haastrup, P.: A consequence model for chlorine and ammonia based on a fatality index approach. *J. Hazardous Mater.* 29 (1992) p. 405 – 425
- [4] Caffo, B.: Exact hypothesis tests for log-linear models with exactLoglinTest, *J. Stat. Software*, 17 (2006), issue 7
- [5] Carol, S. J. A. Vilchez and J. Casal: A new approach to the estimation of the probable number of fatalities in accidental explosions *Safety Science*, Volume 39, Issue 3, December 2001, Pages 205-217
- [6] Coleman, L.: Frequency of man-made disasters in the 20th century. *Journal of Contingencies and Crisis Management* 14 (2006), no 1, p. 3 – 11
- [7] De Weger, D., C.M. Pietersen and Reuzel, P.G.J.: Consequences of exposure to toxic gases following industrial disasters, *J. Loss. Prev. Process. Ind.* Vol. 4 (1991), July, p. 272 – 276
- [8] Dobson, A.J.: *An introduction to generalized linear models*, New South Wales, 1994 (Chapman & Hall, reprinted)
- [9] Fairhurst, S. and R.M. Turner: Toxicological assessments in relation to major hazards, *J. Hazardous Mater.* Vol. 33 (1993), p. 215 – 227
- [10] Gøtzsche, P.C. and Johansen, H.K.: House dust mite control measures for asthma: systematic review, *Allergy* vol 63 (2008), p. 646–659
- [11] Gratt, L.B.: The definition of risk and associated terminology for risk analysis, In: J.J. Bonin and D.E. Stevenson (Eds), *Advances in risk analysis* 7 (1987), 675–680
- [12] Ihaka, R., R. Gentleman , “R: a language for data analysis and graphics” *J. of Computational and Graphical Statistics* 5 (1996), nr. 3, 299 – 314

- [13] Kaplan, S., Garrick, B.J.: On the quantitative definition of risk, *Risk Analysis*, Vol. 1 (1981) nr. 1, p. 11–27
- [14] Larsen, R.J.; Marx, M.L.: *An introduction to mathematical statistics and its applications*, second edition, New Jersey, 1986 (Prentice-Hall)
- [15] Marshall, V.C., How lethal are explosions and toxic escapes? *The Chemical Engineer*, August 1977, 573–577
- [16] Rocard, P and Smets, H., “A Socio-economic Analysis of Controls on Land Use around Hazardous Installations,” *The Geneva Papers on Risk and Insurance*, 17, pp. 468-484, October, 1992.
- [17] Shekelle, P.G., Woolf, S.H., Eccles, M. and Grimshaw, J.: Developing guidelines *BMJ* vol. 318 (1999), p. 593 - 596

7 Appendix A: data extracted from Brockhoff et al. (1992)

Table 8: Sub-set A – data on accidents involving release of chlorine and ammonia

Year	Place	Hazardous material	Toxic release [toxic Mg]	Scenario related fatalities	Population density class
1917	Wyandotte	Chlorine	150	1	U
1936	Johannesburg	Chlorine	25	1	U
1944	Brooklyn	Chlorine	0,5	0	U
1947	Chicago	Chlorine	170	0	U
1963	Philedelphia	Chlorine	10	0	U
1975	Niagara Falls	Chlorine	300	4	U
1978	Youngstown	Chlorine	500	8	U
1947	Rauma	Chlorine	300	19	I
1962	Cornwall	Chlorine	290	0	I
1979	Estarreja	Chlorine	20	0	I
1961	La Barre	Chlorine	285	1	R
1976	Baton Rouge	Chlorine	950	0	R
1963	Brandtsville	Chlorine	85	0	R
1968	Lievin	Ammonia	17	6	U
1969	Crete	Ammonia	77	8	U
1970	West Virginia	Ammonia	75	0	U
1973	Potchefstroom	Ammonia	38	18	U
1975	Texas City	Ammonia	50	0	U
1976	Enid	Ammonia	500	0	U
1976	Houston	Ammonia	19	6	U
1976	Landkrona	Ammonia	180	2	I
1976	Unknown	Ammonia	1	0	I
1970	Blair	Ammonia	153	0	R
1971	Floral	Ammonia	570	0	R
1973	Kansas	Ammonia	244	0	R
1974	McPharson	Ammonia	360	0	R
1981	Minnesota	Ammonia	50	0	R
1987	Lampoul G.	Ammonia	4	0	R

U = urban; I = industrial and R = rural

Table 9: Sub-set B – data on accidents involving release of chlorine without information on population density

Year	Place	Toxic release [toxic Mg]	Scenario related fatalities
1917	Wyandotte	150	1
1936	Johannesburg	25	1
1944	Brooklyn	0,5	0
1947	Chicago	170	0
1963	Philedelphia	10	0
1975	Niagara Falls	300	4
1978	Youngstown	500	8
1947	Rauma	300	19
1962	Cornwall	290	0
1979	Estarreja	20	0
1961	La Barre	285	1
1976	Baton Rouge	950	0
1963	Brandtsville	85	0
1914	Chrome	70	0
1926	St Auban	250	19
1928	Asbotan	20	0
1929	Syracuse	240	1
1934	Niagara Falls	155	1
1935	Griffith	280	0
1939	Zarnesti	250	60
1940	Mjodalen	75	3
1949	Freeport	45	0
1950	Billingham	5	0
1952	Walsum	150	7
1956	Lake Charles	27	0
1957	Runcorn	25	0
1961	Billingham	120	0
1966	La Spezia	70	0
1967	Newton	530	0
1969	Cleveland	10	2
1970	Javle	20	0
1973	Loos	155	0
1981	Puerto Rico	20	0
1981	Mexico	110	29
1983	Louisiana	5	0
1983	Louisiana	15	0

8 Appendix B: example of calculations for sub-set B in R

```
> # Brockhoff et al., 1992; log-linear for chlorine fatalities
> # baseline classifications
> # S1,j >100; Xi 0, 1-9, >=10
> hazard <- data.frame (S1 =c(-1,-1,-1,1,1,1),
+ X =c(-1,0,1,-1,0,1), Y =c(15,3,0,7,7,4))
>
> # frequencies after categorising
> # Function Pearson Statistic
> pearson<-function(obs,pred){sum(((obs-pred)^2)/pred)}
>
> # model of mutual independence of S1 and X (Model S1X)
> fmod <- glm(Y ~ S1 + X, family = poisson, data = hazard)
> summary(fmod)
```

Call:

```
glm(formula = Y ~ S1 + X, family = poisson, data = hazard)
```

Deviance Residuals:

```
 1    2    3    4    5    6
1.1131 -0.8902 -2.0453 -1.3188  0.9311  1.1705
```

Coefficients:

```
      Estimate Std. Error z value Pr(>|z|)
(Intercept) 1.572e+00 2.054e-01  7.655 1.93e-14 ***
S1          -6.481e-13 1.667e-01 -3.89e-12 1.000000
X           -8.341e-01 2.400e-01 -3.476 0.000509 ***
```

```
Signif. codes:  0 '***' 0.001 '**' 0.01 '*' 0.05 '.' 0.1 ' ' 1
```

(Dispersion parameter for poisson family taken to be 1)

```
Null deviance: 24.402 on 5 degrees of freedom
Residual deviance: 10.191 on 3 degrees of freedom
AIC: 34.621
```

Number of Fisher Scoring iterations: 5

```
> exp(predict(fmod))
 1    2    3    4    5    6
11.091673 4.816654 2.091673 11.091673 4.816654 2.091673
```

>

```
> #### Exact tests ####
```

>

```
> library(exactLoglinTest)
```

```
> set.seed(1)
```

>

```
> #S1X
```

```
> mce <- mceexact(Y ~ S1 + X, data=hazard,nosim=10^5)
```

```
> summary(mce)
```

```
Number of iterations = 83024
T degrees of freedom = 3
Number of counts = 6
df = 3
Next update has nosim = 1e+05
Next update has maxiter = 1e+05
Proportion of valid tables = 0.83024
```

```
      deviance Pearson
observed.stat 1.019115e+01 8.3941498579
pvalue        2.224643e-02 0.0295767511
mcse          2.934483e-04 0.0003832667
```

Basis for Risk Management of Vehicle Bridges Located on Seismic Zones

David De-León-Escobedo, David Joaquín Delgado-Hernández

Engineering School, Autonomous University of the State of Mexico, Cerro de Coatepec, Ciudad Universitaria, Toluca, México, C.P. 50130, Tel: +52-01-722-214-0534 Ext. 1097, Fax: +52-01-722-214-0534 Ext. 1014 e-mail: daviddelen@gmail.com

Abstract: Because of their location on seismic zones, some important vehicle bridges are exposed to damages and collapses with the subsequent potential fatalities and economic losses for the country. The magnitude of these losses underlines the need for a rational planning and risk mitigation national policy. Current scientific and technological advances support the risk and reliability concepts and tools to formulate the basis for a decision system with the capabilities to generate strategies to measure and control the structural risk of critical bridges located on seismic zones with high population density and important traffic volume. These criteria and tools may help to support the decision-making process where engineers select a design type or an inspection and maintenance schedule. Also, the safety assessment of bridges exposed to seismic risk involves a significant amount of uncertainty and a probabilistic treatment is mandatory. Quantitative descriptions of the seismic hazard and the risk involved due to the bridge importance constitute basis for the management of mitigation measures to optimize limited resources for bridge protection in a national level. In this paper, the acceptable failure probability for important bridges is calculated throughout the expected cost of failure consequences. Also, the bridge failure probability is calculated for a typical example in Mexico City. The expected life-cycle cost serves as a comparative measure of cost-effectiveness and it is formulated in terms of the bridge seismic hazard and the potential consequences of failure. These consequences are from the physical loss of the bridge to the human casualties and economical cost of the loss of service, which are estimated in monetary terms. The bridge reliability is an essential component of risk and, for a given structural type is estimated in a simplified way by using Monte Carlo simulation techniques in order to account for the uncertainties in an explicit way. Initial and failure cost curves are determined for all possible soil accelerations and expected costs conditional to these accelerations are obtained. The unconditional life-cycle cost is calculated by convolution considering the seismic hazard curve of the site. The procedure is illustrated throughout a bridge on the soft soil of Mexico City. The results may

be extended for generating risk management policies to improve the current Mexican codes and to enhance the practices on bridge design and maintenance on seismic zones. **Keywords:** Seismic hazard, vulnerability, risk and reliability, vehicles bridge, Mexico.

1 Introduction

Several authors have presented their views about the purpose of designing a structure [16]. For example, it has been argued [4] that “the objective of a design process is to reach an acceptable probability that the designed structures will behave satisfactorily during their lifetimes. Therefore they are designed to withstand all possible loads and deformations during construction and normal use”. Meli [12] sustains that the structural safety is defined during the design process, when the designer must verify that the resistance is over the demands that will act over it during its lifetime. Such descriptions have implicit the concept of structural reliability.

According to Meli [12], the reliability of a structure is associated to a certain cost which should be minimized to balance safety with cost. Therefore, an optimization process should be performed where the objective function must include the initial cost of the work and the cost of the potential damages and other consequences in case a failure occur. Therefore, if C_t is the total cost of the structure, C_i the initial cost, C_d the cost of failure consequences and P_f the failure probability:

$$C_t = C_i + C_d \cdot P_f \quad (1)$$

2 Acceptable Failure Probability

By recognizing the uncertainties inherent in the design process, especially the seismic hazard, it has been proposed [11], to appraise bridge performance by using the expected life-cycle assessment. In the offshore technology [18], the expected life-cycle cost $E[C_t]$, is expressed in terms of the initial cost C_i , and the expected failure/damage cost $E[C_d]$.

$$E[C_t] = C_i + E[C_d] \quad (2)$$

Where:

$$E[C_d] = PVF(P_f)C_d \quad (3)$$

And PVF is the present value factor. Given that this formulation includes all possible adverse events, either failure or damage that may occur within the bridge lifetime, the PVF considers all those potentially damaging events not just the worst scenario. Also, the average damage cost C_d is composed by the costs of consequences:

$$C_d = C_r + C_f + C_e \quad (4)$$

Where C_r is the repair/restitution cost, C_f is the cost related to fatalities and C_e is the economic loss due to the service interruption, user costs, while the bridge is repaired or rebuilt. PVF depends on the net annual discount rate r and the bridge lifetime T :

$$PVF = \frac{1 - \exp(-rT)}{r} \quad (5)$$

If the initial cost C_i is expressed as a function of the failure probability [17], the expected lifecycle cost becomes a function of the failure probability.

$$E[C_t] = C_1 - C_2 \ln(P_f) + PVF(P_f)C_d \quad (6)$$

The acceptable (optimal) failure probability may then be calculated by minimizing the expected life-cycle cost respect the failure probability.

$$\frac{\partial E[C_t]}{\partial P_f} = 0 \quad (7)$$

$$P_f = \frac{0.434C_2}{PVF[C_d]} \quad (8)$$

The acceptable failure probability depends inversely of the cost of consequences which means that, according to the bridge importance, the safety requirement should be stricter as those consequences increase. Also, the requirement may be expressed in terms of the bridge reliability index.

$$\beta_a = \Phi^{-1}(1 - P_f) \quad (9)$$

According to previous results [9], the cost of consequences has been normalized to the initial cost and $C_2/C_i = 0.08$ for typical bridges. Also, for $T = 200$ years and $r = 0.08$, the bridge acceptable reliability has been plotted against the cost ratio C_d/C_i (see Figure 1). For the bridge considered here, it has been estimated that the costs of consequences is 800 times the initial cost (because of the high traffic volume) and, therefore, the acceptable bridge reliability β_a is approximately 3.84.

3 Bridge Reliability Theoretically

From well known structural reliability theory, the bridge reliability may be calculated [3] with expression (10):

$$\beta = \frac{E(G)}{\sigma_G} \quad (10)$$

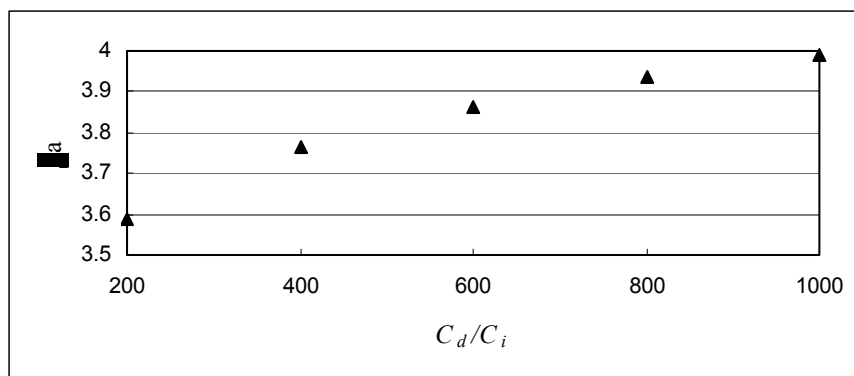


Fig. 1 Bridge acceptable reliability as a function of the ratio C_d/C_i

Where G is the bridge limit state considering its exposure to seismic loads, $E(G)$ the expected value of such limit state and σ_G its standard deviation. Although the bridge is a complex structural system, from previous analyses for typical bridges [9], the limit state has been conservatively approximated in terms of the failure of the most critical structural element. It was found that this element is one of the main piles and it is subject to a combination of axial load and bending. Therefore, G is calculated as:

$$G = 1 - \left[\frac{P_A}{P_R} + \frac{M_A}{M_R} \right] \quad (11)$$

Where P_A is the maximum acting axial load, P_R the axial resistant force, M_A the maximum acting moment and M_R the resistant moment of the critical cross section. Given that P_A and M_A are a consequence of the random earthquakes that may occur during the bridge lifetime, these effects are random variables. Also, from the variability of materials properties, the resistances P_R and M_R are also random. The standard deviation σ_G is:

$$\sigma_G \approx \sqrt{\sum_{i=1}^4 \left(\frac{\partial G}{\partial X_i} \right)^2 \sigma_{x_i}^2} \quad (12)$$

In Equation (12), X is the vector of acting and resisting axial loads and moments, such that, $X_1 = P_A$, $X_2 = P_R$, $X_3 = M_A$ and $X_4 = M_R$, and the derivatives are evaluated on the mean values. Therefore:

$$\sigma_G \approx \sqrt{\frac{\sigma_{P_A}^2}{\bar{P}_R^2} + \left(\frac{\bar{P}_A}{\bar{P}_R^2} \right)^2 \cdot \sigma_{P_R}^2 + \frac{\sigma_{M_A}^2}{\bar{M}_R^2} + \left(\frac{\bar{M}_A}{\bar{M}_R^2} \right)^2 \cdot \sigma_{M_R}^2} \quad (13)$$

Where σ_{MR} , σ_{MA} , σ_{PR} and σ_{PA} are the standard deviations of the resistant and acting moments, and the resistant and acting axial loads, respectively.

4 Application on Selected Bridge

The structure is a vehicles' bridge built on the Benito Juarez International airport area, Mexico City, in the transition seismic zone III, and it is aimed at improving traffic conditions. The bridge has a 400 m total span divided into 16 segments of 25 m each. The structural modelling was made through a finite element-based commercial software [13] and the images of the main structural members are shown in Figures 2 and 3. Essentially, the main structural components of the bridge are: the transverse cap, two piers, the footing and the piles.



Fig. 2 Main supports of the bridge

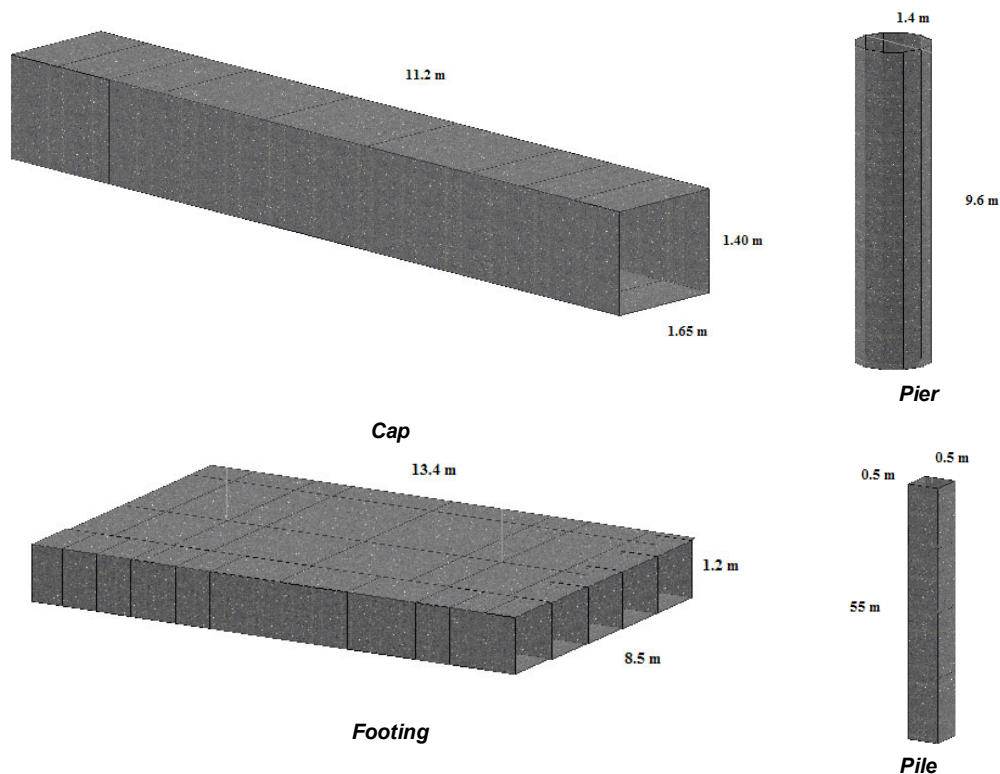


Fig. 3 Main bridge components

Figure 4 shows the plant location and dimensions of the piers and piles. The mean reinforced concrete properties are $f'c = 250 \text{ kg/cm}^2$ and $f_y = 4200 \text{ kg/cm}^2$.

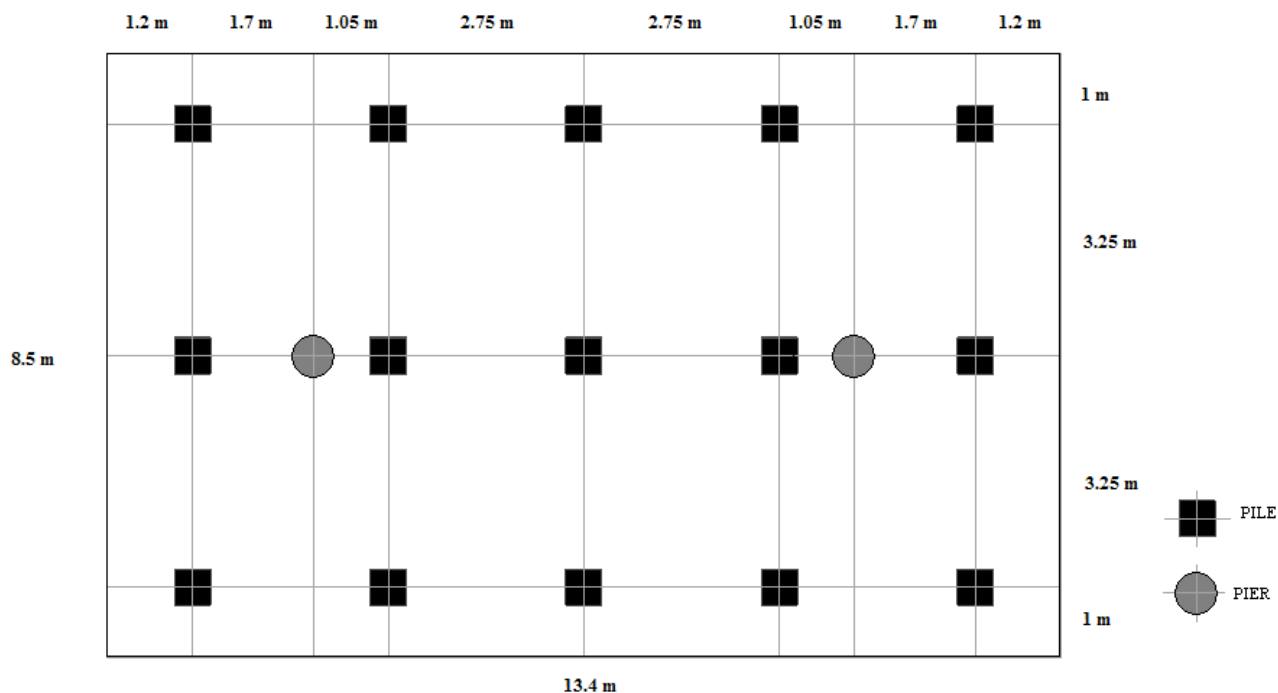


Fig. 4 Main bridge components

4.1 Bridge Reliability Practically

A family of bridge designs were obtained [5] by varying the original design dimensions and steel areas. These designs allowed for a series of alternative designs to measure the variation of reliability with cost under specified seismic intensities. The bridge designs were analyzed under given maximum seismic coefficients c/g , using the typical spectral form for Mexico City, and according to the range of intensities as reported in Mexican seismic hazard and failure rates studies [10].

Table 4.1 shows a sample of the results obtained by varying the seismic coefficients from $0g$ to $0.6g$ at each $0.15g$ and for specific design alternatives (in this case a pier). The Table contains the seismic coefficient, the rebars size, number of rebars, mean values of maximum axial load and moment and axial and moment resistances, reliability index β and the initial costs obtained.

Table 4.1 Sample of the calculations for cost-reliability curve (pier)

c/g	Rebar size ("8)	No Re-bars	P_A (T)	P_R (T)	M_A (T*m)	M_R (T*m)	β	C_i (10^3 USD)
0	22	11	228.97	817.77	529.78	541.29	3.28	6338.4
0.15	26	11	227.4	947.43	575.51	618.62	3.68	6918.6
0.3	28	11	225.82	1026.46	621.24	656.23	3.44	7193.6
0.45	30	11	225.82	1075.38	666.97	689.22	3.37	7468.7
0.6	32	11	222.67	1171.87	712.7	722.25	3.33	7743.7

Five alternative designs and the five maximum intensities shown in Table 4.1, were considered and the corresponding reliability indices and initial costs were calculated. For the standard deviations, it was used $CV_A = 0.25$ and $CV_R = 0.1$, and the following simplifications were made [9]:

$$CV_A = \frac{\bar{P}_A}{\sigma_{P_A}} = \frac{\bar{M}_A}{\sigma_{M_A}} \tag{14}$$

$$CV_R = \frac{\bar{P}_R}{\sigma_{P_R}} = \frac{\bar{M}_R}{\sigma_{M_R}} \tag{15}$$

All the curves in the family shown in Figure 5 are conditional to the occurrence of the indicated intensity. In order to obtain the unconditional curve, the ordinates of the conditional curves need to be weighted by the occurrence probabilities according to the seismic hazard curve for Mexico City [10] (see Figure 6).

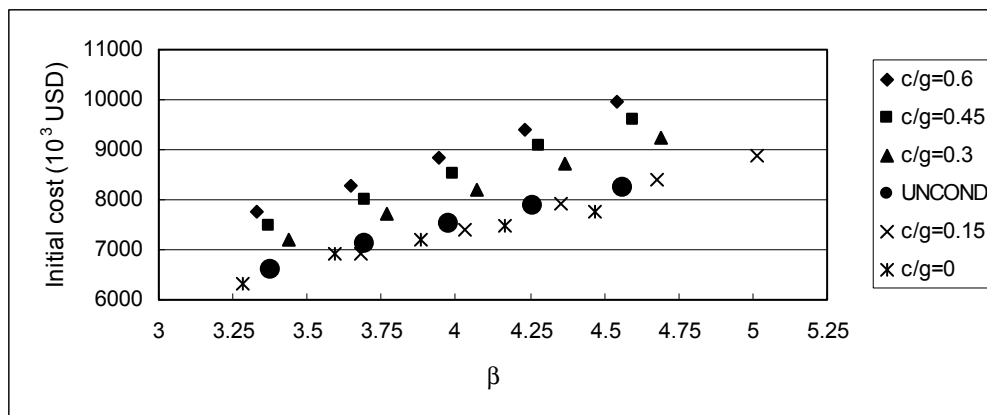


Fig. 5 Family of conditionals and unconditional initial cost curves for a bridge on the zone III, Mexico City

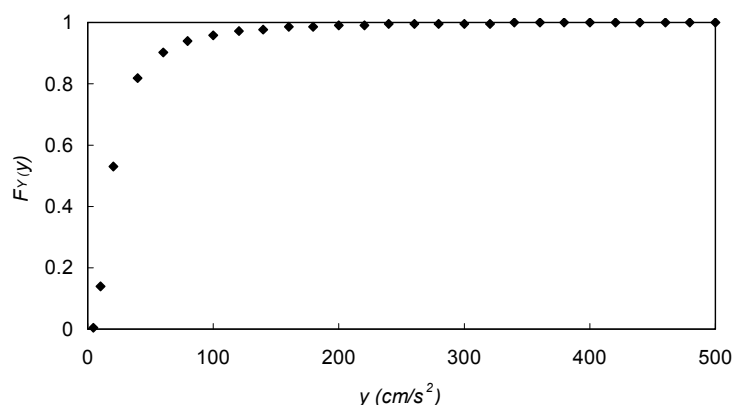


Fig. 6 Annual cumulative probability of seismic intensities in Mexico City

4.2 Expected Failure Cost and Expected Life-Cycle Cost Curves

By considering that, for the bridge under study, the damage/failure cost is 800 times the initial cost, the expected failure cost and expected life-cycle cost are calculated. The results are shown in Figure 7.

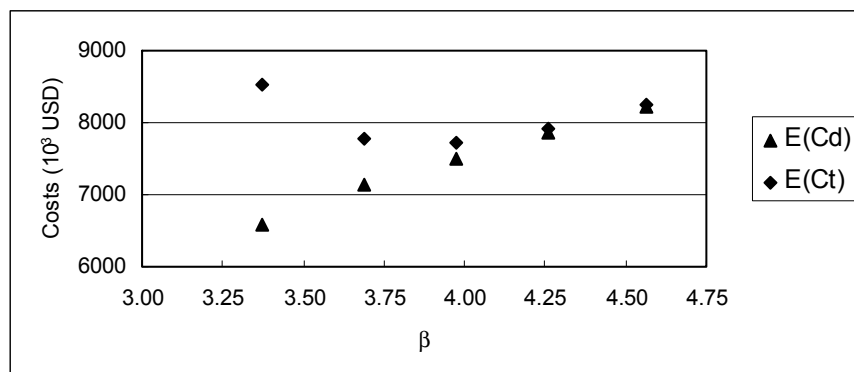


Fig. 7 Expected cost of failure and expected life-cycle cost

5 Discussion

The actual design, the one at the middle of the 5 alternative designs, has a reliability index of 3.98 which is slightly over the optimal of 3.84, according to Figures 1 and 7. Also, it is noted that the unconditional curve resulted between the conditionals for 0.15g and 0.3g showing that the optimal seismic design coefficients is somewhere between these intensities. The influence of the above mentioned intensities is explained by the incremental occurrence probabilities that appear in the annual cumulative probability curve shown in Figure 6.

The high value of the optimal reliability index is due to the very high failure consequences for the bridge, located on a heavily populated area with an almost permanent strong traffic. It is observed that the optimal reliability index, as indicated by the minimum of the expected life-cycle curve in Figure 7, is very close to the one derived from Figure 1.

6 Conclusions

Some risk and reliability calculations have been performed for a typical reinforced concrete vehicles' bridge in Mexico City. Because of the heavy traffic and the large human lives at risk, the cost of consequences is very large (800 that of the initial cost). The bridge may be classified as one with very important failure consequences. The optimal reliability index is, therefore, 3.84. It was found that the bridge has a reliability index slightly over (3.98) the optimal one.

The analyses were simplified by considering only the most critical member (a pier). Further studies should be performed to measure the actual redundancy and all the other potential failure modes (see the following section). Also, additional research should be undertaken to generalize the results and update the current Mexican bridge design code. The risk-based formulation may be used to study other infrastructure works and other hazards in Mexico.

7 Further research

Bayesian Belief Nets (BBNs) can be used to carry out both risk and reliability analysis in bridges such as the one under study. Basically, BBNs are directed acyclic graphs whose nodes represent random variables and whose arcs depict probabilistic relationships amongst them. In fact, they have been applied in a large scale model for air transport safety [1]. Here, nodes represent continuous and/or discrete random variables and arcs represent rank and conditional rank correlations between parents and children.

To build the net, failure bridge modes should be identified and then arranged in a logical way within the BBN. In an effort to build such a net, the authors propose to divide the variables in three groups: causes, failure modes and consequences.

In terms of the causes, the next variables could be included: poor design, poor construction materials, lack of maintenance, seismic activity, wind activity, and rainfall rate. Then, the following failure modes may be considered: rupture during construction, failure during operation, pier break, cap break, footing failure, pile break, slab failure. Finally, the resulting consequences could be: life loss, economic loss and environmental impact.

Again, further research is needed to determine which of the previous factors are more significant for bridges. Using statistical data from documented bridge ruptures, the probability of failure for each mode could be quantified. Then, the correlation between variables should be estimated, and finally the results of the quantitative model (BBN) should be compared with real events, in order to calibrate the model. It is important to mention that the authors are currently working in such a model.

8 Acknowledgments

The authors thank the participation of Dr. Jesus Valdes-Gonzalez for his advise, as well as that of both Elizabeth Camacho-Zepeda and Leticia García-Cuarenta. Thanks also go to the Science and Technology Mexican Council (CONACYT) for the financial support given to carry out this research, and to the Autonomous University of the State of Mexico.

9 References and Bibliography

- [1] Ale, B.J.M.; Bellamy, L.J.; Boom, R. van der; Cooper, J.; Cooke, R.M.; Goossens, L.H.J.; Hale, A.R.; Kurowicka, D.; Morales, O.; Roelen, A.L.C.; Spouge, J.; Further developments of a causal model for air transport safety (CATS); building the mathematical heart, In: Proceedings of ESREL, Stavanger, Norway, 25-27 June, 2007, 1431-1439
- [2] Ang, A.; De Leon, D.: Modeling and Analysis of Uncertainties for Risk-Informed Decisions in Infrastructures Engineering. *Journal of Structure and Infrastructure Engineering*, 1(2005), 19-31
- [3] Ang, A.; Tang, W.; *Probability concepts in engineering*. John Wiley, US, 2007
- [4] Agarwal, J.; Protecting existing structures against unforeseen events, In: Procs. of Applications of Statistics and Probability in Civil Engineering, Der Kiureghian, Madana & Pestana (eds), Millpres, Netherlands, 2003, 775-780.
- [5] AASHTO; Standard Specifications for Highway Bridges, American Association of State Highway and Transportation Officials, US, 2002
- [6] BS 8800; Guide to Occupational Health and Safety Management Systems, British Standard Institutions (BSI), UK, 1996
- [7] Canto-Contreras, J.T.; Alamilla-López, J.L.; Análisis de Confiabilidad de Estructuras de Varios Grados de Libertad, Memorias del XII Congreso Nacional de Ingeniería Estructural, León, Guanajuato, Mexico, 2000
- [8] DDF; Estudios sobre sismicidad en el valle de México, Secretaría General de Obras, Departamento del Distrito Federal, México, 1988
- [9] De León, D.; Ang, A.; Manjarez, L.; Confiabilidad estructural y medidas de riesgo del puente Tampico bajo cargas de viento. *Revista Ingeniando*, Colegio de Ingenieros Civiles del Estado de México, 9(2007), 21-26
- [10] Esteva, L.; Ruiz, S.; Seismic failure rates of multistory frames. *Journal of Structural Engineering*, ASCE, 115(1989), 268-284
- [11] Frangopol, D.M.; Kong, J.S.; Gharaibeh, E.S.; Reliability-based life-cycle management of highway bridges. *Journal of Computing in Civil Engineering*, ASCE, 15(2001), 27-34
- [12] Meli, R.; *Diseño estructural*. Limusa, México, 1994
- [13] RAM Advanse; *Structural Analysis Software*. 8th Version, Bentley Systems, US, 2006

- [14] RCDF; *Reglamento de Construcciones para el Distrito Federal*. Trillas, México, 2004
- [15] Renn, O.; The Role of Risk Perception for Risk Management. *Reliability Engineering & System Safety*, 59(1998), 49-62
- [16] Rosenblueth, E.; Esteva, L.; “Reliability basis for some Mexican codes”. In: Probabilistic design of Reinforced Concrete Building, *ACI Public. SP-31*, ACI, Detroit, Mich., 1972, 1-42
- [17] Rosenblueth E.; Optimum reliabilities and optimum design. *Structural Safety*, 3(1986), 69-83
- [18] Stahl, B.; Reliability Engineering and Risk Analysis. In: Planning and design of fixed offshore platforms, McClelland., B. and Reifel., M. (Eds), VNR, New York, 1986

Evaluating the Characteristics of Marine Pipelines Inspection Data Using Probabilistic Approach

Z. Mustafa^{1,2}, G. Shams¹, P.H.A.J.M van Gelder¹

¹ Section of Hydraulic Engineering, Faculty of Civil Engineering and Geosciences, Delft University of Technology, Delft, The Netherlands

² Civil Engineering Department, Universiti Teknologi PETRONAS, Perak, Malaysia

Abstract: This paper presents a probabilistic approach on analyzing internal corrosion defects formed in a Malaysian gas pipeline using an *intelligent pigging* (IP) device. The significant parameters of IP data and their characteristics in the pipeline are analysed through correlation and multivariate regression methods. Some insensitive parameters like the defect circumferential width which is normally ignored in the current design codes is given high priority in this analysis. These governing parameters are later evaluated to produce a new dimensionless limit state function that can best describe the characteristics of the defects. Results from the probabilistic analysis are compared to the results from the existing pipeline failure assessment codes.

1 Introduction

Marine pipelines, a complex system comprises a total length of thousands of kilometers, have been the most practical and low price means of transporting hydrocarbon in the offshore oil and gas industry. As the structure operates with time, it is exposed to many types of defects. The typical form of defect is the corrosions, as shown in Fig. 1, which may occur in the form of individual pits, colonies of pits, general wall-thickness reduction, or in combinations. Inspection for corrosions in pipelines is normally conducted using an *Intelligent Pigging* (IP) (Fig. 2), a probe that records any internal and external defects that developed along the pipelines. It is able to report the size of the defects with respect to its orientation and location.

2 Case study

A 128 km steel pipeline type API 5LX-65 located at the east coast of Malaysia (Fig. 3) was selected for the analysis. The pipeline transports gas from offshore to onshore. 554 internal corrosion defects of various types were reported by the IP. The IP summarized comprehensive data on the corrosion defect parameters, represented by the pipeline defect depth (d), longitudinal length (l) and circumferential width (w) as well as the defects orientation and location. Descriptive statistics of the IP data for this pipeline is as shown in

Table 1. The wall loss was calculated up to 30% from the actual wall thickness. Fu and Kirkwood (1995) numerically classified defects in this pipeline as shallow ($d/t < 0.30$), short ($l/D < 0.20$) and broad ($w/t > 0.50$) type of corrosions.

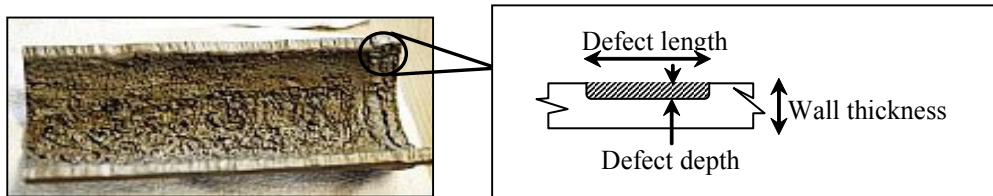


Fig. 1: Internal corrosions in pipelines

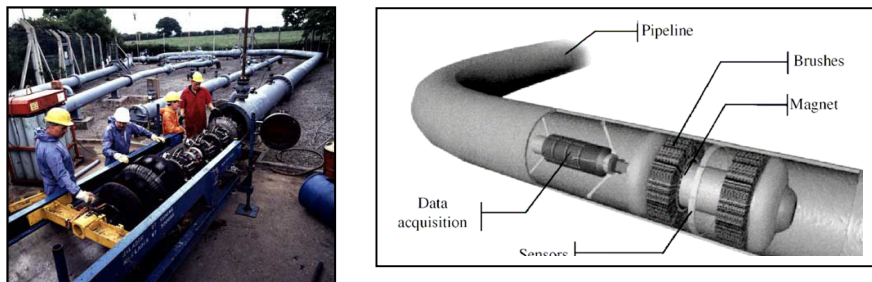


Fig. 2: Inline inspection using an *intelligent pigging* (IP) tool to detect the external and internal metal losses in pipeline cross sections [Photo courtesy of TRANSCO]

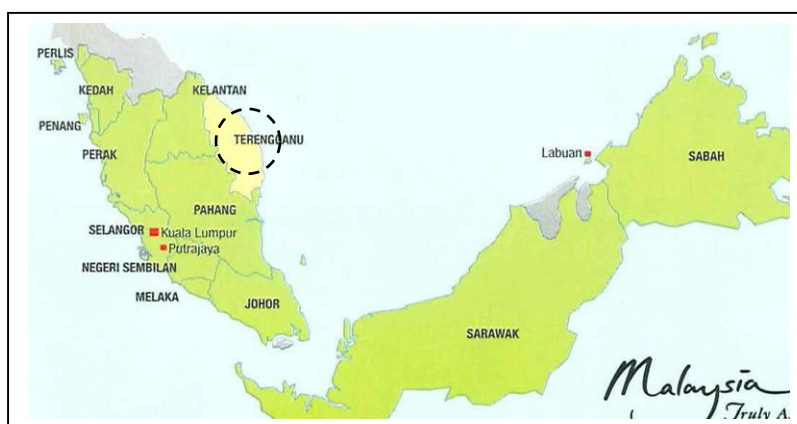


Fig. 3: Location of the pipeline selected in the study

Tab. 1 Descriptive statistics of the IP data for pipeline API 5LX-65

Symbol	Variable Description	Unit	Distribution deviation	Mean value	Standard variation
d	Defect depth	mm	Weibull	1.90	1.19
l	Defect longitudinal length	mm	Exponential	32.64	23.52
w	Defect circumferential width	mm	Gamma	36.76	33.17

 Tab. 2: *Failure pressure* (PF) models used to compute remaining strength of pipeline subjected to corrosion

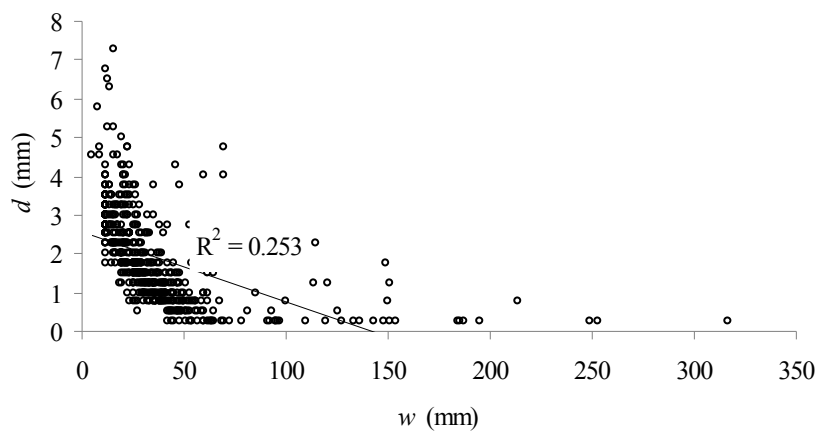
Failure pressure models	Failure pressure expression, PF	Bulging factor, M
Modified ASME B31G	$PF = 1.11 \frac{2(SMYS + *69)t}{D} \left[\frac{1 - 0.85(d/t)}{1 - 0.85(d/t)/M} \right]$	$M = \sqrt{1 + 0.63 \left(\frac{l}{D}\right)^2 \left(\frac{D}{t}\right) - 0.0034 \left(\frac{l}{D}\right)^4 \left(\frac{D}{t}\right)^2}$ <p style="text-align: center;">for $\sqrt{\left(\frac{l}{D}\right)^2 \left(\frac{D}{t}\right)} \leq 50$</p> $M = 3.3 + 0.032 \left(\frac{l}{D}\right)^2 \left(\frac{D}{t}\right)$ <p style="text-align: center;">for $\sqrt{\left(\frac{l}{D}\right)^2 \left(\frac{D}{t}\right)} > 50$</p>
DNV RP F101	$PF = \frac{2SMTS t}{D - t} \left[\frac{1 - (d/t)}{1 - (d/t)/M} \right]$	$M = \sqrt{1 + 0.31 \left(\frac{l}{\sqrt{Dt}}\right)^2}$
SHELL-92	$PF = \frac{1.8SMTS t}{D} \left[\frac{1 - (d/t)}{1 - (d/t)/M} \right]$	$M = \sqrt{1 + 0.805 \left(\frac{l}{D}\right)^2 \left(\frac{D}{t}\right)}$
RSTRENG	$PF = \frac{2SMTS t}{D} [1 - (d/t)/M]$	$M = \sqrt{1 + 0.63 \left(\frac{l}{D}\right)^2 \left(\frac{D}{t}\right) - 0.0034 \left(\frac{l}{D}\right)^4 \left(\frac{D}{t}\right)^2}$

3 Regression analysis of corrosion defects

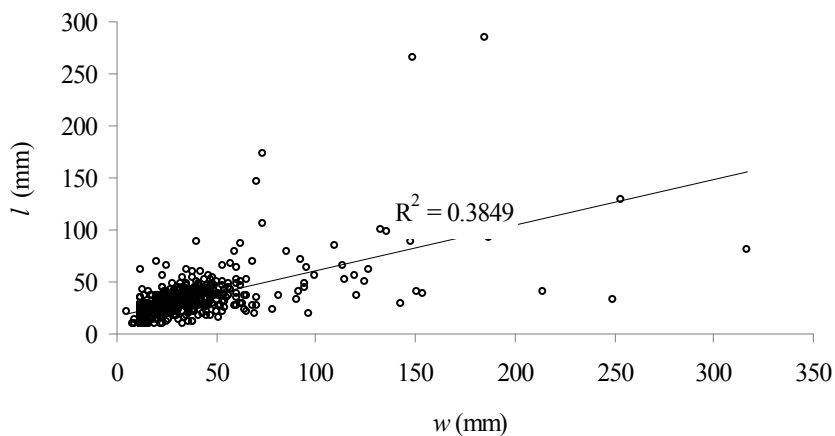
Several regression analysis techniques were carried out on the pipeline IP data. The aim of the analysis was to examine the relative importance of the parameter defect circumferential width, w . This is due to the fact that the existing design codes/equations of *failure pressure* (PF) models (Table 2), which are used to compute the remaining strength of pipeline subjected to corrossions, have omitted the w term while only the defect depth, d and longitudinal length, l terms are used as the governing parameters.

3.1 Bivariate regression

Preliminary work on the regression analysis involved bivariate computation between two parameters. Even though poor negative correlation was noticed between d and w (Fig. 4a), but l and w seemed to have high correlation between each other, as shown in Fig. 4b. Regardless of poor correlation between w and d (25%), good correlation between w and l (39%) is expected to provide good relationship between w and d indirectly. This will be further analyzed using the multivariate function.



(a) Defect depth d vs. defect circumferential width, w



(b) Defect longitudinal length, d vs. defect circumferential width, w

Fig. 4: Bivariate regressions for pipeline API 5LX-65

3.2 Multivariate regression

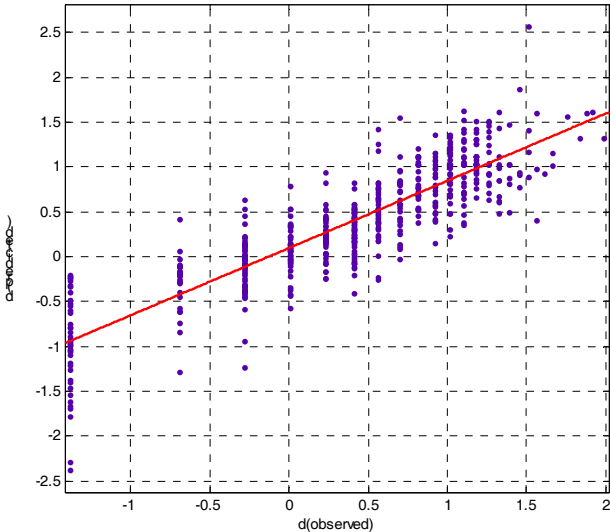
The results from Section 3.1 have supported the idea to further expand the analysis using the multivariate function. The aim of the analysis was to examine the relative importance of the predictor variable w with respect to d . In addition, since the PF models as proposed by the Modified ASME B31G, DnV or SHELL 92 codes (Table 2) have incorporated the d and l terms, so it is wise to examine the degree of correlation between d and w with the inclusive of l into the multivariate analysis. Many trials were made in choosing the best regression model to determine the best equation describing the dependency of d , l and w terms. The parameter d was chosen as the criterion variable while l and w were the predictor variables. It was found that the nonlinear model as given by equation (1) produced the best results.

$$d = 3.3139 l^{0.4393} w^{-1.3071} \quad (1)$$

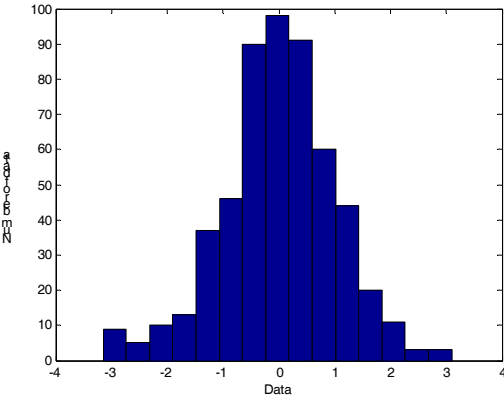
The best fit between $d_{predicted}$ and $d_{observed}$ which results in R^2 value of 75% as shown by Fig. 5a revealed that most of the data were correlated between each other, and this value is statistically very good and acceptable. A histogram and residuals for the data were also plotted for better understanding on the results.

The multivariate regressions carried out for pipeline API 5LX-65 above have resulted with promising founding. In order to support this hypothesis, another multivariate regression analysis was also conducted for another type of corrosion scenario. Similar pipeline with 307 external corrosion defects were analyzed and the results were later compared with the internal defects obtained earlier. Fig. 6a-c below present the best regression results using a nonlinear model as well, as shown in equation (2), with R^2 between the $d_{predicted}$ and $d_{observed}$ of nearly 79%, which is also statistically very good and acceptable. This outcome has affirmed results established in the previous internal corrosion scenario. These two founding from multivariate regression analysis has acknowledged the fact that w is highly dependent upon d and l .

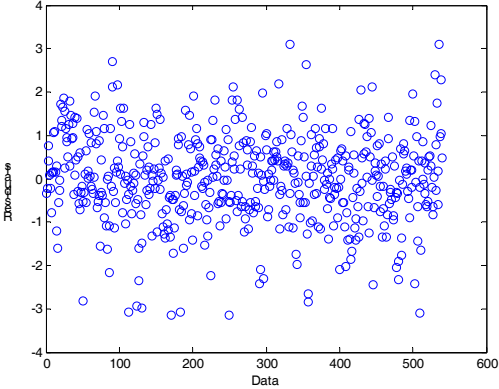
$$d = 1.9156 l^{0.5667} w^{-0.8118} \quad (2)$$



(a)

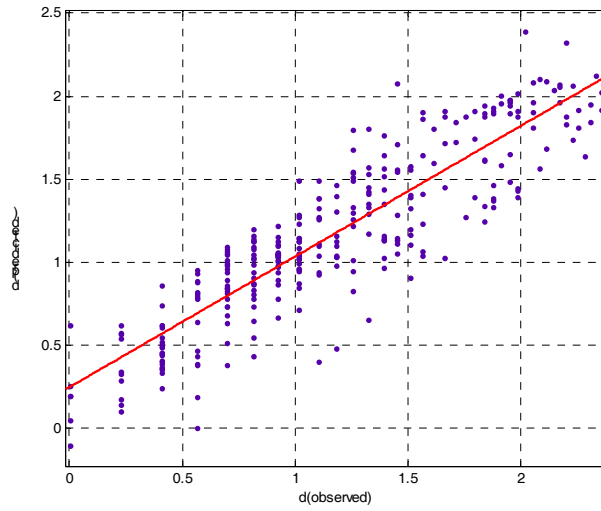


(b)

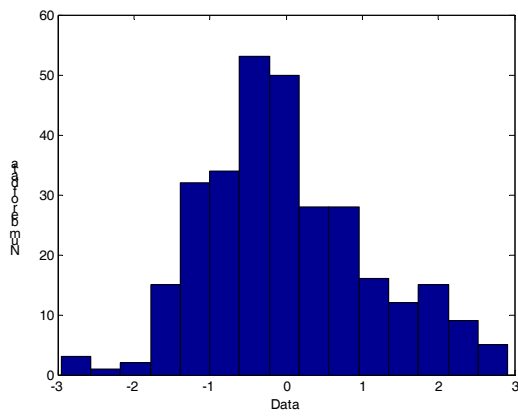


(c)

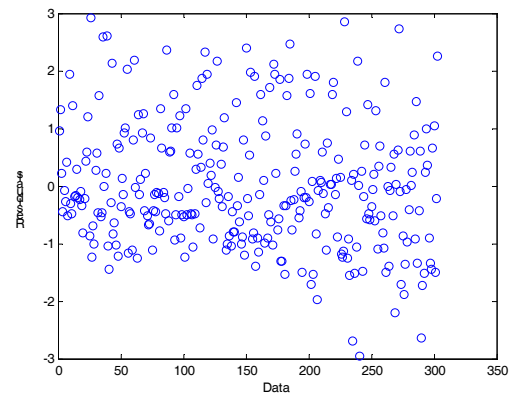
Fig. 5: Results obtained from multivariate regression analysis for pipeline API 5LX-65 containing internal defects (a) Comparison between predicted and observed data (b) Histogram of the standardised residual (c) Residuals



(a)



(b)



(c)

Fig. 6: Results obtained from multivariate regression analysis for pipeline API 5LX-65 containing external defects (a) Comparison between predicted and observed data (b) Histogram of the standardised residual (c) Residuals

4 Limit state function formulation

Results from Section 3 earlier have recognized the importance of defect circumferential width, w as one of the governing parameters representing the characteristics of corrosions in marine pipelines. Since the PF models have ignored this term when determining the remaining strength of pipelines subjected to corrosions, there is a necessity to formulate another equation which takes into account the w term. One of the well known methods in the field of Hydraulics Engineering called the Buckingham- π Theorem was applied to develop the corresponding equation for the above-mentioned problem. A brief discussion on this method is presented in the next section.

4.1 Dimensionless parameters selection

The Buckingham- π Theorem is a method that forms dimensionless parameters from several possible governing parameters for a certain scenario under investigation. It is one approach applied to select the most significant parameters describing the characteristics of the scenario while omitting the less ones. Interested readers are recommended to refer to book chapter on *Dimensional Analysis* from any *Hydraulics* or *Fluid Mechanics* books for further discussion about this method.

For this case study in particular, seven parameters that are assumed to significantly contribute to the remaining strength of pipelines subjected to corrosions were selected, namely burst pressure (P_b), specified minimum tensile strength ($SMTS$), pipeline wall thickness (t), diameter (D), defect depth (d), defect longitudinal length (l) and defect circumferential width (w). It is important to highlight that the IP device is unable to compute P_b for any pipelines, thus this can best be determined through experimental or numerical studies. Therefore, the P_b database for this study utilized DnV Technical Report (1995). This report is a compilation of laboratory tests of corroded pipelines from four institutions, namely American Gas Association (AGA), NOVA, British Gas and University of Waterloo. These participants have conducted many experimental tests for longitudinally corroded pipes under internal pressure for different corrosion defect depths, longitudinally lengths and circumferential widths. Out of the 151 burst pressure database reported, only 31 of them was utilized in this work after considering the suitability of the current and reported work.

From the Buckingham- π Theorem, four dimensionless parameters were identified, namely $P_b/SMTS$, t/D , d/t and l/w . The selection of these terms was also technically supported by literatures. For instance, Fu and Kirkwood (1995) in their work denoted the dimensionless term d/t represents the corrosion shape (parabolic, rectangular) in particular, while l/D symbolizes the length of the corrosion model (pitting, grooving or uniform).

The dependency between the four dimensionless parameters was later formulated using the multivariate regression analysis once again and the nonlinear model was chosen to best describe the parameters, as given in equation (3). This equation is also known as the equation describing the remaining strength (R) of the corroded pipeline.

$$\frac{P_b}{SMTS} = \left(\frac{t}{D}\right)^{0.8442} \left(\frac{d}{t}\right)^{-0.0545} \left(\frac{l}{w}\right)^{-0.0104} \quad (3)$$

Fig. 7a-c presents statistical description of the multivariate regression analysis that formed this equation. The R^2 value between the $(P_b/SMTS)_{\text{predicted}}$ and $(P_b/SMTS)_{\text{observed}}$ was found to give good correlation with a value of 53%, as shown in Fig. 7a. A histogram and residuals for the data were also plotted for better understanding on the results.

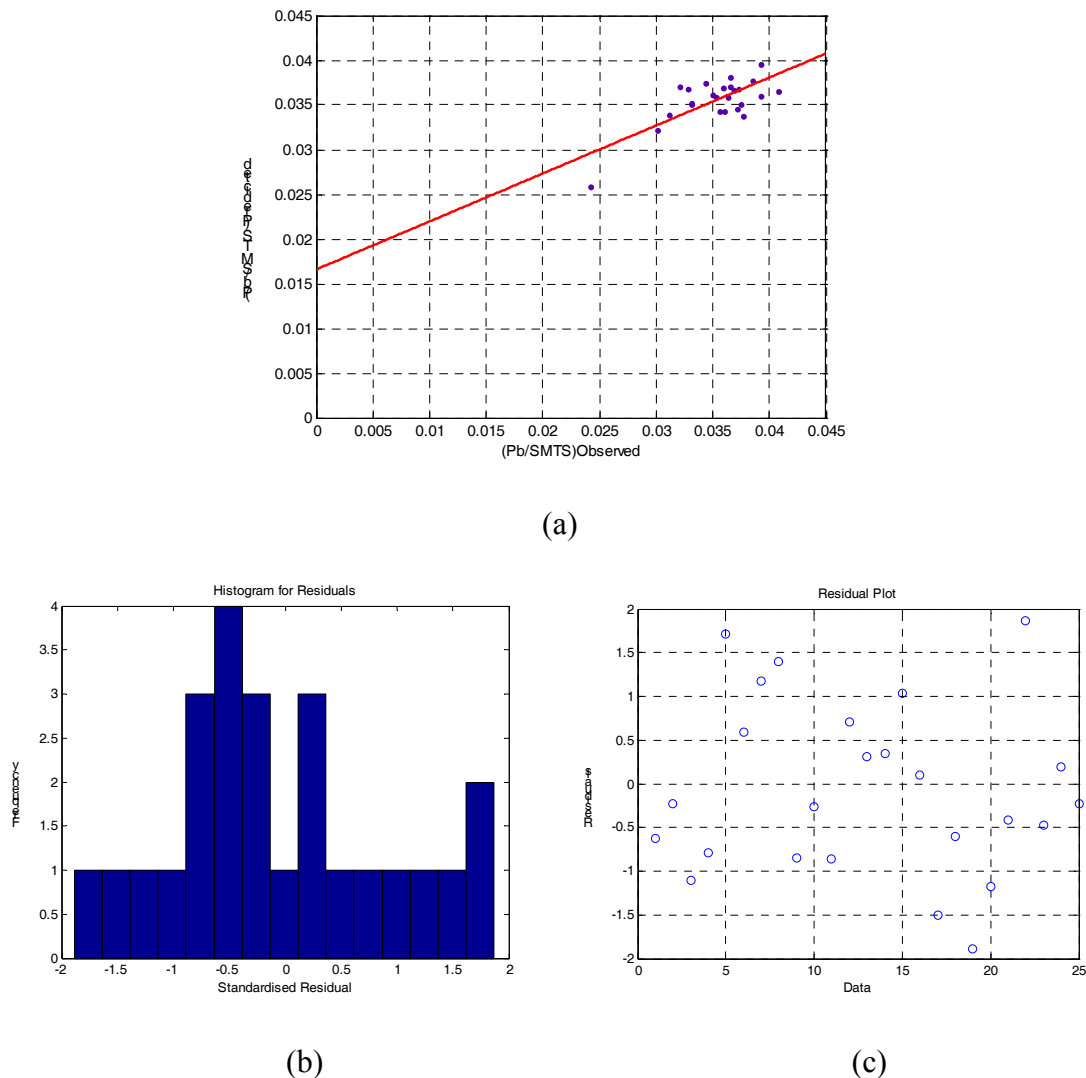


Fig. 7: Results obtained from multivariate regression analysis for the dimensionless limit state function equation (a) Comparison between predicted and observed data (b) Histogram of the standardised residual (c) Residuals

4.2 Reliability computation

This section presents the computation of probability of failure (P_f) for pipeline API 5LX-65. Besides results from this study, the failure pressure (PF) models in Table 1 and another recent study by Teixeira *et. al.* (2008) were included for comparisons. It is important to highlight here, however, that the PF models are completely deterministic, in which the equations are mostly represented by safety factors. Moreover, Teixeira *et. al.* (2008) had chosen partial deterministic equation in their limit state equation. In principle, any theoretical equations represented by safety factors should not be treated in a probabilistic manner (Mustaffa *et. al.*, 2009). Most of the literatures are somewhat contradict to this idea, as seen in Ahammed & Melchers (1994, 95, 96, 97), Ahammed (1998), Pandey (1998), Caleyó *et. al.* (2002), Lee *et. al.* (2003, 06), Santosh *et. al.* (2006), Lee *et. al.* (2006), Khelif *et. al.* (2007) and many more. These include studies on offshore and onshore pipelines transporting either hydrocarbon or water. Thus the approach used in Section 3 is considered to be feasible for this study purpose.

As mentioned earlier, the dimensionless equation (3) above will be used to represent the remaining strength (R) of the corroded pipelines while pipeline operating pressure, P_o will be used as the load (S). Following the strength term, this load was also made dimensionless by dividing it with the $SMTS$. Thus, the limit state function equation, Z can be written as,

$$Z = R - S \quad (4)$$

Inserting equation (3) into (4), the final limit state function equation is given by,

$$Z = \left[\left(\frac{t}{D} \right)^{0.8442} \left(\frac{d}{t} \right)^{-0.0545} \left(\frac{l}{w} \right)^{-0.0104} \right] - \frac{P_o}{SMTS} \quad (5)$$

The limit state is described by $Z = 0$. The probability of failure (P_f) is then given by equation (6). Failures takes place when the failure surface falls in the region of $Z < 0$ while $Z > 0$ is a survival region.

$$P_f = P(Z \leq 0) = P(L \geq S) \quad (6)$$

The P_f in equation (6) was simulated using the analytical approximation methods called First Order Reliability method (FORM) incorporated in the Prob2B software. Apart from data taken from Table 1, other random variables used for P_f computations for equation (5) and PF models in Table 2 are presented in Table 3.

Tab. 3 Random variables for API 5LX-65 pipeline reliability analysis

Variable			Distribution	Mean value	Standard deviation
Symbol	Description	Unit			
D	Diameter	mm	Normal	711.2	21.3
T	Wall thickness	mm	Normal	25.1	1.3
$SMTS$	Specified minimum tensile strength	MPa	Normal	530.9	37.2
$SMYS$	Specified minimum yield stress	MPa	Normal	448.2	31.4
P_o	Operating pressure	MPa	Normal	14 - 30	1.4 - 3.0

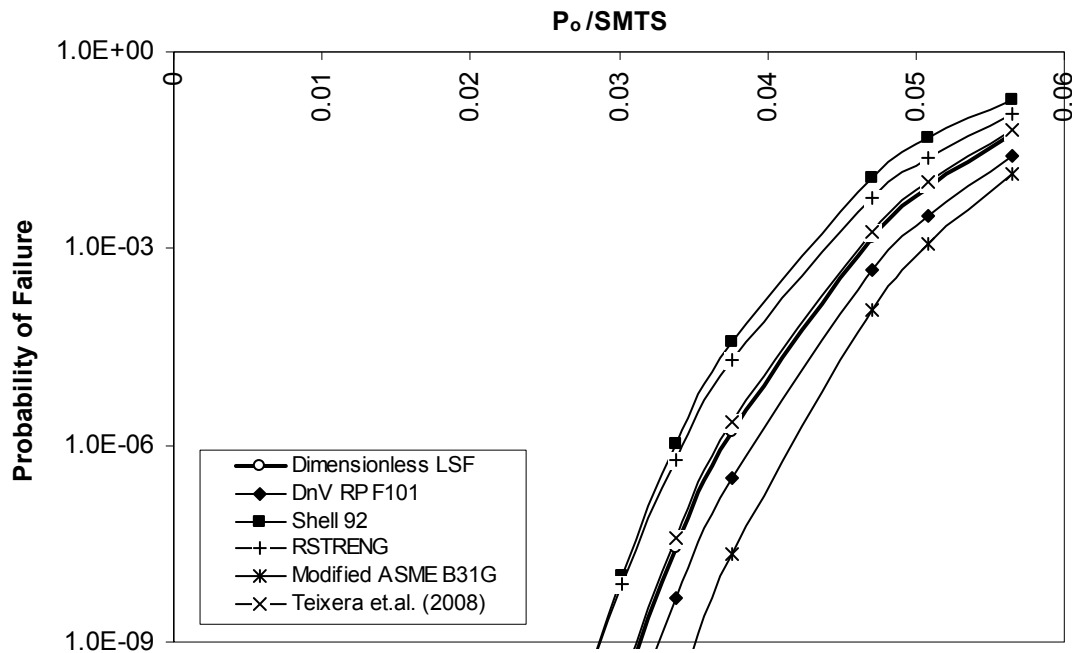


Fig. 7: Probability of failure, P_f for different design codes

Fig. 7 presents the probability of failure computed using equation (5) for different dimensionless load terms. The results were compared with the existing PF models taken from different design codes, namely DnV RP F101, Modified ASME B31G, Shell 92 and RSTRENG. A recent work by Teixeira *et. al.* (2007) was also included in the graph. A common trend seemed to appear from all plots, in which the probability of failure increases as the loads increases. The graph indicates that Shell 92 produced the highest probability of failure with respect to load exerted to the pipeline as compared to others, while the Modified ASME B31G was the lowest. The present work turned out to lie in between the two extremes; lower than the Shell 92, RSTRENG and Teixeira *et. al.* (2007), while higher than the DnV RP F101 and Modified ASME B31G. It seemed that the reliability of cor-

roded pipelines computed from the three lower codes were overestimated while the two higher codes were underestimated when compared to the current work.

This hypothesis may be true because the extra term w included in the present work has made the analysis more comprehensive and complete to represent the whole corrosion area. From the past until the present, there have been many arguments about the parameters represented by those codes, particularly the selection for corrosion shapes and a summary of this discussion can be found in Bjørnøy and Marley (2001). The best solution to overcome all doubts pertaining to corrosion shapes is to include its actual size when analysing it, thus by adding the w term, one is looking at a severe scenario of corrosion sizes.

5 Conclusions

This study evaluates the significance of the circumferential width term, w of corrosion defects in marine pipelines using the regression analysis. The dimensionless limit state function developed using this term has showed favourable results. The analysis has showed that the probability of failure of the present work was lower than the Shell 92, RSTRENG and Teixeira *et. al.* (2007), while higher than the DnV RP F101 and Modified ASME B31G. This indicates that the this study approach is able to provide better judgement on the reliability of corroded pipeline because it has incorporated all the important parameters (d , l , w) governing the characteristics and development of corrosions. It is proven that the w term should not be given less consideration when assessing the reliability of corroded pipelines.

The study is still in a preliminary stage, thus require more improvements. It may be interesting to see the discrepancies when separately analysing the IP data according to different types of corrosions rather than summarizing all IP data as a whole. It may be wise then to consider forming one model that can suit all corrosions scenario in different pipelines.

6 Acknowledgement

The authors would like to thank Petroliam Nasional Berhad (PETRONAS), Malaysia and Taye B. Chanyalew for providing data for this project, which was financed by Universiti Teknologi PETRONAS, Malaysia. Also, special thanks to AliReza Amiri-Simkooei for his preliminary technical support.

References

- [1] Ahammed, M. and Melchers, R. E.: Reliability of Underground Pipelines Subjected to Corrosion. *Journal of Transportation Engineering*, (1994), Vol. 120, No. 6, pp 989-1002.
- [2] Ahammed, M. and Melchers, R. E.: Probabilistic Analysis of Pipelines Subjected to Pitting Corrosion Leaks. *Engineering Structures*, (1995), Vol. 17, No. 2, pp 74-80.
- [3] Ahammed, M. and Melchers, R. E.: Reliability Estimation of Pressurised Pipelines Subject to Localised Corrosion Defects. *International Journal of Pressure Vessels and Piping*, (1996), Vol. 69, pp 267-272.
- [4] Ahammed, M. and Melchers, R. E.: Probabilistic Analysis of Underground Pipelines Subjected to Combined Stresses and Corrosion. *Engineering Structures*, (1996), Vol. 19, No. 12, pp 988-994.
- [5] Ahammed, M.: Probabilistic Estimation of Remaining Life of a Pipeline in the Presence of Active Corrosion Defects, *International Journal of Pressure Vessels and Piping*, (1998), Vol. 75, pp 321-329.
- [6] Bjørnøy, O. H. and Marley, M. J.: Assessment of Corroded PipelinesL Past, Present and Future, *The 11th International Offshore and Polar Engineering Conference (ISOPE)*, (2001), Vol. 2, pp. 93-101.
- [7] Caleyó, F., Gonzalez, J. L. and Hallen, J. M.: A Study on the Reliability Assessment Methodology for Pipelines with Active Corrosion Defects, *International Journal of Pressure Vessels and Piping*, (2002), Vol. 79, pp. 77-86.
- [8] Det Norske Veritas: Reliability-Based Residual Strength Criteria for Corroded Pipes. *Technical Report*, (1995).
- [9] Fu, B. and Kirkwood, M. K.: Predicting Failure Pressure of Internally Corroded Linepipe Using the Finite Element Method, *The 14th International Conference on Offshore Mechanics and Arctic Engineering (OMAE)* (1995), Vol. 5, pp 175-184.
- [10] Khelif, R., Chateauneuf, A., and Chaoui, K.: Reliability-Based Assessment of Polyethylene Pipe Creep Lifetime, *International Journal of Pressure Vessels and Piping* (2007), Vol. 84, pp 697-707.
- [11] Lee, O. S., Pyun, J. S., and Kim, D. H.: Effect of Boundary Conditions of Failure Pressure Models on Reliability Estimation of Buried Pipelines, *International Journal of the Korean Society of Precision Engineering*, (2003), Vol. 4, No. 6.
- [12] Lee, O. S., Kim, D. H. and Choi, S. S.: Reliability of Buried Pipeline Using a Theory of Probability of Failure, *Solid State Phenomena*, (2006), Vol. 110, pp 221-230.
- [13] Lee, S. M., Chang, Y. S., Choi, J. B., and Kim, Y. J.: Probabilistic Integrity Assessment of Corroded Gas Pipelines, *Journal of Pressure Vessel Technology*, (2006), Vol, 128, pp 547-555.

- [14] Mustaffa, Z., Shams, G., Van Gelder, P.H.A.J.M. and Vrijling, J. K.: Risk Assessment of Aging Marine Pipelines: A Probabilistic Approach, *International Conference on Environment*, Malaysia, (2008), pp 167.
- [15] Mustaffa, Z., Van Gelder, P.H.A.J.M. and Vrijling, J. K.: A Discussion of Deterministic vs. Probabilistic Method in Assessing Marine Pipeline Corrosions, *The 19th International Offshore and Polar Engineering Conference (ISOPE)* (2009), Vol.4, pp 653-658.
- [16] Pandey, M. D.: Probabilistic Models for Condition Assessment of Oil and Gas Pipelines, *NDT&E International*, (1998), Vol. 31, No. 5, pp 349-358.
- [17] Santosh, Vinod, G., Shrivastava, O. P., Saraf, R. K., Ghosh, A. K. and Kushwaha, H. S.: Reliability Analysis of Pipelines Carrying H₂S for Risk Based Inspection of Heavy Water Plants, *Reliability Engineering and System Safety* (2006), Vol. 91, pp 163-170.
- [18] Teixeira, A. P., Soares, C. G., Netto, T. A. and Estefen, S. F.: Reliability of Pipelines With Corrosion Defects, *International Journal of Pressure Vessels and Piping* (2008), Vol. 85, pp 228-237.
- [19] Van Gelder, P.H.A.J.M.: Statistical Methods for the Risk-Based Design of Civil Structures, *Delft University of Technology*, 1999, p. 249.

Eurocode road traffic load models for weight restricted bridges

D. Proske¹, S. Loos²

¹ Institute of Mountain Risk Engineering, University of Natural Resources and Applied Life Sciences, Vienna

² Ingenieurbüro Lopp, Weimar, Germany

Abstract: Road traffic weight restricted historical bridges are common in Germany. However often it is unclear how many road users follow these restrictions and what the road weight distributions looks like. Therefore in the German city of Dresden a weight by motion, for road traffic was installed on a weight restricted bridge. This weighting machine included a software package for identification of single vehicles based on their measured axle loads. This package ran for several months/years, over which time data were collected. The data collected has been used to extend the current road traffic load concept of the Eurocode and the German DIN-reports, to weight restricted bridges. Carrying out Monte Carlo Simulation and estimating internal forces due to road loading have achieved this. The load calibration factor α has then been determined for weight-restricted bridges. Furthermore load calibration factors for other weight restrictions have been estimated based on a mixture of measured and estimated load distributions. Finally a comparison with the unrestricted Eurocode road traffic model and the Auxerre load has been carried out.

1 Introduction

1.1 Current state

Civil engineers have to forecast road traffic for future decades during the planning and design of road bridges. To simplify this task, different traffic load models are included in codes of practice. Load models try to model traffic loads on bridges, on the one hand precisely and on the other hand with a limited amount of work required by engineers. Good models fulfil both requirements at the same time. The last requirement especially, is often questioned when Eurocode 1 traffic load models consider many different load combina-

tions. Independent from this criticism, the intensive scientific work behind the models is appreciated. Here only exemplarily the works by Merzenich & Sedlacek (1995) are mentioned.

The road traffic model of the current German DIN-reports 101 is heavily based on the Eurocode 1 model, especially ENV 1991-3. This road traffic model is valid for bridges with a maximum overall span of 200 m and a maximum width of 42 m. A dynamic load factor is already considered in the characteristic loads if necessary. In contrast to the ENV 1991-3 the German DIN-report 101 considers only three road traffic load models: load model 1 for twin axle and uniformly distributed loads; load model 2 for single axle with short structural elements and load model 4 to describe the human scum. A further load model found in the ENV 1991-3 considering special Lorries has not been considered in the German DIN-report 101.

Tab. 1: gives characteristic traffic load values for load model 1 and Table 2 shows the distribution of the loads on a roadway according to the current DIN-report 101 and the historical DIN 1072

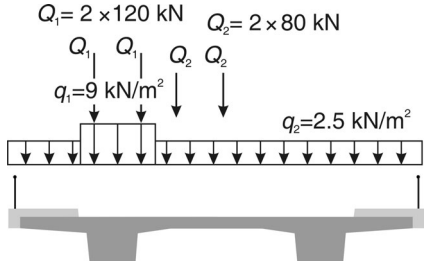
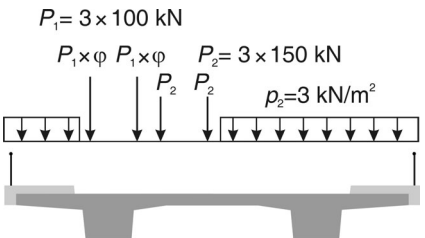
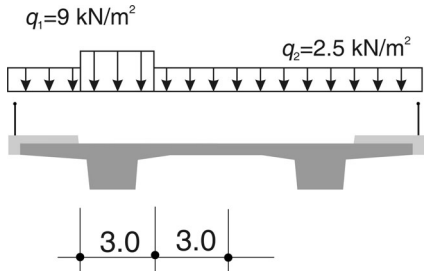
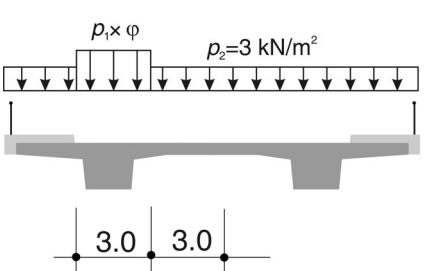
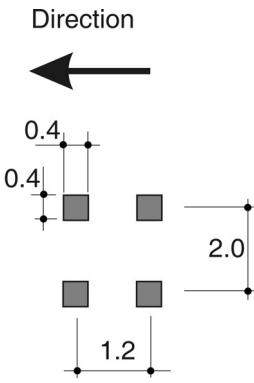
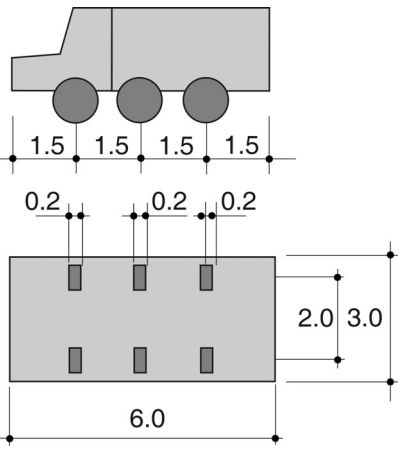
Load position	Twin axle			Uniform distributed load	
	Axle load Q_{ik} in kN	Reduction factor α_{Qk}	$Q_{ik} \times \alpha_{Qk}$	q_{ik} in kN/m ²	Reduction factor α_{qk}
Lane 1	300	0.8	240	9.0	1.0
Lane 2	200	0.8	160	2.5	1.0
Lane 3	100	0.0	0	2.5	1.0
Further lanes	0	-	0	2.5	1.0
Remaining areas	0	-	0	2.5	1.0

1.2 Former road traffic load models (DIN 1072)

The road traffic model of the historical DIN 1072 includes two bridge standard classes: the bridge class 60/30, which is used for new motorways, highways, city roads (most roads) and the bridge class 30/30, which is used for secondary roads. The bridge class 60/30 includes, just like the load model 1 a main, a secondary lane and remaining areas. The main lane is exposed to a uniform load of 5 kN/m² (p_1) and six single loads of the SLW 60 (Heavy Load Vehicle). Furthermore in the DIN 1072 the loads are dependent on the span and the coverage, which are increased by a dynamic load factor. The secondary lane is exposed to a uniform distributed load of 3 kN/m² and single loads of the SLW 30. No dynamic load factor is applied to the secondary lane or to the remaining areas. The remaining areas are though, also exposed to a uniform distributed load of 3 kN/m². In contrast to the Eurocode or DIN-report 101 load model, the uniform distributed loads do not continue in the area of the SLW. Table 2 permits the comparison of the different load patterns according to the DIN-report 101 and the DIN 1072.

Beside the two standard bridge classes the DIN 1072 has introduced further bridge classes (BK 16/16, BK 12/12, BK 9/9, BK 6/6, BK 3/3) for checking or re-calibration. Additionally historical load models for standard 20 tonne and 8 tonne Lorries can be found in literature (Leliasky 1982).

Tab. 2: Characteristic loads for load model 1 according to the DIN-report 101 and DIN 1072 (60/30)

DIN-report 101	DIN 1072
<p>Characteristic loads for load model 1 in the area of the twin axle</p>  <p>$Q_1 = 2 \times 120 \text{ kN}$ $Q_2 = 2 \times 80 \text{ kN}$</p> <p>$q_1 = 9 \text{ kN/m}^2$ $q_2 = 2.5 \text{ kN/m}^2$</p>	<p>Characteristic loads for load model 1 in the area of the SLW (Heavy Load Vehicle)</p>  <p>$P_1 = 3 \times 100 \text{ kN}$</p> <p>$P_2 = 3 \times 150 \text{ kN}$</p> <p>$p_2 = 3 \text{ kN/m}^2$</p>
<p>Characteristic loads for load model 1 outside the area of the twin axle</p>  <p>$q_1 = 9 \text{ kN/m}^2$ $q_2 = 2.5 \text{ kN/m}^2$</p> <p>3.0 3.0</p>	<p>Characteristic loads for load model 1 outside the area of the SLW (Heavy Load Vehicle)</p>  <p>$p_1 \times \phi$ $p_2 = 3 \text{ kN/m}^2$</p> <p>3.0 3.0</p>
<p>Geometry of twin axle</p>  <p>Direction</p> <p>0.4 0.4 2.0</p> <p>1.2</p>	<p>Geometry of SLW (Heavy Load Vehicle)</p>  <p>1.5 1.5 1.5 1.5</p> <p>0.2 0.2 0.2</p> <p>6.0</p> <p>2.0 3.0</p>

The DIN 1072 has offered a wide range of different characteristic road traffic loads and therefore permitted a fine gradation for the usage of historical bridges. This gradation cannot be found either in the Eurocode or in the German DIN-report 101. If the codes of practice no longer offer special load patterns for weight restricted historical bridges, it would be helpful to develop different characteristic road traffic loads for them. This is because historical bridges still contribute heavily to the bridge stock in industrialized countries (Proske & van Gelder 2009).

Tab. 3: Characteristic loads for re-calibration classes of DIN 1072 including the figure of the load vehicle (bottom)

Bridge class		16/16	12/12	9/9	6/6	3/3
Overall load in kN of the lorry		160.00	120.00	90.00	60.00	30.00
Front wheels	Wheel load in kN	30.00	20.00	15.00	10.00	5.00
	Contact width in m	0.26	0.20	0.18	0.14	0.14
Back wheels	Wheel load in kN	50.00	40.00	30.00	20.00	10.00
	Contact width in m	0.40	0.30	0.26	0.20	0.20
Single axle	Wheel load in kN	110.00	110.00	90	60.00	30.00
	Contact width in m	0.40	0.40	0.30	0.26	0.20
Uniform distributed load p_1 in kN/m ²		5.00	4.00	4.00	4.00	3.00
Uniform distributed load p_2 in kN/m ²		3.00	3.00	3.00	2.00	2.00

As a basis for such a development many different theoretical scientific works about road traffic models can be used. Relevant work has been carried out by König & Gerhardt (1985), Spaethe (1977), Schütz (1991), Krämer & Pohl (1984), Pohl (1993), Puche & Gerhardt (1986), Bogath (1997), Bogath & Bergmeister (1999), Ablinger (1996), Crespo-Minguillón & Casas (1997), COST-345 (2004), Allaix et al. (2007), Vrouwenvelder & Waarts (1993) and Prat (2001).

Different road models are used besides the Eurocode load model, in other countries, for example the HA-KEL and HB load model in Great Britain, the HB-17 load model in the US or the load model T 44 and L 44 in Australia. These models will not be considered here.

1.3 Preliminary considerations

The great diversity of load models is partially caused by the high number of influencing parameters on the traffic load prediction models. The development of traffic load models is, of course, strongly related to the essential properties of road traffic. Road traffic is and will be for an indefinite period the most important means of traffic: it offers high speed, high usability by the masses, all usability and omnipresence. On roads, every non-railtied vehicle can always reach, every road developed goal. And the number of road-developed goals is immense compared to all other means of traffic. These advantages of roads cause major drawbacks for the road traffic models, since the numbers of influencing parameters is extremely high. To develop models, which can be used by engineers under practical conditions, requires the number of input parameters to be strongly restricted. Table 4 shows some load influencing factors classified in to four groups.

Tab. 4: Load influencing factors for the estimation of the characteristic road traffic loads according to Schütz (1991)

Traffic intensity	Traffic flow	Vehicle group	Single vehicle
<ul style="list-style-type: none"> • Average daily traffic intensity • Average daily heavy traffic intensity • Maximum hourly traffic intensity 	<ul style="list-style-type: none"> • Vehicle distance • Lane distribution • Velocity 	<ul style="list-style-type: none"> • Frequency of single vehicle types 	<ul style="list-style-type: none"> • Number of axles • Axle loads • Axle distances • Vibration properties

Additionally to traffic parameters, further parameters describing the structural conditions of bridges have to be considered. Such parameters are the statical system or the quality of the roadway. The quality of the roadway can be considered in terms of local, regular and irregular bumpiness. A classification of the quality of the roadway in terms of the road class is given in Table 5.

Tab. 5: Roadway quality based on road classes (Merzenich & Sedlacek 1995)

Road class	Roadway quality
Highway	Excellent
Federal Highway	Good up to very good
State road	Good
Country road	Average

After the identification of significant input parameters, realistic values for these parameters have to be found. These values are usually identified by traffic measurements. However, although many measurement stations on highways exist, the number on country roads, where historical arch bridges usually are, is rather limited. In Germany in 1991, about 300 measurement stations were placed on highways and federal highways, but only 15 measurement stations could be found on country roads. Table 6 shows some state road measurement locations in the German federal state of Saxony.

Tab. 6. Automatic permanent road traffic counting devices in the German federal state of Saxony. Average traffic numbers from the years 1998 to 2003. Only state roads, higher roads are excluded and on communal roads are no devices installed.

Road Nr.	Location	Number of vehicles per 24 hours	Number of heavy vehicles per 24 hours	Ratio of heavy vehicles to overall number of vehicles in %*
242	Hartmannsdorf	9,356	736	7.9
302	Arnoldsgrün	3,322	188	5.7
309	Tiefenbrunn	1,869	52	2.8
100	Prischwitz	2,942	243	8.3
165	Kimitzschtal	1,831	102	5.6
95	Wittichenau	3,920	240	6.1
87	Riesa	3,979	167	4.2
36	Minkwitz	5,064	360	7.1
38	Liebertwolkwitz	17,869	1,136	6.4
24	Sitzenroda	3,426	309	9.0

*The heavy vehicle ratio has decreased in the last years. It is assumed, that the heavy trucks are using more the highways instead of the state roads. However, this depends also very much on the road fees charged.

On the European level the majority of traffic measurements are also carried out on highways. This is especially true with regards to the planning and completion of the development of an international European traffic load model, which focused heavily on high lorry traffic density measurements of long distance traffic. These measurements were used to define classes of Lorries. Merzenich & Sedlacek (1995) have proposed four different lorry classes (Table 7).

Tab. 7: Lorry classes according to Merzenich & Sedlacek (1995)

Class	Description of lorry	Representative lorry	Example
Class 1	Lorry with two axes	Two-axle vehicle	
Class 2	Lorry with more than two axes	Three-axle vehicle	
Class 3	Semi-trailer truck	Two axle truck with three axle semi-trailer	
Class 4	Tractive units	Three-axle vehicle with two axle trailer	

Within the classes a bimodal random distribution of the mass of vehicles is observed as Fig. 1 shows (Geißler 1995, Quan 2004). This distribution consists of a distribution for the weight of the unloaded lorry and a distribution for the loaded lorry. Pohl (1993) considers in his model this distribution of the weight of loaded and unloaded lorries whereas other authors consider the axle loads as randomly distributed variables (Fig. 2). An overview regarding these different models can be found in Geißler (1995).

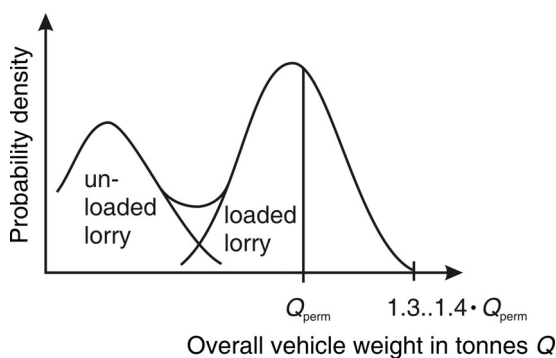


Fig. 1: General bimodal random distribution of the overall vehicle weight (Geißler 1995, Quan 2004)

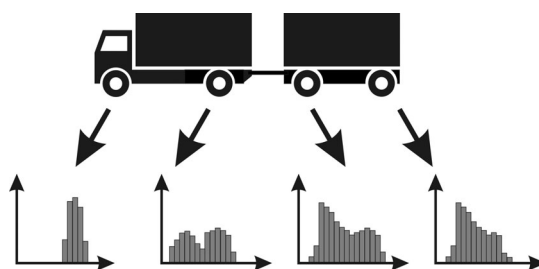


Fig. 2: General bimodal random distribution of the axle load (Geißler 1995)

Based on the limitation of the current Eurocode or DIN-report (i.e. neglecting models for weight restricted bridges), an extension of the Eurocode road traffic model should be introduced. However, the general procedure outlined in the Eurocode for the development of traffic models should continue to be used. The goal of the following presented research is the development of α -factors, which can be applied to the Eurocode traffic model 1 to permit the re-computation of load restricted bridges.

To develop such a model, as suggested earlier, measurement data is required. Traffic measurements were therefore carried out for the Dresden weight restricted (15 tonnes) “Blue wonder” bridge. The axle weight measurement was processed (including identification of vehicle types) through use of software. Such identification is mainly based on axle distances, but also on the correlation between axle loads, as suggested by Cooper (2002). Results of the weight-in-motion measurements of heavy weight vehicles are shown in Fig. 3.

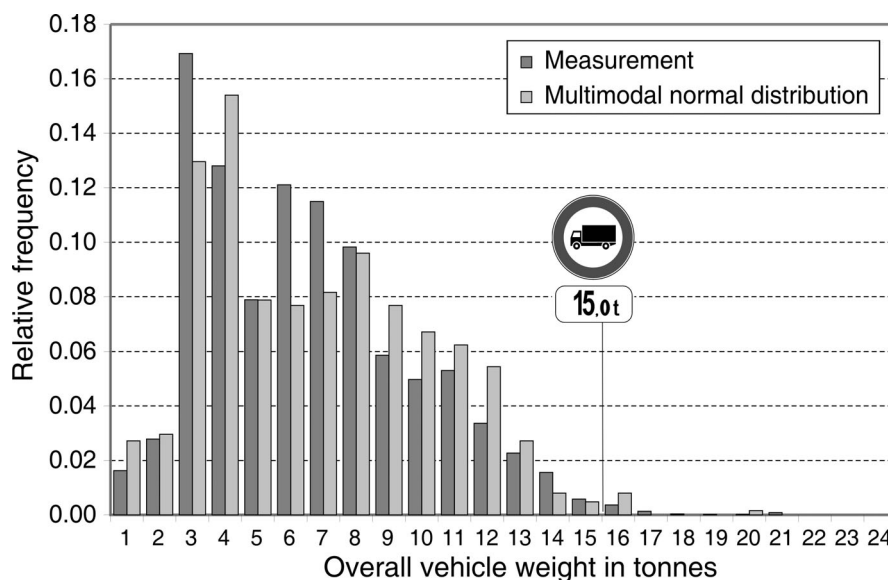


Fig. 3: The relative frequency of the measured overall vehicle weight and adjusted multimodal normal distribution of heavy weight vehicles in October 2001, for the “Blue wonder” bridge, Dresden

2 Development of new load classes

2.1 Methods applied

The factors to be developed should deliver traffic models, which are comparable to the recalibration classes of the DIN 1072. The number inside the class of the DIN 1072 gave the weight restriction for the lane, such as bridge class 30/30, 16/16 and 12/12.

Besides the input data from measurement, a Monte-Carlo-Simulation is required. The input for the simulation is the breakdown of the heavy vehicle measured data into four lorry types (standard lorry or truck, truck with trailer, semi-trailer and busses). Since the meas-

urement data from the “Blue wonder” did not include all relevant information, further data was taken from Merzenich & Sedlacek (1995). The approximation of the axle load distribution was calculated using a bi-modal distribution.

In general, the α -factors were determined by the following steps:

- Simulation of the vehicle type based on the traffic contribution of the “Blue wonder” bridge data.
- Simulation of the overall vehicle weight based on the vehicle weights calculated/measured for the “Blue wonder” bridge data.
- Simulation of the axle load contributions to the overall vehicle weight, based on the work by Merzenich & Sedlacek (1995).
- Computation of the axle loads, based on the overall vehicle weight and the axle load contribution.
- Simulation of the axle distances, based on Merzenich & Sedlacek (1995).
- Computation of the maximum bending moment for a single span beam.

There are some simplifications included in the simulation process. For example, five-axle-vehicles are simplified, so that the fifth axle has the same weight as the fourth axle. Also, the decisive load pattern was identified by iteration. The simulation itself was repeated 5000-times for one length of a single span beam. Of course, the length of the single span beam was varied. The simulation yielded to a frequency distribution for the maximum bending moment of a single-span beam of a certain length. Parallel to the approximation of the frequency data by a normal distribution, a log-normal distribution was also applied. The characteristic traffic load value is assumed as a value with a 1,000-year return period of this distribution (Merzenich & Sedlacek 1995).

Following the computation of the maximum bending moment by the simulation process, the α -factor was computed by the required adaptation of the standard traffic model 1, according to the Eurocode 1 and the DIN-report 101. The standard traffic model 1, including the α -factor, should give comparable results in terms of moments as the simulated computation.

Besides flowing traffic conditions, traffic jam conditions also have to be considered. Traffic jam conditions are mainly relevant for long-span conditions and have to be considered in the computation of the factors.

The described procedure was applied for the bridge class 16/16 (the class of the “Blue wonder”). However for the bridge class 12/12 and 30/30 the procedure had to be changed slightly, since measurements were only based on the bridge class 16/16.

For the bridge class 12/12 the mean value of the measurement data from the “Blue wonder” bridge was multiplied by $12/16=0.75$. The standard deviation and the contribution of

the different vehicle types of the traffic were kept constant. For the adaptation of the bridge class 30/30 this procedure was again extended. Based on measurements from the “Blue wonder” and “Auxerre-traffic” (Fig. 4), a new overall traffic weight distribution was constructed, changing mean values, standard deviation and the contribution of different vehicle types to the traffic from the “Blue wonder” bridge traffic (Fig. 5). Then again the simulation was repeated.

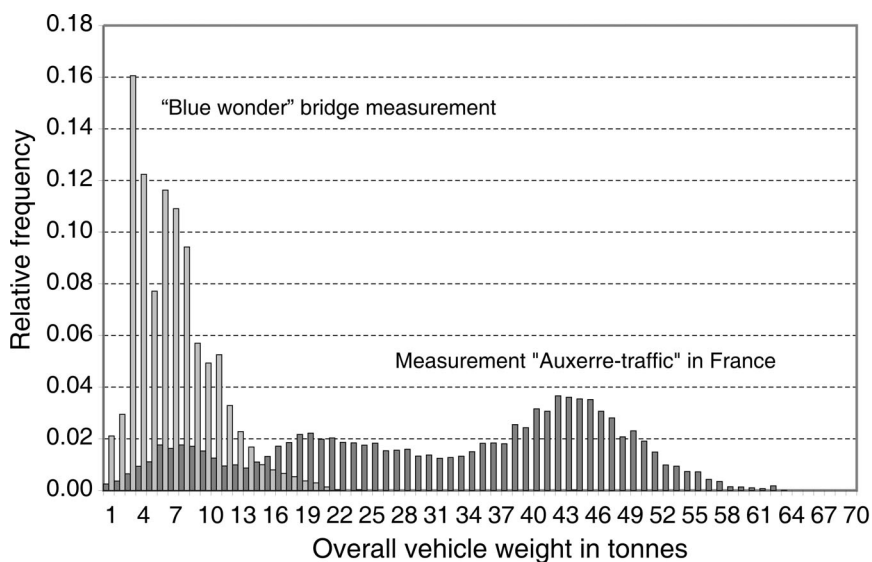


Fig. 4: Comparison of overall vehicle weights measured at the “Blue wonder” bridge in Dresden and at the “Auxerre-traffic” in France. The later was mainly used for the development of the Eurocode traffic model 1

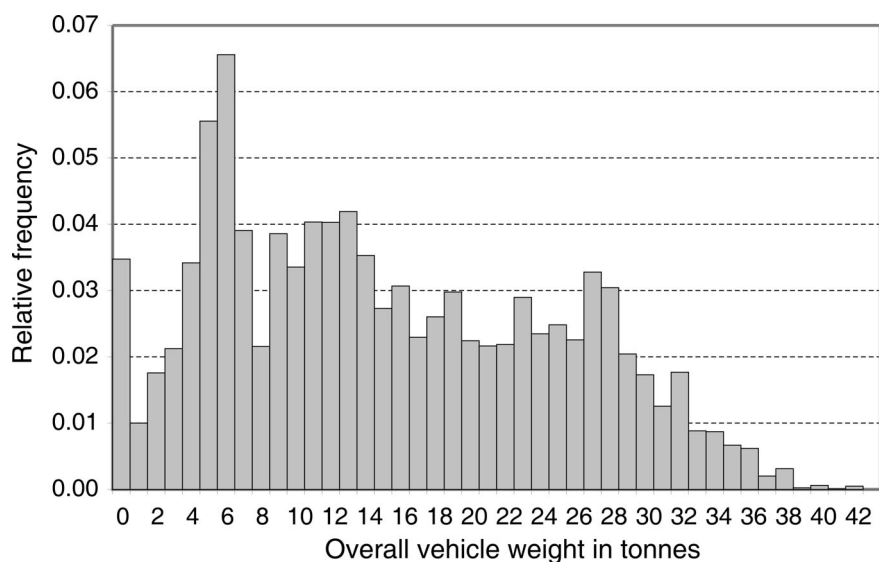


Fig. 5: Development of an synthetically traffic distribution for the bridge class 30/30 based on measurements from the „Blue wonder“ in Dresden and from the „Auxerre-traffic“ in France

To prove the adopted approach, the α -factor of 1.0 for unified traffic loads (used in the traffic model 1 of the Eurocode) was verified for “Auxerre-traffic” (Fig. 6). For the axle load a value of 0.9 was found. This slight difference can be interpreted as an additional safety element. The computed α -factors are summarized in Table 8.

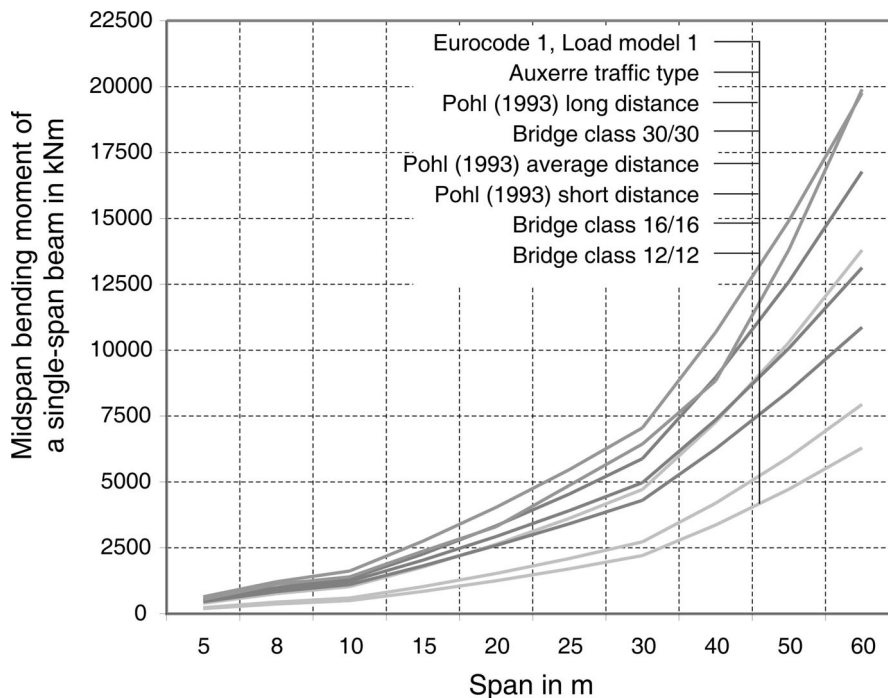


Fig. 6: Maximum bending moments caused by characteristic traffic loads including dynamic load factor. The bridge classes here are equivalents of the former DIN 1072 bridge classes in terms of the DIN 101-report or Eurocode 1 traffic models

Tab. 8: Characteristic loads for recalibration classes of DIN 1072

Bridge class	Roadway quality	Lane 1		Lane 2	
		α_{Q1}	α_{q1}	α_{Q2}	α_{q2}
3/3*	Average	0.10	0.22		
6/6*	Average	0.20	0.24		
9/9*	Average	0.25	0.26		
12/12	Good	0.30	0.28	0.20	1.00
	Average	0.30	0.30	0.25	1.00
16/16	Good	0.35	0.30	0.35	1.00
	Average	0.35	0.40	0.45	1.00
30/30	Good	0.55	0.70	0.50	1.00
	Average	0.60	0.70	0.80	1.00
Simulation Auxerre	Good	1.0	0.90	1.00	1.00
Load model 1 DIN 101	0.80	1.00	0.80	1.00	

* First drafts

2.2 Extension

To provide further control of the suggested factors the results should also be compared with the road traffic model by Pohl (1993). Pohl distinguishes between long distance, aver-

age distance and short distance traffic. Long distance traffic represents more or less heavy vehicle traffic on German highways. Average traffic can be found on federal highways and on country roads; and short distance traffic can be found on weight-restricted routes. Therefore the simulation procedure using the model of Pohl is slightly different to the simulation procedure explained above. Furthermore in our simulation the short distance traffic is separated into two types (Lorry type 1 through 4 or type 1 and 2 according to Table 7).

Fig. 6 shows the characteristic maximum bending moment of a single span beam for different spans and different load models. It permits a direct comparison of the load model by Pohl, the Eurocode model and the suggested variation of the Eurocode model.

The factors given in Table 8 depend on the roadway quality. Usually this property is not given in codes, however, here it is assumed that for country roads lower roadway quality can be found and this has significant impact on the chosen α -factor due to the dynamic properties. Here the model from Merzenich & Sedlacek (1995) has been applied. In general, different roadway qualities have a greater influence on the second lane than the main lane.

3 Conclusion

It should be stated here, that the factors applied in this study are a much more appropriate method for the re-computation of historical bridges than the sometimes found simple diminishing factors of the Eurocode load model 1 (of 0.9, 0.8, 0.7...) as was suggested, for example, in Vockrodt (2005). Applying these factors of 0.9, 0.8 or 0.7 to the Eurocode model 1 violates general assumptions of the statistical properties of the model 1.

Besides the presented schema further adaptations of the Eurocode model 1 are known. Such an additional adaptation has been presented by Novák et al. (2007).

A different proposal for the consideration of local traffic conditions for the load traffic models has been shown by Bailey & Hirt (1996). This method shows the corresponding stochastic basis much stronger than the Eurocode model 1. The major problem of this schema is probably the capturing of the data and, as stated in the beginning, the simple and practical application of the traffic model. The authors assume that their presented model fulfills both, an accurate modeling and a simple application for the engineer.

4 References

- [1] Ablinger, W. (1996): Einwirkungen auf Brückentragwerke – Achslastmessungen und stochastische Modelle, Diplomarbeit, Institut für konstruktiven Ingenieurbau, Universität für Bodenkultur

- [2] Allaix, D.L.; Vrouwenvelder, A.C.W.M. & Courage, W.M.G. (2007): Traffic load effects in prestressed concrete bridges. 5th International Probabilistic Workshop, L. Taerwe & D. Proske (Eds), Ghent, pp. 97-110
- [3] Bailey, S.F. & Hirt, A.H. (1996): Site specific models of traffic action effects for bridge evaluation. J.R. Casas, F.W. Klaiber & A.R. Mari (Eds): Recent Advances in Bridge Engineering. Evaluation, management and repair. Proceedings of the US-Europe Workshop on Bridge Engineering, organized by the Technical University of Catalonia and the Iowa State University, Barcelona, 15-17 July 1996, International Center for Numerical Methods in Engineering CIMNE, pp 405-425
- [4] Bogath, J. & Bergmeister, K. (1999) Neues Lastmodell für Straßenbrücken. Bauingenieur 6, pp 270-277
- [5] Bogath, J. (1997) Verkehrslastmodelle für Straßenbrücken. Dissertation, Institut für konstruktiven Ingenieurbau, Universität für Bodenkultur
- [6] Cooper, D. (2002) Traffic and moving loads on bridges. Dynamic loading and design of structures, A.J. Kappos (Edr), Chapter 8, Spon Press, London, pp 307-322
- [7] COST 345 (2004) European Commission Directorate General Transport and Energy: Procedures Required for the Assessment of Highway Structures: Numerical Techniques for Safety and Serviceability Assessment – Report of Working Groups 4 and 5
- [8] Crespo-Minguillón, C. & Casas, J.R. (1997) A comprehensive traffic load model for bridge safety checking. Structural Safety, 19 (4), pp 339-359
- [9] DIN 1072: Straßen und Wegbrücken, Lastannahmen. Dezember 1985
- [10] DIN-report 101: Einwirkungen auf Brücken. Berlin: Beuth Verlag, 2001
- [11] Eurocode 1: Basis of actions
- [12] ENV 1991-3 Eurocode 1: Grundlagen der Tragwerksplanung und Einwirkungen auf Tragwerke, Teil 3: Verkehrslasten auf Brücken, 1995
- [13] Geißler, K. (1999) Beitrag zur probabilistischen Berechnung der Restnutzungsdauer stählerner Brücken. Dissertation, Heft 2 der Schriftenreihe des Institutes für Tragwerke und Baustoffe an der Technischen Universität Dresden
- [14] König, G. & Gerhardt, H.C. (1985) Verkehrslastmodell für Straßenbrücken. Bauingenieur 60, pp 405-409
- [15] Krämer, W. & Pohl, S. (1984) Der Ermüdungsnachweis in dem Standard TGL 13460/01. Ausgabe 1984 – Grundlagen und Erläuterungen. Die Straße 24, Heft 9, pp 257-263
- [16] Leliavsky, S. (1982) Arches and short span bridges. Design Textbook in Civil Engineering: Volume VII, Chapman and Hall, London

- [17] Merzenich, G. & Sedlacek, G. (1995) Hintergrundbericht zum Eurocode 1 - Teil 3.2: Verkehrslasten auf Straßenbrücken. Forschung Straßenbau und Straßenverkehrstechnik. Bundesministerium für Verkehr, Heft 711
- [18] Novák, B.; Brosge, B.; Barthel, K. & Pfisterer, W. (2007) Anpassung des Verkehrslastmodells des DIN FB-101 für kommunale Brücken, Beton- und Stahlbetonbau 102, Heft 5, pp 271-279
- [19] O'Connor, A. & O'Brien, E.J. (2005) Traffic load modelling and factors influencing the accuracy of predicted extremes. Canadian Journal of Civil Engineering 32, pp 270-278
- [20] Pohl, S. (1993) Definition von charakteristischen Werten für Straßenverkehrsmodelle auf der Basis der Fahrzeuge sowie Fraktilwerte der Lasten des Eurocode 1-Modells; Forschungsbericht Bundesanstalt für Straßenwesen
- [21] Prat, M. (2001) Traffic load models for bridge design: recent developments and research. Progress in Structural Engineering and Materials 3, pp 326-334
- [22] Proske, D. & van Gelder, P. (2009) Safety of historical arch bridges, Berlin: Springer
- [23] Puche, M. & Gerhardt, H.C. (1986) Absicherung eines Verkehrslastmodells durch Messungen von Spannstahlspannungen. Bauingenieur 61, pp 79-81
- [24] Quan, Q. (2004) Modeling current traffic load, safety evaluation and SFE analysis of four bridges in China. Risk Analysis IV, C.A. Brebbia (Edr.) Wessex Institute of Technology Press, Southampton
- [25] Schütz, K.G. (1991) Verkehrslasten für die Bemessung von Straßenbrücken, Bauingenieur 66, pp 363-373
- [26] Spaethe, G. (1977) Beanspruchungskollektive von Straßenbrücken, Die Straße 17, Heft 4, pp 241-246
- [27] Vockrodt, H.-J. (2005) Instandsetzung historischer Bogenbrücken im Spannungsfeld von Denkmalschutz und modernen historischen Anforderungen. 15. Dresdner Brückenbausymposium, Technische Universität Dresden, pp 221-241
- [28] Vrouwenvelder, A.C.W.M. & Waarts, P.H. (1993) Traffic loads on bridges. Structural Engineering International 3, pp 169-177

Comparison of current probabilistic approaches for budget estimating for transportation projects

P. Bakhshi¹, A. Touran²

¹ Ph.D. Student, Dept. of Civil & Env. Engrg., Northeastern University, Boston, MA 02115

² Assoc. Prof., Dept. of Civil & Env. Engrg., Northeastern University, Boston, MA 02115

Abstract: Cost overrun and schedule delays have plagued transportation projects in various parts of the world for the past several decades. Research has shown that this is due to many different reasons including optimistic original estimates, lack of scope definition at the start of the project, increase in scope during the project development phase due to pressure from project stakeholders, errors in estimation, and lack of appropriate contingency budget. In the past few years, many agencies have resorted to the use of probabilistic means to quantify the uncertainties associated with project cost and schedule.

In this paper, we examine two probabilistic approaches developed and used in the United States and Europe. In the first approach, we review the method used by the Federal Transit Administration (FTA) of the U.S. Department of Transportation. FTA requires a formal risk assessment for all new transit projects. In this method, various project cost components are treated as random variables and are *ranged* according to predetermined values to explicitly model the variability of each major cost component. The sum of these cost components will be a distribution that represents the total cost. In the second approach, the British Department for Transport suggests increasing project contingency in order to cope with the *optimism bias* in infrastructure transportation projects. This is done by considering a cumulative distribution function of the amounts of overruns in previous projects and specifying a confidence limit for the project at hand for establishing a revised budget.

The two methods discussed above have similarities; they both consider the probabilistic nature of the project costs and establish budget levels by explicitly considering this variability. This paper evaluates these two methods and makes a quantitative comparison of the results obtained by these methods. This is accomplished by analyzing the cost performance data of a group of major transit projects in the United States, applying the two methodologies, comparing and analyzing the results. The problem areas of these approaches are discussed and recommendations are made to optimize the use of these techniques. The paper will be useful for owner agencies that are in charge of planning and executing large transit projects in the face of cost uncertainty.

1 Introduction

Cost overrun and schedule delays have plagued transportation projects in various parts of the world for the past several decades (Flyvbjerg 2002). Research has shown that this is due to many different reasons including optimistic original estimates, lack of scope definition at the start of the project, increase in scope during the project development phase due to pressure from project stakeholders, errors in estimation, and lack of appropriate contingency budget (Booz.Allen & Hamilton 2005). In the past few years, many agencies have resorted to the use of probabilistic means to quantify the uncertainties associated with project cost and schedule.

In this paper, we examine two probabilistic approaches developed and used in the United States and Europe. Applications of these approaches in transit projects are illustrated. In the first approach, we review the method used by the Federal Transit Administration (FTA) of the U.S. Department of Transportation. FTA requires a formal risk assessment for all new transit projects. In this method, various project cost components are treated as random variables and are *ranged* according to predetermined values to explicitly model the variability of each major cost component. The sum of these cost components will be a distribution that represents the total cost. These sums are calculated with different assumptions regarding the correlations among cost components and are used to establish budget contingencies. In the second approach, we examine the British Department for Transport method that suggests increasing project contingency in order to cope with the *optimism bias* present in infrastructure transportation project cost estimates. This is done by considering a cumulative distribution function of the amounts of overruns in previous projects and specifying a confidence limit for the project at hand for establishing a revised budget. The purpose of the paper is to illustrate the probabilistic approaches currently used in transportation industry. We will not critically examine theoretical foundations of these approaches as that would require space beyond the scope of this paper.

2 Federal Transit Administration (Top-down) model

2.1 Top-down model background

Federal Transit Administration (FTA) of the U.S. Department of Transportation (DOT) sponsors and provides technical support assistance to local transit authorities to carry out their transit projects. FTA, through a set of documented Project Guidance (PG) manuals and procuring the services of Project Management Oversight Contractors (PMOCs), provides oversight assistance to transit authorities. Among the PGs, PG-40 “Risk Management Products and Procedures” (March 2007) is used for conducting risk analysis of all new transit projects. This probabilistic risk assessment, referred to as Top-down model, is a “holistic view of all risks associated with the projects” rather than listing all risks in a risk register. FTA approach asserted that assessment of project risks considering discrete risk events could not capture the variability that is witnessed in current transit projects (Sillars and O’Connor 2008). The PG’s stance was that to focus on significant but few risk

items instead of project risk as a whole may be masking risks that are unconsidered or individually small, but in total have a significant impact on the final cost.

2.2 Top-down model methodology

FTA classifies all costs of a new start transit project into ten Standard Cost Categories (SCC), SCC-10 to SCC-100 (Fig. 1).

Standard Cost Categories for Capital Projects (Rev.11a, June 4, 2008)	
10 GUIDEWAY & TRACK ELEMENTS (route miles)	40.06 Pedestrian / bike access and accommodation, landscaping 40.07 Automobile, bus, van accessways including roads, parking lots 40.08 Temporary Facilities and other indirect costs during construction
10.01 Guideway: At-grade exclusive right-of-way 10.02 Guideway: At-grade semi-exclusive (allows cross-traffic) 10.03 Guideway: At-grade in mixed traffic 10.04 Guideway: Aerial structure 10.05 Guideway: Built-up fill 10.06 Guideway: Underground cut & cover 10.07 Guideway: Underground tunnel 10.08 Guideway: Retained cut or fill 10.09 Track: Direct fixation 10.10 Track: Embedded 10.11 Track: Ballasted 10.12 Track: Special (switches, turnouts) 10.13 Track: Vibration and noise dampening	50 SYSTEMS 50.01 Train control and signals 50.02 Traffic signals and crossing protection 50.03 Traction power supply: substations 50.04 Traction power distribution: catenary and third rail 50.05 Communications 50.06 Fare collection system and equipment 50.07 Central Control
20 STATIONS, STOPS, TERMINALS, INTERMODAL (number)	60 ROW, LAND, EXISTING IMPROVEMENTS 60.01 Purchase or lease of real estate 60.02 Relocation of existing households and businesses
20.01 At-grade station, stop, shelter, mall, terminal, platform 20.02 Aerial station, stop, shelter, mall, terminal, platform 20.03 Underground station, stop, shelter, mall, terminal, platform 20.04 Other stations, landings, terminals: Intermodal, ferry, trolley, etc. 20.05 Joint development 20.06 Automobile parking multi-story structure 20.07 Elevators, escalators	70 VEHICLES (number) 70.01 Light Rail 70.02 Heavy Rail 70.03 Commuter Rail 70.04 Bus 70.05 Other 70.06 Non-revenue vehicles 70.07 Spare parts
30 SUPPORT FACILITIES: YARDS, SHOPS, ADMIN. BLDGS	80 PROFESSIONAL SERVICES (applies to Cats. 10-50) 80.01 Preliminary Engineering 80.02 Final Design 80.03 Project Management for Design and Construction 80.04 Construction Administration & Management 80.05 Professional Liability and other Non-Construction Insurance 80.06 Legal; Permits; Review Fees by other agencies, cities, etc. 80.07 Surveys, Testing, Investigation, Inspection 80.08 Start up
40 SITEWORK & SPECIAL CONDITIONS	90 UNALLOCATED CONTINGENCY
40.01 Demolition, Clearing, Earthwork 40.02 Site Utilities, Utility Relocation 40.03 Haz. mat'l, contam'd soil removal/mitigation, ground water treatments 40.04 Environmental mitigation, e.g. wetlands, historic/archeologic, parks 40.05 Site structures including retaining walls, sound walls	100 FINANCE CHARGES

Fig. 1: Standard Cost Categories (SCC), USDOT

Costs in SCC 90, Unallocated Contingency, and SCC 100, Financial Charges, are not considered in the Top-down procedure. The remained categories should be carefully reviewed to identify all allocated contingencies and escalation. These contingencies are removed from the estimate to arrive at the Base Cost Estimate (BCE) in each category. The approach assumes that each cost category follows a lognormal distribution that can be identified by estimating the 10th and 90th percentile values of each cost component. The BCE is usually considered to be the 10th percentile of the lognormal distribution. The 90th percentile of the distribution is estimated from Eq. (1):

$$90^{th} \text{ Percentile of the Distribution} = \beta * 10^{th} \text{ Percentile of the Distribution} \tag{1}$$

β is dependent on the level of risk in project delivery stages and ranges from 1.0 to 2.5 and above. A β value of 1.0 means that there is no risk associated with the BCE. The more the project progresses, the smaller the value of β . Having the 10th and 90th percentile of each cost components and using Lognormal Distribution equations, the mean and standard deviation of each cost component are calculated (Eqs. (2)-(7)). In these equations, μ and σ

are parameters of the underlying normal distribution; mean and variance of the lognormal distribution are given in Eqs. (6) and (7).

$$x_a = \text{Optimistic Estimate \%} = \text{Cost of } 10^{\text{th}} \text{ Percentile in Each SCC} \quad (2)$$

$$x_b = \text{Pesimistic Estimate \%} = \text{Cost of } 90^{\text{th}} \text{ Percentile in Each SCC} \quad (3)$$

$$\mu = \frac{1}{2} \text{Ln}(x_a x_b) - \frac{[\phi^{-1}(a) + \phi^{-1}(b)]}{2} \sigma \quad (4)$$

$$\sigma = \text{Ln}\left(\frac{x_a}{x_b}\right) / [\phi^{-1}(b) - \phi^{-1}(a)] \quad (5)$$

$$\text{Mean} = e^{\mu + \sigma^2 / 2} \quad (6)$$

$$\text{Variance} = e^{2\mu + \sigma^2} (e^{\sigma^2} - 1) \quad (7)$$

The sum of these cost components that represents the total cost is calculated using the Central Limit Theorem and assuming normality for the sum of lognormal components. The cumulative distribution is formed once with the assumption that all cost categories are completely correlated, $r=1.0$, and once with the assumption that there is no correlation, $r=0$. Note that the assumption of normality is not correct when components are fully correlated. Indeed, it can be proven that the total will follow a lognormal distribution. A “First Order Approximation” distribution which is the final product of the proposed top-down approach is created by finding the one-third point of the total difference in variance between two aforementioned distributions. This process is applied at project cost components and several scenarios are run at the beginning of various project phases.

2.3 How to assign β values to different SCCs at the various project delivery stages

Based on the historical data and lesson learned from previous transit projects, a set of recommended β values is suggested by PG-40. It is risk analyst’s responsibility to find the most appropriate β factors to assign to each SCC considering the unique and specific characteristics of every project.

1. Requirement risks: those associated with definition of basic project needs and transit system requirements to meet those needs ($\beta \geq 2.5$);
2. Design risks: those involved with engineering design of the transit system ($2.5 > \beta \geq 2.0$);
3. Market risks: those associated with procurement of construction services and other system components ($2.0 > \beta \geq 1.75$);
4. Construction risks: those associated with the actual construction of the systems ($1.75 > \beta \geq 1.05$).

The guidelines provide specific β values to be applied to various Standard Cost Categories (SCC) of the transit project. The values of β may vary through project implementation at each key stage of project development. These recommendations would be used in the next section to assign the β ’s at three different stages of the project completion.

2.4 Applying the Top-down model to U.S. data

The value of β will vary from project to project and depending on the level of project development. As the project design progresses, the values of β tend to decrease. However, one can estimate an average β for the average transit project in the United States. The objective here is to calculate the average range for U.S. transit projects costs using the guidelines provided in PG-40. We have identified 51 transit projects in the U.S. (30 heavy rail and 21 light rail) for which actual costs were reported (Booz.Allen & Hamilton 2003 and 2004). Using these cost data, the breakdown of costs for the average of these 51 transit projects are calculated for various cost categories. The result is illustrated in Fig. 2.

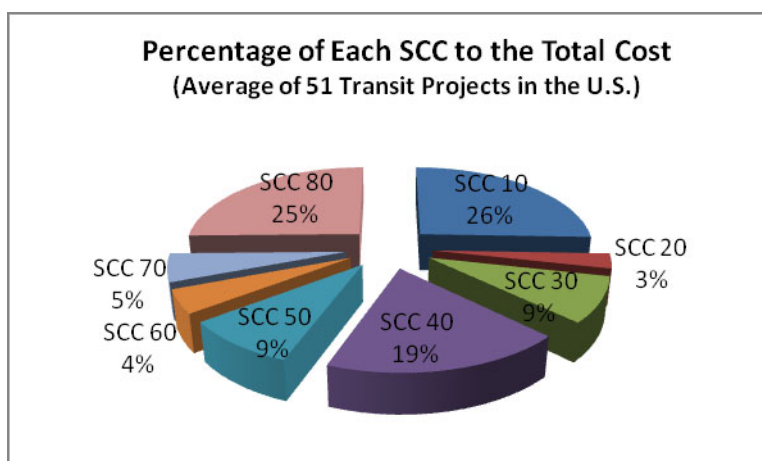


Fig. 2: Percentage of each scc to the total cost

The β factors using the FTA recommendations are assigned for three different key phases of a project. These three phases are: Draft Environmental Impact Statement (DEIS), Preliminary Engineering (PE), and Final Design (FD). These phases are commonly used for transit project development in the US and are roughly equivalent to Conceptual Design, Preliminary Engineering, and Final Design phases of a project development. These values are given in Table 1. It can be seen that following this procedure, for example at the PE stage, the average β value is 2.2. This means that the 90th percentile cost is more than twice as large as the 10th percentile cost.

Tab. 1: β Values assigned to each cost category at three key phases of a transit project

SCC	Average of 30 HRT Project	Average of 21 LRT Project	Average of 51 Transit Projects	% of Each SCC to Total Cost	Beta @DEIS	Beta @PE	Beta @FD	
SCC 10	\$191,915,256	\$145,732,385	\$172,660,755	25.55%	2.50	2.25	2.00	
SCC 20	\$20,763,234	\$16,594,973	\$19,427,829	2.88%	2.50	2.25	2.00	
SCC 30	\$61,752,584	\$51,401,222	\$58,640,064	8.68%	2.50	2.25	2.00	
SCC 40	\$179,590,760	\$42,208,831	\$125,482,165	18.57%	2.77	2.50	2.22	
SCC 50	\$62,638,602	\$56,277,600	\$61,219,753	9.06%	2.50	2.25	2.00	
SCC 60	\$26,399,332	\$35,113,473	\$30,587,258	4.53%	4.37	3.93	3.50	
SCC 70	\$38,409,454	\$32,770,106	\$36,809,117	5.45%	1.87	1.68	1.50	
SCC 80	\$198,569,935	\$123,061,639	\$170,827,849	25.28%	1.87	1.68	1.50	
Total					Weighted Average of Beta			
				\$675,654,790	100%	2.44	2.20	1.96

For the average transit project, the 10th percentile is assumed to be the value of BCE and the 90th percentile is calculated using Eq. (1). Values of mean and standard deviation in each category are calculated using Eqs. (2)-(7).

Then, all SCCs are summed to generate Total Cost assuming independence and perfect correlation among cost BCEs. In both cases, following the FTA guide, the mean of the total cost is assumed to be a Normal distribution. The result is given in Table 2.

Tab. 2: 10th Percentile, 90th percentile, mean and standard deviation of each cost category

SCC	10th Percentile	DEIS Stage			PE Stage			FD Stage		
		90th Percentile	Mean	Std. Dev.	90th Percentile	Mean	Std. Dev.	90th Percentile	Mean	Std. Dev.
SCC 10	25.6%	63.9%	43.07%	15.90%	57.5%	40.30%	13.08%	51.1%	37.49%	10.33%
SCC 20	2.9%	7.2%	4.85%	1.79%	6.5%	4.53%	1.47%	5.8%	4.22%	1.16%
SCC 30	8.7%	21.7%	14.63%	5.40%	19.5%	13.69%	4.44%	17.4%	12.73%	3.51%
SCC 40	18.6%	51.4%	33.45%	13.84%	46.4%	31.30%	11.56%	41.2%	29.04%	9.26%
SCC 50	9.1%	22.7%	15.27%	5.64%	20.4%	14.29%	4.64%	18.1%	13.29%	3.66%
SCC 60	4.5%	19.8%	11.17%	7.00%	17.8%	10.35%	5.94%	15.8%	9.54%	4.96%
SCC 70	5.4%	10.2%	7.68%	1.90%	9.2%	7.21%	1.47%	8.2%	6.76%	1.08%
SCC 80	25.3%	47.3%	35.62%	8.83%	42.5%	33.45%	6.84%	37.9%	31.36%	4.99%
Total (Correlated)			165.73%	60.30%		155.12%	49.44%		144.43%	38.94%
Total (Independent)			165.73%	25.28%		155.12%	20.79%		144.43%	16.43%

Following the Top-down model process, cumulative normal distributions for each phase assuming completely correlated and independent are formed and the first order approximation curves are generated (Fig. 3).

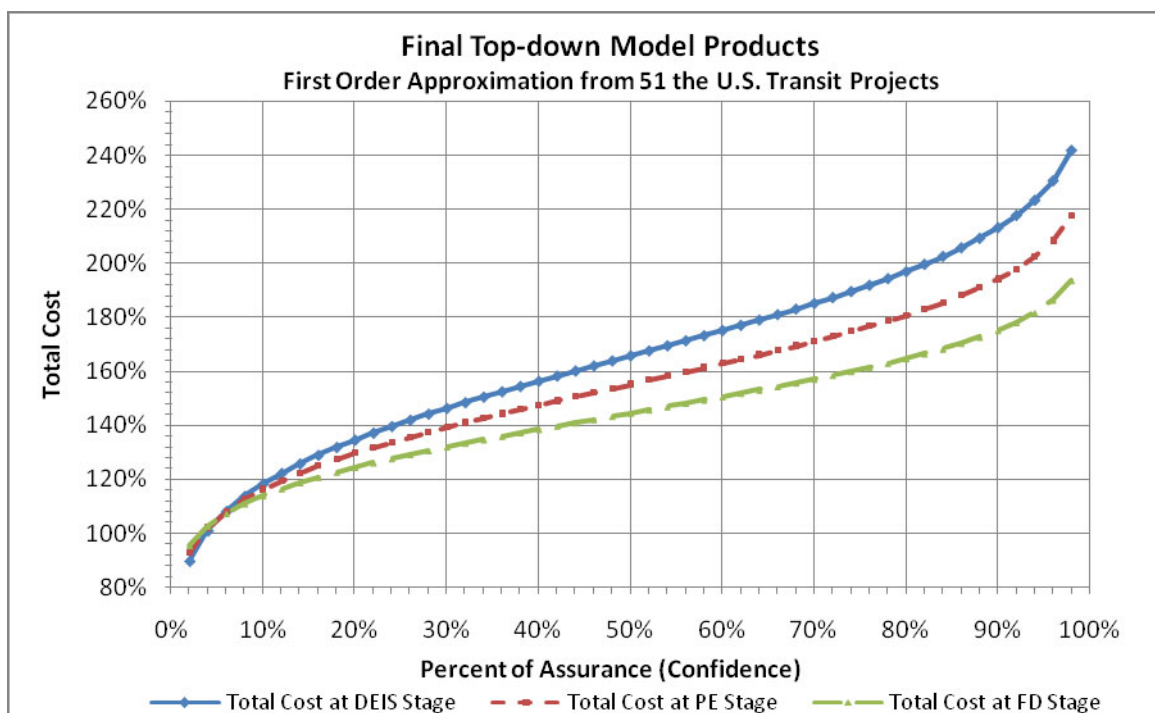


Fig. 3: Final Top-down Model curves (Total Required Budget) at three different phases of a transit project

Using Fig. 3, if an agency wants to establish project budget at the “Final Design” phase of a project, in order to have 85% confidence that the budget is sufficient, it should allocate a budget equal to 1.69 of initial cost estimate (Total BCEs). It should be noted that since in a transit project, a contingency budget is added to the Base Cost Estimate (BCE), and this contingency varies according to the project phase, the amount of uplift compared to the budgeted estimate should be smaller. For example, a typical contingency added to the BCE at the Final Design phase is about 10%. This means that according to the Optimism Bias Approach, this estimated budget should be increased by $1.69/1.1 = 1.54$ (or 54%). Since transit projects usually are costly, it means that the agency must provide and block a huge amount of money to ensure the sufficiency of budget. Fig. 4 is a modified version of Fig. 3. The X axis is converted to the “Acceptable Chance of Cost Overrun”, 100% - Percent of Assurance (Confidence), and Y axis to “Required Uplift” (or the amount needed to be added to the base cost), Total Cost - 100%. This modification was done to make Fig. 4 similar to the final product of British Department for Transport (Optimism Bias) Model. We will be comparing the outcome of this analysis with the British approach later in this paper. As an example, increasing the base budget by 69% (at the Final Design phase), will mean that there is a 15% chance that the budget would not be sufficient, *i.e.*, there will be a cost overrun.

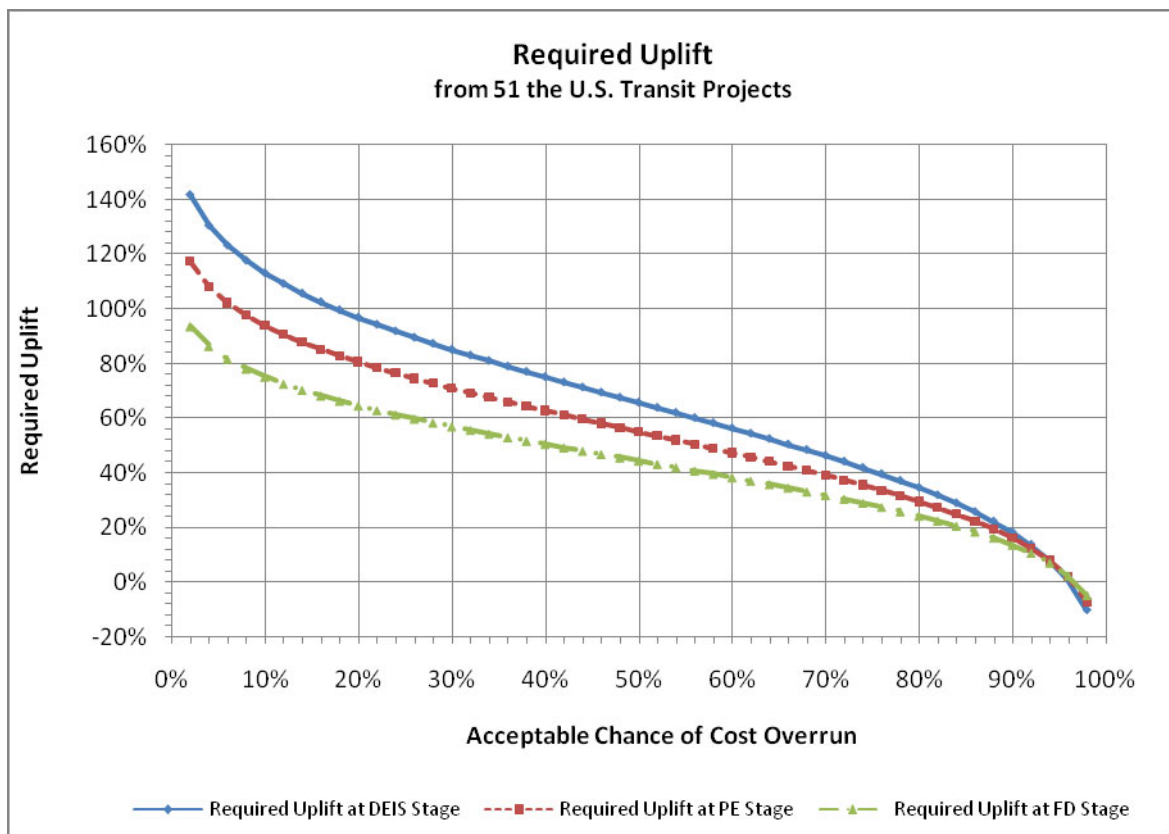


Fig. 4: Converted Curves of the Top-down Model to show the required uplift

3 The British Department for Transport (Optimism Bias) model

3.1 Optimism Bias model background

The second approach examined for this research is the British Department for Transport approach in dealing with optimism bias in capital project cost estimates. This approach is based on work done by Flyvbjerg and COWI (2004) and reported by Flyvbjerg (2006). According to Flyvbjerg *et al* (2002; 2005; 2006), psychological (optimism bias) and political explanations (strategic misrepresenting due to political and organizational pressure) are responsible for much of the inaccuracy in transportation cost forecasting. Reference class forecasting method is based on theories of decision-making under uncertainty. "Reference class forecasting does not try to forecast the specific uncertain events that will affect the particular project, but instead places the project in statistical distribution of outcomes from the class of reference projects." (Flyvbjerg 2006).

According to *Supplementary Green Book* (2003): "There is a demonstrated, systematic tendency for project appraisers to be overly optimistic. To redress this tendency, appraisers should make explicit, empirically based adjustments to the estimates of a project's costs, benefits, and duration... It is recommended that these adjustments be based on data from past projects or similar projects elsewhere". To this end, the British Department for Transport (DfT) and HM Treasury published a guide: "Procedures for dealing with Optimism Bias in Transport Planning" based on the work conducted by Flyvbjerg and COWI to establish a guide for selected reference classes of transport infrastructure projects to prevent cost overrun. This approach is hereafter called "Optimism Bias Model" method in this paper.

3.2 The Optimism Bias Model methodology

In the DfT guide, transportation projects have been divided into a number of distinct groups. These groups include road, rail, fixed links, buildings, and IT projects and have been selected in order to have statistically similar risk of cost overrun based on the study of an international database of 260 transportation projects. In this paper, we are interested in rail projects because the transit projects that we analyzed for the US case were almost exclusively rail projects.

In the DfT guide, cost overrun is defined as the difference between actual cost (final cost) and estimated costs which is the forecasted costs at the time of approval of/decision to build a project in percentage of estimated costs. Where the approval point is not clear in the project planning process, the closest available estimate is used. For each category, the probability distribution for cost overrun as the share of projects with a given maximum cost overrun was created. Having established the empirical cumulative probability distribution, uplifts are set up as a function of the level of risk that the DfT is willing to accept regarding cost overrun. "Uplift" is the term used to show the amount that the original estimate needs to be increased to arrive at the project budget for a given level of certainty with respect to cost adequacy. If the DfT wants to accept a higher risk, then a

lower uplift is required. The readers are referred to the British DfT (2004) and Flyvbjerg (2006) for a thorough description of the Optimism Bias methodology.

3.3 Applying Optimism Bias model to U.S. data

To generate a reference class, 22 transit projects across the U.S. were selected. The objective here is to apply the Optimism Bias Model approach to these projects and then compare the results with the results of applying the USDOT approach to the same data. These projects were part of a study conducted under a research project where the co-author was a team member of the research group (Booz.Allen 2005). As part of this research effort, cost overruns for 22 major transit projects were calculated considering estimated budgets at various stages of these projects. For each project, the cost overrun/underrun was calculated at the DEIS, PE, and FD stages by comparing these estimates with actual cost of projects. Although, DfT calculates the cost overrun relative to the estimate at the point of approval of/decision to build, in order to compare FTA and DfT models, here cost overrun has been calculated at: DEIS, PE, and FD stages. PE can be considered equivalent to the time that British agencies prepare their initial budgets. In this way, we can compare these two models. It should be noted that the main criteria in selecting these 22 projects for inclusion in the original study was the availability of data. In other word, the research team was not trying to identify and select projects that were notorious for cost overrun or delay. Following the abovementioned process, the cumulative probability distribution for cost overrun as the percentage of projects with a given maximum cost overrun is formed (Fig. 5); then the required uplift curve is calculated (Fig. 6).

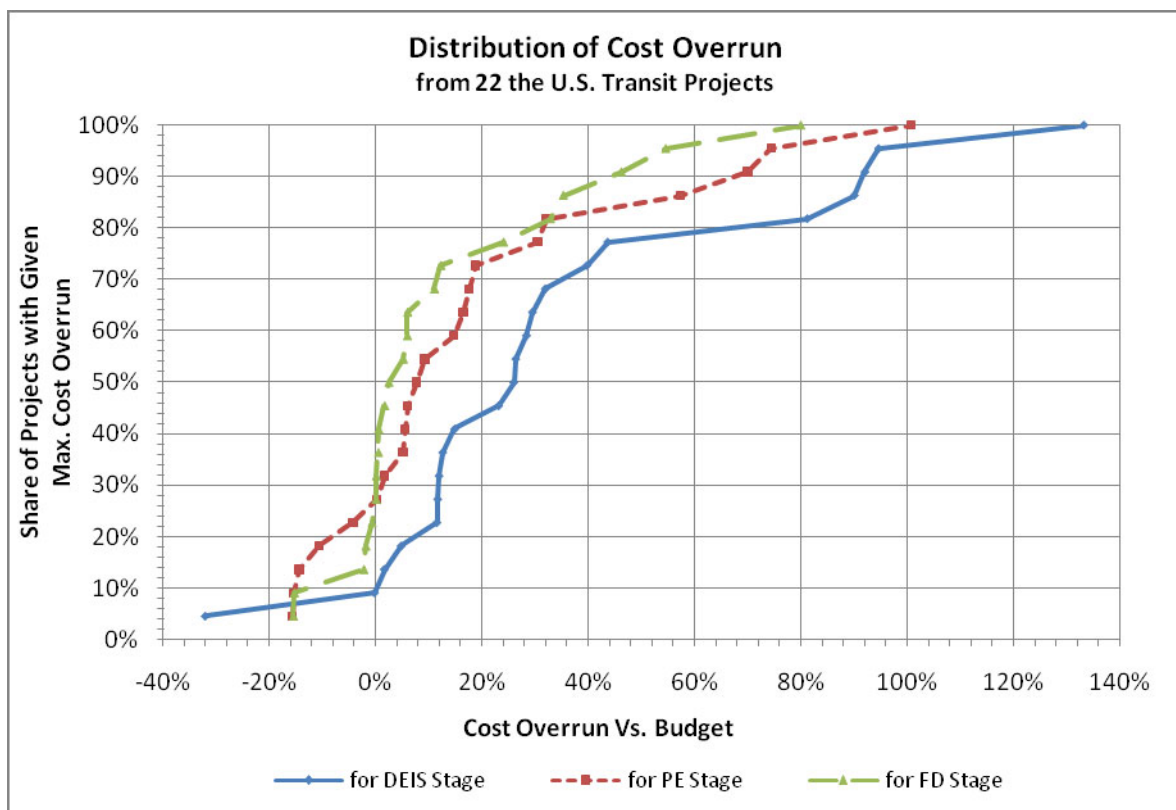


Fig. 5: Probability distribution of cost overrun at three different stages of a project

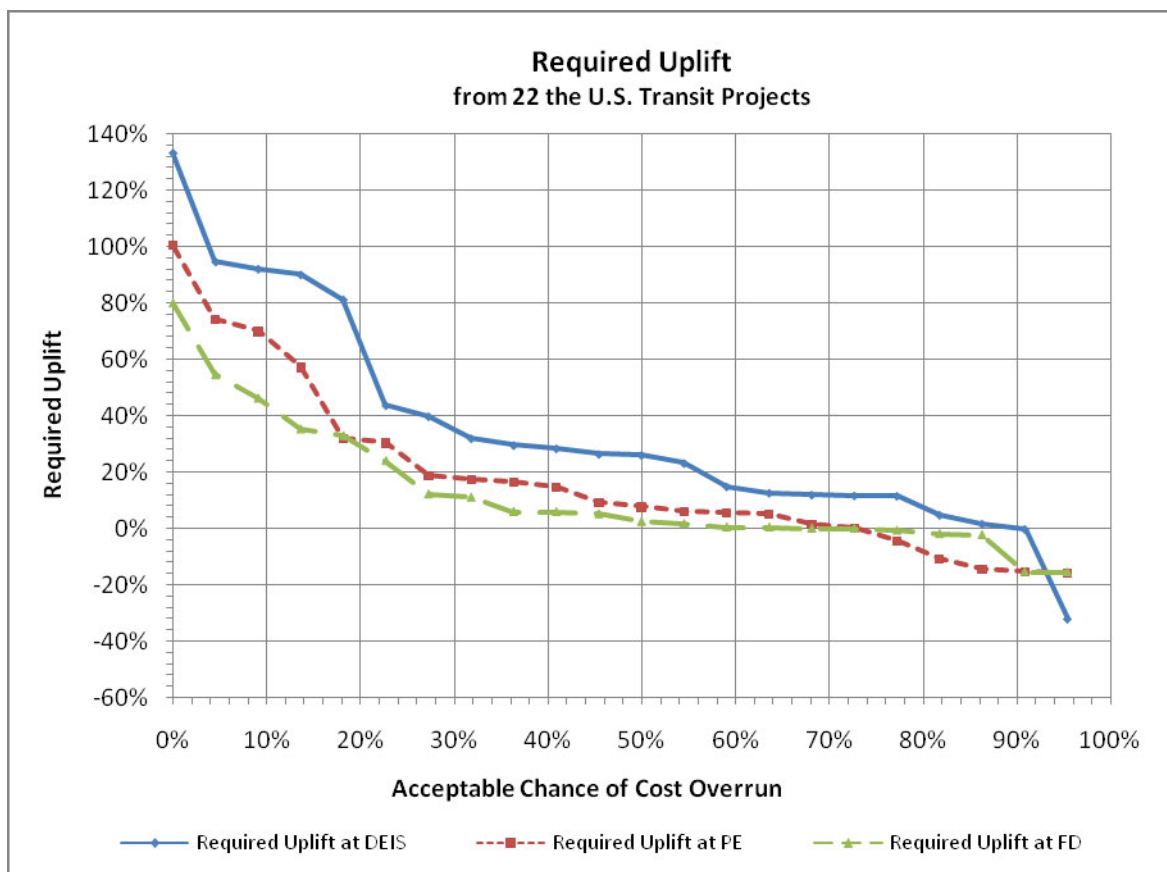


Fig. 6: Required Uplifts at Three Different Stages of a Project

Fig. 6 illustrates that based on the selected U.S. projects, if a transit agency decides to apply the method suggested by the DfT and to accept a 10% chance of cost overrun for its project, the required uplift is 91.61% at the DEIS phase, 67.36% at the PE phase, and 44.01% at the FD phase. It demonstrates that the more project progresses, due to the decreasing level of uncertainty, the less uplift is required.

4 Comparison of Top-down and Optimism Bias models

In previous sections, we applied two different probabilistic approaches to a group of transit projects in the U.S. Although, the Optimism Bias approach used in the U.K. only considers the cost estimate at the approval of/decision to built stage of a project to calculate cost overrun, in order to evaluate β values of Top-down model used in the U.S., we have calculated cost overrun at three phases of DEIS, PE, and FD. Comparing Fig. 4 and Fig. 6 shows that required uplift for 50% confidence at PE stage is 55.12% with Top-down model and 7.70% with the Optimism Bias approach. Table 3 lists the required uplift with 50% confidence at three stages of the project with two approaches.

Tab. 3: Required uplift with 50% Acceptable Chance of Cost Overrun with two approaches

Model	Required Uplift with 50% Confidence		
	DEIS	PE	FD
Top-Down approach	65.73%	55.12%	44.43%
Optimism Bias approach	25.96%	7.70%	2.37%

Comparing these results show that the Top-Down approach established a much larger budget for the project. It should be realized that establishing too conservative a budget is not necessarily desirable because by tying excessive funds for projects, other candidate projects will be deprived of the necessary funds. From Top-down Methodology, we remember that β is defined as the ratio between 90th percentile and 10th percentile of the cumulative cost distribution. So using data in Fig. 5, we can construct equivalent β values for the Optimistic Bias approach by calculating the ratio between the 10th and 90th percentile points. In Table 4, the calculated β values are compared with weighted average of β values recommended by the Top-down model (computed in Table 1).

Tab. 4: Comparison of the β values in two approaches

Key Stages	Optimism Bias			Top-down
	10 th Percentile	90 th Percentile	β	Weighted Average β
DEIS	1.001	1.916	1.91	2.44
PE	0.847	1.674	1.97	2.20
FD	0.872	1.440	1.65	1.96

As stated before, reviewing Table 4 shows that β values from Optimism Bias approach where the data come from historical data are significantly smaller than the β recommended by the Top-down approach. Looking at β s for Optimism Bias approach illustrates that the values of β at PE stage is greater than DEIS where it should be normally smaller. This anomaly might be due to the nature of the projects in the sample and the relative small sample size. This is due to the greater number of projects that have had cost underrun at the PE stage possibly due to scope reduction.

5 Conclusion

Optimism Bias and Top-Down approaches are suggested (and used) for transit project development in the U.S. and the U.K. Both these approaches have positive and negative aspects. First, the Top-down model selects large values of β in order to prevent cost overrun which results in establishing a budget far larger than historical actual costs. Optimism Bias approach is based on historical data but does not consider unique features and characteristic of individual projects. It gives an estimate of the actual cost based on a set of peer projects without considering the location and special condition of each projects. The positive aspect of both approaches is the explicit consideration of uncertainty in cost estimating and budgeting. The authors' suggestion is to refine these approaches and come

up with a probabilistic method that considers the unique characteristics of each project without tying up huge capital in order to prevent potential cost overruns. It seems that more research is needed in this area since over the past several decades, preventing cost overrun and accuracy in cost estimate has not been improved substantially.

6 References

- [1] Booz-Allen & Hamilton. (2003). "Light Rail Transit Capital Cost Study Update." Federal Transit Administration, Washington, D.C.
- [2] Booz-Allen & Hamilton. (2004). "Heavy Rail Transit Capital Cost Study Update." Federal Transit Administration, Washington, D.C.
- [3] Booz-Allen Hamilton (2005). "Final Report: Managing Capital Costs of Major Federally Funded Public Transportation Projects", Project G-07, Transit Cooperation Research Program. (TCRP), McLean, VA, November.
- [4] Federal Transit Administration. (2007). "Risk Management Products and Procedures", PG# 40, March 29.
- [5] Federal Transit Administration. (2003). "Risk Assessment and Mitigation Procedures", PG# 22, December 8.
- [6] Fyvbjerg, B. (2006). "From Nobel Prize to Project Management: Getting Risk Right", Project Management Journal, August, P5-15.
- [7] Fyvbjerg, B. (2005). "Design by Deception: The Politics of Megaprojects Approval", Harvard Design Magazine, Spring/Summer, 22, pp. 50-59.
- [8] Fyvbjerg, B., Holm, M. K. S., and Buhl, S. L. (2002). "Underestimating Costs in Public Works Projects: Error or Lie?", *Journal of the American Planning Association*, Summer, 68(3), pp. 279-295.
- [9] HM Treasury of the U.K. (2003). *Supplementary Green Book Guidance: Optimism Bias*, London, U.K.
- [10] Sillars, D. and O'Connor, M. (2008). "Risk-Informed Project Oversight at the FTA", TRB 2008 Annual Meeting.
- [11] The British Department for Transport. (2004). "Procedure for Dealing with Optimism Bias in Transport Planning", Guidance Document, June.

Risk Assessment of Petroleum Pipelines using a combined Analytical Hierarchy Process - Fault Tree Analysis (AHP-FTA)

Alex. W. Dawotola, P.H.A.J.M van Gelder, J.K Vrijling
Faculty of Civil Engineering and Geosciences, Delft University of Technology,
Stevinweg 1, 2628CN Delft, the Netherlands

Abstract: This paper proposes a combined Analytic Hierarchy process (AHP) and Fault Tree Analysis (FTA) to support the design, construction, inspection and maintenance policy of oil and gas pipelines by proposing an optimal selection strategy based on the probability of failure and consequences of failure. To quantitatively analyze the probability of a safety hazard obtained from AHP, a Fault Tree Analysis (FTA) is proposed. With the AHP-FTA, the most crucial failure mode of the pipeline is estimated by AHP and further analyzed by FTA. The methodology is an improvement in the existing qualitative risk assessment of oil pipelines. Furthermore, with enhanced accuracy in risk assessment, considerable cost savings in the design, construction, inspection and maintenance planning of the pipeline may be achieved.

1 Introduction

1.1 Pipeline Risk Assessment

Pipelines carry products that are very vital to the sustenance of national economies and remain a reliable means of transporting water, oil and gas in the world. Like any other engineering facility, petroleum pipelines are subject to different degrees of failure and degradation. Pipeline failures are often fatal and very disastrous. It is therefore important that they are effectively monitored for optimal operation, while reducing failures to acceptable safety limit. There has been an increased awareness on risk assessment of transportation pipelines both in the industry and academia, Allouche and Bowman (2006) due to the continuous need for cost minimization and safety maximization.

Risk assessment of petroleum pipelines entails the study of failures and consequences of pipelines in terms of possible damage to property, human hazards, and the environment. Ideally, most pipeline operators ensure that during the design stage, safety provisions are created to provide a theoretical minimum failure rate for the life of the pipeline. There are approaches such as corrosion control and routine based maintenance to ensure reliability of pipelines during service.

Transmission pipelines are complex in nature, and their risk analysis could be simplified by using a hierarchical approach, Huipeng Li (2007). However, little has been achieved on hierarchical risk analysis of petroleum pipelines, as an aid to decision analysis, which is required in making inspection and maintenance decisions. AHP is a promising method for this application. AHP, developed by Saaty fundamentally works by using opinions of experts in developing priorities for alternatives and the criteria used to judge the alternatives in a system, Saaty (1999). The outcome is a relative scale which gives managers a rational basis for decision making. It has found applications in diverse industries, such as agriculture, Quresh and Harrison (2003), oil and gas, Dey et al (2004), Al-Khalill (2005), Nonis et al (2007), Brito and Almeida (2009), and the public sector, Dey (2002). Majority of AHP applications in pipelines sector, Dey et al (2004), Al-Khalill (2005), Brito et al (2009) have concentrated mainly on qualitative risk analysis and there has not been adequate application of AHP in achieving quantitative risk assessment.

The focus of this paper is the introduction of a framework that implements combined analytic hierarchy process and fault tree analysis for quantitative risk assessment of petroleum pipelines. The combined AHP-FTA is particularly suitable where sufficient data is lacking to carry out a full scale Fault Tree Analysis. The case study of cross-country oil and gas pipelines is used to illustrate the proposed methodology.

1.2 What is risk?

Quantitatively, risk is a function of an event, its probability and associated consequences. Kaplan and Garrick (1981) discussed a risk triplet and argued that risk analysis consists of an answer to the three questions:

- (i) What can go wrong?
- (ii) How can it happen?
- (iii) What are the consequences?

And the set, R of the above three questions can be mathematically represented as:

$$R = \{s_i, p_i, x_i\}, i = 1, 2, \dots, N \quad (1)$$

Where s_i is an event or an occurrence.

p_i is the probability of s_i and x_i is the consequence of s_i

2 AHP-FTA Methodology for Risk Assessment

The combined AHP-FTA model methodology comprise of implementation of Analytic hierarchy process followed by a Fault Tree analysis. AHP is used in the decision making to estimate the likelihood of an event, by establishing relative importance of each contributing factors, while Fault Tree Analysis is directed at the important failure criteria identified by AHP.

The analytical hierarchy process consists of the following basic steps:

- Problem formulation – the ultimate goal of the AHP is defined. In this paper, it is the determination of risk due to oil spillage from petroleum pipeline. After the goal definition, contributing factors to the failure are then identified. If applicable, these factors are further divided into 1 or 2 sub factors. The major factors and sub factors responsible for product loss from a pipeline are presented in Fig. 1.
- Facility segmentation – The pipeline is divided into different sections based on their peculiar similarities. The different sections are the alternatives of the decision making process.
- Collection of pipeline information - Required features for the pipelines is divided into physical data, construction data, operational data, inspection data and Failure history. This information is documented for the hierarchical analysis.
- The next step is the development of a hierarchy structure, which consists of the goal of the risk assessment, the failure factors and subfactors, if applicable and the pipeline stretches.
- In the last step of the analytical hierarchy process, data of the pipelines are made available to a number of experts who the carry out a pairwise comparison of the pipeline segments with respect to each risk factor (failure criteria). The outcome of the comparison is a matrix that ranks the pipeline stretches in order of the likelihood of failure.
- Consistency check: AHP provides the possibility of checking the logical consistency of the pairwise matrix by calculating the consistency ratio (CR). AHP judgement is acceptable if CR is less than 0.1

Given a weight vector, $\vec{w} = \begin{bmatrix} w_1 \\ w_2 \\ w_n \end{bmatrix}$ obtained from a decision matrix, $A = \begin{bmatrix} a_{11} & a_{12} & a_{1n} \\ a_{21} & a_{22} & a_{2n} \\ a_{31} & a_{32} & a_{3n} \end{bmatrix}$,

the consistency of the decision matrix is calculated as follows:

Multiply matrix A by the weight vector \vec{w} to give vector, \vec{B}

$$\vec{B} = \vec{A} \cdot \vec{w} = \begin{bmatrix} b_1 \\ b_2 \\ \vdots \\ b_n \end{bmatrix} \quad \text{Where,} \quad \begin{aligned} b_1 &= a_{11}w_1 + a_{12}w_2 + \dots + a_{1n}w_n \\ b_2 &= a_{21}w_1 + a_{22}w_2 + \dots + a_{2n}w_n \\ &\vdots \\ b_n &= a_{n1}w_1 + a_{n2}w_2 + \dots + a_{nn}w_n \end{aligned} \quad (2)$$

Divide each element of vector, \vec{B} with the corresponding element in the weight vector

$$\vec{w} \text{ to give a new vector } \vec{c}: \begin{bmatrix} b_1/w_1 \\ b_2/w_2 \\ \vdots \\ b_n/w_n \end{bmatrix} = \begin{bmatrix} c_1 \\ c_2 \\ \vdots \\ c_n \end{bmatrix} \quad (3)$$

$$\lambda_{\max} \text{ is the average of the elements of vector } \vec{c}: \lambda_{\max} = \frac{1}{n} \sum_{i=1}^n c_i \quad (4)$$

$$\text{Consistency Index is then calculated using, } CI = \frac{\lambda_{\max} - n}{n - 1} \quad (5)$$

Where n is order of the decision matrix and λ_{\max} is obtained from equation (4) above.

$$\text{Using equation (4), Consistency Ratio is calculated as, } CR = \frac{CI}{RI} \quad (6)$$

Where RI is the random index, and its value is obtained from table 1 below.

Tab 1: Random index table

n	3	4	5	6	7	8	9	>9
RI	0.58	0.9	1.12	1.24	1.32	1.41	1.45	1.49

Other measures of consistency have been defined. For example, J. Mustajoki and R.P.Hämäläinen (2000) give a Consistency Measure (CM) of between 0 to 1 using the Multi Attribute Value Theory inherent in their Web-HIPRE software. A CM of 0.2 is considered acceptable.

Consistency Measure is calculated using,

$$CM = \frac{2}{n(n-1)} \sum_{i>j} \frac{\bar{r}(i,j) - \underline{r}(i,j)}{(1 + \bar{r}(i,j))(1 + \underline{r}(i,j))} \quad (7)$$

Where $\bar{r}(i,j) = \max a(i,k)a(k,j)$, $k \in \{1, \dots, n\}$ is the extended bound of the comparison matrix element $a(i,j)$, and $\underline{r}(i,j)$ is the inverse of $\bar{r}(i,j)$. CM gives an indication of the size of the extended region formed by the set of local preferences, when $w_i \leq \bar{r}(i,j)w_j$ for all $i, j \in \{1, \dots, n\}$

- Fault tree analysis of important failure factors: Fault Tree Analysis of the most important failure factor is carried out to determine acceptability of risk. Using the FTA and AHP results, the overall failure probability is then calculated.

Fig. 1: Development of a hierarchy of failure of pipeline

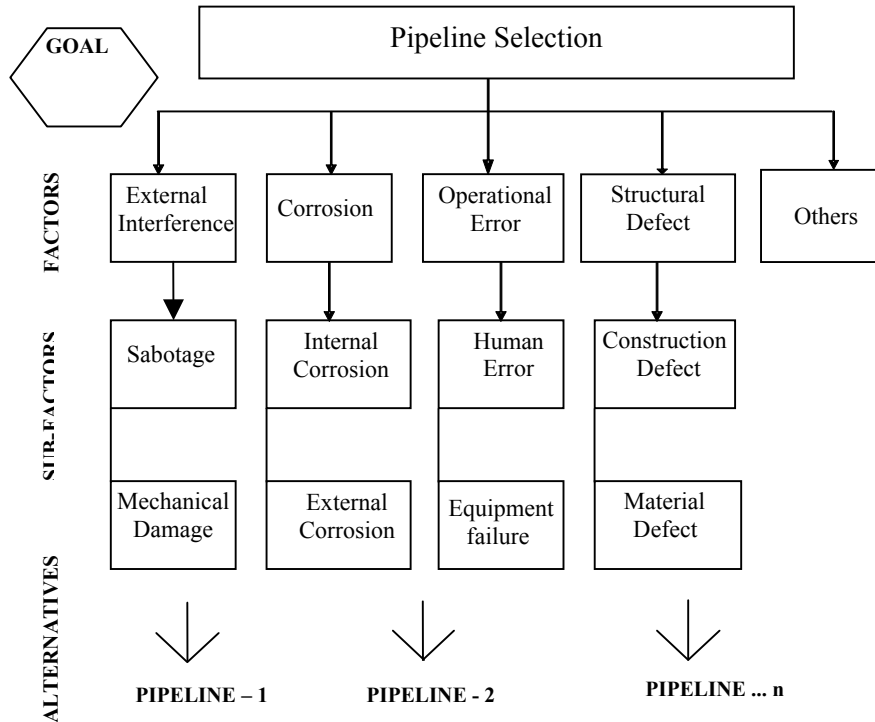
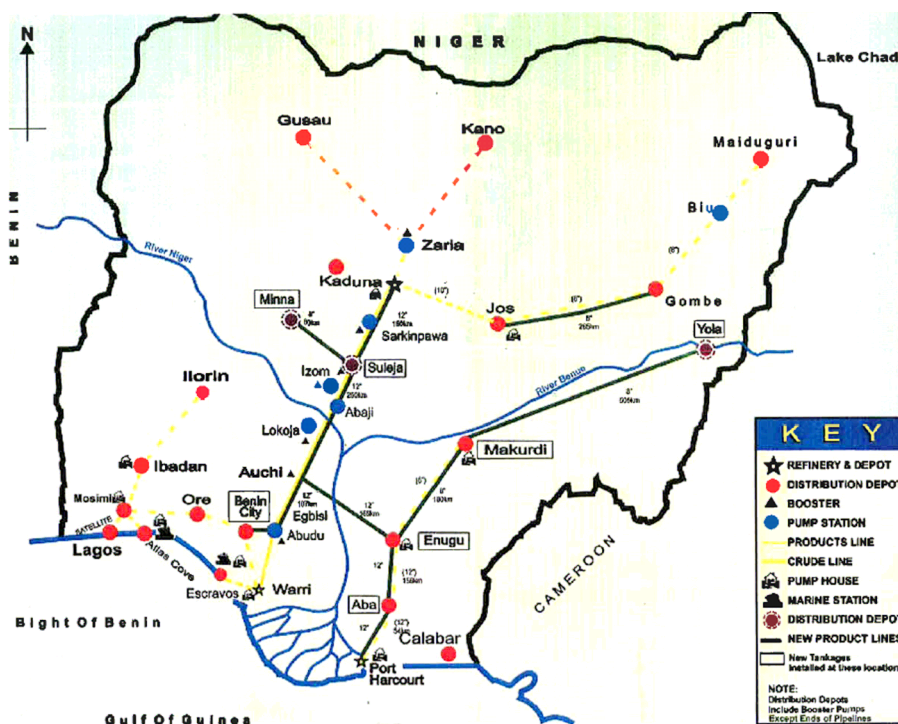


Fig. 2: Map of Nigeria showing Petroleum Pipeline Network, NEITI (2006)



3 AHP-FTA Pipeline risk assessment – A case study

3.1 Introduction

Oil and gas pipelines located in 3 different parts of Nigeria: EL Pipeline (Escravos), AB Pipeline (Warri), and AZ Pipeline (Benin) (Fig. 2) were considered as a case study. A summary of the characteristics of the pipelines are shown in tab. 2 below. The goal of the research is to conduct a risk assessment of given pipelines using Analytical Hierarchy Process (AHP) method. This is achieved by determining the relative contribution of different failure factors to the overall pipeline failure. Pipeline failure is defined as loss of structural integrity of pipeline which may lead to unintended products loss.

Based on literature research conducted, Adebayo and Dada (2008), L.P.E YO-Essien (2008), NNPC (2008) five factors have been identified as being mostly responsible for pipeline failures in Nigeria, namely external interference, corrosion, structural defects, operational defects, and other minor failures.

A total of six pipeline experts participated in the expert judgement study on risk assessment of the petroleum pipelines. The affiliations of the experts are in the following organisations: Shell International, Chevron Exploration, BJ Services, Nigeria Petroleum Development Company (NPDC), Nigeria National Petroleum Company (NNPC), and SBM Offshore. Attributes of the pipelines and a pipeline historical failure records sheet containing defining characteristics of the pipelines were made available to the experts with an AHP questionnaire.

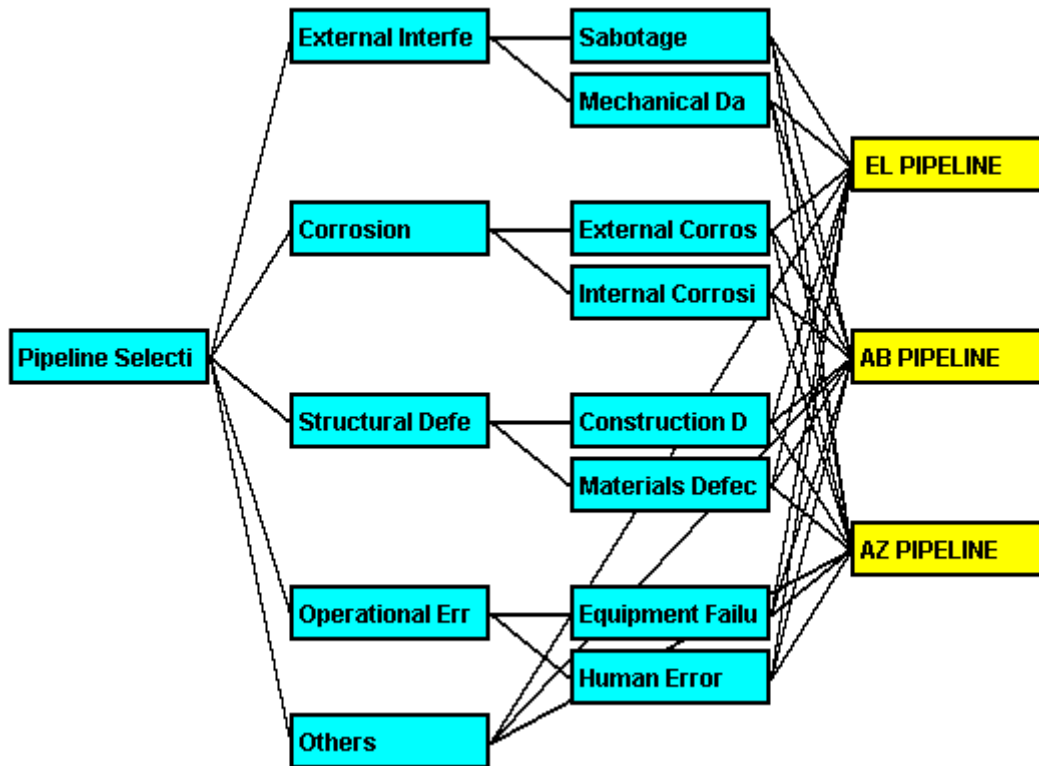
Tab 2: Summary of the attributes of Pipelines

Pipeline Attributes	EL PIPELINE	AB PIPELINE	AZ PIPELINE
Primary Service	Gas	Crude Oil	Crude Oil
Year of commission	1989	1996	2002
Type of Coating	Concrete Weight	Polykene Wrap	Polykene Wrap
Length	340km	4km	18km
Nominal Diameter	24"	4"	6"
Design Pressure	100bar	207bar	207bar

3.2 Construction of hierarchy

A hierarchy tree of the three pipelines is constructed using the Web-HIPRE software, J. Mustajoki and R.P.Hämäläinen (2000). The tree (fig. 3) contains information on the goal (Risk Based Pipeline selection), criteria (failure factors) and sub-criteria (sub division of failure factors). The decision alternatives are the three pipelines under consideration.

Fig. 3: Hierarchy tree for the risk assessment of EL Pipeline, AB Pipeline and AZ Pipeline



3.3 Results of Pairwise comparison

Individual expert opinion on the pairwise comparison of factors responsible for pipeline failures are separately collected and combined group wise using the geometric mean method, Aczel and Saaty (1983). The overall group weights for the failure factors are shown below in tab.3.

Tab. 3: Pair wise ranking of failure criteria and likelihood of failure of the three pipelines

Factors	Likelihood	Sub-Factors	Likelihood	EL Pipeline	AB Pipeline	AZ Pipeline
External Interference	0.607	Sabotage	0.525	0.271	0.179	0.076
		Mechanical Damage	0.081	0.051	0.019	0.011
Corrosion	0.214	External Corrosion	0.153	0.093	0.041	0.018
		Internal Corrosion	0.061	0.009	0.021	0.031
Structural Defects	0.066	Construction Defect	0.045	0.023	0.014	0.009
		Materials Defect	0.021	0.006	0.007	0.008
Operational Error	0.069	Equipment failure	0.050	0.009	0.018	0.024
		Human error	0.019	0.003	0.007	0.009
Others	0.044					

The overall consistency measure (CM) of the group matrix is 0.195 which is considered consistent with the 0.2 stated by R.P.Hämäläinen (2009).

Fig 4: Relative ranking of factors responsible for Pipeline Failure

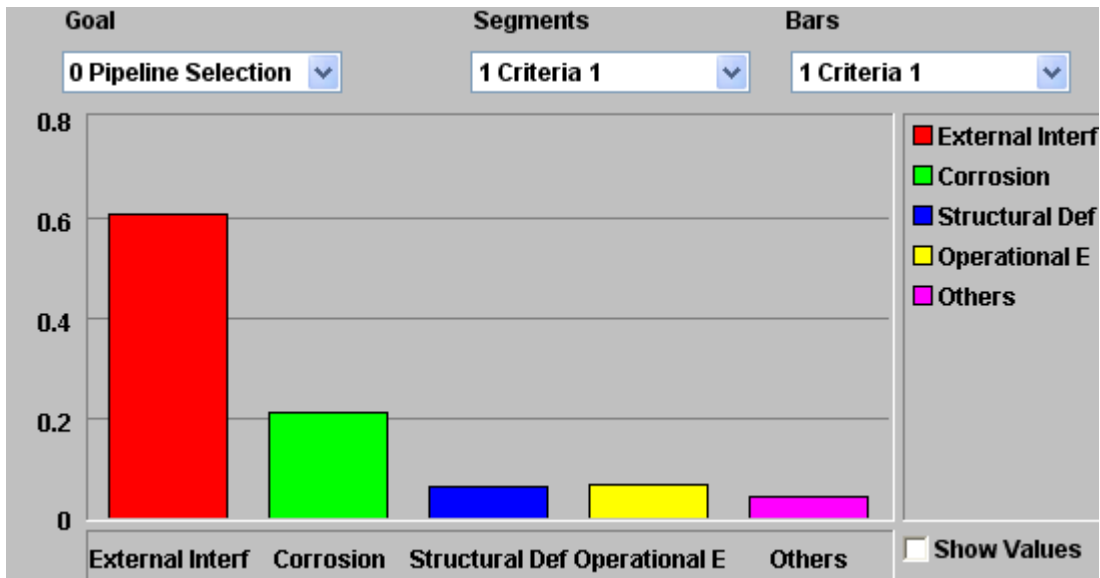
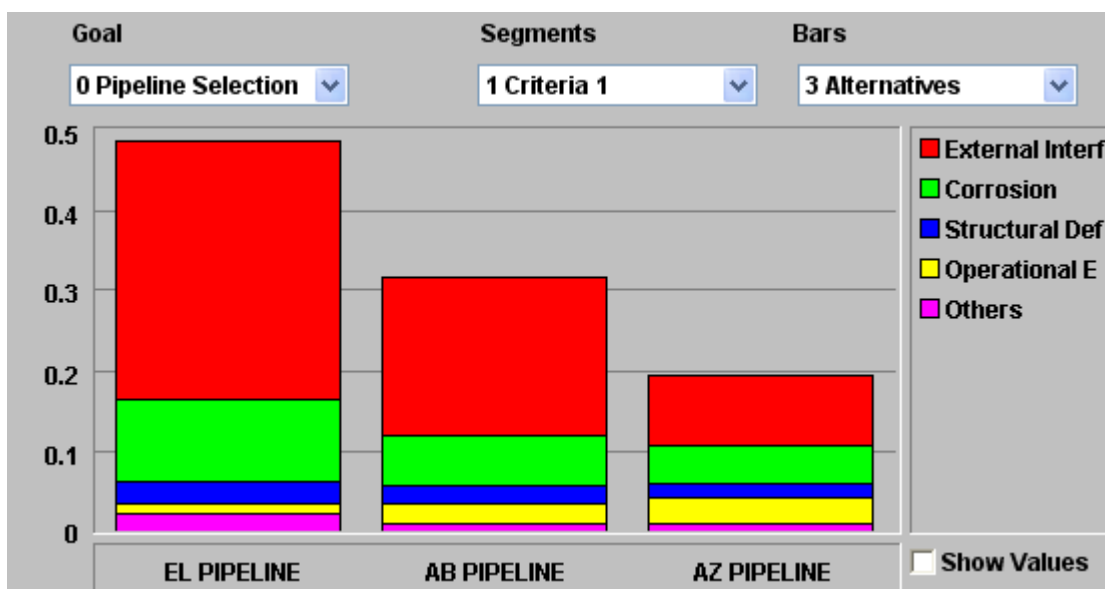


Fig 4 shows that the most significant failure criterion for the pipelines is external interference followed by corrosion, with relative likelihood of failure of 0.607 and 0.214 respectively.

Fig 5: Pairwise comparison of risk levels of EL Pipeline, AB Pipeline and AZ Pipeline



From Fig.5 it can be seen that sabotage remains the most significant failure criterion for the three pipelines. EL Pipeline is the most vulnerable among the three pipelines. This is expected considering its proximity to the Niger-Delta region of Nigeria.

3.4 Fault Tree analysis

The failure probability of petroleum pipeline is modelled as sum of failure probability due to external interference, corrosion, construction defect, operational errors and other minor failures.

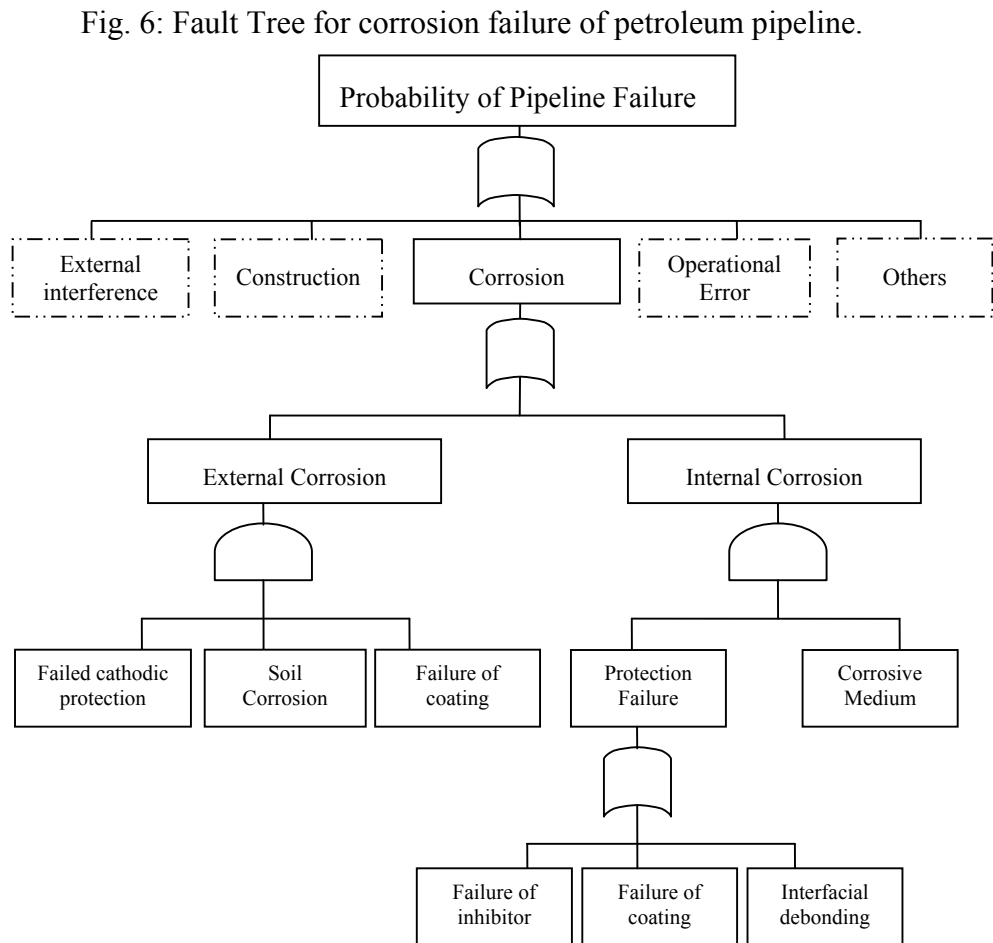
$$\begin{aligned}
 P(\text{Total failure of pipeline}) = & \\
 & P(\text{failure of pipeline due to corrosion}) + \\
 & P(\text{failure of pipeline due to external interference}) + \\
 & P(\text{failure of pipeline due to construction defect}) + \\
 & P(\text{failure of pipeline due to operational error}) + \\
 & P(\text{failure of pipeline due to other minor failures}) \tag{8}
 \end{aligned}$$

However, based on table 3, once the probability of failure of one of the factors is known, the total probability, $P(\text{Total failure of petroleum pipeline})$ can be determined.

For example, using

$$P(\text{failure of pipeline due to corrosion}) = 0.214 * P(\text{Total failure of pipeline}) \tag{9}$$

$P(\text{failure of pipeline due to corrosion})$ can be determined from parameters in the fault tree (Fig. 6). The outcome from Fault tree is a quantitative data which would be valuable information in determining individual or societal risk acceptance, Vrijling et al (2004).



4 Conclusions

This paper proposes a combined AHP-FTA methodology for risk assessment of cross country pipelines. We achieve a number of important conclusions.

A ranking methodology has been presented which uses available data and structured judgment to select operating pipeline based on the risk of failure. The results can be further used to achieve a quantitative risk analysis through the implementation of fault tree analysis. The approach is capable of reducing the rigour of quantitative risk analysis by focusing on the most important criteria.

The fault tree analysis of AHP Failure criterion would be further investigated in future works and be compared to available failure data. A major setback of the approach is the subjective nature of the AHP methodology and a structured expert judgement study will be investigated in the future.

References

- [1] J. Aczel, T.L. Saaty, "Procedures for synthesizing ratio judgements", *Journal of Mathematical Psychology* 27 (1983), pp 93 - 10
- [2] A. Adebayo, A.S Dada 2008 "An Evaluation of the causes of oil pipeline incidents In Oil and Gas Industries in Niger Delta Region of Nigeria", *J. Eng. Applied Sci.*, 3(3): pp 279-281
- [3] M Al-Khalil1 et al 2005 "Risk-Based Maintenance Planning of Cross-Country Pipelines", *J of Performance of Constructed Facilities*. Vol 19 No 2 pp 124-131.
- [4] E.N.Allouche and A.L. Bowman 2006 "Holistic Approach for Assessing the Vulnerability of Buried pipelines to Earthquake Loads", *Natural Hazards Review*. Vol 7 No 1 pp12-18
- [5] A.J. Brito and A.T de Almeida 2009, "Multiattribute risk assessment for risk ranking of natural gas pipelines", *Reliability Engrg and Sys Safety* 94 pp187-198
- [6] P.K Dey 2002 "Benchmarking project management practices of Caribbean organizations using analytic hierarchy process", *Benchmarking: An international journal*, Vol 9 No 4.
- [7] P K Dey et al 2004 "Risk -based maintenance model for offshore oil and gas pipelines: a case study", *Journal of Quality in Maintenance Engineering*, Vol. 10 Number 3 pp. 169-183.
- [8] R.P.Hämäläinen: "Introduction to Value theory analysis", *eLearning Resources*, System Analysis Laboratory, www.eLearning.sal.hut.fi (visited October 2, 2009)

- [9] Huipeng Li 2007, “Hierarchical Risk Assessment of water supply systems”, *PhD thesis, Loughborough University, Leicestershire, UK*
- [10] J. Mustajoki and R.P.Hämäläinen: “Web-HIPRE: Global decision support by value tree and AHP analysis”, *INFOR*, Vol. 38, no. 3, Aug. 2000, pp. 208-220
- [11] NEITI (2006) “Report on the process and audit 1999-2004 refineries and product importation”, Appendix A: Schematics, NEITI Nigeria.
- [12] NNPC 2008, “Annual Statistical Bulletin”, *Corporate Planning and Development Division (CPDD)*, NNPC, 2008.
- [13] C.N Nonis et al 2007 “Investigation of an AHP Based Multicriteria weighting scheme for GIS routing of cross country pipeline projects”, *24th int. sym. on aut. and rob. in constr.*
- [14] M.E. Quresh, S.R. Harrison 2003, “Application of the Analytical Hierarchy process to Riparian Revegetation Policy options”, *Small-scale Forest Economics, Mgt. and Policy* 2(3).
- [15] T.L. Saaty 1999, “The seven pillars of the Analytic Hierarchy Process”, in proc. *ISAHP*, Kobe.
- [16] L.P.E Yo-Essien 2008, “Oil Spill Management in Nigeria: Challenges of Pipeline Vandalism in the Niger Delta Region of Nigeria”, in Proc. Int. Petr. Env. Conf., 2008.
- [17] J.K. Vrijling et al 2004 “A framework for risk criteria for critical infrastructures: fundamentals and case studies in the Netherlands”, *Journal of Risk Research* 7 (6), pp 569–579.

Part VI

Probabilistic Modelling For Geotechnical Engineering

Updating piping probabilities with survived loads

Timo Schweckendiek^{1,2}, Wim Kanning¹

¹ Section of Hydraulic Engineering, Delft University of Technology, Delft, Netherlands

² Unit Geo-engineering, Deltares, Delft, Netherlands

Abstract: Piping, also called under-seepage, is an internal erosion mechanism, which can cause the failure of dikes or other flood defence structures. The uncertainty in the resistance of a flood defence against piping is usually large, causing high probabilities of failure for this mechanism. A considerable part of this uncertainty is of epistemic nature, which can be reduced by incorporating extra information. It is shown how the knowledge of historically survived water levels, the main load factor, can be integrated into the probability distribution of the piping resistance variables by means of Bayesian Updating. The effects are demonstrated by means of a realistic numerical example.

1 Introduction

Piping, also called under-seepage, is an internal erosion mechanism, which can cause the failure of dikes or other flood defence structures. This failure mechanism is particularly relevant for river dikes on sandy subsoil, typical conditions in flood protection systems in delta areas. In recent years, the issue of piping received special attention in the Netherlands. Results from the FLORIS (FLOod Risks and Safety in the Netherlands) project, a nation-wide flood risk analysis applying a reliability analysis to the entire flood defence system, indicate that in some regions the probability of failure due to piping is very high, far greater than acceptable. A large part of the uncertainty causing these high probabilities of failure stem from knowledge (epistemic) uncertainty in the piping resistance and the subsoil conditions. This uncertainty can, in principle, be reduced by incorporating extra information. This paper deals with one specific source of information, the knowledge of historically survived load conditions. A survived load can be interpreted as an incomplete load test. This knowledge can be integrated into the probability distribution of the piping resistance variables by means of Bayesian Updating. The effects are demonstrated by means of a realistic numerical example.

2 Bayesian Updating based on survived loads

2.1 Bayesian Updating

Let Θ be the random variable for the parameter of a distribution of the quantity of interest X , with a *prior* PDF $f_{\Theta}(\theta)$. Based non the evidence ϵ the *posterior* distribution can be determined by Bayes' theorem (Bayes [2]):

$$f_{\Theta}(\theta|\epsilon) = \frac{P(\epsilon|\theta)f_{\Theta}(\theta)}{\int_{-\infty}^{\infty} P(\epsilon|\theta)f_{\Theta}(\theta)} \quad (1)$$

where $P(\epsilon|\theta)$ is the probability of observing the evidence, given parameter $\Theta = \theta$, also called the *likelihood* $\mathbb{L}(\theta)$. Eq. (1) may also be written in simplified form with the inverse of the denominator expressed as normalizing constant k :

$$f_{\Theta}(\theta|\epsilon) = k\mathbb{L}(\theta)f_{\Theta}(\theta) \quad (2)$$

The uncertainty in the estimation of the parameter can be included in the calculation of the probability of the quantity of interest X . By “integrating out” the uncertainty in θ , we obtain a composite distribution, the so called *Bayesian distribution* of X :

$$\tilde{f}_X(x) = \int_{-\infty}^{\infty} f_X(x|\theta)f_{\Theta}(\theta)d\theta \quad (3)$$

Thus, using $f_{\Theta}(\theta|\epsilon)$ in Eq. (3) results in the updated Bayesian distribution of X . It is emphasized that, in contrast to frequentist approaches, the Bayesian distribution includes both, aleatory and epistemic uncertainties. Therefore, the variance (spread) of such a distribution is in general larger than the variance of the “true” distribution $f_X(x)$, and therefore probably larger than frequentist estimates of the variance. For the remainder of this paper, the Bayesian distribution $\tilde{f}_X(x)$ is used to account for the (total) uncertainty in X in uncertainty, reliability or decision analyses. For sake of simplicity, in the following the tilde is omitted and the distribution of X is just referred to as $f_X(x)$. For a more detailed discussion and examples it is referred to Benjamin and Cornell [3], Ang and Tang [1] and Tang [7].

2.2 Likelihood based on survived loads

Analogue to Bayesian parameter estimation survival analysis, the likelihood function of resistance parameters based on a survived load condition is the probability of survival or non-failure, given the survived load and the parameters. The load may be univariate and known exactly in the simplest case, it may also be a load combination (multivariate) and uncertain, e.g. due to measurement, transformation or model uncertainties.

To give an insightful example, contemplate the simple case of the *limit state function* $Z = R - S$ (R = resistance, S = solicitation or load). The likelihood function of R , given the historically survived load S^* can be formulated as:

$$\mathbb{L}(\theta) = P(R > S^*) = 1 - F_R(S^*|\theta) \quad (4)$$

More generally, for a *limit state function* $Z = g(\mathbf{X})$, where \mathbf{X} is the vector of random variables with parameters θ , the likelihood function is given by the probability of Z assuming positive values, given the survived load S^* :

$$\mathbb{L}(\theta) = P(Z > 0|\theta, S^*) = 1 - P_{f|\theta, S^*} = 1 - \int_{-\infty}^{\infty} I_{Z < 0} f_{\mathbf{X}}(\mathbf{x}) d\mathbf{x} \quad (5)$$

where $I_{(\cdot)}$ is the indicator function. Thus, determining the likelihood function requires solving a classical structural reliability problem, conditional on the observed load for the feasible range of resistance parameters. The prior information on either R or \mathbf{X} , respectively on their distributions parameters, may stem from either engineering or expert judgment or from any other source of data, such as measurements of load and strength properties.

3 Application to piping

3.1 Simple piping model

To illustrate the concept described above and its effects on reliability considerations, the piping model first established by Bligh [4] is adopted (see Fig. 1).

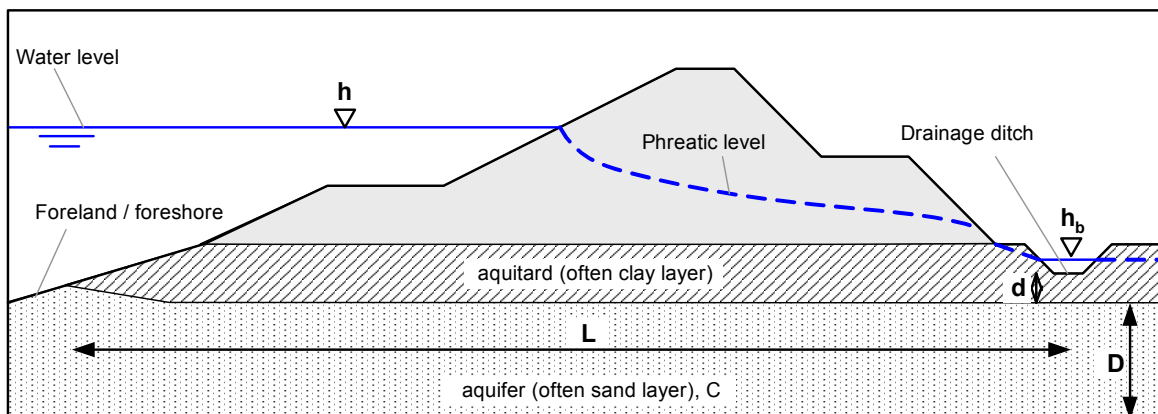


Fig. 1: Illustration of schematic geometry and parameters for heave and piping

The limit state function (LSF) for the adopted model is given by:

$$Z = L - m_C C(h - h_b - 0.3d) \quad (6)$$

with	L	piping length [m]
	C	Bligh's Creep parameter [-] (erosion resistance)
	m_C	factor for model uncertainty associated with C
	h	water level (main load) [m+NAP]
	h_b	landside water level [m+NAP]
	d	thickness of aquitard at exit point [m]

The formulation is similar to Steenbergen and Vrouwenvelder [6], re-written in a form that is linear in all parameters. Using this piping model, we implicitly make the following assumptions:

- If the maximum head difference exceeds the critical head difference, failure occurs (i.e., time-dependent effects in the piping mechanism are disregarded).
- No cumulative effect, i.e. there is no cumulative damage or “fatigue” effect.
- Piping can occur directly, i.e. there is no dependence on other mechanisms such as uplift. This assumption is realistic in the absence of blanket layers or for thin blanket layers with very low uplift resistance.

3.2 Uncertainties in piping resistance

Tab. 1 shows design values C_d of the piping resistance parameter C for different soil types according to TAW [8].

Tab. 1: Creep factors for piping rules

Soil type	Median grain diameter [μm] ¹	C_d (Bligh) [-]
Silt	< 105	
Very fine sand	105 – 150	18
Very fine sand (mica)		18
Medium-fine sand (quartz)	150 – 210	15
Medium-coarse sand	210 – 300	
Very coarse sand	300 – 2000	12
Fine gravel	2000 – 5600	9
Medium-coarse gravel	5600 – 16000	
Very coarse gravel	> 16000	4

¹indications in accordance with NEN 5104 (September 1989)

The modeling of uncertainties in piping resistance for this study is adopted from the FLORIS project (VNK) in the Netherlands (Rijkswaterstaat [5]). Since the tabulated design values C_d are conservative by definition, it is assumed that the underlying distribution of the uncertain variable has a lognormal distribution with moments $C \sim LN(\mu_C, \sigma_C)$ with $\mu_C = C_d/1.5$ and $\sigma_C = 0.1 C_d = 0.15\mu_C$ (c.o.v. of 15 %).

In order to account for the model uncertainty related to C , a model factor m_C is used (multiplicative model). It expresses the imperfection of C to represent the resistance against piping; even knowing the values of all resistance variables including C exactly, one could not predict the critical head difference with certainty. Its distribution is assumed to be $m_C \sim N(1, 0.15)$.

The other resistance variable, the piping length L is commonly modeled by means of a Normal distribution, too. The mean value is based on measurements or “educated guesses”, best on the data available of geometry and subsurface. A realistic value to account for the uncertainty in the piping length is a c.o.v. of 10%, resulting in $L \sim N(\mu_L, 0.1 \mu_L)$. One could also count d (thickness of the blanket layer) to the resistance variables in the piping performance function. In the examples treated in this paper d is treated deterministically.

4 Numerical Example

The concept described above is illustrated by means of a numerical example. The chosen parameters are realistic and very similar to the real data of a location in the Eastern part of the Netherlands. The a-priori parameters are shown Tab. 2. In the subsequent sections, modifications of this case are presented and the varying assumptions are defined at the beginning of each section.

Tab. 2: A-priori parameters (NAP = Normaal Amsterdams Peil: reference level)

Variable	Distribution	Parameters / moments
C [-]	Lognormal	$\mu_C = 15.0$ $\sigma_C = 2.0$
m_C [-]	Normal	$\mu_{m_C} = 1.0$ $\sigma_{m_C} = 0.15$
L [m]	Normal	$\mu_L = 30.0$ $\sigma_L = 3.0$
h [m+NAP]	Gumbel	$\alpha = 8.27$ $\beta = 0.406$
h_b [m+NAP]	deterministic	$h_b = 7.5$
d [m]	deterministic	$d = 0.8$

In the subsequent examples it is assumed that a water level with a 100 year return period of $h^* = 10.14$ [m+NAP] has been observed and no piping failure has occurred.

4.1 One uncertain resistance variable (case 1)

For sake of illustration, the first case is simplified with respect to the general case. Only C is considered uncertain on the resistance side, L and m_C are considered deterministic with their respective mean values. In order to be able to compare the cases, the standard deviation of C is chosen as $\sigma_C = 3.0$, which can be shown is approximately equivalent to the combined distribution of $m_C \cdot C$ with their original parameters from Tab. 2. The uncertainty in C is assumed to be of epistemic nature and can, in principle be reduced. It is noted that these assumptions were only made for sake of illustration and are not realistic.

The likelihood function of C can be formulated as:

$$\mathbb{L}(C) = P(Z > 0|\epsilon) = P(L - m_C C (h^* - h_b - 0.3d) > 0|C) \quad (7)$$

Since C was the only variable considered random in this case, the likelihood function is deterministic may be re-written as:

$$\mathbb{L}(C) = \begin{cases} P(Z > 0|C) = 1 & \text{if } C < C_c \\ P(Z > 0|C) = 0 & \text{if } C \geq C_c \end{cases} \quad (8)$$

with $C_c = L/(h^* - h_b - 0.3 * d) =$ critical Bligh parameter [-]

In other words, the survival of h^* has proven that C must be smaller than C_c . Fig. 2 illustrates that the observed water level had a low yearly exceedance probability (1 %) and that the critical (i.e. “proven”) resistance value was relatively high (low C values mean high resistance). That implies that a large part of the probability mass of C can be redistributed, in fact the part with values greater than $C_c = 12.51$ [-].

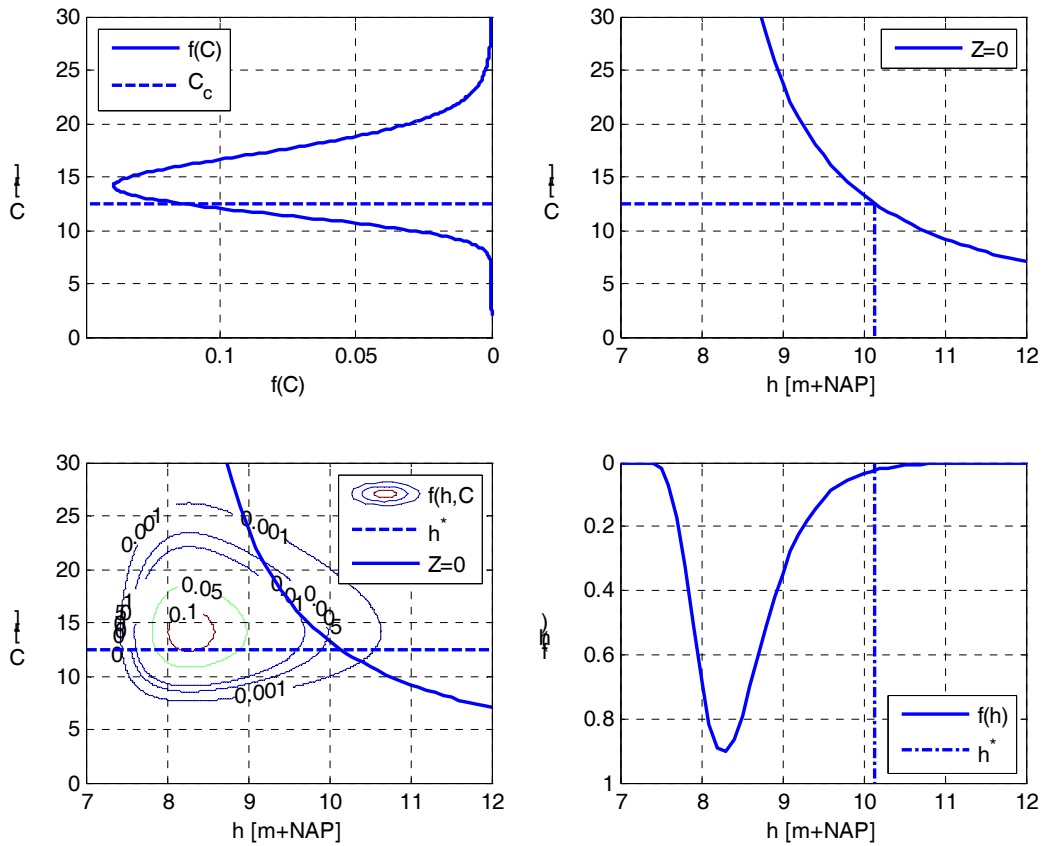
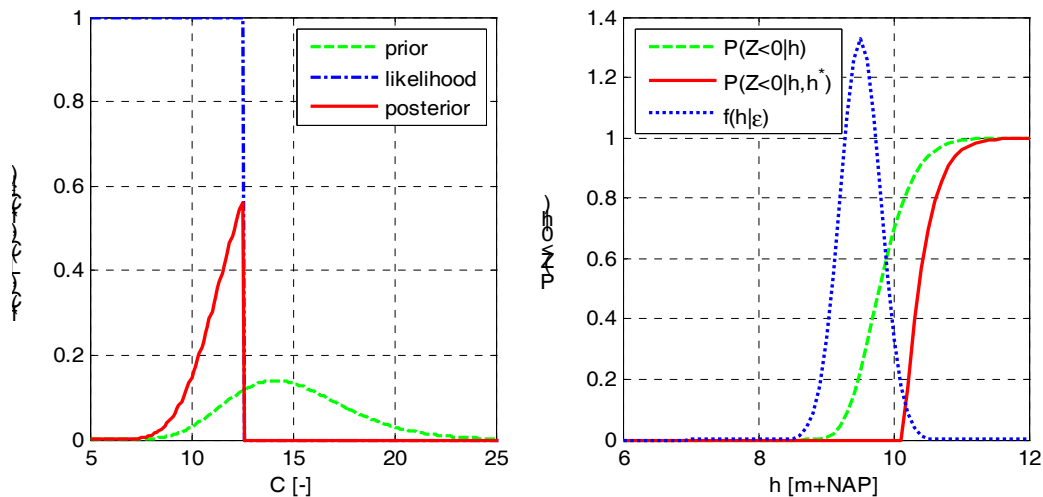


Fig. 2: Prior $f(h,C)$, observed water level, and critical C (case 1)

The effect of updating can be appreciated in the posterior distribution of C (see Fig. 3 (a)) and the updated fragility curve ($P\{Z < 0|h\}$). In fact, the posterior distribution of C is the prior distribution truncated at C_c (and normalized).



(a) Prior and posterior distribution of C (b) Prior and posterior fragility curves

Fig. 3: Updated distribution of C and fragility curves (case 1)

In Fig. 3 (b), an example of a short term prediction with expectation $E[h|\epsilon] = 9.5$ [m+NAP] and standard prediction error of $\sigma_{h|\epsilon} = 0.3$ [m] (typical for about 3 days lead time on rivers)

was plotted together with the fragility curves in order to appreciate the impact of the updating procedure on short-term predictions.

There is also an effect of the updated resistance on the reliability. As indicated in Tab. 3, the probability of failure using the water level distribution of the yearly maxima (long-term) decreases by a factor of 5. The effect on the short-term reliability with the scenario of a water level prediction as in Fig. 3 is even much more significant, though for water level predictions higher than the observed survived level the effect may vanish.

Tab. 3: Prior and posterior probabilities of failure (case 1)

		with $f(C)$	with $f(C \epsilon)$
with $f(h)$ (long-term)	Probability of failure P_f	3.1 E-2	6.1 E-3
	Reliability index β	1.86	2.51
with $f(h \epsilon)$ (short-term)	Probability of failure P_f	2.8 E-1	4.1 E-3
	Reliability index β	0.59	2.63

4.2 One uncertain resistance variable and model uncertainty (case 2)

In the second case, model uncertainty is added as uncertainty, whilst the piping length L is still treated deterministically. As mentioned, with the parameters in Tab. 2, the aggregate uncertainty of $m_C \cdot C$ is practically equivalent to the uncertainty of C in the previous case. This way the results can be compared well.

When several uncertain variables or parameters are involved, one has to be careful with the definition of the likelihood function. The basic question is, which variables can be updated and which ones cannot. E.g. epistemic uncertainties can be updated, whilst intrinsic uncertainties cannot. In this particular example, the fact of survival provides information about the actual value of C , whilst it does not provide information on the model uncertainty. In fact, the model uncertainty weakens the effect of updating C . The likelihood function is again:

$$\mathbb{L}(C) = P(Z > 0|\epsilon) = P(L - m_C C (h^* - h_b - 0.3d) > 0|C) \quad (9)$$

However, in this case, it is a stochastic function, since m_C is uncertain. The likelihood function and the posterior distribution are shown in Fig. 4 (a). The same figure also shows that the posterior distribution is well described by a lognormal distribution with moments $\mu_{C|\epsilon} = 13.4$ and $\sigma_{C|\epsilon} = 1.54$ (Fig. 4). The impact on the probability of failure is much less compared to case 1 (see Tab. 4), this is mainly due to the (irreducible model uncertainty).

Tab. 4: Prior and posterior probabilities of failure (case 2)

		with $f(C)$	with $f(C \epsilon)$
with $f(h)$ (long-term)	Probability of failure P_f	3.1 E-2	1.8 E-2
	Reliability index β	1.86	2.09
with $f(h \epsilon)$ (short-term)	Probability of failure P_f	2.8 E-1	1.4 E-1
	Reliability index β	0.59	1.08

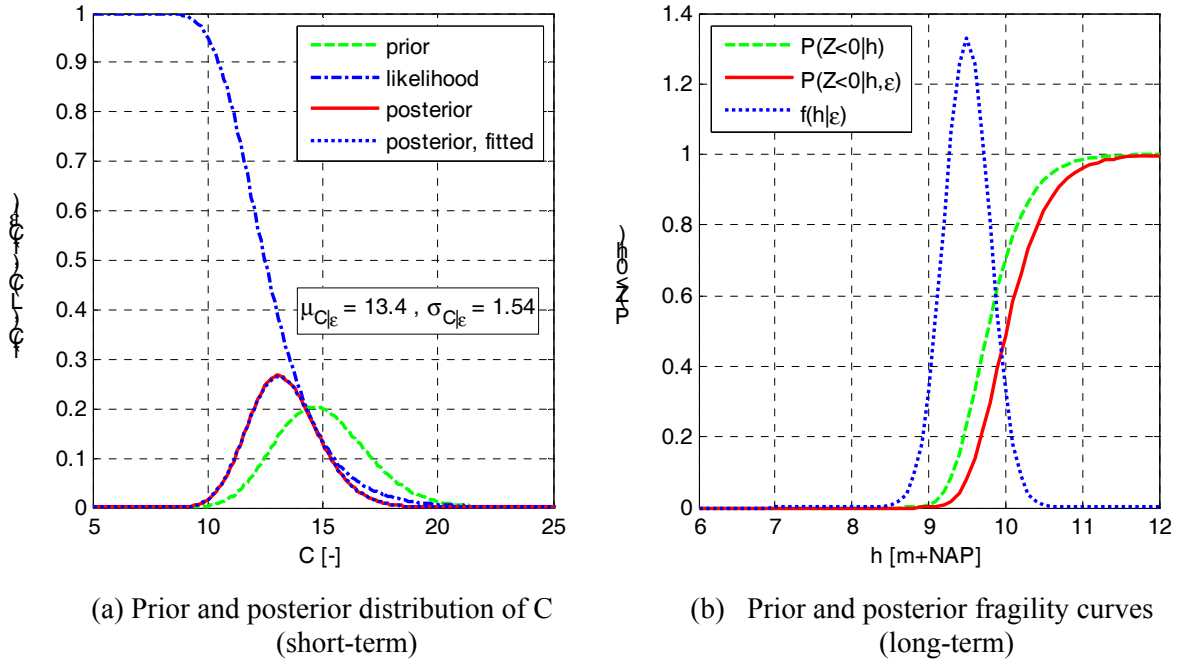


Fig. 4: Updated distribution of C and fragility curves (case 2)

The effect on the fragility curve in Fig. 4 is much less for the present case with model uncertainty, which is also reflected in the lesser impact on the short-term reliability in Tab. 4.

4.3 Two uncertain resistance variables (case 3)

In the third case, two uncertain resistance variables, C and L are considered, whilst model uncertainty is disregarded ($m_C = 1$, deterministic). The aggregate uncertainty in C and L is again comparable to the previous cases, so the impact on the reliability can be compared, too. The uncertainty in C and L is assumed to be purely epistemic, similar to case 1, however in this case the likelihood function is two-dimensional:

$$\mathbb{L}((C, L) = P(Z > 0 | \epsilon) = P(L - m_C C (h^* - h_b - 0.3d) > 0 | C, L) \quad (10)$$

Without model uncertainty, a line can be determined, given the survived water level, that separates the combinations of C and L that should have failed under this loading from those that are still possible. This is illustrated in Fig. 5 (a). The parameter combinations on the upper left hand side of the limit state line ($Z = 0 | h^*$) have practically been proven to be impossible, given the observation of survival. In the Bayesian Updating process this probability mass is re-distributed to the lower right hand side (see Fig. 5 (b)), as becomes also clear by rewriting the deterministic likelihood function in the following form:

$$\mathbb{L}(C, L) = \begin{cases} P(Z > 0 | C) = 1 & \text{if } L/C < (h^* - h_b - 0.3d) \\ P(Z > 0 | C) = 0 & \text{if } L/C \geq (h^* - h_b - 0.3d) \end{cases} \quad (11)$$

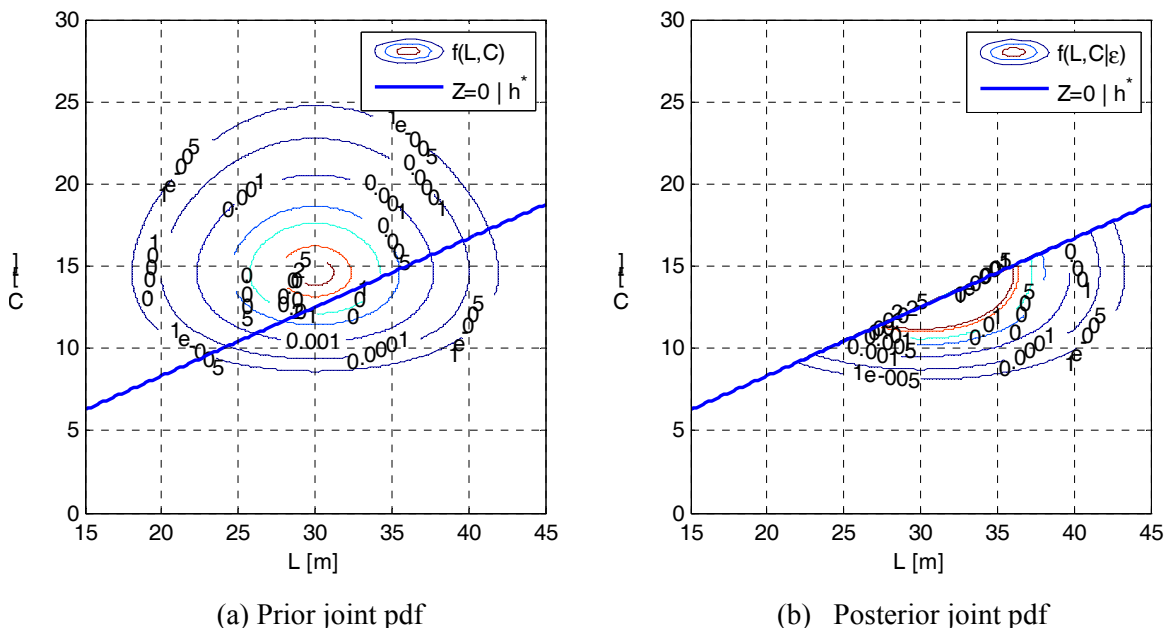


Fig. 5: Prior and posterior joint probability density of C and L

Having determined the posterior joint probability density, we can determine the posterior marginal distributions of C and L (in general: $f_X(x) = \int_y f_{X,Y}(x,y)dy$), see Fig. 6. The posterior moments differ significantly from the prior ones.

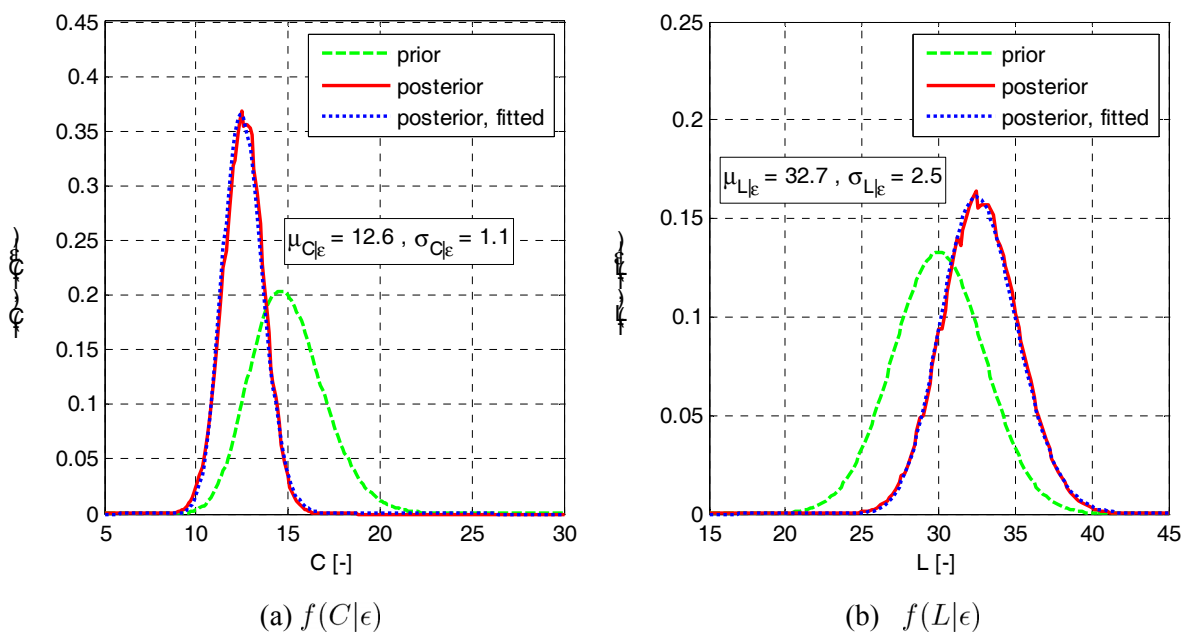


Fig. 6: Posterior marginal distributions of C and L (case 3)

Using the posterior distributions, one has to be very careful, since the posterior marginal distributions are not independent anymore, even though the prior marginal distributions were assumed to be independent. The safest way to use the updated information in further analyses is using the joint pdf directly, whether it has been determined numerically or by simulation (e.g. Markov Chain Monte Carlo). If that is not possible, the correlation structure has to be taken care of in any other suitable manner.

In the current analysis, the posterior reliability analyses have been carried out using numerical integration of the joint pdf $f(C, L|\epsilon)$ (fourth column in Tab. 5). In order to demonstrate the error using independent marginal distributions, these results are given in the last column of the same table ($f(C|\epsilon)f(L|\epsilon)$).

Tab. 5: Prior and posterior probabilities of failure (case 3)

		with $f(C, L)$	with $f(C, L \epsilon)$	with $f(C \epsilon)f(L \epsilon)$
with $f(h)$ (long-term)	Probability of failure P_f	3.1 E-2	6.4 E-3	7.5 E-3
	Reliability index β	1.86	2.49	2.43
with $f(h \epsilon)$ (short-term)	Probability of failure P_f	2.8 E-1	5.5 E-3	
	Reliability index β	0.59	2.54	

It is remarkable that the posterior probabilities of failure, i.e. the effects of updating the resistance variables, are practically the same as in case 1. This can be explained by the fact that, on the one hand, the aggregate uncertainty in the resistance was practically equal, and, on the other hand, despite of having two uncertain variables in the absence of model uncertainty we could assign probability zero to some regions of the parameter space of C and L , just as in case 1.

Also the effect on the fragility curve (see Fig. 7) is very much similar to case 1 due to the same reasons. This is also reflected in the posterior values for short term reliability (water level prediction) in Tab. 5.

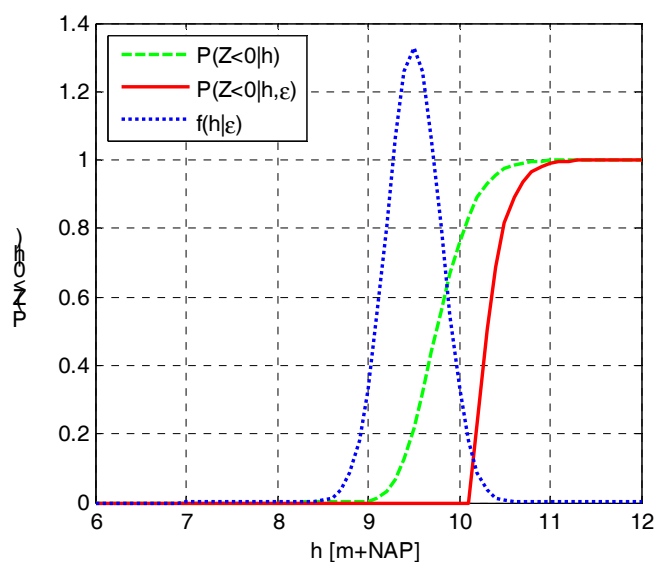


Fig. 7: Prior and posterior fragility curves (case 3)

4.4 Two uncertain resistance variables and model uncertainty (case 4)

In the last case, all random variables are treated as uncertain as specified at the beginning of this section. Notice that the total uncertainty is different and that the results cannot be compared to the previous cases directly anymore.

The likelihood function is the same as in the previous case 3 (eq. 10), however, in this case it is a stochastic function. In the previous case, the likelihood function distinguished sharply between zero and one probability, in the current case it is a smooth function (see Fig. 8 (a)).

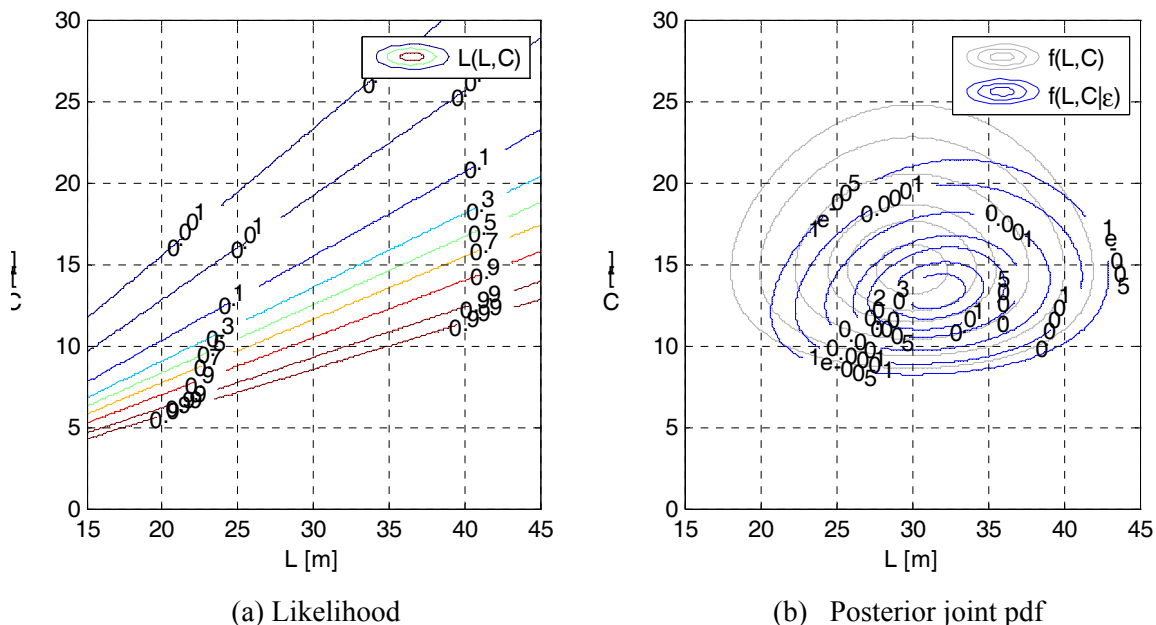


Fig. 8: Contours of likelihood function and posterior distribution (case 4)

The posterior marginal distributions and their statistical moments are displayed in Fig. 9. Neither the shift in mean value nor the decrease in variance is as significant as in case 3. The model uncertainty weakens the updating effect, as already shown in case 2.

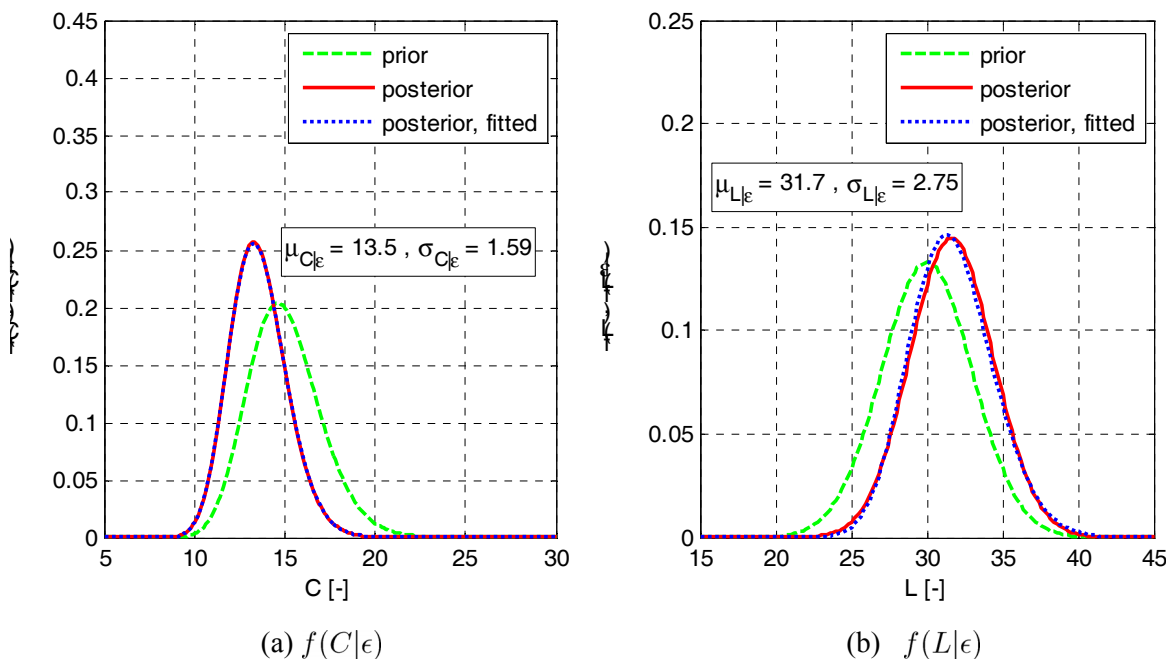


Fig. 9: Posterior marginal distributions of C and L (case 4)

The posterior marginal distributions again follow well their original distribution types.

Tab. 6: Prior and posterior probabilities of failure (case 4)

		prior	posterior
with $f(h)$ (long-term)	Probability of failure P_f	3.7 E-2	1.6 E-2
	Reliability index β	1.79	2.13
with $f(h \epsilon)$ (short-term)	Probability of failure P_f	2.9 E-1	1.1 E-1
	Reliability index β	0.54	1.20

The effect on the reliability is similar to case 2 (see Tab. 6), even though the two cases are not perfectly comparable anymore due to the difference in total (aggregate) prior uncertainty. Differences could be due to the accuracy of the numerical solution procedure. The same holds for the fragility curves presented in Fig. 10.

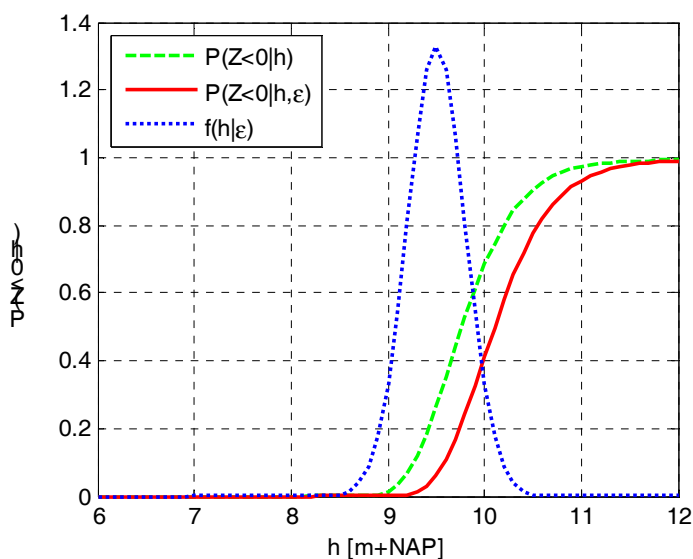


Fig. 10: Prior and posterior fragility curves (case 4)

Notice that so far all calculations have been carried out mainly by means of numerical integration techniques. The last case is a four-dimensional problem and requires already considerable calculation effort and computer memory. Higher dimensional problems might require the use of alternative techniques, such as Markov Chain Monte Carlo sampling.

5 Conclusions and outlook

Bayesian statistics have been applied to update the probability distributions of resistance variables based on survived load conditions in a structural reliability problem. The key to the problem is establishing a suitable likelihood function. This is usually the probability of survival or non-failure, given the observed load, which itself may be uncertain e.g. due to measurement errors. From the simplified numerical example we can conclude that in the most simplified and rather artificial form (case 1: only epistemic uncertainty in one resistance variable, certain load observation) the impact of updating is significant. In the more realistic cases including model uncertainty, the effect of updating is much less pronounced. It is interesting to see that the number of variables to be updated itself does not influence

the effect of updating, if the total variance is kept the same, only intrinsic or non-reducible uncertainties like the model uncertainty in cases 2 and 4 do. The more uncertainty of the latter type is present in a problem, the lesser the value of information of survival of observed load. The updated fragility curves show that the effect may still be interesting for operational forecasting purposes, when the short-term expectation of the load is still below the observed survived load.

The presented approach is currently being extended to come to a more comprehensive and realistic assessment and updating for the piping mechanism. Aspects to be included in the near future are combined failure due to uplift and piping, geological anomalies (probability of weak spots), spatial variability or more specific observations regarding the occurrence of uplift and piping mechanisms (e.g. water and sand boils). Furthermore, the approach is not restricted to survival observations, is also suitable for any kind of measurement or observation, for which we can establish a likelihood function of the resistance variables.

6 References

- [1] Ang, A.H.-S. and W.H. Tang, *Probability Concepts in Engineering*. 2nd edition ed. 2007, New York: Wiley.
- [2] Bayes, T., *An Essay towards solving a Problem in the Doctrine of Chances*. Philosophical Transactions of the Royal Society of London, 1763. **53**: p. 370-418.
- [3] Benjamin, J.R. and C.A. Cornell, *Probability, Statistics and Decision for Civil Engineers*. 1970, New York: McGraw-Hill.
- [4] Bligh, W.G., *Dams, barrages and weirs on porous foundations*. Eng. News, 1910. **64**(Dec.): p. 708.
- [5] Rijkswaterstaat, *Flood Risks and Safety in the Netherlands (Floris)*. 2005.
- [6] Steenbergen, H.M.G.M. and A.C.W.M. Vrouwenvelder, *Theoriehandleiding PC-Ring - Deel A: Mechanismebescrijvingen (2003-CI-R0020)*. 2003, TNO Bouw: Delft, The Netherlands.
- [7] Tang, W.H., *A Bayesian Evaluation of Information for Foundation Engineering Design*, in *International Conference on Applications of Statistics and Probability to Soil and Structural Engineering*. 1971, Hong Kong University Press: Hong Kong.
- [8] TAW, *Technical Report on Sand Boils (Piping)*. 1999, Technical Advisory Committee on Flood Defences: Delft, The Netherlands. p. draft English version, August 2002 (original in Dutch).

Contributions to probabilistic soil modelling

Maximilian Huber¹, Axel Moellmann¹, András Bárdossy², Pieter A. Vermeer¹

¹University of Stuttgart, Institute of Geotechnical Engineering,
Pfaffenwaldring 35, 70569 Stuttgart, Germany

²University of Stuttgart, Institute of Hydraulic Engineering,
Department of Hydrology & Geohydrology Pfaffenwaldring 35, 70569 Stuttgart, Germany

Abstract: In order to capture the varying soil properties, the EUROCODE 7 offers different methods. The most general possibility to incorporate soil variability is the fully probabilistic approach. However, the probabilistic characterisation of the soil is crucial. Within this contribution, basics of describing spatial soil variability are presented. The results of experiments to evaluate soil variability are compared to results presented in literature. Furthermore, a case study has been carried out using the random finite element method.

1 Soil Variability

Geological processes and man-made influences cause fluctuations of properties within soil layers. Several researchers have investigated this soil variability in their work. PHOON & KULHAWY categorised the uncertainty of soil properties in their work [21, 22] in order to model soil variability. Similar investigations have been carried out by other researchers like BAECHER & CHRISTIAN [4], ORR [18], ASOAKA & GRIVAS [3], POPESCU [23], VANMARCKE [33] and many others.

1.1 Random fields

In this contribution random fields are used to describe spatial variability as presented by VANMARCKE [32] or BAECHER & CHRISTIAN [4]. According to BAECHER & CHRISTIAN [4] the application of random field theory to geotechnical issues is based on the assumption that the spatially variable of concern is the realization of a random field, which can be defined as a joint probability distribution [8].

The spatial dependency of a random field can be expressed via an autocorrelation function $\rho(\tau)$. Herein τ is the lag between the points. If a random field X_i has mean μ_X and variance σ_X^2 then the definition of the autocorrelation $\rho(\tau)$ is as shown in equation (1). Herein $E(X)$ is the expected value operator.

$$\rho(\tau) = \rho(-\tau) = \frac{E[(X_i - \mu_X) \cdot (X_{i+\tau} - \mu_X)]}{\sigma_{X_i} \cdot \sigma_{X_{i+\tau}}} \quad (1)$$

To make things more general, one can also compare the ranks of a series instead of the single values of a random field. This concept is a more general concept in analyzing spatial patterns. The interested reader is referred to HOLLANDER & WOLFE [14] and JOURNAL & HUIJBREGTS [16].

If the autocorrelation function only depends on the absolute separation distance of \mathbf{x}_i and \mathbf{x}_j the random field is called isotropic. Another assumption is ergodicity. Ergodicity means that the probabilistic properties of a random field can be completely estimated from observing one realization of that field [26]. Like for many approaches in Natural Sciences, stationarity is an assumption of the model, and may only be approximately true. Also, stationarity usually depends upon scale. According to BAECHEER & CHRISTIAN [4], within small region, such as a construction site, soil properties may behave as if drawn from a stationary process; whereas, the same properties over a larger region may follow this assumption. By definition, autocorrelation functions are symmetric and bounded. Another assumption is the separability of the autocovariance function according to VANMARCKE [32]. Separable autocovariance function can be expressed as a product of autocovariance of lower dimension fields. VANMARCKE [32] as well as RACKWITZ [26] offer various models for autocorrelation functions.

1.2 Geostatistics

In the field of geostatistics the spatial dependence is described via a so called variogram. The so-called semivariance γ is defined as the expected squared increment of the values between two locations according to WACKERNAGEL [35]. For practitioners BAKER ET AL. [5] describes explains the variogram in equation 2.

$$\gamma(\tau) = \frac{1}{2 \cdot n} \sum_i^n (f(x_i) - f(x_i + \tau))^2 \quad (2)$$

In Fig. 1 the correlation distance is introduced. Within the correlation distance two points are correlated according to the autocorrelation function or variogram. VANMARCKE [32] quantifies a correlation structure via the so-called scale of fluctuation. This scale of fluctuation is defined as an integral over the whole length from minus to plus infinity.

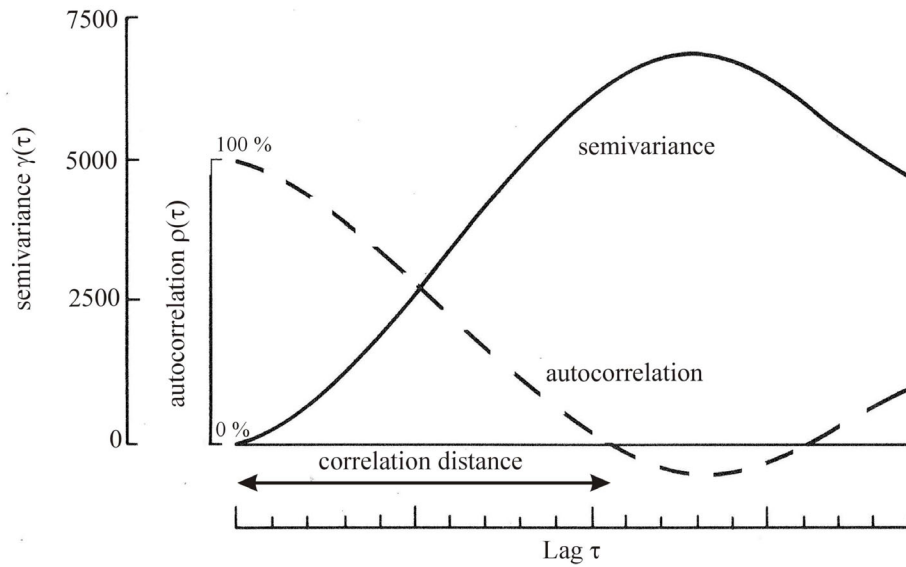


Fig. 1: Relationship between semivariance and autocorrelation according to CLARK [9]

1.3 Consideration of variability in geotechnical design

EUROCODE 7 [19] offers different methods of calibrating partial safety factors for solicitation and resistance to incorporate soil variability as shown in Fig. 2. The full probabilistic analysis is the most general and accurate method.

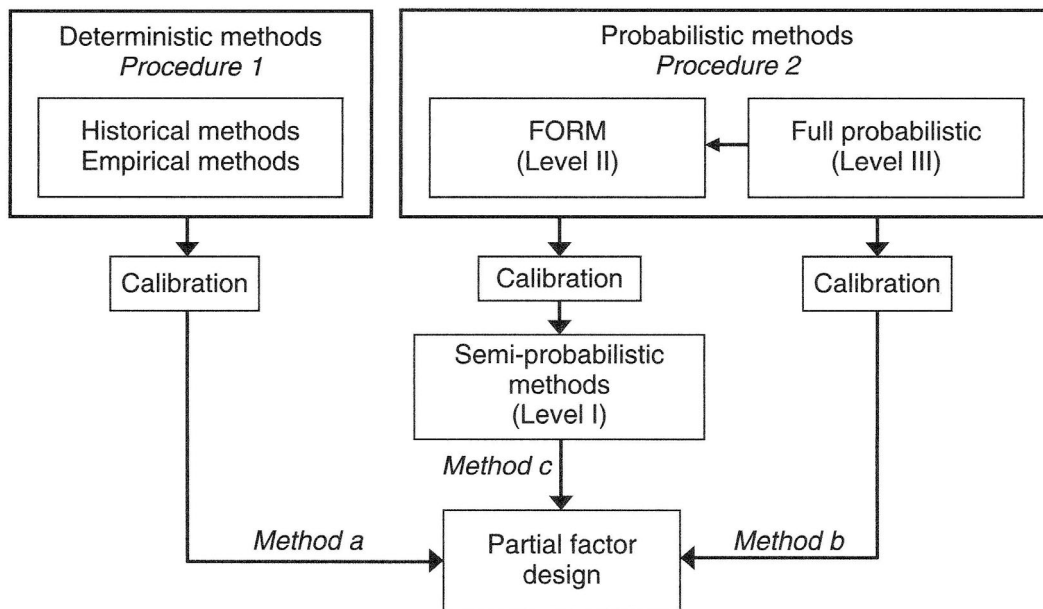


Fig. 2: Overview of the use of reliability methods in EUROCODE 7 [20]

2 Evaluation of spatial variability

In order to apply probabilistic models for reliability analysis in geotechnics one has to characterize soil in a probabilistic way. PHOON & KULHAWY [21, 22] evaluated geotechnical properties on an exhaustive data set. Their emphasis was on describing a coefficient of variation. The coefficient of variation describes the relationship between standard deviation and mean of property. A fruitful literature review resulted in the Tab. 1. Specifications from BAKER ET AL. [5] have been updated with other sources as shown in Tab. 1.

Tab. 1: Summary of autocorrelation distances

Source		Correlation distance θ
ASOAKA & GRIVAS [3]	Undrained shear strength	$\theta_v = 2.5 - 6.0$ m
MULLA [17]	Penetrometer resistance	$\theta_h = 40.0 - 70.0$ m
RONOLD [28]	Shear strength	$\theta_v = 2.0$ m
UNLU ET AL. [31]	Permeability	$\theta_h = 12.0 - 16.0$ m
SOULIE ET AL. [29]	Shear strength	$\theta_v = 2.0$ m $\theta_h = 20.0$ m
REHFELD ET AL. [27]	Permeability	$\theta_v = 3.2$ m $\theta_h = 25.0$ m
HESS ET AL. [12]	Permeability	$\theta_v = 0.2 - 1.0$ m $\theta_h = 2.0 - 10.0$ m
CHAISSON ET AL. [7]	Cone resistance	$\theta_v = 1.5$ m
VROUWENVELDER & CALLE [34]	Cone resistance	$\theta_h = 20 - 35$ m
POPESCU ET AL. [25]	Cone resistance	$\theta_v = 0.8 - 1.8$ m
JAKSA ET AL. [15]	Dilatometer	$\theta_h = 0.5 - 2.0$ m

2.1 Experiments for evaluating variability

One can deduce from studying Tab. 1 that most of the investigations have been carried out in terms of cone resistance and permeability. By studying the publications it turns out that the investigations have mainly been carried out in clay and in sandy soils. In order to gain more knowledge in probabilistic characterisation of soil and rock and to apply fully probabilistic calculations as proposed in the EUROCODE [19], experiments have been carried out.

2.1.1 Experimental setup

The experiments have been conducted within an urban tunnelling site. During the tunnelling construction process at the Fasanenhofunnel in Stuttgart 45 horizontal borings have been carried out as shown in Fig. 3. These horizontal borings were grouped within a geological homogeneous layer of mudstone with a separation distance of 2.5 m. The elevation of the boreholes is varied according to the gradient of the tunnel. Therefore the first and the last borehole have a difference in the elevation approximately 2.5 m.

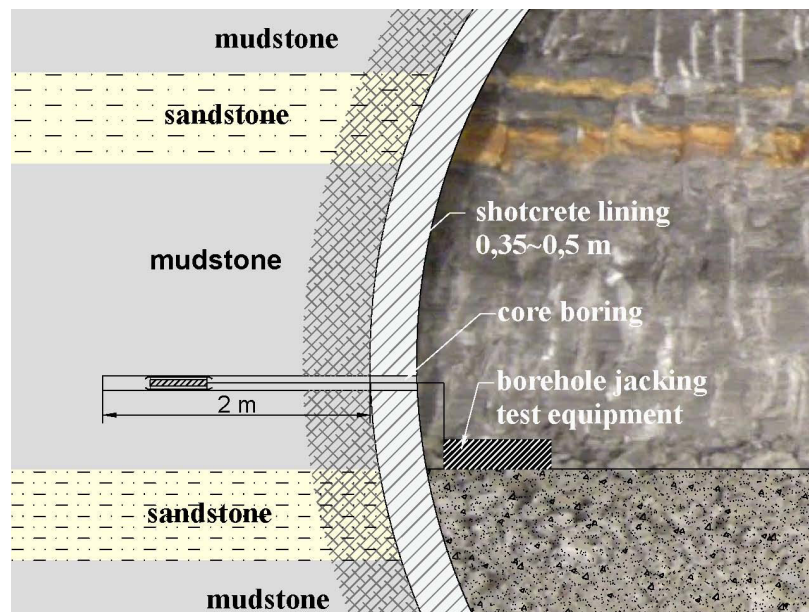


Fig. 3: Testing scheme in the tunnel

In every borehole a borehole deformation test has been carried out at an approximate depth in the borehole axes of 1.35 m. Fig. 4 shows the equipment of the borehole deformation test as described in DIN 4094-5 [1]. Within this test to half-shells are pressed diametrically against the walls of a borehole. Three different loading cycles have been executed. The pressure was raised up to three different levels of 1,000 kN/m², 2,000 kN/m² and 3,000 kN/m². During this loading process the deformation of the half-shells was measured as illustrated in Fig. 5.

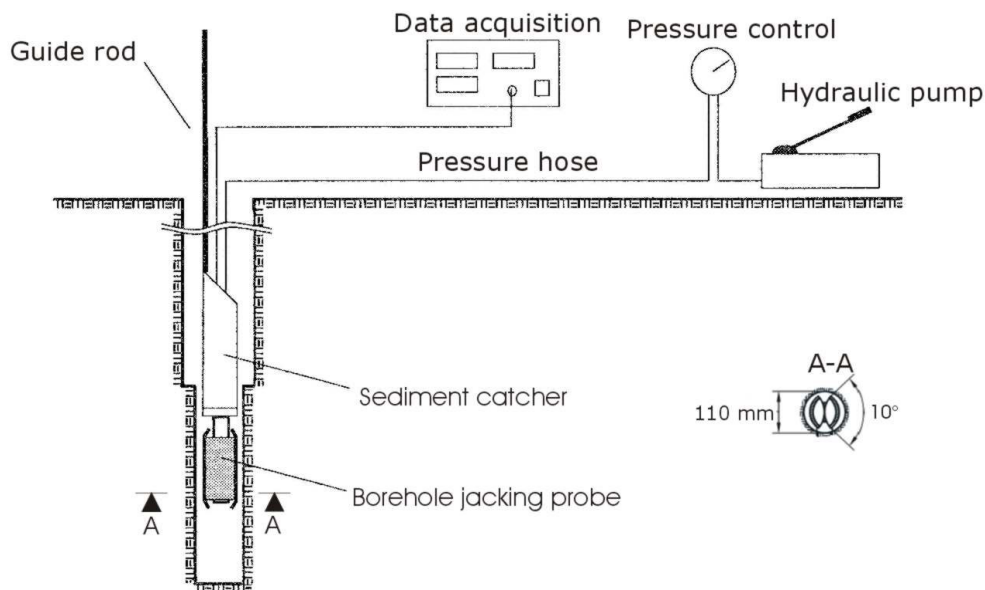


Fig. 4: Testing Equipment as described in DIN 4094-5 [1]

2.1.2 Experimental Results

The evaluation of the modulus of elasticity has been carried out according to DIN 4094-5 [1]. When looking at the results shown in Fig. 5, one would not conclude that the layer of mudstone was defined as homogeneous. The broad spectrum of results can be deduced from the spatial variability of the stiffness as well as to the varying content of CaCO_3 and MgCO_3 in the mudstone. In order to capture these results correctly statistical methods have been used as recommended in JOURNAL & HUIJBREGTS [16].

The results of the statistical evaluation of the measurements are shown in Fig. 6. The lognormal distribution function was accepted to represent the measurements after the Kolmogorov-Smirnov-Test as described in FENTON & GRIFFITHS [10].

To evaluate the correlation structure of the stiffness properties different approaches have been used. According to the very little skewed distribution shown in Fig. 6 one can deduce a similar correlation length. In Fig. 7 the variogram shows at a distance between 15 m and 20 m a nearly horizontal plateau. A similar answer can be drawn from the correlation function and from the rank correlation function in Fig. 7 (bottom). The results of the correlation distances are summarized in Tab. 2. The comparison with the results of the literature review is difficult. As mentioned above, there is only a very limited knowledge of stochastic soil properties about the modulus of elasticity presented in scientific literature. Only JAKSA ET AL. [15] did comparable tests in sandy soil. The outcome is very different from the findings of the test carried out in mudstone. The correlation distance has nearly the same dimension as the tunnel diameter. Studying FENTON & GRIFFITHS [10], one can be seen that the critical correlation length has nearly the same dimension as the building.

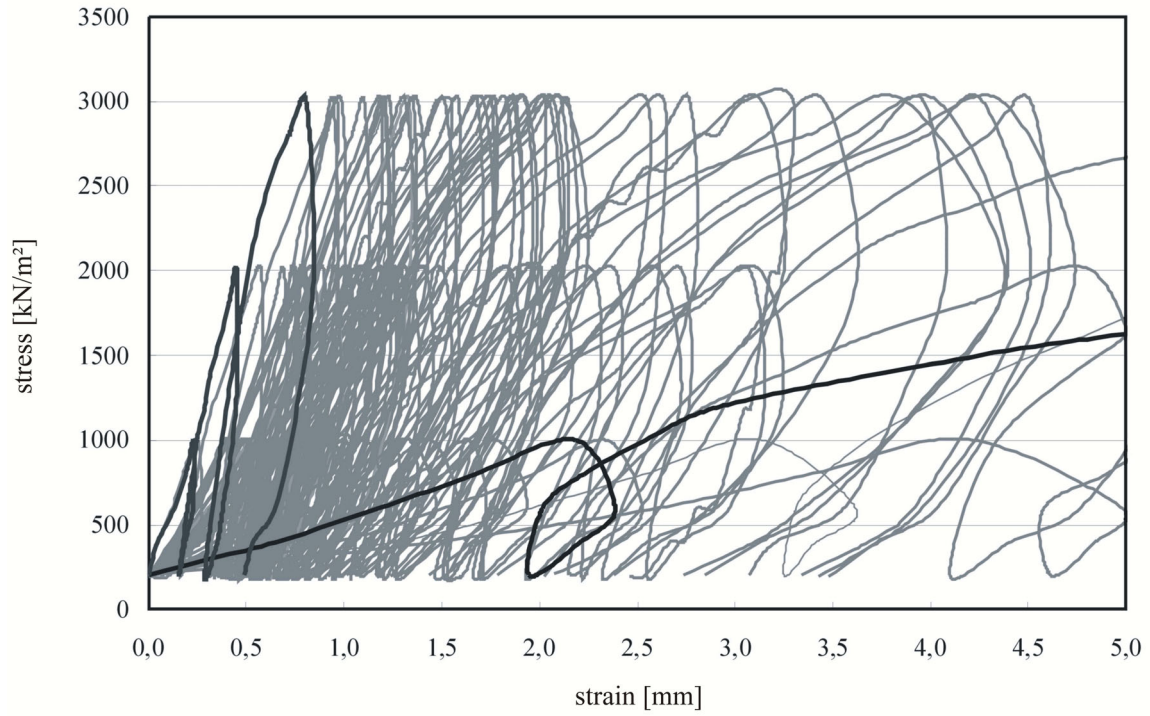
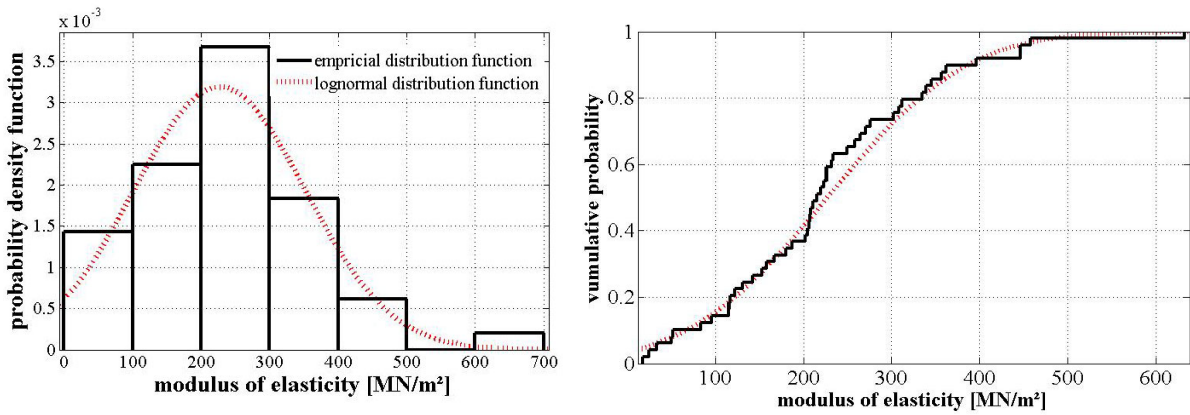


Fig. 5: Experimental results of all experiments



(a) probability density

(b) cumulative probability

Fig. 6: Statistical results of the measurements of the third loading cycle

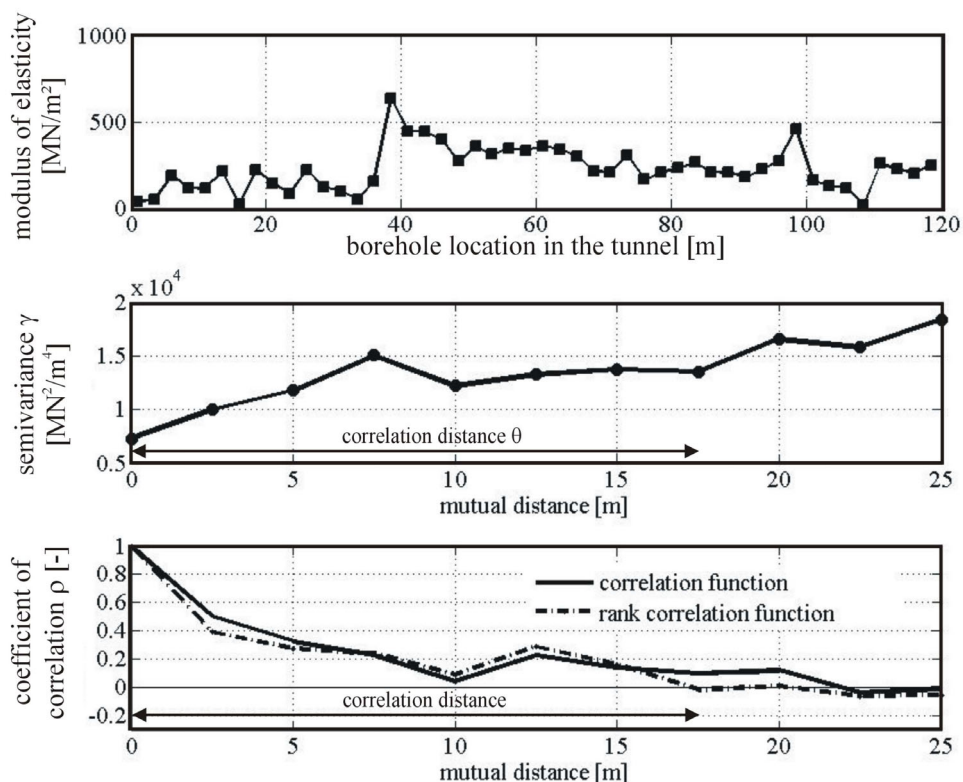


Fig. 7: Analysis of the covariance structure of the third loading cycle for the spatial distribution of the modulus of elasticity (top) using semi-covariance (middle), correlation function and rank correlation function (bottom)

Tab. 2: Results of experiments with assumed lognormal distribution for the modulus of elasticity

		mean	coefficient of variation	correlation distance
1 st cycle	loading	124 MN/m ²	0,54	10 m
	reloading	660 MN/m ²	0,64	10 - 15 m
2 nd cycle	loading	229 MN/m ²	0,53	10 - 15 m
	reloading	432 MN/m ²	0,57	10 - 15 m
3 rd cycle	loading	229 MN/m ²	0,59	15 - 20 m
	reloading	397 MN/m ²	0,61	15 - 20 m

3 Case study on probabilistic modelling

Several scientists are working in the field of developing and improving probabilistic soil modelling procedures. FENTON & GRIFFITHS [10] are very present through their publication in Random Finite Element modelling. Herein random fields are mapped on a finite element mesh in order to detect the behaviour of a geotechnical structure under spatially varying properties. In terms of random field representation as well as mapping strategies other authors have to be mentioned like POPESCU ET AL. [24], BREYSSE [6] or HICKS & SAMY [13].

In order to perform RANDOM FINITE ELEMENT modelling, an implementation was done on this into the commercial finite element code Plaxis [2]. The generation of correlated random fields with connected mean values via Cholesky decomposition was adapted from BAECHER & CHRISTIAN [4] and POPESCU ET AL. [25]. The mapping of the random field onto the Finite Element mesh was performed via the midpoint method detailedly described by SUDRET & KIUREGHIAN [30].

This program was used for a case study of a strip footing on spatially varying soil with the above mentioned implementation. With this program similar results as presented in FENTON & GRIFFITHS [10] and POPESCU ET AL. [24] could be achieved. For this case study an isotropic, normally-distributed random field was chosen. The resulting bearing capacity is also normally-distributed as shown in Fig. 8b. If one varies the correlation length of the random field, it can be found for which value that the bearing capacity is the lowest as published by FENTON & GRIFFITHS [10].

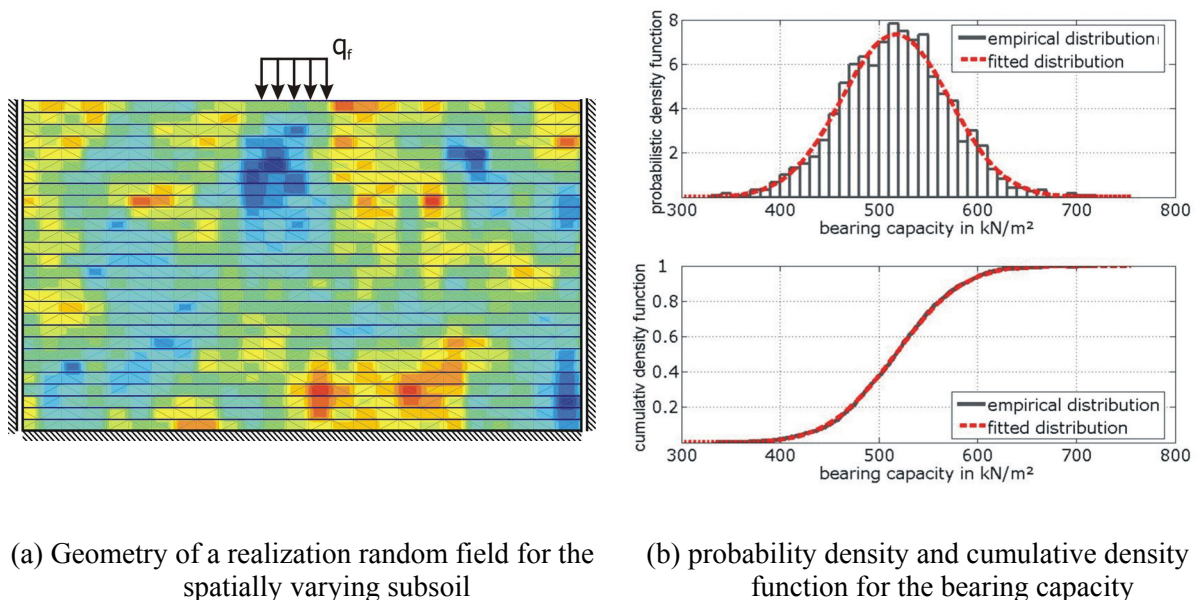


Fig. 8: Input and output of the case study on the behaviour of a strip-footing on random soil

4 Summary and Conclusions

In this article a contribution to probabilistic soil modelling was presented. Experiments have been carried out to investigate in-situ soil properties. These properties have been analyzed with random fields. Moreover, an implementation of random finite element method into a finite element code has been made and was presented through a small case study.

Further research has to be done in both fields of probabilistic soil modelling. On the one hand additional investigations have to be carried out in order to gain more knowledge in describing mechanical soil properties. On the other hand further research has to be done with respect to random field modelling. By now geotechnical scientists just use random fields with connected mean values. It may be useful to perform investigations with random field generations with connected extreme values as proposed by GOMEZ-HERNANDEZ & WEN [11] in order to describe the behaviour of soil in a better way.

5 Acknowledgements

These investigations were friendly supported by Prof. Dr.-Ing. habil H. Schad (Materialprüfungsanstalt Universität Stuttgart - Division 5 Geotechnics) through consulting, support and fruitful discussions. Moreover we thank Dipl.-Ing. C.-D. Hauck (Stadt Stuttgart, Tiefbauamt), who allowed us to carry out the experiments on-site.

6 References

- [1] DIN 4094-5: Geotechnical field investigations - part 5: Borehole deformation tests, June 2001.
- [2] R. Al-Khoury, K.J. Bakker, P.G. Bonnier, H.J. Burd, G. Soltys, and P.A. Vermeer. *PLAXIS 2D Version 9*. 2008.
- [3] A. Asoaka and D.A. Grivas. Spatial variability of the undrained strength of clays. *ASCE, Journal of Engineering Mechanics*, 108(5):743 – 756, 1982.
- [4] G.B. Baecher and J.T. Christian. *Reliability and statistics in geotechnical engineering*. John Wiley & Sons Inc, 2003.
- [5] J. Baker, E. Calle, and R. Rackwitz. Joint committee on structural safety probabilistic model code, section 3.7: Soil properties, updated version. August 2006.
- [6] D. Breyse. Probabilistic Formulation of Damage-Evolution Law of Cementitious Composites. *Journal of Engineering Mechanics*, 116:1489, 1990.

- [7] P. Chiasson, J. Lafleur, M. Soulié, and K.T. Haw. Characterizing spatial variability of clay by geostatistics. *Canadian Geotechnical Journal*, 32:1–10, 1995.
- [8] G. Christakos. *Random field models in earth sciences*. Academic Pr, 1992.
- [9] I. Clark. *Practical Geostatistics*. Applied Science Publishers LTD, 1979.
- [10] G.A. Fenton and D.V. Griffiths. Risk assessment in geotechnical engineering. 2008.
- [11] J.J. Gómez-Hernández and X.H. Wen. To be or not to be multi-gaussian? - A reflection on stochastic hydrogeology. *Advances in Water Resources*, 21(1):47–61, 1998.
- [12] K.M Hess, S.H. Wolf, and M.A. Celia. Large scale natural gradient tracer test in sand and gravel, cape cod, Massachusetts 3. hydraulic conductivity variability and calculated macrodispersivities. *Water Resources Research*, 28:2011–2017, 1992.
- [13] M.A. Hicks and K. Samy. Influence of heterogeneity on undrained clay slope stability. *Quarterly Journal of Engineering Geology & Hydrogeology*, 35(1):41–49, 2002.
- [14] M. Hollander and D.A. Wolfe. *Nonparametric statistical methods*. New York: John Wiley, 1973.
- [15] M.B. Jaksa, K.S. Yeong, K.T. Wong, and S.L. Lee. Horizontal spatial variability of elastic modulus in sand from the dilatometer. In *9th Australia New Zealand Conference on Geomechanics*, volume I, pages 289–294, Auckland, 2004.
- [16] AG Journel and C.J. Huijbregts. *Mining geostatistics*. Academic Press, London, 1978.
- [17] D.J Mulla. Estimating spatial patterns in water content, matric suction and hydraulic conductivity. *Soil Science Society*, 52:1547–1553, 1988.
- [18] T.L.L Orr. Probabilistic characterization of Irish till properties. In B.O. Skipp, editor, *Risk and reliability in ground engineering*, pages 126–133, London, November 1993. Institution of Civil Engineers, Thomas Telford.
- [19] T.L.L. Orr. *Eurocode 7 - A code for harmonised geotechnical design*. 2002.
- [20] K.-K. Phoon (editor). *Reliability-Based Design in Geotechnical Engineering - Computations and Applications*. Taylor & Francis, 2008.
- [21] K.-K. Phoon and F.H. Kulhawy. Characterization of geotechnical variability. *Canadian Geotechnical Journal*, 36:612–624, 1999.

- [22] K.-K. Phoon and F.H. Kulhawy. Evaluation of geotechnical property variability. *Canadian Geotechnical Journal*, 36:625–639, 1999.
- [23] R. Popescu. *Stochastic variability of soil properties: data analysis, digital simulation, effects on system behaviour*. PhD thesis, Princeton University, 1995.
- [24] R. Popescu, G. Deodatis, and A. Nobahar. Effects of random heterogeneity of soil properties on bearing capacity. *Probabilistic Engineering Mechanics*, 20(4):324 – 341, 2005.
- [25] R. Popescu, J.H. Prevost, and E. H. Vanmarcke. Numerical simulations of soil liquefaction using stochastic input parameters. In *Proceedings of the 3rd International Conference on Recent Advances in Geotechnical Earthquake Engineering and Soil Dynamics*, 1995.
- [26] R. Rackwitz. Reviewing probabilistic soils modelling. *Computers and Geotechnics*, 26(3-4):199–223, 2000.
- [27] K.R. Rehfeldt, J.M. Boggs, and L.W. Gelhar. Field study of dispersion in a heterogeneous aquifer, 3-d geostatistical analysis of hydraulic conductivity. *Water Resources Research*, 28(12):3309–3324, 1992.
- [28] M. Ronold. Random field modeling of foundation failure modes. *Journal of Geotechnical Engineering*, 166(4), April 1990.
- [29] M. Soulié, P. Montes, and V. Silvestri. Modeling spatial variability of soil parameters. *Canadian Geotechnical Journal*, 27:617–630, 1990.
- [30] B. Sudret and A. Der Kiureghian. Stochastic finite element methods and reliability: a state-of-the-art report. Technical report, University of California at Berkeley, 2000.
- [31] K. Unlu, D.R. Nielsen, J.W. Biggar, and F. Morkoc. Statistical parameters characterizing variability of selected soil hydraulic properties. *Soil Science Society Am Journal*, 54:1537–1547, 1990.
- [32] E.H. Vanmarcke. *Random fields: analysis and synthesis*. The M.I.T., 3rd edition, 1983.
- [33] E.H. Vanmarcke. Stochastic finite elements and experimental measurements. *Probabilistic Engineering Mechanics*, 9:103–104, 1994.
- [34] T. Vrouwenvelder and E. Calle. Measuring spatial correlation of soil properties. *Heron*, 48(4):297–311, 2003.
- [35] H. Wackernagel. *Multivariate geostatistics: an introduction with applications*. Springer, 3rd edition, 2003.

Reliability of Reinforced Masonry Walls Subjected To In-Plane Shear

E. Brehm¹, J. E. Dickie² and S. L. Lissel³

1 Research associate, PhD candidate, Institute for Concrete and Masonry Structures, Technische Universität Darmstadt, Petersenstr. 12, 64287 Darmstadt, Germany, brehm@massivbau.tu-darmstadt.de

2 PhD student, Department of Civil Engineering, The University of Calgary, 2500 University Drive NW, Calgary, AB, T2N 1N4, Canada

3 Associate Professor, Department of Civil Engineering, The University of Calgary

Abstract: Masonry shear walls are the major lateral load-carrying elements in masonry structures. Due to the fact that failure of the member might directly be followed by collapse of the structure, reliability analysis of masonry walls subjected to in-plane shear is important. Nevertheless, reliability of these members has not been subjected to extensive research due to the complex load-carrying behaviour. In this paper, an approach for the assessment of the reliability of masonry walls subjected to in-plane shear using analytical models is examined. An example wall is designed according to Canadian codes and subsequently analysed using probabilistic methods. The reliability of the wall will be determined and a parameter study will be performed. In the last step, partial safety factors for the safe design of masonry walls subjected to in-plane shear will be recommended.

1 Introduction

The key objective in structural design is the design of sufficiently safe and reliable structures. While safety commonly refers to the absence of hazards, reliability is a calculable value that can be determined by probabilistic methods. In current structural design codes, the demands of safety are accommodated by the use of partial safety factors which can be derived from probabilistic analysis. Unlike other materials in construction, the reliability of masonry members has not been subjected to extensive research in the past. Recent research (see [1]) showed the necessity for a probabilistic approach to masonry structures.

Masonry walls subjected to in-plane shear exhibit complex load carrying behaviour which is difficult to describe by analytical models. Hence, finite element analysis combined with software for reliability analysis have been preferred in the past. However, since the numerical modeling of masonry is also difficult and a large database of experiments is required for the calibration of the FE model, in this paper several analytical approaches will be compared to test data and assessed

2 Reliability of Structures

The most important requirement for structures is reliability. The term reliability concerns every aspect of a structure; structures have to be reliable when it comes to load bearing capacity as well as serviceability. In design, every parameter is uncertain to some extent. The uncertainty may be in the strength of materials as well as in dimensions and quality of workmanship. All parameters, further referred to as basic variables, influence the properties of a member. Reliability is linked to the probability that a member will exceed a certain limit state. This can be described by so called limit state functions. For ultimate limit state, the limit state function can be written as follows:

$$Z_{(R,E)} = R - E \tag{1}$$

with R resistance
 E load effect

In the case where $R = E$, the ultimate limit state is reached. It can be seen from this equation that the safety of a member can be defined as the difference between the resistance and load effect. It has to be noted that R and E are independent random variables in many cases, so they have to be described by means of stochastics. Therefore a stochastic model, mostly consisting of a probability distribution and the corresponding moments (e.g. mean, standard deviation) is required for every basic variable.

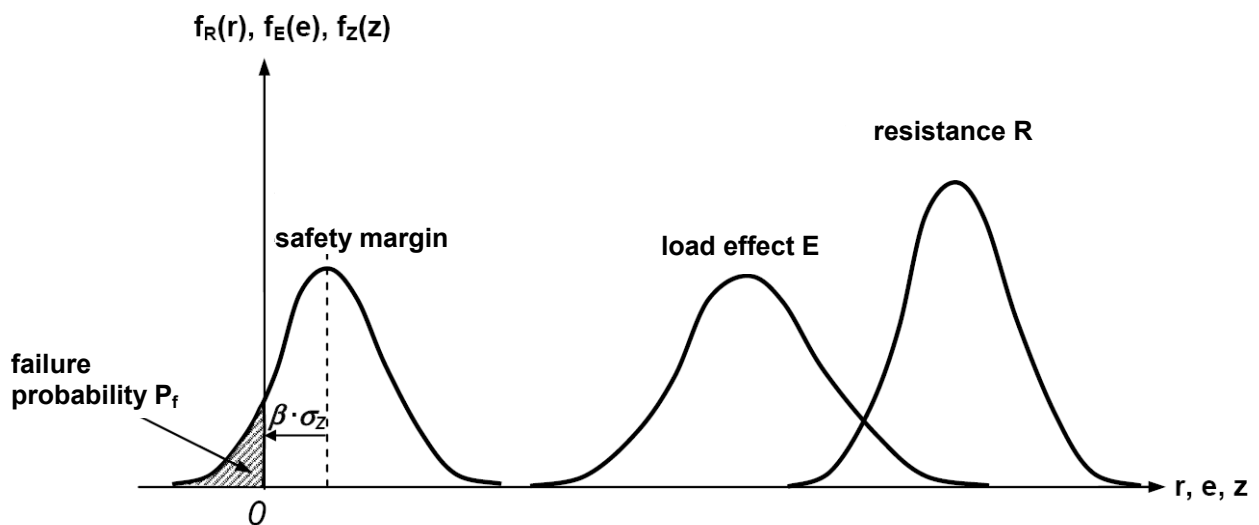


Figure 1: Definition of failure probability [1]

The failure probability can be computed by probabilistic methods such as SORM (Second Order Reliability Method) or Monte Carlo-simulation. For further information, see [2].

For the description of the resistance, proper models are required that describe the load carrying behaviour realistically. Contrary to design models, a model that underestimates the load carrying behaviour is not sufficient for probabilistic analysis.

To find a measure for reliability that can be defined independently from the type of distribution of the basic variables, the reliability index β_R according to [3] has proven useful. The major advantage of this definition is that only the mean, m_Z , and standard deviation, σ_Z , of the basic variables need to be known.

$$\beta_R = \frac{m_Z}{\sigma_Z} \tag{2}$$

with m_Z mean of Z
 σ_Z Standard deviation of Z

With this measure, target reliabilities can be defined. Ideally, target reliabilities are based on a complex optimization process accounting for aspects of safety as well as economic requirements. In the past, target reliability has mostly been determined on an empirical basis. Since the target reliability has a major influence on safety factors, setting too large of a target reliability will lead to uneconomic design. More information can be found in [1], [4] and [5].

The Joint Committee on Structural Safety (JCSS) [6] gives the target reliabilities depending on the failure consequences as shown in Table 1.

Table 1: Target reliabilities according to [6] for an observation period of 1 year

relative cost for enhancing the structural reliability	failure consequences		
	Minor ^{a)}	Average ^{b)}	Major ^{c)}
large	$\beta=3.1 (P_f \approx 10^{-3})$	$\beta=3.3 (P_f \approx 5 \cdot 10^{-4})$	$\beta=3.7 (P_f \approx 10^{-4})$
medium	$\beta=3.7 (P_f \approx 10^{-4})$	$\beta=4.2 (P_f \approx 10^{-5})$ ^{d)}	$\beta=4.4 (P_f \approx 5 \cdot 10^{-6})$
small	$\beta=4.2 (P_f \approx 10^{-5})$	$\beta=4.4 (P_f \approx 5 \cdot 10^{-5})$	$\beta=4.7 (P_f \approx 10^{-6})$

^{a)} e.g. agricultural building
^{b)} e.g. office buildings, residential buildings or industrial buildings
^{c)} e.g. bridges, stadiums or high-rise buildings
^{d)} recommendation for regular cases according to JCSS 2001

These target reliabilities are considered to be sufficient for most cases and will be taken as reference for further calculations. Another recommendation is given by the German code DIN 1055-100 [7]. There, a value of $\beta_{target} = 4.7$ is given for a 1 year observation period.

A full probabilistic approach for design is difficult since stochastic models have to be known for all basic variables and good prediction models are required. To simplify design, the semi-probabilistic partial safety concept is applied in most design codes. In this con-

cept, the partial safety factors for different basic variables make it possible to account for different scatter of the variables. A typical application of partial safety factors is presented by the following equation:

$$\gamma_E \cdot E \leq \frac{R}{\gamma_R} \quad (3)$$

with R resistance
 E load effect
 γ_E partial safety factor on load effect
 γ_R partial safety factor on resistance

3 Shear strength of masonry walls

Masonry members subjected to shear show a complex load-carrying behaviour. There is, however, a general consensus on the three main in-plane failure modes in masonry which include: flexural failure (tension at the heel or crushing at the toe), sliding failure in one or multiple bed joints, and diagonal tensile failure of the panel, which may be combined with sliding failure of the joints. Cracks are typically diagonal and stepped in nature, but may also traverse through units as shown below.

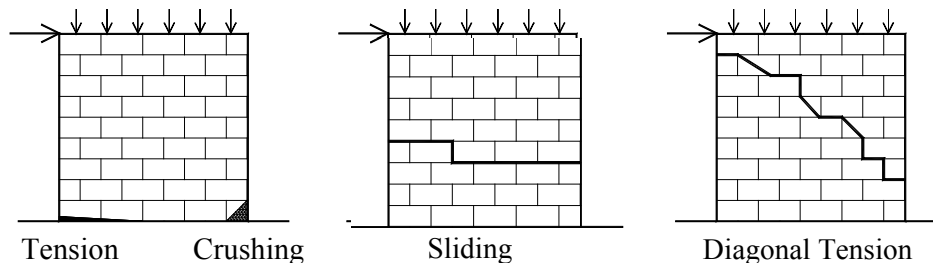


Figure 2: Typical failure modes for in-plane shear failure of masonry

For further information on the load-carrying behaviour of masonry walls subjected to in-plane shear, see [8] and [9].

4 Analysed wall

The wall analysed consists of hollow concrete blocks with dimensions and properties chosen to make shear failure become dominant. The hollow blocks are fully grouted to achieve full bond with the vertical reinforcement which prevents flexural and sliding failure. Horizontal reinforcement is assumed to be placed in every second bed joint, at a spacing of 400 mm. The axial load applied to the walls was determined assuming a 20 cm reinforced concrete slab spanning over 5 m and supporting dead and live loads of 4.8 kPa each. This results in an axial load of 12.5 kN/m dead load and 12.5 kN/m live load applied to the wall. The wall is designed to reach its full diagonal shear capacity at a horizontal load of 135kN.

Fully grouted hollow concrete block
 $f_m' = 10 \text{ MPa}$
 $A_{sh} = 127 \text{ mm}^2$
 (spacing of 400 mm)
 $A_{sv} = 607 \text{ mm}^2$
 $N_D = 25 \text{ kN}$
 $N_L = 25 \text{ kN}$
 Design according to CSA S304.1-04

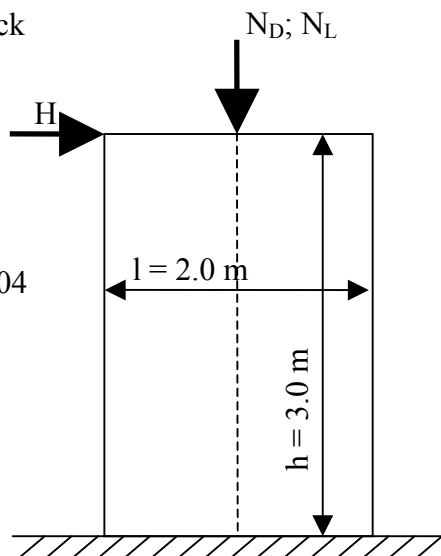


Figure 3: Analysed wall panel

5 Choice of Shear model

Every model is uncertain and so there has to be a random variable in the reliability analysis taking into account the deviations of the prediction model. This basic variable is referred to as model uncertainty on the resistance. To obtain realistic results in the reliability analysis, the most realistic model has to be chosen. In order to find an appropriate model, i.e. the one which gives the least uncertain prediction, several prediction models for the shear capacity of unreinforced masonry panels were evaluated by comparison with test data. Here, models from several international standards and some scientific models were analysed.

The Canadian masonry standard, CSA S304.1-04 [10], provides equations for determining the shear strength based on diagonal and sliding failure. Although not explicitly stated, there is an expectation that walls also be designed for in-plane flexural shear resistance. The US standard, ACI 530-08/TMS 402-08/ASCE 5-08 [11], is the most similar to the Canadian standard. The only difference is that the US standard only includes provisions for sliding shear for reinforced sections for autoclaved aerated concrete masonry. The Australian standard, AS 3700-2004 [12], is more simplistic and bases the masonry shear stress solely on the aspect ratio of the wall. It accounts for neither axial load nor for sliding shear failure. The New Zealand standard, NZS 4230-2004 [13], is one of the more complex models. This model accounts for the shear resistance provided by the masonry, reinforcement, and axial load. Eurocode 6 [14] also accounts for the shear resistance provided by these three sources, but does not account for sliding failure. Anderson and Priestley [15] proposed yet another shear model after a review of the equations proposed by Shing et al. [16] and Matsumura [17]. The equation was developed using statistical data fitting. It accounts for the degradation of shear strength when the wall is subjected to cyclic loading into the inelastic range. This equation also accounts for all three types of shear failure. The National Earthquake Hazards Reduction Program (NEHRP) developed an equation similar

to that of Anderson and Priestley, but with an additional factor, $M/(VL)$, to account for the wall aspect ratio. Finally, Voon and Ingham [18] developed the most recent shear model. This model is based on that of NEHRP, but with some modifications. The masonry shear resistance includes a parameter to account for longitudinal steel. The shear resistance provided by axial loading was modified to account for a compression strut at an angle to the wall axis. This results in a greater contribution from squat walls than provided by slender walls. For shear resistance provided by reinforcement, the effective depth was reduced due to the assumption that reinforcement at the ends of the wall is not developing.

Evaluation of the test-to-prediction ratio gives the stochastic parameters presented in Table 2. The database consists of test results from walls with large reinforcement ratios. It is found that the model according to Anderson and Priestley [15] gives the best prediction due to the small CoV and was therefore chosen for further study.

Table 2: Stochastic parameters for $V_{\text{test}}/V_{\text{prediction}}$ for various models

	CSA S304.1 -04	ACI 530-08	AS 3700- 2001	NZS 4230- 2004	EC 6	Anderson & Priest- ley	NEHRP (1997)	Voon & Ingham
St. Dev.	0.44	0.40	0.68	0.36	0.39	0.16	0.38	0.30
Mean	2.05	1.65	1.64	1.60	1.39	0.97	1.45	1.32
CoV	0.22	0.25	0.41	0.23	0.28	0.17	0.26	0.23

6 Stochastic Model

Every basic variable in the chosen model has to be represented by a stochastic model. Commonly, stochastic data requires large databases. Since probabilistic analysis is gaining more and more acceptance within the construction industry, the number of stochastic models that can be found in the literature increases. In particular, values for material strength can be found more easily since strength tests are part of the quality control of producers. However, some values such as cohesion are difficult to find due to lack of data. The reliability analysis was executed using the following limit state function for shear failure:

$$g(x) = R - E = \Theta_{R,s} \cdot \left(0.24 \cdot \sqrt{f'_m} \cdot l \cdot t + 0.25 \cdot (N_D + N_L) + 0.5 \cdot A_{sh} \cdot f_s \cdot \frac{0.8 \cdot l}{s} \right) - \Theta_E \cdot H \quad (4)$$

with	$\Theta_{R,s}$	model uncertainty resistance
	Θ_E	model uncertainty load effect
	f'_m	compressive strength of masonry
	N_D	axial force due to dead load
	N_L	axial force due to live load
	f_s	strength of reinforcing steel
	l	wall length
	t	wall thickness
	A_{sh}	cross-section of reinforcing steel
	s	spacing of reinforcement
	H	horizontal load

The model uncertainties are always major parameters in a reliability analysis. Here, the model uncertainty for shear resistance $\Theta_{R,s}$ has been chosen on the basis of test data (see previous paragraph). The model uncertainty for the load effect Θ_E is chosen according to the JCSS Probabilistic Model Code [19].

The horizontal load H is modelled by the *Gumbel* distribution. This is the extreme value distribution of the group of exponential distributions, which includes the *Gaussian* distribution, and therefore the *Gumbel* distribution is widely used in probabilistic design. Additionally, it allows different observation periods T to be considered due to its properties concerning variability over time. It was found that while the mean increases the standard deviation stays the same for different observation periods. This leads to decreasing CoV (CoV is the ratio of standard deviation to the mean) for longer observation periods. Furthermore, the 98%-quantile of a 1-year observation is close to equal to the mean of the 50-year observation, as seen in Figure 4.

Many codes give the unfactored wind load as the one occurring once in 50 years. This is taken as the basis for the analysis and this wind load is converted to the wind load for a 1-year observation.

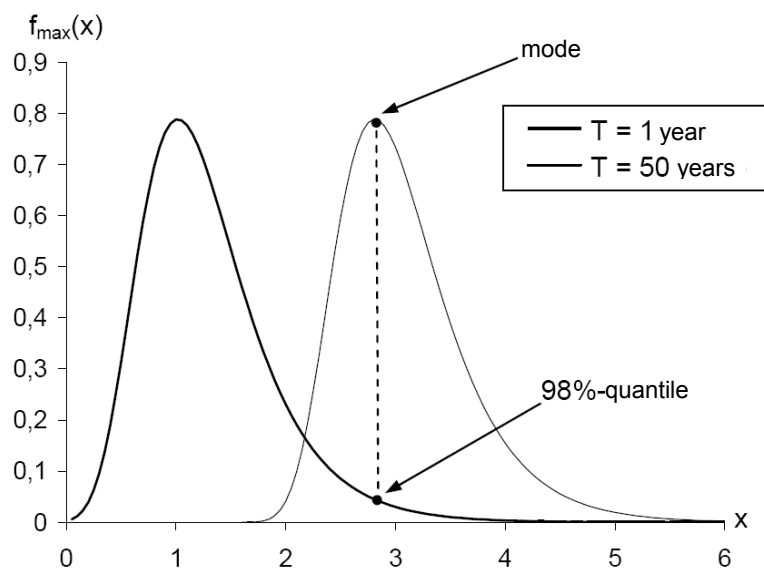


Figure 4: Gumbel distribution for different observation periods [1]

The mean values for dead and live load are also chosen to represent the characteristic values according to current codes on the basis of the distributions and coefficients of variation (*CoV*) given in Table 3.

The stochastic model includes four kinds of probability distributions: the aforementioned *Gumbel*, and the *Gaussian*, *lognormal* and *Gamma* distributions. The *Gaussian* distribution allows for negative and positive values and is widely used within every field of engineering. However, negative values for material strength and other parameters are not logical. Therefore, the *lognormal* distribution which only permits positive values is used for mate-

rial strengths and model uncertainties. The *Gamma* distribution is used to determine the point-in-time value of the live load and so to account for favourable effects

Table 3: Stochastic Model Parameters

Basic variable	Type of distribution	Mean	CoV
$\Theta_{R,s}$	lognormal	0.97 [-]	17 %
Θ_E	lognormal	1.0 [-]	10 %
H	Gumbel	0.075	31 %
f_s	lognormal	430 MN/m ²	4 %
f_m	lognormal	14.1 MN/m ²	20 %
N_G	Gaussian	0.025 MN	3 %
l	constant	2.0 m	-
t	constant	0.19 m	-
h	constant	3.0 m	-
A_{sh}	constant	127.0 mm ² ^{a)}	-
A_{sv}	constant	607.0 mm ²	-

^{a)} spacing of 400 mm

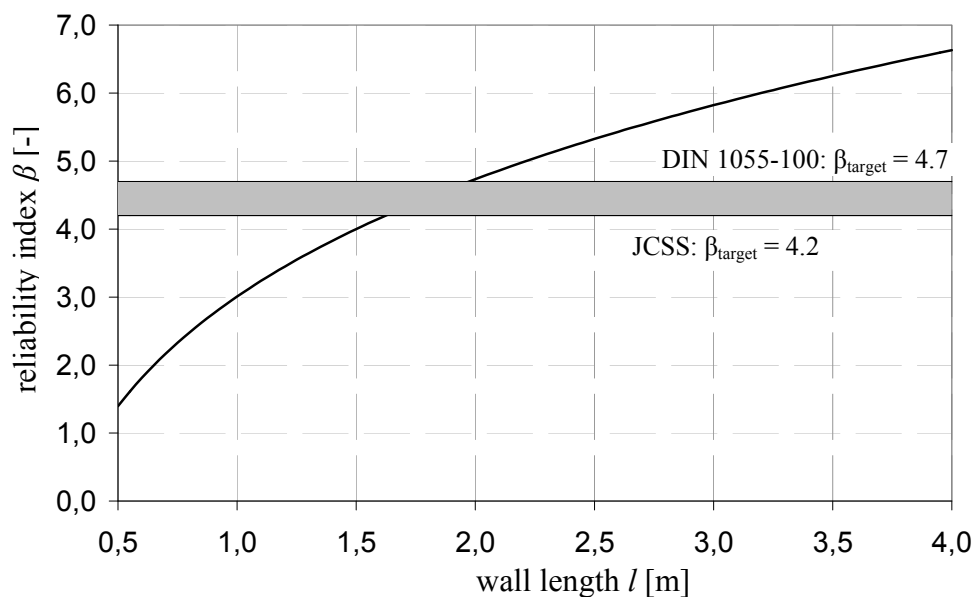
The parameters have been estimated on the basis of [19] and [20]. For the parameters of the distribution of the masonry compressive strength, refer to [1] and [22].

7 Results and assessment

The reliability analysis was performed using the Software COMREL [23] which includes various procedures. For this analysis, SORM was used.

The governing parameter of a masonry wall subjected to in-plane shear is the wall length l_w . In Figure 5, the reliability index β is shown versus the wall length. It can be seen, that the reliability increases non-linearly with growing wall length. Additionally, it can also be seen that the wall length of 2.0 m is enough to provide sufficient reliability since the target reliabilities according to DIN 1055-100 and JCSS are exceeded for $l = 2.0$ m. To reach the target reliabilities, wall lengths of 1.64 m (JCSS) and 1.98 m (DIN 1055-100) are sufficient. Further research and development of the prediction models therefore might lead to economic enhancement of the walls.

Flexural failure was also included in the analysis but did not dominate due to the design of the wall. The analysis was executed for an observation period of one year.


 Figure 5: Reliability index β vs. wall length

Another outcome of the reliability analysis is determination of the sensitivity values α_i . These values define the design value of a basic variable together with the reliability value β and the standard deviation σ . The sensitivity values can be seen as a measure for the influence of a basic variable on the reliability; the larger the sensitivity, the larger the influence. As expected, the horizontal load H is the parameter with the largest influence. DIN 1055-100 gives an estimate for the sensitivity of load effects of $\alpha_E = 0.8$. The obtained value meets this recommendation. The model uncertainties have the second largest influence which underlines the importance of precise prediction models.

 Table 4: Sensitivity values for $H_k = 135$ kN

Basic variable	Sensitivity value α
$\Theta_{R,s}$	0.44
Θ_E	-0.27
H	-0.83
f_s	0.03
f_m	0.19
N_D	0.02
N_L	0.04

Additionally, the values α_i can be used to calculate the partial safety factors. These are defined as follows:

$$\gamma_E = \frac{E_d}{E_k} \quad (5)$$

$$\gamma_R = \frac{R_k}{R_d} \quad (6)$$

where E_d is the factored load effect, E_k is the corresponding characteristic value, R_d is the factored resistance and R_k is the characteristic value of the resistance.

The characteristic values represent quantiles of the respective probability distribution of a basic variable. The design values can be determined depending on the sensitivity values, the target reliability, mean and standard deviation of every basic variable. Since every distribution requires different equations, refer to [20] for further information.

The obtained partial safety factors can be taken from Table 5. Compared to the recommendations of CSA S304.1-04, it can be seen that the required factor on the horizontal load to reach the target reliability according to the JCSS [6] is larger than the recommendation. However, the larger safety factor on the masonry strength equalizes the effects of the small safety factor on the horizontal load.

Table 5: Partial Safety Factors for $\beta_{target} = 4.2$

Basic variable	Partial Safety Factor	Recommendation of CSA S304.1-04
H	1.78	1.50
f_m	1.25	1.667
f_s	1.26	1.176
N_D	0.75	0.90

Note that the live load is not to be applied in design since it is acting favourably. However, it was included in the reliability analysis to account for the permanently existent part of the live load. So, neglecting the live load in design is an additional element of safety.

8 Conclusion

In this paper, the reliability of a reinforced masonry shear wall was analysed. Therefore, several models were compared to test data to find an appropriate theoretical model for analysis. The model of Anderson & Priestley [15] was found to provide the best match to the experimental data available. A stochastic model was set up and the analysis was performed by application of SORM. The reliability index β was computed and compared to recommended values. It was found that the wall provides sufficient reliability so that further optimization is possible. Partial safety factors were provided and compared to the recommendations of the CSA.

9 References

- [1] Glowienka, S. (2007) "Zuverlässigkeit von Mauerwerkswänden aus großformatigen Steinen", doctoral thesis, Institut für Massivbau, Technische Universität Darmstadt, Germany, in German
- [2] Melchers, R. E. (1999) "Structural Reliability Analysis and Prediction", John Wiley & Sons Ltd., Chichester, England
- [3] Benjamin, J. R. and Cornell, C. A. (1970) "Probability, Statistics and Decisions for Civil Engineers" McGraw-Hill Book Company, New York
- [4] Rackwitz, R. (2004) „Zuverlässigkeit und Lasten im konstruktiven Ingenieurbau“, TU Munich, Munich, Germany
- [5] Rosenblueth, E. and Mendoza, E. (1971) "Optimization in Isostatic Structures" Journal of the Eng. Mech. Division, ASCE, 97, EM6
- [6] JCSS (2001) "Probabilistic Assessment of Existing Structures", RILEM Publications, S.A.R.L.
- [7] DIN 1055-100 (2001) "Einwirkungen auf Tragwerke - Teil 100: Grundlagen der Tragwerksplanung - Sicherheitskonzept und Bemessungsregeln", Beuth Verlag, Berlin
- [8] Kranzler, T. (2008) "Tragfähigkeit überwiegend horizontal beanspruchter Aussteifungsscheiben aus unbewehrtem Mauerwerk", doctoral thesis, Institut für Massivbau, Technische Universität Darmstadt, Darmstadt, Germany
- [9] Lissel, S.L., Shrive, N.G., and Page, A.W. (2000) "Shear in Plain, Bed Joint Reinforced and Post-tensioned Masonry" Canadian Journal of Civil Engineering, Vol. 27, pp. 1021-1030
- [10] CSA S304.1-04 (2004) "Design of Masonry Structures," Mississauga, ON.
- [11] TMS 402-08/ACI 530-08/ASCE 5-08 (2008) "Building Code Requirements for Masonry Structures," Boulder, CO
- [12] AS 3700-2001 (2001) "Masonry Structures," Sydney, Australia
- [13] NZS 4230:2004 (2004) "Design of Reinforced Concrete Masonry Structures," Wellington, NZ
- [14] Eurocode 6 (2003) "Design of Masonry Structures," Brussels
- [15] Anderson, D.L. and Priestley, M.J.N. (1992) "In Plane Shear Strength of Masonry Walls," 6th Canadian Masonry Symposium, Saskatoon, SK
- [16] Shing, P.B., Schuller, M., Hoskere, V.S., and Carter, E. (1990) "Flexural and Shear Response of Masonry Walls", ACI Structural Journal, Vol 87 No 6, Nov.-Dec.

- [17] Matsumura, A. (1987) "Shear Strength of Reinforced Hollow Unit Masonry Walls", Proceedings, 4th North American Masonry Conference, Los Angeles, CA.
- [18] Voon, K.C., and Ingham, J.M. (2007) "Design Expression for the In-Plane Shear Strength of Reinforced Concrete Masonry," Journal of Structural Engineering, Vol. 133, pp. 706-713
- [19] JCSS (2003), "Probabilistic Model Code", online available at www.jcss.ethz.ch
- [20] Spaethe, G. (1992) "Die Sicherheit tragender Baukonstruktionen" Springer, Vienna
- [21] Gumbel, E. J. (1958) "Statistics of Extremes" Columbia University Press, New York
- [22] Schueremans, L. (2001) "Probabilistic evaluation of structural unreinforced masonry", doctoral thesis, Catholic university of Leuven, Leuven, Belgium
- [23] RCP (2004) "STRUREL, a Structural Reliability analysis program system" RCP GmbH, Munich
- [24] Graubner, C.-A., Brehm, E. and Glowienka, S. (2008) "Economic Potentials of Probabilistic Optimization Methods", Beton- und Stahlbetonbau, Volume 103, ISSN 0005-9900, Ernst & Sohn, Berlin, in English

The subset simulation applied to the reliability analysis of a nonlinear geotechnical finite element model

Iason Papaioannou¹, Holger Heidkamp², Alexander Düster³, Stefan Kollmannsberger¹, Ernst Rank¹, Casimir Katz²

¹Chair for Computation in Engineering, Technische Universität München, Germany

²SOFiSTiK AG, Oberschleißheim, Germany

³Numerical Structural Analysis with Application in Ship Technology, Technische Universität Hamburg-Harburg, Germany

Abstract: This paper presents an application of the subset simulation method to the finite element reliability assessment of a deep circular tunnel. The tunnel is assumed to be surrounded by weak rock with uncertain material properties. For the spatial variability of the uncertain parameters the midpoint method is utilized. Depending on the assumed correlation length, the above stochastic discretization method may lead to a very large number of random variables. In such cases, most Monte Carlo variants prove to be inefficient in computing small failure probabilities, which are typical in structural engineering. However, the subset simulation method overcomes this problem by expressing the failure probability as a product of larger conditional probabilities, which are estimated by applying an efficient Markov chain Monte Carlo technique. The reliability analysis is performed using a reliability tool, which is being developed as part of the SOFiSTiK finite element software package.

1 Introduction

A general trend for reliable and economical design has led to the inclusion of safety concepts for the consideration of uncertainties in the design and analysis procedures. In geotechnical engineering, these uncertainties stem to a large extent from the stochastic properties of the materials within the soil mass. However, the widely applied conventional safety factor concept lacks a well-defined procedure for taking the uncertainties of different material properties into account. Such a more accurate approach is offered by the reliability analysis concept, providing the means for an accurate estimation of the true margins of safety. In this context, the impact of the uncertainties is expressed by the probability of non-successful performance, corresponding to the failure event.

In reliability analysis, the uncertain parameters are regarded as a set of random variables with corresponding probability distributions. The failure event is then expressed by using a performance function, defined in terms of these random variables. In industrial applications, the performance function may depend on the result of a finite element (FE) calculation. Naturally, the computational time needed for the FE calculation may be considerable. This underlines the importance of using reliability algorithms, which are able to provide accurate probabilities within a minimum number of performance function evaluations.

Moreover, in cases where the spatial variability of the parameters is considered important, each stochastic parameter is represented by a random field, additionally defined by a correlation structure. In such cases, the discretization of the random fields may lead to a very large number of random variables. A review on how to process such high-dimensional problems is given by SCHUËLLER et al. in [15]. In this work we use the subset simulation method, introduced by AU & BECK [1]. This method is offering a solution to this dimensionality curse, by applying an efficient Markov chain Monte Carlo method to simulate intermediate conditional failure events. The method is designed for the estimation of small failure probabilities, which are typical in civil engineering.

The presented application is focused on the performance of the subset simulation in the reliability analysis of a geotechnical application. The uncertainties in the soil material properties are expressed by a set of random variables and the spatial variability of the most important variables is described by a homogeneous random field. A series of comparisons illustrates the influence of the spatial variability and the correlation length of the random field on the reliability.

2 Random fields

2.1 Formulation

A random field $X(\mathbf{t})$ may be defined, in the context of this work, as a random function, which assigns a random variable at each point of a continuous space, in terms of the location vector \mathbf{t} . Moreover, $X^i(\mathbf{t})$ denotes a particular realization of the field and $X(\mathbf{t}_i)$ the random variable at the location \mathbf{t}_i .

We define the expectation of any function $h(\mathbf{X})$ of the random variables $\mathbf{X} = [X(\mathbf{t}_1) X(\mathbf{t}_2) \dots]^T$ in terms of the random field $X(\mathbf{t})$ as:

$$E[h(\mathbf{X})] = \int_{\Omega} h(\mathbf{x}) f_x(\mathbf{t}, \mathbf{x}) d\mathbf{x} \tag{1}$$

where $f_x(\mathbf{t}, \mathbf{x})$ is the joint probability density function (PDF) of the random variables $X(\mathbf{t}_i)$ and Ω is the infinite-dimensional domain of definition of the variables $X(\mathbf{t}_i)$. The *mean* of the random field is defined as:

$$\mu(\mathbf{t}) = E[X(\mathbf{t})] \tag{2}$$

Furthermore, the *autocorrelation* function and the *autocovariance* function are defined respectively by:

$$\rho(\mathbf{t}_i, \mathbf{t}_j) = E[X(\mathbf{t}_i)X(\mathbf{t}_j)] \quad (3)$$

and

$$\gamma(\mathbf{t}_i, \mathbf{t}_j) = E\{[X(\mathbf{t}_i) - \mu(\mathbf{t}_i)][X(\mathbf{t}_j) - \mu(\mathbf{t}_j)]\} \quad (4)$$

The variance at location \mathbf{t}_i is expressed as:

$$\text{Var}[X(\mathbf{t}_i)] = \gamma(\mathbf{t}_i, \mathbf{t}_i) \quad (5)$$

A random field is said to be *homogeneous* if its statistical properties are invariant to a shift of the origin. A direct consequence of this is that the mean and variance are constant over space and that the random field is uniquely defined by the autocorrelation function, now depending on the distance τ between two locations:

$$\rho(\tau) = E[X(\mathbf{t} + \tau)X(\mathbf{t})] \quad (6)$$

Several models of the autocorrelation function for the description of homogeneous random fields have been proposed, e.g. see VANMARCKE [17]. Alternatively, a more accurate correlation structure may be calculated using measured data. In this work, the following exponential autocorrelation function is chosen:

$$\rho(\tau) = \exp\left(-\frac{\tau}{\lambda L}\right) \quad (7)$$

where L is the problem's characteristic length and λ is a dimensionless constant. λL is referred to as the correlation length. In practical terms, $\lambda L/2$ roughly characterizes the distance between two locations below which the field is effectively correlated.

2.2 Discretization

In the discretization procedure, the continuous random field $X(\mathbf{t})$ is approximated by the discrete $\hat{X}(\mathbf{t})$, defined by means of a finite set of random variables X_i . Several methods have been proposed for the discretization of random fields into random variables (see SUDRET & DER KIUREGHIAN [16] for a review). In this study, the *midpoint method*, proposed by DER KIUREGHIAN & KE [3], is adopted, due to its well-defined application to non-Gaussian random fields. This method requires a stochastic finite element (SFE) mesh, which may be independent of the finite element mesh for the deterministic part of the analysis. According to this method, the value of the random field $X(\mathbf{t})$ over each SFE i is represented by its value at the midpoint of the element:

$$X_i = X(\mathbf{t}_i) \quad (8)$$

where \mathbf{t}_i is the location of the midpoint (centroid) of the element. The statistical properties of the random variable X_i are then obtained from equations (2)-(5).

If the random field is homogeneous, the mean and the variance of the random variable X_i are not affected by the discretization and therefore are equal to their constant values over the entire field. The correlation matrix of the random variables is generated by computing the distances τ_{ij} between the midpoints of each element and substituting to equation (6). The random field is thus reduced to a vector \mathbf{X} of *correlated* random variables.

3 Reliability analysis

Let \mathbf{X} denote the K -dimensional vector of basic random variables with known marginal probability distributions and correlations. Let $g(\mathbf{X})$ be the performance function with negative values defining the failure event. The probability of failure may be computed by:

$$P_f = \text{Prob}\{g(\mathbf{X}) \leq 0\} = \int_{g(\mathbf{x}) \leq 0} f_{\mathbf{X}}(\mathbf{x}) d\mathbf{x} \quad (9)$$

where $f_{\mathbf{X}}$ is the joint PDF of the random variables \mathbf{X} .

To facilitate the implementation of the reliability algorithms, a transformation of the random variables from the original random variable space to the equivalent standard normal space of uncorrelated random variables (transformed space) $\mathbf{U} = T(\mathbf{X})$ is performed, by applying the Nataf transformation, as described in DER KIUREGHIAN & LIU [4]. The problem then reduces to that of computing:

$$P_f = \int_{G(\mathbf{u}) \leq 0} \varphi_{\mathbf{U}}(\mathbf{u}) d\mathbf{u} \quad (10)$$

where $\varphi_{\mathbf{U}}$ is the K -dimensional standard normal joint PDF and $G(\mathbf{U})$ is the performance function in the transformed space.

3.1 First Order Reliability Method (FORM)

The FORM is an approximation method, according to which the integration domain in equation (9) is approximated by the tangent of the limit state $G(\mathbf{u}) = 0$ of the performance function at the design point \mathbf{u}^* . This is the point of the limit state function with minimum distance to the origin of the transformed space. The reliability index β is defined by the Euclidean norm of \mathbf{u}^* . In other words, the reliability index represents the distance of the most probable failure point from the mean value of the random variables. The probability of failure is then approximated with respect to β as:

$$P_f \approx \Phi(-\beta) \quad (11)$$

where $\Phi(\cdot)$ is the standard normal cumulative distribution function (CDF).

The design point is determined by applying an iterative procedure, which requires the evaluation of the performance function and its gradient at each step. The gradient evaluation is performed by applying the finite difference method at the current iteration step. A series of algorithms, described in PAPAIOANNOU et al. [10, 11], have been implemented for this purpose. In this work, the standard HLRF method, introduced by HASOFER & LIND [6] and further developed for the application to non-Gaussian random variables by RACKWITZ & FIESSLER [12], is applied.

The sensitivity of the performance function with respect to the random variables is expressed by the influence coefficients α_i evaluated at the design point according to DITLEVSEN & MADSEN [5]:

$$\alpha_i = \frac{\nabla G(u_i^*)}{\|\nabla G(\mathbf{u}^*)\|} \quad (12)$$

The coefficients α_i represent the directional cosines along the coordinate axes U_i . This sensitivity measure is helpful for estimating the most important uncertain parameters, in terms of their influence on the reliability.

3.2 Subset simulation

The subset simulation (SubS) is an adaptive simulation technique developed by AU & BECK [1], which is shown to be efficient especially in high dimensions. This method is based on the standard Monte Carlo simulation (MCS) but overcomes its well known inefficiency in estimating small probabilities, by expressing the failure probability as a product of larger conditional probabilities. This is achieved by expressing the failure event F , corresponding to the failure region defined by $G(\mathbf{u}) \leq 0$, as the intersection of M intermediate failure events:

$$F = \bigcap_{i=1}^M F_i \quad (13)$$

where $F_1 \supset F_2 \supset \dots \supset F_M = F$. The probability of failure is estimated by applying the definition of conditional probability, resulting in:

$$P_f = \text{Prob}\{F_1\} \prod_{i=2}^M \text{Prob}\{F_i | F_{i-1}\} \quad (14)$$

Each of these events is defined as $F_i = \{G(\mathbf{u}) \leq G_i\}$, where $G_i > \dots > G_M = 0$. The values of G_i are chosen adaptively so that the estimates of the conditional probabilities correspond to a given value p_0 . The probability of F_1 is computed by applying the crude MCS method, e.g. see RUBINSTEIN [13]. This is done by simulating N samples at the standard normal space and taking as G_1 the $[(1 - p_0)N]$ th largest value among the samples $\{G_{1,k}: k = 1, \dots, N\}$. The samples for which $G(\mathbf{u}) \leq G_1$ are used for the simulation of F_1 , by applying a Markov chain Monte Carlo technique, called the Metropolis-Hastings algorithm (see METROPOLIS et al. [9] and HASTINGS [7]). This procedure is repeated until the maximum

level M is reached, for which the threshold $G_M = 0$ is given. The failure probability is therefore calculated by:

$$P_f = p_0^{M-1} \text{Prob}\{F_M | F_{M-1}\} \quad (15)$$

where the conditional probability $\text{Prob}\{F_M | F_{M-1}\}$ is equal to the number of samples for which $G(\mathbf{u}) \leq 0$ over the total number of samples N simulated at F_{M-1} .

The choice of p_0 and the number of samples at each step N may in principle be arbitrary. However, the choice of N should be large enough to give an accurate estimation of p_0 . To this end, the following empirical expression may be used:

$$N \geq \frac{10}{p_0} \quad (16)$$

A graphical representation of the method, applied for the reliability assessment of a convex performance function in a 2D standard normal space, is shown in Fig. 1 for $p_0 = 0.1$ and $N = 400$.

The superiority of the SubS over the crude MCS in high-dimensional problems is illustrated in AU et al. [2], where the method is applied for the solution of a series of reliability benchmark problems, proposed by SCHUËLLER & PRADLWARTER [14].

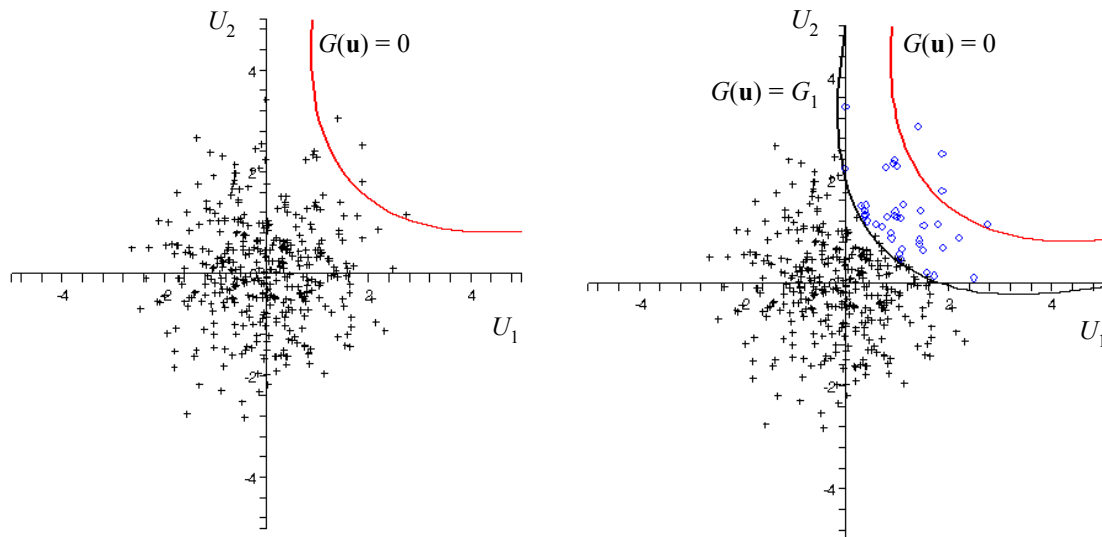
4 Application

4.1 Numerical model

The presented application focuses on the reliability analysis of a deep circular tunnel. The scope of the numerical model is the evaluation of the vertical displacement at the uppermost point of the tunnel's circumference. The rocky soil surrounding the tunnel is spread within an $80 \times 80 \text{ m}$ bounded block and the tunnel's diameter is taken as 6.6 m . The soil is modelled in the SOFiSTiK program, using plain strain finite elements (FE). The material parameters are taken as independent random variables, described by probability distributions, as shown in Table 1. For the specific weight the normal distribution was chosen, while for the remaining parameters the lognormal and beta distributions were utilized due to their advantage in defining lower and upper bounds. For example, the Young's modulus must take positive values and the Poisson's ratio may not be larger than 0.5. The tunnel's support is modelled by a constant pressure $P = 5000 \text{ kN/m}^2$ distributed at the tunnel's circumference.

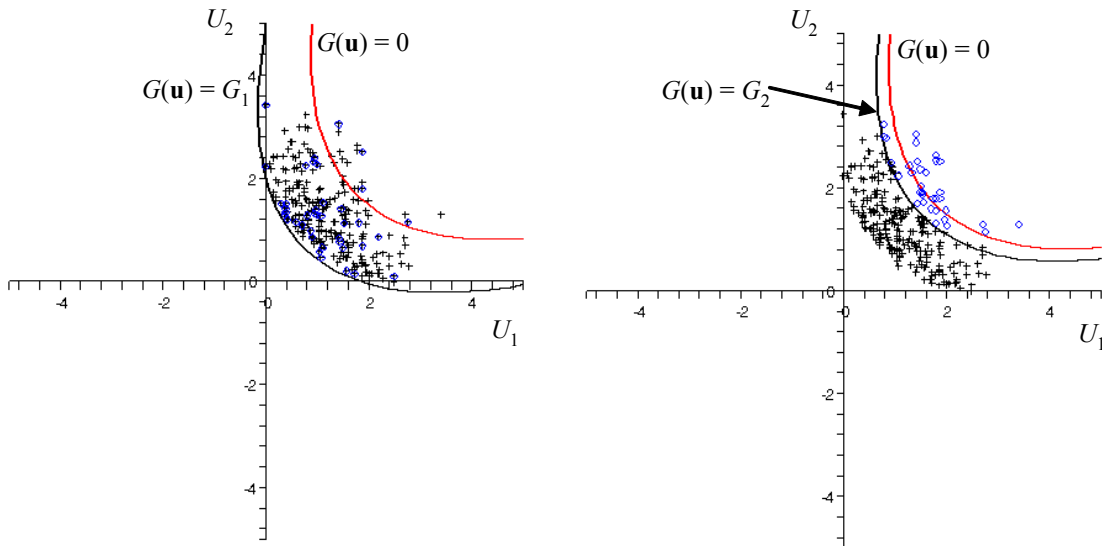
The performance function is chosen such that the inward displacement of the tunnel's circumference does not exceed a threshold of 0.04 m :

$$g(\mathbf{x}) = 0.04 - u_{in}(\mathbf{x}) \quad (17)$$



(a) Monte Carlo simulation

(b) Determination of the first threshold G_1



(c) Markov chain simulation of the intermediate failure domain

(d) Determination of the second threshold G_2

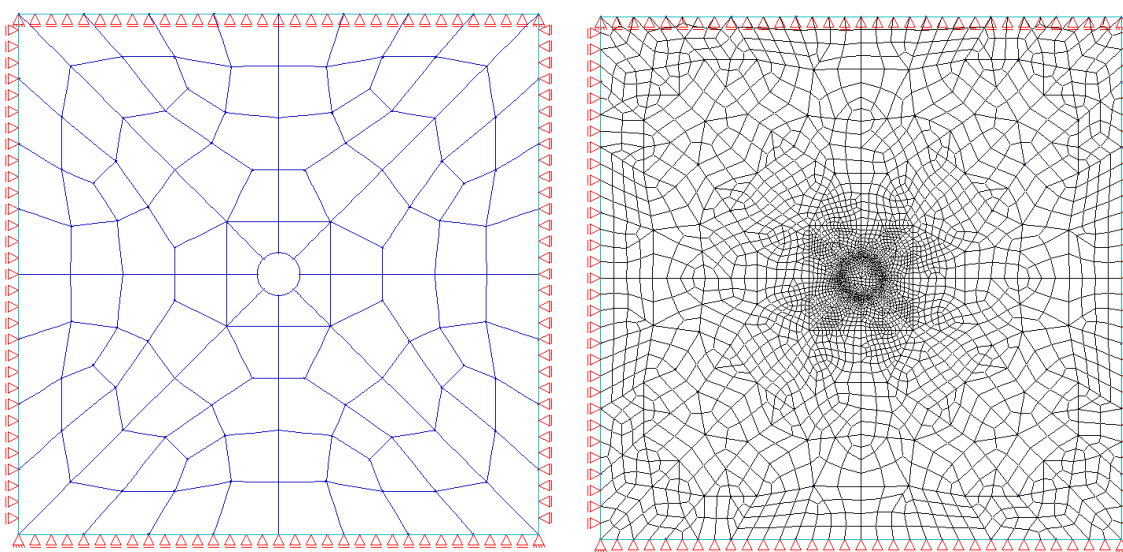
Fig. 1: Graphical representation of the SubS method in a 2D standard normal space

The displacement of the tunnel is determined by a numerical evaluation of the ground-support equilibrium point (see HOEK et al. [8]). To this end, a FE analysis is performed in two steps. First, the modelling of the in-situ stress state is carried out. Since the tunnel is assumed to be deep, the self-weight of the soil can be ignored and the in-situ stress state can be modelled by a constant hydrostatic pressure, due to the stresses resulting from an assumed 1100 m overburden load. Then the elements corresponding to the circular tunnel are removed and the supporting pressure is applied by performing a nonlinear computation. The material model used is an elastic-perfectly plastic model with non-associative plastic flow and zero dilatancy, while the yield surface is defined by the Mohr-Coulomb criterion. The choice of the material model is motivated by matching the prerequisites for which an analytical ground reaction curve can be derived (see HOEK et al. [8]).

Tab. 1: Uncertain material parameters

Parameter	Distribution	Mean	CoV
Specific weight γ [kN/m^3]	Normal	27.0	5%
Young's modulus E [MPa]	Lognormal	5000.0	25%
Poisson's ratio ν	Beta(0.0, 0.5)	0.2	10%
Friction angle φ [$^\circ$]	Beta(0.0, 45.0)	39.0	10%
Cohesion c [MPa]	Lognormal	3.7	20%

The spatial variability of the material parameters is described by a homogeneous random field. The validity of this assumption is supported by the fact that the tunnel is deep and therefore the statistical properties may be taken as constant over space. In addition, a unified correlation length for the vertical and horizontal directions is assumed. Hence, the spatial variability may be defined by the exponential autocorrelation function, given in equation (7). The random field is discretized applying the midpoint method. The resulting SFE mesh consists of 113 deterministic finite element patches. In Fig. 2 the stochastic and deterministic finite element meshes are shown. Fig. 3 depicts colour plots of a realization of the Young's modulus' random field for different chosen correlation lengths.



(a) Stochastic finite element mesh

(b) Deterministic finite element mesh

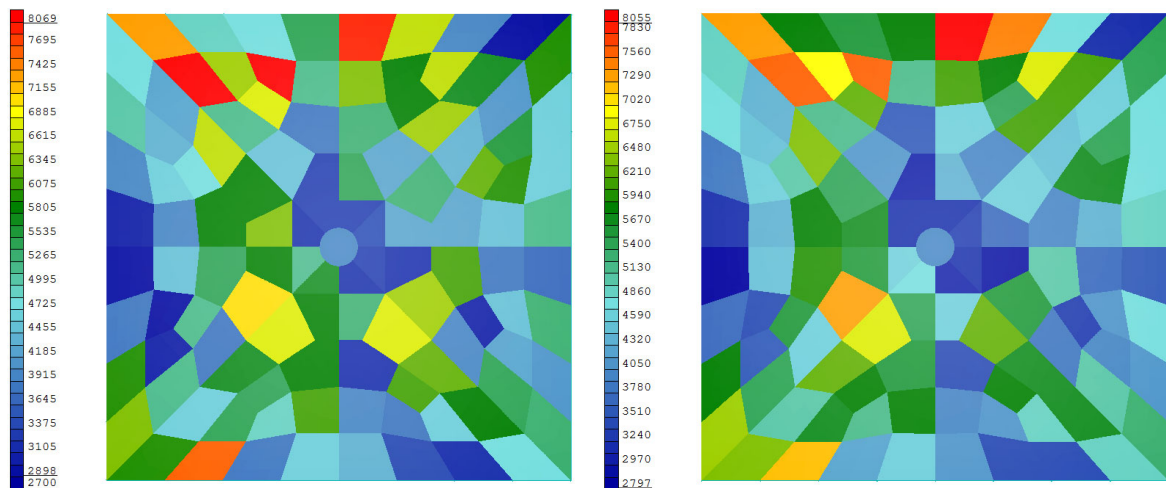
Fig. 2: Stochastic and deterministic finite element mesh

4.2 Computational approach

The consideration of the spatial variability of the uncertain parameters increases the computational cost for the reliability evaluation, due to the additional number of random variables emerging from the random field discretization. On the other hand, the representation of a spatially varied stochastic parameter by a single random variable implies a perfectly correlated random field, which is an approximation. It is therefore essential to judge whether it is necessary to consider all the distributed parameters as random fields. This

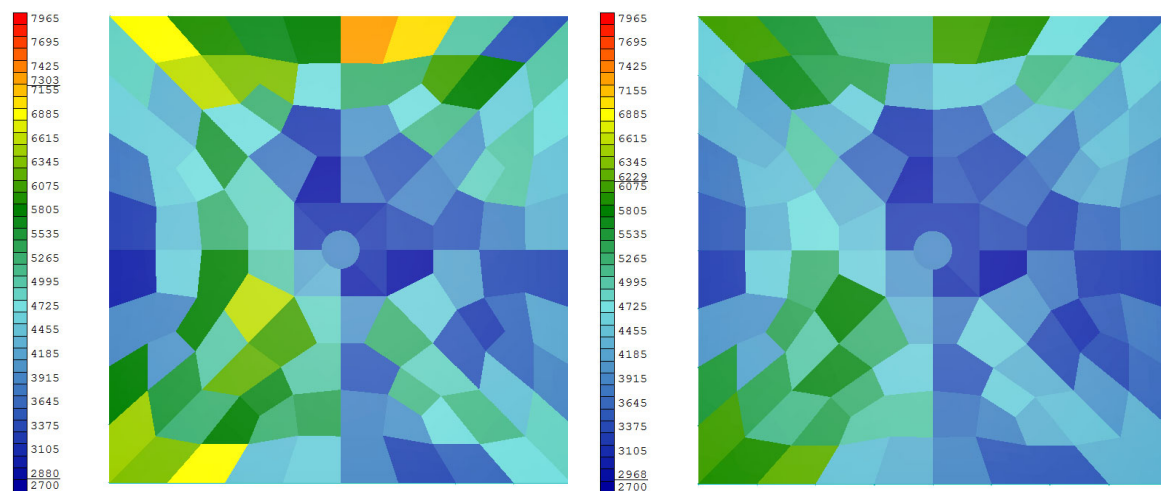
decision may be determined with the help of a sensitivity measure, such as the influence coefficients, defined in equation (12). According to this idea only the spatial variation of the most important parameters, i.e. with larger impact on the reliability, is considered.

To this end, a two step scheme is followed. First, the reliability analysis is performed applying the FORM and ignoring the spatial variability of the material parameters, therefore regarding all parameters as random variables. Then, the most influential parameters are discretized using the SFE mesh, shown in Fig. 2(a), and the reliability analysis is carried out applying the in high dimensions more efficient SubS.



(a) Correlation length $\lambda L = 5 m$

(b) Correlation length $\lambda L = 10 m$



(c) Correlation length $\lambda L = 20 m$

(d) Correlation length $\lambda L = 40 m$

Fig. 3: The same realization of the Young's modulus' lognormal random field in [MPa] for different correlation lengths

4.3 Results and discussion

In the first step, where all parameters are regarded as random variables, the FORM converged in 16 iterations, requiring a total number of 96 performance function evaluations.

The results were verified by the SubS with a chosen $p_0 = 0.1$. The number of samples for each conditional probability was set to 500. Three levels were adequate for the estimation of the failure probability, requiring 1400 performance function evaluations.

The FORM gave a good approximation, although slightly overestimating the reliability, as shown in Table 2. In Fig. 4, the influence coefficients are plotted. As expected, the Young's modulus E is the dominant variable. In addition, the friction angle φ and the specific weight γ appear to have a considerable influence, while the sensitivity upon the rest of the variables is negligible.

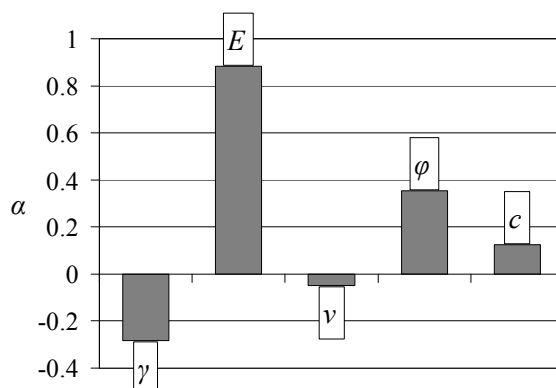


Fig. 4: Influence coefficients

In the second step, the SubS method was applied for the progressive consideration of the influence of the spatial variability of the most important random variables on the reliability. The correlation length was first set to $\lambda L = 5 m$. The results are shown in Table 2. It can be observed that the consideration of E , the parameter with the highest influence, improves the reliability estimation significantly, while the improvement from an additional consideration of the less influential φ is much less important.

In Fig. 5, the reliability index is plotted for different values of the correlation coefficient λ and the consideration of the Young's modulus E as a random field. The degree of correlation in the cases considered is illustrated by the realizations of the random field, shown in Fig. 3. The plot shows that as λ increases and thus the random field becomes more correlated, the reliability index approaches the value computed in the fully correlated case, where all parameters are regarded as random variables. Hence, it may be concluded that neglecting the spatial variation of the uncertain material parameters will lead to an underestimation of the tunnel's reliability. This may be quantified in the extreme case of a poorly correlated random field ($\lambda L = 5 m$) with a rough 20% relative error. Such a misestimation of the reliability in the design phase may have considerable economical impact on the structural design. On the other hand, the combination of regarding as random fields only the most important uncertain parameters and applying the efficient SubS method for the reliability estimation can give a reliable estimation with an affordable additional computational cost.

Tab. 2: Progressive consideration of the random fields for a correlation length of $\lambda L = 5 m$

Random field consideration	B		P_f	
	FORM	SubS	FORM	SubS
All parameters as random variables	2.414	2.358	7.886×10^{-3}	9.199×10^{-3}
Only φ as random field	-	2.390	-	8.420×10^{-3}
Only E as random field	-	2.949	-	1.600×10^{-3}
E and φ as random fields	-	3.046	-	1.160×10^{-3}

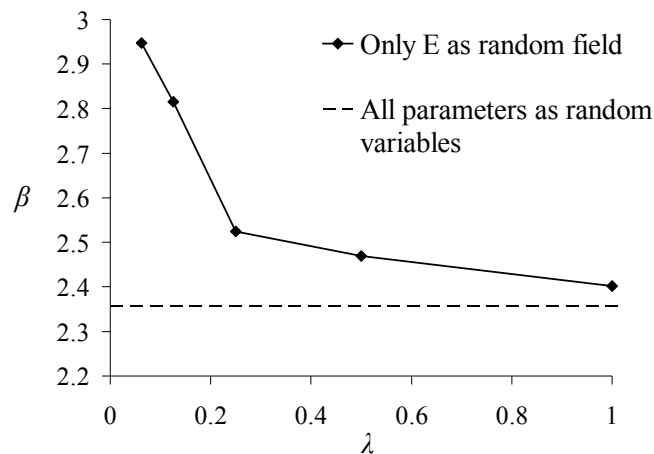


Fig. 5: Influence of the correlation length on the reliability

5 Conclusion

In this study, the subset simulation method was applied for the reliability analysis of a nonlinear tunnel finite element model. The uncertain material parameters of the soil were regarded as random variables and the spatial variability of the parameters with the highest influence on the reliability were modelled by a homogeneous random field. Therefore, the number of random variables resulting from the random field discretization was reduced, without losing accuracy in the reliability estimation. In addition, the subset simulation required only 1400 performance function evaluations, confirming its efficiency in high-dimensional problems.

It was also shown, that not accounting for the spatial variability of distributed uncertain parameters, such as the soil material properties, may lead to errors in the reliability estimation. These errors become more important in cases of poorly correlated random fields. It is therefore of practical interest to include spatial variability considerations in the reliability estimation, particularly when this may be achieved with a minimum additional computational cost.

6 References

- [1] Au, S.K.; Beck, J.L.: Estimation of small failure probabilities in high dimensions by subset simulation. *Probabilistic Engineering Mechanics* 16(4), (2001), pp 83-91
- [2] Au, S.K.; Ching, J.; Beck, J.L.: Application of subset simulation methods to reliability benchmark problems. *Structural Safety* 29(3), (2007), pp 183-193
- [3] Der Kiureghian, A.; Ke, J-B.: The stochastic finite element method in structural reliability. *Probabilistic Engineering Mechanics* 3(2), (1988), pp 83-91
- [4] Der Kiureghian, A.; Liu, P-L.: Structural reliability under incomplete probability transformation. *Journal of Engineering Mechanics ASCE* 112(1), (1986), pp 85-104
- [5] Ditlevsen, O.; Madsen, H.O.: *Structural Reliability Methods*. Chichester: John Wiley & Sons, 1996
- [6] Hasofer, A.M.; Lind, N.C.: Exact and invariant second moment code format. *Journal of Engineering Mechanics ASCE* 100, (1974), pp 111-121
- [7] Hastings, W.K.: Monte Carlo sampling methods using Markov chains and their applications. *Biometrika* 57(1), (1970), pp 97-109
- [8] Hoek, E.; Kaiser, P.K.; Bawden, W.F.: *Support of Underground Excavations in Hard Rock*. Rotterdam: Balkema, 1995
- [9] Metropolis, N.; Rosenbluth, A.W.; Rosenbluth, M.N.; Teller, A.H.; Teller, E.: Equations of state calculations by fast computing machines. *Journal of Chemical Physics* 21(6), (1953), pp 1087-1092
- [10] Papaioannou, I.; Heidkamp, H.; Düster, A.; Rank, E.; Katz, C.: Towards efficient reliability methods with applications to industrial problems. In: Topping, B.H.V.; Papadrakakis, M. (eds.): *Proceedings of the Ninth International Conference on Computational Structures Technology*. Stirlingshire: Civil-Comp Press, 2008, Paper 106
- [11] Papaioannou, I.; Heidkamp, H.; Düster, A.; Rank, E.; Katz, C.: Integration of reliability methods into a commercial finite element software package. In: Furuta, H. (ed.): *Proceedings of the 10th International Conference on Structural Safety and Reliability ICOSSAR 2009*. Osaka, 2009
- [12] Rackwitz, R.; Fiessler, B.: Structural reliability under combined random load sequences. *Computers and Structures* 9(5), (1978), pp 484-494
- [13] Rubinstein, R.Y.: *Simulation and the Monte Carlo Method*. New York: John Wiley & Sons, 1981

- [14] Schuëller, G. I.; Pradlwarter, H. J.: Benchmark study on reliability estimation in higher dimensions of structural systems – An overview. *Structural Safety* 29(3), (2007), pp 167-182
- [15] Schuëller, G. I.; Pradlwarter, H. J.; Koutsourelakis, P. S.: A critical appraisal of reliability estimation procedures for high dimensions. *Probabilistic Engineering Mechanics* 19(4), (2004), pp 463-474
- [16] Sudret, B.; Der Kiureghian, A.: *Stochastic Finite Elements and Reliability: A State-of-the-Art Report*. University of California, Berkeley, 2000 – Technical Report no UCB/SEMM-2000/08
- [17] Vanmarcke, E.H.: *Random Fields: Analysis and Synthesis*. Cambridge, MA: MIT Press, 1983

A modified approach to the polluter-pays-principle that accounts for the value of groundwater resources and its impact on statistical decision-making

Evan K. Paleologos

Department of Environmental Engineering, Technical University of Crete, Chania

Abstract: In environmental statistical decision-making a probabilistic model of success/failure, as well as, a loss function of the consequences of each potential action are defined in order to reach an optimal decision. The current interpretation of the polluter-pays-principle provides for a description of the environmental cost, and hence for loss functions, which are limited to the cost of construction and operation, as well as of remediation in the event of failure. Our work proposes an extension to the polluter-pays-principle and hence of the loss function, which for the case of pollution of groundwater resources accounts for the lost value of water. The lost value of groundwater is defined as the reduction in value resulting from the change of use of an aquifer's water from potable to irrigation water, which is what is returned after remediation. Our study develops an expression that accounts for this reduction in value, normalized for the subsidized pricing that exists for different uses of water.

The impact of our extended loss function in decision-making is studied through the case where the selection of the type of bottom liner in municipal landfills is considered. In this case, when the cost of pollution was considered to be equal to the clean-up cost the lowest-protection technology was preferred. When the lost value of groundwater was incorporated, the conclusions of the decision-making analysis shifted, and the highest level technology became the most profitable alternative. It appears that the effect of the extended PPP through the incorporation of the lost value of groundwater is sufficient to guide, voluntarily, environmental practices toward the selection of safer technologies.

1 Introduction

The Polluter Pays Principle (PPP) refers to the requirement that the cost of pollution should be borne by the person or organization causing the pollution. The practical application of the principle relates to the economic obligations, the liabilities, and the rules of competition and subsidies, in case of environmental damage. The meaning of the principle remains open in its interpretation and application, especially regarding the nature and the extent of the costs to be borne [3].

The principle appeared first at the international level in the 1972 Recommendation by the Organization for Economic Co-operation and Development (OECD) Council on Guiding Principles concerning International Economic Aspects of Environmental Policies. This endorsed the principle in a limited way, that is, the polluter should bear the cost of pollution prevention and control measures, which are deemed necessary by public authorities for the protection of the environment. This initial recommendation did not explicitly apply the PPP to the cost of environmental damages. Article 4 of the 1972 Recommendation stated [8]: *“The principle to be used for allocating costs of pollution prevention and control measures to encourage rational use of scarce environmental resources and to avoid distortions in international trade and investment is the so-called “Polluter-Pays Principle”. This principle means that the polluter should bear the expense of carrying out the above mentioned measures decided by public authorities to ensure that the environment is in an acceptable state. In other words, the cost of these measures should be reflected in the cost of goods and services which cause pollution in production and/or consumption. Such measures should not be accompanied by subsidies that would create significant distortions in international trade and investment.”* This standard or weak PPP as a guiding principle across countries arose from the need to safeguard international competitiveness of firms, which had to face implementation of the PPP at the domestic level.

In 1989 the PPP evolved into what is called *extended or strong* PPP with the OECD Council Recommendation on the Application of the Polluter-Pays Principle to Accidental Pollution [9]. This extended the principle to an operator of a hazardous installation, who should bear the cost of reasonable measures to prevent and control accidental pollution from the installation. Article 11 of the 1989 Recommendation appears to include also the clean-up costs and the rehabilitation of the polluted environment in its extended definition of the PPP by stating that: *“A further specific application of the Polluter-Pays Principle consists in charging, in conformity with domestic law, the cost of reasonable pollution control measures decided by the authorities following an accident to the operator of the hazardous installation from which pollution is released. Such measures taken without undue delay by the operator or, in case of need, by the authorities would aim at promptly avoiding the spreading of environmental damage and would concern limiting the release of hazardous substances (e.g., by ceasing emissions at the plant, by erecting floating barriers on a river), the pollution as such (e.g., by cleaning or decontamination), or its ecological effects (e.g., by rehabilitating the polluted environment).”*

The PPP has achieved the status of customary international law among the member states of the EU, the United Nations Economic Commission for Europe (UNECE), and the Organization for Economic Co-operation and Development (OECD). The PPP is one of the bases of the environmental policy of the European Community, with the 1997 Treaty Establishing the European Community, under Title XIX Environment, article 174.2 stating that: *“Community policy on the environment ... shall be based on the precautionary principle and on the principles that preventive action should be taken, that environmental damage should as a priority be rectified at source and that the polluter should pay.”*

However, at this stage the PPP does not appear to have achieved the status of customary international law governing environmental issues among all countries, but rather, with the exception of the above organizations, it is perceived to apply at the domestic level [11]. This was shown by the 1992 Rio Declaration, where a more limited language was utilized in the text (Principle 16): *“National authorities should endeavor to promote the internalization of environmental costs and the use of economic instruments, taking into account the approach that the polluter should, in principle, bear the cost of pollution, with*

due regard to the public interest and without distorting international trade and investment.”

On the positive side the PPP had the effect to discourage poor environmental practices and define the allocation of environmental costs within a country, as well as, promote economic efficiency and justice, and the harmonization of international environmental policies [1]. On the negative side its broad and not sharply defined scope has raised issues about its application. Some of the limitations of the PPP include: Small households and subsistence farmers, who in most cases cannot bear the cost of environmentally friendly practices; small and medium size firms serving local markets, which find it difficult passing the higher cost to their domestic market; exporters to developing countries, who find it hard to pass the environmental cost to such markets.

2 Modified Polluter-Pays-Principle

2.1 Lost Value of Groundwater

Groundwater resources constitute an important component of available freshwater, providing on a worldwide basis 50% of the potable water, 20% of the irrigation water, and 15% of the water needs for industrial use. This distribution is highly variable depending on a continent, a region, or a country, with groundwater providing, for example, 70% of the potable water in Europe, 20-25% in North America and Africa, and less than 20% in Asia. Within Europe this use ranges from almost 100% in Austria and Denmark to 60% in Belgium, France, and the Netherlands. At the same time exploitation of groundwater resources has increased dramatically; for example, this was increased by 54% (1950-75) in the United Kingdom, by 70% (1970-77) in Denmark, and tripling in Australia during 1970-2000. In addition to the overexploitation challenges exist relative to pollution activities. The situation is accentuated by poor management practices, which delegate fresh and ground water resources to a variety of agencies leading to rivalries and inefficiencies [2].

An important aspect is the significant time lag of overdraft or pollution problems, which would require groundwater management plans extending way beyond an electoral time-frame [12]. Groundwater differs from surface water in that it does not flow toward a single topographic outlet of a watershed, where the impact of human activities can be measured, but its discharge is influenced by the topography, hydrogeology, and the recharge and discharge to and from an area. This discharge can be directed toward neighboring wells, or to down-gradient lakes or streams, or through the subsurface environment to neighboring water basins. The time span when problems become obvious differs significantly from that of surface water. Groundwater velocities can range from a few meters per year, in poorly producing aquifers, to hundreds of meters in sandy, gravelly, or karstic aquifers making pollution effects appear years or decades after an initial release. Furthermore, rehabilitation is costly and long, and in most cases it has proven to be highly inefficient.

In view of the above and the projected water stress or scarcity conditions¹, which are expected to affect more than 2.8 billion people by 2025, and about 40% of the projected global population by 2050 it is reasonable to provide interpretations to the PPP, which extend the notion of pollution liability, and are better equipped to address future extreme water shortage conditions [United Nations Environment Programme (UNEP), [14]].

Current probabilistic environmental decision-making analyses are customarily performed by treating the cost of pollution as equal to the cost of remediation of an environmental damage. But in most cases remediation of the damage *does not always return the full value* of a good that has been affected. Groundwater, before a pollution event, exists, in the majority of cases, as *drinking water*, but after remediation returns as *irrigation water*.

The irrigation water can be argued that it will, eventually, return to the aquifer and with its infiltration through the soil reach its original quality. However, the fact remains that for a significant time period (of the order of decades or more) groundwater has faced a degradation of its quality, and correspondingly, a reduction in its value as a result of pollution and clean-up activities. Hence, the first stipulation proposed here toward the extension of the polluter-pays-principle reads as follows [10]:

$$\text{Lost Value of Groundwater} = \text{Value of Drinking Water} - \text{Value of Irrigation Water} \quad (1)$$

One then could, in principle, proceed as follows to assess the lost value of groundwater. The example of an existing groundwater plume from a Massachusetts military installation [7] is utilized here to perform some elementary calculations. This plume has affected 1.8 billion gallons of groundwater or equivalently 6,813,000 m³ of water. In each country public water utilities have detailed charges for different water uses. For example, in Greece, on the average, drinking water is charged at a rate of 0.38 Euros per 1m³, whereas the price of irrigation water ranges from 0.02 Euros to 0.08 Euros per 1m³ [6]. Using the most conservative value of 0.08 Euros per 1m³, for the irrigation water, this would return a lost value of groundwater for the above plume of:

$$\text{Lost value of groundwater} = (0.38 - 0.08) \times 6,813,000 = 2 \text{ million Euros}$$

This calculation, although useful in order to illustrate that the assessment of the lost value of groundwater can be done easily, is incorrect in providing a true measure of the value lost. The absolute prices for drinking and irrigation water do not reflect open market conditions, but subsidized prices. Each society provides cheap water to its population as a result of a historical evolution that has viewed water as a free public good. To use these prices, in absolute terms, for the evaluation of the lost value of groundwater, would mean that a society essentially subsidizes a polluter for practices that are not in compliance with its regulatory framework.

The correct approach to address the issue of water subsidies is to use the *ratio, M*, of drinking to irrigation water prices to reflect the socially acceptable, at each time period, relative value of the water depending on its use. For example, again using data from Greece, the ratio of the value of drinking to irrigation water lies between 5 : 1 up to 20 : 1, depending on the region. The second stipulation is, then, as follows:

The ratio of the subsidized prices, of drinking to irrigation water, reflects the

¹ An area faces water stress when water supplies fall below 1700 m³ per person, annually, and water scarcity when the respective volume falls below 1000 m³.

$$\text{relative value of each use of water that is socially acceptable} \quad (2)$$

The last stipulation is based on the premise that no rational entity pays for repairs, if the value of the good that is returned, is not at least equal to the amount paid to fix it. The amounts spent for remediation at different sites and countries would not have made sense if the retrieved value of the water at each location was not such as to justify this expenditure. This can be summarized as follows:

$$\begin{aligned} & \text{The amount paid for remediation, in each case and at each location, represents,} \\ & \text{at a minimum, the value of the water recovered} \end{aligned} \quad (3)$$

The assessment of the lost value of groundwater, as a result of a pollution event, based on these three stipulations can be summarized as follows². If, at a specific location, the cost of remediation of polluted groundwater is B, and at the same area the ratio of prices of drinking and irrigation water is M then:

B: is the value of irrigation water returned after remediation;

M B: is the value of the drinking-water-quality affected groundwater;

and then the Lost Value of Groundwater is: $MB - B = (M-1) B$.

This means that the expanded cost of pollution, incorporating the lost value of groundwater, is expressed as:

$$\begin{aligned} \text{Total Cost of Pollution} &= \text{Remediation Cost} + \text{Lost Value of GW} = \\ & B + (M-1) B = MB \end{aligned} \quad (4)$$

2.2 Case Study: Decision-Making Analysis for Landfill Bottom Liner

We proceed now to illustrate the above concepts by analyzing the selection of a bottom liner for a municipal waste landfill. The evaluation will proceed first in the customary fashion, i.e., considering that the environmental cost equals the remediation cost, and subsequently, the additional cost of the lost value of groundwater will be included to determine the impact of the modified polluter-pays-principle on the optimal selection.

The bottom liner constitutes, perhaps, the most important component for limiting leaks to the environment with the density, sampling frequency, and resolution of the monitoring system being the other critical factor in the design, if an early response to contamination is to be desired. There exist three types of bottom liners with the first two having similar effectiveness and costs, which will be considered as a single option, and the third type, the double liner, which is a combination of the other two, costing more and providing an extra level of protection. For the bottom liner of an average landfill with an area of 100 acres (1 acre = 4,047 m²) data from the State of Illinois give in 2003 the average construction cost to be [4]: Type I: \$9,420,100; Type II: \$7,988,300; and Type III \$14,342,400. The cost difference between the two options is about 5 million Euros (about \$6 million from the Illinois data).

² Alternatively, one could arrive at the lost value of groundwater by calculating the amount needed (or a portion thereof) to treat the affected volume in order to bring the irrigation water to drinking water quality standards.

The probability of failure *for limited contamination leaks*, defined as those not exceeding 2 million Euros in remediation costs, will be considered to be about $\theta=0.3$. Recent data from the State of Wyoming [13] have shown that from a total of 53 active municipal waste landfills in that State 12 have polluted the groundwater. The remediation cost of the groundwater per site was estimated to vary between \$500,000 and \$2.5 million. The higher number of \$2.5 million or about 2 million Euros will be considered to correspond to the remediation cost of a limited pollution event, i.e., a situation that is expected to occur, with a significant probability, based on historical experience. The numbers from the State of Wyoming correspond to a 23% probability of failure for active municipal waste landfills, constructed under regulations similar or more stringent than those of the *European Directive 1999/31/EC on the Landfill of Waste*. This is lower than a 40% failure quoted by U.S. EPA., and hence our selection of $\theta=0.3$ constitutes a compromise between these two estimates.

In order to illustrate the impact of incorporating the lost value of groundwater in the decision-making process the analysis will be kept at the simplest possible level, without consideration of the attitude of an organization to risk (and hence without the employment of utility functions, risk tolerance etc.), with a simple loss function, and without proceeding to a Bayesian framework, which would be appropriate for a more detailed analysis.

Even at the qualitative level though, it should be noted that there exists a significant difference of viewpoint between a private and a public entity. Given that the construction cost difference between the two options of bottom liner is 5 million Euros, if a private entity feels confident (because of the monitoring system installed etc.) that in the event of a contamination leak this will not prove to be catastrophic (remediation costs will not exceed 2 million Euros), then it is clear that, with the exception of a regulatory requirement, a private entity does not have any incentive to voluntarily select the second option of the double liner. In the case of a limited pollution event, even if it were certain that the bottom liner would leak in a limited fashion ($\theta=1.0$), a private entity would select, rationally, the least expensive option.

In contrast a public entity, even without considering the broader policy mandate for protection of the resources and the environment for future generations, has also a financial interest in selecting the higher level of protection afforded by the double liner. The difference of 3 million Euros between the construction cost of the options and the remediation cost of a limited leak corresponds to the cost of hiring 2-3 permanent technical personnel with annual (low) salary of 25,000 Euro for 35 years (without considering the cost of retirement, health coverage and other benefits). As a point of reference the State of Wyoming employs 230 people in the Department of Environmental Quality, with 80 of these people working in the division of solid waste (about 1.5 people per active landfill). The external cost of additional hires, of monitoring and regulating potential contamination leaks from landfills, can be compensated by the selection of technologies that provide increased levels of protection.

Limited Pollution Event (Remediation cost less than 2 million Euros): For a limited leak a private organization does not need to mathematically analyze the options since the cost difference between the technologies and the remediation activities does not warrant selection of the second option, the double liner. We will however proceed with a simple probabilistic cost-benefit analysis to establish the level of insurance, which is profitable to be considered by a private organization in the event of a leak.

The probability space can be described by the Bernoulli random variable:

$$X = \begin{cases} 1 & \text{Success(Pollution) Probability } \theta \\ 0 & \text{Failure Probability } 1-\theta, \end{cases} \quad (5)$$

and the action space, for a private entity that has decided that it is not worth to exceed the regulatory requirements, which are satisfied with the first option, and hence does not invest in the double liner, is simply given by:

- Action A(0): The organization does not purchase insurance for a limited pollution event
- Action A(1): The organization purchases insurance for a limited pollution event (6)

Let us designate with B the cost of pollution, and with C the cost of insurance, which would cover entirely the remediation cost, up to 2 million. A simple loss function is given in Table 1.

Tab. 1: Loss Function L(θ, A)

Event	Action: A(0)	Action: A(1)	Probability: P(X)
Pollution	B	C	θ
No Pollution	0	C	1-θ

The expected loss, with respect to X, for actions A(0) and A(1) is given, respectively, by:

$$\langle L(\theta, A(0)) \rangle = B \theta, \text{ and } \langle L(\theta, A(1)) \rangle = C,$$

and at the neutral point, when no action is preferable to the other, the probability $\theta = C/B$. For the values of $\theta=0.3$, and $B=2$ million this returns a value of $C=600,000$ Euros. Hence, a private organization can select either to face, with probability 30%, a potential remediation cost that can reach 2 million Euros, or spend up to 600,000 for insurance (or on any other measures, such as an extensive monitoring system), which will cover it up to 2 million for clean-up costs (or equivalently, minimize clean-up costs with an early detection).

Catastrophic Pollution Event (Remediation cost exceeds 2 million Euros): But what is of interest primarily to an organization is the possibility of a catastrophic pollution, the remediation cost of which can exceed by far a historically expected, limited level of pollution. In other terms, assuming that a private entity is unwilling to select the more expensive (and not mandated, at least in most States of U.S.A. and in Europe) double liner system what is the level of pollution and, correspondingly, of the remediation costs that may convince a private organization to, voluntarily, alter its decision? Industrial or chemical or medical waste (for example, expired medication, which is routinely disposed in domestic waste) has found its way in many municipal landfills and in such cases remediation costs can reach tens of millions.

We consider again expression (5), where now instead of the “no pollution” event we substitute the event “zero-base pollution,” i.e., any event, which falls within the range of historically, limited-scope pollution incidents, and whose remediation cost is relatively small compared to that of a catastrophic event, will be considered a “zero-base pollution” event. In our case, any remediation cost below 2 million, which historically has been

shown to occur with a significant probability (especially, if one considers the 50-70 year period of liability of a landfill), and which an organization should be capable to absorb is considered to be a “zero-base remediation cost”. In expression (5) the case of pollution represents now a catastrophic event, where the remediation cost, B, above a “zero-base remediation cost” is significant. We designate again with C the amount that a private entity wants to investigate whether it is worthwhile to spend in order to protect itself from the likelihood of a catastrophic leak.

The action space is phrased now in more general terms:

Action A(0): The organization selects the minimum mandated type of bottom liner and does not take measures in anticipation of a catastrophic event

Action A(1): The organization does take measures for a catastrophic pollution event (7)

The loss function, with the appropriate definitions of actions and events that apply to the catastrophic case, remains the same as in Table 1. Since the probability of a catastrophic failure is much smaller than the value of 30%, which was inferred from a record of limited pollution incidents, a value of $\theta=0.1$ is utilized. Hence, if the catastrophic cost reaches B=10 million (this amount is in excess of any amount needed for limited remediation) then the amount C that a private organization should be willing to spend in anticipation of a catastrophic spill is 1.0 million. Correspondingly, when B=20 million then C=2.0 million. This range of 10 to 20 million of remediation costs has historically been expended at sites for municipal waste where, either industrial, and/or chemical waste have been deposited (either accidentally or purposefully), or where the inadequacy of the monitoring system did not allow for early detection.

Hence, a private organization will benefit by expending 1 to 2 million above the cost of the EU regulatory requirement of bottom liner to protect itself from the possibility of a catastrophic event. It is clear that, even for what is considered catastrophic pollution for municipal waste landfills, the above amounts do not reach the additional cost of a double liner system and no profit-based organization would voluntarily select this option. The amounts of 1 to 2 million can also be viewed as the price difference that can make the double liner system competitive.

Modified Probabilistic Decision-Making Analysis: Our elementary analysis can now be repeated using the modified cost of pollution from expression (4). For a *limited pollution event*, with all the parameters of the problem remaining the same, i.e., probability of failure $\theta = 0.3$, and remediation cost of B = 2 million, and assuming a conservative ratio of prices for drinking to irrigation water of M=6, the new, total cost of pollution becomes 12 million. Upon substitution of this amount for the case of limited pollution the amount of 3.6 million is returned for C, the cost of additional measures that is worth for a private organization to spend. This indicates that, even for limited pollution events, which previously did not merit investigation of the double liner system, the use of this liner, when the cost of pollution is properly accounted for, makes economic sense. For *catastrophic pollution events*, with a probability of failure $\theta=0.1$, when the remediation cost is 10 million the modified analysis returns C=6 million, and when remediation costs reach 20 million then C becomes 12 million. Not only the double liner system, which previously would not have been considered, becomes now a profitable alternative but, in addition, a substantial amount for additional measures should be allocated by a private organization.

3 Conclusions

The conduct of probabilistic decision-making analyses for sanitary landfills, based on real data, is hindered by many problems. The type of waste deposited, and the function of a landfill, even in the case of a municipal waste landfill, which by law should receive only “...waste from households, as well as other waste which, because of the nature or composition is similar to waste from household...” (Article 2 of 1999/31/EC) can vary in practice. Many municipal waste landfills have either accidentally or purposefully received waste in violation of this mandate. This translates into pollution problems and correspondingly to remediation costs that can vary significantly, depending on whether a municipal waste landfill was constructed carefully and had good control of the type of waste received. Decision-analyses are faced then with the problem of either assuming a proper construction and operation of a landfill and hence bracketing a potential future remediation cost within a reasonable range that, usually, does not exceed one to two million dollars or allow, based on the history of many landfills, for regulatory violations and hence use much higher potential remediation costs for calculations. Since, what is of interest is to select the various elements before the construction of a landfill, this unknown future practice at a landfill means that a decision analysis may, in one case, suffer from underestimation, and in the other case of, overestimation of future costs and consequences.

Even for elements of the decision problem that are better controlled, such as the construction costs, these can vary from one country to another, and in different regions of a country. Significant cost overruns of initial construction estimates exist and, especially, for public projects these can make the conclusions of decision analyses that are based on the initial cost estimates questionable. The effectiveness of the elements of a landfill depends very much on the experience of the personnel that is used during the construction process, and this presents a difficulty in the estimation of the probability of failure of a system. Historical data indicate that, even for landfills that have been constructed under recent regulations and which, to the extent known, have been within the regulatory mandate of receiving only domestic waste the probability of limited failure (for remediation activities that do not surpass 2 million dollars) exceeds 20 percent.

Standard decision-making analyses equate the “cost of pollution” simply to the cost of remediating a site. Our analysis has illustrated that based on this premise, even for catastrophic costs of the order of tens of millions of dollars (which for municipal waste landfills represent the extreme case of non-compliance, poor construction, etc.) no profit-based organization has an incentive to voluntarily select a higher, and environmentally safer, technological alternative. Hence, this limited definition of what constitutes cost of pollution would lead rationally, without any externalities, an organization to pick the lowest-protection technology, barring a regulatory change.

The contribution of this article is to provide an extended definition of the Polluter-Pays Principle by including in this the lost value of groundwater. The lost value of groundwater results from the change of use of groundwater, from potable water, before a pollution event, to irrigation water, which is what is returned after remediation. Based on the stipulation that the remediation amount expended corresponds to the value of the groundwater affected (and which is returned as irrigation water), and the argument that the ratio of the subsidized prices of drinking water to irrigation water is truly representative of the relative value assigned to these uses by society, the total cost of pollution can be calculated. This

cost, which is the sum of the remediation cost and the lost value of groundwater, can be given, simply, by the expression of $M \times B$, where M is the ratio of the subsidized prices of drinking to irrigation water, and B is the remediation cost at the site where these prices for the water apply. Although the total cost of pollution in most cases extend to other components as well (value of resources, ecosystems etc.), which need to be assessed, the current modification provides a step forward for a more rational accounting of environmental costs.

This extended definition of pollution cost has as a consequence the alteration of the conclusions of a cost-benefit probabilistic analysis. Even for limited pollution events, which in our case did not merit an analysis for the selection of a technological option, the more expensive, and environmentally safer, double liner system appears to be the most profitable alternative. For more expensive remediation efforts, not only the highest technology becomes the preferred choice but there exists, additionally, a substantial margin for implementation of supplementary measures, such as insurance, denser monitoring network etc.

It appears that the incorporation of the lost value of groundwater in the definition of the PPP is sufficient to guide, voluntarily, toward the selection of safer environmental practices.

3.1 Literature

- [1] Bugge H. C. (1996). "The principles of polluter pays in economics and law", in Eide E. and van der Bergh R. (eds) *"Law and Economics of the Environment"*, Oslo: Juridisk Forlag.
- [2] Darnault (ed.), C.J.G. (2008). *"Overexploitation and contamination of shared groundwater resources,"* Springer.
- [3] De Lucia, Vito (Lead Author); Richard Reibstein (Topic Editor). (2008). "Polluter pays principle." In: *Encyclopedia of Earth*. Eds. Cutler J. Cleveland (Washington, D.C.: Environmental Information Coalition, National Council for Science and the Environment). [First published in the Encyclopedia of Earth January 28, 2007; Last revised August 22, 2008; Retrieved August 30, 2009].
- [4] Illinois EPA (Environmental Protection Agency). (2003). *A Study of the Merits and Effectiveness of Alternate Liner Systems at Illinois Landfills*. A research paper submitted in fulfillment of House Resolution 715 of the State of Illinois 92nd General Assembly, 58 pp.
- [5] Jaynes, E.T. (2003). *Probability Theory: The Logic of Science*. Cambridge: Cambridge University Press, pp. 758.
- [6] Latinopoulos, P. (2005). Valuation and pricing of irrigation water: An analysis in Greek agricultural areas. *Global NEST Journal* **7(3)**: 323-335.
- [7] Massachusetts Military Reservation Installation Restoration Program (MMR IRP), *Groundwater Plumes. Landfill 1 (LF-1) Groundwater Plume*. www.mmr.org/cleanup/plumes.htm (accessed July 18, 2009).

- [8] OECD. (1972). [*Recommendation of the council on guiding principles concerning international economic aspects of environmental policies*](#). Council Document no. C(72)128. Paris: Organization of Economic Cooperation and Development.
- [9] OECD. (1989). [*Recommendation of the Council concerning the Application of the Polluter-Pays Principle to Accidental Pollution C\(89\)88*](#). Paris: Organization of Economic Cooperation and Development.
- [10] Paleologos, E.K. (2008). "The lost value of groundwater and its influence on environmental decision-making," *Jour. of Risk Analysis*, Vol. 28(4), pp. 939-950.
- [11] Sands, P., (2003). *Principles of international environmental law*, 2nd edition, Cambridge University Press.
- [12] Sophocleous, M. (2002). Interactions between groundwater and surface water: The state of the science, *Hydrogeology Journal*, vol. 10, pp. 52-67.
- [13] Wyoming Department of Environmental Quality (DEQ). (2004). Solid and Hazardous Waste Division. March 9, 2004. *Remediation at Municipal Landfills*. Draft Policy Paper: pp. 1-4.
- [14] UNEP: <http://www.unep.org/dewa/assessments/ecosystems/water/vitalwater/21.htm>

List of Probabilistic Workshops/Symposiums in this series


TECHNISCHE UNIVERSITÄT DRESDEN
Fakultät Bauingenieurwesen

1. Dresdner Probabilistik-Symposium – Sicherheit und Risiko im Bauwesen



Dresden, 14. November 2003


TECHNISCHE UNIVERSITÄT DRESDEN
Fakultät Bauingenieurwesen

2. Dresdner Probabilistik-Symposium – Sicherheit und Risiko im Bauwesen



Dresden, 12. November 2004


BCU
Universität für Bodenkultur Wien
Department für Bodenbau & Naturgefahren

3rd Probabilistic Workshop
Technical Systems
Natural Hazards

Schriftenreihe des Departments
 Nr. 7 November 2005



Konrad Bergmeister
 Dieter Richmann
 Alfred Straus



4th International Probabilistic Symposium
12th-13th October 2006
BAM, Berlin

Federal Institute for Material Research and Testing (BAM), Berlin
 University of Natural Resources and Applied Life Sciences, Department of Civil Engineering and Natural Hazards, Vienna
 Academia Morska Szczecin






5th International Probabilistic Workshop
Luc Taerwe & Dirk Proske
Editors

28-29 November 2007
Ghent, Belgium

acco

32. Darmstädter Massivbauseminar



6th International Probabilistic Workshop
Graubner, Schmidt & Proske
Editors

26-27 November 2008
Darmstadt, Germany